



FACULTY OF SCIENCE AND TECHNOLOGY

MASTER'S THESIS

Study programme / specialisation: Structural Engineering and Materials Science	The <i>spring</i> semester, 2023 Open
Authors: Vetle Chyba Norstad Herman Fossan-Waage Vaka	
Supervisor at UiS: Professor Dimitrios Pavlou External supervisors: Maria Teige Kristoffer Johansen	
Thesis title: Integration of a skid and hatch-based launch and recovery system for ROVs on USVs	
Credits (ECTS): 30	
Keywords: ROV, USV, SKID, LARS, hatch	Pages: 92 + appendix: 187 Stavanger, 15.06.2023

Design of a Skid and Hatch-Based Launch and Recovery System for ROVs on USVs

Vetle Chyba Norstad

Herman Fossan-Waage Vaka

Faculty of Science and Technology
Department of Mechanical and Structural Engineering and Material Science
Master of Science Thesis, Spring 2023
NO-4021 Stavanger, Norway

15.06.2023

Preface

This Master thesis marks the end of the studies in the Structures and Materials program at the University of Stavanger (UiS). We are grateful to DeepOcean for providing us with this opportunity and for their support throughout this innovative project. Maria Teige and Kristoffer Johansen from DeepOcean have been involved as our contact persons and advisors, offering valuable insights and guidance.

We extend our sincere gratitude to Professor Dimitrios Pavlou for serving as our project supervisor. Pavlou has been a constant source of support and technical expertise, providing invaluable guidance during the research phases and how to conduct a design project. His knowledge and mentorship have played a significant role in the success of our work.

Vetle Chyba Norstad

Herman Fossan-Waage Vaka

Haugesund, June 2023

Summary

Subsea surveying plays a crucial role in the oil and gas industry by facilitating the maintenance, repair, and inspection of underwater equipment and infrastructure. As the demand for sustainable offshore oil and gas resources grows, there is an urgent need for cost-effective and efficient surveying methods. To address this, the use of Unmanned Surface Vessels (USVs) for launching and recovering remotely operated vehicles (ROVs) has emerged as a promising solution. Developing a specialized Launch and Recovery System (LARS) for USVs can significantly enhance survey operations, resulting in longer ROV operation durations, reduced reliance on support vessels, and improved overall efficiency.

The primary objective of this thesis is to design an efficient LARS for ROVs using USVs. This involves the development of a hatch and skid that enable seamless transitions between the USV and the ocean. Modifications will be made to an existing survey skid to ensure its suitability, and static analysis will be conducted to validate the designs and identify areas for improvement. Various design options and materials will be explored to withstand impact loads and optimize performance.

This study's development of the new LARS system along with its components and design considerations, holds significant potential to advance subsea surveying technology. It can enable safer and more efficient exploration and maintenance of offshore oil and gas resources while promoting the sustainable development of offshore energy.

Sammendrag

Undervanns undersøkelser er en essensiell del av olje- og gassindustrien, og muliggjør vedlikehold, reparasjon og inspeksjon av utstyr og installasjoner på havbunnen. Med den økende etterspørselen etter offshore olje- og gassressurser, er det et større behov for kostnadseffektive og effektive metoder for å vedlikeholde og kartlegge havbunnsressurser. For å imøtekomme dette behovet har bruken av ubemannede overflatefartøy (USV-er) for utsetting og henting av fjernstyrte undervannsfarkoster (ROV-er) blitt sett på som en lovende løsning. Utviklingen av et spesialisert system for utsetting og henting (LARS) for USV-er kan betydelig forbedre undersøkelsesoperasjoner, noe som resulterer i økt driftstid for ROV-er, redusert avhengighet av støttefartøy og forbedret effektivitet.

Hovedmålet med denne avhandlingen er å designe en effektiv LARS for ROV-er ved bruk av USV-er. Dette innebærer utvikling av en luke og en ROV ramme som muliggjør sømløs overgang mellom USV-en og havet. Det vil bli gjort modifikasjoner på en eksisterende ramme for å sikre dens egnethet, og statiske analyser vil bli utført for å validere designene og identifisere områder for forbedring. Forskjellige designalternativer og materialer vil bli utforsket for å tåle støtbelastninger og optimalisere ytelsen.

Dette studiets utvikling av det nye LARS-systemet sammen med dets komponenter og design har betydelig potensial for å fremme teknologien innen undervannsundersøkelser. Det kan muliggjøre sikrere og mer effektiv utforskning og vedlikehold av offshore olje- og gassressurser samtidig som det fremmer bærekraftig utvikling av offshore energi.

Table of contents

SUMMARY	VI
SAMMENDRAG	VII
FIGURES	XI
TABLES	XIV
ABBREVIATIONS.....	XV
VARIABLES	XVI
1 INTRODUCTION	1
1.1 BACKGROUND.....	1
1.2 DEEPOCEAN.....	2
1.3 LITERATURE REVIEW	2
1.4 KYSTDESIGN SUPPORTER WORK-CLASS ROV	4
1.5 OCEAN CHALLENGER USV.....	4
1.6 OBJECTIVES	5
1.7 SKID REQUIREMENTS	5
1.8 HATCH REQUIREMENTS.....	7
2 METHOD.....	8
2.1 DESIGN AND STRUCTURAL ANALYSIS	8
2.2 TOOLS	8
2.2.1 <i>Autodesk Inventor</i>	8
2.2.2 <i>Autodesk Nastran</i>	8
2.2.3 <i>Mathcad Prime</i>	8
2.3 STANDARDS.....	8
3 PRELIMINARY DESIGN.....	9
3.1 HATCH DESIGN.....	9
3.1.1 <i>Structural analysis of preliminary hatch</i>	10
3.2 SKID.....	12
3.2.1 <i>Improvements to be made from existing skid</i>	13
3.2.2 <i>Preliminary skid</i>	15
3.2.3 <i>Structural analysis of preliminary skid</i>	16
3.3 MATERIALS	17
3.3.1 <i>S165M W1.4418</i>	17
3.3.2 <i>6082-T6</i>	18
3.3.3 <i>API 5L X65</i>	18
3.3.4 <i>S420N</i>	18
3.3.5 <i>Strenx 700 OME</i>	18
3.3.6 <i>Polyethylene High density (PEHD) 1000</i>	18
3.3.7 <i>Ethylene-propylene diene monomer (EPDM)</i>	19
3.3.8 <i>Fasteners</i>	19
3.3.9 <i>Material properties and partial factors</i>	19
3.4 SURFACE TREATMENT	20
4 LOADS.....	21
4.1 ASSUMPTIONS AND LIMITATIONS	21
4.2 DESIGN PARAMETERS	21
4.2.1 <i>Free body diagram of ROV and hatch</i>	21
4.2.2 <i>Wave kinematics</i>	22
4.2.3 <i>USV kinematics</i>	23
4.2.4 <i>Resulting kinematics for the water, USV and ROV</i>	24
4.3 KINETIC- AND ELASTIC POTENTIAL ENERGIES	24

4.3.1	<i>Kinetic- and elastic potential energy of impact</i>	24
4.3.2	<i>Damping of rubber</i>	25
4.4	DETERMINING THE ENERGY TRANSFER LOAD FROM THE ROV	26
4.5	ENVIRONMENTAL LOADS	27
4.5.1	<i>Hydrodynamic forces</i>	27
4.5.2	<i>Buoyancy force</i>	29
4.5.3	<i>Permanent force</i>	29
4.6	SUM OF FORCES ACTING ON THE HATCH	29
4.7	LOAD CASES AND LOAD FACTORS.....	30
4.8	DETERMINING BOLT CAPACITY AND WELD STRESSES	31
4.8.1	<i>Fasteners</i>	31
4.8.2	<i>Welded connections</i>	31
4.8.3	<i>Design of fillet welds with directional method</i>	32
5	STRUCTURAL ANALYSIS	35
5.1	ANALYSIS SETUP	35
5.2	HATCH	35
5.2.1	<i>Hatch analysis</i>	37
5.2.2	<i>ULS-a LCA</i>	37
5.2.3	<i>Support loads</i>	41
5.2.4	<i>Stresses, deformation, and pin forces</i>	42
5.3	SKID.....	42
5.3.1	<i>Model</i>	42
5.3.2	<i>Skid analysis</i>	44
5.3.3	<i>Load case 1</i>	45
5.3.4	<i>Load case 4</i>	48
5.3.5	<i>Calculations of selected structural items</i>	50
5.4	CRITICAL LOAD BEARING WELDS	54
5.4.1	<i>Critical weld 1</i>	55
5.4.2	<i>Critical weld 2</i>	55
5.4.3	<i>Critical weld 3</i>	57
5.4.4	<i>Critical weld 4</i>	57
5.4.5	<i>Critical weld 5</i>	58
5.4.6	<i>Critical weld 6</i>	59
5.4.7	<i>Summary of calculations for critical load bearing welds</i>	59
5.5	INTEGRITY OF EPDM AND PEHD 1000	60
5.6	SUMMARY OF KINETIC AND ELASTIC POTENTIAL ENERGIES	60
6	FINAL DESIGN	62
6.1	HATCH	62
6.2	SKID.....	64
6.2.1	<i>Review of centre of gravity</i>	67
6.3	COMBINED SYSTEM	68
7	CONCLUSION	69
8	BIBLIOGRAPHY	70

Figures

Figure 1 Conventional LARS for survey and construction vessels [2]	1
Figure 2 DeepOcean’s patent WO2022/035322A1 for launch and recovery of underwater units or vehicles [6].	3
Figure 3 Kystdesign Supporter ROV	4
Figure 4 Operational concept for launch and recovery of ROV from USV, source: DeepOcean.	5
Figure 5 Hatch designs included in DeepOcean’s patent WO2022/035322A1 [6].	9
Figure 6 Preliminary hatch model	10
Figure 7 Preliminary hatch model with constraints and fQ at centre of the outmost pipe.	11
Figure 8 Preliminary hatch stress map top view.	11
Figure 9 Preliminary hatch stress map bottom side pipe connections.	12
Figure 10 Preliminary hatch stress map topside pipe connections.	12
Figure 11 Existing skid improvements front view	13
Figure 12 Existing skid improvements rear view	14
Figure 13 Existing skid improvements bottom view	14
Figure 14 Preliminary skid design front view	15
Figure 15 Preliminary skid design bottom view	15
Figure 16 Stress map preliminary skid beam starboard side view	16
Figure 17 Stress map preliminary skid starboard side view of bolted connections.	17
Figure 18 System overview	21
Figure 19 FBD of ROV with skid	22
Figure 20 FBD of hatch.	22
Figure 21 Annotations for the components acting on the hatch.	22
Figure 22 Applied fQ locations for determining elastic potential energy of hatch.	26
Figure 23 Hatch model split into pipes, box beams and T-bars, for calculating separate hydrodynamic loads.	28
Figure 24 Stresses σ_{\perp} , σ_{\parallel} , τ_{\perp} and τ_{\parallel} , acting on the throat section of a fillet weld [23].	32
Figure 25 Meshed model of the hatch.	35
Figure 26 Constraints in hatch hinge and pipe support.	36
Figure 27 Symmetry constraints to hatch model.	36
Figure 28 Applied environmental loads on structural hatch model.	37

Figure 29 Stress map hatch ULS-a LCA top view	38
Figure 30 Stress map hatch ULS-a LCA bottom view	38
Figure 31 Stress map hatch ULS-a LCA hinge of T-bars	39
Figure 32 Stress map hatch ULS-a LCA bottom.....	39
Figure 33 Stress map hatch ULS-a LCA T-bar connection bottom view	40
Figure 34 Stress map hatch ULS-a LCA T-bar top view	40
Figure 35 Stress map Hatch ULS-a LCA T-bar bottom view	41
Figure 36 Skid stress analysis model top view.....	42
Figure 37 Skid applied load case locations.	43
Figure 38 Skid model constraints annotations.....	43
Figure 39 Skid symmetry meshed model with constraints and fasteners, port side.....	44
Figure 40 Skid symmetry meshed model with constraints and fasteners, starboard side.....	44
Figure 41 Stress map load case 1 top view.....	46
Figure 42 Stress map load case 1 max stress.....	46
Figure 43 Stress map case 1 impact zone front view	47
Figure 44 Stress map load case 1 impact zone side view bolt connections.....	47
Figure 45 Stress map load case 4 top view.....	48
Figure 46 Stress map load case 4 max stress.....	49
Figure 47 Stress map load case 4 impact zone side view	49
Figure 48 Meshed model with forces and constraints of doppler with INS holder	50
Figure 49 Stress map doppler with INS holder top view	51
Figure 50 Meshed model with forces and constraints of MUX pod drawer with dummy MUX.....	52
Figure 51 Stress map MUX pod drawer max stress	52
Figure 52 Meshed model with forces and constraints of Top beam with dummy beam attached.....	53
Figure 53 Stress map top beam	53
Figure 54 Critical load bearing welds in the bottom part of the skid	54
Figure 55 Critical load bearing welds in the hatch.....	54
Figure 56 Critical weld section 1	55
Figure 57 Critical weld section 2	55
Figure 58 Critical weld section 2 equivalent cross section	56
Figure 59 Bending moment calculation model for critical weld section 2.....	56

Figure 60 Critical weld section 3	57
Figure 61 Critical weld section 4	57
Figure 62 Critical weld 4 cross section A	58
Figure 63 Critical weld 4 cross section B.....	58
Figure 64 Equivalent cross section of critical weld 4 cross section A	58
Figure 65 Critical weld section 6	59
Figure 66 Contact region during impact between ROV and hatch, with annotation of rubber profiles, front view	60
Figure 67 Impact between ROV and hatch at LCF, side view	61
Figure 68 Final hatch design square beam cross section view	62
Figure 69 Final hatch design pipe materials.....	63
Figure 70 Final hatch design cross section view of joint reinforcement	63
Figure 71 Final hatch design cross section view EPDM rubber and PEHD	64
Figure 72 Final hatch design cross section view hinged beam.....	64
Figure 73 Final skid design top view sensor placement.....	65
Figure 74 Final skid design top view multibeam and lasers	65
Figure 75 Final skid design front view ROVINS and MUX.....	66
Figure 76 Final skid design impact dampers.....	66
Figure 77 Annotation of COG reference point.....	67
Figure 78 Visual representation of COG in skid side and top view	67
Figure 79 Combined system ROV with skid angled on hatch side view	68
Figure 80 Combined system ROV with skid flat on hatch side view.....	68

Tables

Table 1 Kystdesign Supporter ROV specifications.....	4
Table 2 Ocean Challenger USV specifications	4
Table 3 Sensor function- and placement	6
Table 4 Applied materials.	19
Table 5 Kinematics for the water, ROV and USV	24
Table 6 Deformation in hatch with deformation loads.....	27
Table 7 Hydrodynamic forces acting on the hatch.....	29
Table 8 Load factors for ULS according to [19].	30
Table 9 Resulting forces applied to hatch with load factors applied.....	30
Table 10 Resulting support loads for hatch analysis.	41
Table 11 Resulting stresses, deformation, and pin forces for hatch analysis.	42
Table 12 Resulting stresses, deformation, and fastener forces for skid analysis.....	45
Table 13 Resulting support loads for skid analysis.	45
Table 14 Stress analysis results for doppler with INS holder.....	50
Table 15 Stress analysis results for MUX pod drawer	51
Table 16 Stress analysis results for Top beam	53
Table 17 Results from weld check calculations	59
Table 18 Kinetic and elastic potential energies in the ROV, hatch and skid	60
Table 19 COG of skid with sensors.....	67

Abbreviations

Abbreviations	Description
CAD	Computer Aided Design
CTD	Conductivity, Temperature and Density
EPDM	Ethylene-propylene diene monomer
FBD	Free Body Diagram
LARS	Launch and Recovery System
PEHD	Polyethylene High density
PHINS/ROVINS	iXblue INS
ROV	Survey Remotely Operated Vehicle
ROV	Work-Class Remotely Operated Vehicle
RTS	Rental Technology & Services AS
TMS	Tether Management System
TSS	Teledyne Pipe tracking System
Tx/Rx	Transponders/Responders
ULS	Ultimate Limit State
USV	Unmanned Surface Vessel

Variables

A	=	Load area [m ²]
A_s	=	Stress area [mm ²]
E	=	Young's modulus [GPa]
E_c	=	Effective compression modulus [N/m]
E_k	=	Kinetic energy of ROV [J]
F	=	Force [N]
F_B	=	Design buoyancy load [kN]
F_E	=	Design environmental load [kN]
F_G	=	Design permanent load [kN]
F_Q	=	Design energy transfer load [kN]
F_Q	=	Design energy transfer load [kN]
$F_{v,Ed}$	=	Design shear force
$F_{v,Rd}$	=	Design shear capacity
F_x	=	Force in the local x-direction [kN]
F_y	=	Force in the local y-direction [kN]
g	=	Gravity [m/s ²]
F_z	=	Force in the local z-direction [kN]
H_S	=	Significant wave height [m]
K_c	=	Compressive spring rate of rubber [N/m]
L_{rb}	=	Length load area [m]
L_{USV}	=	Length of USV [m]
M	=	Bending moment [Nmm]
m	=	Mass of item [m]
S_b	=	Block shape factor [-]
S_f	=	Shape factor [-]
S_t	=	Tube shape factor [-]
T	=	Torsion [Nmm]
T_z	=	Zero-up-crossing wave period [s]
t	=	Thickness of rubber material [m]
U_{el}	=	Elastic potential energy of hatch [J]
u	=	Total displacement [mm]
V	=	Volume of item [m ³]
W_{ey}	=	Section modulus [mm ³]
W_p	=	Polar section modulus [mm ³]
W_{rb}	=	Width of rubber block [m]
a	=	Effective throat thickness [mm]
a_1	=	Incline angle of hatch [degrees]
$a_{n.USV}$	=	USV acceleration normal to hatch [m/s ²]
a_r	=	Relative acceleration between ROV/Water and USV hatch
a_v	=	Correction for the cut-off area, = 0.6 for class 8.8 screws [-]
$a_{v.ROV}$	=	ROV acceleration normal to hatch [m/s ²]
$a_{v.USV}$	=	USV vertical acceleration [m/s ²]
$d_{COG,ROV}$	=	Distance from water plane to centre of gravity of submerged part of the ROV [m]
$d_{COG.ROV}$	=	Distance to COG of ROV [m]
d_c	=	Compressive displacement [m]
d_c	=	Compressive displacement [mm]
d_i	=	Inner diameter of rubber tube [m]
d_o	=	Outside diameter of rubber tube [m]
f_A	=	Added mass force [kN]
f_B	=	Buoyancy force [kN]
f_D	=	Drag force [kN]

f_G	=	Permanent weight force [kN]
f_I	=	Inertial force [kN]
f_Q	=	Energy transfer load [kN]
f_u	=	Ultimate tensile strength [MPa]
$f_{u.haz}$	=	Ultimate tensile strength for HAZ in aluminium [MPa]
f_y	=	Yield strength [MPa]
$f_{y.haz}$	=	Yield strength for HAZ in aluminium [MPa]
l_W	=	Total length of the longitudinal fillet welds [mm]
l_{W1}	=	Weld length 1 [mm]
l_{W2}	=	Weld length 2 [mm]
l_{W3}	=	Weld length 3 [mm]
l_{eff}	=	Effective length of the longitudinal fillet welds [mm]
m_{ROV}	=	Mass of ROV [kg]
m_a	=	Added mass [kg]
u_s	=	Total displacement [mm]
$v_{h.USV}$	=	USV horizontal velocity [knots]
$v_{n.ROV}$	=	ROV velocity normal to hatch [m/s]
v_r	=	Relative velocity between ROV/Water and USV hatch
$v_{v.ROV}$	=	ROV vertical velocity [m/s]
γ_{2M}	=	Partial factor welds and joints [-]
γ_B	=	Partial factor buoyancy load [-]
γ_E	=	Partial factor environmental load [-]
γ_G	=	Partial factor permanent load [-]
γ_L	=	Partial factor load [-]
γ_{M1}	=	Partial factor material [-]
γ_Q	=	Partial factor variable functional load [-]
η_h	=	Utilization of horizontal weld [-]
η_s	=	Utilization of weld section [-]
η_v	=	Utilization of vertical weld [-]
σ_{\parallel}	=	Normal stress parallel to the weld axis [MPa]
σ_{\perp}	=	Normal stress perpendicular to the throat section [MPa]
σ_{vm}	=	Von Mises stress [MPa]
τ_{\parallel}	=	Shear stress acting on the throat section parallel to the weld axis [MPa]
τ_{\perp}	=	Shear stress acting on the throat section perpendicular to the weld axis [MPa]
C_A	=	Added mass coefficient of submerged part of item [-]
C_D	=	Drag coefficient in oscillatory flow of submerged part of item [-]
S	=	Projected area normal to the force direction [m ²]
v	=	Impact velocity between USV and ROV during recovery [m/s]
ζ	=	Characteristic wave amplitude [m]
ρ	=	Density of sea water [kg/m ³]
ϕ	=	Elastomer compression coefficient [-]

1 Introduction

The introduction will provide a comprehensive overview of the thesis, including its claims, significance, methodology, existing design, as well as defining the objectives and requirements.

1.1 Background

Subsea surveying plays a vital role in the oil and gas industry for maintenance, repair, and inspection tasks on subsea installations and equipment. With the depletion of onshore reserves, there has been an increased demand for offshore oil and gas exploration, leading to more offshore drilling operations. [1].

Traditionally, subsea surveying has been performed using remotely operated vehicles (ROVs) launched from large construction- and specialized ROV support vessels. However, the operational expenses associated with these large ships have driven the search for more cost-effective surveying methods [1]. One such approach is the use of Unmanned Surface Vessels (USVs) to launch and recover ROVs. This method allows for longer ROV operation durations, reduces the reliance on support vessels, and improves survey efficiency.

Ensuring the protection of sensors during the launch and recovery process is up most important for an effective LARS (Launch and Recovery System). In the harsh ocean environment, where the conditions can be challenging, protecting the sensors from damage becomes crucial. These sensors are not only essential for collecting high-quality data but can also be expensive to replace. Thus, the design of the LARS system must prioritize the preservation of these sensitive components.

To achieve this, careful consideration needs to be given to the implementation of a robust skid and hatch solution. The skid serves as a dedicated platform attached to the ROV, providing a secure base for the sensors and other equipment. Its purpose is to shield the sensors during the challenging launch and recovery phases, mitigating the risk of any potential damage. Meanwhile, the hatch, positioned aft of the vessel, should facilitate the smooth entry, and exit of the ROV without compromising the integrity of skid including sensors.

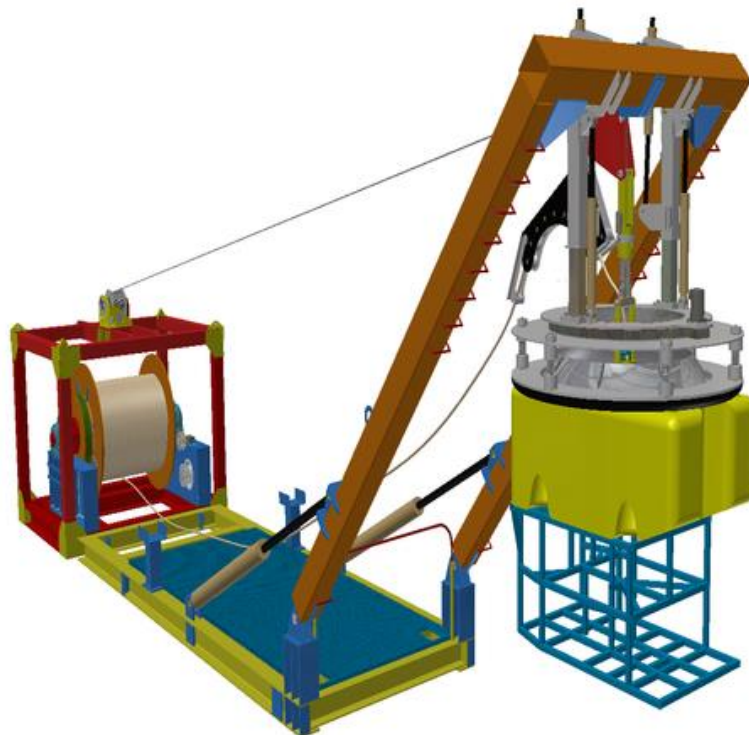


Figure 1 Conventional LARS for survey and construction vessels [2]

The conventional LARS for ROVs is comprised of four key components, shown in Figure 1: a A-frame, a winch system, an umbilical cable, and a tether management system (TMS). The A-frame is mounted on the vessel's deck and provides a platform for the winch system, which is deploying and retrieving the ROV from the water.

The umbilical cable is connected to the ROV and the winch system, providing the communication and power link between the ROV and the vessel. During operation, the manages the umbilical cable to ensure it remains free from entanglement or damage.

However, using a traditional LARS system for USVs can present challenges that make up the reason for the new type of LARS. These challenges have been presented by DeepOcean and are as follows:

- **Smaller vessel:** Due to its limited length of only 26.9 m, a traditional LARS A-frame cannot be installed over the side of the smaller vessel as it would compromise the vessel's stability.
- **Moonpool Challenges:** Smaller vessels face challenges in using a moonpool for launching and recovering ROVs. The vessel's reduced size can cause the frequency of movements to increase, requiring the use of a TMS to add weight to the ROV in the water, enabling the winch to maintain CT and control the ROV movements.
- **Increased Complexity:** Operating an unmanned ROV system on a smaller vessel can be complex. Fewer components are desirable to ensure smooth operation, but adding a TMS, for example, can increase complexity, making it challenging to operate and maintain the system on a USV.
- **Large Movements:** When a small vessel is in motion or experiencing rough seas, the movements of the vessel will be much larger than a traditional 100m long supply vessel. The largest movements will be aft and to have a A-frame with a snubber reeling in the ROV would lead to high possibility of uncontrolled collision between ROV and the snubber. ROV is neutral in water and will follow the movements of the waves. In launch or recovery where the ROV and vessel are experiencing large movements in opposite phase, the risk of the snubber or vessel colliding destructively with the ROV is large. The winch will not be fast enough to secure the ROV into the snubber in large movements.
- **Solution:** With vessel forward speed and pushing the ROV into the sea, one makes sure that there are no objects above the ROV at any stage of the launch. With vessel speed forward and towing the ROV with a moving sheave wheel, one makes sure that there are no objects above the ROV at any stage of the recovery.

1.2 DeepOcean

DeepOcean AS is a prominent player in the subsea services sector and has made reducing its carbon footprint a high priority. Based in Oslo and founded in 1999, the company offers a variety of services to the oil and gas, offshore renewables, and subsea mineral and surveying for a variety of clients. These services include subsea trenching and cable laying, inspection, repair, maintenance, and subsea intervention. DeepOcean's fleet includes support vessels, cable laying vessels, and subsea construction vessels equipped with the latest technology, such as ROVs and trenching systems [3]. DeepOcean is presently in search of a solution to conduct surveys using a combination of an USV and a ROV.

1.3 Literature review

While both USVs and ROVs have been used extensively for various tasks, there is a relatively small amount of literature on the combined use of these two technologies for surveying applications in the oil and gas sector. One possible reason for this is that the use of USVs and ROVs together, is a combination of technologies that still is unexplored and requires specialized equipment and software with rules and regulations. However, there is research and patents on this matter as discussed below.

SINTEF

The Artifex project's part "Task 1.2" describes a LARS for a ROV including bumper bars and a docking mechanism, enabling launch and recovery in rough sea conditions. The report also considered the use of a moon pool, providing additional safety and stability. Results showed that minimizing the moments of inertia in pitch and roll and placing the LARS systems as close as possible to the COG of the vessel could minimize heave motion at the ROV and LARS locations at 2 m significant wave height (SWH) [4].

Patent EP3448748A1

The patent titled "EP3448748A1" was filed by Kongsberg Maritime AS and relates to a USV together with a ROV. The invention relates to a system that can be used for IMR and other subsea operations.

Reach Subsea

Reach Subsea is a provider of subsea services, offering a range of solutions for subsea IMR. The company is committed to future-proofing subsea services through remote and autonomous operations [5] and are working with Kongsberg Maritime AS on this matter.

Kongsberg Maritime AS

A leading supplier of technology and services for the offshore and subsea services. Kongsberg Maritime is the company behind the patent "EP3448748A1." Reach Subsea will utilize this patent to provide its subsea services for ROV operations with Kongsberg's USVs.

DeepOcean has also patented a LARS for underwater units or vehicles, as seen in their patent WO2022/035322A1 in Figure 2. With their long experience in subsea operations and a strong focus on innovative technological solutions, DeepOcean holds a strategic advantage in pioneering advancements and addressing this issue. Consequently, this thesis aims to provide valuable additional insights to the ongoing research in this field.

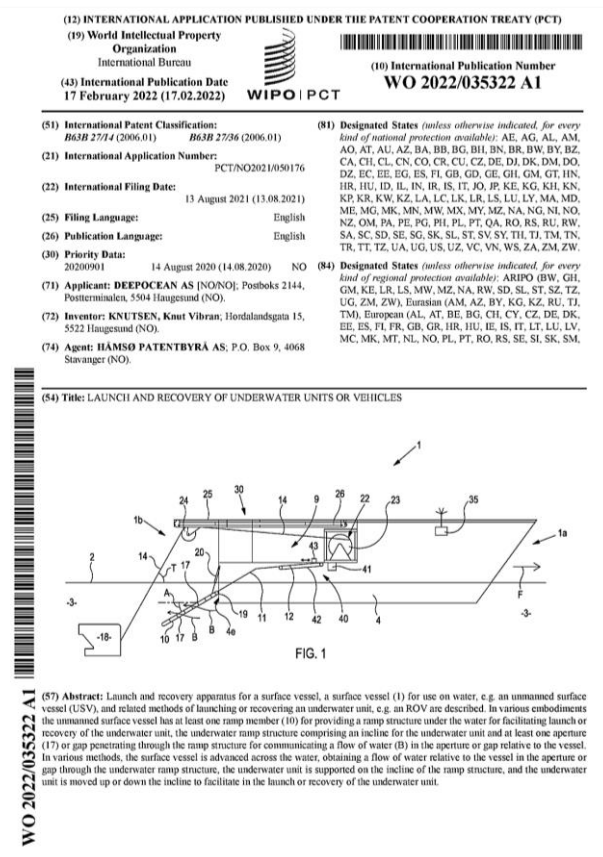


Figure 2 DeepOcean's patent WO2022/035322A1 for launch and recovery of underwater units or vehicles [6].

1.4 Kystdesign Supporter Work-Class ROV

The skid is specifically designed for the Kystdesign Supporter ROV 3000, as depicted in Figure 3, which has a frame lift capacity of 3000 kg. The specifications and dimensions of the ROV are provided in Table 1. DeepOcean has informed us that the Supporter ROV features a specialized hinged umbilical connector at the ROV. This unique design allows the umbilical to be angled both horizontally from the aft and vertically, as shown in Figure 4.

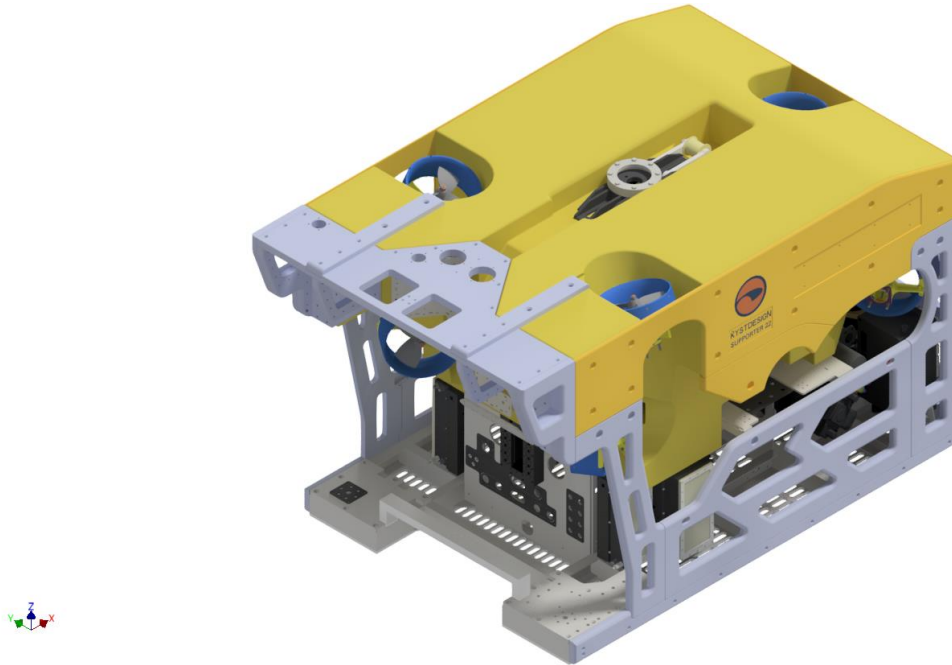


Figure 3 Kystdesign Supporter ROV

Table 1 Kystdesign Supporter ROV specifications

Description	Specification
Dimensions	L x W x H = 2.5 x 1.7 x 1.65 m
Tare weight	2450 kg
Through frame lift capacity	3000 kg
COG from top without skid	-0.90 m

1.5 Ocean Challenger USV

The USV Ocean Challenger is smaller and lighter compared to typical survey vessels, and it holds great value for this research. Unfortunately, as the nature of the vessel is undisclosed at the time of this report, we are unable to provide images or specific calculations. However, DeepOcean has provided dimensions listed in Table 2 that are sufficient for load calculations and determining skid specifications.

Table 2 Ocean Challenger USV specifications

Description	Size [m]
Length	26.9
Max width of hatch fastenings aft	5.2
Max width of aft opening in vessel	3.4
Max width of garage for ROV on vessel	2.0

1.6 Objectives

The primary goal of this project is to develop a LARS that can effectively launch and recover a ROV in offshore environments using a USV, as seen in Figure 4. The following tasks will be undertaken to achieve this objective:

- Evaluate the placement of sensors within the skid to ensure their protection during the launch and recovery processes.
- Consider suitable design options and materials that can effectively withstand and mitigate impact loads, safeguarding the sensors against damage or misalignment during launch and recovery.
- Develop a hatch design that facilitates the smooth launch and recovery of an ROV with the skid, ensuring efficient operation and minimizing potential risks.
- Modify an existing survey skid to make it compatible and functional within the new LARS system, allowing for seamless integration with the hatch.
- Conduct static simulations of the ROV skid and hatch to validate their designs and identify any potential issues or areas for improvement.
- Review the new gravity COG for the skid.
- Generate comprehensive 3D models of the ROV skid and hatch components, providing a detailed visualization of their structure and configuration.
- Produce technical drawings of the hatch and skid, providing guidelines for manufacturing and assembly processes.

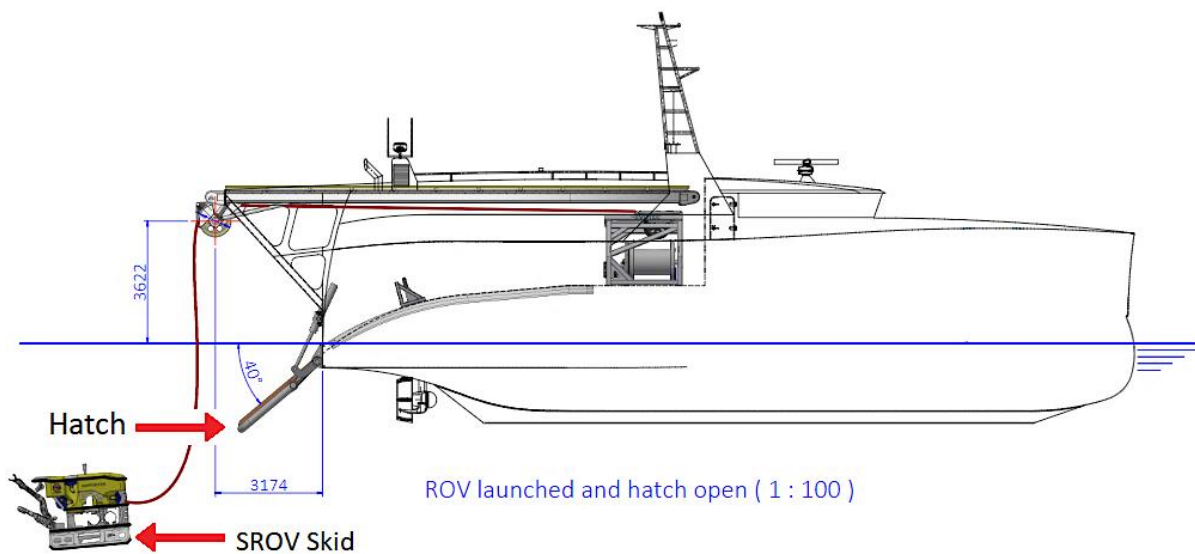


Figure 4 Operational concept for launch and recovery of ROV from USV, source: DeepOcean.

1.7 Skid requirements

The design of the skid plays a crucial role in ensuring the successful launch, recovery, and stability of the ROV. Several factors need to be considered during its design process, including impact forces and sensor placement. To mitigate the impact forces experienced by the skid, force-absorbing materials like rubber are strategically placed at critical impact points.

To ensure stability during launch and recovery operations, the skid should be designed with a low centre of gravity.

This can be achieved by positioning the heavier components of the skid at the bottom. A low centre of gravity not only enhances stability but also reduces the skid's susceptibility to tipping over, especially in rough sea conditions.

Additionally, the ROV skid should incorporate a low-friction material on its bottom surface, facilitating easy dragging onto the vessel during recovery. This material should be highly durable and resistant to abrasion to withstand the demanding marine environment.

The survey skid must fulfil the following requirements:

- Accommodate key sensors utilized in surveying operations.
- Securely fastening of sensors, with special care to acoustic sensors.
- Protecting and reducing loads the sensors during launch and recovery.
- Be implemented as a part of the LARS.
- The contact material should be corrosion and abrasion resistant.
- Simple design to reduce risk of repeated operation failure.
- Enable attachment to the Kystdesign Supporter ROV.
- Low-friction material on its contact surface.

The Survey Skid is designed to carry many sensors, but the main ones used for weight measurements in the skid are listed in Table 3. The weights of the sensors are according to Appendix A.

Table 3 Sensor function- and placement

Sensor	No.	Function	Placement	Total weight in air [Kg]	Total weight in water [kg]
SAIV CTD	2	Determining physical properties of the sea water	Horizontally between the MBES heads	6	2
Transponders	2	Underwater acoustic positioning and data link	Mounted on the top survey frame	10	4
ROVINS c/w Nortek DVL	1	Inertial navigation system with doppler	Mounted on the front of the ROV	15	6.2
Dual-head MBES	2	Determine the topography of the seabed	Mounted on the top survey frame	32.4	11.8
Alignment Lasers	3	Determine distance from deviance to ROV	Mounted on the top frame	5	6
SSS transducers	2	Detection of debris and other obstructions	Centre port and starboard	10	4
SBS	1	Imaging of sediment layers and buried objects	Centre bottom	30	10
RTS Gen5 MUX	1	subsea data transfer unit	Centre	32	14
DigiQuarts	2	Depth sensor	Mounted front bottom	2	1
Camera booms	2	Visual inspection	Centre front	92	56
Camera / light on booms	2	Visual inspection	Centre front	10	4

1.8 Hatch requirements

The hatch plays a critical role in protecting the ROV and its components during launch, recovery, and operation. It is designed to withstand impact and hydrodynamic forces. Additionally, the hatch should also incorporate a low-friction material on its top surface, facilitating easy dragging of the ROV onto the vessel during recovery. To fulfil its purpose effectively, the hatch needs to meet the following requirements:

- Ensure a smooth and seamless transition between the ROV skid and the USV during launch and recovery.
- Be implemented as a part of the LARS.
- Withstand environmental loads.
- Withstand resulting loads associated with launch and recovery of the ROV.
- Simple design to reduce risk of repeated operation failure.
- The material should be corrosion and abrasion resistant.

2 Method

This chapter will explain the theory and methods used in this thesis, including equations, symbols, notations, coefficients, descriptions, and the tools used.

2.1 Design and structural analysis

Ultimate Limit State (ULS) principle of limit state design is used to assess the maximum load carrying capacity of specific structural elements based on the allowable stress limit.

2.2 Tools

In this section, the key tools utilized throughout this thesis for conducting Finite Element Analysis (FEA) and calculations, are discussed.

2.2.1 Autodesk Inventor

Autodesk Inventor Professional 2023 is a computer aided design (CAD) software used for 3D modelling, simulation, and visualization. Autodesk Inventor is used in this project to create 3D models of the skid components, an assembled 3D model of all the components, and create technical drawings of the parts. Build 359 was the build during the time of the project.

2.2.2 Autodesk Nastran

Autodesk Nastran, an Autodesk-provided finite element solver plug-in for Inventor, was selected as the software for conducting linear static analysis. This choice allowed for exploring multiple scenarios and testing ideas efficiently when transitioning from design modifications to analysis. The version utilized during the project was 17.1.2.33.

2.2.3 Mathcad Prime

Mathcad was used during this project for the purpose of presenting calculations, as this is a more efficient and tidier way to present calculations in the report. The version utilized during the project was 9.0.0.0.

2.3 Standards

Following discussions with DeepOcean, an agreement was reached to use the Eurocode as the guiding framework for the design process. The design process relied on the following standards:

- EN 1993-1-1 General rules and rules for buildings: This standard is used as a basis for the overall design of the hatch and skid.
- EN 1993-1-8 Design of joints: This standard provides guidelines for the design of joints and welds.
- DNVGL-ST-N001 Marine Operations: This standard is recommended by DeepOcean for determining the material factor for welds and joints.
- DNV-RP-C205 Environmental Conditions: This standard provides information on the environmental conditions that the hatch and skid will be subjected to, including the loads applied to the hatch. We have used this standard to ensure that the hatch and skid are designed to withstand the expected environmental conditions.
- ISO 2768-1:1989 General tolerances — Part 1: Tolerances for linear and angular dimensions without individual tolerance indications
- NORSOK M-101 Structural steel fabrication. Rev. 5, October 2011
- NORSOK M-102:2015 Structural aluminium fabrication. Edition 2, April 2015

3 Preliminary design

This chapter provides an overview of the preliminary design phase, which includes modification, function, and material selection.

3.1 Hatch design

The patent [6] involves a range of hatch designs, as illustrated in Figure 5. Considering this, the choice of the hatch design was primarily guided by factors such as hydrodynamic forces and the necessity for a seamless transition between the ROV and the hatch. With these considerations in mind, a hatch with a geometry resembling that shown in FIG. 2A was selected. This design incorporates the necessary functionality for launching and recovering an ROV equipped with a skid, facilitating transverse transport across the hatch and onto the USV.

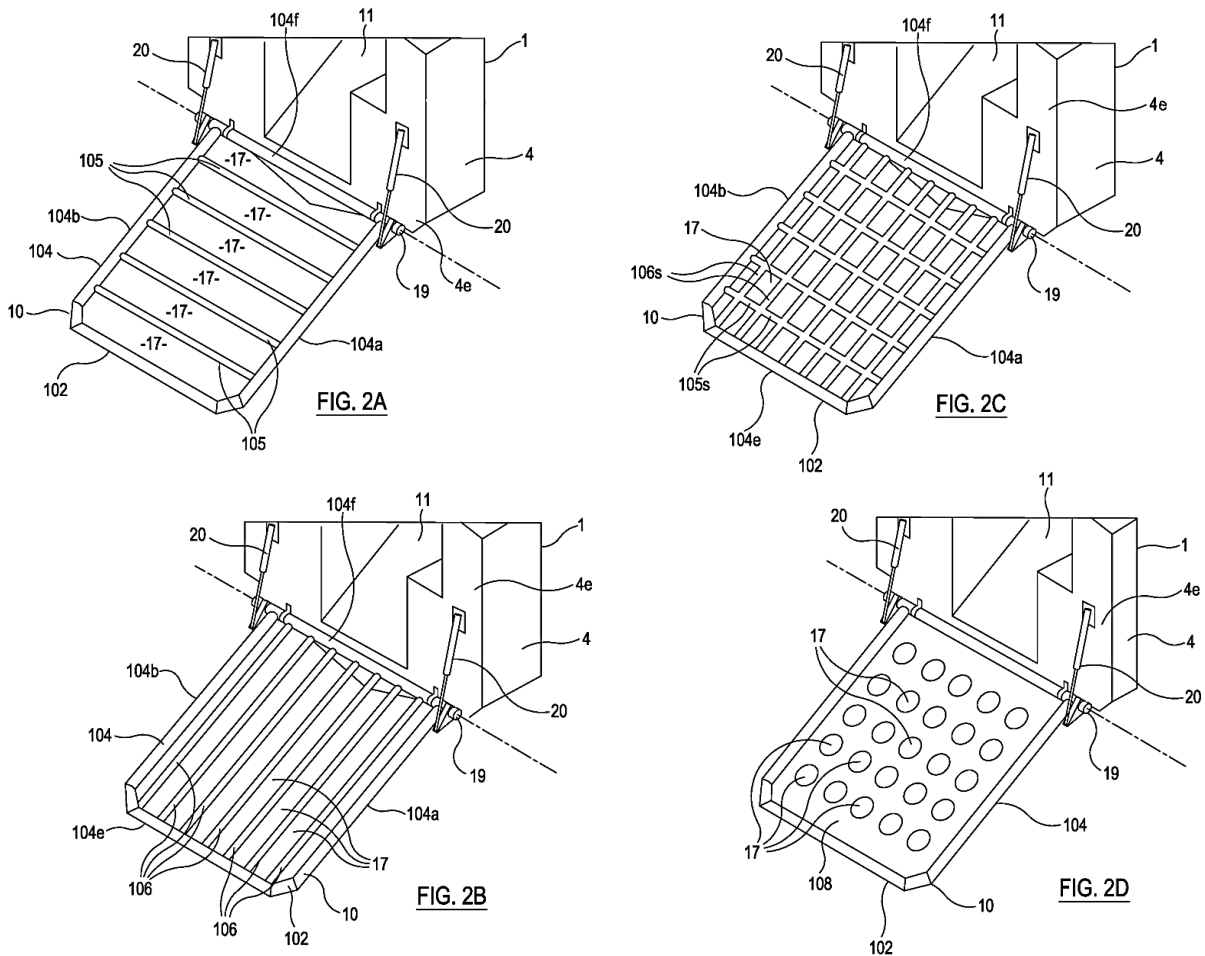


Figure 5 Hatch designs included in DeepOcean’s patent WO2022/035322A1 [6].

The preliminary hatch design is presented in Figure 6, featuring a maximum width of 5.20 m. This width was determined based on the vessel’s maximum width as outlined in The USV Ocean Challenger is smaller and lighter compared to typical survey vessels, and it holds great value for this research. Unfortunately, as the nature of the vessel is undisclosed at the time of this report, we are unable to provide images or specific calculations. However, DeepOcean has provided dimensions listed in Table 2 that are sufficient for load calculations and determining skid specifications.

Table 2. The placement of hinges was determined without complete knowledge of the precise geometric entities of the hydraulic arm locations on the USV. Nonetheless, the design allows for flexible adjustment along both the port and starboard sides to accommodate different configurations.

In addition, the length of the hatch is established at 3.22 m, taking into consideration various factors such as the length of the ROV, the impact perspective of hydrodynamic forces, and the strain energy in the hatch structure resulting from the loads, discussed further in chapter 4 Loads.

It is important to note that a longer hatch would lead to increased bending- and hydrodynamic forces, hence the decision to set the length at 3.22 m to mitigate these effects.

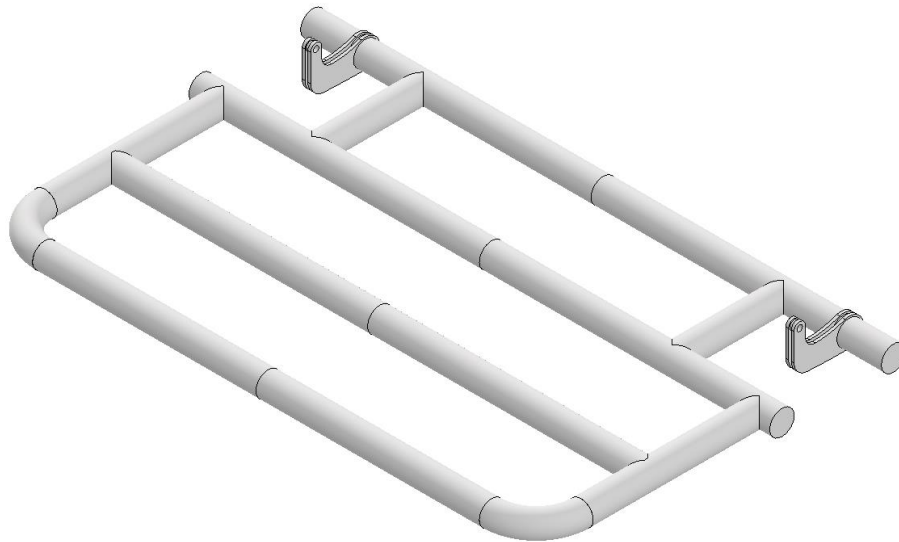


Figure 6 Preliminary hatch model

3.1.1 Structural analysis of preliminary hatch

The model of the preliminary hatch with fixed radial supports in the hinge holes, and fixed radial and axial constraints in the pipe connected to the vessel, shown in Figure 7. The impact load of the ROV, representing the energy transfer load f_Q , is placed at the out most part of the hatch, resulting in the largest strain energy possible. Welded contacts are used, which Prevents contacting regions from sliding, separating, or closing.

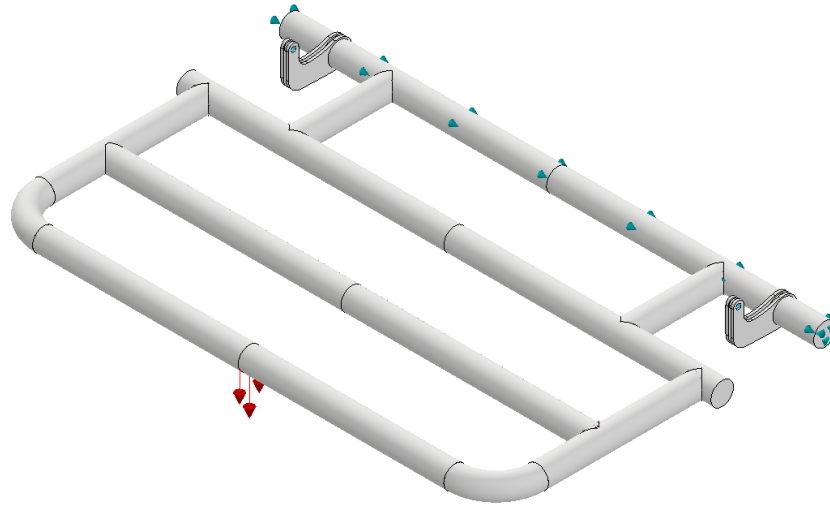


Figure 7 Preliminary hatch model with constraints and f_Q at centre of the outmost pipe.

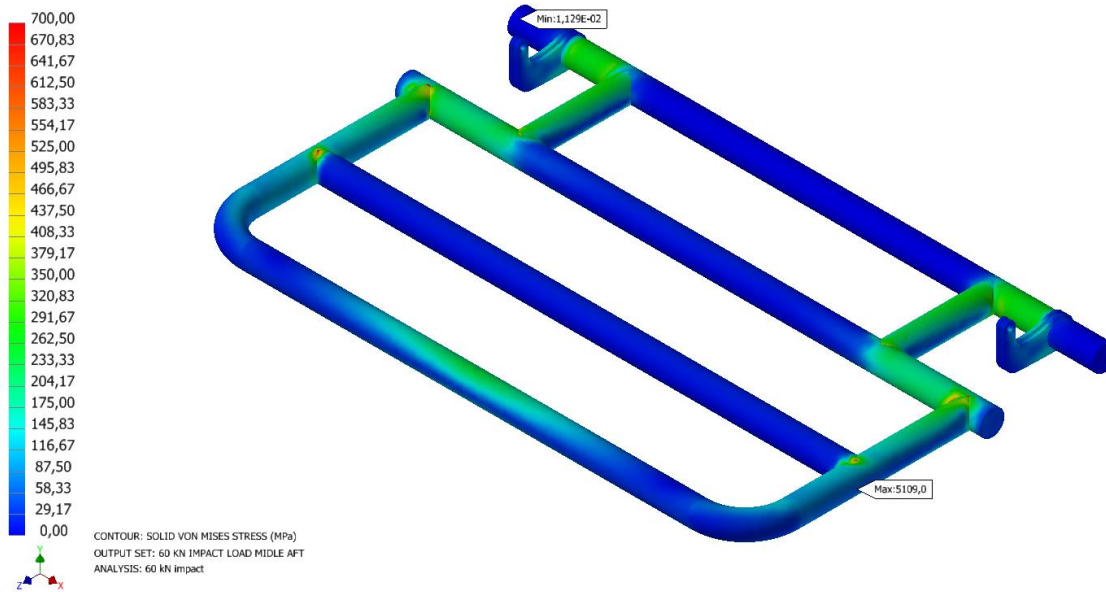


Figure 8 Preliminary hatch stress map top view.

The general view, shown in Figure 8, provides a complete view of how the load is transmitted from the point of impact to the hinges and constraints. Additionally, the analysis reveals significant stress concentrations in the areas where the pipes are welded. Upon closer examination, as shown in Figure 9 and Figure 10, stress concentrations are observed at the top and bottom of the pipe cross-section, particularly where the greatest bending moment is exerted.

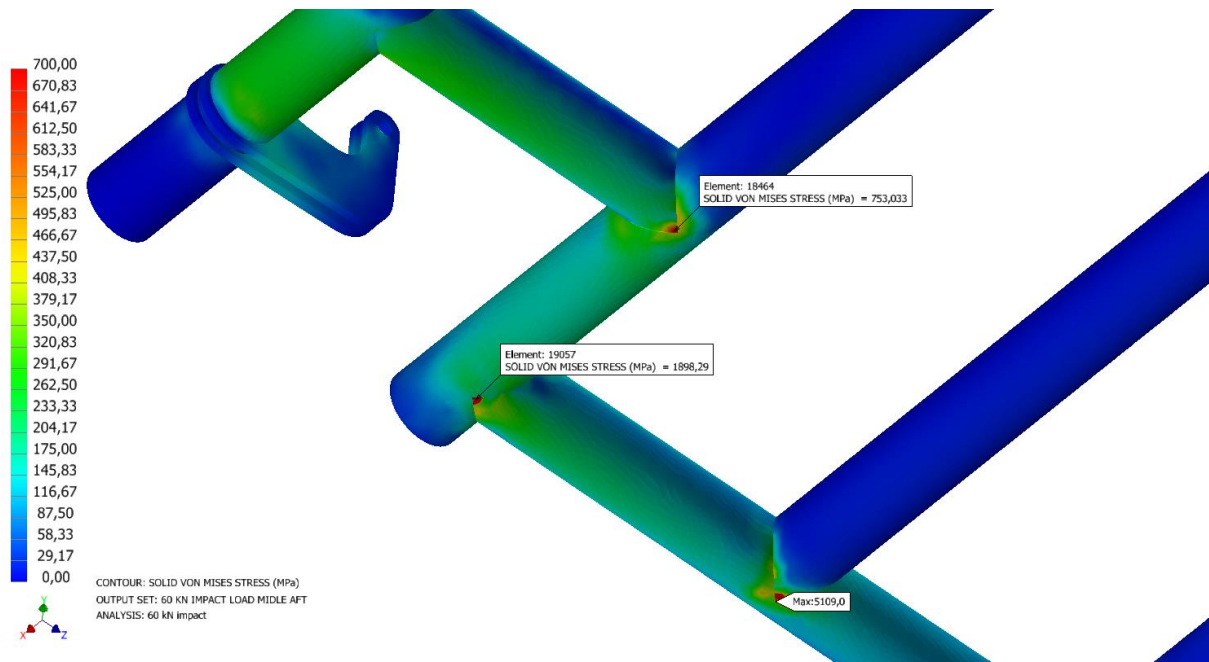


Figure 9 Preliminary hatch stress map bottom side pipe connections.

These findings serve as the foundation for material selection and design improvements. For instance, the addition of more material in these high-stress areas which will be further discussed in detail in Chapter 6: Final design.

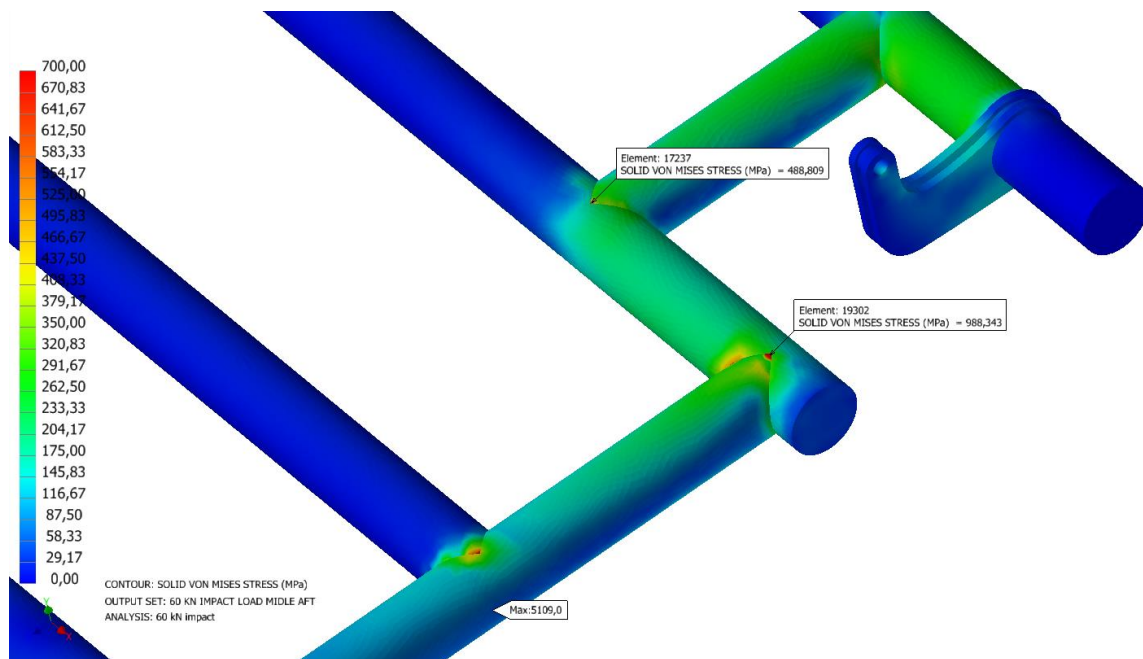


Figure 10 Preliminary hatch stress map topside pipe connections.

3.2 Skid

The preliminary skid is based on the existing survey skid that DeepOcean has designed. By using this as a base, a new design can effectively be implemented without making a completely new design.

3.2.1 Improvements to be made from existing skid

The pipe tracker feature has been excluded from the current skid design to avoid increasing its complexity and width. However, the necessary bolt holes and arrangements for attaching a pipe tracker to the skid have been retained for potential future use.

As shown in Figure 11, the camera booms have also been rearranged inside the skid, eliminating the extended section that previously connected them to the skid.

To further optimize the skid's width, the sensors and lasers on the top beam have been repositioned towards the centre, allowing the multi beam echosounder (MBEs) heads to be moved closer to the beam's centre as well. The side scanner is also deemed to be lowered and implemented in the vertical beams to reduce width. This adjustment, as shown in Figure 12, contributes to a reduction in the skid's overall width. These modifications ensure that the skid remains within the maximum width requirements specified in Table 2, allowing it to fit within the ROV garage on the USV.

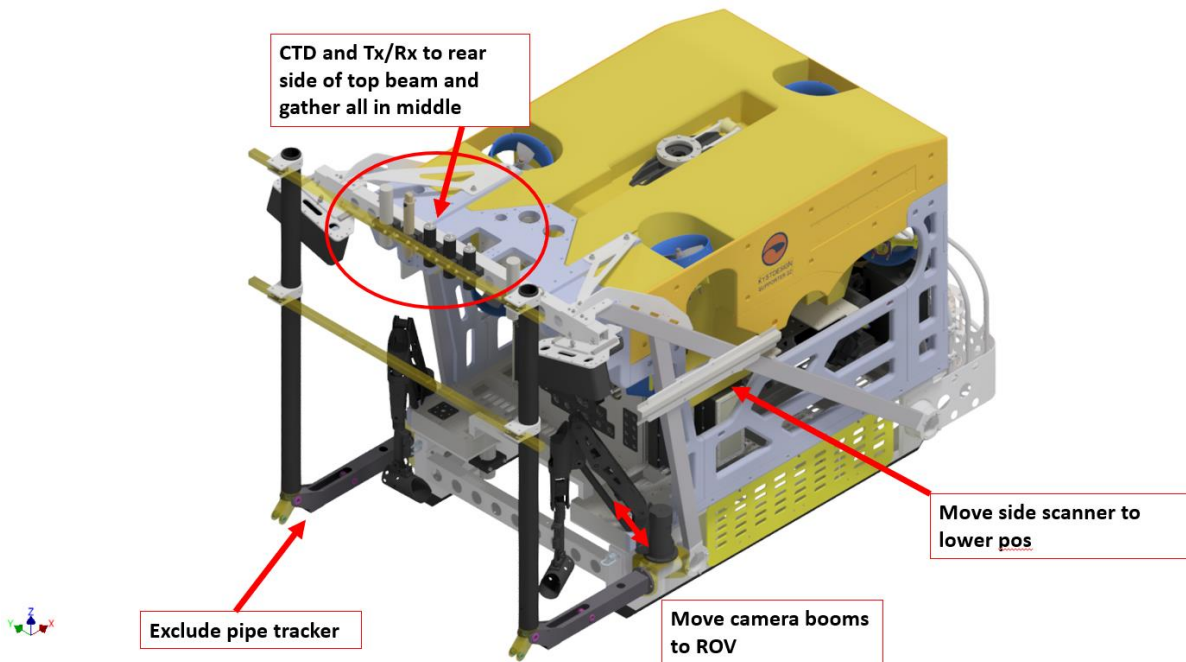
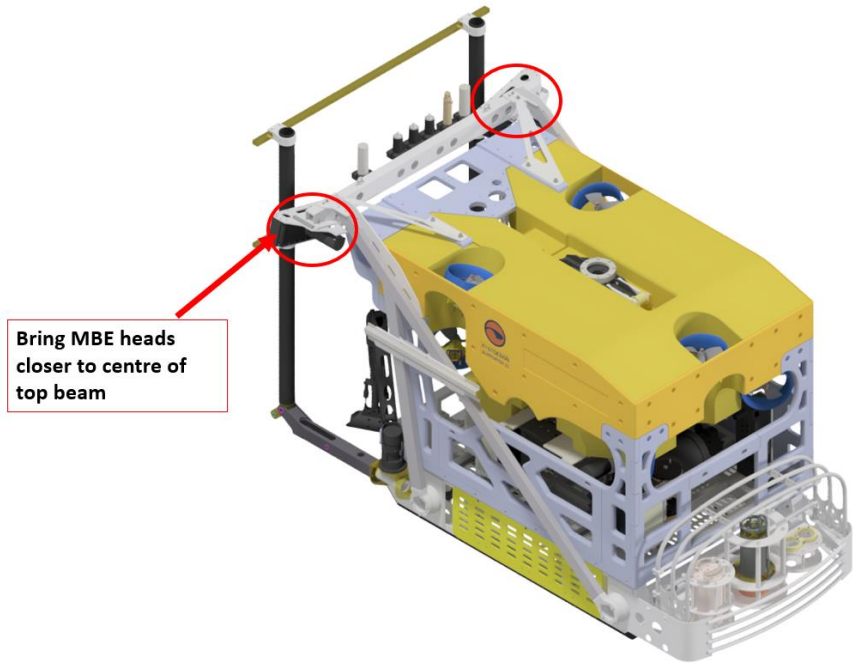


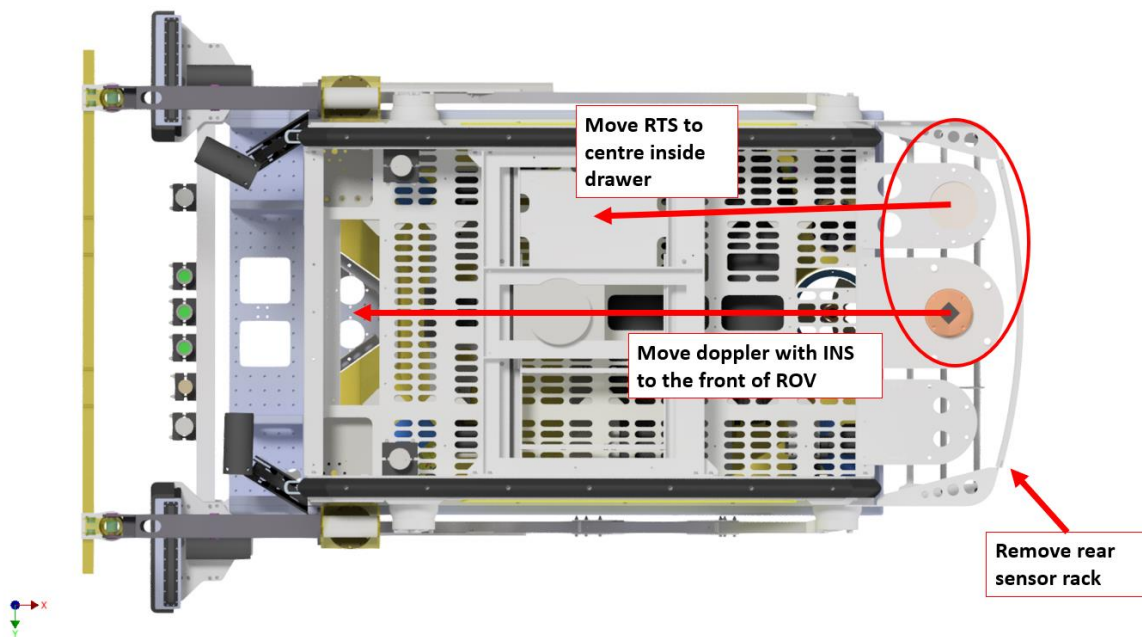
Figure 11 Existing skid improvements front view



Bring MBE heads closer to centre of top beam

Figure 12 Existing skid improvements rear view

The most significant modification involves the elimination of the rear sensor rack, as shown in Figure 13. The rear section of the skid is particularly vulnerable to substantial forces during impacts, which could potentially damage both the structure and the doppler and RTS sensors. To address this concern, the sensors are relocated within the skid itself. The doppler sensor is moved to the front end, ensuring its unobstructed line of sight to the sea bottom. Meanwhile, the RTS sensor is positioned in the drawer area at the centre of the skid. This reconfiguration ensures the protection and optimal placement of these sensors.



3.2.2 Preliminary skid

The new structure of the preliminary skid, excluding the sensors, is shown in Figure 14. Notable modifications include the presence of a sensor holder at the front to facilitate the doppler with INS. The top beam has been shortened and altered. The rubber material on the sides has been extended towards the rear to ensure enhanced protection during the recovery. To address loads during recovery, a cross beam has been introduced. Additionally, the RTS holder has been placed within a modified drawer.

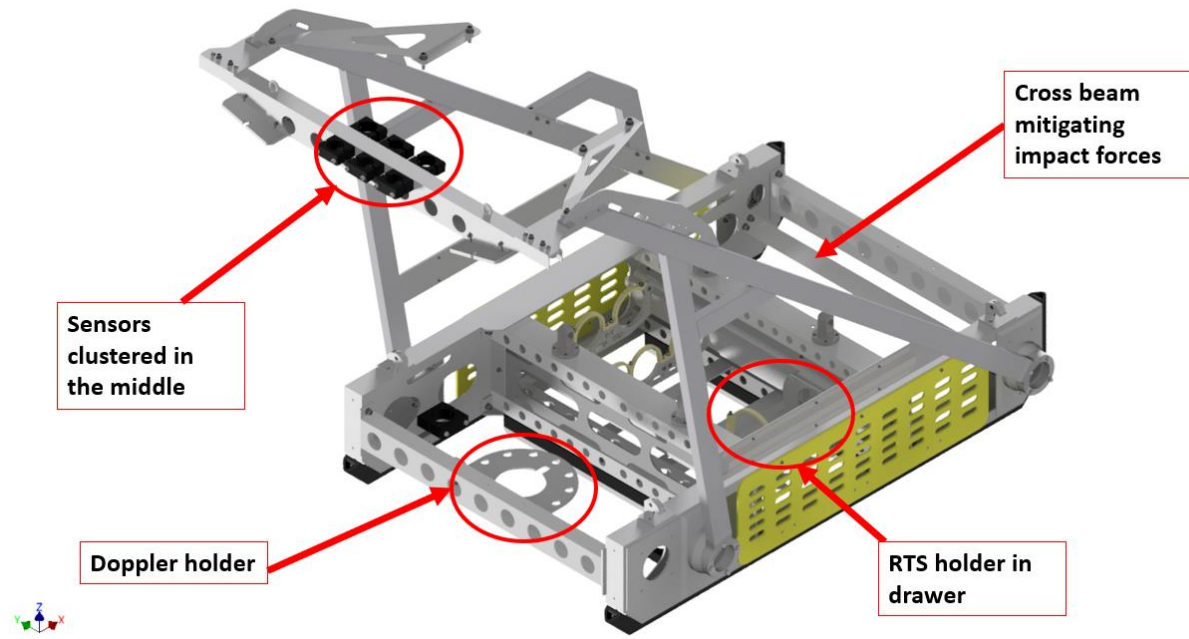


Figure 14 Preliminary skid design front view

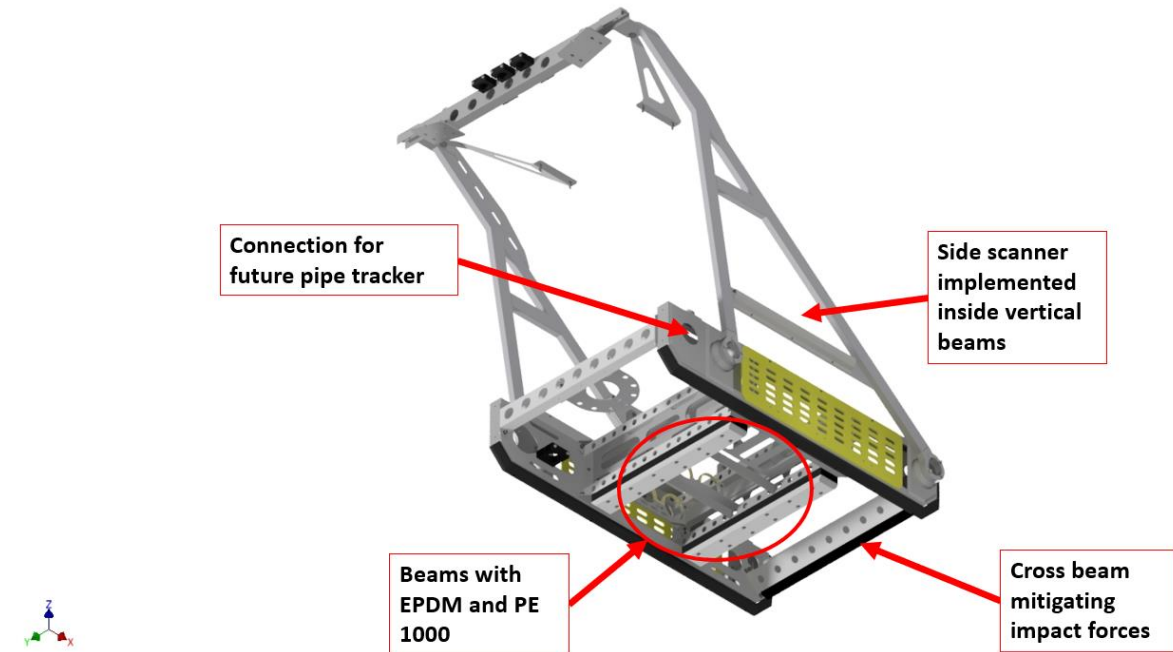


Figure 15 Preliminary skid design bottom view

The implementation of the side scanner involves incorporating it inside the vertical beams that connect to the top beam. To improve overall strength, additional beams have been added to the middle bottom

section, while EPDM rubber is utilized for damping purposes and PE 1000 is employed for low friction and abrasion resistance sliding during recovery. In consideration of stress levels in the bolt holes due to the notch effect, the size of the bolts for the main structure has been increased from M12 to M16.

3.2.3 Structural analysis of preliminary skid

The preliminary skid model incorporates fixed translation support in the z-direction within the corner locks. The probes are designed with fixed rotation in both the x and z-directions, as well as fixed translation in all axes. The design energy transfer load F_Q , defined in Chapter 4.7, is considered for ULS-b. Welded contacts are employed for welds, while bolted connections utilize sliding surfaces.

Note that the structural analysis of the preliminary skid serves as a concise overview, focusing on the main issues rather than providing a detailed explanation. A more comprehensive analysis is provided in Chapter 5: Structural analysis.

The skid is primarily subjected to loads on the cross beams, where impacts are most likely to occur, corresponding with load case 4. One notable observation is that the cross beam, which incorporates EPDM and PE 1000 materials, does not effectively distribute the load. This results in high stresses at the welded and bolted connections, exceeding the maximum allowable stress limit. Additionally, the force transfer to the probes is not directed optimally, as it initially goes horizontally towards the bolt connections and then transitions vertically and horizontally again towards the probe locations. Therefore, significant bending moments are generated in the bolted connections, necessitating further attention, and addressing. Figure 16 illustrates this stress distribution in the preliminary skid beam from a starboard side view.

On the contrary, on the opposite side of the beam, where the threaded part of the bolts is connected to the S420N reinforcement plates, the maximum stress is 111.74 MPa, which falls below the allowable stress limit. This is demonstrated in Figure 17.

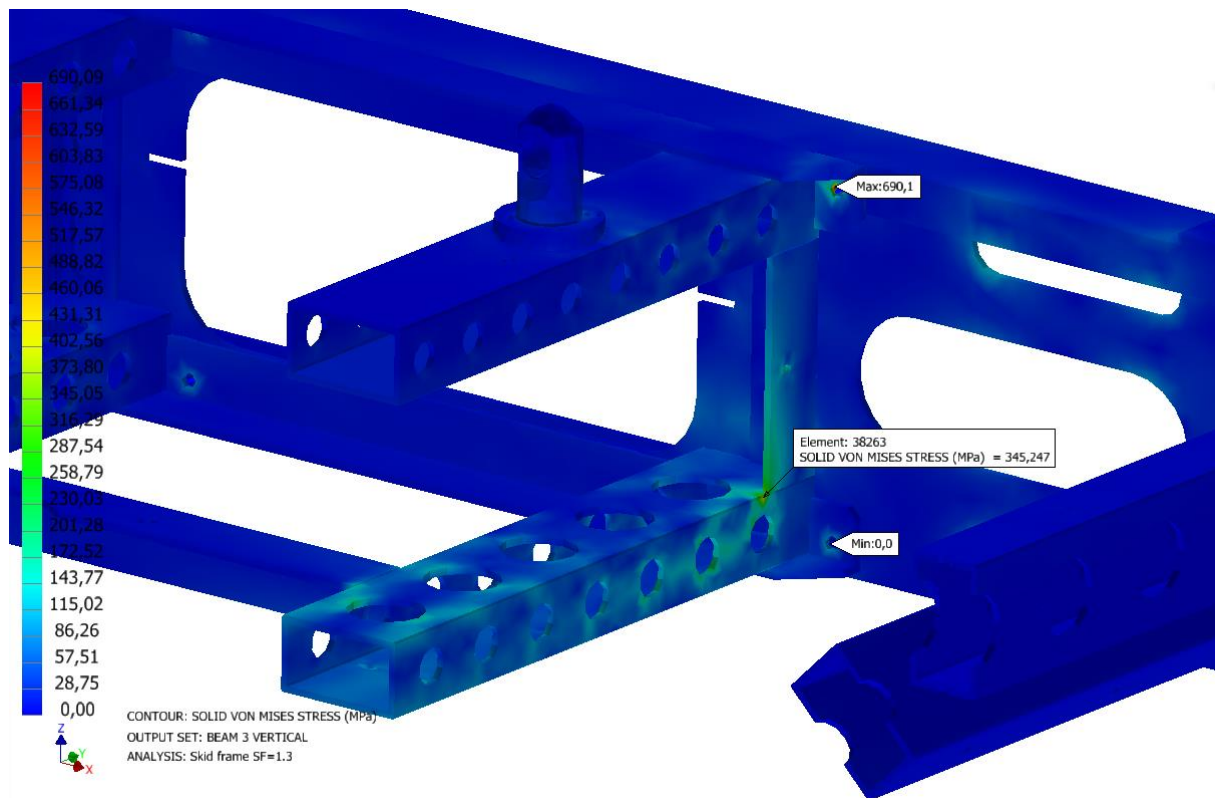


Figure 16 Stress map preliminary skid beam starboard side view

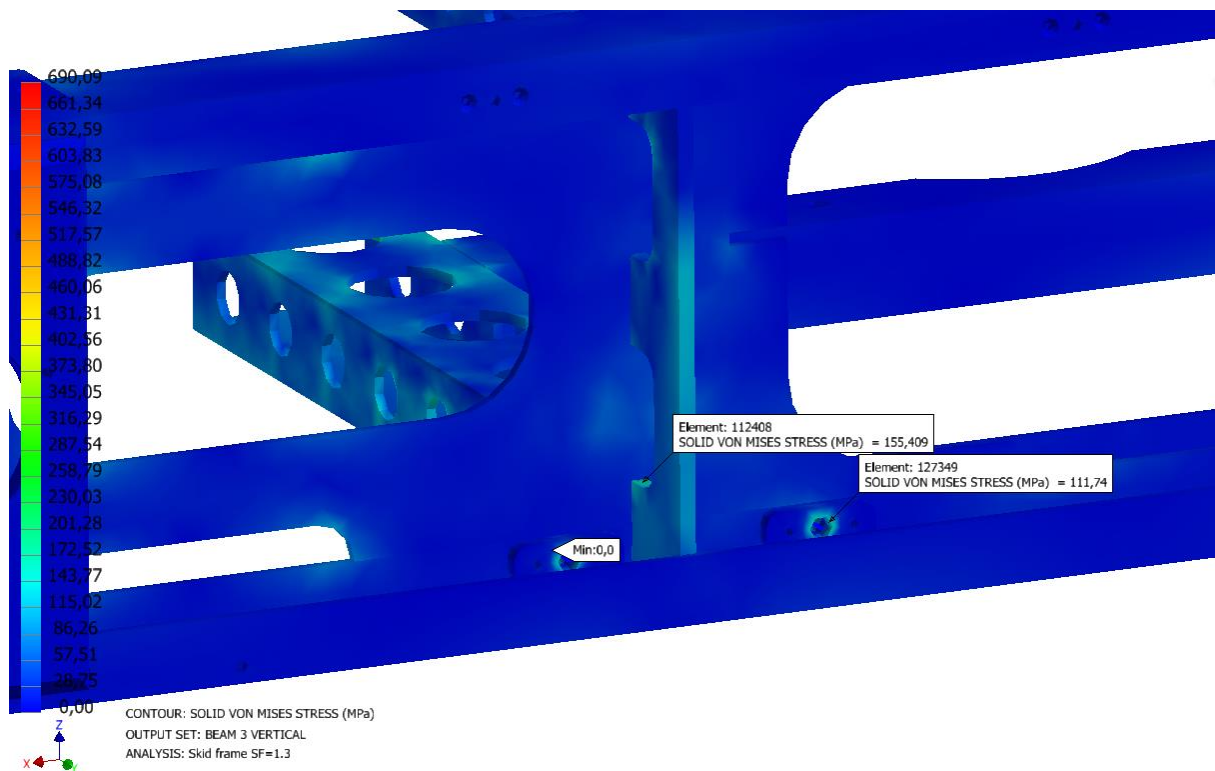


Figure 17 Stress map preliminary skid starboard side view of bolted connections

3.3 Materials

After the preliminary study is conducted, the material selection is done. When considering the material selection for the hatch, it is important to recognize that while the argument in favour of using stainless steels or duplex steel for their corrosion resistance is valid, there are other critical factors that heavily influence the choice of materials, such as price and strength. A widely acknowledged factor is that stainless steel generally comes with a higher price tag compared to carbon steel, often approximately four to five times the material cost. Additionally, the cost of stainless steel tends to increase as alloying elements are added.

Moreover, it is worth noting that surface coatings offer an alternative approach to combat corrosion. By implementing suitable coatings, the need for high-cost corrosion-resistant materials can be reduced, discussed in Chapter 3.4: Surface treatment. Consequently, the significance of corrosion resistance in the material selection process becomes less prominent. Considering these factors, choosing carbon steel for certain applications in the hatch may prove to be a more cost-effective, particularly when corrosion resistance can be effectively addressed through alternative means such as surface coatings [7].

3.3.1 S165M W1.4418

S165M W1.4418 is a high-grade martensitic stainless steel known for its exceptional mechanical properties and corrosion resistance. Widely used in demanding industries, such as offshore and is used for the docking probes in the ROV skid. The probes are an existing part of the skid and will therefore remain as a part of the new skid. The material properties are according to Appendix B.

3.3.2 6082-T6

Aluminium 6082-T6 is a heat-treated AlMgSi alloy renowned for its exceptional strength-to-weight ratio, favourable welding characteristics, and corrosion resistance, making it a popular choice for offshore structural applications.

When welding a heat-treatable alloy, the process of annealing at a sufficiently high temperature effectively eliminates the hardening effect caused by previous heat treatments. Consequently, it is crucial to consider the strength of the Heat-Affected Zone (HAZ) when designing welded joints for aluminium. The HAZ typically experiences a significant reduction in yield strength. This consideration becomes particularly important for T4 and higher aluminium alloys, especially those belonging to the 6xxx series, as employed in the skid structure [8]. As a result, load-bearing elements are joined using A4-80 bolts instead of relying solely on welding. This approach ensures the integrity and reliability of the joint. The material properties are according to Appendix C.

3.3.3 API 5L X65

API 5L X65 steel is a suitable choice for the lower stress areas of the hatch due to its favourable combination of properties, including good ductility, corrosion resistance, and cost-effectiveness.

The material has been widely used in various industries, including the offshore and marine sectors, due to its excellent ductility, which is important for areas subjected to high impact loads [9]. The material exhibits good toughness, reducing the risk of brittle fracture and enhancing structural integrity. This makes it a viable option for the pipes used with a relative lower stress areas of the hatch without compromising the required mechanical and corrosion resistance properties. The material properties are according to Appendix D [10].

3.3.4 S420N

S420N structural steel has been chosen for the T-bars in the hatch due to its high yield strength, ensuring the required strength and structural integrity.

Additionally, S420N steel is used for reinforcement plates in the bolted connections of the skid. It offers greater strength than 6062-T6 aluminium, reducing stresses in the bolt holes. However, when steel bolts are connected to aluminium, there is a risk of galvanic corrosion. This occurs due to the electrochemical reaction between the dissimilar metals, with aluminium being more prone to corrosion. This could compromise the connection integrity [11].

To address this issue, DeepOcean implements sacrificial anodes on the ROV. These anodes divert corrosion away from critical components, preserving the connection integrity. By using sacrificial anodes, the long-term performance and reliability of the structures are ensured. Material properties are detailed in Appendix E.

3.3.5 Strenx 700 OME

Strenx 700 OME is an ideal choice for the high-stress areas of the hatch, where resulting stresses are significant. Developed for load-bearing structures in the offshore and marine Industry, it offers exceptional ductility, toughness, and weldability. This makes it well-suited for allowing displacements in the hatch, while also being highly resistant to abrasion and wear, providing good durability [12]. The material properties are according to Appendix F.

3.3.6 Polyethylene High density (PEHD) 1000

PEHD 1000, which is a type of high-density polyethylene, is used as the top layer of the hatch and the bottom layer of the skid, for the sliding contact surfaced. The long linear chains present in PEHD 1000 contribute to its exceptional impact strength, abrasion resistance, toughness, and resistance to stress cracking, surpassing other types of polyethylene. Additionally, it exhibits good impact strength even at

extremely low temperatures, along with high resistance to cyclic fatigue and stress cracking. PEHD 1000 also has a low coefficient of friction, offering smooth sliding and good corrosion resistance, making it suitable for the application [13]. The material properties are according to [14] and Appendix G.

3.3.7 Ethylene-propylene diene monomer (EPDM)

EPDM rubber is an excellent choice for damping impact, and therefore used to dampen the impact in both the skid and hatch. The high elasticity and flexibility of EPDM allow it to effectively absorb and dissipate impact and allow for a 500% elongation at break, reducing the risk of damage or deformation to the hatch structure and skid. Furthermore, EPDM rubber exhibits excellent resistance to environmental factors such as UV radiation, ozone, and moisture, ensuring long-term performance and durability in marine environments [15]. The material properties are according to Appendix H.

3.3.8 Fasteners

In the construction of the skid and hatch components, only stainless steel A4-grade fasteners are used. These fasteners are austenitic and alloyed with chromium, nickel, and molybdenum, making them highly corrosion resistant. This specific grade of stainless steel is chosen for its exceptional resistance to corrosion in seawater environments, making it highly suitable for the application.

However, when these stainless-steel fasteners meet aluminium, a galvanic reaction occurs, like what was discussed in the previous chapter regarding S420N steel. This reaction arises due to the dissimilar metals and can lead to galvanic corrosion. To counteract the risk of galvanic corrosion, sacrificial anodes in the ROV mitigate this issue. This ensures the long-term durability and integrity of the skid and hatch components. The material properties are according to Appendix I.

3.3.9 Material properties and partial factors

The materials employed in this report are listed in Table 4. DeepOcean's practice for partial factors concerning welds and connections, on the other hand, follows the guidelines outlined in reference [16]. It should be noted that this practice deviates from the previously mentioned reference [17], as it is replaced $\gamma_{2M} = 1.25$ to $\gamma_{2M} = 1.3$.

Table 4 Applied materials.

Material	Description	Ultimate tensile strength [MPa]	Yield strength [MPa]	Young's modulus [GPa]	Material factor	Material factor welds/joints
		f_u	f_y	E	γ_{M1}	γ_{2M}
Strenx 700 OME	High stress pipes and parts	780	700	210	1.15	1.30
API 5L X65	Pipes general	531	448			
S420N	T-profiles	520	420			
S165M W1.4418	Docking probe	950	750	70	1.25	
6068-T6	Structure skid	300 (185) ^a	255 (125) ^a	210	-	
8.8 Fasteners	Fasteners	800	640	$2.14 \cdot 10^{-3}$	-	
EPDM	Rubber damping	-	4 (25) ^b	0.7	1.15	-
PEHD 1000	Low friction material	44	20			-

^{a)} Aluminium has separate HAZ values for ultimate tensile strength $f_{u, haz}$ and yield strength $f_{y, haz}$ used for weld capacity calculations.

^{b)} EPDM has increased yield strength up to 25 MPa with additives [11].

3.4 Surface treatment

As mentioned in the previous Chapter 3.3: Materials, the hatch components, specifically the structural steel S420N and Strenx 700 OME, do not possess any good corrosion resistance. Considering the placement of the hatch in the splash zone, it is recommended, as stated in reference [18], that carbon and stainless steels in this zone should be coated with a protective system known as 7A. This system typically involves a two-component epoxy or polyester-based coating.

4 Loads

This chapter will discuss the design load of the skid and hatch, including estimation of the loads, design specifications, assumptions, and simplifications.

4.1 Assumptions and limitations

This thesis focuses on static simulations and calculations in relation to the launch and recovery procedure. The dynamic forces experienced by the ROV are not considered, thereby excluding the impact of motion and variations in velocity. Additionally, the hydraulic aspect of the hatch has not been incorporated, i.e., in a fixed, lowered position.

Highest forces occur under recovery of the ROV, i.e.:

- Point of impact are centred in the middle section of the cross going beams in the skid.
- Slamming forces are neglected, due to its absence when the hatch is lowered into the water.
- Varying drag coefficients neglected i.e., marine growth etc.
- Environmental forces acting on the skid are neglected.
- Assume that the ROV follow the water surface in periodic waves.
- Assume that the hatch is moving normal to the water, i.e., the forces work normal to the hatch.
- When the ROV comes to a stop at the hatch, the added drag forces could be considered, but the impact force is greater than the added drag, and therefore neglected.
- When using the relative velocity formulation for the drag forces, additional hydrodynamic damping is not included, according to [19].

4.2 Design parameters

Launch and recovery must be carried out with sea waves at $H_G < 3$ m. The USVs speed when recovering the ROV will also need to be $v_{h.USV} < 0.5$ m/s (0.97 knot), and the relative velocity between the USV hatch and ROV during impact must be $v < 0.45$ m/s in accordance with the findings in Chapter 4.2.2: Wave kinematic and 4.3: Kinetic- and elastic potential energies.

4.2.1 Free body diagram of ROV and hatch

Figure 18 provides a system overview of the recovery phase, offering a representation of the key components involved.

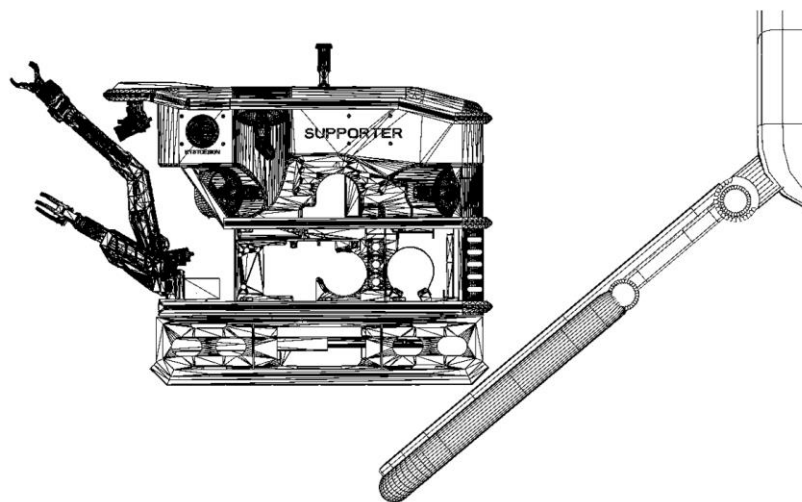


Figure 18 System overview

To further analyse the load distribution, Figure 19 and Figure 20 present the free body diagrams (FBDs) for the ROV and hatch respectively. These diagrams illustrate the forces, including the load exerted on the skid and hatch during impact, referred to as the energy transfer load f_Q , as well as the environmental loads f_E , discussed further in this chapter. To ensure the structural integrity in areas where the possibility of impact is greatest, the energy transfer load will be applied to various locations on the skid, explained further in Chapter 5: Structural analysis. This load will be directed both vertically and horizontally, allowing for assessment of the structural response. By applying the energy transfer load in these critical zones, the design can effectively address the potential impact scenarios and optimize the skid's ability to withstand the impact.

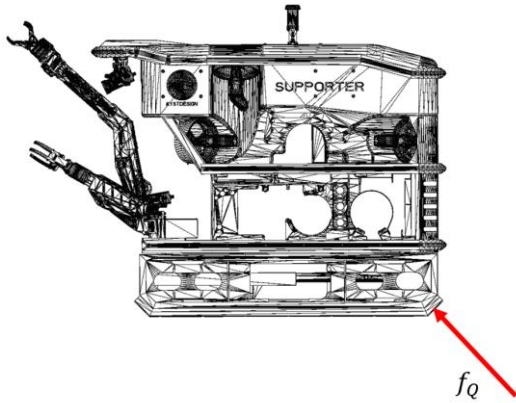


Figure 19 FBD of ROV with skid

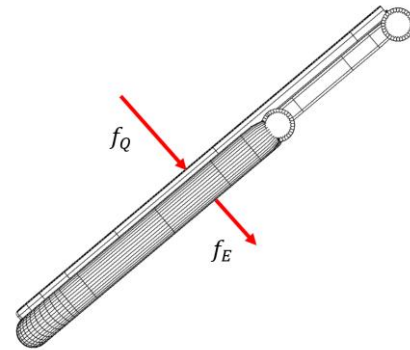


Figure 20 FBD of hatch

4.2.2 Wave kinematics

To determine the hydrodynamic forces acting on the hatch, the vertical velocity $v_{v,ROV}$ and acceleration $a_{v,ROV}$ of the ROV, the assumption is that the ROV follows the waterline in the oscillating flow. In this scenario, the ROV's velocity and acceleration are considered equal to that of the water particles. The angles of components relative to the hatch is shown in Figure 21.

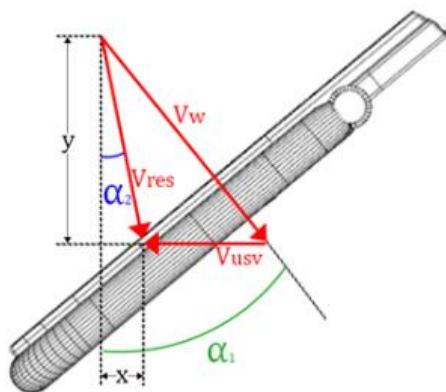


Figure 21 Annotations for the components acting on the hatch.

First the characteristic wave amplitude ζ and the zero-up-crossing wave period T_z , is to be calculated using equation (1) and (4).

$$\zeta = 0.9 \cdot H_S \tag{1}$$

And

$$T_z \approx 3.39 \cdot H_S^{1/2} \quad (2)$$

Then the vertical acceleration and velocity $a_{v,ROV}$ and $v_{v,ROV}$ can be calculated with equations (4) and (3):

$$a_{v,ROV} = \zeta * \left(\frac{2\pi}{T_z}\right)^2 \cdot e^{-\frac{4\pi^2 d_{COG,ROV}}{T_z^2 \cdot g}} \quad (3)$$

$$v_{v,ROV} = \zeta \cdot \left(\frac{2\pi}{T_z}\right) \cdot e^{-\frac{4\pi^2 d_{COG,ROV}}{T_z^2 \cdot g}} \quad (4)$$

and normal to the hatch:

$$a_{n,ROV} = a_{v,ROV} \cdot \cos(a_1) \quad (5)$$

$$v_{n,ROV} = v_{v,ROV} \cdot \cos(a_1) \quad (6)$$

where:

$v_{v,ROV}$	=	vertical velocity of ROV [m/s]
$a_{v,ROV}$	=	vertical acceleration of ROV [m/s ²]
$v_{n,ROV}$	=	velocity normal to hatch
$a_{n,ROV}$	=	Acceleration normal to hatch
$d_{COG,ROV}$	=	distance from water plane to centre of gravity of submerged part of the ROV [m]
ζ	=	characteristic wave amplitude [m]
T_z	=	zero-up-crossing wave period [s]
$d_{COG,ROV}$	=	distance to COG of ROV [m]
g	=	gravity [m/s ²]
a_1	=	incline angle of hatch [degrees]
a_2	=	angle of decomposed components [degrees]
H_S	=	significant wave height [m]

4.2.3 USV kinematics

The vertical acceleration of the Ocean Challenger USV is estimated through calculations described in [20]. This estimation of vertical accelerations $a_{v,USV}$ considers the combined value of the USV horizontal speed, $v_{h,USV}$, and significant wave height H_S . When $v_{h,USV}\sqrt{L_{USV}} < 3$, the vertical acceleration of the USV $a_{v,USV}$ can be calculated with equation (7).

$$a_{v,USV} = 6 \cdot \frac{H_S}{L_{USV}} \left(0.85 + 0.35 \cdot \frac{v_{h,USV}}{\sqrt{L_{USV}}} \right) \cdot g \quad (7)$$

and normal to the hatch:

$$a_{n.USV} = a_{v.USV} \cdot \sin(a_1) \quad (8)$$

where:

- L_{USV} = length of USV [m]
 $v_{h.USV}$ = horizontal velocity of USV [knots]

4.2.4 Resulting kinematics for the water, USV and ROV

The calculations for the kinematics are shown in Appendix J.

Table 5 Kinematics for the water, ROV and USV

Kinematics					
Water / ROV		USV		Relative	
$a_{n.ROV}$ [m/s ²]	$v_{v.ROV}$ [m/s]	$a_{n.USV}$ [m/s ²]	$v_{v.USV}$ [m/s]	v_r [m/s]	a_r [m/s ²]
-2.12	-2.59	4.60	0.26	-2.84	-6.72

4.3 Kinetic- and elastic potential energies

Several aspects of the design incorporate dynamic responses, which necessitate the calculation of kinetic and elastic potential energies. This includes evaluating the kinetic energy associated with the ROV and determining how this energy is absorbed within the system.

4.3.1 Kinetic- and elastic potential energy of impact

To calculate the force exerted by the ROV onto the skid, the kinetic energy and elastic energy absorbed in the hatch is used. The kinetic energy of the ROV with a given mass, the added mass and velocity can be calculated with equation (9) [11].

$$E_k = \frac{1}{2} \cdot (m_{ROV} + m_a)v^2 \quad (9)$$

where:

- E_k = kinetic energy of ROV [J]
 m_{ROV} = mass of ROV [kg]
 m_a = added mass [kg]
 v = Impact velocity between USV and ROV during recovery [m/s]

The elastic potential energy stored in the hatch during impact, is equal to the force times the displacement of the hatch and is calculated with equation (10).

$$U_{el} = \frac{1}{2} f_Q d \quad (10)$$

where:

- U_{el} = Elastic potential energy of hatch [J]
 d = displacement [m]

If only the elastic force does the work, the total mechanical energy is conserved and can be written as:

$$E_k = U_{el} \quad (11)$$

By knowing the kinetic energy of the ROV, we can estimate what kind of energy the hatch needs to absorb. This is done by applying the energy transfer load, f_Q , to the preliminary design of the hatch, till equation (11) is fulfilled.

4.3.2 Damping of rubber

This chapter focuses on the design of rubber components for efficient impact damping. The calculations are based on [15], for simple geometries bonded to rigid components. The same principle used to calculate the elastic potential energy in the hatch, is used with the rubber components. Equation (12) links the compression spring rate K_c , to the variables involved in the product dimensioning.

$$K_c = \frac{F_Q}{d_c} = \frac{AE_c}{t} \quad (12)$$

where:

K_c	=	compressive spring rate of rubber [N/m]
d_c	=	compressive displacement [m]
A	=	load area [m ²]
E_c	=	effective compression modulus [N/m]
t	=	thickness of rubber material [m]

Taking equation (12) and solving for the compressive displacement d_c , we get equation (13). With the calculated displacements, the resulting elastic potential energy U_{el} , can be obtained with equation (10).

$$d_c = \frac{F_c \cdot t}{A \cdot E_c} \quad (13)$$

The effective compression modulus E_c for the rubber material experiencing bidirectional strain, is given by equation (14).

$$E_c = E_0(1 + \phi S_f^2) \quad (14)$$

where:

d_c	=	compressive displacement [mm]
E	=	Young's modulus [GPa]
ϕ	=	elastomer compression coefficient [-]
S_f	=	shape factor [-]

The shape factor S is a mathematical function representing the influence of component geometry on the compression modulus. Specifically, it quantifies the relationship between the area of a single loaded surface and the overall surface area available for bulging [15]. Shape factor for the rectangular rubber blocks S_b , is obtained with equation (15).

$$S_b = \frac{\text{load area}}{\text{bulge area}} = \frac{(L_{rb}) \cdot (W_{rb})}{2t(L_{rb}) + 2t(W_{rb})} \quad (15)$$

And for hollow tube profiles, the shape factor S_t is calculated with equation (16).

$$S_t = \frac{(d_o - d_i)L_{rb}}{2\pi \left[\frac{(d_o)^2}{4} - \frac{(d_i)^2}{4} \right]} \quad (16)$$

where:

- S_b = block shape factor [-]
- S_t = tube shape factor [-]
- L_{rb} = length load area [m]
- W_{rb} = width of rubber block [m]
- d_o = outside diameter of rubber tube [m]
- d_i = inner diameter of rubber tube [m]

4.4 Determining the energy transfer load from the ROV

A load of 60 kN is resulting in the required elastic potential energy in the hatch during impact. This load is an energy transfer load f_Q , and is the force resulting in the hatch elastic potential energy equal to the kinetic energy of the ROV, and the skid is designed for. The locations exerted to this force is shown in Figure 22, with results in Table 6. For calculations see Appendix K.

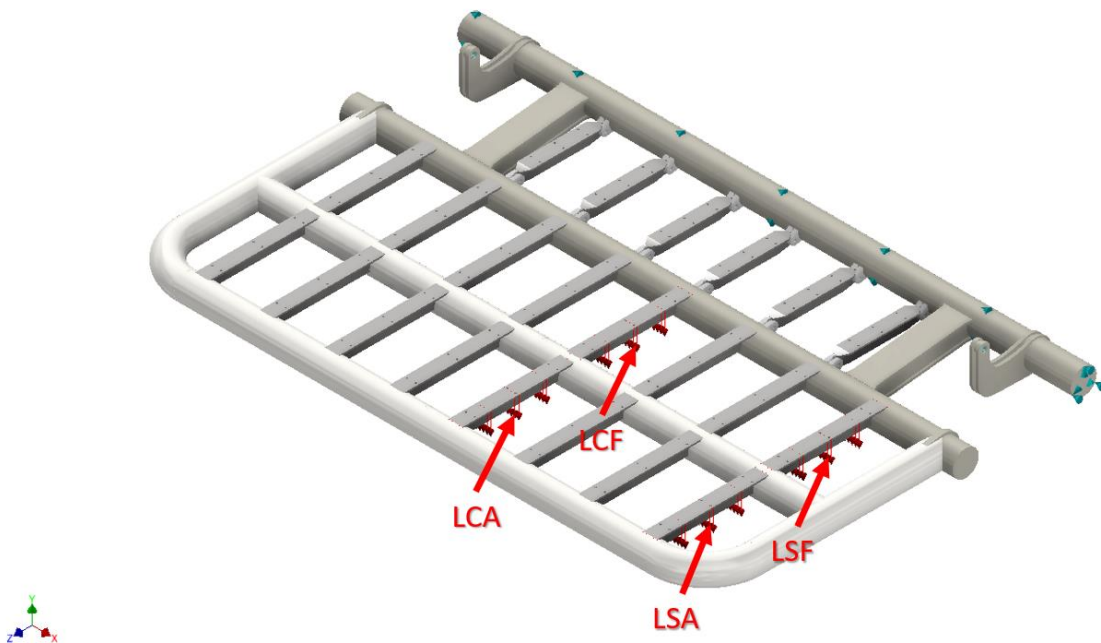


Figure 22 Applied f_Q locations for determining elastic potential energy of hatch.

Table 6 Deformation in hatch with deformation loads

Load placement	Description	f_Q [kN]	U_{el} [J]	Deformation [mm]			
				Total	X-axis	Y-axis	Z-axis
LCA	Load centre aft	60	376.8	-12.56	0.25	-12.56	0.22
LCF	Load centre forward	60	179.7	-5.99	0.15	-5.98	0.19
LSA	Load starboard aft	60	443.4	-14.78	0.42	-14.77	0.30
LSF	Load starboard forward	60	243.9	-8.13	0.27	-8.13	0.26

4.5 Environmental loads

The environmental loads are calculated according to [21] with calculations in Appendix L.

4.5.1 Hydrodynamic forces

The hydrodynamic force on the hatch is calculated with the Morison's equation according to [21]. It is the sum of the inertia force proportional to acceleration and a drag force proportional to the square of velocity, and neglects gradients of fluid particle velocities and accelerations in the direction relative to the member. The inertial force f_I due to the motion of a floating body disrupting the movement of the waves, is calculated with equation (17). Here the velocity of water is equal to the velocity of ROV, i.e., $v_{n,ROV}$ and is used for the inertia force.

$$f_I = \rho V v_{n,ROV} \quad (17)$$

where:

$$\begin{aligned} f_I &= \text{inertial force [kN]} \\ \rho &= \text{density of sea water [kg/m}^3\text{]} \\ V &= \text{volume of item [m}^3\text{]} \end{aligned}$$

The added mass force f_A due to the displacement and acceleration of the surrounding fluid, is calculated with equation (18).

$$f_A = \rho C_A V a_r \quad (18)$$

where:

$$\begin{aligned} f_A &= \text{added mass force [kN]} \\ C_A &= \text{added mass coefficient of submerged part of item [-]} \\ a_r &= \text{relative acceleration [m/s}^2\text{]} \end{aligned}$$

The characteristic drag force f_D on an object is calculated with equation (19).

$$f_D = \frac{1}{2} \cdot \rho C_D S (v_r \cdot \sin \alpha_1)^2 \quad (19)$$

where:

$$\begin{aligned} f_D &= \text{drag force [kN]} \\ \rho &= \text{density of sea water [kg/m}^3\text{]} \\ C_D &= \text{drag coefficient in oscillatory flow of submerged part of item [-]} \\ S &= \text{projected area normal to the force direction [m}^2\text{]} \end{aligned}$$

The total hydrodynamic force acting on the object is then the sum of the discussed forces and denoted as the environmental loads.

$$f_E = f_I + f_A + f_D \quad (20)$$

The hydrodynamic forces depend largely on the geometric entity, therefore the pipes, box beams and T-bars with damper material, have been calculated separately with their respective volume and area seen in Figure 23.

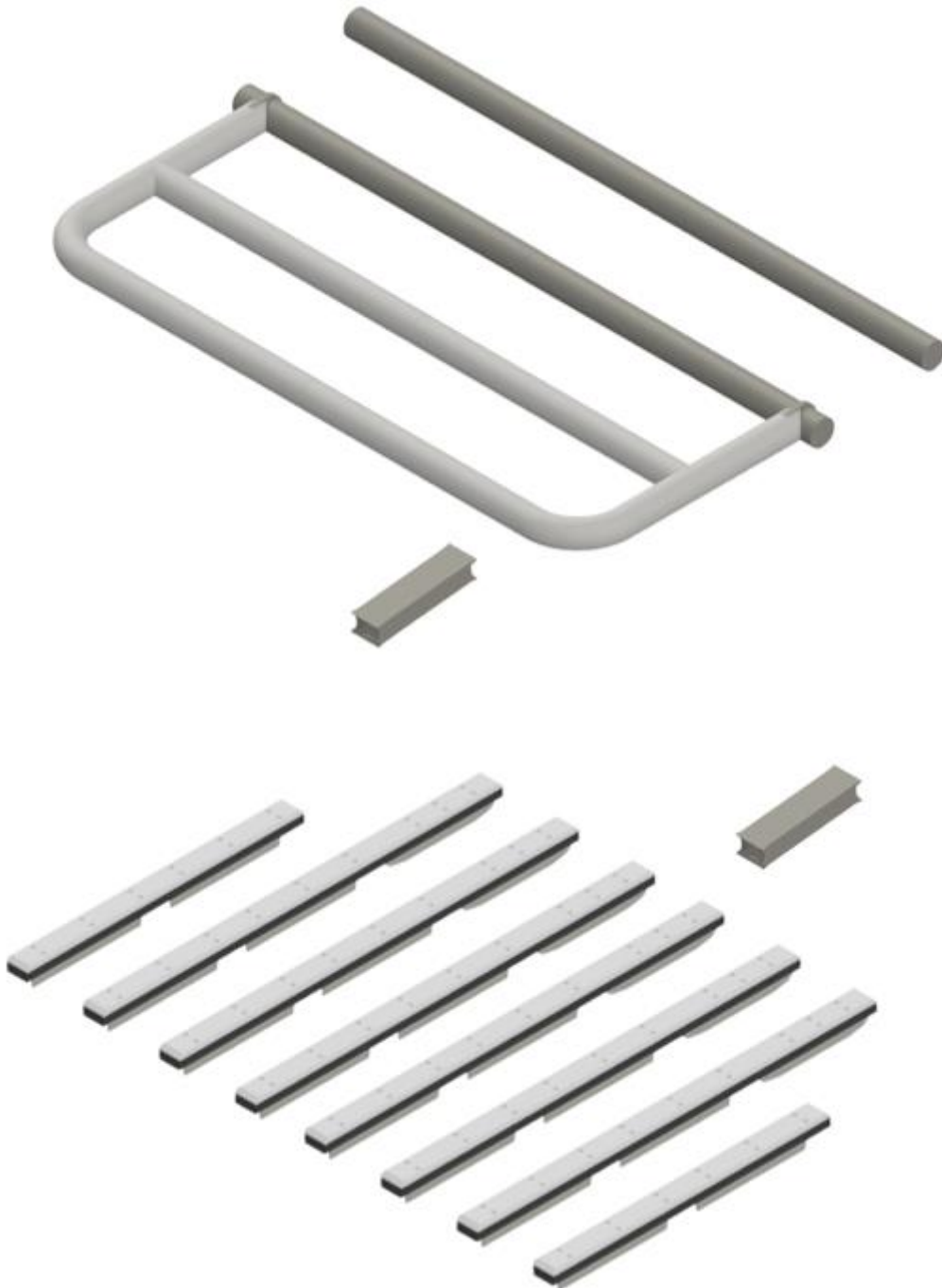


Figure 23 Hatch model split into pipes, box beams and T-bars, for calculating separate hydrodynamic loads.

4.5.2 Buoyancy force

The buoyancy force is calculated according to [19] with equation (21). The displaced volume of the hatch is calculated with Inventor and used as input.

$$f_B = \rho g V \quad (21)$$

where:

$$f_B = \text{buoyancy force [kN]}$$

4.5.3 Permanent force

The permanent forces, F_G , is the weight of the structure times the gravity calculated with equation (22).

$$f_G = mg \quad (22)$$

where:

$$f_G = \text{Permanent weight force [kN]}$$

$$m = \text{mass of item [m]}$$

4.6 Sum of forces acting on the hatch

The hydrodynamic coefficients on each of the respective elements in the hatch are listed in Table 7.

Table 7 Hydrodynamic forces acting on the hatch.

Item	Forces [kN]					
	f_D	f_A	f_I	f_B	f_G	f_Q
General pipes	-21.37	-1.24	-0.39	0.19	-	-
T-bars with dampers	-2.60	-3.51	-0.76	3.52	-	-
Box beam	-1.83	-0.23	-0.43	0.20	-	-
Hatch general	-	-	-	-	-20.60	60
Sum	-25.8	-4.98	-1.58	3.91	-20.60	-60

4.7 Load cases and load factors

The hydrodynamic forces listed in Table 7 are categorised into the following:

- Permanent G f_G
- Variable functional Q f_Q
- Environmental E $f_E = f_D + f_A + f_I$
- Buoyancy B f_B

These are applied into different load cases ULS-a and ULS-b with their own load factor listed in Table 8. Where a permanent load G causes favourable load effects as in this case buoyancy, a load factor $\gamma_B = 1.0$ is used for this load in load conditions.

Table 8 Load factors for ULS according to [19].

Load Condition	Load factors			
	γ_G	γ_Q	γ_E	γ_B
ULS-a	1.3	0.7	0.7	1.0
ULS-b	1.0	1.3	1.3	1.0

The load factors in Table 8 are used to determine the design forces listed in Table 9, and are as follows:

$$F_G = f_G \cdot \gamma_G$$

$$F_Q = f_Q \cdot \gamma_Q$$

$$F_E = f_E \cdot \gamma_E$$

$$F_B = f_B \cdot \gamma_B$$

Table 9 Resulting forces applied to hatch with load factors applied.

Load condition	Design force [kN]				Sum [kN]
	F_G	F_Q	F_E	F_B	
ULS-a	-26.78	-42.00	-22.65	3.91	-87.52
ULS-b	-20.60	-78.00	-42.07	3.91	-136.76

4.8 Determining Bolt Capacity and Weld Stresses

This chapter focuses on how the calculation and analysis of bolt capacity and weld stresses is done.

4.8.1 Fasteners

The bolted connections are categorized as Type A shear connections, which involves screws with strength classes ranging from 4.6 to 10.9. Notably, no preloading or additional measures for contact surface preparation are necessary for Category A connections. The design shear force $F_{v,Ed}$ applied to these connections, should not exceed the design shear capacity $F_{v,Rd}$ calculated with equation (23) according to [17].

$$F_{v,Rd} = \frac{a_v \cdot f_u \cdot A}{\gamma_{M2}} \quad (23)$$

And for tension capacity $F_{t,Rd}$ in the bolts, equation (24) is used.

$$F_{t,Rd} = \frac{0.9 \cdot f_u \cdot A_s}{\gamma_{M2}} \quad (24)$$

where:

- $F_{v,Rd}$ = design shear capacity
- $F_{v,Ed}$ = design shear force
- a_v = correction for the cut-off area, = 0.6 for class 8.8 screws [-]
- A_s = stress area according to [11] [mm²]

In Inventor Nastran, $F_{v,Ed}$ and $F_{v,Rd}$ are calculated with two methods. One method is to use beam elements and calculate maximum von Mises stress σ_{vm} , which includes the local x, y, and z axes. A second method is also used, where the support loads in the bolt holes, are calculated using constraint forces generated in Nastran analysis.

4.8.2 Welded connections

According to [22], the calculation of welds is required in structural design. Welds are considered critical load bearing elements in structural applications, and their design and calculation are necessary to ensure the structural integrity. The Eurocode distinguished from EN-1993-1-8 for steel structures, and EN-1999-1-1 for aluminium structures [17] [23]. In this case the welded parts of the hatch are a steel structure, and for the skid, an aluminium structure.

4.8.2.1 Design of fillet welds

In the design of fillet welds, the governing section is determined by the throat section. The throat section's area is calculated based on the effective weld length and the effective throat thickness of the weld. The effective length l_{eff} of a fillet weld is set equal to the length of the fillet where it reaches its full size. This can be assumed to be the actual length of the weld minus two times the effective throat thickness a , as stated in equation (25).

$$l_{eff} = l_w - 2a \quad (25)$$

where:

- l_{eff} = effective length of the longitudinal fillet welds [mm]
- l_w = total length of the longitudinal fillet welds [mm]
- a = effective throat thickness [mm]

4.8.3 Design of fillet welds with directional method

The forces that must be transmitted by a fillet weld shall be resolved into stress components with respect to the throat section seen in Figure 24, where:

- σ_{\perp} is the normal stress perpendicular to the throat section;
- σ_{\parallel} is the normal stress parallel to the weld axis;
- τ_{\perp} is the shear stress acting on the throat section perpendicular to the weld axis;
- τ_{\parallel} is the shear stress acting on the throat section parallel to the weld axis;

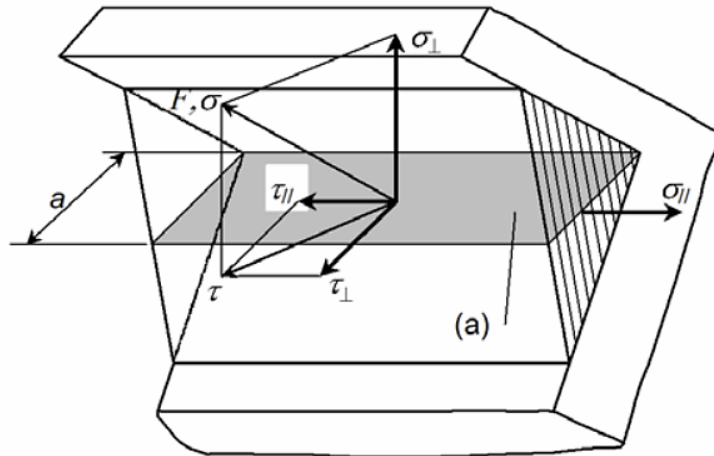


Figure 24 Stresses σ^{\perp} , σ^{\parallel} , τ^{\perp} and τ^{\parallel} , acting on the throat section of a fillet weld [23].

For axial loading, the perpendicular stress is calculated with equation (26):

$$\sigma_{\perp} = \frac{F}{l_{eff} \cdot a \cdot \sqrt{2}} \quad (26)$$

For axial loading when bending moment is introduced, the perpendicular normal stress is calculated with equation (27):

$$\sigma_{\perp} = \frac{M}{\sqrt{2} \cdot W_{ey}} \quad (27)$$

For shear forces, the normal and parallel shear stress is equal, and calculated with equation (28):

$$\tau_{\perp} = \tau_{\parallel} = \frac{F}{a \cdot l_{eff}} \quad (28)$$

And for when torsion applied, the parallel shear stress is calculated with equation (29):

$$\tau_{\parallel} = \frac{T}{W_p} \quad (29)$$

where:

- F = Force [N]
- M = bending moment [Nmm]
- T = torsion [Nmm]
- W_{ey} = section modulus [mm³]
- W_p = polar section modulus [mm³]

Welds are evaluated and examined in both horizontal and vertical sections, as well as their entire section. This involves considering the moment through the horizontal welds by creating a force couple, while the vertical welds bear the vertical load.

Additionally, in weld connections subjected to torsional load, it is assumed that the weld cross-section experiences torsional shear stress solely.

4.8.3.1 Capacity of welds in steel structures

The design capacity of a fillet weld is deemed satisfactory if both of the following conditions are met in equation (30):

$$\sigma_{vm} = \sqrt{\sigma_{\perp}^2 + 3(\tau_{\perp}^2 + \tau_{\parallel}^2)} \leq \frac{f_u}{\beta_w \gamma_{m2}} \quad \text{and} \quad \sigma_{\perp} \leq \frac{0.9f_u}{\gamma_{m2}} \quad (30)$$

According to [17], welds between parts with different steel grades should be dimensioned based on the properties of the material with the lowest strength. Thereafter the utilization of the horizontal η_h , vertical η_v and the whole connection η_c is calculated with the ratio of von Mises stress and allowed stress according to equation (30).

4.8.3.2 Capacity of fillet welds in aluminium welds

The design capacity of welds in aluminium structures, the design capacity of a fillet weld is deemed satisfactory if both of the following conditions are met in equation (31). The method and utilization are the same as described in the previous chapter 4.8.3.1 Capacity of welds in steel structures.

$$\sqrt{\sigma_{\perp}^2 + 3(\tau_{\perp}^2 + \tau_{\parallel}^2)} \leq \frac{f_{u,haz}}{\gamma_{m2}} \quad (31)$$

where:

$f_{u,haz}$ = characteristic strength of weld metal according to [23] [N/mm²]

5 Structural analysis

This chapter provides an in-depth explanation of the structural analysis conducted on the skid and hatch components. It covers the Nastran simulation setup and presents stress maps for a comprehensive understanding of the structural behaviour.

5.1 Analysis setup

To accurately capture the behaviour of the system, various contact models were employed during the analysis:

- General Contact: This model represents standard nonlinear surface contact, considering friction if specified.
- Welded Contact: This model prevents sliding, separating, or closing between contacting regions that are welded.
- Bi-Directional Slide: This model allows sliding between contacting regions while preventing separation or closure. It assumes a zero coefficient of friction.

For the contact surfaces between the aluminium profiles, a frictional coefficient of $\mu_F = 0.3$, as specified in [17], was utilized.

The fasteners were analysed using the Inventor Nastran bolts function. This function resembles stiff bars that accurately reflect the dimensions of the actual bolts being analysed. By conducting this analysis, reaction forces, including axial forces and shear forces in the local y and z-directions, were determined. It is important to note that the pre-torque values for the bolts were followed as per the specifications provided in [11].

5.2 Hatch

A linear static analysis was performed using the finite element symmetry model shown in Figure 25. The model is divided into 4 property groups according to their material properties. The model consists of a total of 165236 nodes and 83006 elements. The model contains 56 contact regions, where the structure has welded contacts, and the bolted connections are configured as frictionless.

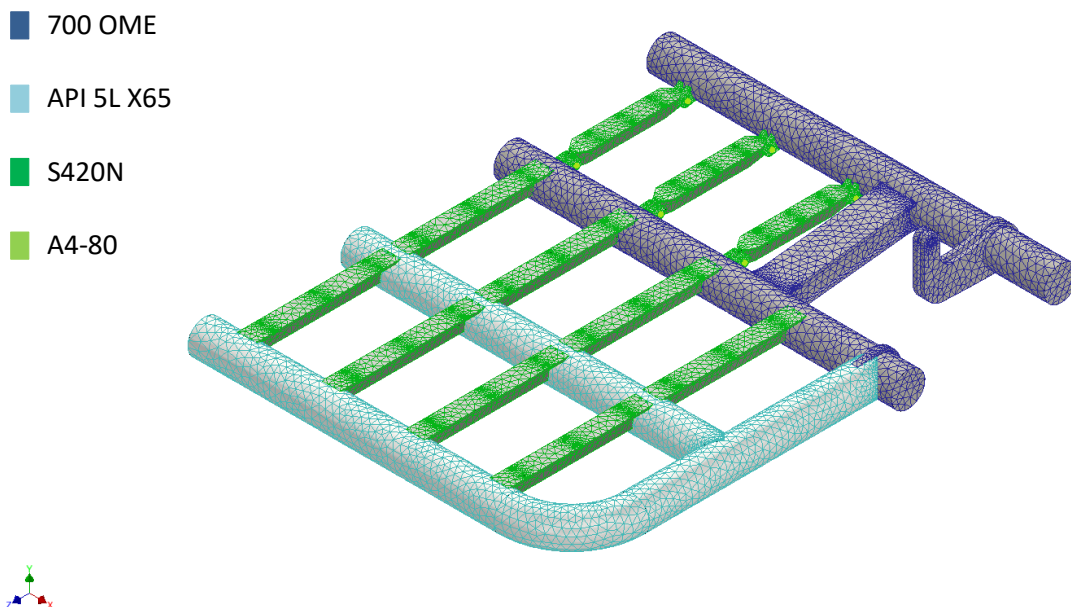


Figure 25 Meshed model of the hatch.

The constraints are shown in Figure 26, where the hinge holes are constrained in radial direction, and the pipe constrained in radial and axial direction. Figure 27 shown the symmetry constraints about the x-axis, with fixed rotation around y and z-axis, and translation in the x-axis.

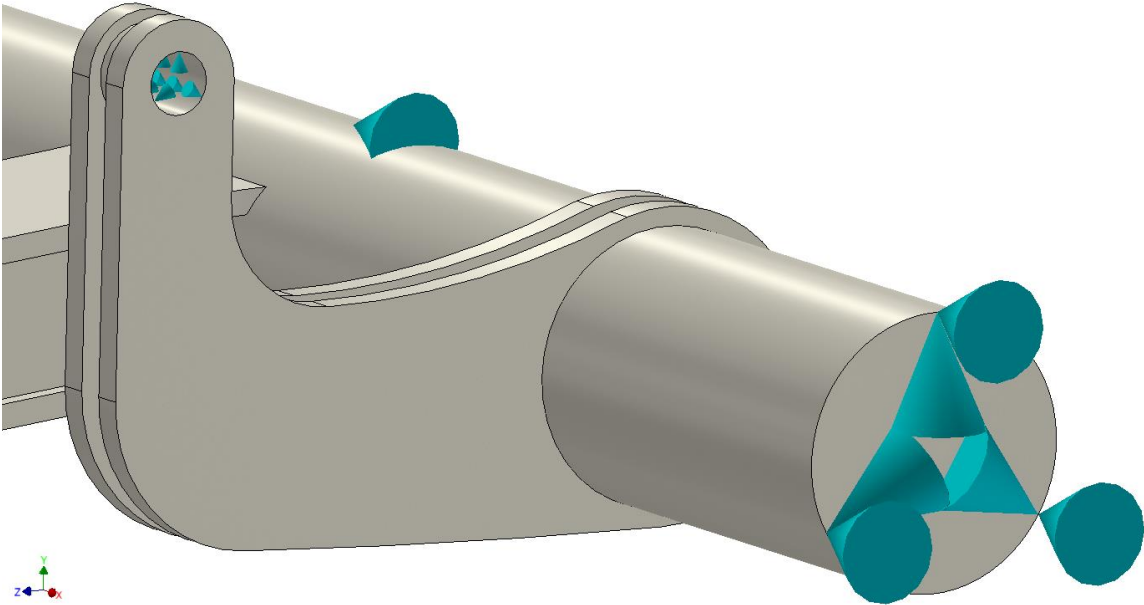


Figure 26 Constraints in hatch hinge and pipe support.

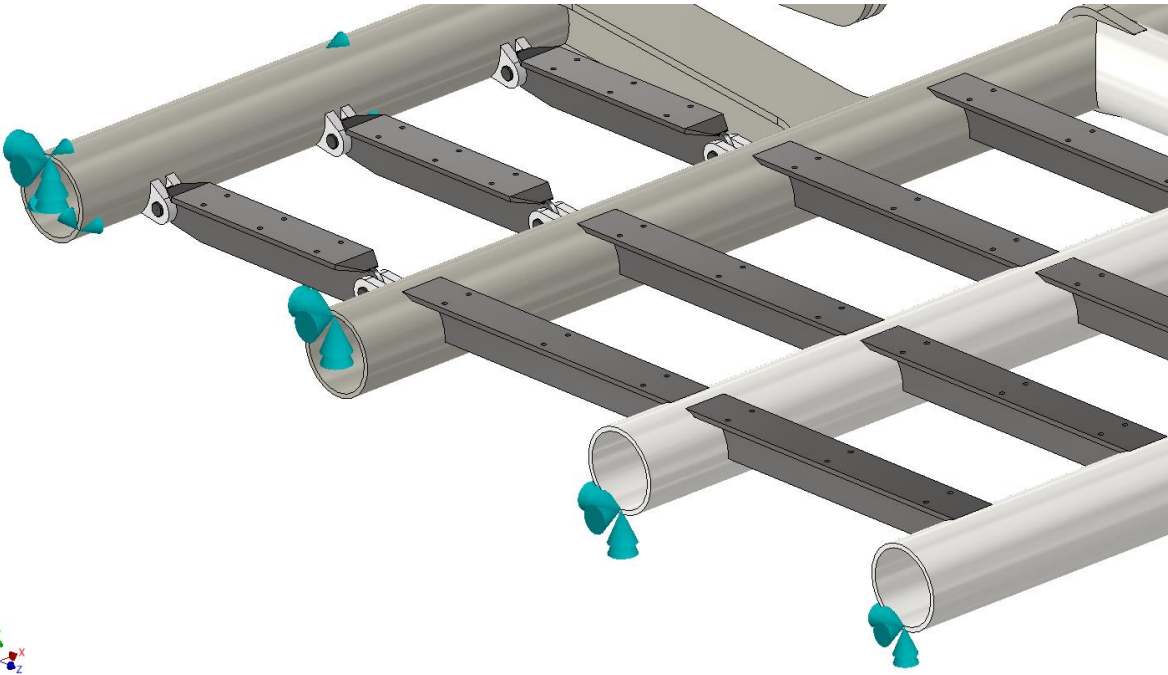


Figure 27 Symmetry constraints to hatch model.

The loads applied to the model is shown in Figure 28. The loads are applied to all members of the hatch, summing up to the total respective magnitude as listed in Table 9.

- Hydrodynamic forces F_E
- Buoyancy force F_B
- Permanent force F_G

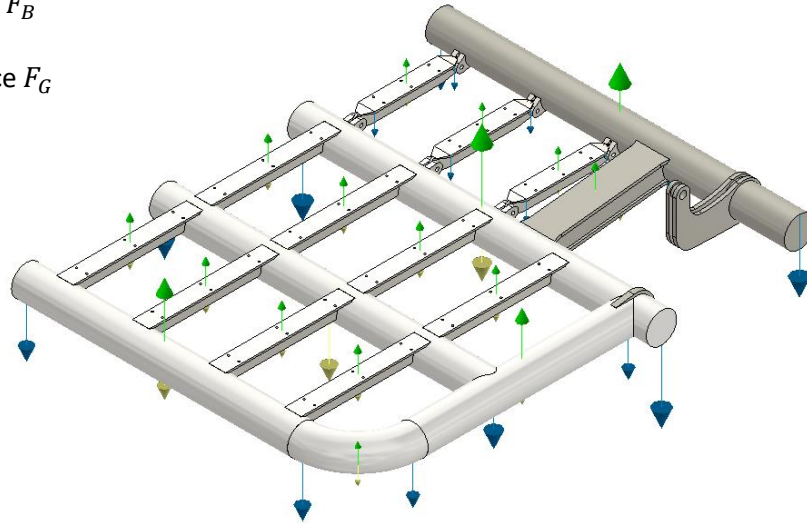


Figure 28 Applied environmental loads on structural hatch model.

5.2.1 Hatch analysis

The load cases from Table 8 are combined with the load locations from Table 6, to form the 8 different load cases to be applied to the hatch. The ULS-a LCA load case results in the largest reaction forces, stresses, and displacements, and will be presented in this part if the report. The remaining 7 load cases are listed in Appendix M.

5.2.2 ULS-a LCA

Local max stress, seen in Figure 29 and Figure 30, may be assumed to be caused by caused by notch effects in construction details and/or an issue with the FEA model in Nastran, as discussed with DeepOcean. This stress does however not coincide with the weld stress calculations in chapter 5.4.4.

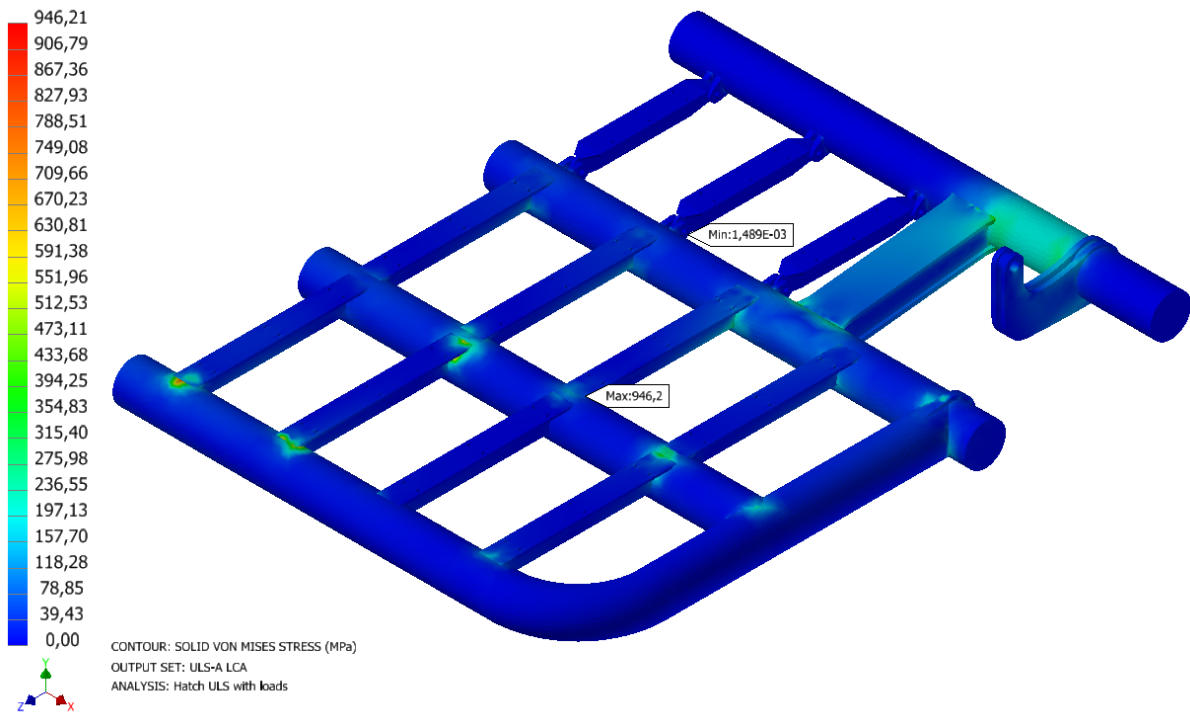


Figure 29 Stress map hatch ULS-a LCA top view

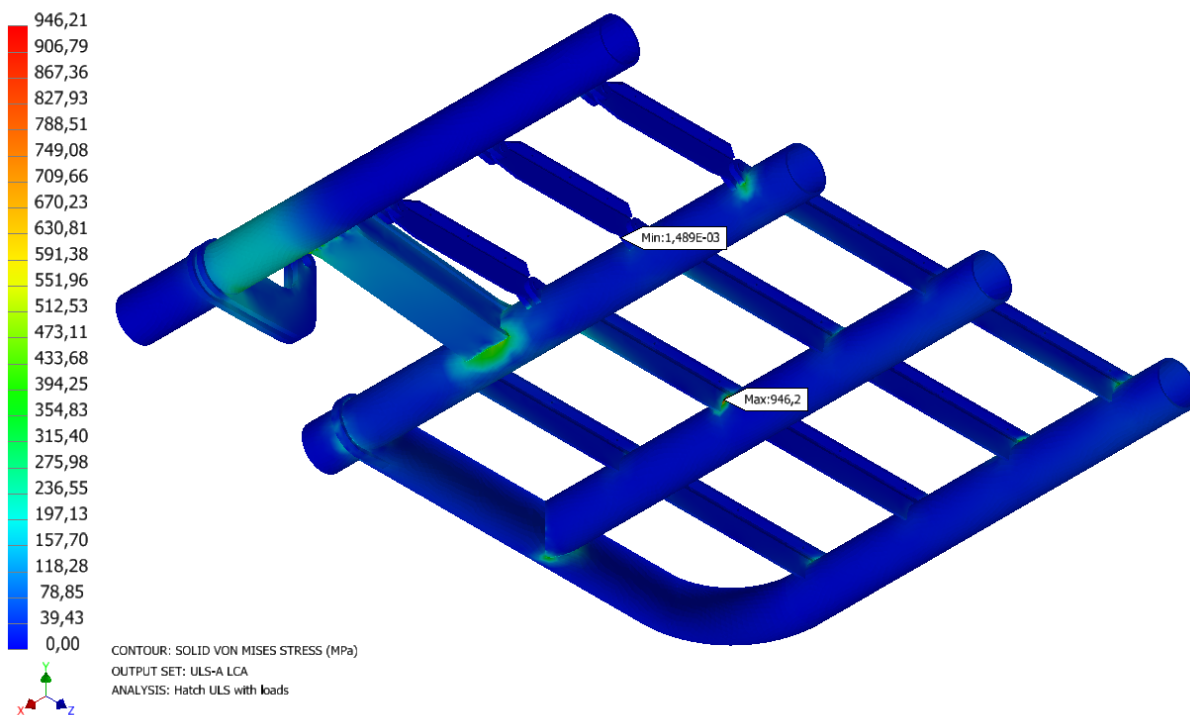


Figure 30 Stress map hatch ULS-a LCA bottom view

As seen in Figure 31, the stresses are focused on one side of the pinned T-bar connection weld, with stresses below allowed stress. Figure 32 show the bottom side of the hatch, experiencing the compressive and other torsional stresses, with acceptable results.

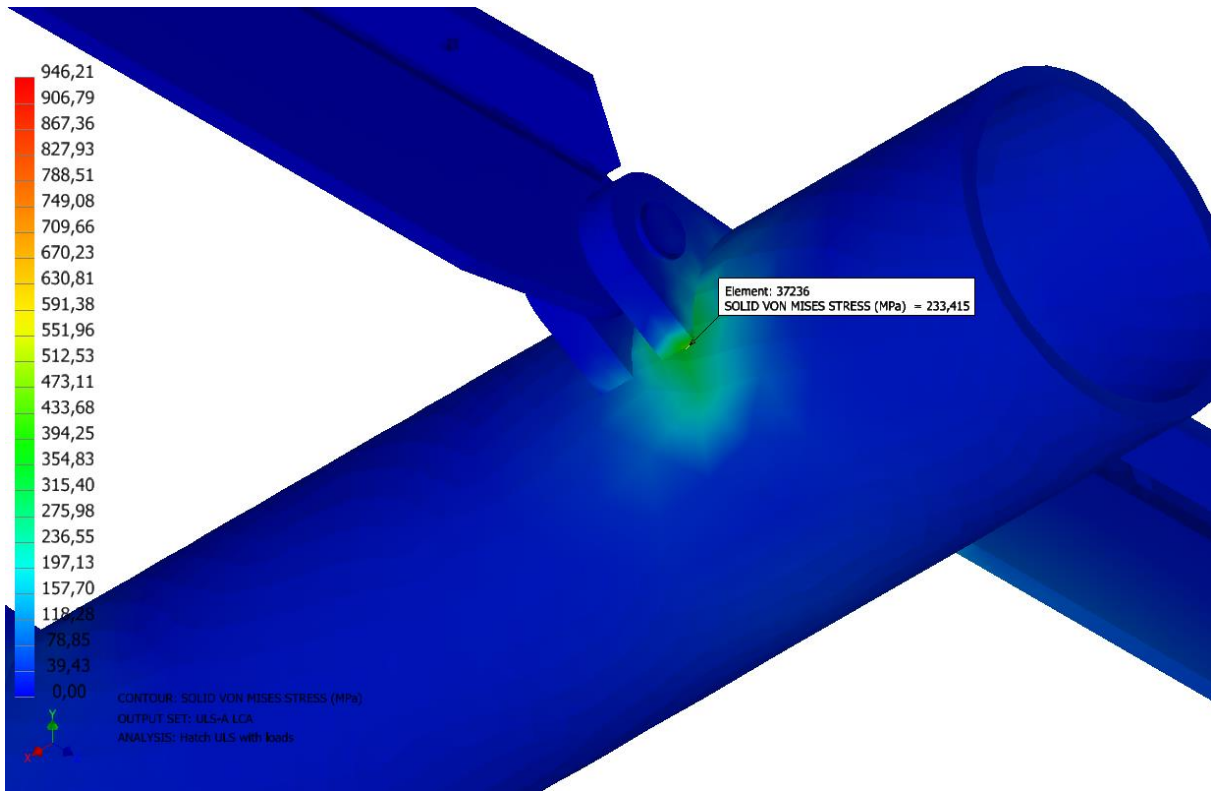


Figure 31 Stress map hatch ULS-a LCA hinge of T-bars

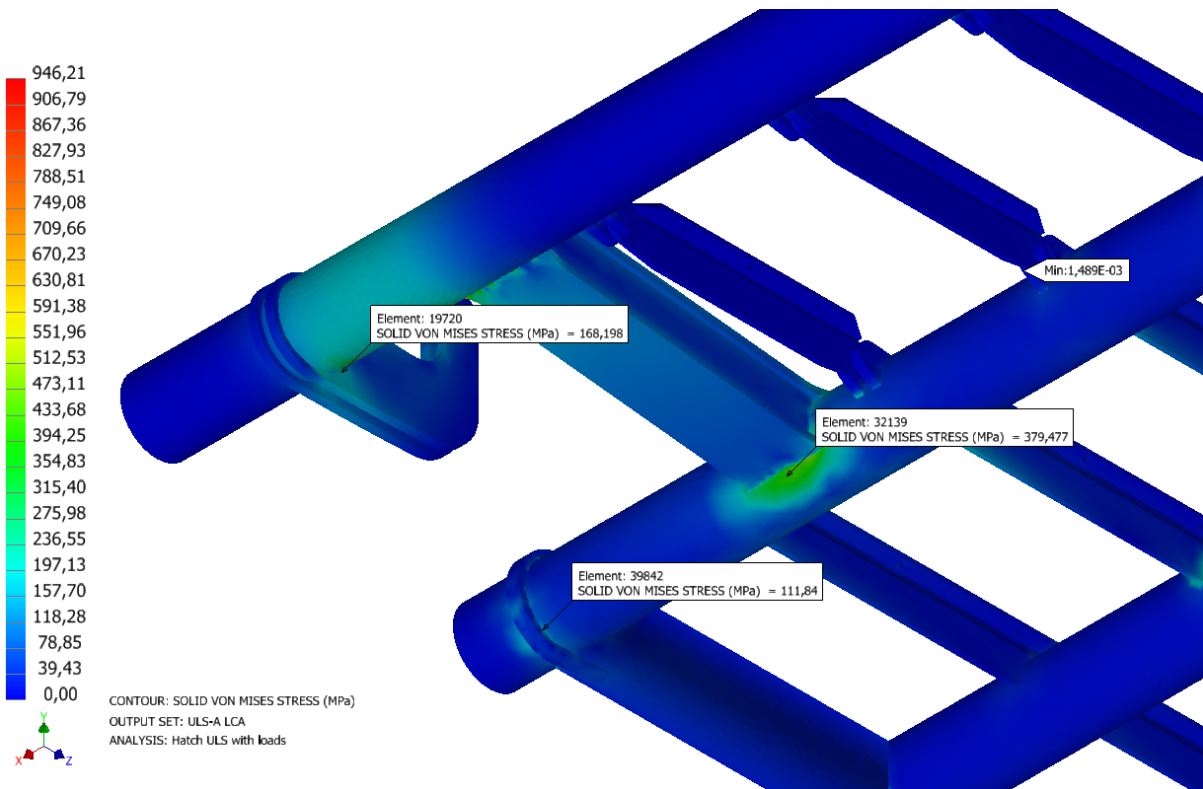


Figure 32 Stress map hatch ULS-a LCA bottom

The max stress concentration, seen in Figure 33, display stresses above allowed stress. It also shows a node close to the max stress with only 114,57 Mpa. The max stress does not coincide with the weld stress calculations in chapter 5.4.4. Figure 34 also shows similar stress distributions.

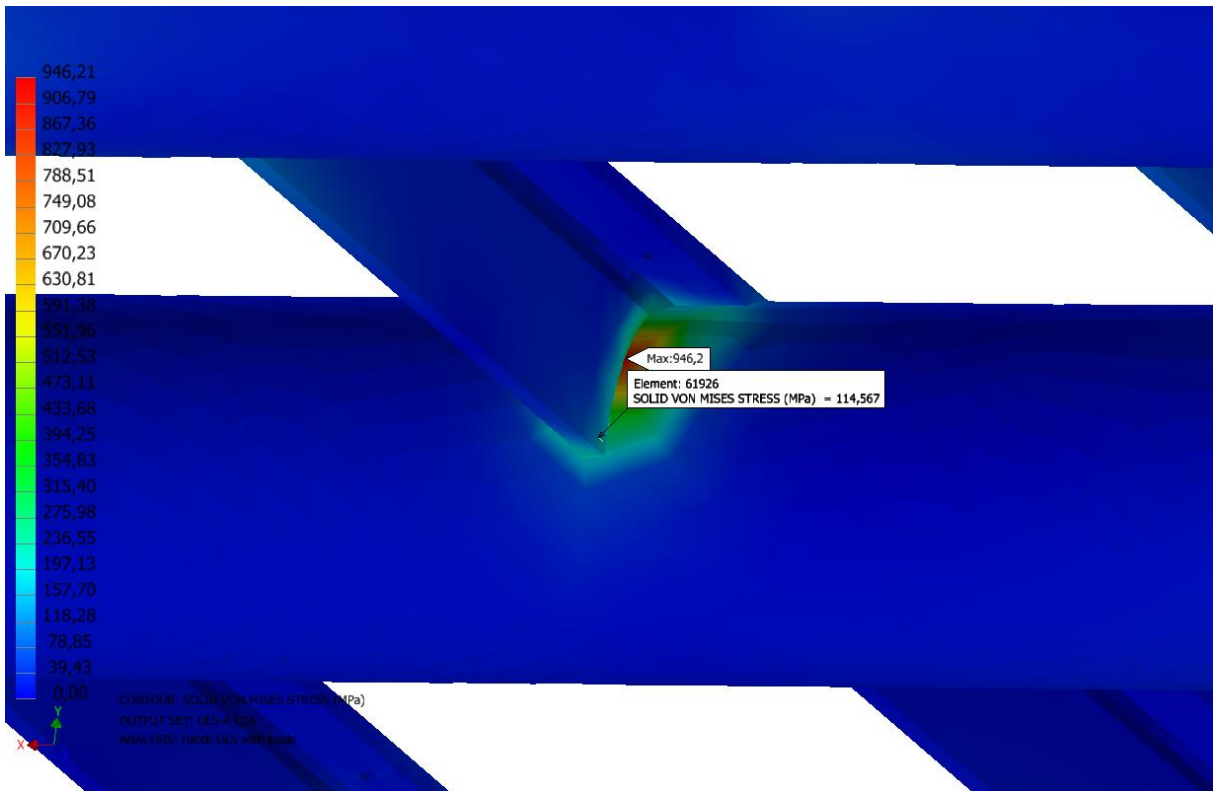


Figure 33 Stress map hatch ULS-a LCA T-bar connection bottom view

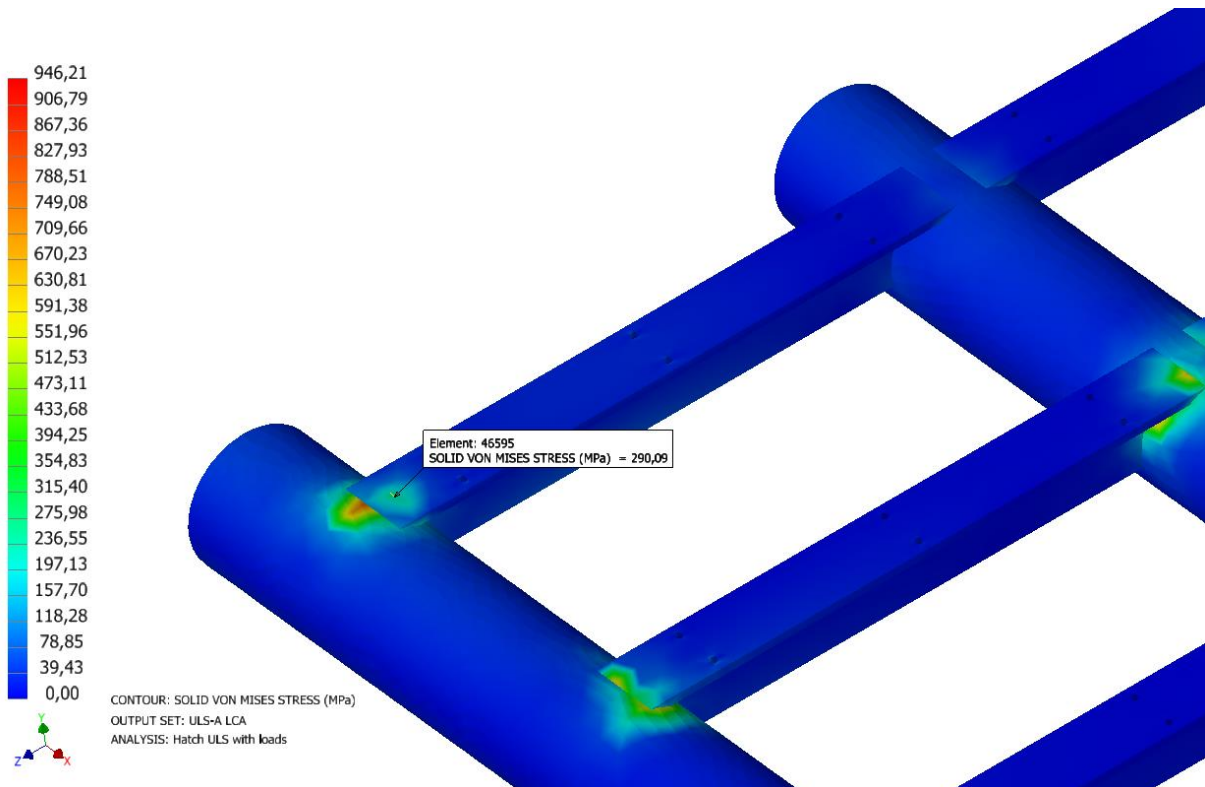


Figure 34 Stress map hatch ULS-a LCA T-bar top view

The peak stresses in the T-bars, also shown in Figure 35, have a large range of von mises stresses. As stated, the weld calculations do not coincide with the FEA results. A welded connection would increase the stress area, reducing the notch effect and ultimately reducing the stress concentrations.

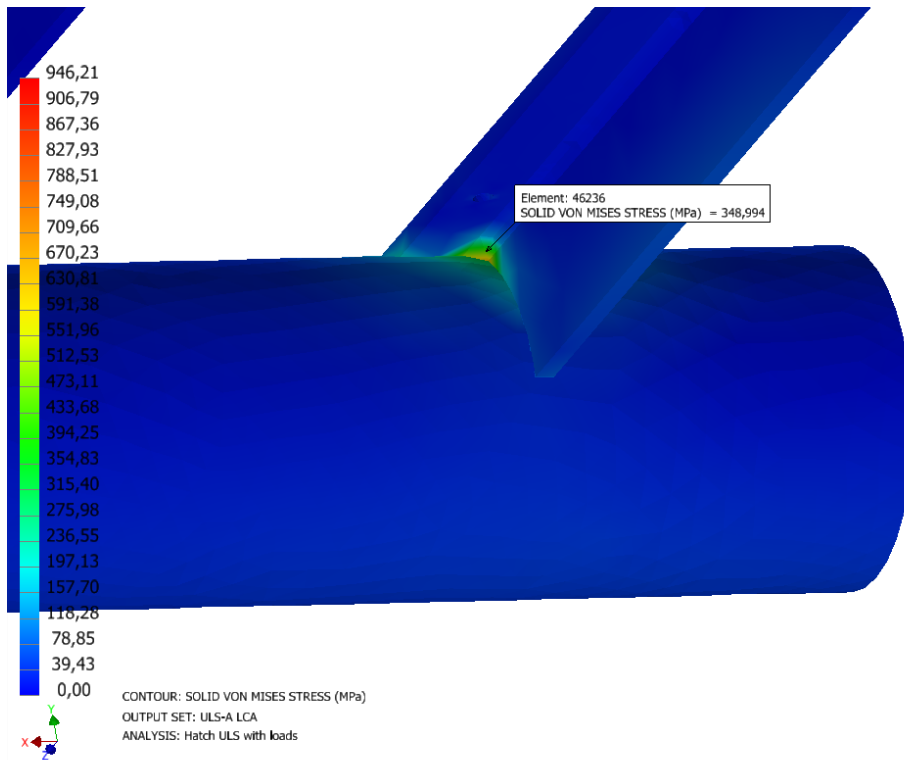


Figure 35 Stress map Hatch ULS-a LCA T-bar bottom view

5.2.3 Support loads

The resulting support loads are listed in Table 10. The hand calculations presented in Appendix O for the support loads, yield comparable results for both the hinge and pipe support. This consistency indicates that the stress analysis exhibits a reasonable level of accuracy and reliability.

Table 10 Resulting support loads for hatch analysis.

Support loads [kN]								
Load case	Hinge				Pipe support			
	F_x	F_y	F_z	Total	F_x	F_y	F_z	Total
ULS-a LCA	0.00	234.64	56.01	241.23	7.29	-171.03	-56.01	180.12
ULS-a LCF	0.00	133.52	31.85	137.26	5.31	-69.91	-31.85	170.08
ULS-a LSA	0.00	234.51	55.98	241.10	3.97	-170.91	-55.98	179.89
ULS-a LSF	0.00	177.38	42.33	182.36	0.32	-113.78	-42.33	121.40
ULS-b LCA	0.00	234.21	55.91	240.79	6.71	-165.61	-55.91	174.92
ULS-b LCF	0.00	190.54	45.47	195.89	6.55	-121.94	-45.47	130.31
ULS-b LSA	0.00	234.11	55.88	240.69	4.17	-165.52	-55.88	174.75
ULS-b LSF	0.00	190.16	45.38	195.51	1.37	-121.57	-45.38	129.77

5.2.4 Stresses, deformation, and pin forces

The resulting stresses, deformations and pin forces are listed in Table 11. Only the largest $F_{v,Ed}$ is considered for the pins, as these are only exposed to shear forces. The forces experienced by the clevis pins, $F_{v,Ed}$ is quite a lot smaller than $F_{v,Rd}$, suggesting that smaller pins would have been sufficient.

Table 11 Resulting stresses, deformation, and pin forces for hatch analysis.

Load case	Von Mises σ_{vm} [Mpa]	Total displacement u [mm]	Forces on clevis pins	
			$F_{v,Ed}$ [kN]	$F_{v,Rd}$ [kN]
ULS-a LCA	946.00	55.67	3.62	167.00
ULS-a LCF	505.19	30.71	6.73	
ULS-a LSA	935.51	53.39	4.57	
ULS-a LSF	553.91	33.12	1.58	
ULS-b LCA	921.22	54.15	3.46	
ULS-b LCF	616.12	37.56	2.44	
ULS-b LSA	913.00	52.29	4.28	
ULS-b LSF	619.47	36.70	1.92	

5.3 Skid

During the analysis of the skid using Inventor Nastran, it is important to focus only on the components that directly impact the structural analysis. This means excluding certain components that are not of interest, such as sensors, non-linear materials like rubber, and other elements that do not contribute to the structural analysis objectives. By removing these components from the analysis, a simplified model that can be effectively analysed.

5.3.1 Model

The bottom part of the skid structure is the part experiencing the loads, and therefore isolated in a model seen in Figure 36.

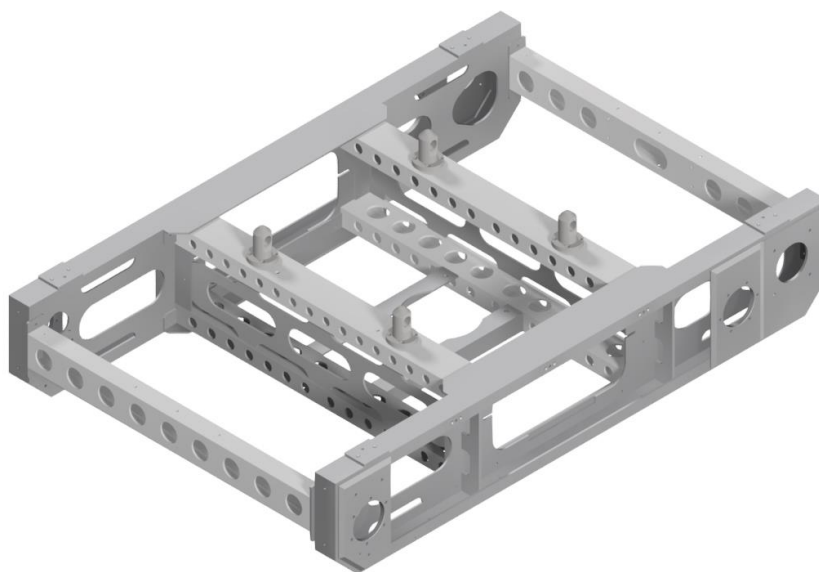


Figure 36 Skid stress analysis model top view

The critical locations of interest are illustrated in Figure 37. These specific areas are where potential collisions are anticipated and expected to occur.

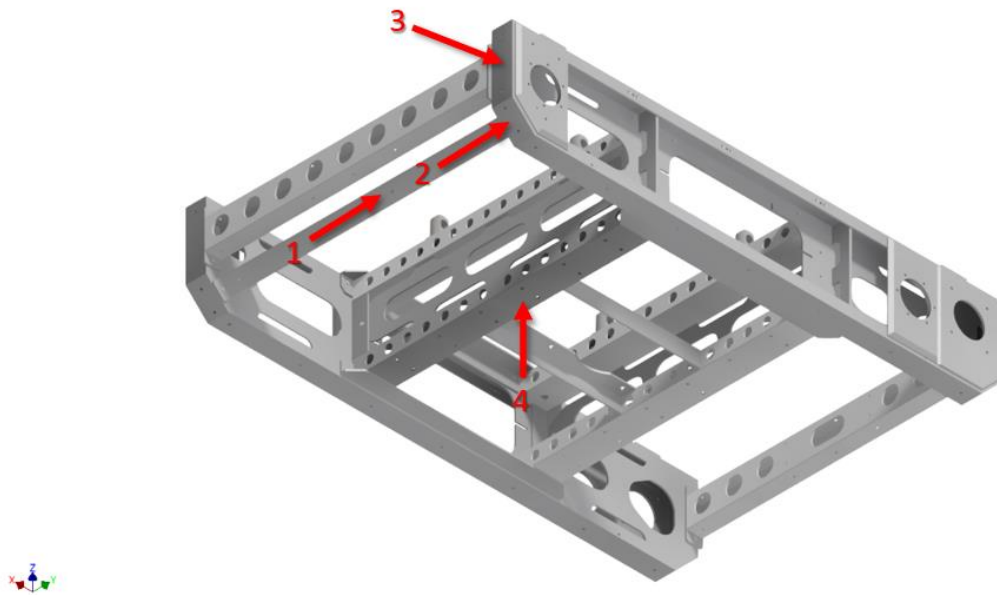


Figure 37 Skid applied load case locations.

The model is constrained in the four corner locks and the four probes, shown in Figure 38. The corner locks are constrained only in the z-direction, while the probes constrained in all axes except rotation around the y axis.

- Corner locks
- Probes

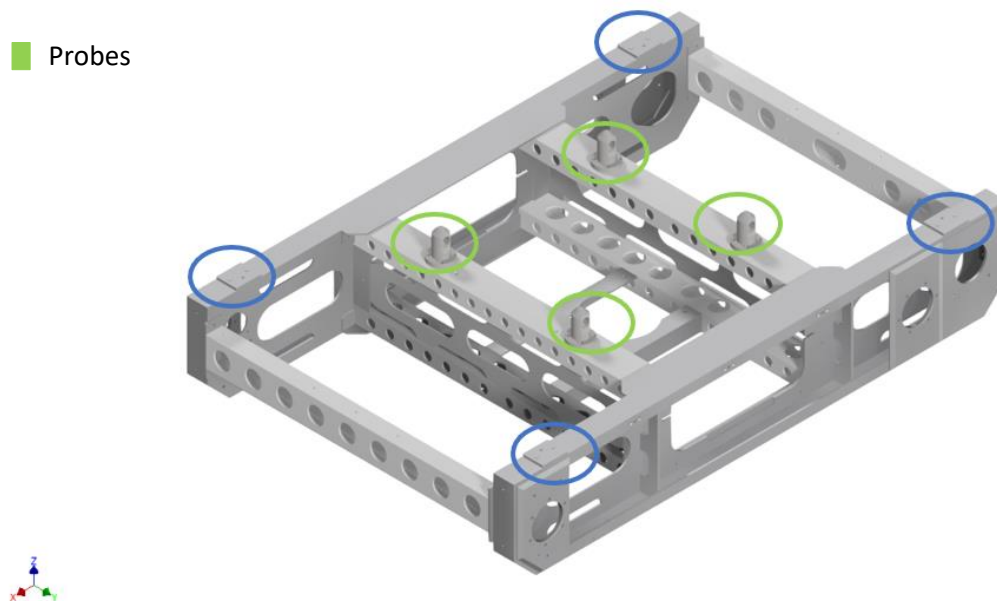


Figure 38 Skid model constraints annotations

5.3.2 Skid analysis

Symmetry is used to efficiently reduce simulating times. The finite element mesh is shown in the Figure 39. The model consists of a total of 278327 nodes and 139033 elements, with symmetric constraints in all the beam sections in the local y-direction, seen in Figure 39. The materials are shown in Figure 40.

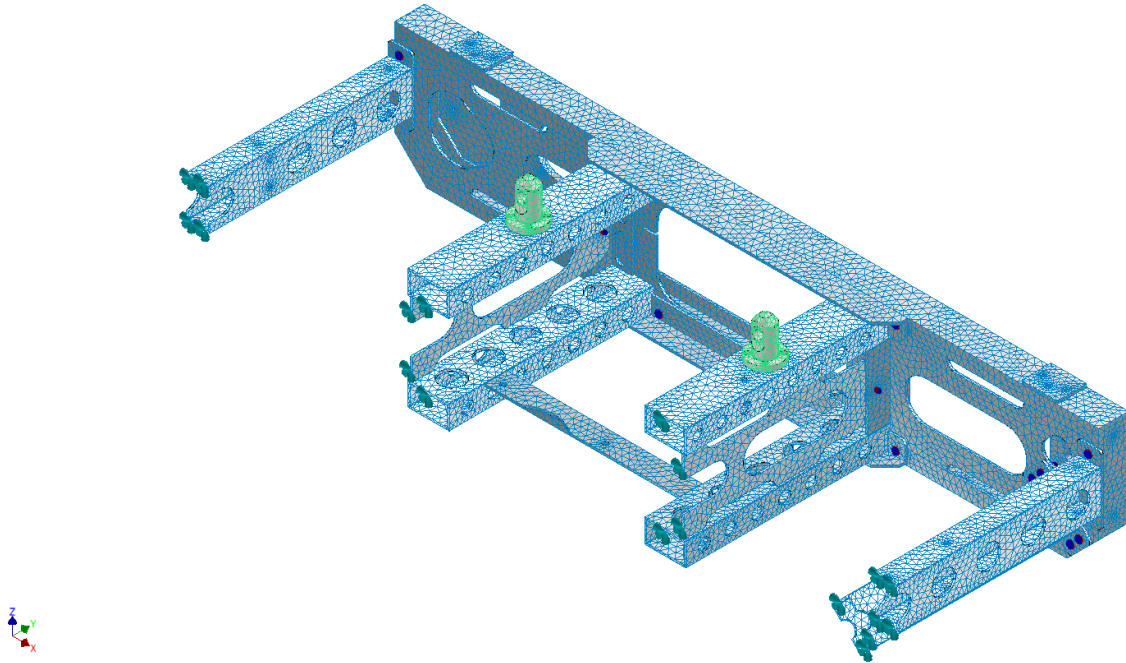


Figure 39 Skid symmetry meshed model with constraints and fasteners, port side.

- 6062-T6
- S165M W1.4418
- S420N

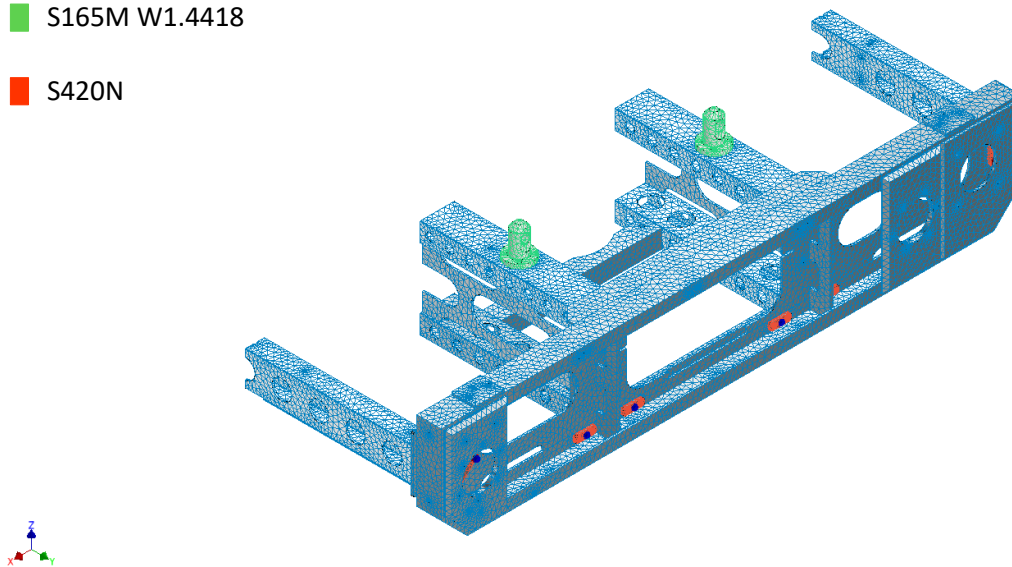


Figure 40 Skid symmetry meshed model with constraints and fasteners, starboard side.

The stresses, displacements, and forces resulting from the analysis are summarized in Table 12, while the reaction forces are provided in Table 13. The significant capacity of the bolts is attributed to their larger sizes, which were intentionally chosen to mitigate the notch effect in the bolt holes and consequently reduce the stresses.

Table 12 Resulting stresses, deformation, and fastener forces for skid analysis.

Load case	Partial factor	F_Q [kN]	Von Mises σ_{vm} [Mpa]	Total displacement u [mm]	Fasteners [kN]			
					$F_{v,Ed}$	$F_{t,Ed}$	$F_{v,Rd}$	$F_{t,Rd}$
1	γ_Q	78 kN	290.75	4.67	3.50	16.59	57.97	86.95
2			278.67	0.86	3.02	16.47		
3			338.28	1.19	4.31	18.08		
4			247.85	1.96	2.06	16.16		

Table 13 Resulting support loads for skid analysis.

Support loads [kN]								
Load case	Probes				Corner locks			
	F_x	F_y	F_z	Total	F_x	F_y	F_z	Total
1	14.51	-0.23	2.68	14.76	0	0	-22.96	22.96
2	13.80	-0.60	2.67	14.07	0	0	-24.43	24.43
3	19.97	-0.47	3.58	19.97	0	0	-4.89	4.89
4	0.083	-0.85	-27.72	27.73	0	0	-7.06	7.06

Load case 1 and 4 are the most likely to occur in operation scenario. These two load cases are presented in the following two chapters, while the other load cases are to be found in the Appendix P.

5.3.3 Load case 1

In this load case, the primary stresses are concentrated around the bolted connections, as depicted in Figure 41. The maximum stresses are observed in the bolt holes, where the S340N steel reinforcement plate is located. These findings align with the preliminary analysis and are within an acceptable stress range of 290.70 MPa, which is below the allowable stress limit.

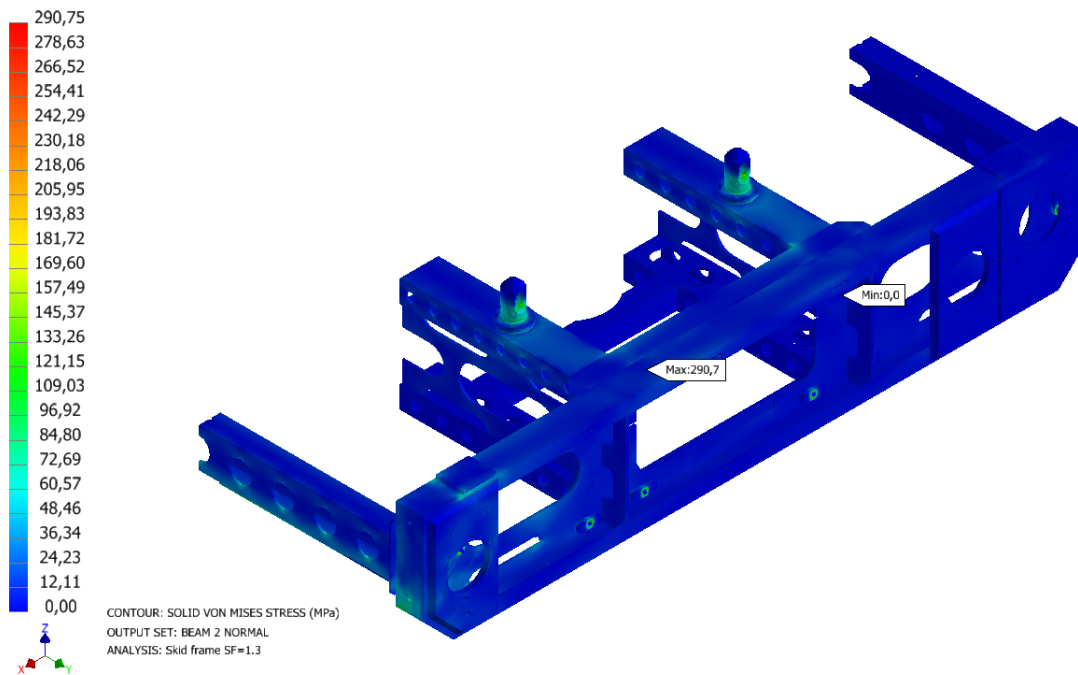


Figure 41 Stress map load case 1 top view

Figure 42 shows the max stress of 290.70 MPa which is below the allowable stress limit.

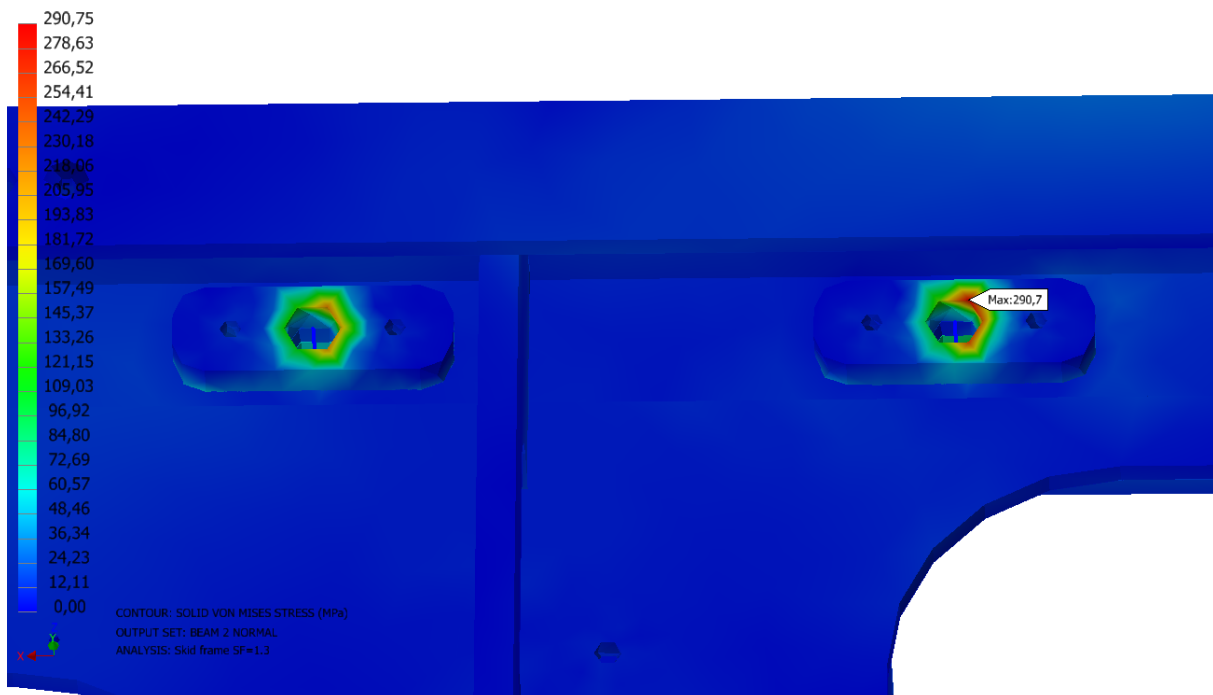


Figure 42 Stress map load case 1 max stress

Figure 43 show the beam where the load is applied. The beam and surrounding material yield good results, and display a stress of 177.03, which is below allowed stress limit.

The stresses in the bolt holes, shown in Figure 44, display a stress of 184.56 MPa, which is below allowed stress limit.

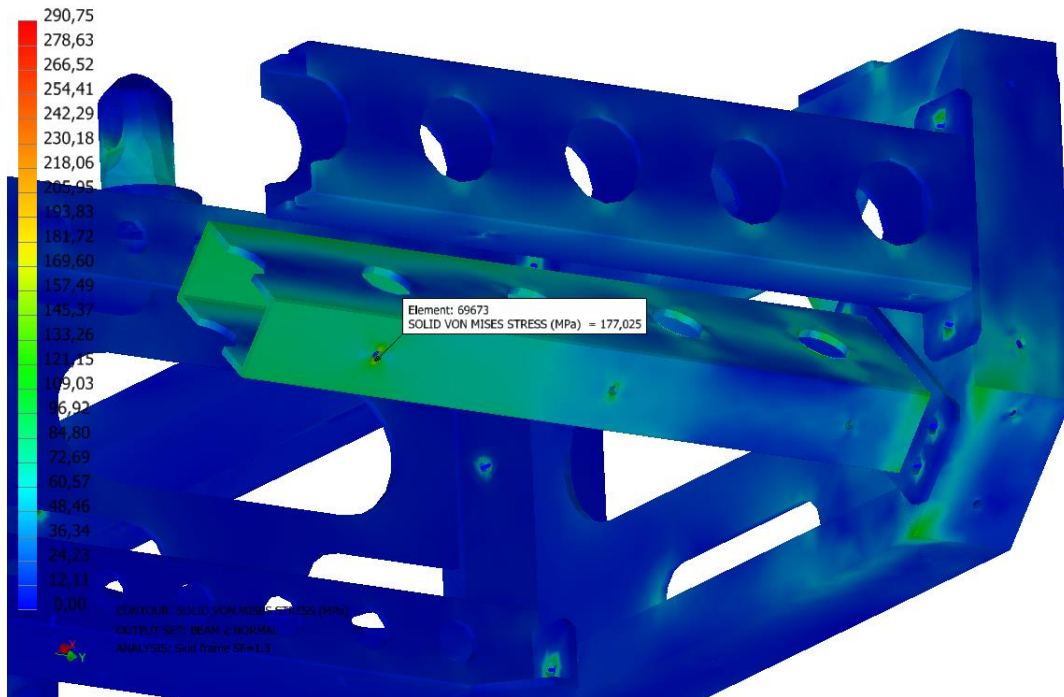


Figure 43 Stress map case 1 impact zone front view

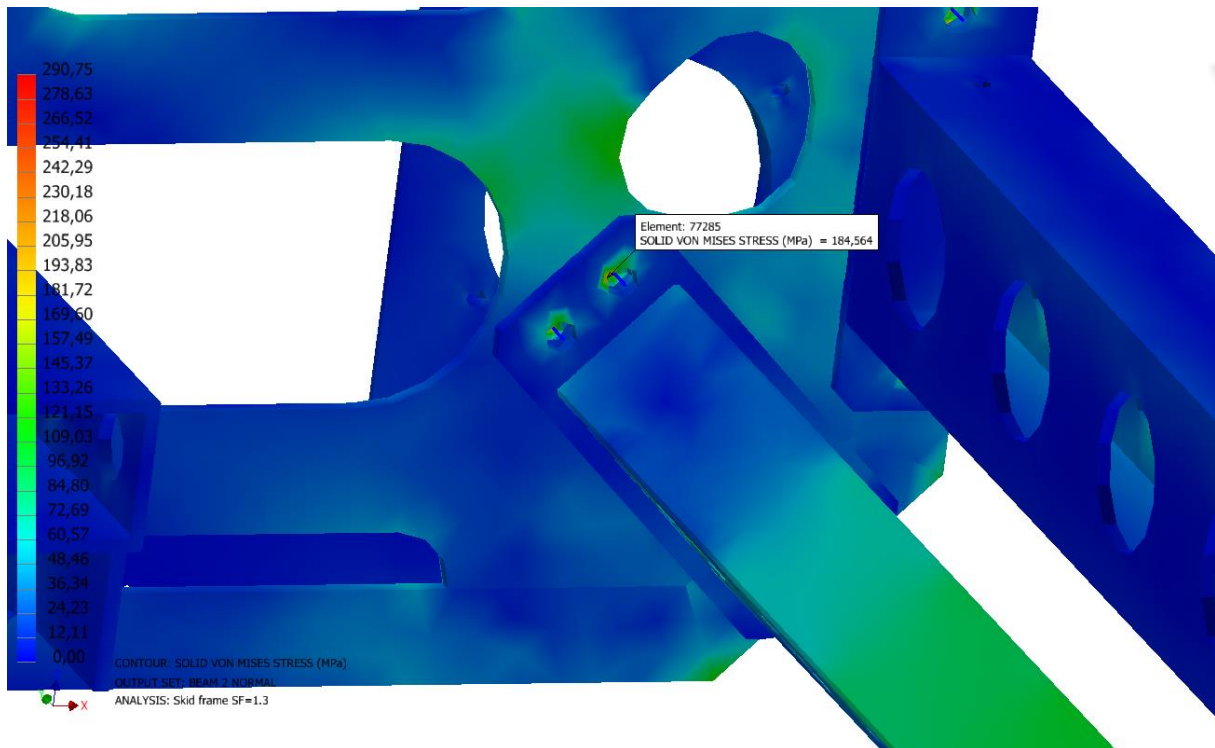


Figure 44 Stress map load case 1 impact zone side view bolt connections

5.3.4 Load case 4

In this load case, the primary stresses are like load case 1, where the bolted connections, as depicted in Figure 45, display the maximum stresses. This stress is of magnitude 247.90 MPa which is below the allowable stress limit. Here the added material between the beams distributes the load vertically up two the probes, effectively mitigating the energy transfer load. Resolving the issue found in Chapter 3.2.3: Structural analysis of preliminary skid.

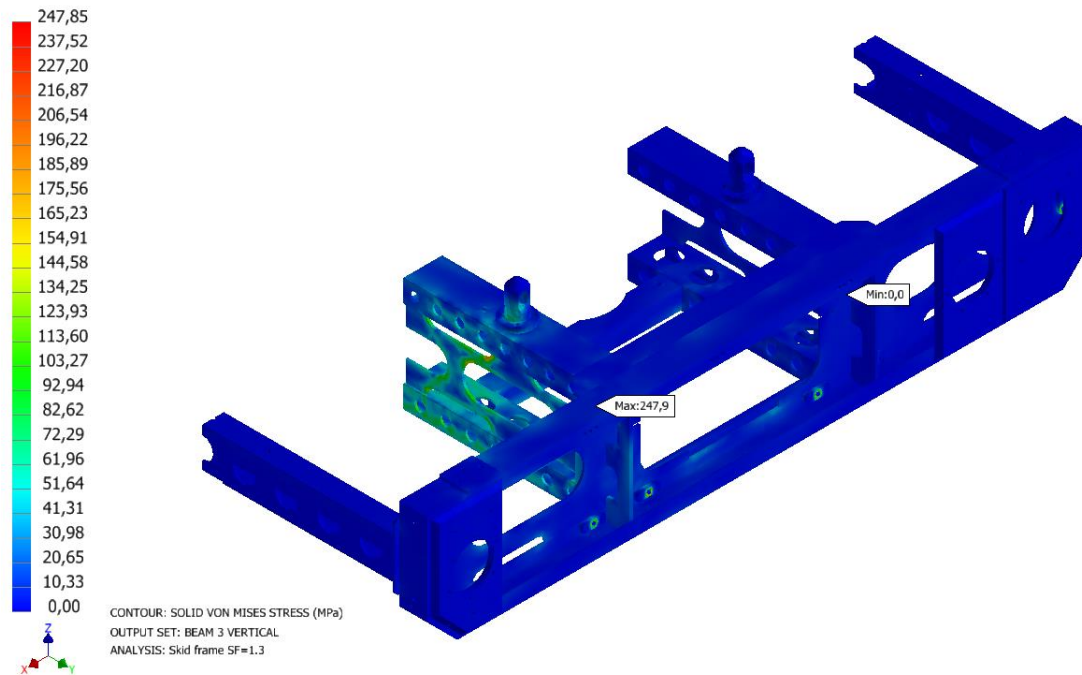


Figure 45 Stress map load case 4 top view

A closer look at the max stress in shown in Figure 46, where the S420N reinforcement plates are located. The material added to mitigate the load, seen in Figure 47, have acceptable stresses of 161.88 MPa, which is below the allowable stress limit.

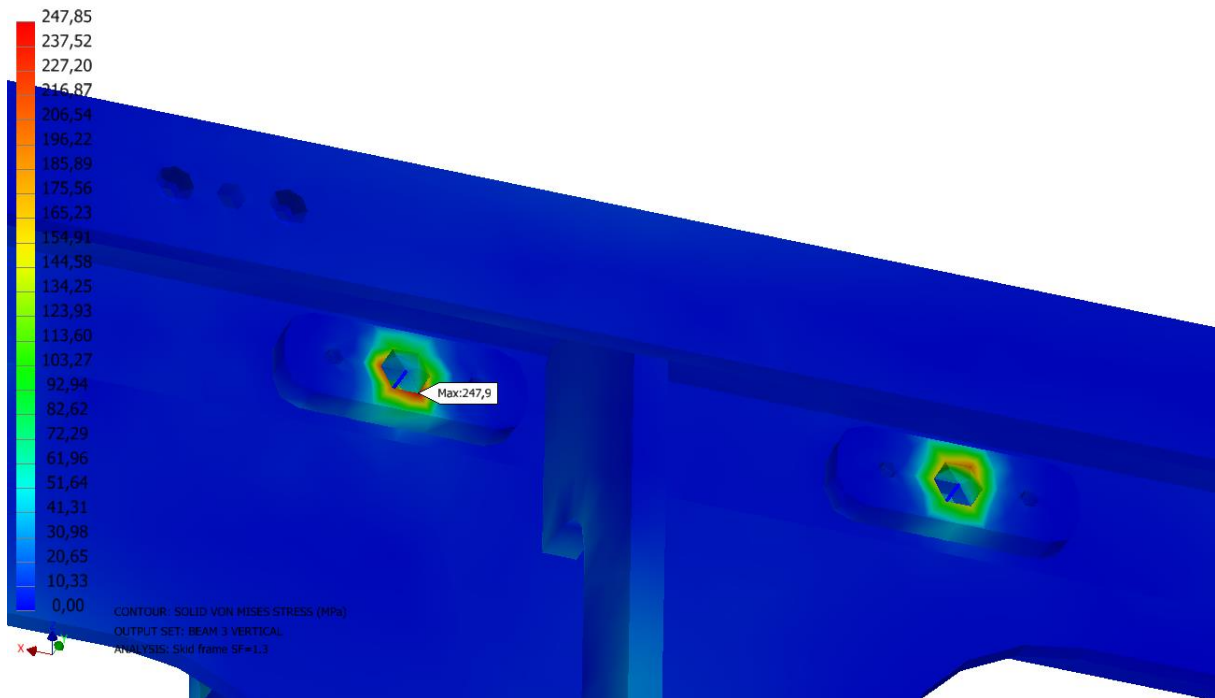


Figure 46 Stress map load case 4 max stress

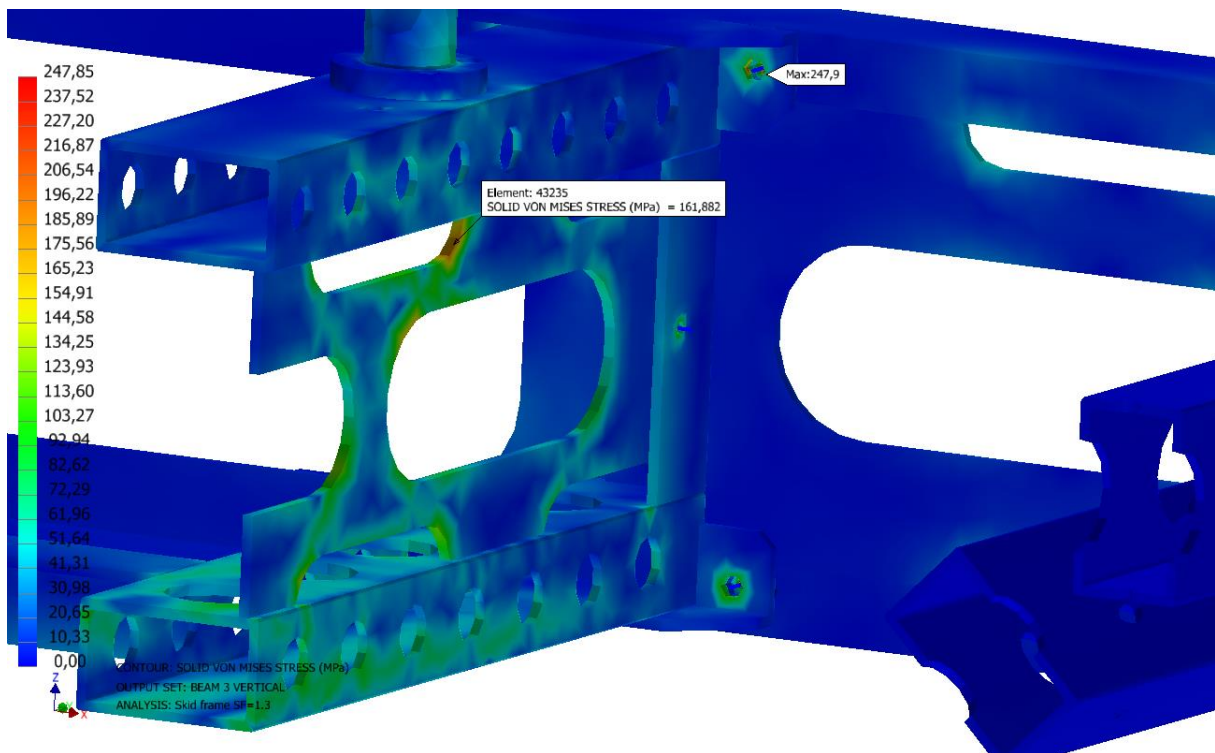


Figure 47 Stress map load case 4 impact zone side view

5.3.5 Calculations of selected structural items

Parts of the skid that have been made and/or modified have been analysed to ensure structural integrity. This includes the holder for the Doppler with INS, the drawer for the MUX and the top beam which holds the MBE heads, lasers, CTD and Tx/Rx. The applied forces to the models are calculated with equation (11), with the partial factor γ_Q applied. The kinetic energy of the sensor and relative impact velocity is used, for calculations see Appendix Q.

5.3.5.1 Doppler with INS holder

The analysis includes the examination of the Doppler with INS holder, as shown in Figure 48 with results listed in Table 14.

The maximum displacement observed for this item is 2.55 mm. Furthermore, the maximum von Mises stress of 114.98 MPa, is within the allowable stress limit. Additionally, the fasteners utilized in this configuration are found to be within the allowed design capacity, ensuring their suitability for the intended purpose. It is worth noting that the fasteners used are generally the ones used in the skid, making consistent fasteners throughout the skid, there is enhanced efficiency and convenience in manufacturing, assembly, and maintenance activities.

Table 14 Stress analysis results for doppler with INS holder

Partial factor	Load [kN]	Von Mises σ_{vm} [Mpa]	Total displacement u [mm]	Fasteners [kN]			
				$F_{v,Ed}$	$F_{t,Ed}$	$F_{v,Rd}$	$F_{t,Rd}$
-	1.18	88.44	1.96	0.56	0.90	21.42	32.12
γ_Q	1.53	114.98	2.55	0.73	1.16		

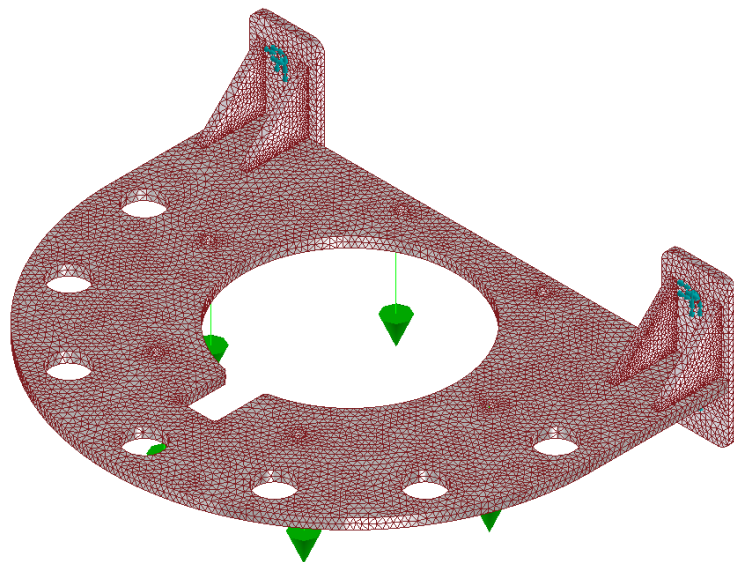


Figure 48 Meshed model with forces and constraints of doppler with INS holder

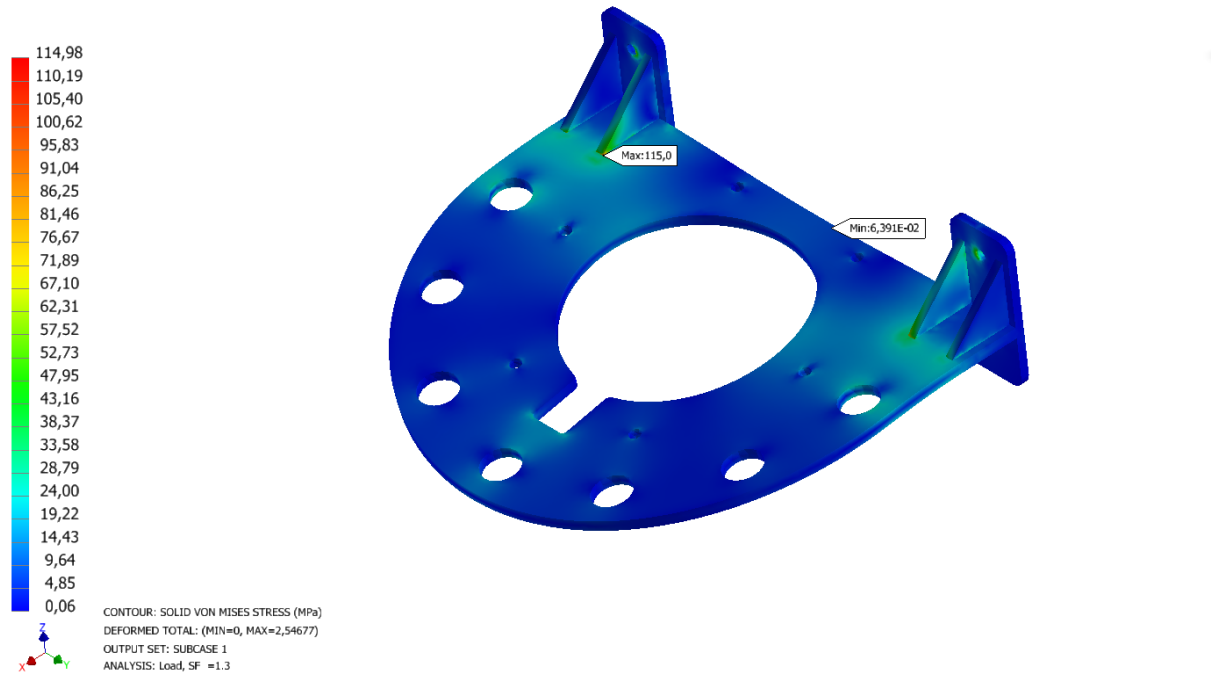


Figure 49 Stress map doppler with INS holder top view

5.3.5.2 MUX pod drawer

The analysis includes the Mux Pod Drawer with a dummy model of the MUX included, as shown in Figure 50. This was done to simulate the correct force distribution and resulting axial displacements. The maximum displacement for this item is 1.71 mm. Additionally, the maximum von Mises stress of 155.86 MPa is within the allowable stress limit.

Table 15 Stress analysis results for MUX pod drawer

Partial factor	Load [kN]	Von Mises σ_{vm} [Mpa]	Total displacement u [mm]
-	2.6	119.89	1.37
γ_Q	3.38	155.86	1.71

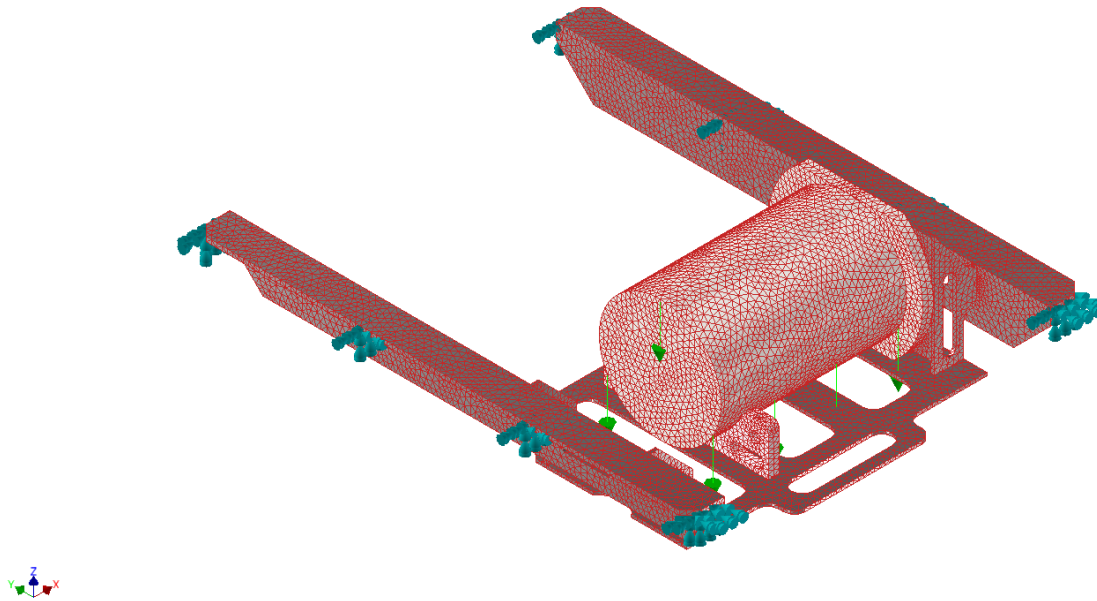


Figure 50 Meshed model with forces and constraints of MUX pod drawer with dummy MUX

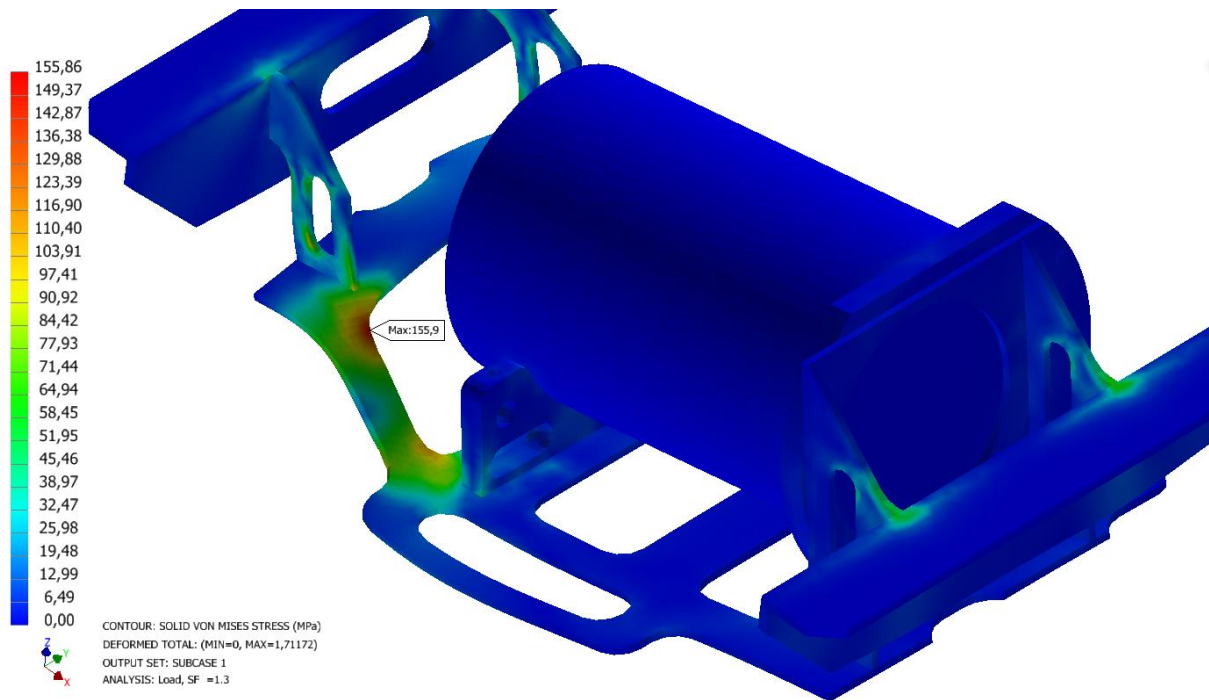


Figure 51 Stress map MUX pod drawer max stress

5.3.5.1 Top beam

The analysis includes the examination of the top beam, with a dummy model of the beam included as shown in Figure 52. This was done to simulate the correct force distribution and resulting forces in the bolts. The maximum displacement displayed for this item is 1.69 mm. Additionally maximum von Mises stress of 155.16 MPa, which is within the allowable stress limit. The fasteners utilized in this configuration are found to be within the allowed design capacity, ensuring their suitability for the intended purpose.

Table 16 Stress analysis results for Top beam

Partial factor	Load [kN]	Von Mises σ_{vm} [Mpa]	Total displacement u [mm]	Fasteners [kN]	
				$F_{t,Ed}$	$F_{t,Rd}$
-	2.13	119.35	1.40	0.877	32.12
γ_Q	2.77	155.16	1.69	1.14	

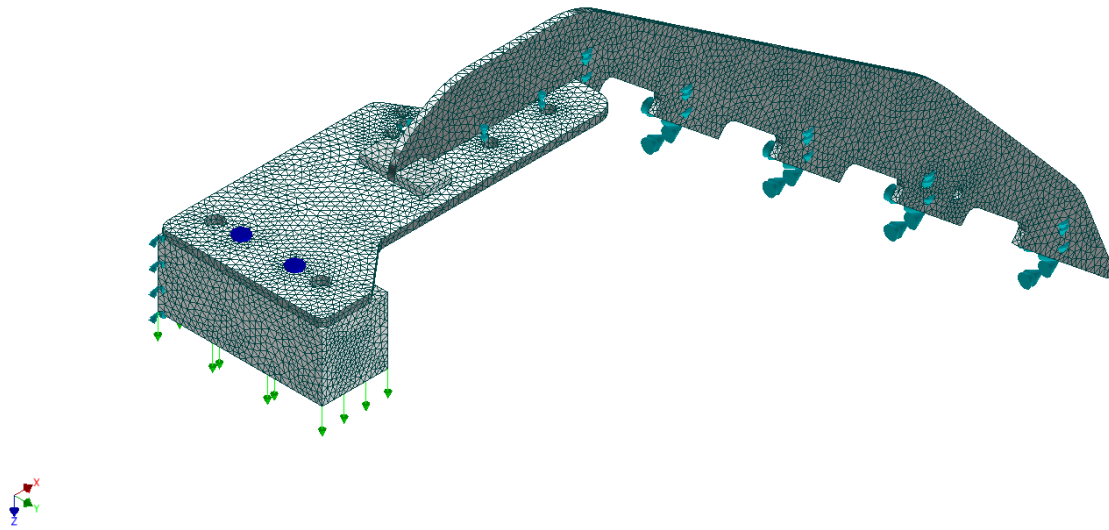


Figure 52 Meshed model with forces and constraints of Top beam with dummy beam attached.

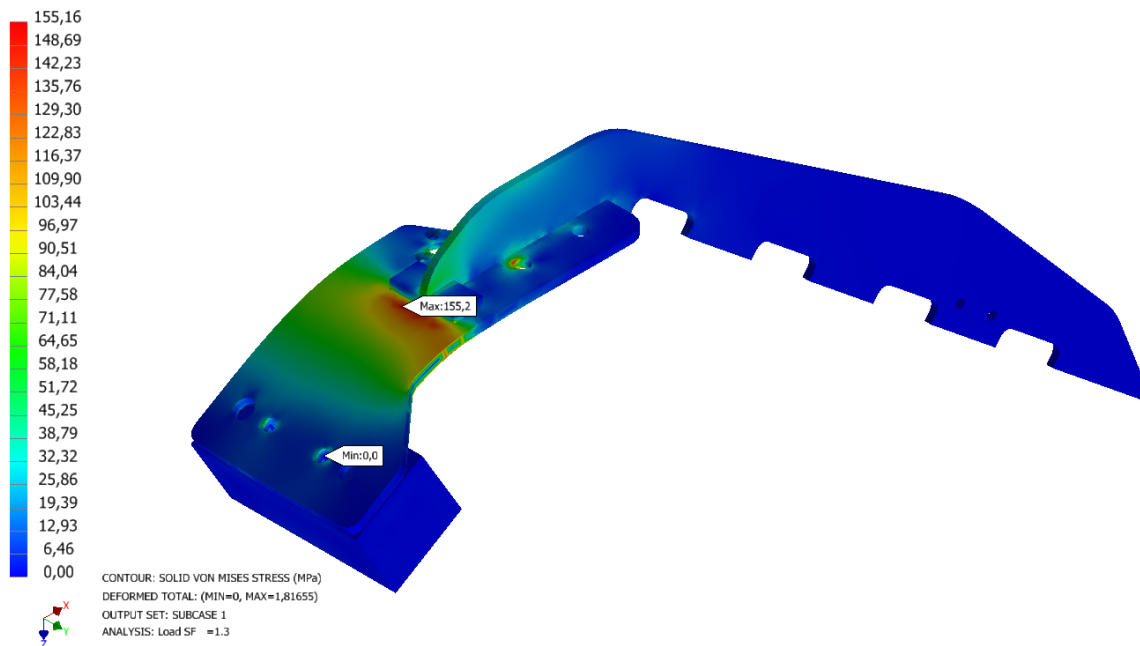


Figure 53 Stress map top beam

5.4 Critical load bearing welds

A total of six crucial load-bearing welds require examination in the analysis. In the skid, two cross beams contribute to load cases 1 and 4, as depicted in Figure 54. The load applied to these welds is obtained from Table 9.

Moving on to the hatch, there are four significant load-bearing welds that warrant examination, as shown in Figure 55. To determine the maximum load-bearing capacity, the sum of forces in the ULS conditions is applied. This includes considering both ULS-a and ULS-b scenarios, resulting in a combined point load exerted at the outermost part of the hatch.

Detailed analysis of the welds is presented in the subsequent subchapters, with the calculations for each weld provided in the appendices. The results of these analyses are then consolidated and presented in Table 17.

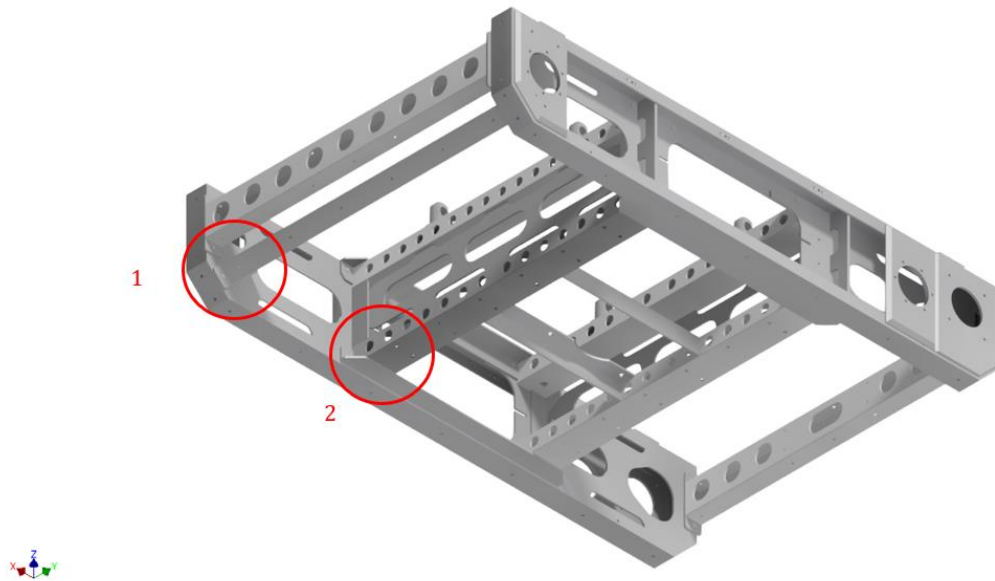


Figure 54 Critical load bearing welds in the bottom part of the skid

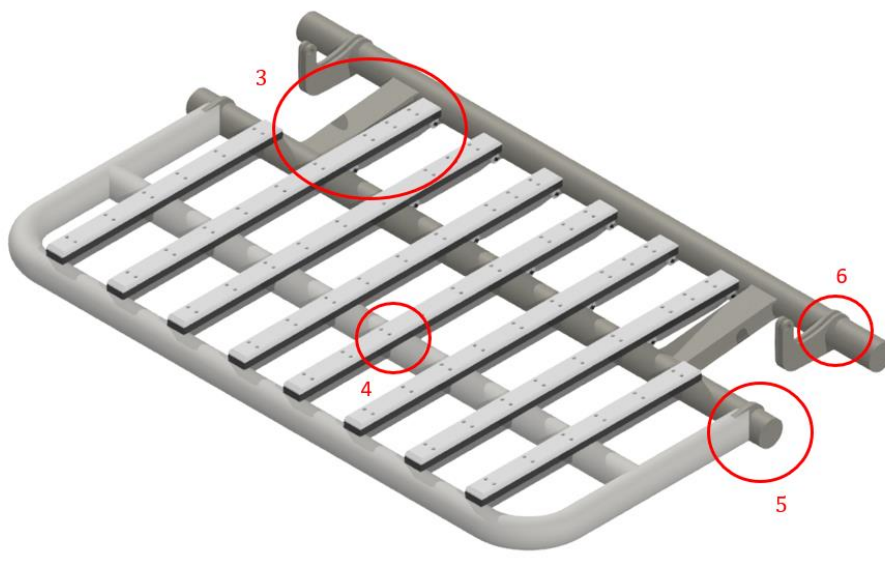


Figure 55 Critical load bearing welds in the hatch

5.4.1 Critical weld 1

For critical weld 1, it is assumed that there is a fixed support at each end of the weld, and the load is applied at $L/2$ of the beam. This configuration helps determine the weld's response to bending moments. Critical weld 1 experiences bending forces along the horizontal weld length, l_{w2} . Additionally, shear forces act on the vertical weld length, l_{w1} . Detailed calculations for these bending and shear forces can be found in Appendix S.

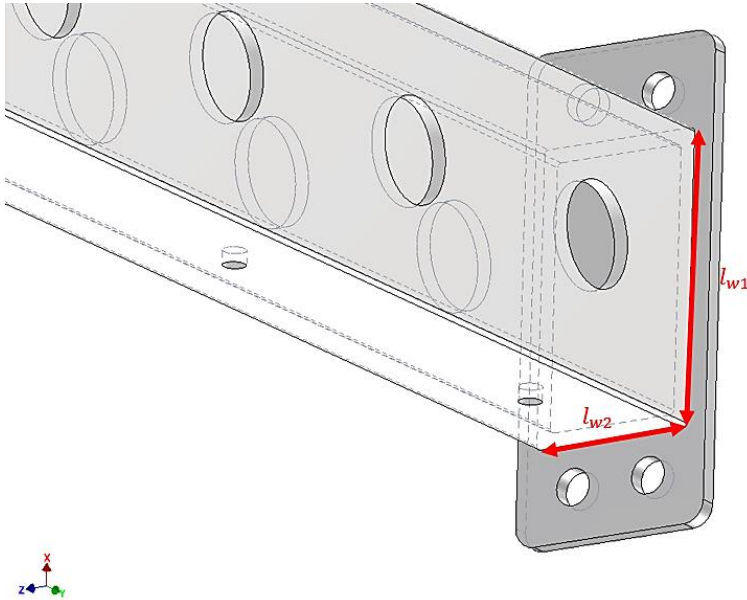


Figure 56 Critical weld section 1

5.4.2 Critical weld 2

The calculation of this weld is more complicated due to the presence of l_{w3} in the local z-plane, as illustrated in Figure 37. To simplify the hand calculations for this weld, the weld section is approximated as an equivalent square beam. This approximation neglects l_{w3} and considers only l_{w1} and l_{w2} from the lower and upper parts of the skid section, as shown in Figure 58. In a conservative approach, the moment is primarily presented in the horizontal welds, which are arranged in a force couple configuration to counteract the moment. Vertical loads, on the other hand, are primarily supported by the vertical welds.

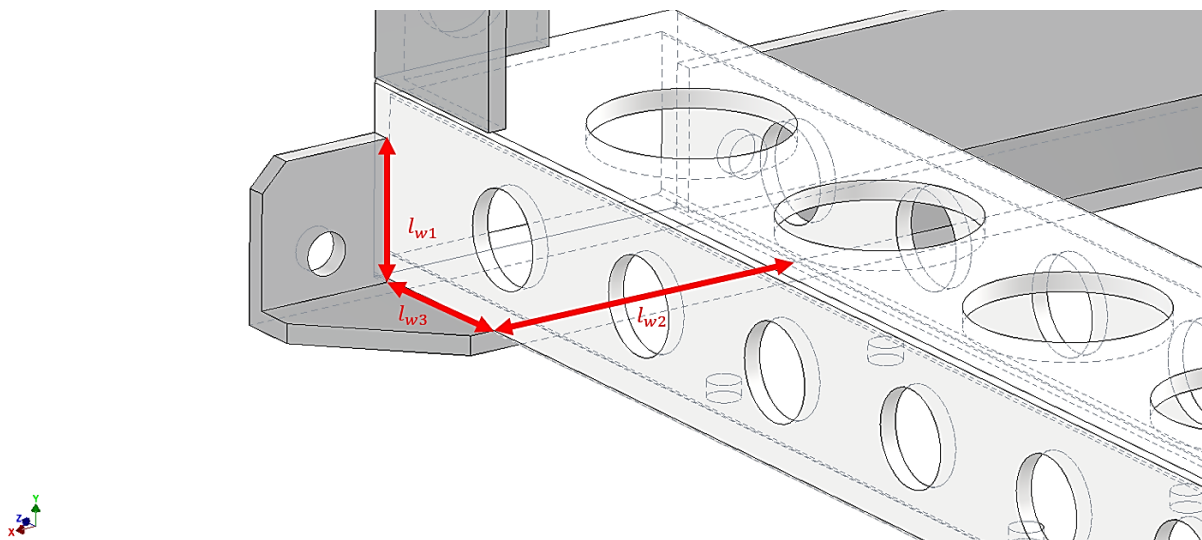


Figure 57 Critical weld section 2

The model exhibits symmetry, which allows for dividing the load present in each weld into two equal parts. The load is applied at $L/2$ of the beam, ensuring even distribution of forces along the weld. To simplify the calculations further, the two connected beams in the vertical section are approximated as a rectangular beam. This approximation facilitates the analysis and evaluation of the weld's structural behaviour as if it was a welded beam.

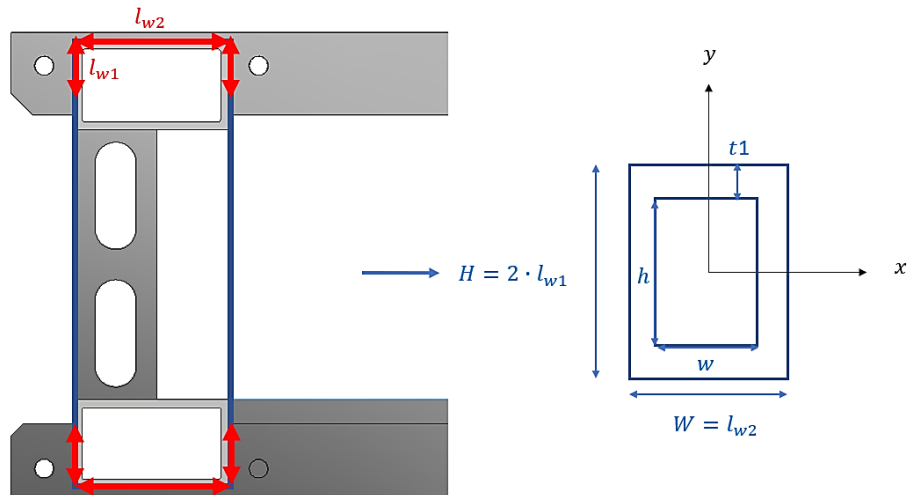


Figure 58 Critical weld section 2 equivalent cross section

The moment needed for the weld calculations were calculated using Inventor Nastran, with constraints at each side of the square profiles, seen in Figure 59. See Appendix T for calculations.

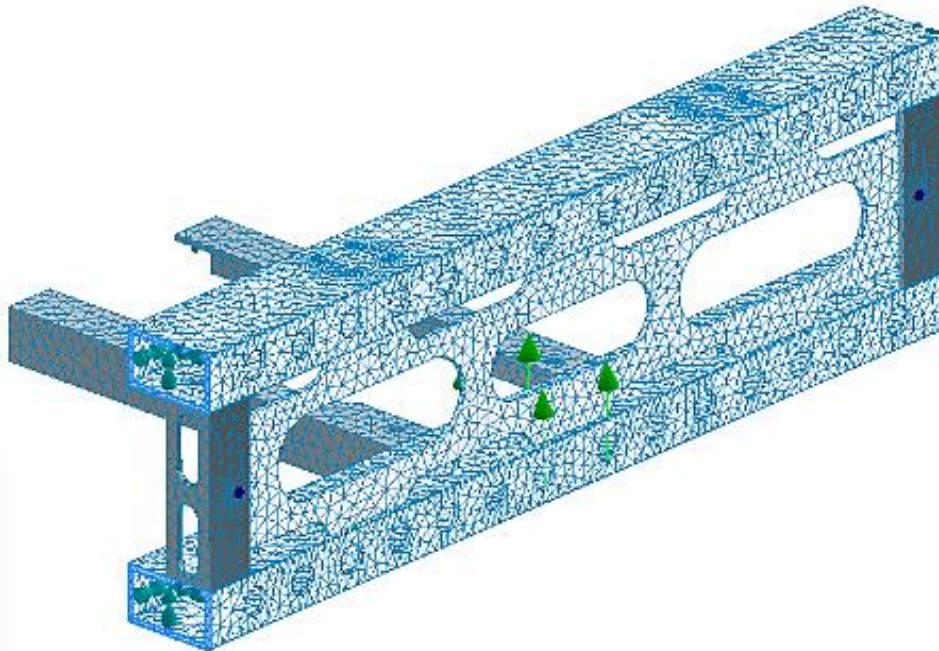


Figure 59 Bending moment calculation model for critical weld section 2.

5.4.3 Critical weld 3

In the analysis of the box beam weld cross section, seen in Figure 60, the weld is simplified it as a rectangular weld for simplicity and ease of calculation. To ensure a conservative approach, the moment is typically taken by the horizontal welds by creating a force couple to counteract the moment. On the other hand, the shear forces are supported by the vertical welds. This ensures that the load distribution within the box beams is appropriately accounted for. The presence of two box beams in the hatch is dividing the load in half, distributing it evenly between the beams. See Appendix U for calculations.

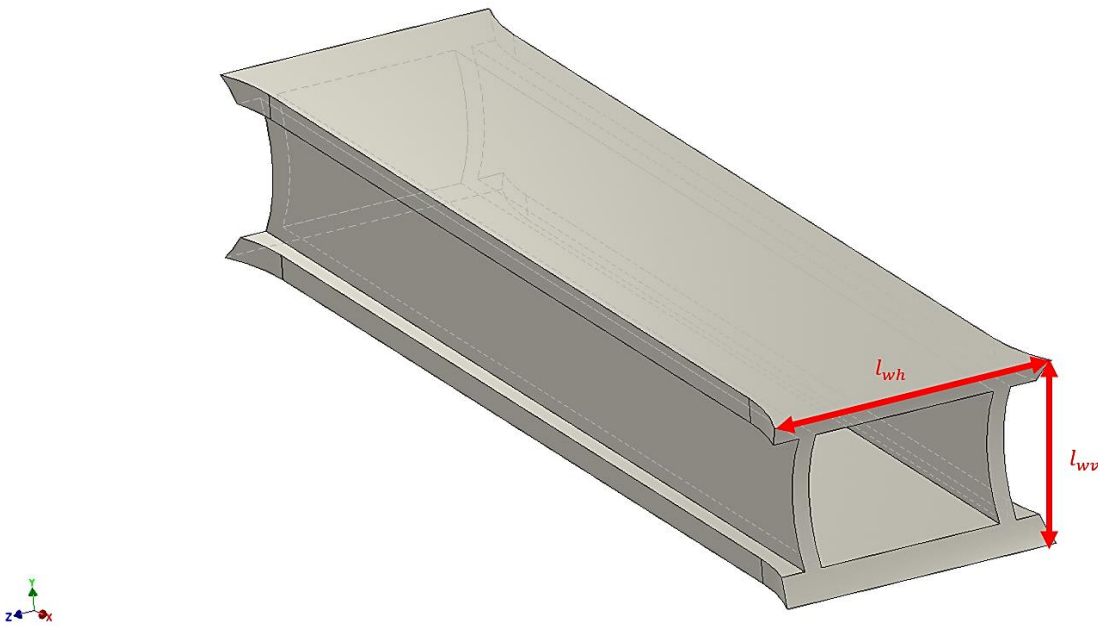


Figure 60 Critical weld section 3

5.4.4 Critical weld 4

In the analysis of the T-bar welds, seen in Figure 61, the weld is simplified as a plane weld due to its curvature. A conservative approach is taken where the moment is primarily handled by the horizontal weld, while the vertical weld handles the vertical load. The T-bar with the highest moment is determined through calculations. It is assumed that the load is evenly distributed across all eight beams and two pipes. For calculations see Appendix V.

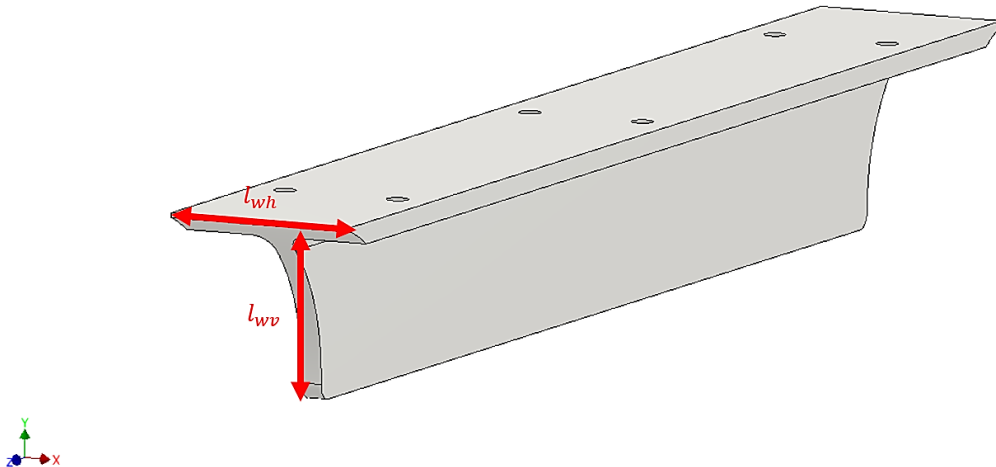


Figure 61 Critical weld section 4

5.4.5 Critical weld 5

The calculation of this weld is complicated due to the configuration of the weld in all axes. To simplify the analysis of the weld, it is separated into two cross section A and B seen in Figure 62 Figure 63. For section A, the curvature of the cross section in the z-plane is simplified and made equivalent to a flat cylinder cross section, seen in Figure 64. In this configuration it is assumed that cross section A only experience bending moment resulting in normal forces at the bottom and top of the cross section.

For cross section B, it is assumed that only torsional forces are acting on the cross section resulting in pure shear stress. Moreover, the load exerted on the weld is divided between the two hinges present in the hatch. This division of load helps ensure proper load distribution. For calculations see Appendix W.

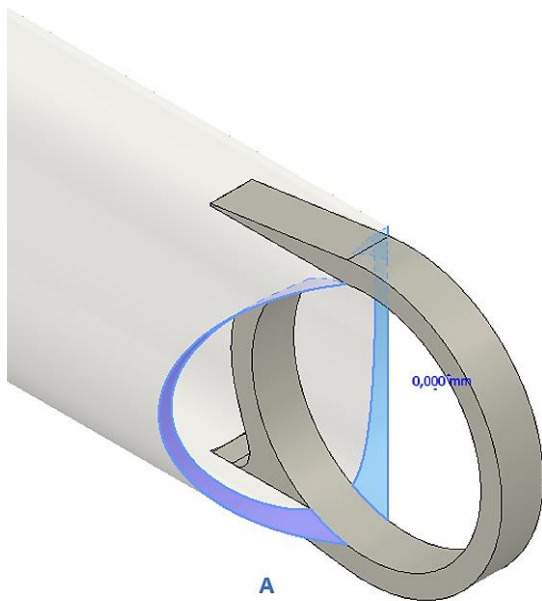


Figure 62 Critical weld 4 cross section A

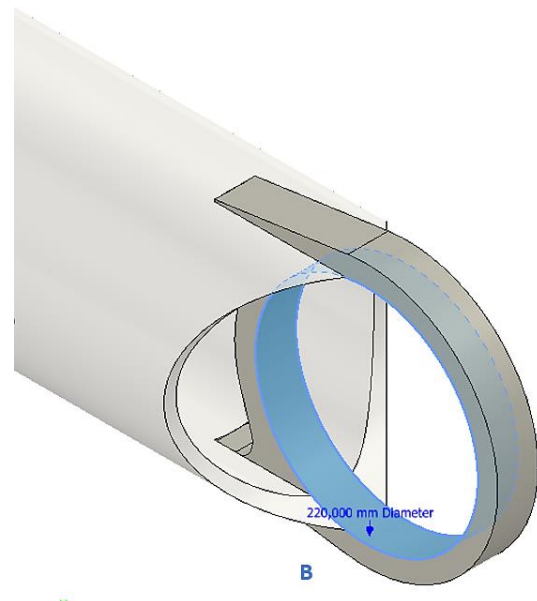


Figure 63 Critical weld 4 cross section B

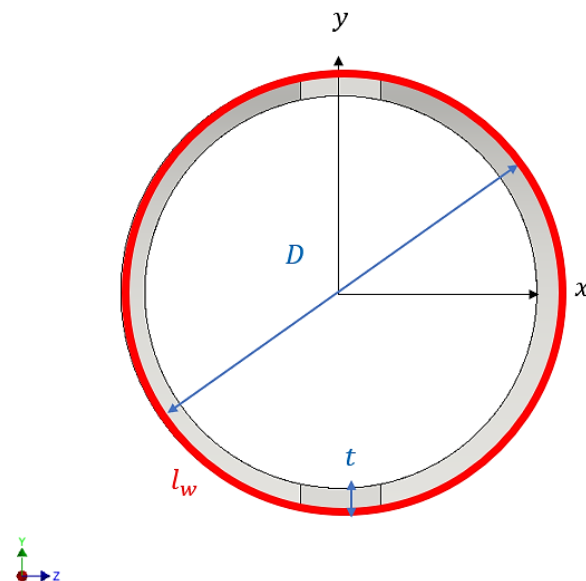


Figure 64 Equivalent cross section of critical weld 4 cross section A

5.4.6 Critical weld 6

In a similar fashion as critical weld 5 section B, certain assumptions and considerations are made. Firstly, it is assumed that both welds in this section experience an equal torsional force. Secondly, the largest value between the sum of ULS-a and ULS-b is determined and applied. Lastly, the load in this section is divided by the two hinges present in the hatch, distributing the force accordingly. For calculations see Appendix X.

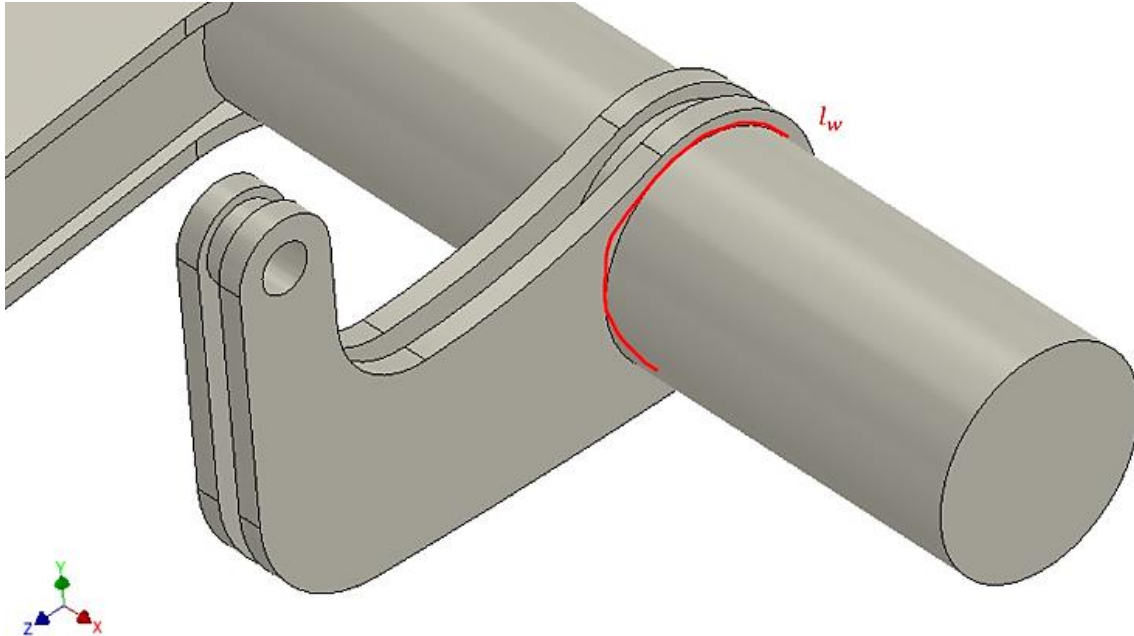


Figure 65 Critical weld section 6

5.4.7 Summary of calculations for critical load bearing welds

All welds exhibit satisfactory utilization, except for critical weld 4, which has a utilization of 1.01, seen in Table 17. However, this deviation is particularly small and therefore regarded negligible, allowing it to be disregarded.

Table 17 Results from weld check calculations

Critical weld	Allowed stress [MPa]	Von Mises σ_{vm} [Mpa]			Utilization [-]		
		Horizontal weld	Vertical weld	Connection weld	Horizontal weld	Vertical weld	Connection weld
1	142.31	130.20	68.10	99.8	0.92	0.48	0.70
2	142.31	0.10	122.40	44.00	0.00	0.86	0.31
3	538.46	524.40	55.20	170.4	0.97	0.10	0.32
4	323.08	276.30	68.10	106.10	0.86	0.21	0.33
5	344.62	-	-	153.90	-	-	0.45
				47.00			0.14
6	538.46			140.90	-	-	0.26

5.5 Integrity of EPDM and PEHD 1000

According to DeepOcean, it is not a common practice to perform calculations specifically for thermoplastics and elastomers like EPDM. However, given the application of EPDM as an intermediate layer between PEHD 1000 and structural components, it can be considered resilient against the energy transfer load F_Q , that are concentrated in such a small area, where stress levels would exceed the maximum allowable stress of 3.48 MPa (and 21.74 MPa for EPDM with additives).

Furthermore, when considering the PEHD 1000, with its allowable stress of 17.39 MPa, with F_Q applied, an area smaller than 4485 mm² could lead to a stress above allowed stress limit.

5.6 Summary of kinetic and elastic potential energies

Calculating the kinetic and elastic potential energies with equation (9) and (10), with added mass with equation (18), elastic energies in the hatch from Table 6, the summation of energies can be listed, seen in Table 18. For calculations see Appendix Y.

Table 18 Kinetic and elastic potential energies in the ROV, hatch and skid

Hatch		Skid		U_{El} [J]				E_k [J]	
				Square rubber profile	Hollow rubber profile	Sum		Minimum	Maximum
						Minimum	Maximum		
LCA	376.80	LC 1	140.10	332.27	37.93	575.70	1181.44	555.58	1175.43
LCF	179.70	LC 2	25.80						
LSA	443.40	LC 3	35.70						
LSF	243.90	LC 4	58.80						

Figure 66 demonstrates the occurrence of minimum and maximum elastic potential energies when considering the contact of rubber profiles during impact.

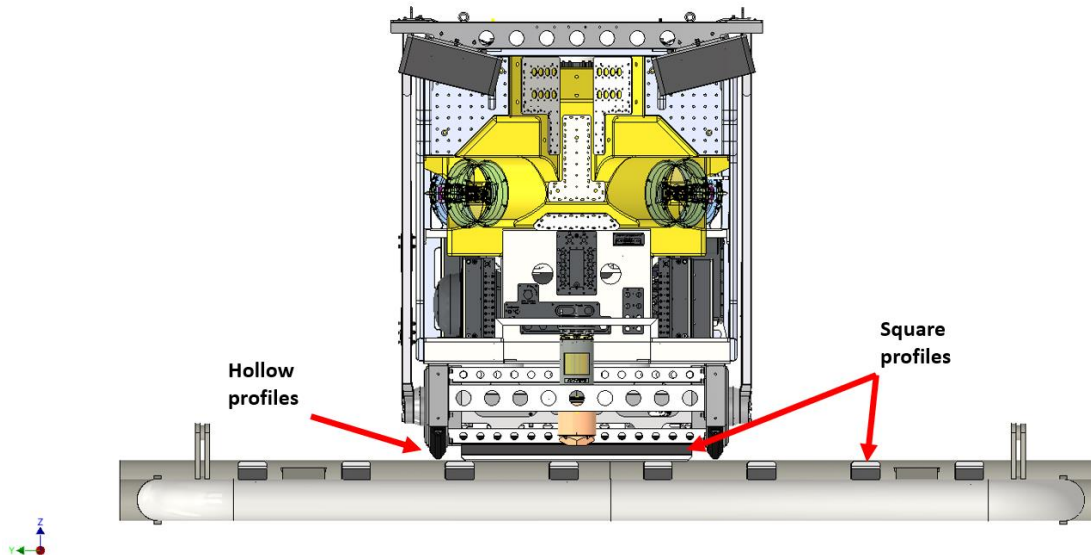


Figure 66 Contact region during impact between ROV and hatch, with annotation of rubber profiles, front view

Minimum elastic potential energy absorbed during impact between ROV and hatch (Square profile meets hollow profile at LCF on hatch, see Figure 67) is 575.7 J, with a relative velocity between USV

and ROV during recovery of $v = 0.44$ m/s. This makes sure that $E_k < U_{El}$ for the whole section of the hatch and skid. This is then set as the operational limit.

Maximum elastic potential energy absorbed during impact between ROV and hatch (Square profile meets square profile at LSA on hatch) is 1181.44 J, with a relative velocity between USV and ROV during recovery of $v = 0.64$ m/s. For this scenario to occur, the ROV must hit the hatch at the out most part, assuring the largest deformation.

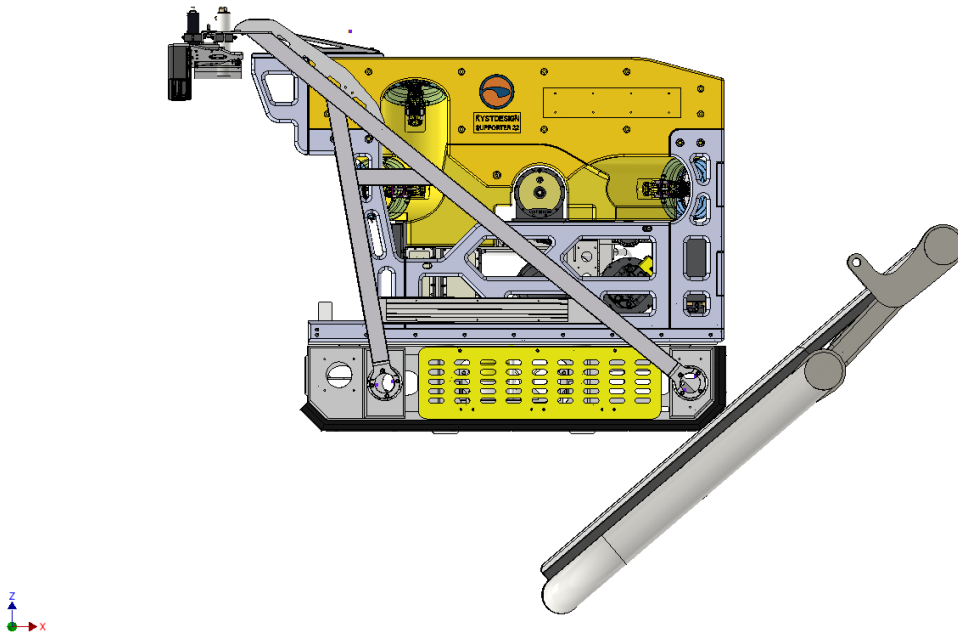


Figure 67 Impact between ROV and hatch at LCF, side view

6 Final design

This chapter will include the final design and reasoning for the changes done according to the preliminary design.

6.1 Hatch

The primary consideration in the final design of the hatch was its ability to elastically deform and absorb the energy transfer load. The hatch needed a balance of flexibility and strength to withstand not only the weight of the ROV and skid but also the hydrodynamic forces.

After careful evaluation, we strategically chose circular pipes for their consistent strength and reduced weak points. However, in areas requiring higher moment resistance and greater moment of inertia around the neutral axis, we utilized square pipes as seen in Figure 68. This dual approach ensured both overall strength advantages and enhanced performance in meeting specific demands.

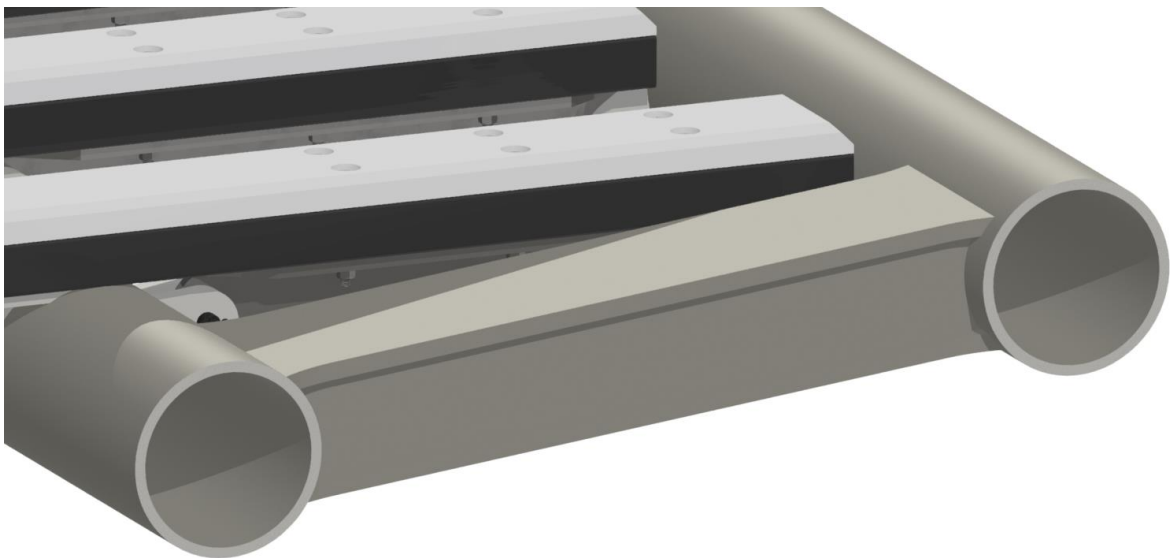


Figure 68 Final hatch design square beam cross section view

To meet the requirements for deformation, a combination of different materials was needed, as seen in Figure 69.

For areas with higher stress levels, Strenx 700 OME was chosen. However, considering the cost of this material, it would not be practical to employ Strenx 700 OME throughout the entire hatch. To keep costs down, the remaining sections of the hatch were designed with API 5L X65. This approach allowed for a balance between strength requirements and cost considerations.

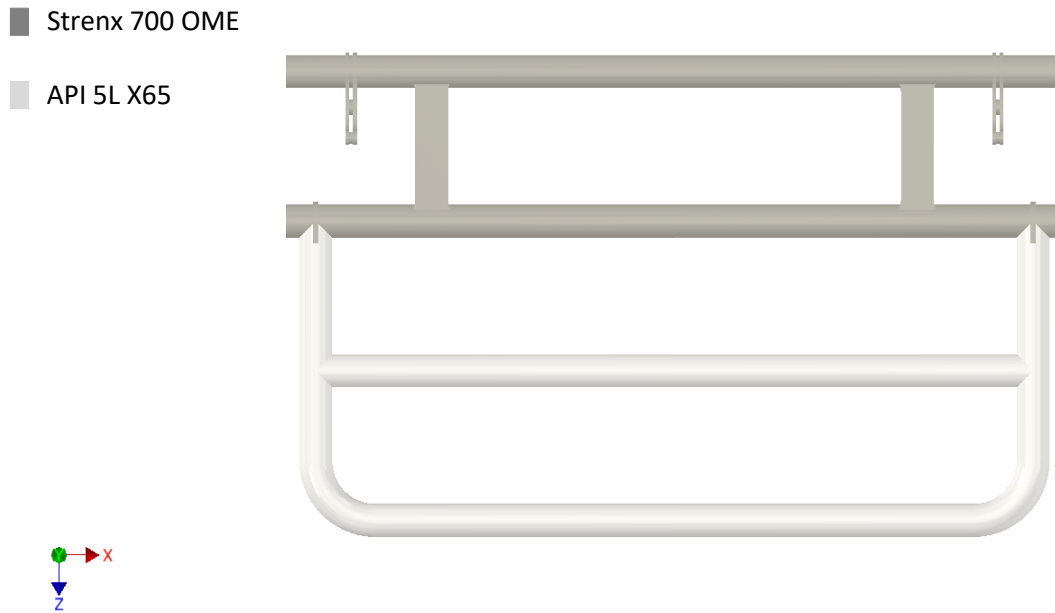


Figure 69 Final hatch design pipe materials

Recognizing that the joints posed a vulnerability in our structure, it was decided to reinforce these areas by adding additional material, as seen in Figure 70. This resulted in a more evenly distributed stress, eliminating the weak points, and increasing the overall strength and durability of the structure in this area.

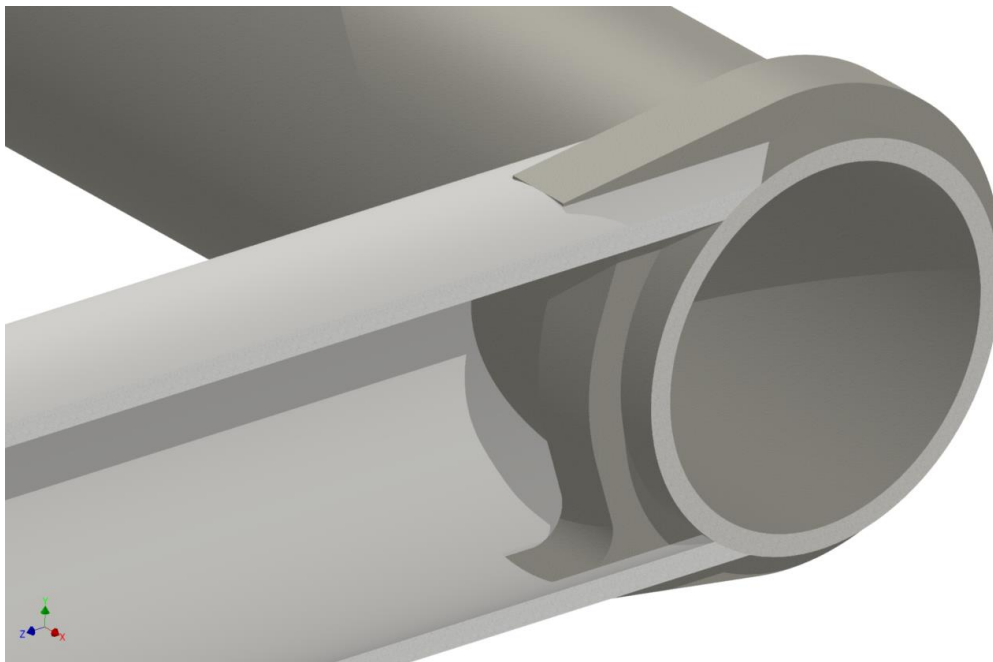


Figure 70 Final hatch design cross section view of joint reinforcement

To reduce the load between the skid and hatch during recovery of the ROV, it was decided to design a dampening material on top of the hatch. To absorb impact while keeping friction to a minimum, EPDM was used in combination with PEHD 1000, as seen in Figure 71. It was also decided to make the longitudinal beams at the top of the hatch hinged, as seen in Figure 72, to allow for further deformation to absorb the energy transfer load. Drawings for the hatch are shown in Appendix Z.

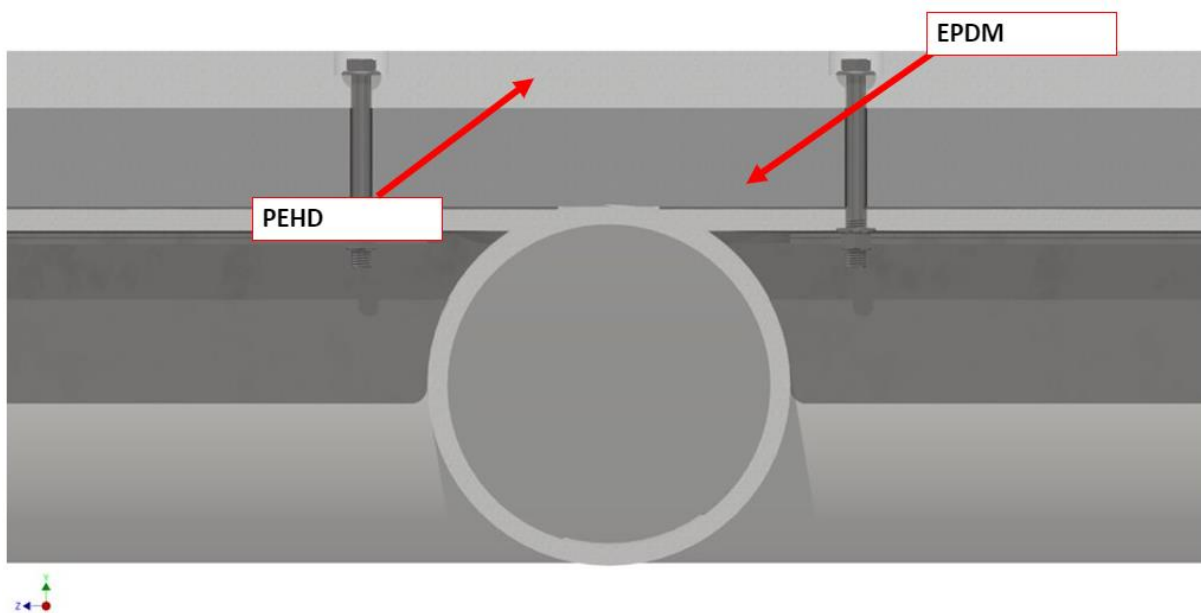


Figure 71 Final hatch design cross section view EPDM rubber and PEHD 1000

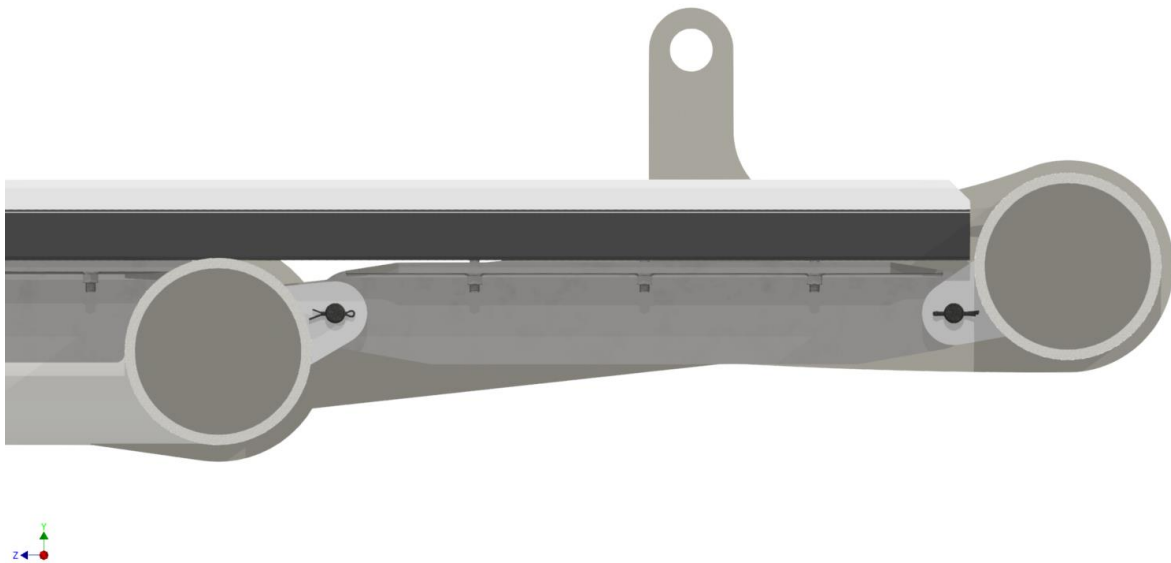


Figure 72 Final hatch design cross section view hinged beam.

6.2 Skid

The sensors proved to be the determining factor in the final design's outcome, as seen in Figure 73. This was due to the need of complying with the operational limitations of the sensors while keeping them protected. The energy transfer load led to the need for an impact absorbing material and structure.

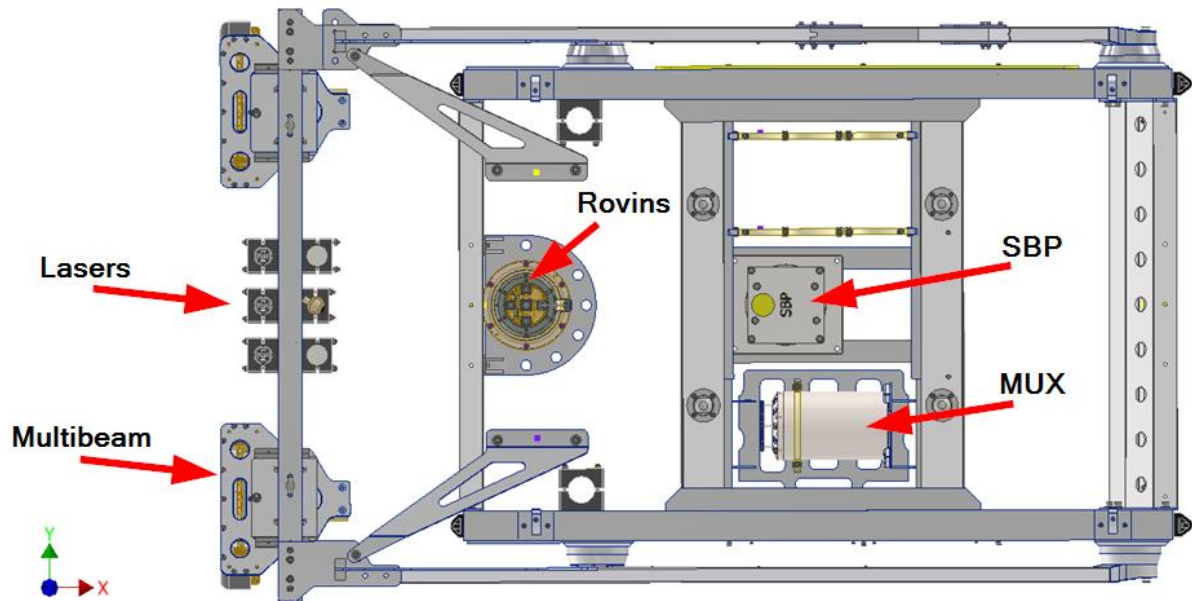


Figure 73 Final skid design top view sensor placement

The protection of the lasers, CTD, Tx/Rx and multibeam, as shown in Figure 74, required attention. The main concern was the positioning of the multibeams, which extended beyond the main frame, making them susceptible to impacts from the skid's sides hitting the USV during recovery. To address this issue, adjustments were made by relocating the lasers, CTD and Tx/Rx. This was achieved by shifting the beam that held all the sensors at the top of the skid slightly forward, in the x-direction according to Figure 74. Consequently, the lasers were clustered towards the centre of the beam. The CTD and Tx/Rx were relocated to the rear of the beam. This arrangement enabled the multibeams to be brought closer together, effectively eliminating the problem of them protruding beyond the sides of the skid.

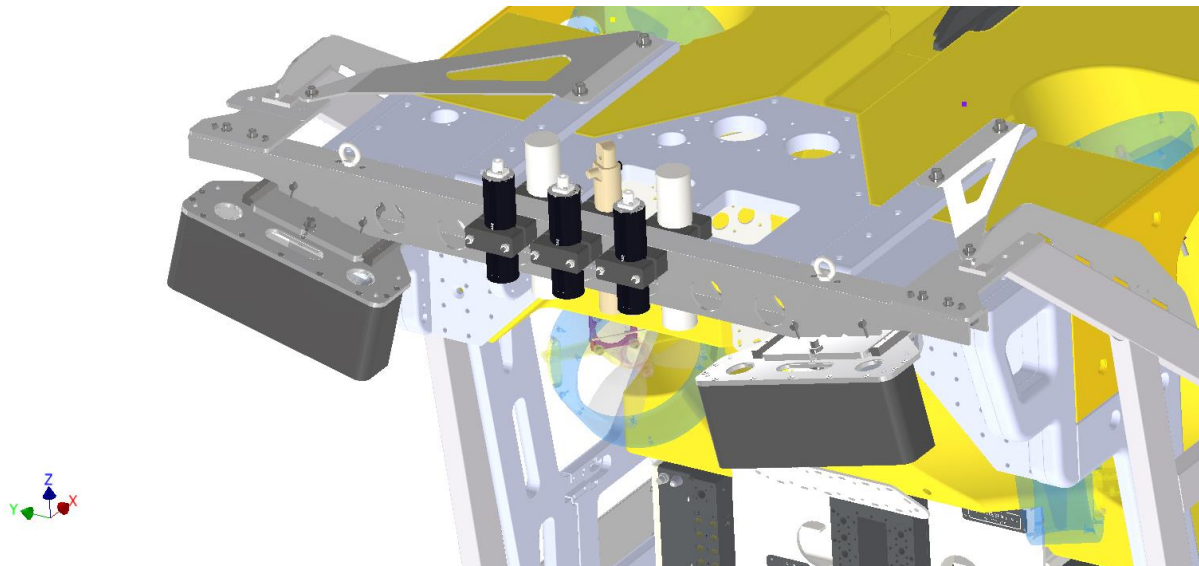


Figure 74 Final skid design top view multibeam and lasers

Due to the ROV's rear-end retrieval, the arrangement of the ROVINS, MUX, and Pipe Tracker Accumulators, as seen in Figure 12 and Figure 13, needed reorganization due to the high-impact area. As the decision was made to exclude the pipe tracker from this design, the associated accumulators were no longer deemed essential and subsequently disregarded. The ROVINS was repositioned to the

front of the skid, as seen in Figure 75. This adjustment was made to ensure that the ROVINS had an unobstructed downward line of sight to effectively register the seabed. As for the MUX, serving as a central hub for connecting all the sensor cables, it was decided that laying it down on its side and fitting it into a drawer at the centre of the skid, as illustrated in Figure 75, would be the most suitable arrangement as this would require easy access during installation or maintenance.

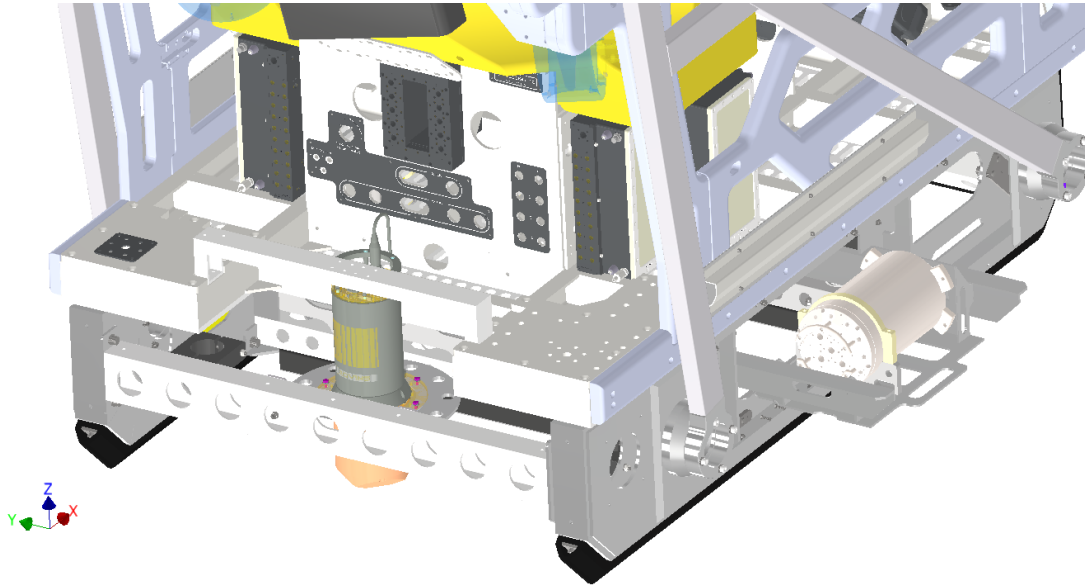


Figure 75 Final skid design front view ROVINS and MUX

To mitigate impact forces and protect the sensors from misalignment, a combination of rubber and PEHD 1000 was used beneath the skid, as seen in Figure 76. Rubber was applied to areas likely to make initial contact with the hatch, providing an additional layer of protection. The PEHD 1000 material was implemented in conjunction with rubber to the area expected to slide against the hatch after the initial contact once primary impact forces had already been absorbed. This approach fulfilled the initial goal of minimizing friction while ensuring effective impact reduction. Drawings for the skid are shown in Appendix AA.

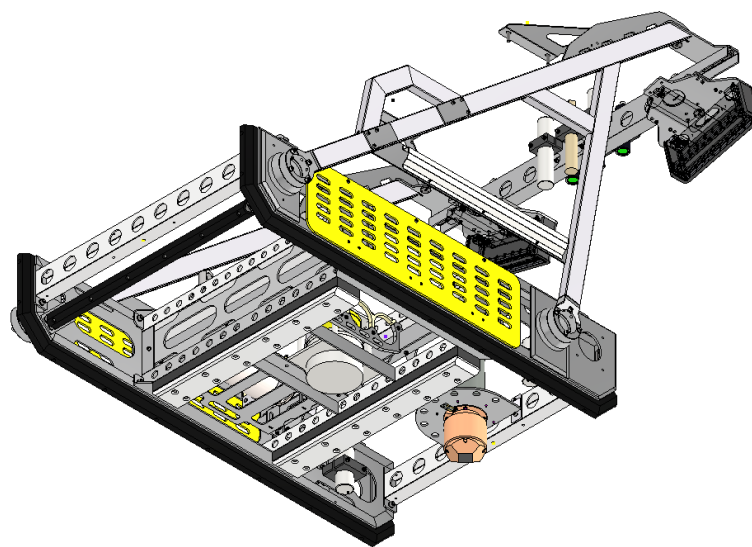


Figure 76 Final skid design impact dampers

6.2.1 Review of centre of gravity

The COG is measured from a reference point shown in Figure 77, with dimensions tabulated in Table 19. The new COG position is also visualised in Figure 78.

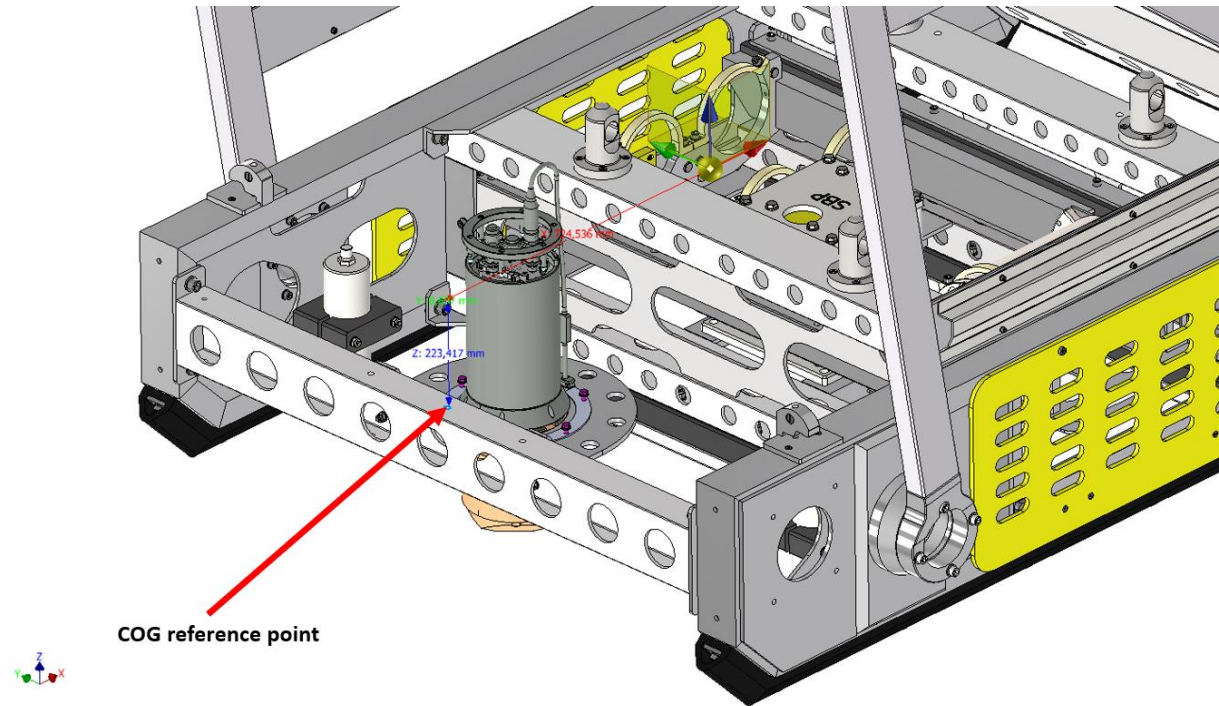


Figure 77 Annotation of COG reference point

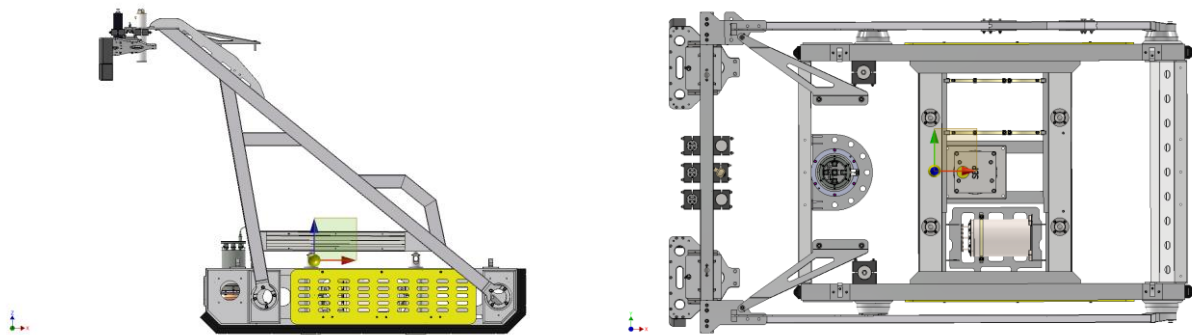


Figure 78 Visual representation of COG in skid side and top view

Table 19 COG of skid with sensors

New COG	Coordinates [mm]		
	x	y	z
	724.54	8.61	223.42

6.3 Combined system

The combined skid and hatch system, as seen in Figure 79, demonstrates how these two elements work together to form a LARS. Figure 80 shows a 13 mm clearance between the skid and hatch in the z-direction, which is designed to reduce friction by ensuring that only the PEHD 1000 materials are in contact with each other during operation.

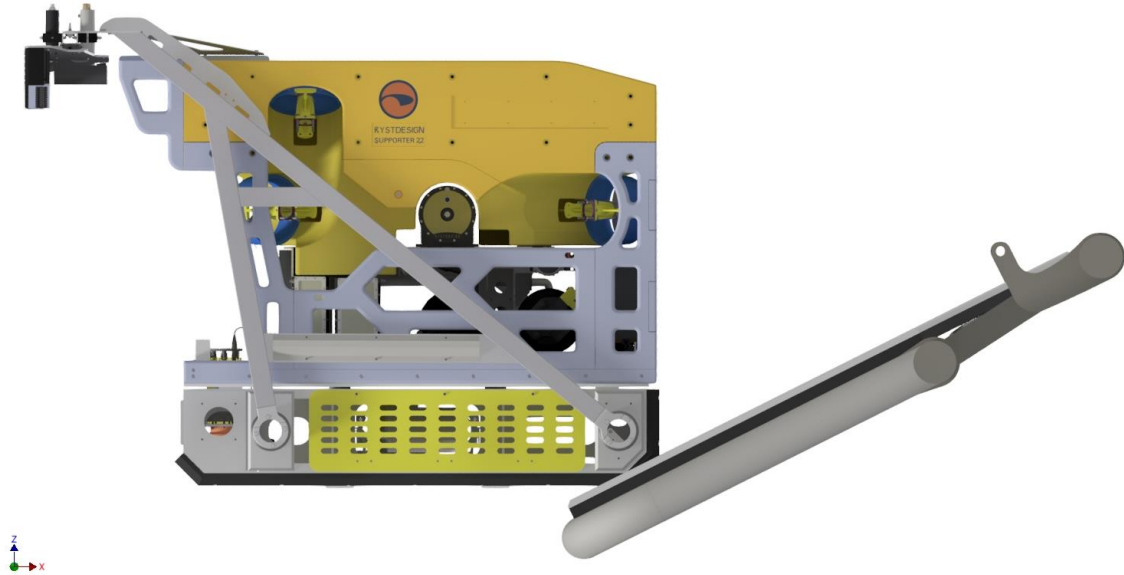


Figure 79 Combined system ROV with skid angled on hatch side view

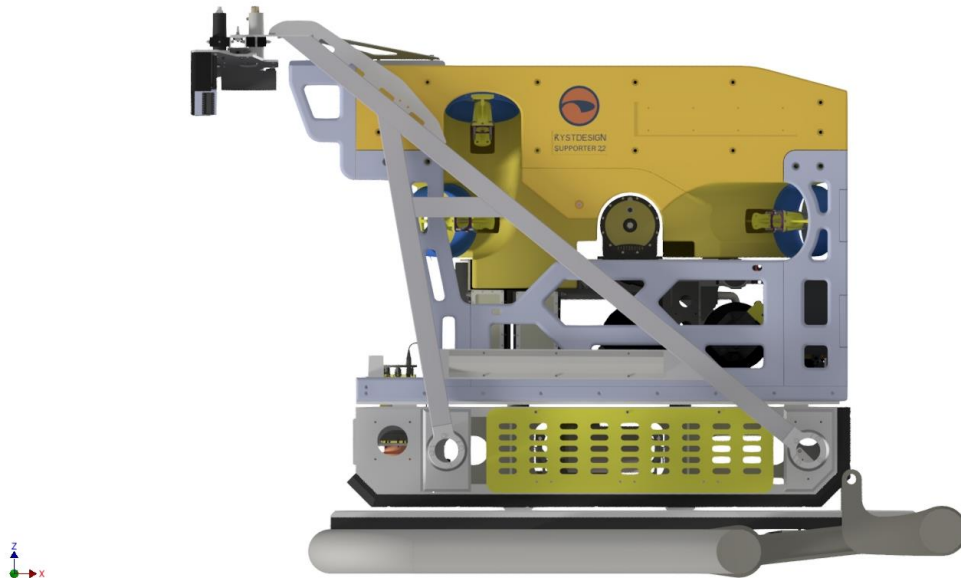


Figure 80 Combined system ROV with skid flat on hatch side view

7 Conclusion

The structural analysis of the hatch has revealed important findings regarding its performance under specific scenarios. In the case of ULS-a LCA, which involves the skid impacting the lowest beam with one leg at its centre, dimensional changes were observed. The maximum total displacement measured in this case was 55.67 mm. However, the von Mises stress reached 946.00 MPa in the section where the T-bar is welded, surpassing the allowable stress limit. On the other hand, the weld stress analysis for this section indicated a stress level of 276.30 MPa for the horizontal section of the weld and 68.10 MPa for the vertical section. The utilization values for these stresses were 0.86 and 0.21, respectively.

Similarly, the analysis of the skid focused on Load case 3, where the skid experiences horizontal impact on the port and starboard sides of the structure in the longitudinal direction. In this scenario, a displacement of 1.19 mm was measured, and the maximum von Mises stress reached 338.28 MPa. The utilization value for this stress was determined to be 0.93.

The skid and hatch have been specifically designed to withstand wave heights up to $H_s \leq 3$ m, with a maximum relative velocity of $v = 0.44$ m/s between the ROV and the USV during recovery. It is crucial for the ROV and USV to be corresponding in terms of wave period during the recovery process to ensure safe launch and retrieval. However, further attention is needed for the side scanners, as they are susceptible to impact during ROV recovery.

It is important to acknowledge that although the structural designs have undergone significant development through static simulations, they are not the final designs for the USVs. Additional analysis, such as practical testing and dynamic simulations, must be conducted to validate and refine the proposed solutions. These further steps will ensure the completion of a robust and reliable LARS design for the USV.

8 Bibliography

- [1] Y. Bai and B. Qiang , Subsea Engineering Handbook, Oxford: Elsevier Science & Technology, 2012.
- [2] West Marine Technologies, “LARS for Free Swimming ROV Systems,” [Online]. Available: http://wmt.com.sg/product_uri/rov-lars/free-swim-lars/. [Accessed 24 05 2023].
- [3] DeepOcean, “About DeepOcean,” [Online]. Available: <https://www.deepocean.com/about/about-us>. [Accessed 20 January 2023].
- [4] W. Caharija, “Artifex Final Project Report,” SINTEF, 2021.
- [5] Reach Subsea, “Future proofing subsea,” [Online]. Available: <https://reachsubsea.no/future-proofing-subsea-services-through-remote-and-autonomous-operations/>. [Accessed 02 February 2023].
- [6] K. V. Knutsen, “Launch and recovery of underwater units or vehicles”. Norway Patent WO 2022/035322 A1, 17 Februar 2022.
- [7] W. D. Callister and D. G. Rethwisch, “Callister's Materials Science and Engineering,” Callister's Materials Science and Engineering, 2020.
- [8] S. Kou, Welding Metallurgy, NJ 07030: John Wiley & Sons, Inc., 2003.
- [9] American Petroleum Institute, “Specification for Line Pipe,” 2004.
- [10] The American Society of Mechanical Engineers, “B31.3 - Process piping,” 2022.
- [11] R. Gomeringer, F. Wieneke and M. Heinzler, Mechanical and Metal Trades Handbook, Haan-Gruiten: Verlag Europa-Lehrmittel, 2018.
- [12] SSAB, “Strenx 700 OME Data sheet”.
- [13] M. Chanda, Plastics technology handbook, Clemson, South Carolina: Taylor & Francis Group, 2018.
- [14] Astrup, “PE / PP,” [Online]. Available: <https://astrup.no/content/download/12576/80427/version/1/file/PEHD+1000+natur.pdf>. [Accessed 24 05 2023].
- [15] A. N. Gent, Engineering with Rubber, Ravenna: Hanser Publishers, 2012.
- [16] Det Norske Veritas, “DNV-ST-N001 Marine operations and marine warranty,” 2018.
- [17] Standard Norge, Eurocode 3: Design of steel structures - Part 1-8: Design of joints, 2005.
- [18] Norsk Standard, “NORSOK M-501 Surface preparation and protective coating,” 2012.
- [19] Det Norske Veritas, “DNV-RP-H103 Modelling and analysis of marine operations,” 2017.
- [20] Det Norske Veritas, “DNV-RU-HSLC Pt.3 Ch 1 Design principles, design loads”.
- [21] Det Norske Veritas, “DNV-RP-C205 Environmental conditions and environmental loads”.
- [22] Standard Norge, “Eurocode 3: Design of steel structures - Part 1-1: General rules and rules for buildings”.

[23] Standard Norge, “Eurocode 9: Design of aluminium structures - Part 1-1: General structural rules”.

Appendices

Integration of a skid and hatch-based launch and recovery system for ROVs on USVs

Vetle Chyba Norstad

Herman Fossan-Waage Vaka

Faculty of Science and Technology
Department of Mechanical and Structural Engineering and Material Science
Master of Science Thesis, Spring 2023
NO-4021 Stavanger, Norway

15.06.2023

Table of contents

APPENDIX A	SENSOR'S SPECIFICATIONS	3
APPENDIX B	MATERIAL PROPERTIES FOR S165M W1.4418	4
APPENDIX C	MATERIAL PROPERTIES FOR 6082-T6	5
APPENDIX D	MATERIAL PROPERTIES FOR API 5L X65.....	6
APPENDIX E	MATERIAL PROPERTIES FOR S420N	7
APPENDIX F	MATERIAL PROPERTIES FOR STRENX 700 OME.....	8
APPENDIX G	MATERIAL PROPERTIES FOR PEHD 1000	9
APPENDIX H	MATERIAL PROPERTIES FOR EPDM	10
APPENDIX I	MATERIAL PROPERTIES FOR FASTENERS	11
APPENDIX J	ROV AND USV KINEMATICS.....	13
APPENDIX K	KINETIC AND ELASTIC POTENTIAL ENERGIES CALCULATIONS.....	15
APPENDIX L	HYDRODYNAMIC FORCES ON HATCH	17
APPENDIX M	HATCH STRESS ANALYSIS.....	19
	ULS-A LCF.....	19
	ULS-A LSA	21
	ULS-A LSF	24
	ULS-B LCA	27
	ULS-B LCF.....	30
	ULS-B LSA.....	33
	ULS-B LSF	36
APPENDIX O	HAND CALCULATIONS OF HATCH	39
APPENDIX P	SKID STRESS ANALYSIS	41
	LOAD CASE 2	41
	LOAD CASE 3	42
APPENDIX Q	FORCE CALCULATIONS OF SELECTED STRUCTURAL ITEMS	45
APPENDIX S	WELD CHECK OF CRITICAL WELD 1	1
APPENDIX T	WELD CHECK OF CRITICAL WELD 2	3
APPENDIX U	WELD CHECK OF CRITICAL WELD 3	6
APPENDIX V	WELD CHECK OF CRITICAL WELD 4	9
APPENDIX W	WELD CHECK OF CRITICAL WELD 5	12
APPENDIX X	WELD CHECK OF CRITICAL WELD 6	15
APPENDIX Y	DAMPING OF RUBBER MATERIALS.....	17
APPENDIX Z	HATCH DRAWINGS.....	21
APPENDIX AA	SKID DRAWINGS.....	40

Appendix A Sensor’s specifications

DeepOcean Survey Skid Guideline



4.3.7 Weight Budget for Survey Skid and Sensors

Table 4-1 - Survey Sensor including weight in air and water

Sensors	No.	Weight air (Kg)	Weight water (Kg)	Total weight air (Kg)	Total weight water (Kg)	Installed on Skid (Kg)	Comments
R2Sonic 2024 MBES	2	16.,2	5.9	32.4	11.8	Front	
ixBlue ROVINS	1	15	6.2	15	6.2	Aft	
Nortek DVL	1	2.7	1.7	2.7	1.7	Aft	
TSS Electronic pod	1	10	2	10	2	Front	
TSS PSU pod	1	10	2	10	2	Front	
TSS Coils	3	15	4.75	45	14.25	Front	
SSS/SBP Electronic pod	1	15	5	15	5	Center	Estimated
SBP TX	1	30	10	30	10	Center	Estimated
SBP Hydrophones	2	3	1	6	2	Front	Estimated
SSS Transducers	2	5	2	10	4	Center	Estimated
SAIV CTD	2	3	1	6	2	Front	Estimated
Laser	1	5	2	5	2	Front	Estimated
DigiQuartz	2	1	0.5	2	1	Front	Estimated
RTS Gen5 MUX	1	32	14	32	14	Aft	
Camera / light on Booms	2	5	2	10	4	Front	Estimated
Transponders	2	5	2	10	4	Front	Estimated
Camera booms	2	46	28	92	56	Front	Estimated
Sum sensor weight				333.1 kg	141.95kg*		

Appendix B Material properties for S165M W1.4418



Quality Group
Approved by:
Valid from / Revision:
Page:

STAINLESS STEEL FOR FORGING
EOG
09.11.2017/ 01
2 of 2

21F – S165M

QT-XXX	Yield strength R _{p0.2} [MPa]	Tensile strength R _m [MPa]	Fracture Elongation A [%]	Impact Charpy-V @20 °C [J]
QT-900	700	900-1100	14	60
QT-760	550	760-960	14	70

For other dimensions, please contact us. We will be pleased to give you additional information.

Heat treatment

Austenitization at 1000 °C and cooled in air or water, followed by tempering at 560 - 580 °C and air-cooling. The tempering temperature may be adjusted within this temperature range to obtain the desired mechanical properties.

Weldability

S165M belongs to group 7.2, Martensitic stainless steels, according to ISO/TR 15608:2005. The weldability of S165M is good.

Physical properties at room temperature (typical values)

Density, 20 °C [kg/m ³]	Relative magnetic permeability	Coefficient of thermal expansion		Specific heat, 20°C [J/(kg °C)]	Thermal conductivity [W/m °C]	Electrical resistivity [Ωmm ² /m]	Young's modulus, 20 °C [GPa]
		Range [°C]	Coefficient [K ⁻¹]				
7700	-	20 - 100	10.8·10 ⁻⁶	430	15	0.7	200
		20 - 200	10.8·10 ⁻⁶				
		20 - 300	11.2·10 ⁻⁶				
		20 - 400	11.6·10 ⁻⁶				

Appendix C Material properties for 6082-T6

BS EN 1999-1-1:2007+A1:2009
EN 1999-1-1:2007+A1:2009 (E)

Table 3.2a - Characteristic values of 0,2% proof strength f_0 , ultimate tensile strength f_u (unwelded and for HAZ), min elongation A , reduction factors $\rho_{0, haz}$ and $\rho_{u, haz}$ in HAZ, buckling class and exponent n_p for wrought aluminium alloys - Sheet, strip and plate

Alloy EN- AW	Temper ¹⁾	Thick- ness ¹⁾ mm	f_0 ¹⁾	f_u	A_{50} ^{1) 6)}	$f_{0, haz}$ ²⁾	$f_{u, haz}$ ²⁾	HAZ-factor ²⁾		BC ⁴⁾	n_p ^{1), 5)}						
			N/mm ²			%	N/mm ²		$\rho_{0, haz}$ ¹⁾			$\rho_{u, haz}$					
3004	H14 H24/H34	≤ 6 3	180 170	220	1 3	75	155	0,42 0,44	0,70	B	23 18						
	H16 H26/H36	≤ 4 3	200 190	240	1 3			0,38 0,39	0,65	B	25 20						
3005	H14 H24	≤ 6 3	150 130	170	1 4	56	115	0,37 0,43	0,68	B	38 18						
	H16 H26	≤ 4 3	175 160	195	1 3			0,32 0,35	0,59	B	43 24						
3103	H14 H24	≤ 25 12,5	120 110	140	2 4	44	90	0,37 0,40	0,64	B	31 20						
	H16 H26	≤ 4	145 135	160	1 2			0,30 0,33	0,56	B	48 28						
5005/ 5005A	O/H111	≤ 50	35	100	15	35	100	1	1	B	5						
	H12 H22/H32	≤ 12,5	95 80	125	2 4	44	100	0,46 0,55	0,80	B	18 11						
	H14 H24/H34	≤ 12,5	120 110	145	2 3			0,37 0,40	0,69	B	25 17						
5052	H12 H22/H32	≤ 40	160 130	210	4 5	80	170	0,50 0,62	0,81	B	17 10						
	H14 H24/H34	≤ 25	180 150	230	3 4			0,44 0,53	0,74	B	19 11						
5049	O / H111	≤ 100	80	190	12	80	190	1	1	B	6						
	H14 H24/H34	≤ 25	190 160	240	3 6	100	190	0,53 0,63	0,79	B	20 12						
5454	O/H111	≤ 80	85	215	12	85	215	1	1	B	5						
	H14 H24/H34	≤ 25	220 200	270	2 4	105	215	0,48 0,53	0,80	B	22 15						
5754	O/H111	≤ 100	80	190	12	80	190	1	1	B	6						
	H14 H24/H34	≤ 25	190 160	240	3 6	100	190	0,53 0,63	0,79	B	20 12						
5083	O/H111	≤ 50	125	275	11	125	275	1	1	B	6						
		50 < t ≤ 80	115	270	14 ³⁾	115	270			B							
	H12 H22/H32	≤ 40	250 215	305	3 5	155	275	0,62 0,72	0,90	B	22 14						
H14 H24/H34	≤ 25	280 250	340	2 4	0,55 0,62			0,81	A	22 14							
6061	T4 / T451	≤ 12,5	110	205	12	95	150	0,86	0,73	B	8						
	T6 / T651	≤ 12,5	240	290	6	115	175	0,48	0,60	A	23						
	T651	12,5 < t ≤ 80	240	290	6 ³⁾												
6082	T4 / T451	≤ 12,5	110	205	12	100	160	0,91	0,78	B	8						
	T61/T6151	≤ 12,5	205	280	10							125	185	0,61	0,66	A	15
	T6151	12,5 < t ≤ 100	200	275	12 ³⁾									0,63	0,67	A	14
	T6/T651	≤ 6	260	310	6									0,48	0,60	A	25
		6 < t ≤ 12,5	255	300	9									0,49	0,62	A	27
T651	12,5 < t ≤ 100	240	295	7 ³⁾	0,52	0,63	A	21									
7020	T6	≤ 12,5	280	350	7	205	280	0,73	0,80	A	19						
	T651	≤ 40			9 ³⁾												
8011A	H14 H24	≤ 12,5	110 100	125	2 3	37	85	0,34 0,37	0,68	B	37 22						
	H16 H26	≤ 4	130 120	145	1 2			0,28 0,31	0,59		33 33						

1) If two (three) tempers are specified in one line, tempers separated by " | " have different technological values but separated by " / " have same values. (The tempers show differences for f_0 , A and n_p).

2) The HAZ-values are valid for MIG welding and thickness up to 15mm. For TIG welding strain hardening alloys (3xxx, 5xxx and 8011A) up to 6 mm the same values apply, but for TIG welding precipitation hardening alloys (6xxx and 7xxx) and thickness up to 6 mm the HAZ values have to be multiplied by a factor 0,8 and so the ρ -factors. For higher thickness – unless other data are available – the HAZ values and ρ -factors have to be further reduced by a factor 0,8 for the precipitation hardening alloys (6xxx and 7xxx) and by a factor 0,9 for the strain hardening alloys (3xxx, 5xxx and 8011A). These reductions do not apply in temper O.

3) Based on $A (= A_{5,65\sqrt{A_0}})$, not A_{50} .

4) BC = buckling class, see 6.1.4.4, 6.1.5 and 6.3.1.

5) n -value in Ramberg-Osgood expression for plastic analysis. It applies only in connection with the listed f_0 -value.

6) The minimum elongation values indicated do not apply across the whole range of thickness given, but mostly to the thinner materials. In detail see EN 485-2.

Appendix D Material properties for API 5L X65

Table A-1M Basic Allowable Stresses in Tension for Metals (SI Units) (Cont'd)

Numbers in Parentheses Refer to Notes for Appendix A Tables; Specifications Are ASTM Unless Otherwise Indicated

Line No.	Nominal Composition	Product Form	Spec. No.	Type/Grade	UNS No.	Class/Cond./Temper	Size, mm	P-No. (5)	Notes	Min. Temp., °C (6)	Min. Tensile Str., MPa	Min. Yield Str., MPa	Max. Use Temp., °C
37	Carbon steel	Pipe & tube	A139	C	K03004	1	(8b)	A	414	290	149
38	Carbon steel	Pipe & tube	A139	D	K03010	1	(8b)	A	414	317	149
39	Carbon steel	Pipe & tube	API 5L	X42	1	(55)(77)	A	414	290	204
40	Carbon steel	Pipe & tube	A381	Y42	1	...	A	414	290	204
41	Carbon steel	Pipe & tube	A381	Y48	1	...	A	427	331	343
42	Carbon steel	Pipe & tube	API 5L	X46	1	(55)(77)	A	434	317	204
43	Carbon steel	Pipe & tube	A381	Y46	1	...	A	434	317	204
44	Carbon steel	Pipe & tube	A381	Y50	1	...	A	441	345	343
45	Carbon steel	Pipe & tube	A671	CC65	K02403	1	(57)(67)	B	448	241	538
46	Carbon steel	Pipe & tube	A671	CB65	K02800	1	(57)(67)	A	448	241	593
47	Carbon steel	Pipe & tube	A672	B65	K02800	1	(57)(67)	A	448	241	593
48	Carbon steel	Pipe & tube	A672	C65	K02403	1	(57)(67)	B	448	241	593
49	Carbon steel	Pipe & tube	A139	E	K03012	1	(8b)	A	455	359	149
50	Carbon steel	Pipe & tube	API 5L	X52	1	(55)(77)	A	455	359	204
51	Carbon steel	Pipe & tube	A381	Y52	1	...	A	455	359	204
52	Carbon steel	Pipe & tube	A671	CC70	K02700	1	(57)(67)	B	483	262	538
53	Carbon steel	Pipe & tube	A671	CB70	K03101	1	(57)(67)	A	483	262	593
54	Carbon steel	Pipe & tube	A672	B70	K03101	1	(57)(67)	A	483	262	593
55	Carbon steel	Pipe & tube	A672	C70	K02700	1	(57)(67)	B	483	262	593
56	Carbon steel	Pipe & tube	A106	C	K03501	1	(57)	B	483	276	427
57	Carbon steel	Pipe & tube	A671	CD70	K12437	...	≤64	1	(67)	D	483	345	371
58	Carbon steel	Pipe & tube	A672	D70	K12437	...	≤64	1	(67)	D	483	345	371
59	Carbon steel	Pipe & tube	A691	CMSH-70	K12437	...	≤64	1	(67)	D	483	345	371
60	Carbon steel	Pipe & tube	API 5L	X56	1	(51)(55)(71)(77)	A	490	386	204
61	Carbon steel	Pipe & tube	A381	Y56	1	(51)(55)(71)	A	490	386	204
62	Carbon steel	Pipe & tube	A671	CK75	K02803	...	>25	1	(57)(67)	A	517	276	593
63	Carbon steel	Pipe & tube	A672	N75	K02803	...	>25	1	(57)(67)	A	517	276	593
64	Carbon steel	Pipe & tube	A691	CMS-75	K02803	...	>25	1	(57)(67)	A	517	276	593
65	Carbon steel	Pipe & tube	A671	CK75	K02803	...	≤25	1	(57)(67)	A	517	290	371
66	Carbon steel	Pipe & tube	A672	N75	K02803	...	≤25	1	(57)(67)	A	517	290	371
67	Carbon steel	Pipe & tube	A691	CMS-75	K02803	...	≤25	1	(57)(67)	A	517	290	371
68	Carbon steel	Pipe & tube	API 5L	X60	1	(51)(55)(71)(77)	A	517	414	204
69	Carbon steel	Pipe & tube	API 5L	X65	1	(51)(55)(71)(77)	A	531	448	204
70	Carbon steel	Pipe & tube	API 5L	X70	1	(51)(55)(71)(77)	A	565	483	204

Appendix E Material properties for S420N

Materials science: 4.3 Steels, Steel types

131

Weldable fine-grain and quenched & tempered structural steels												
Weldable fine-grained structural steels (selection) cf. DIN EN 10025-3 and DIN EN 10025-4 (2005-04), replaces DIN EN 10113												
Steel type Designation	Material number	DC ¹⁾	Notch impact energy KV ²⁾ in J at temperatures in °C			Tensile strength R_m N/mm ²	Yield strength R_e in N/mm ² for nominal thicknesses in mm			Elongation at fracture A %	Properties, application	
			+20	0	-20		≤ 16	> 16 ≤ 40	> 40 ≤ 63			
Unalloyed quality steels												
S275N S275M	1.0490 1.8818	N M	55	47	40	370–510 370–530	275	265	255	24	High toughness, brittle fracture and aging resistant; weldments in machinery, crane and bridge construction, automotive manufacturing, conveyors	
S355N S355M	1.0545 1.8823	N M	55	47	40	470–630	355	345	335	22		
Alloy high-grade steels												
S420N S420M	1.8902 1.8825	N M	55	47	40	520–680	420	400	390	19		
S460N S460M	1.8901 1.8827	N M	55	47	40	550–720 540–720	460	440	430	17		
¹⁾ DC Delivery condition: N normalized/normalizing rolled M thermomechanically rolled ²⁾ Values apply to V-notch longitudinal test pieces. Assignment of steels: DIN EN 10025-3 → S275N, S355N, S420N, S460N DIN EN 10025-4 → S275M, S355M, S420M, S460M												
Technical properties												
Weldability			Hot workability				Cold workability					
The steels are weldable. Increased strength and product thickness also increase the risk of cold cracks.			Only steels S275N, S355N, S420N and S480N are hot workable.				Cold-bending or edge folding is guaranteed for nominal thicknesses up to 16 mm, if cold-workability is specified in the order.					
Quenched and tempered struc. steels with higher yield strength (selection) cf. DIN EN 10025-6 (2005-02), replaces DIN EN 10137-2												
Steel type Designation ¹⁾	Material number	Notch impact energy KV in J at temperatures in °C			Tensile strength R_m N/mm ²	Yield strength R_e in N/mm ² for nominal thicknesses in mm			Elongation at fracture A %	Properties, application		
		0	-20	-40		> 3 ≤ 50	> 50 ≤ 100	> 100 ≤ 150				
S460Q S460QL	1.8908 1.8906	40	30	–	550–720	460	440	400	17	High toughness, high resistance to brittle fracture and aging stability; highly stressed weldments in machinery, crane and bridge construction, automotive manufacturing, conveyors		
S500Q S500QL	1.8924 1.8909	40	30	–	590–770	500	480	440	17			
S620Q S620QL	1.8914 1.8927	40	30	–	700–890	620	580	560	15			
S890Q S890QL	1.8940 1.8983	40	30	–	940–1100	890	830	–	11			
S960Q S960QL	1.8941 1.8933	40	30	–	980–1150	960	–	–	10			
¹⁾ Q quenched and tempered; QL quenched and tempered, guaranteed minimum values for notched bar impact values to –40 °C												
Technical properties												
Weldability			Hot workability				Cold workability					
The steels are not weldable without limitations. Professional planning of the welding parameters is required. Increased strength and product thickness also increase the risk of cold cracks.			The steels are hot workable up to the temperature limit for stress relief annealing.				Cold-bending or edge folding is guaranteed for nominal thicknesses up to 16 mm, if cold-workability is specified in the order.					

Appendix F Material properties for Strenx 700 OME



Data sheet 2023 Strenx® 700 OME 2017-04-20

Strenx® 700 OME

General Product Description

A structural steel developed for use in demanding load-bearing structures within the Offshore and Marine Industry.

Strenx® 700 OME exceeds the requirements of S690QL, EN 10 025-6. Strenx® 700 OME can be ordered with dual steel grades certificate, where the additional steel grade is defined and approved by one of the Classification Societies listed below.

The dual certification offers You the benefits of excellent mechanical properties, extra tight tolerances, formability and consistency of SSAB Strenx® Guarantees.

Classification society:

- American Bureau of Shipping AB EQ70, 4.8 to 130 mm thickness.
- DNV - GL NV E690, VL E690, 6 to 80 mm thickness.
- Lloyds Register LR EH 69, 8 to 80 mm thickness.

Dimension Range

Strenx® 700 OME is available as plate in thicknesses of 4.0 – 130.0 mm and available in widths up to 3350 mm and lengths up to 14630 mm depending on thickness. More detailed information on dimensions is provided in the dimension program for Strenx® 700 E/F at www.ssab.com.

Mechanical Properties

Thickness (mm)	Yield strength ¹⁾ R _{p0.2} (min MPa)	Tensile strength ¹⁾ R _m (MPa)	Elongation A ₅ (min %)
4.0 - 130.0	700	780 - 930	14

¹⁾ For transverse test pieces according to EN 10 025.

Impact Properties

Grade	Min transverse test, impact energy, Charpy V 10x10 mm tests specimens ¹⁾
Strenx®700 OME	69 J/ -40 °C

¹⁾ Unless otherwise agreed, only transverse impact testing.

Additional Options for Mechanical properties:

Option 1 - Min guaranteed impact energy (J) for transverse testing Charpy V 10x10 mm tests specimens 50 J/ -60°C.

Option 2 - Improved deformation properties perpendicular to the surface. Through- thickness tensile testing according to EN 10 164, Class Z35, Z25 and Z15.

Chemical Composition (ladle analysis)

C ^{*)} (max %)	Si ^{*)} (%)	Mn ^{*)} (max %)	P (max %)	S (max %)	Cr ^{*)} (max %)	Cu ^{*)} (max %)	Ni ^{*)} (max %)	Mo ^{*)} (max %)	B ^{*)} (max %)
0.20	0.10 - 0.55	1.60	0.015	0.003	0.80	0.30	2.0	0.70	0.005

The steel is grain refined. ^{*)} Intentional alloying elements.


Maximum Carbon Equivalent CET(CEV)

Thickness	4 - 30	(30) - 100	(100) - 130
Strenx 700 OME: CET(CEV)	0.38 (0.57)	0.39 (0.58)	0.41 (0.67)

$$CET = C + \frac{Mn + Mo}{10} + \frac{Cr + Cu}{20} + \frac{Ni}{40}$$

$$CEV = C + \frac{Mn}{6} + \frac{Cr + Mo + V}{5} + \frac{Cu + Ni}{15}$$

Appendix G Material properties for PEHD 1000



ASTRUP AS | Telefon: 22 79 15 00 | Faks: 22 79 16 82 | E-post: plast@astrup.no | www.astrup.no

2011
Plast-
katalogen

53

1

2

3

4

5

6

7

8

9

10

11

12

13

14

15

16

17

18

19

20

21

22

23

PEHD

1000

PEHD 1000 ultrahøymolekylær polyetylen high density

Materialegenskaper

PEHD 1000 (ultrahøymolekylær polyetylen high density) er et termoplastisk materiale, det glatteste av alle polyetylen-typene.

Materialet er kjent for gode mekaniske og termiske egenskaper, samt spesielt lav friksjon mot andre materialer. Lav vekt og vannabsorpsjon, samt god kjemikaliebestandighet er også viktige egenskaper.

PEHD 1000 finnes som halvfabrikata i plater, bolt, emnerør og profiler. Bearbeidingsegenskapene (sponende) er gode, men materialet lar seg vanskelig sveise og varmforme.

Anvendelsesområder er:

- Glideplater, glideskinner, foringer, sleider
- Maskindeler til bryggerier og næringsmiddelindustrien
- Filterplater og pumpedeler til kjemisk industri

Noen egenskaper	Norm	Enhet	Natur	Verdi	
				Sort (regen.)	Antistatisk
Egenvekt	DIN 53479	g/cm ³	0,94	0,94	0,96
Strekfasthet v/lyt	DIN 53455	N/mm ²	20	18	20
Strekfasthet v/brudd	DIN 53455	N/mm ²	44	30	35
Slagfasthet	DIN 53453	KJ/m ²	uten brudd	uten brudd	uten brudd
E-modul	DIN 53457	N/mm ²	700		
Brukstemperatur	–	°C	÷200/+80	÷200/+80	÷200/+80
Temperaturutvidelse	ASTM D 896	mm/m/°C	0,20	0,20	0,18
Friksjonskoeffisient	Mot stål	–	0,15	0,20	0,10–0,12
Vannopptak	DIN 53495	%	<0,01	<0,01	<0,01
Elektrisk motstand	ASTM D 257	ohm x cm	>10 ¹⁵	10 ¹²	<10 ⁵
Dielektr. overflatemotstand	DIN 53482	ohm	>10 ¹³	10 ¹¹	<10 ⁸
Brennbarhet	Normal brennbarhet. Avgir ingen farlige stoffer				

For ytterligere egenskaper se tabell side 150–151.

Materialegenskaper 53

Plate, presset, skivet 54

Plate, presset 54

Plate, regenerert, presset 54

Rundbolt, ekstrudert 55

Skinne, regenerert, ekstrudert 56

Appendix H Material properties for EPDM

TABLE 8.1 Material Properties [3]

Shear modulus, G (kPa)	Young's modulus, E_0 (kPa)	Bulk modulus, E_b (MPa)	Material compressibility coefficient, ϕ
296	896	979	0.93
365	1158	979	0.89
441	1469	979	0.85
524	1765	979	0.80
621	2137	1,007	0.73
793	3172	1,062	0.64
1034	4344	1,124	0.57
1344	5723	1,179	0.54
1689	7170	1,241	0.53
2186	9239	1,303	0.52

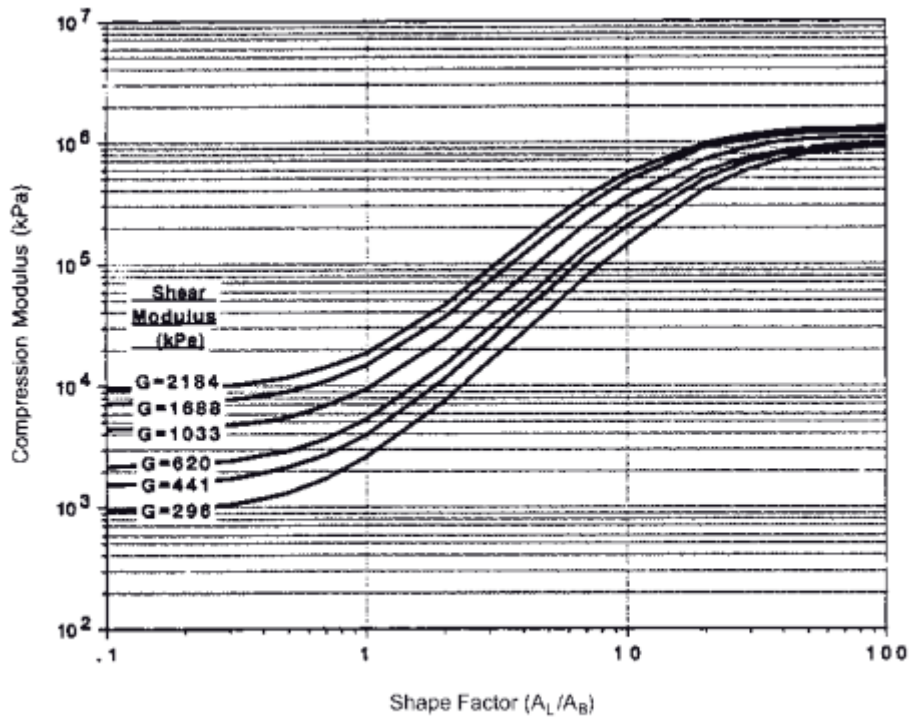


FIGURE 8.4 Compression modulus E_c versus shape factor S for various shear moduli [3]

Screw joint calculations																																																
<p>Joint diagram</p> <p>F_p preload F_a applied force F_c joint clamp force F_s total bolt load f_s bolt extension f_j joint compression Δl</p>				Preselection of shank bolts¹⁾ <table border="1"> <thead> <tr> <th rowspan="2">Load</th> <th colspan="8">Applied force per bolt $F_s^{2)}$ in kN</th> </tr> <tr> <th>2.5</th> <th>4</th> <th>6.3</th> <th>10</th> <th>16</th> <th>25</th> <th>40</th> <th>63</th> </tr> </thead> <tbody> <tr> <td>• static</td> <td>2.5</td> <td>4</td> <td>6.3</td> <td>10</td> <td>16</td> <td>25</td> <td>40</td> <td>63</td> </tr> <tr> <td>• dynamic</td> <td>1.6</td> <td>2.5</td> <td>4</td> <td>6.3</td> <td>10</td> <td>16</td> <td>25</td> <td>40</td> </tr> </tbody> </table>										Load	Applied force per bolt $F_s^{2)}$ in kN								2.5	4	6.3	10	16	25	40	63	• static	2.5	4	6.3	10	16	25	40	63	• dynamic	1.6	2.5	4	6.3	10	16	25	40
Load	Applied force per bolt $F_s^{2)}$ in kN																																															
	2.5	4	6.3	10	16	25	40	63																																								
• static	2.5	4	6.3	10	16	25	40	63																																								
• dynamic	1.6	2.5	4	6.3	10	16	25	40																																								
Property class		5.8, 6.8	M5	M6	M8	M10	M12	M16	M20	M24																																						
		8.8	M5	M6	M8	M10	M10	M16	M20	M24																																						
		10.9	M4	M5	M6	M8	M10	M12	M16	M20																																						
		12.9	M4	M5	M5	M8	M8	M10	M12	M16																																						

¹⁾ It is necessary to check the values of the selected bolts in accordance with VDI Guideline 2230 for instance.
²⁾ For waisted bolts select next higher applied force level.

Preload and tightening torques

Thread	$F^3)$	$A_s^1)$ in mm ²	Shank bolts						$A_w^2)$ in mm ²	Waisted bolts											
			Preload F_p in kN			Tightening torque M_t in N · m				Preload F_p in kN			Tightening torque M_t in N · m								
			Overall coefficient of friction $\mu^4)$									Total coefficient of friction $\mu^4)$									
			0.08	0.12	0.14	0.08	0.12	0.14		0.08	0.12	0.14	0.08	0.12	0.14						
M8	8.8	36.6	18.6	17.2	16.5	17.9	23.1	25.3	26.6	12.9	11.8	11.2	13.6	17.6	19.2						
	10.9		27.1	25.2	24.2	26.2	34	37.2		19	17.3	16.4	20	25.8	28.2						
	12.9		31.9	29.5	28.3	30.7	39.6	43.6		22.2	20.2	19.2	23.4	30.2	33						
M8 x 1	8.8	39.2	20.3	18.8	18.1	18.8	24.8	27.3	29.2	14.6	13.4	12.7	13.6	17.6	19.2						
	10.9		29.7	27.7	26.6	27.7	36.4	40.1		21.5	19.6	18.7	20	25.8	28.2						
	12.9		34.8	32.4	31.1	32.4	42.6	47.1		25.1	23	21.9	23.4	30.2	33						
M10	8.8	58.0	29.5	27.3	26.2	36	46	51	42.4	20.7	18.9	17.9	25	32	35						
	10.9		43.3	40.2	38.5	53	68	75		30.4	27.7	26.4	37	47	51						
	12.9		50.7	47	45	61	80	88		35.6	32.4	30.8	43	55	60						
M10x1.25	8.8	61.2	31.5	29.4	28.3	37	49	54	45.6	22.7	20.9	19.9	27	35	38						
	10.9		46.5	43.2	41.5	55	72	80		33.5	30.6	29.2	40	51	56						
	12.9		54.4	50.6	48.6	64	84	93		39.2	35.9	34.4	46	60	65						
M12	8.8	84.3	43	39.9	38.3	61	80	87	61.7	30.3	27.6	26.3	43	55	60						
	10.9		63	58.5	56.2	90	117	128		44.6	40.6	38.6	63	81	88						
	12.9		73.9	68.5	65.8	105	137	150		52.1	47.7	45.2	74	95	103						
M12x1.5	8.8	88.1	48.2	45	43.2	65	87	96	65.8	35	32.6	31	48	63	69						
	10.9		70.8	66	63.5	96	128	141		52	47.8	45.7	71	93	102						
	12.9		82.7	72.3	74.3	112	150	165		61	56	53.4	83	108	119						
M16	8.8	157	81	75.3	72.4	147	194	214	117	58.4	53.4	51	106	137	150						
	10.9		119	111	106	216	285	314		85.8	78.5	74.8	156	202	221						
	12.9		140	130	124	253	333	367		100	91.8	87.5	182	236	258						
M16x1.5	8.8	167	88	82.2	79.2	154	207	229	128	65.5	60.2	57.4	115	151	166						
	10.9		129	121	116	227	304	336		96.2	88.4	84.5	169	222	244						
	12.9		151	141	136	265	355	394		113	104	99	197	260	285						
M20	8.8	245	131	121	117	297	391	430	182	92	86	82	215	278	304						
	10.9		186	173	166	423	557	615		134	123	117	306	395	432						
	12.9		218	202	194	495	653	720		157	144	137	358	462	505						
M20x1.5	8.8	272	149	138	134	320	433	482	210	113	104	100	242	322	355						
	10.9		212	200	190	455	618	685		160	148	142	345	460	508						
	12.9		247	231	225	533	721	802		188	173	166	402	540	594						
M24	8.8	353	188	175	168	512	675	743	262	136	124	118	370	480	523						
	10.9		268	250	238	730	960	1060		193	177	168	527	682	745						
	12.9		313	291	280	855	1125	1240		225	207	196	617	800	871						
M24x2	8.8	384	210	196	189	545	735	816	295	158	145	139	410	543	600						
	10.9		300	280	268	776	1046	1160		224	207	198	582	775	852						
	12.9		350	327	315	908	1224	1360		263	242	230	682	905	998						

During assembly, the bolts are under tensile and torsional stress. The tightening torque M_t utilizes approx. 90% of the yield strength of the bolt material.

¹⁾ A_s stress area
²⁾ A_w waist cross section
³⁾ F property class of bolt
⁴⁾ $\mu = 0.08$: bolt MoS₂ lubricated
 $\mu = 0.12$: bolt lightly oiled
 $\mu = 0.14$: bolt secured with microencapsulated plastic

Appendix J ROV and USV kinematics

1 USV and ROV kinematics

2 Assumptions

- Only vertical vessel accelerations are considered

3 Input Parameters

Length of USV:	$L_{USV} := 26.9 \text{ m}$
Horizontal velocity of USV:	$v_{h,USV} := 0.972 \text{ knots}$
Significant wave height:	$H_S := 3$
Distance from water plane to COG of ROV:	$d_{COG,ROV} := 0.9 \text{ m}$
Incline angle of hatch:	$\alpha_1 := 40 \text{ deg}$
Gravity:	$g := 9.81$

4 ROV kinematics

Characteristic wave amplitude:	$\zeta := 0.9 \cdot H_S$	$\zeta = 2.7$
Zero-up-crossing wave period:	$T_z := 3.39 \cdot (H_S)^{\frac{1}{2}}$	$T_z := 5.872 \text{ s}$
Vertical acceleration of ROV:	$a_{v,ROV} := -\zeta \cdot \left(2 \cdot \frac{\pi}{T_z}\right)^2 \cdot e^{-\frac{4 \cdot \pi^2 \cdot d_{COG,ROV}}{T_z^2 \cdot g}}$	$a_{v,ROV} = -2.767 \frac{m}{s^2}$
Acceleration normal to hatch:	$a_{n,ROV} := a_{v,ROV} \cdot \cos(\alpha_1)$	$a_{n,ROV} = -2.12$
Vertical velocity of ROV:	$v_{v,ROV} := -\zeta \cdot \left(2 \cdot \frac{\pi}{T_z}\right) \cdot e^{-\frac{4 \cdot \pi^2 \cdot d_{COG,ROV}}{T_z^2 \cdot g}}$	$v_{v,ROV} = -2.586 \frac{m}{s}$
x-component of ROV velocity:	$x := \sin(\alpha_1) \cdot v_{v,ROV}$	$x = -1.662 \frac{m}{s}$
y-component of ROV velocity:	$y := \cos(\alpha_1) \cdot v_{v,ROV}$	$y = -1.981 \frac{m}{s}$
the angle a2:	$\alpha_2 := \text{atan}\left(\frac{x}{y}\right)$	$\alpha_2 = 40 \text{ deg}$
Resulting velocity ROV	$v_r := \frac{x}{\sin(\alpha_2)}$	$v_r = -2.586 \frac{m}{s}$

4 USV kinematics

Vertical acceleration of USV: $a_{v.USV} := 6 \cdot \frac{H_S}{L_{USV}} \left(0.85 + 0.35 \cdot \frac{v_{h.USV}}{\sqrt{L_{USV}}} \right) \cdot g$ $a_{v.USV} = 6.01 \frac{m}{s^2}$

USV acceleration normal to hatch: $a_{vn.USV} := \cos(\alpha_1) \cdot a_{v.USV}$ $a_{vn.USV} = 4.604$

$v_{h.USV} := 0.4 \frac{m}{s}$

USV velocity normal to hatch: $v_{n.USV} := \sin(\alpha_1) \cdot v_{h.USV}$ $v_{n.USV} = 0.257$

4 Relative accelerations and velocities

Relative velocity between USV and ROV: $v_r := v_r - v_{n.USV}$ $v_r = -2.843$

Relative acceleration between USV and ROV: $a_r := a_{n.ROV} - a_{vn.USV}$ $a_r = -6.724$

Created with PTC Mathcad Express. See www.mathcad.com for more information.

Appendix K Kinetic and elastic potential energies calculations

1 Assumptions

- Assume 70% of ROV submerged when at waterline when recovered

2 Input Parameters

Length of ROV: $L := 2.5 \text{ m}$

Width of ROV: $W := 1.7 \text{ m}$

Height of ROV: $H := 1.65 \text{ m}$

Mass of ROV: $m_{ROV} := 3200 \text{ kg}$

Density of sea water: $\rho := 1025 \text{ kg} \cdot \text{m}^{-3}$

Gravity: $g := 1025 \text{ m} \cdot \text{s}^{-2}$

Deformation force exerted onto hatch: $f_Q := 60 \text{ kN}$

Min. relative velocity between USV and ROV during recovery: $v_{r.min} := 0.44 \text{ m} \cdot \text{s}^{-1}$

Max. relative velocity between USV and ROV during recovery: $v_{r.max} := 0.64 \text{ m} \cdot \text{s}^{-1}$

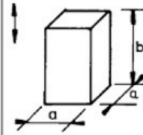
Hatch deformations: $u_h := \begin{bmatrix} 12.56 \\ 5.99 \\ 14.78 \\ 8.13 \end{bmatrix} \text{ mm}$

Skid deformations: $u_s := \begin{bmatrix} 4.67 \\ 0.86 \\ 1.19 \\ 1.96 \end{bmatrix} \text{ mm}$

Elastic potential energy absorbed in square rubber profile: $U_{srp} := 332.27 \text{ J}$

Elastic potential energy absorbed in hollow rubber profile: $U_{hrp} := 37.93 \text{ J}$

3 Ref DNV-RP-N103 Modelling and analysis of marine operations

Body shape	Direction of motion	C_A		V_R	
		b/a	C_A		
Square prisms 	Vertical	1.0	0.68	$a^2 b$	
		2.0	0.36		
		3.0	0.24		
		4.0	0.19		
		5.0	0.15		
		6.0	0.13		
		7.0	0.11		
		10.0	0.08		
		$b \ll a$	0.45		a^3

4 Intermediate Calculations

Reference volume of ROV: $V_r := H^2 \cdot L$ $V_r = 6.806 \text{ m}^3$

Added mass coefficient acc to ref: $C_A := \frac{L}{H} = 1.515$ $C_A := 0.52$

Added mass: $m_a := \rho \cdot C_A \cdot V_r \cdot 0.7$ $m_a = 2539.412 \text{ kg}$

5 Kinetic and elastic potential energy calculations		
Min. kinetic energy of ROV with added mass:	$E_{k.min} := 0.5 \cdot (m_{ROV} + m_a) \cdot v_{r.min}^2$	$E_{k.min} = 555.575 \text{ J}$
Max. kinetic energy of ROV with added mass:	$E_{k.max} := 0.5 \cdot (m_{ROV} + m_a) \cdot v_{r.max}^2$	$E_{k.max} = 1175.432 \text{ J}$
Elastic potential energy of hatch:	$U_h := 0.5 \cdot f_Q \cdot u_h$	$U_h = \begin{bmatrix} 376.8 \\ 179.7 \\ 443.4 \\ 243.9 \end{bmatrix} \text{ J}$
Elastic potential energy of skid:	$U_s := 0.5 \cdot f_Q \cdot u_s$	$U_s = \begin{bmatrix} 140.1 \\ 25.8 \\ 35.7 \\ 58.8 \end{bmatrix} \text{ J}$
Min. elastic potential energy absorbed during impact between ROV and hatch: (Square profile meets hollow profile at LCF on hatch)	$U_{min} := \min(U_h + U_s) + U_{srp} + U_{hrp}$	$U_{min} = 575.7 \text{ J}$
Max. elastic potential energy absorbed during impact between ROV and hatch: (Square profile meets square profile at LSA on hatch)	$U_{max} := \max(U_h + U_s) + 2 \cdot U_{srp}$	$U_{max} = 1181.44 \text{ J}$

Appendix L Hydrodynamic forces on hatch

1 Hydrodynamic forces on hatch

2 Input Parameters

Relative velocity between USV and ROV: $v_r := -2.843 \frac{m}{s}$

Relative acceleration between USV and ROV: $a_r := -6.724 \frac{m}{s^2}$

Water acceleration normal to hatch: $a_w := -2.12 \frac{m}{s^2}$

Density of sea water: $\rho := 1025 \frac{kg}{m^3}$

Diameter of pipes in hatch: $D_p := 220 \text{ mm}$

Length of pipes in hatch: $L_p := 24800 \text{ mm}$

Volume of pipes: $V_p := 0.18 \text{ m}^3$

Projected area of pipes: $S_p := 5.16 \text{ m}^2$

Height of T-bar: $H_T := 150 \text{ mm}$

Width of T-bar: $W_T := 120 \text{ mm}$

Length of all T-bars: $L_T := 3000 \text{ mm}$

Volume of T-bar: $V_T := 0.35 \text{ m}^3$

Projected area of T-bars: $S_T := 0.33 \text{ m}^2$

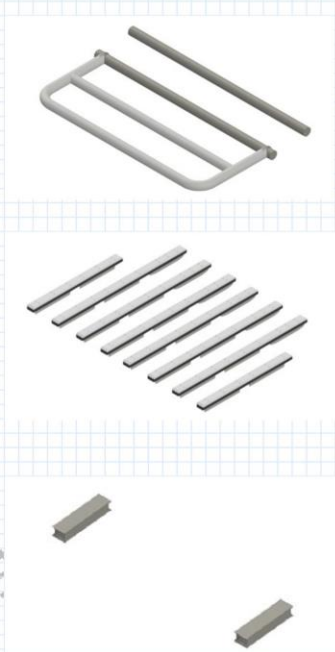
Height of box beam: $H_b := 150 \text{ mm}$

Width of box beam: $W_b := 250 \text{ mm}$

Length of box beam: $L_b := 843 \text{ mm}$

Volume of box beam: $V_b := 0.02 \text{ m}^3$

Surface area of box beam: $S_b := 0.372 \text{ m}^2$



2 Hydrodynamic forces acting on pipes

Added mass coefficient: $\frac{L_p}{D_p} = 112.727$
 $C_{Ap} := 1.00$

Drag coefficient: $\frac{L_p}{D_p} = 112.727$
 $C_{Dp} := 1.00$

Inertia: $F_{Ip} := \rho \cdot V_p \cdot a_w$ $F_{Ip} = -391.14 \text{ N}$

Added mass: $F_{Ap} := \rho \cdot C_{Ap} \cdot V_p \cdot a_r$ $F_{Ap} = -1240.578 \text{ N}$

Drag: $F_{Dp} := 0.5 \cdot \rho \cdot C_{Dp} \cdot S_p \cdot v_r \cdot \text{abs}(v_r)$ $F_{Dp} = -21374.565 \text{ N}$

Geometry	Dimensions	C_a	Reference Volume
Vertical cylinder	$b/2a$		$\pi a^2 b$
	1.2	0.62	
	2.5	0.78	
	5.0	0.90	
	9.0	0.96	
∞	1.00		

Geometry	Dimensions	C_D	
		Sub critical flow $Re_c < 10^5$	Supercritical flow $Re_c > 5 \cdot 10^5$
Circular cylinder normal to flow	L/D		
	2	0.98	0.80
	5	0.62	0.80
	10	0.48	0.82
	20	0.74	0.90
	40	0.82	0.98
	50	0.87	0.99
100	0.98	1.00	

3 Hydrodynamic forcs acting on T-bars with damper material

Added mass coefficient:

$$\frac{H_T}{W_T} = 1.25$$

$$C_{AT} := 1.456$$

Drag coefficient:

$$\frac{L_T}{W_T} = 25$$

$$C_{DT} := 1.90$$

Inertia:

$$F_{IT} := \rho \cdot V_T \cdot a_w$$

$$F_{IT} = -760.55 \text{ N}$$

Added mass:

$$F_{AT} := \rho \cdot C_{AT} \cdot V_T \cdot a_r$$

$$F_{AT} = -3512.214 \text{ N}$$

Drag:

$$F_{DT} := 0.5 \cdot \rho \cdot C_{DT} \cdot S_T \cdot v_r \cdot \text{abs}(v_r)$$

$$F_{DT} = -2597.258 \text{ N}$$

Section through body	Direction of motion	C _d	A _r	Added mass moment of inertia [kg/m ³ ·m ²]		
				$\beta_1 \rho a^3$ or $\beta_2 \rho a b^2$	β_1	β_2
	Vertical	1.0	πa^2			
		1.14		0.1	-	0.147
		1.21		0.2	-	0.15
		1.36		0.5	-	0.15
		1.51		1.0	0.234	0.234
		1.70		2.0	0.15	-
		1.98		5.0	0.15	-
		2.23		∞	0.125	-

Geometry	Dimensions	C _{dis}
	b/H	1.16
	1	1.20
	5	1.90
	10	1.90
	∞	1.90
		$Re > 10^3$

3 Hydrodynamic forcs acting on box beam

Added mass coefficient:

$$\frac{H_b}{W_b} = 0.6$$

$$C_{Ab} := 1.66$$

Drag coefficient:

$$\frac{L_b}{W_b} = 3.372$$

$$C_{Db} := 1.19$$

Inertia:

$$F_{Ib} := \rho \cdot V_b \cdot a_w$$

$$F_{Ib} = -43.46 \text{ N}$$

Added mass:

$$F_{Ab} := \rho \cdot C_{Ab} \cdot V_b \cdot a_r$$

$$F_{Ab} = -228.818 \text{ N}$$

Drag:

$$F_{Db} := 0.5 \cdot \rho \cdot C_{Db} \cdot S_b \cdot v_r \cdot \text{abs}(v_r)$$

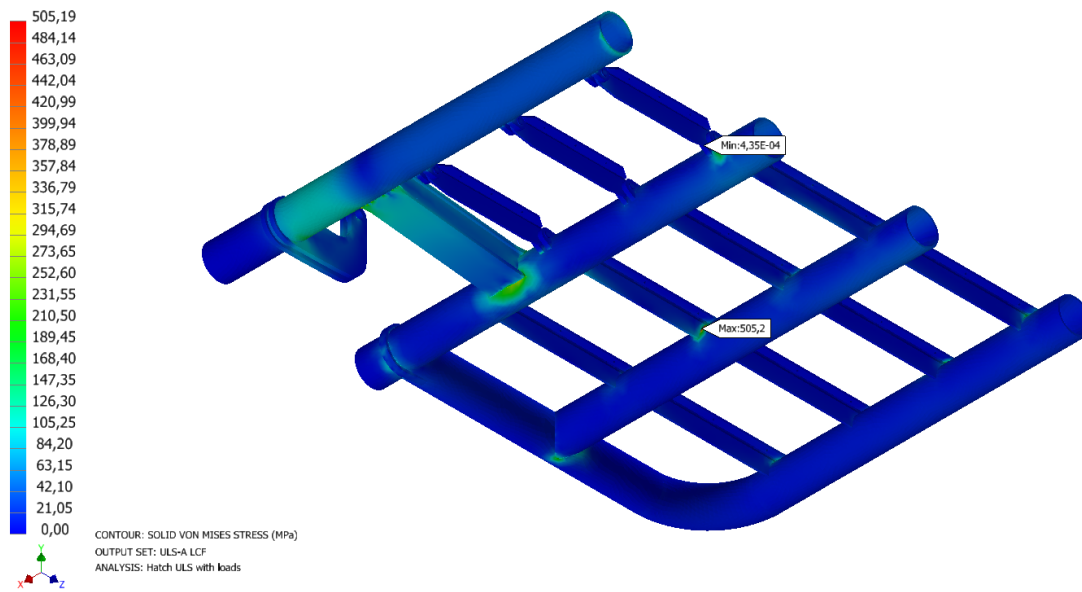
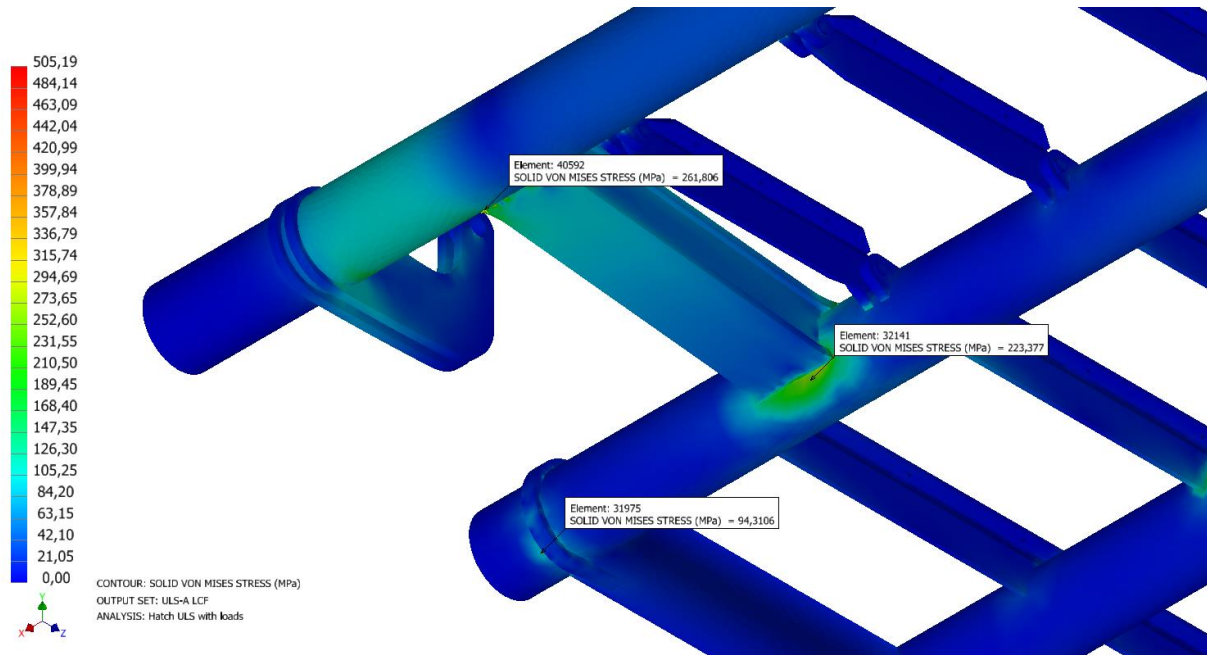
$$F_{Db} = -1833.739 \text{ N}$$

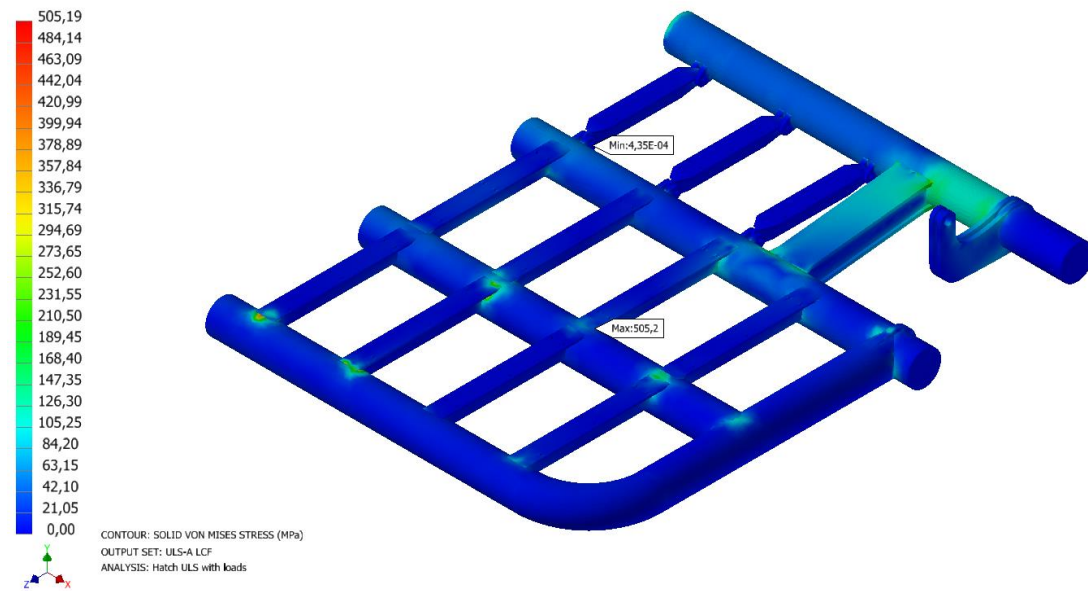
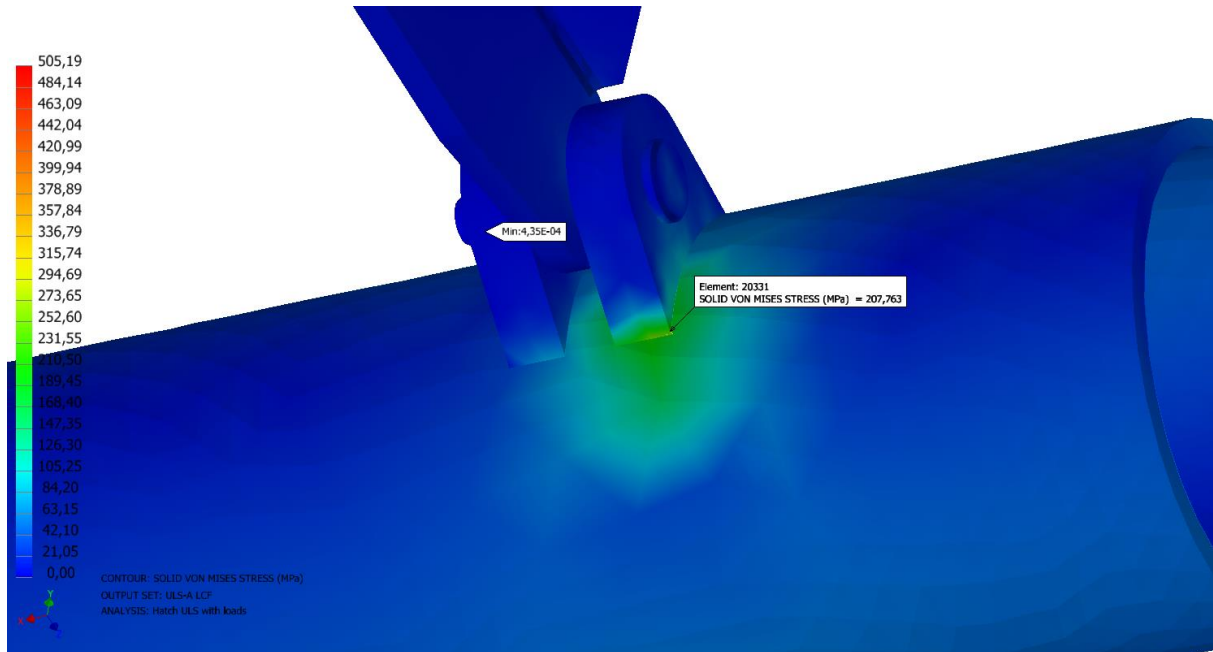
Section through body	Direction of motion	C _d	A _r	Added mass moment of inertia [kg/m ³ ·m ²]		
				$\beta_1 \rho a^3$ or $\beta_2 \rho a b^2$	β_1	β_2
	Vertical	1.0	πa^2			
		1.14		0.1	-	0.147
		1.21		0.2	-	0.15
		1.36		0.5	-	0.15
		1.51		1.0	0.234	0.234
		1.70		2.0	0.15	-
		1.98		5.0	0.15	-
		2.23		∞	0.125	-

Geometry	Dimensions	C _{dis}
	b/H	1.16
	1	1.20
	5	1.90
	10	1.90
	∞	1.90
		$Re > 10^3$

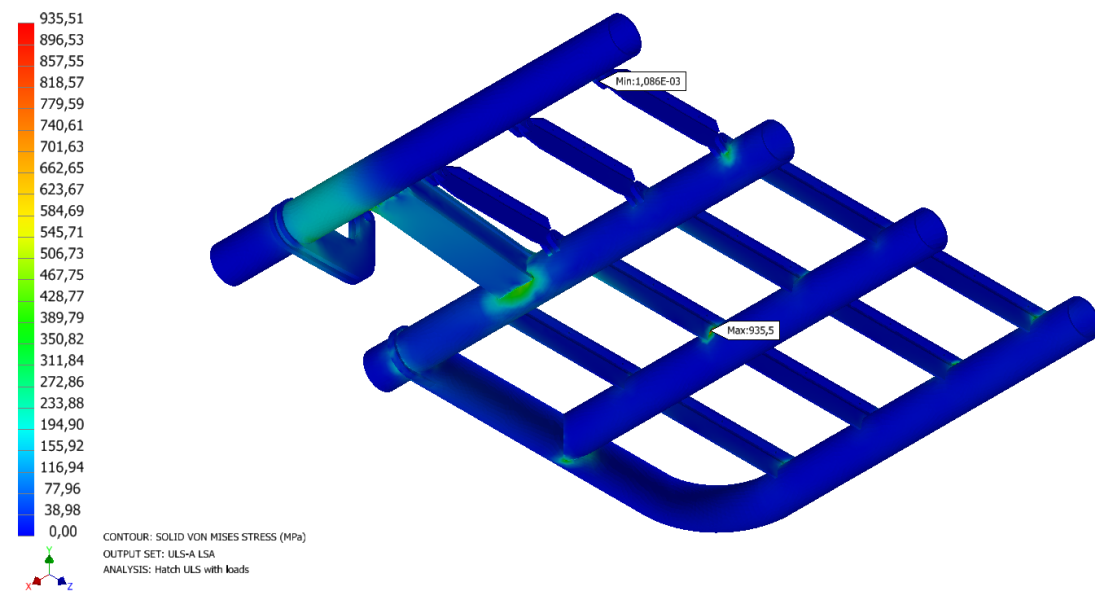
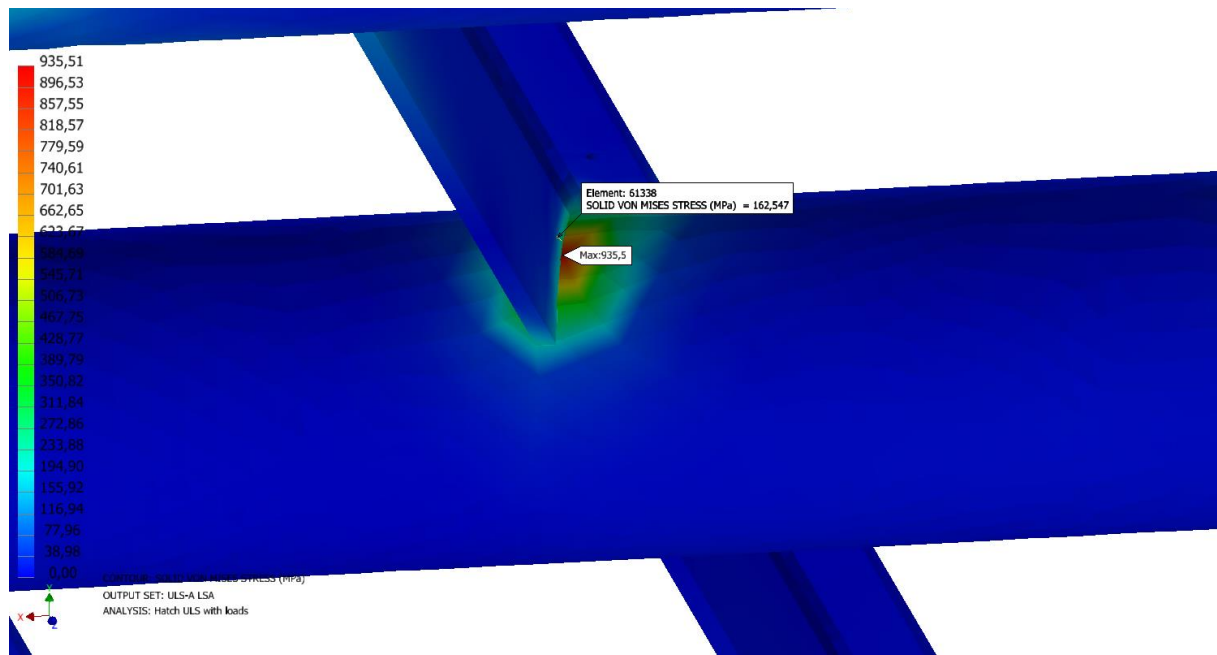
Appendix M Hatch Stress analysis

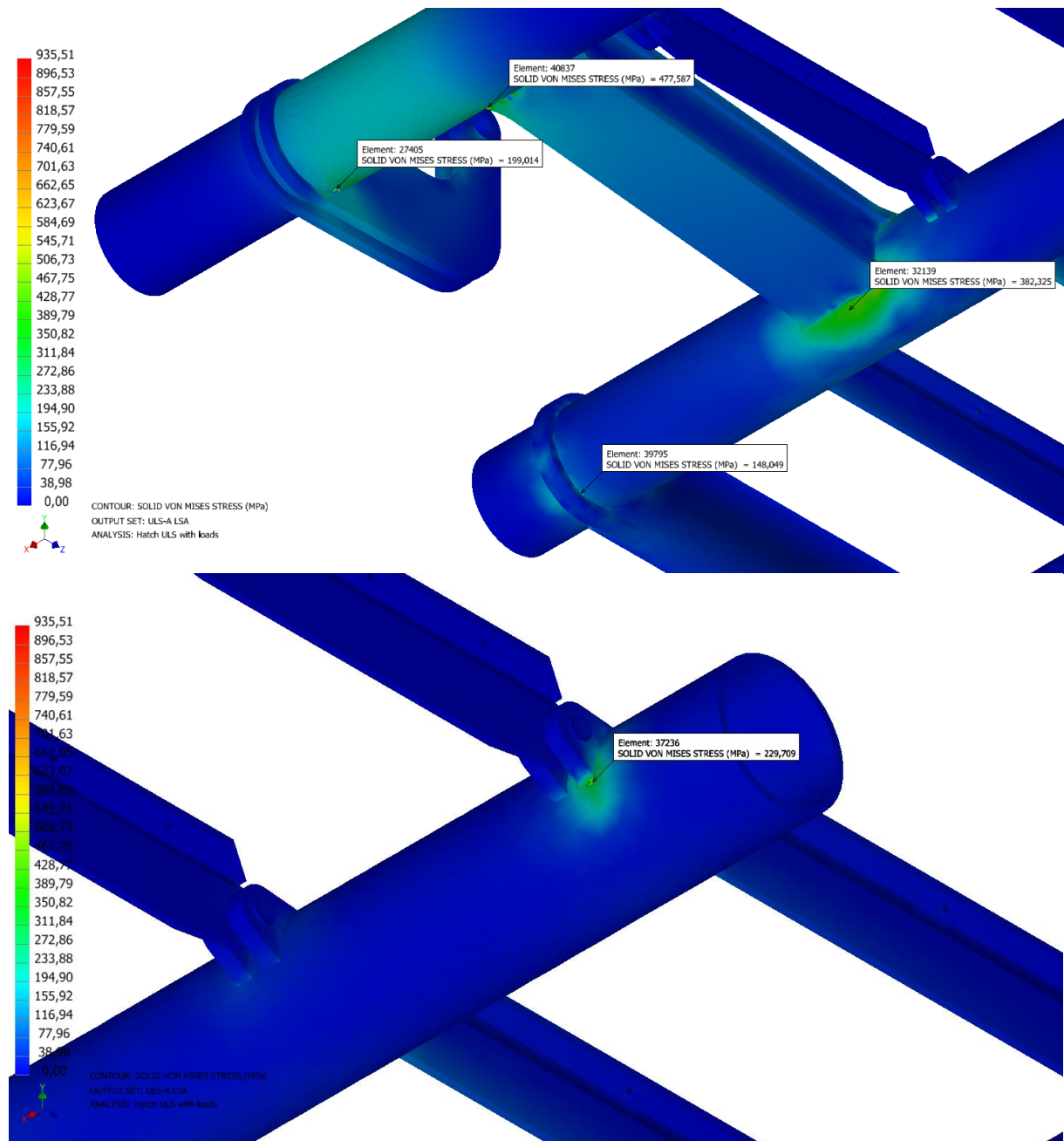
ULS-a LCF

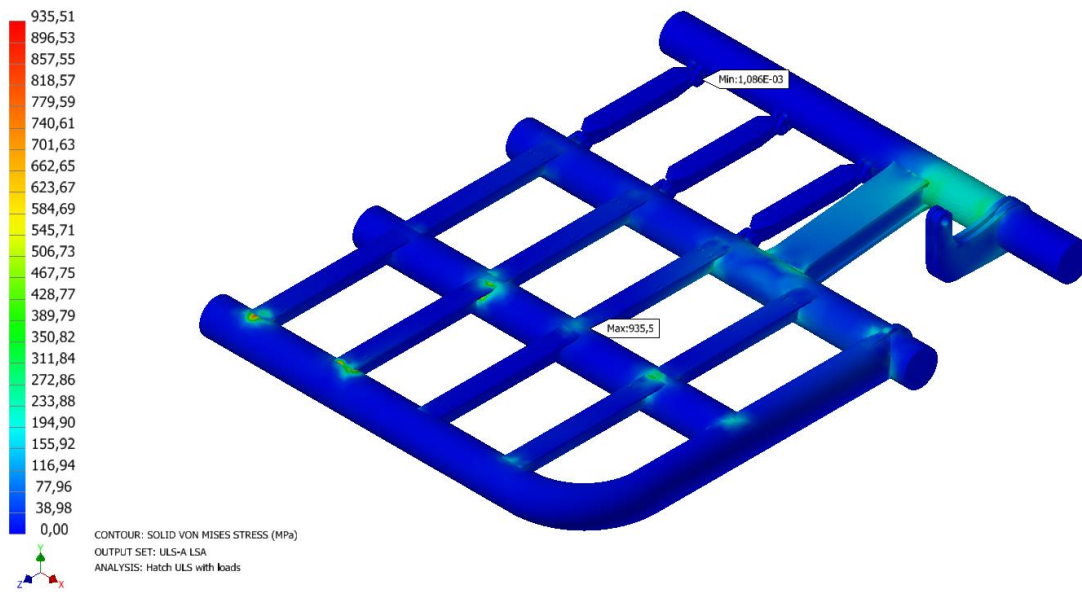




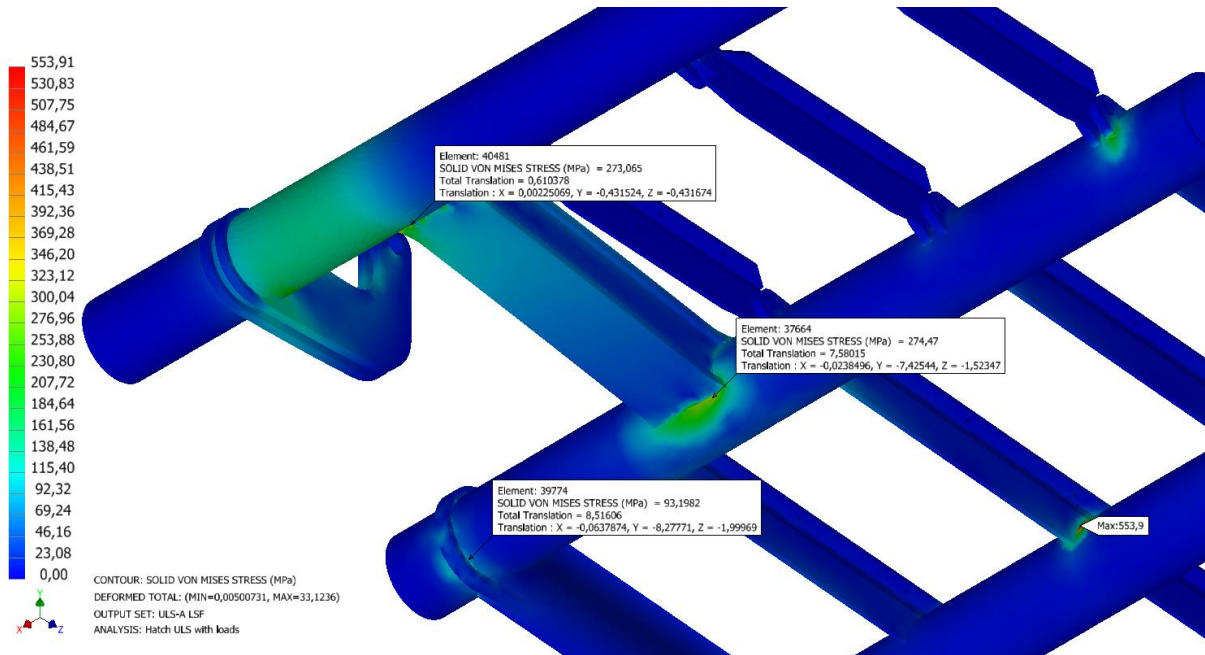
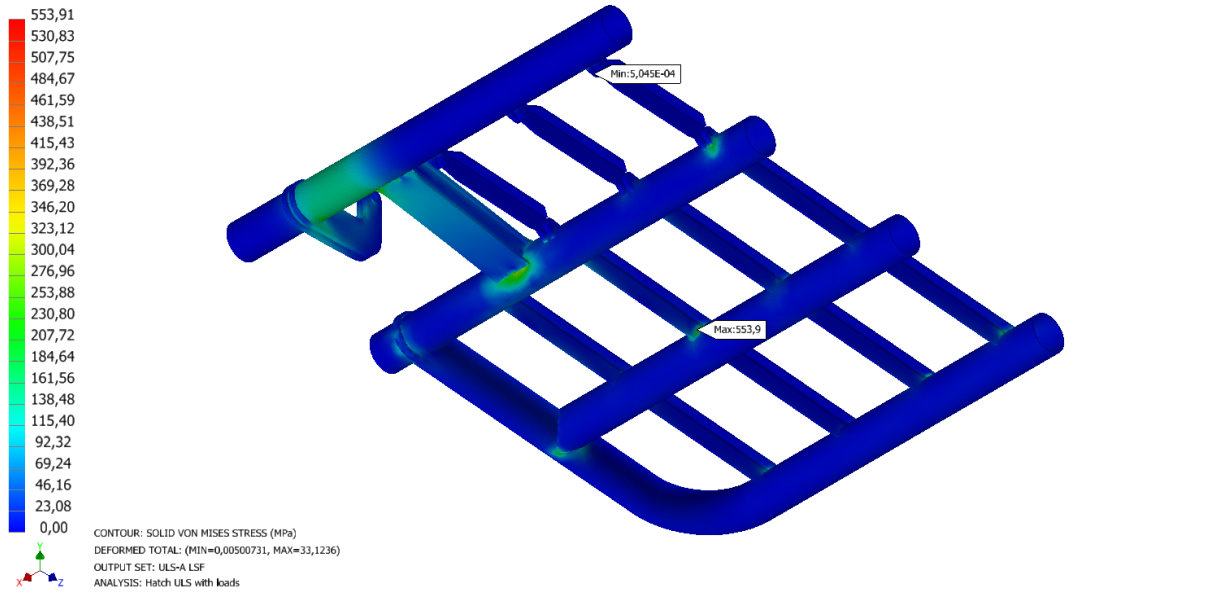
ULS-a LSA

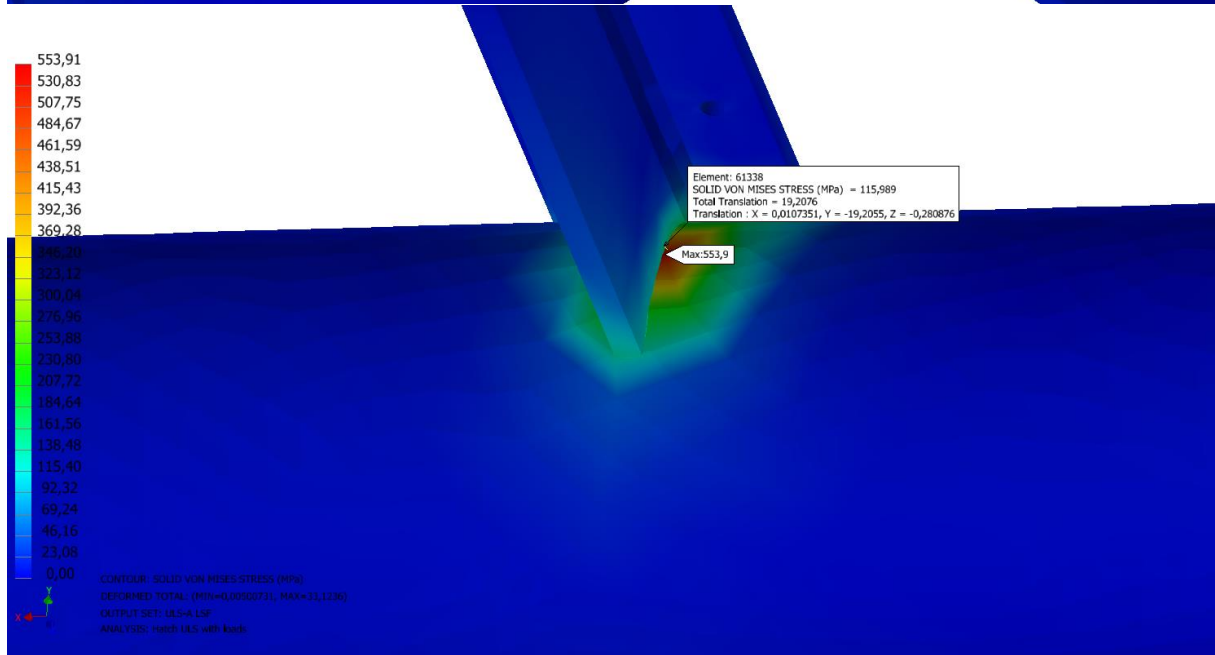
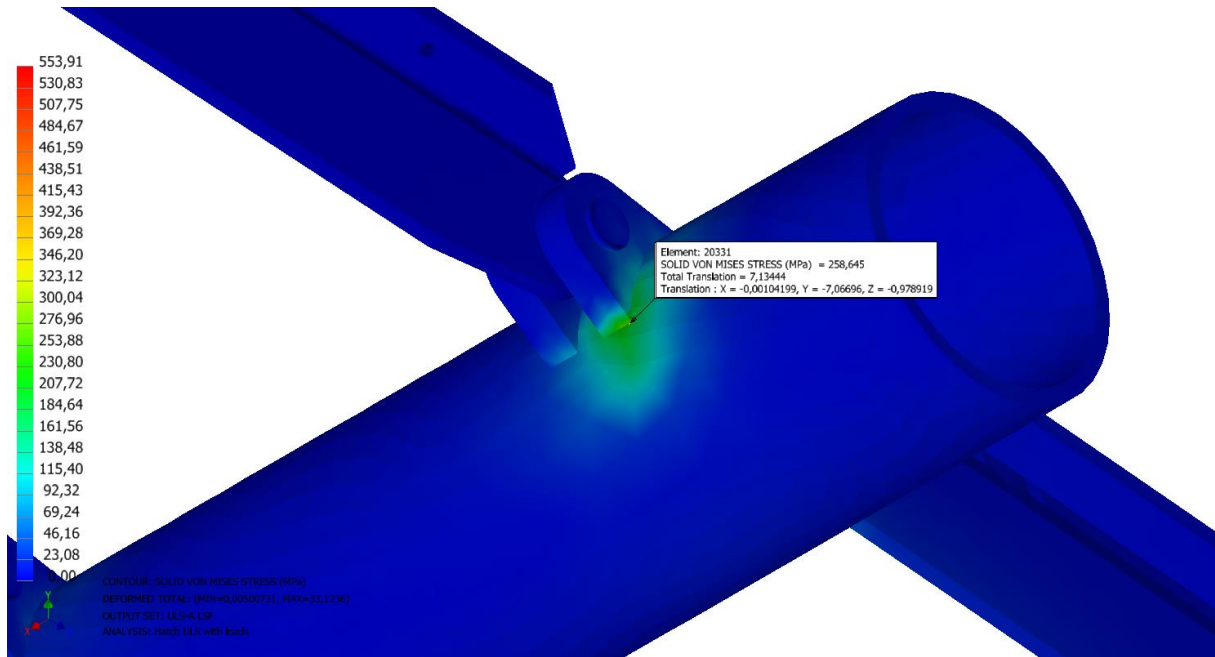


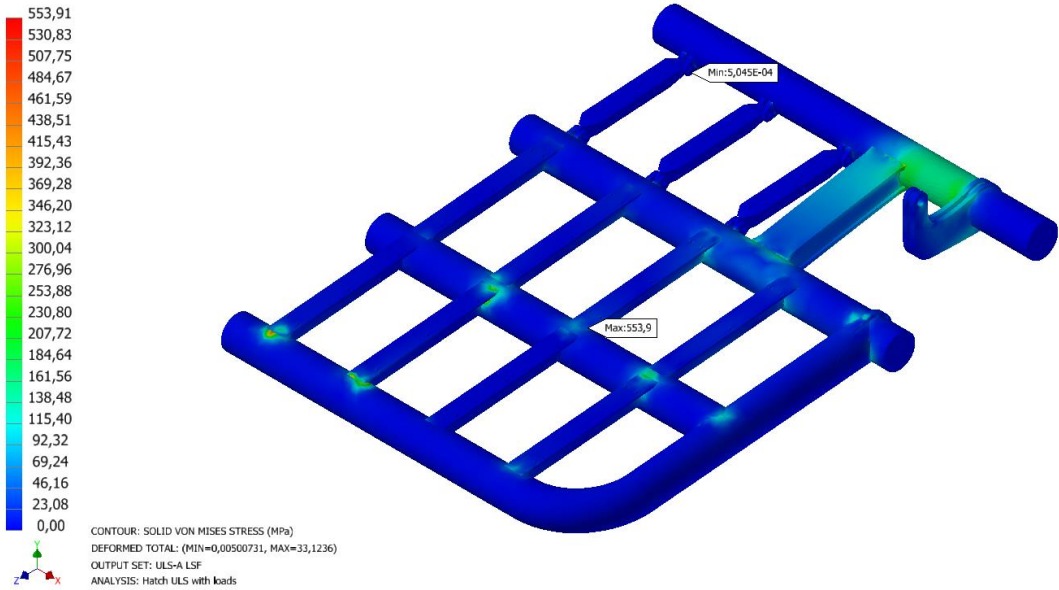




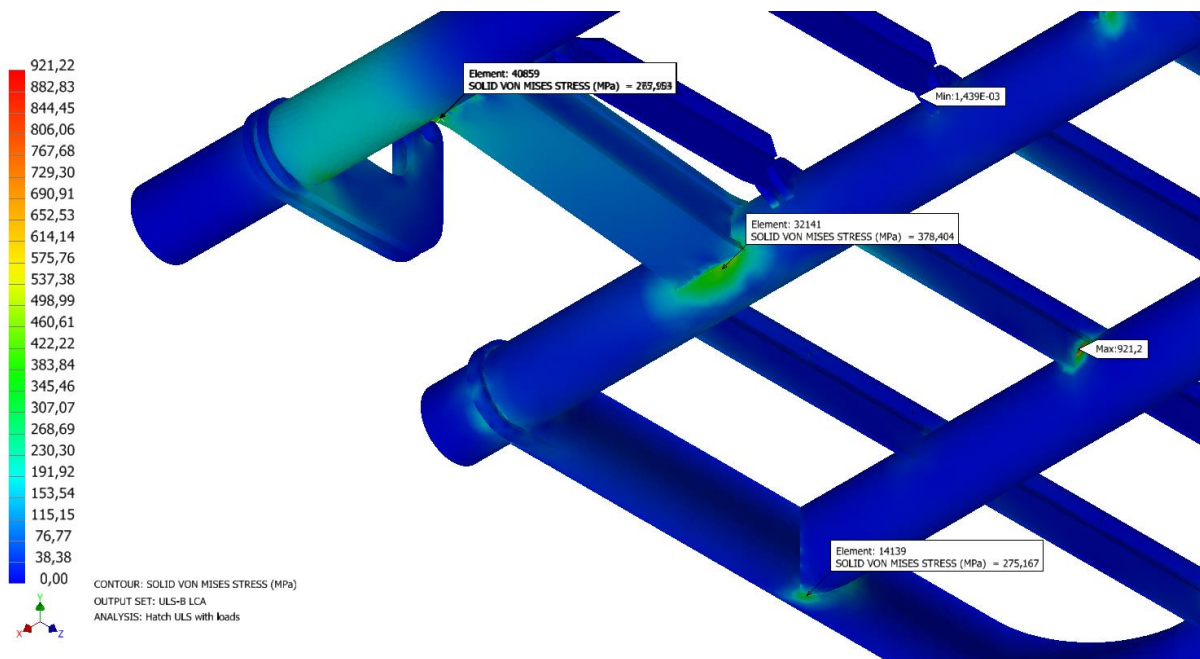
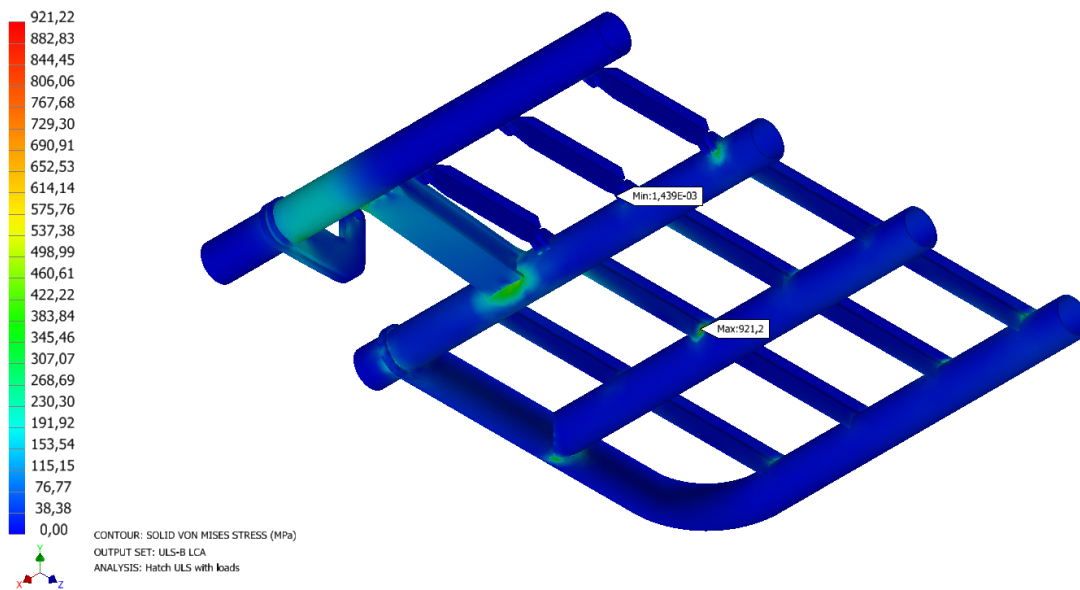
ULS-a LSF

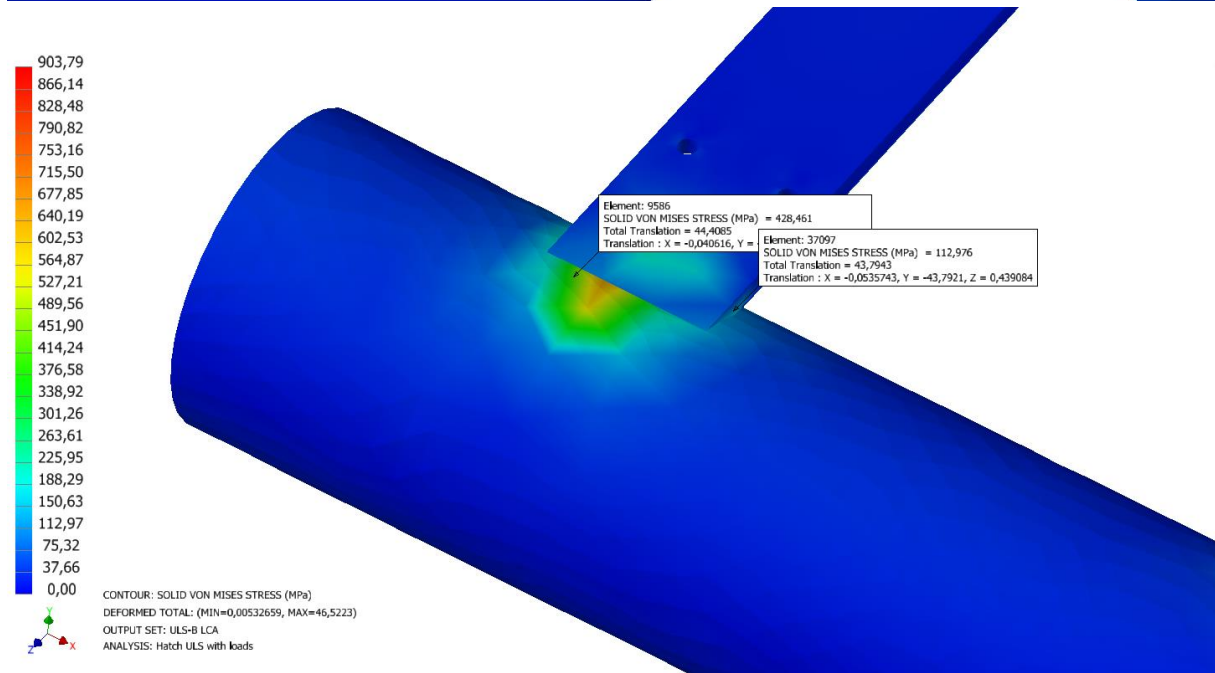
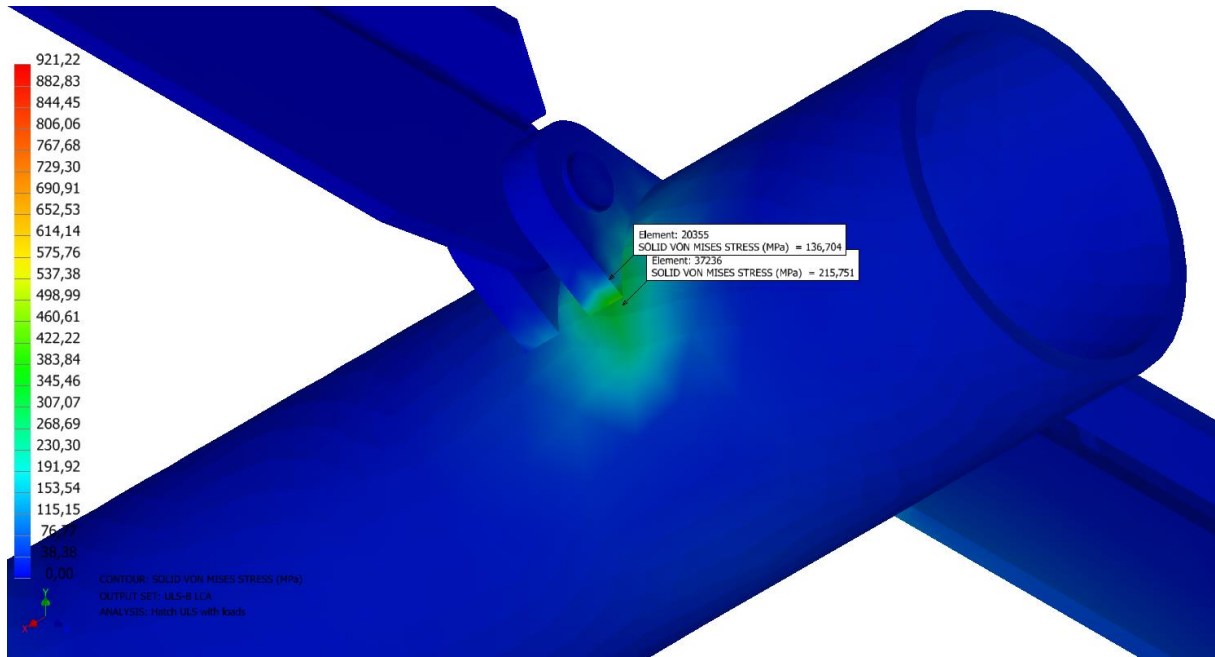


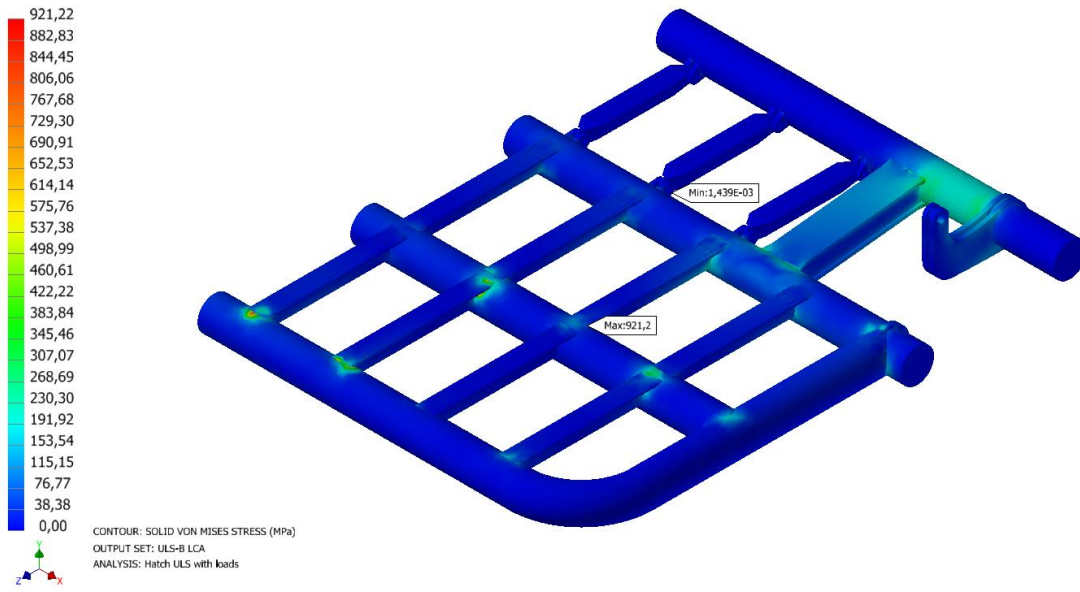




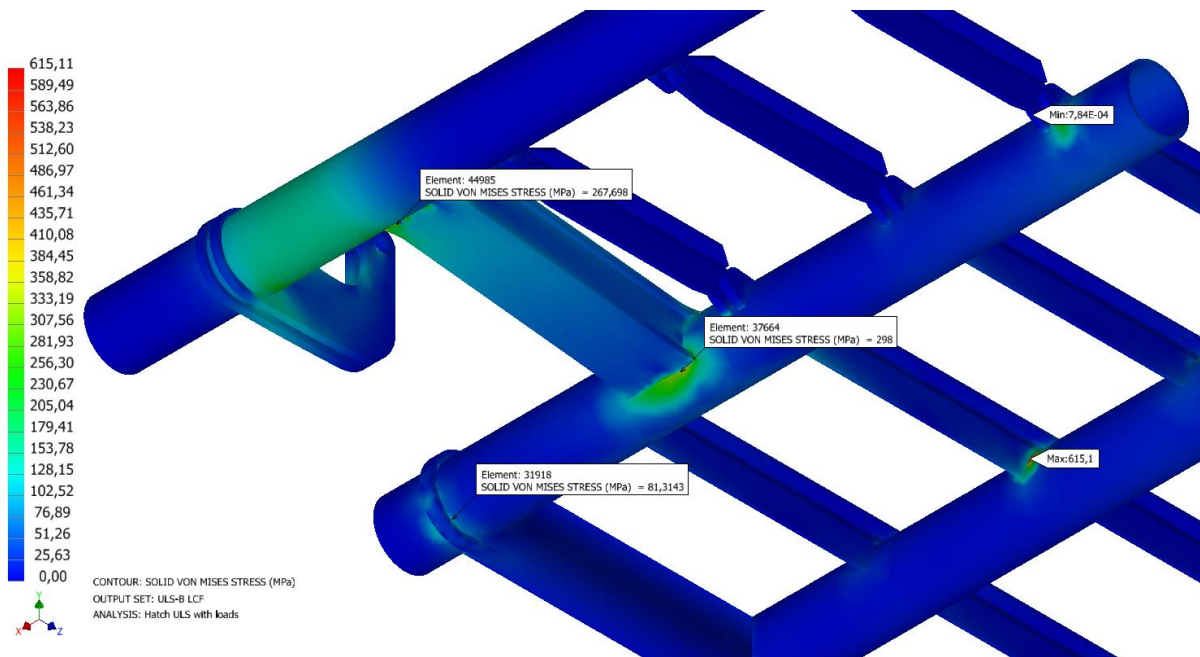
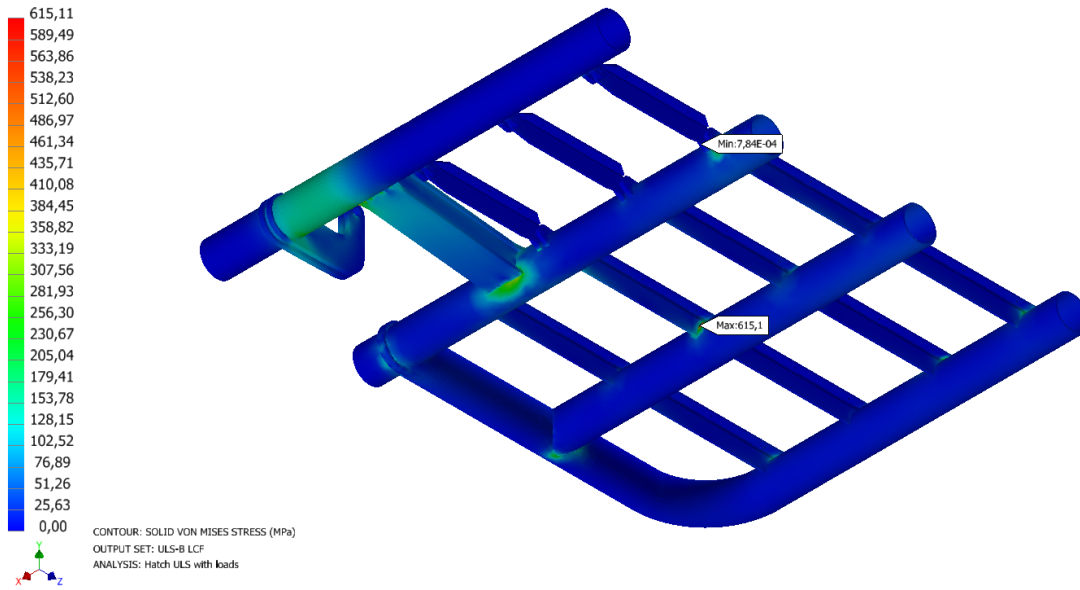
ULS-b LCA

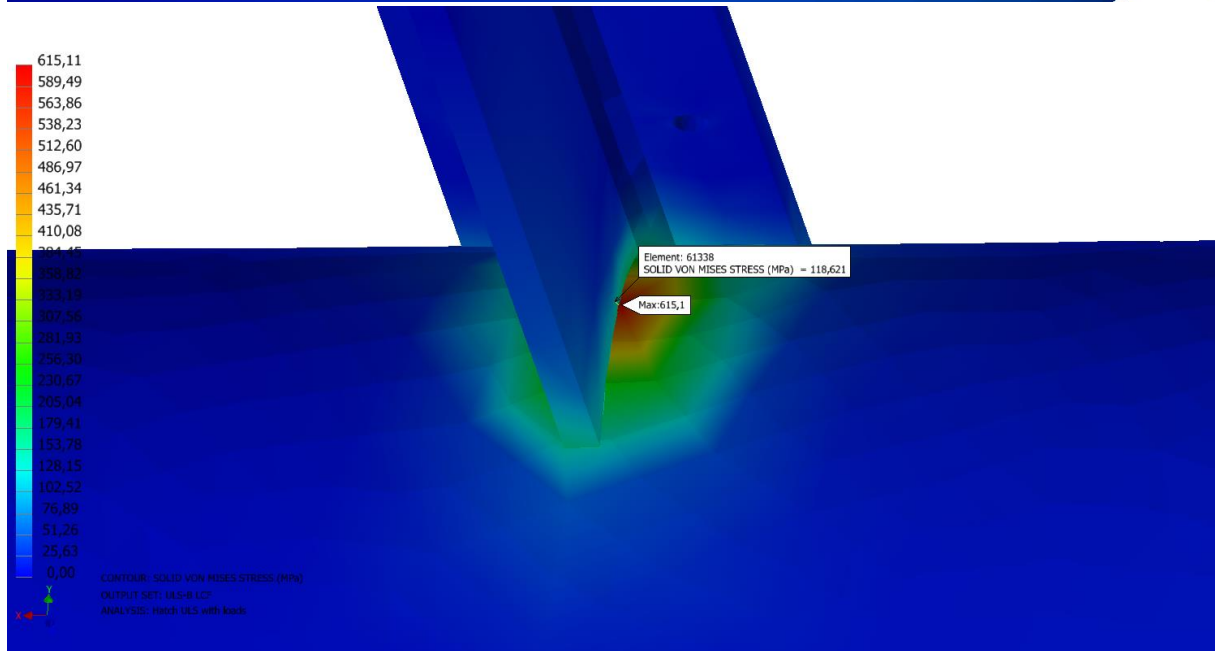
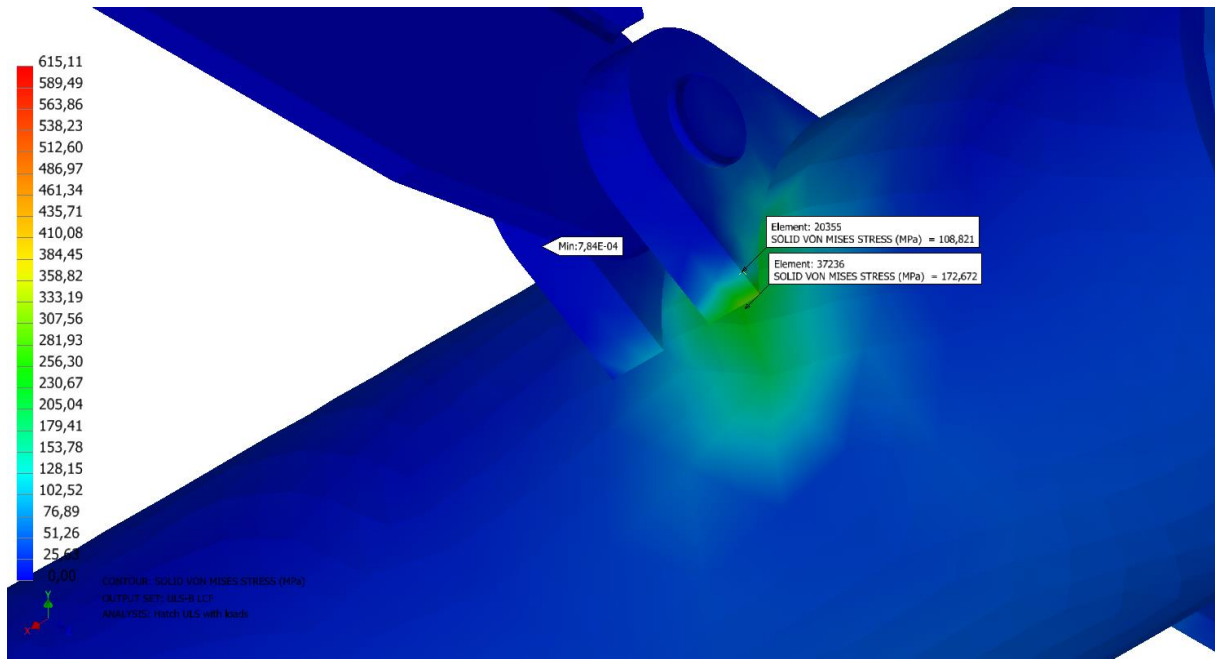


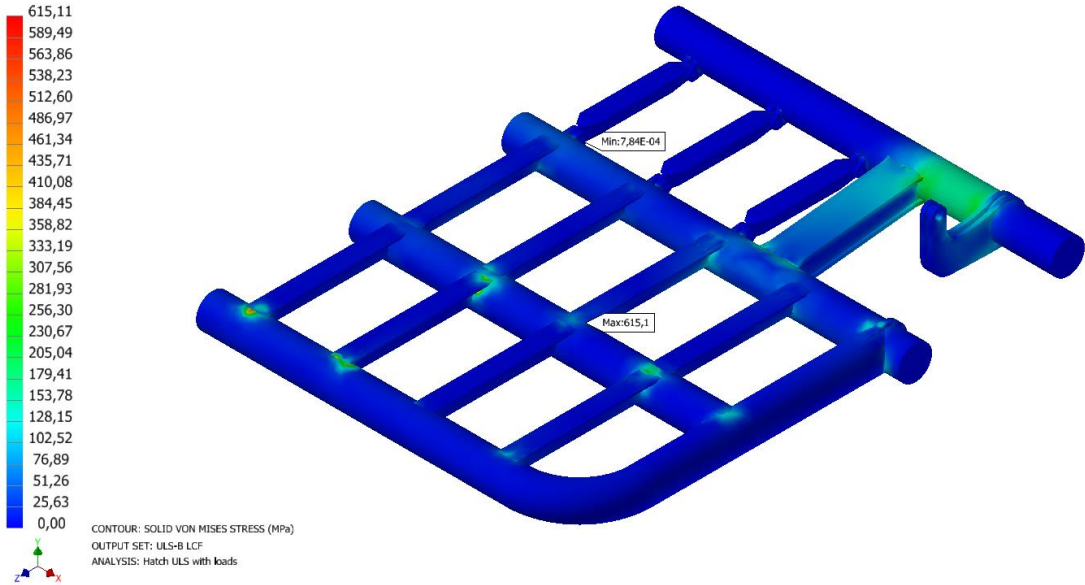




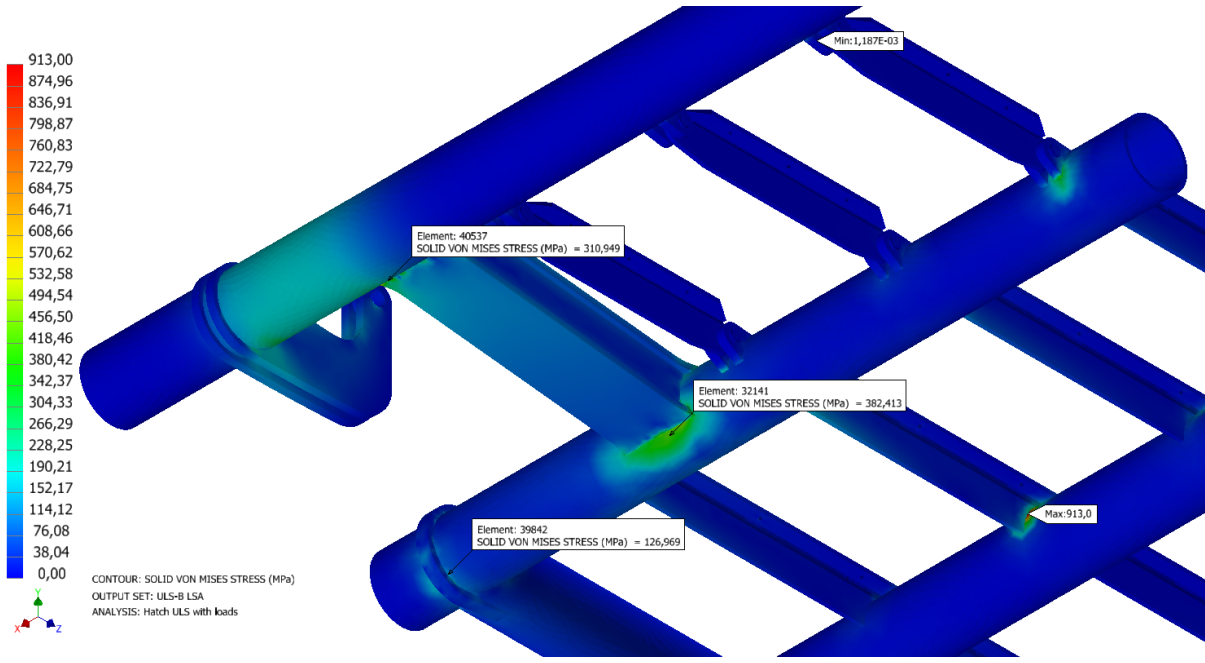
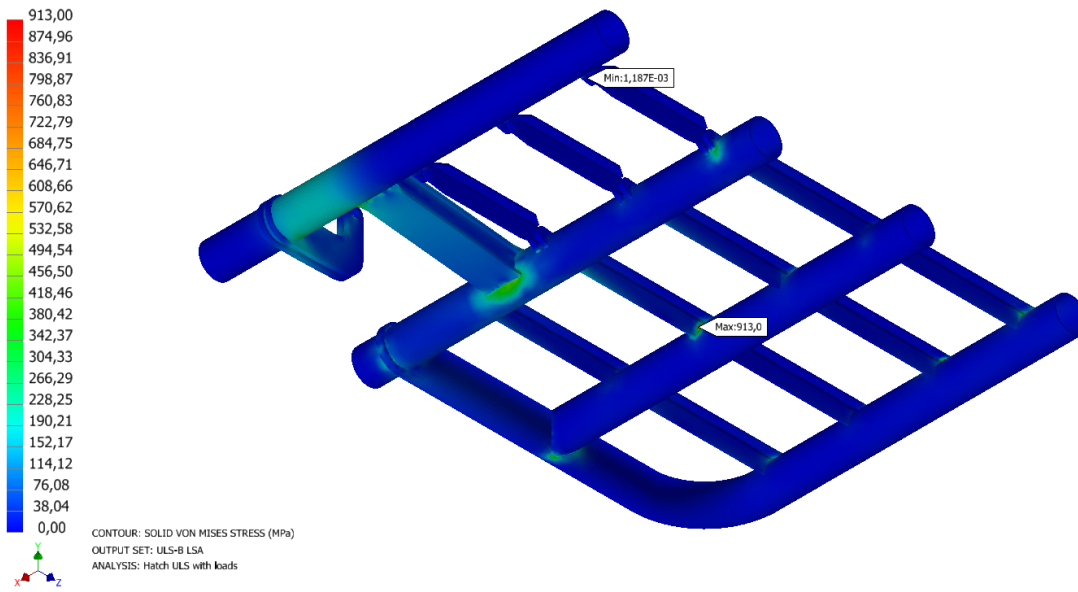
ULS-b LCF

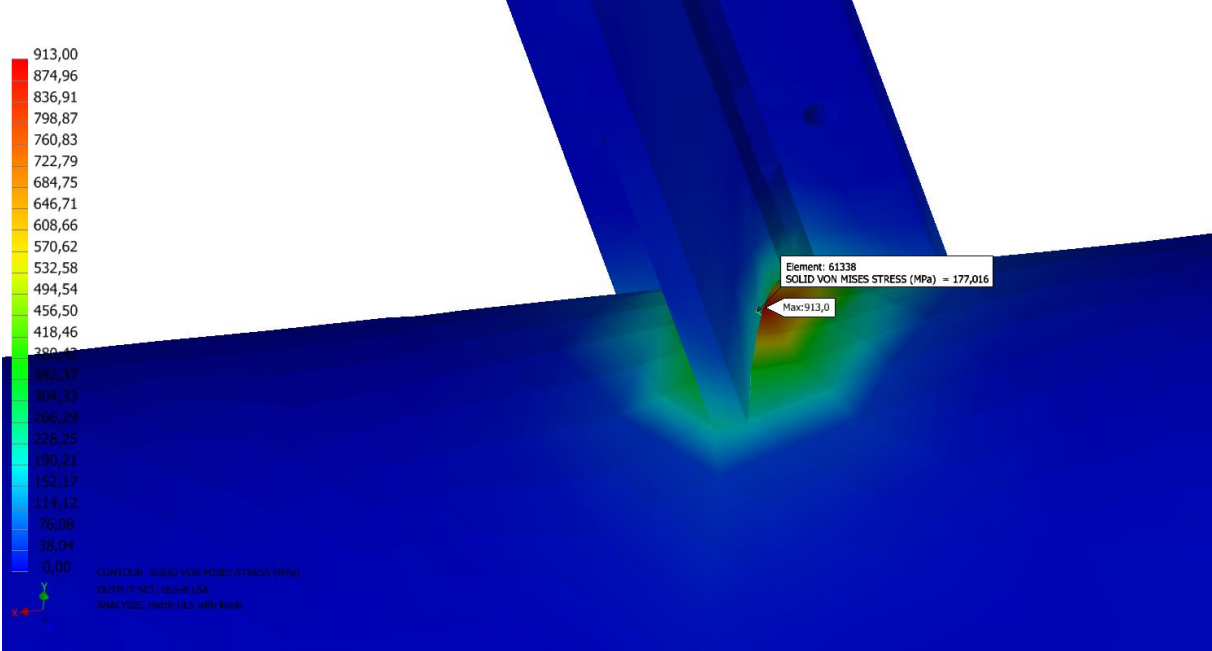
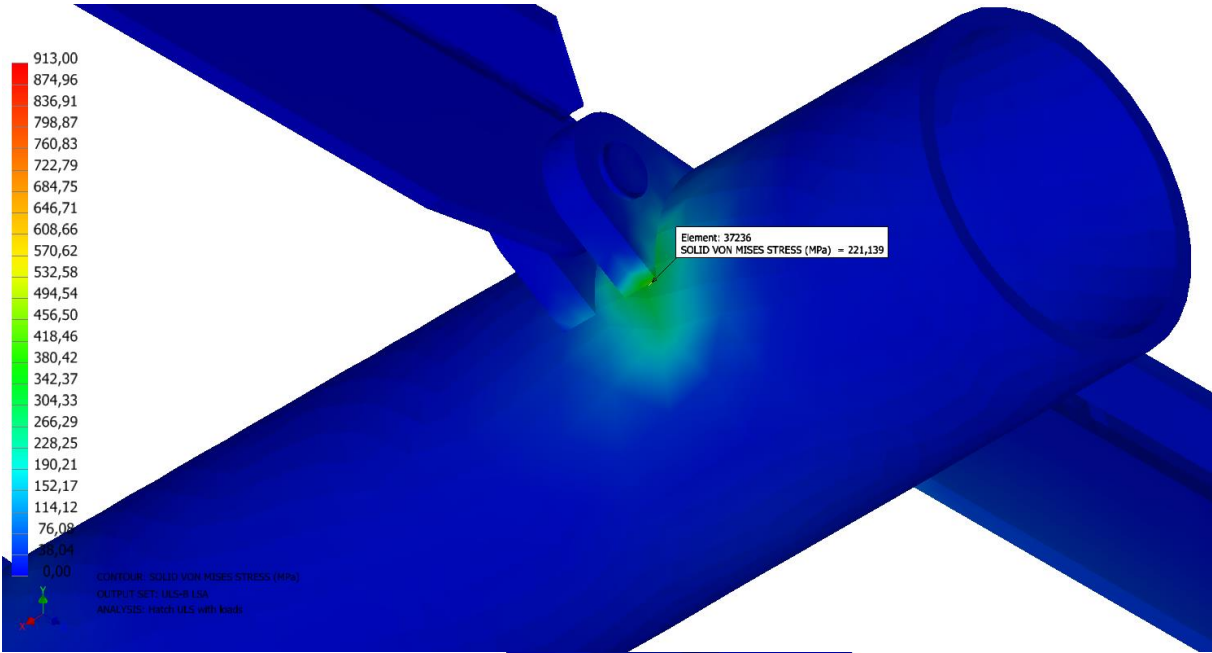


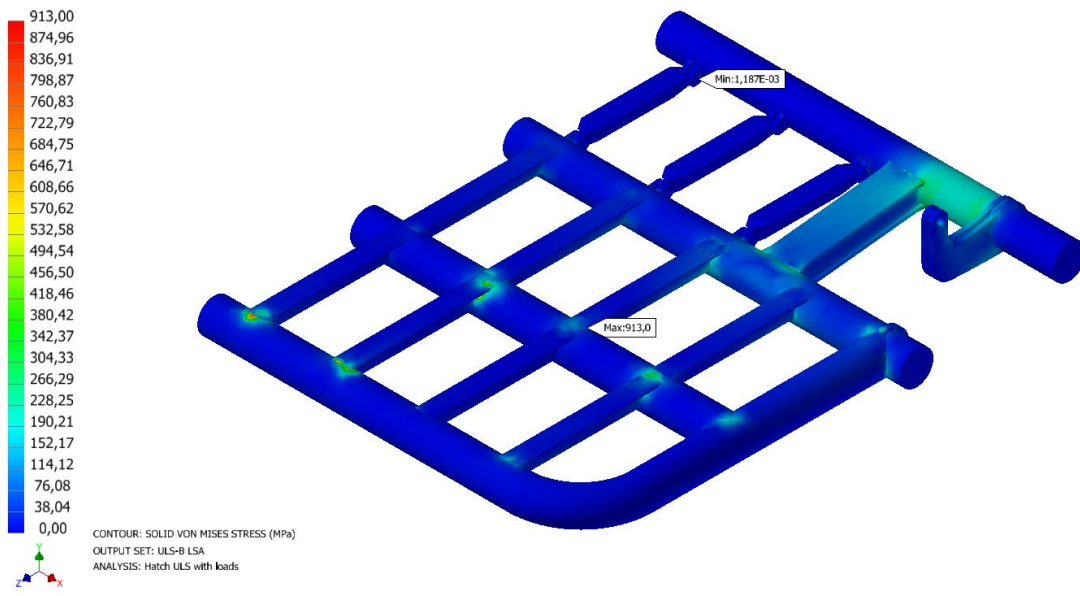




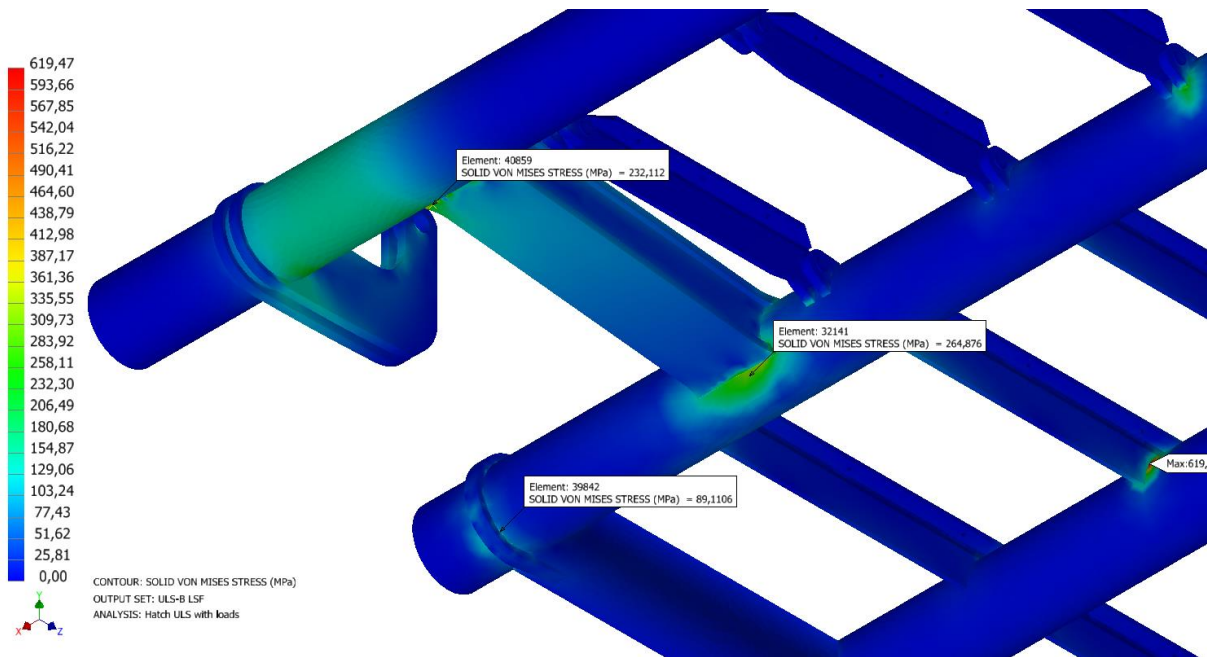
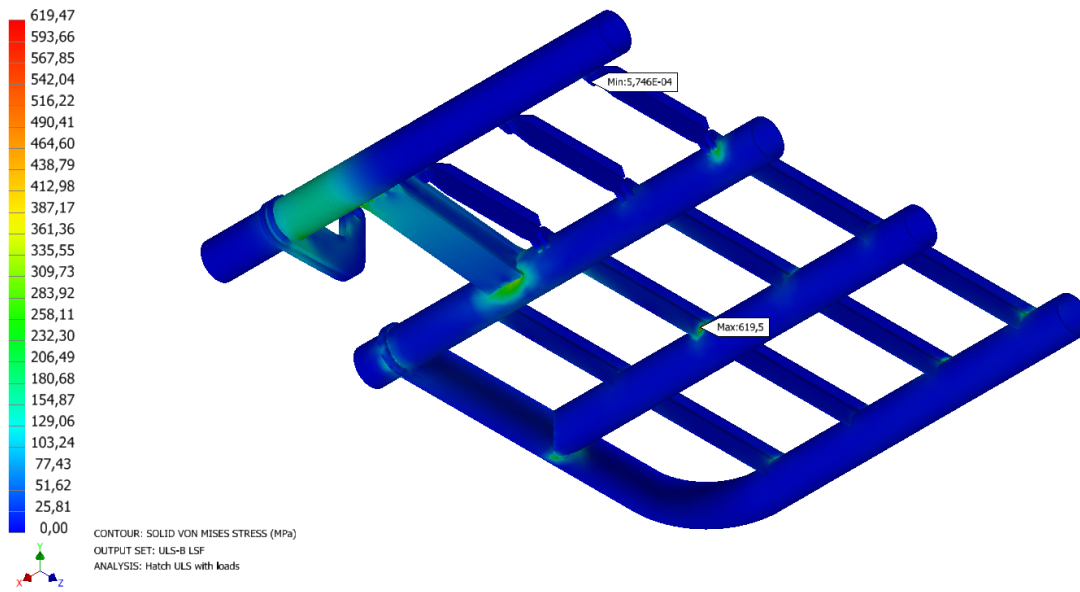
ULS-b LSA



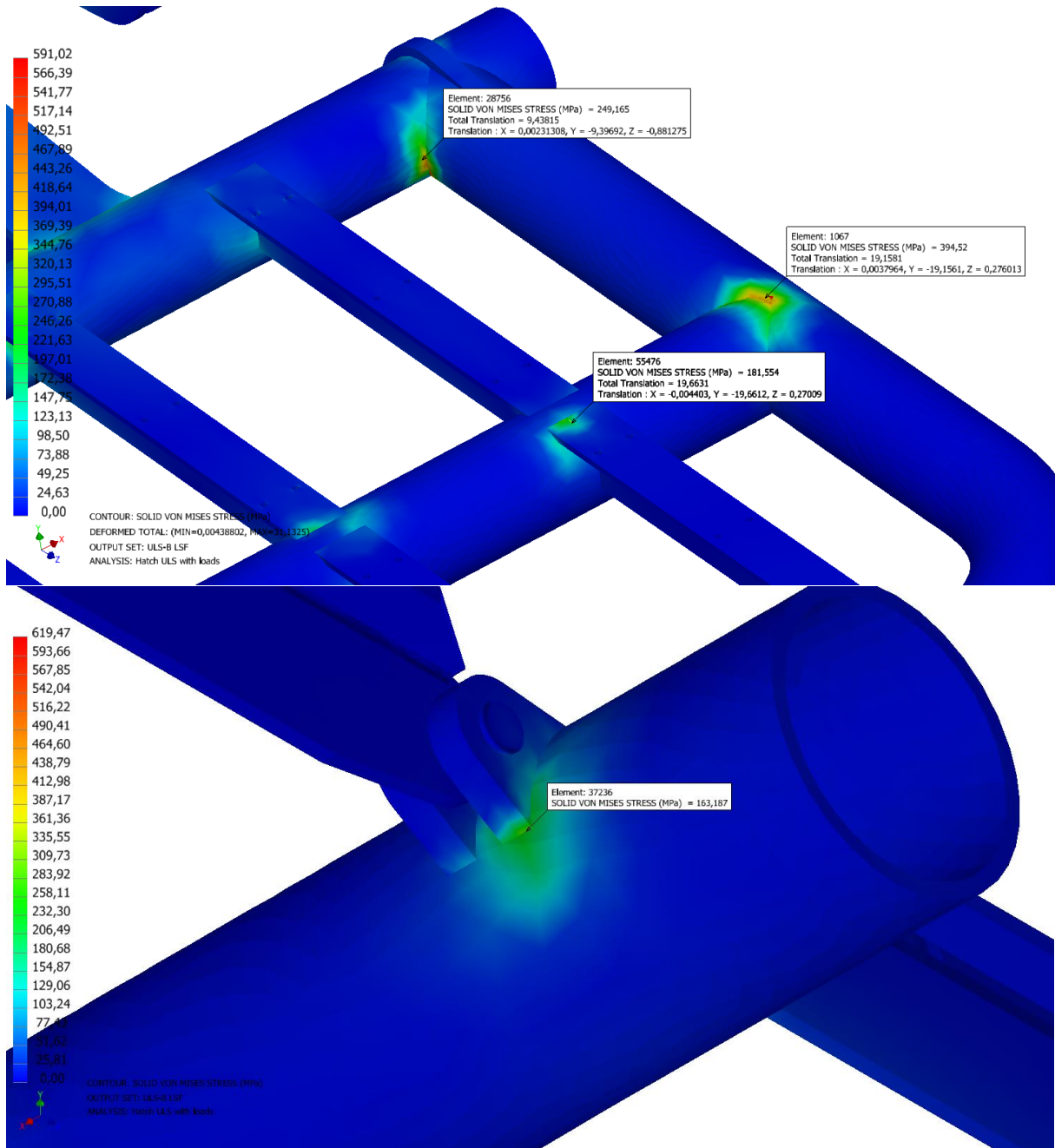


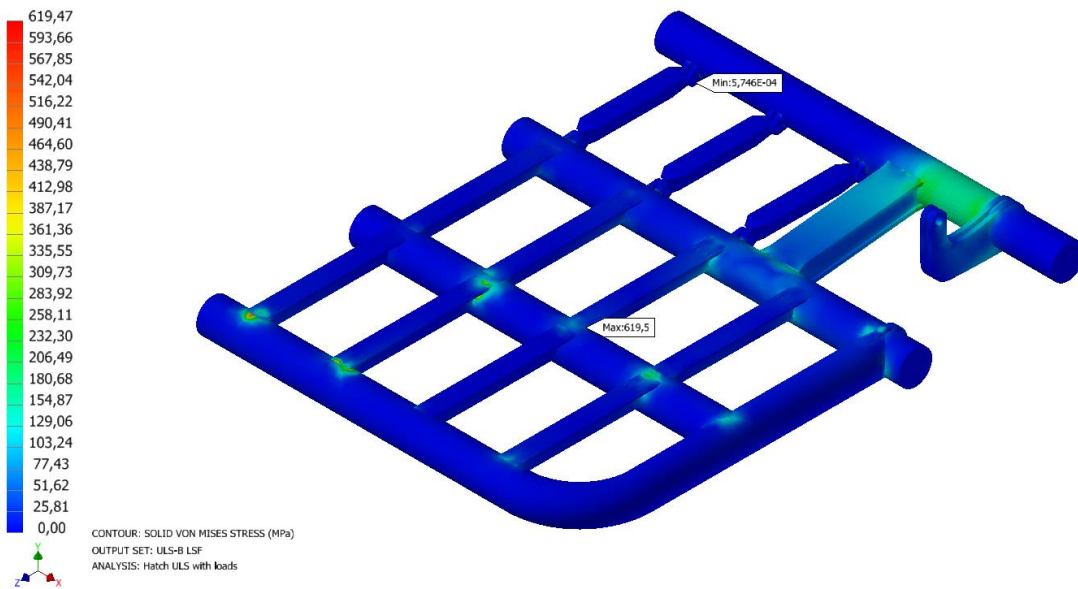
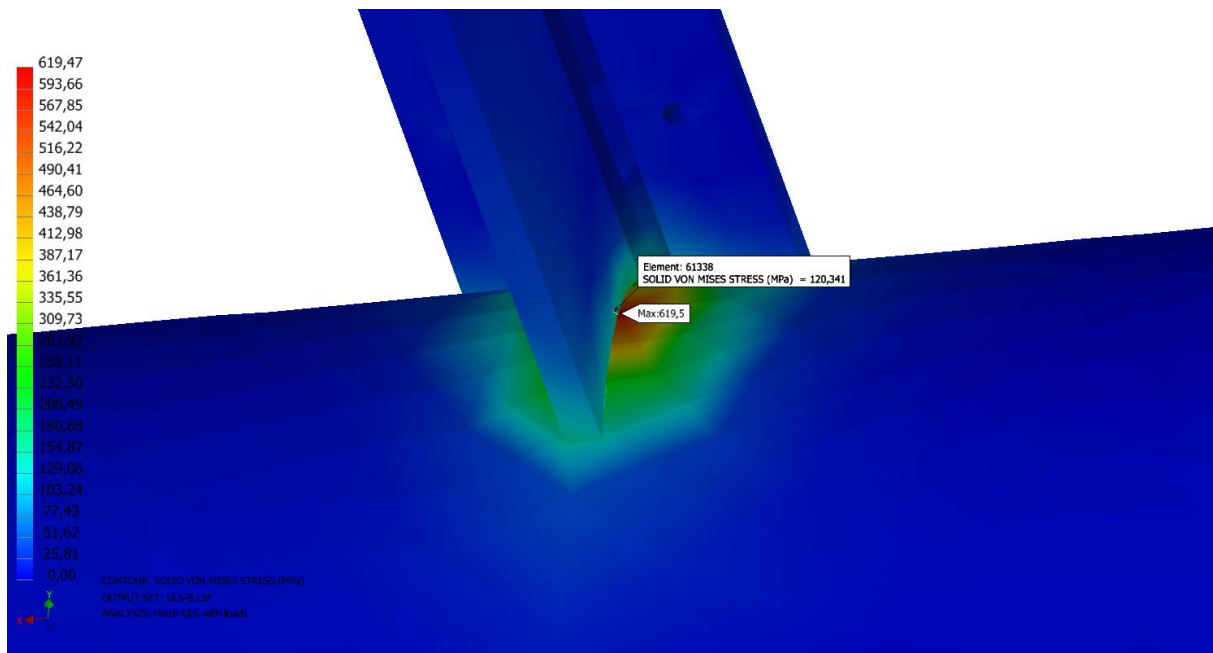


ULS-b LSF



Integration of a Skid and Hatch-Based Launch and Recovery System for ROVs on USVs





Appendix O Hand calculations of hatch

Deformation of hatch with "load center aft" LCA

Length from hinge at vessel to load: $L_L := 3.220 \text{ m}$

Load: $F_1 := 30000 \text{ N}$

E-modulus: $E_{st} := 2 \cdot 10^5 \cdot \text{MPa}$

G-modulus: $G_{st} := \frac{E_{st}}{2 \cdot (1 + 0.3)} = (7.692 \cdot 10^4) \text{ MPa}$

Dimensions of pipe 1 at vessel constraint:

Length of pipe 1 (hinged) experiencing torsion: $L_p := 5200 \text{ mm}$

Outer diameter: $OD_{p1} := 220 \text{ mm}$

Inner diameter: $ID_{p1} := 196 \text{ mm}$

Pipe inner area: $A_i := 7841$

Polar area moment pipe 1: $I_{p,r1} := \frac{\pi \cdot (OD_{p1}^4 - ID_{p1}^4)}{32} = (8.51 \cdot 10^7) \text{ mm}^4$

Polar resistance of moment pipe 1: $W_{p,r1} := \frac{2 \cdot I_{p,r1}}{OD_{p1}} = (7.736 \cdot 10^5) \text{ mm}^3$

Resistance of moment pipe 1: $W_{r1} := \frac{\pi \cdot (OD_{p1}^4 - ID_{p1}^4)}{32 \cdot OD_{p1}} = (3.868 \cdot 10^5) \text{ mm}^3$

Torsion in pipe 1: $T_{p1} := F_1 \cdot L_L = 96.6 \text{ kN} \cdot \text{m}$

Rotate section in pipe 1 (rad): $\alpha_{r1} := \frac{T_{p1} \cdot L_p}{G_{st} \cdot I_{p,r1}} = 0.07674$

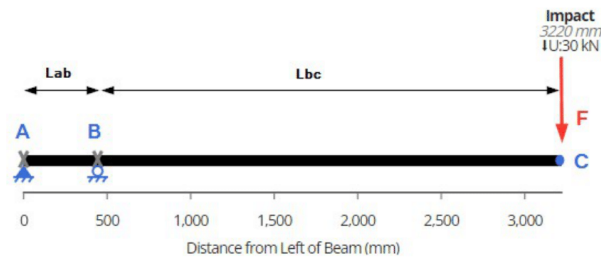
Deformation due to load: $\Delta y_{r1} := \alpha_{r1} \cdot L_L = 247.102 \text{ mm}$

Shear stress in pipe 1: $\tau_{r1} := \frac{T_{p1}}{W_{p,r1}} = 124.872 \text{ MPa}$

Bending stress in pipe 1: $\sigma_{b,r1} := \frac{F_1 \cdot L_p}{W_{r1}} = 403.314 \text{ MPa}$

Von Mises Stress in pipe 1: $\sigma_{eq,p1} := \sqrt{\sigma_{b,r1}^2 + 3 \cdot \tau_{r1}^2} = 457.647 \text{ MPa}$

Beam static calculations



Lengths:

$$L_{ab} := 0.443 \text{ m} \quad L_{bc} := 2.777 \text{ m}$$

Sum of moments around point B:

$$\Sigma M_B := R_a \cdot L_{ab} - F_1 \cdot L_{bc}$$

Reaction force Ra:

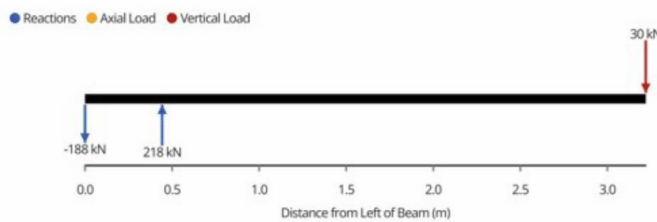
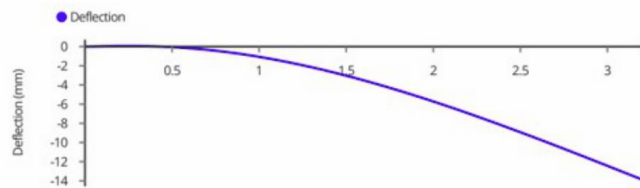
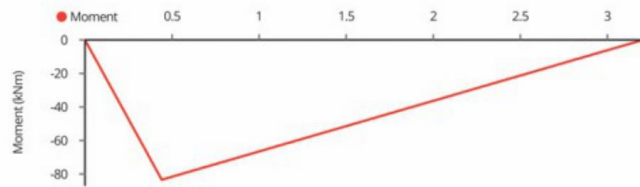
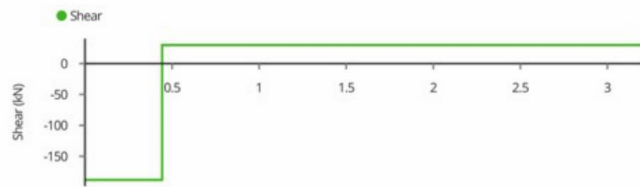
$$R_a := -F_1 \cdot \frac{L_{bc}}{L_{ab}} = -1.881 \cdot 10^5 \text{ N}$$

Sum of forces in y-dir.:

$$\Sigma F_y := R_a + R_b - 30 \text{ kN}$$

Reaction force Rb:

$$R_b := -R_a + 30 \text{ kN} = (2.181 \cdot 10^5) \text{ N}$$



Appendix P Skid stress analysis

Load case 2

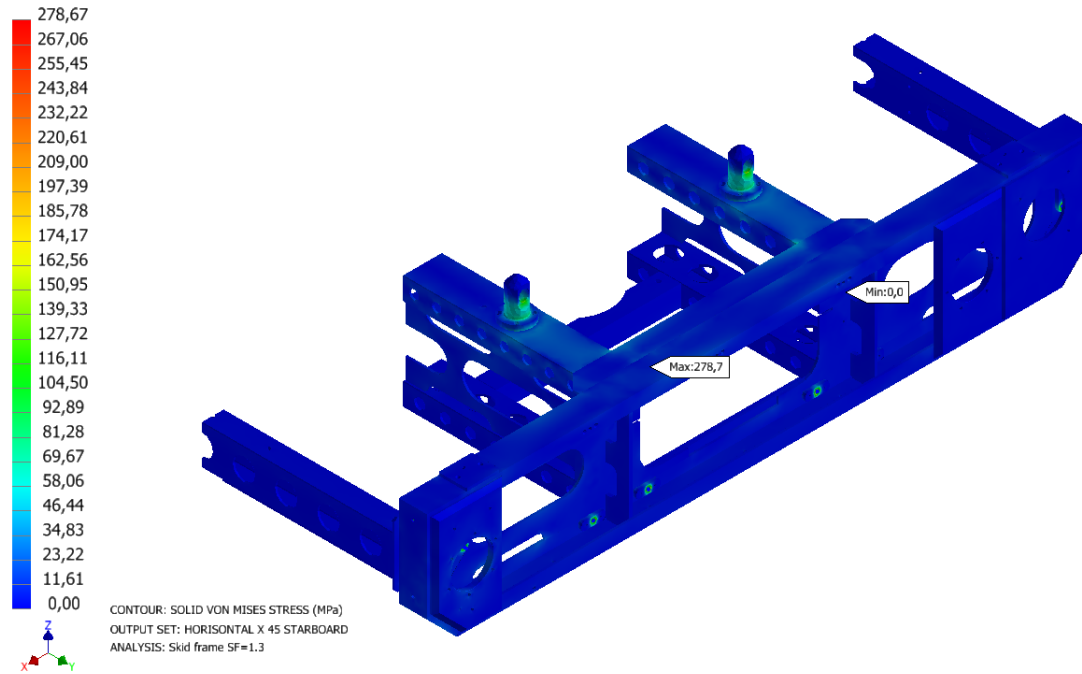


Figure 1 Skid LCI von Mises stress

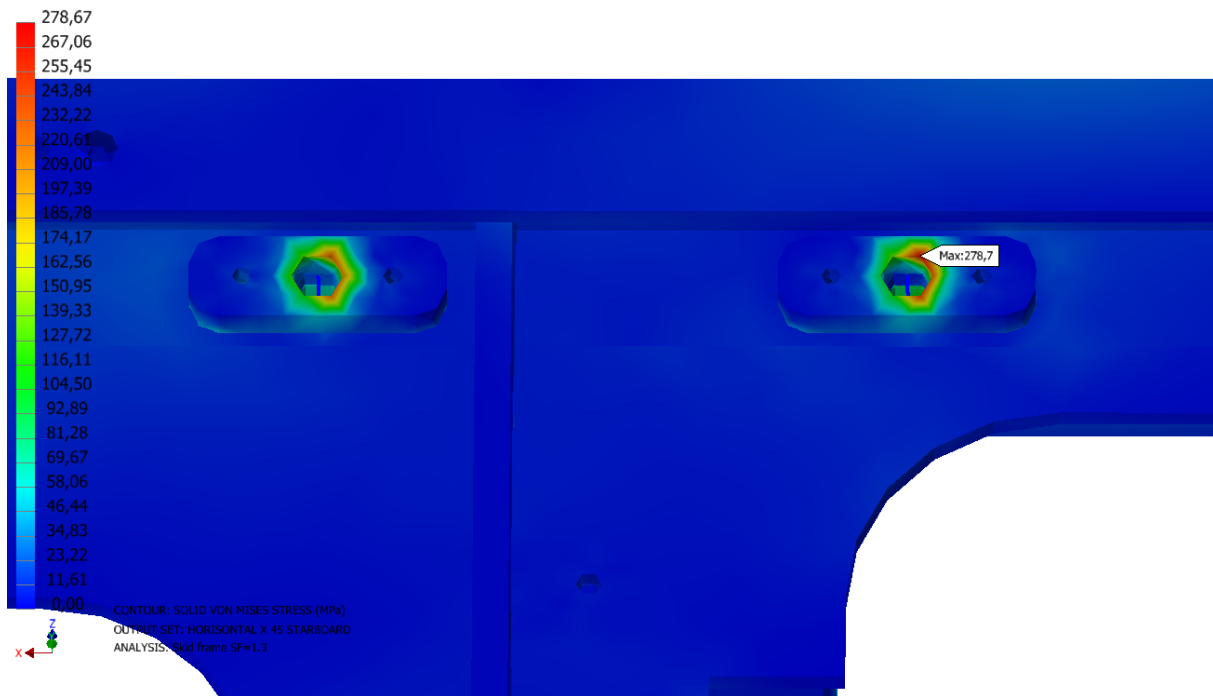


Figure 2 Skid LCI max von Mises stress.

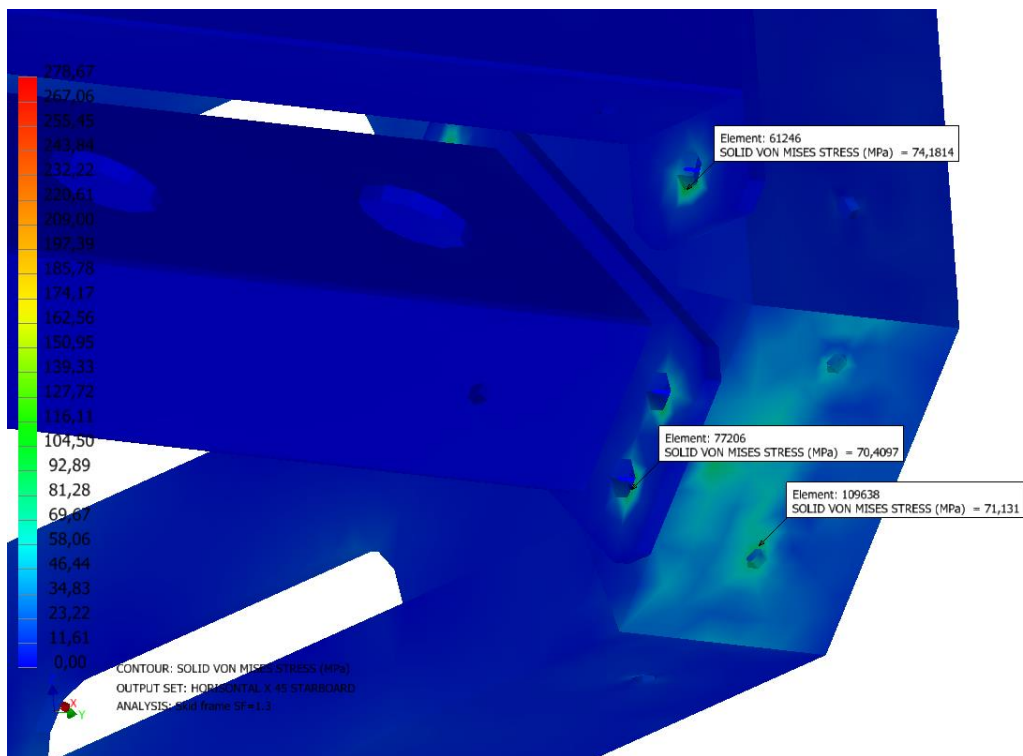


Figure 3 Skid LC1 von Mises stress at load location

Load case 3

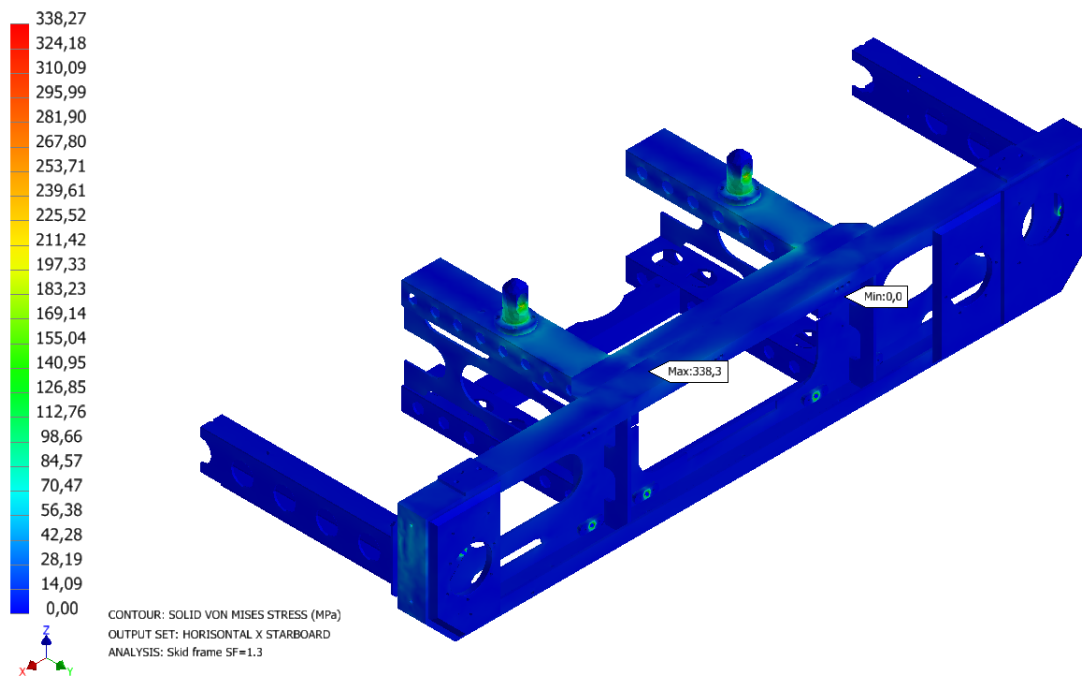
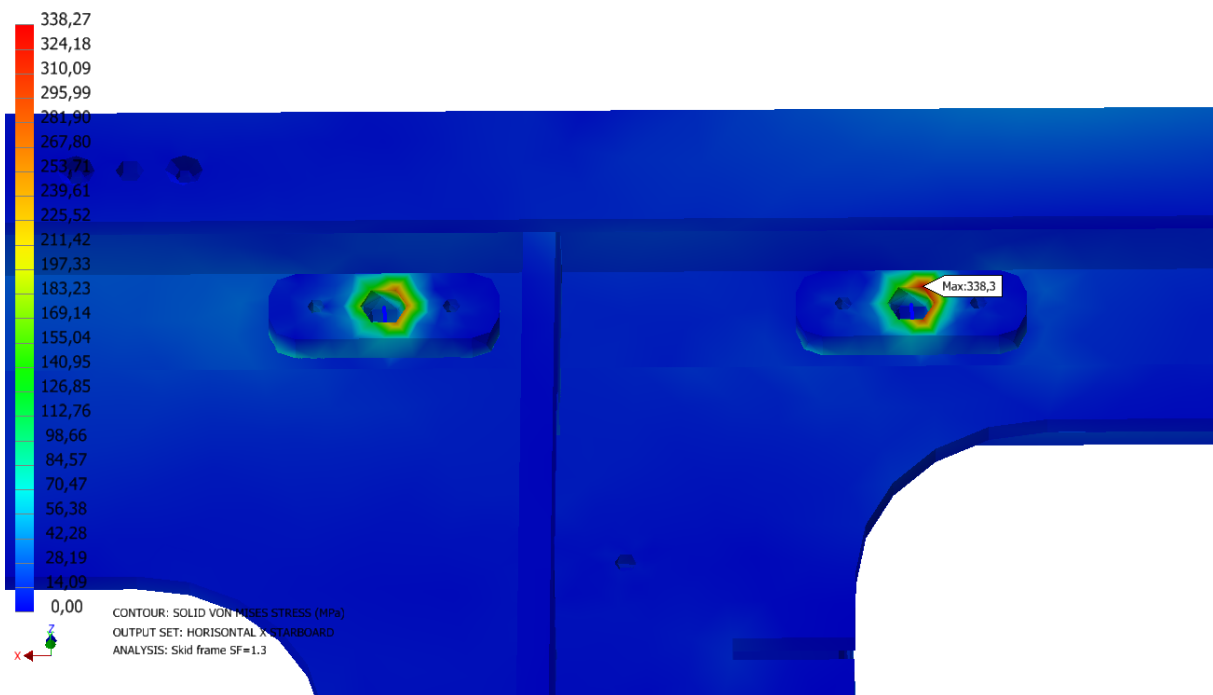
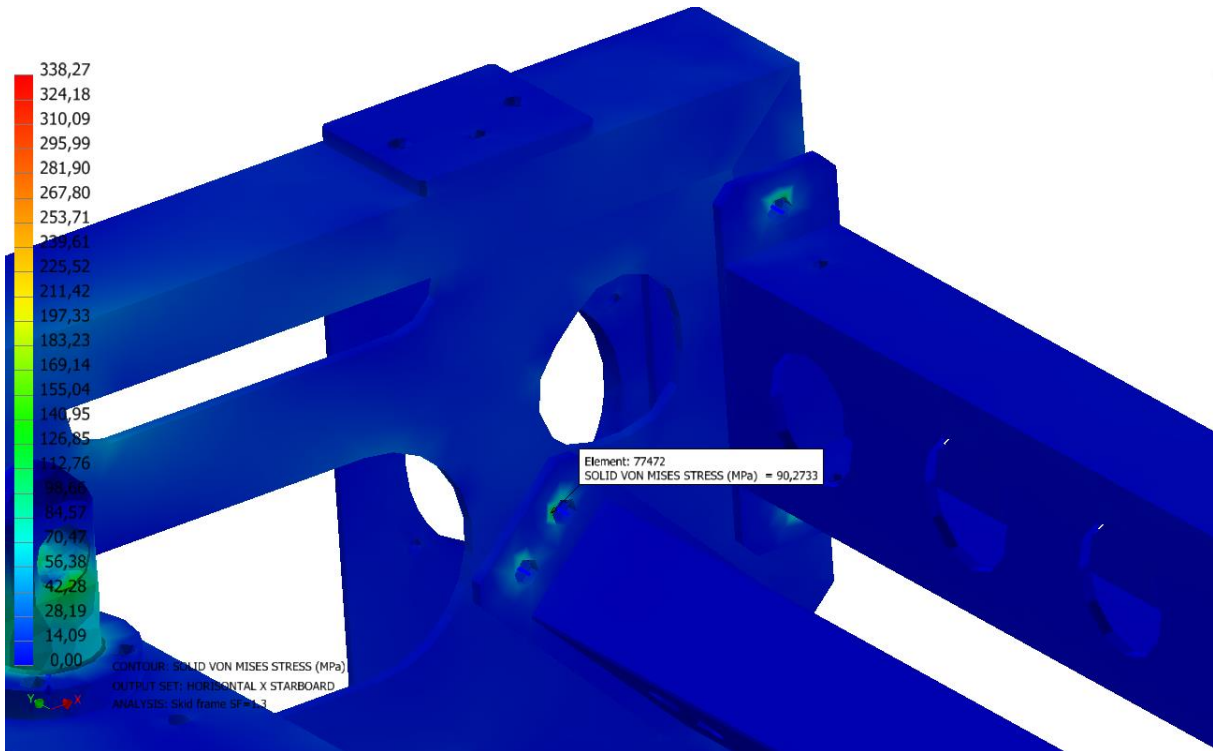
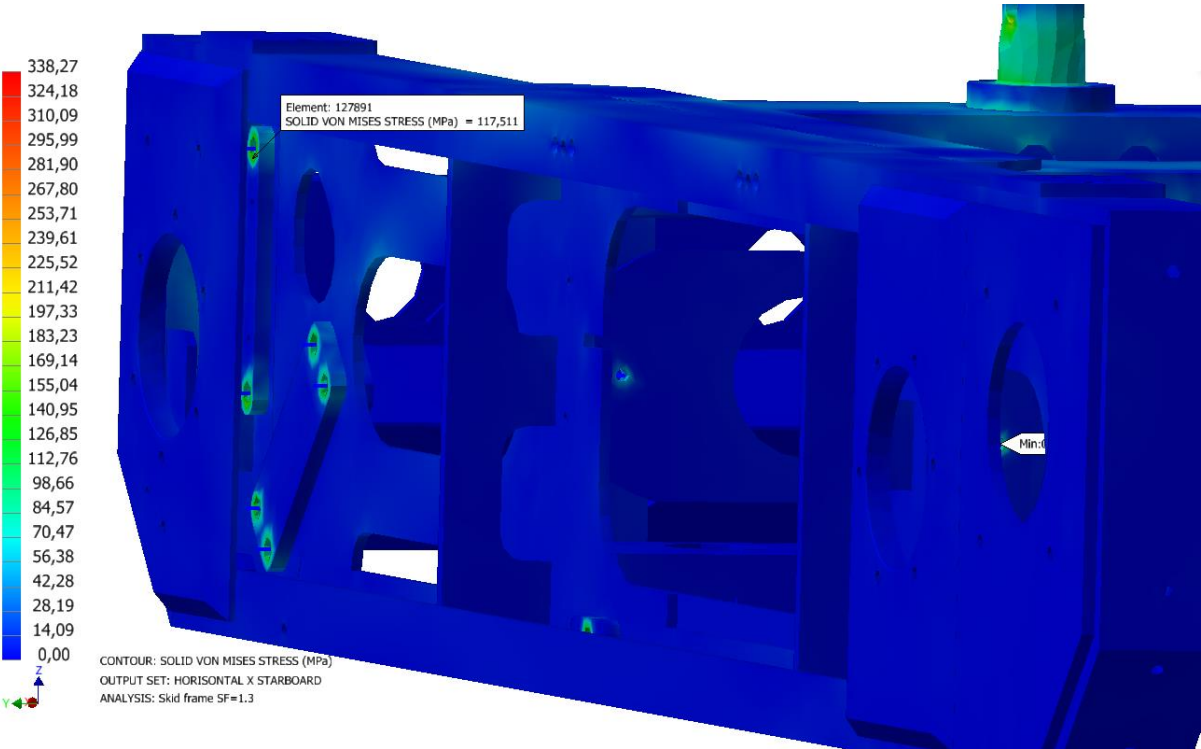


Figure 4 Skid LC2 von Mises stress

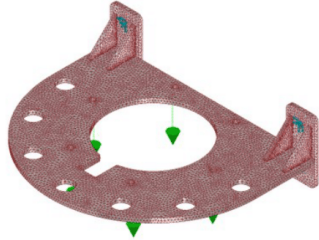




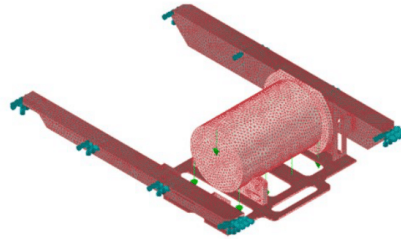
Appendix Q Force calculations of selected structural items

1 Kinetic energy to force calculations for selected parts analysis

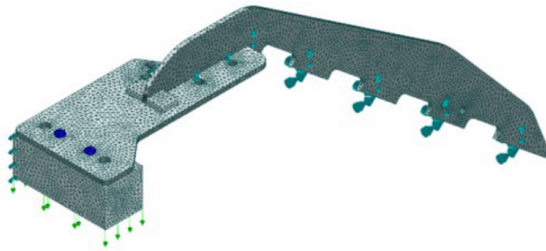
Doppler with INS holder:



MUX drawer:



Top beam:



2 Input Parameters

Relative velocity between USV and ROV:

$$v := 0.45 \frac{m}{s}$$

Weight of MUX:

$$m_{MUX} := 17 \text{ kg}$$

Weight of doppler:

$$m_{Doppler} := 11.4 \text{ kg}$$

Weight of MBE heads:

$$m_{MBE} := 5.7 \text{ kg}$$

Weight of beam:

$$m_B := 12.92 \text{ kg}$$

Weight of lasers:

$$m_{laser} := 2 \text{ kg} \cdot 3 = 6 \text{ kg}$$

Weight of CTD:

$$m_{CTD} := 0.8 \text{ kg}$$

Weight of Tx/Rx:

$$m_{TxRx} := 2 \text{ kg} \cdot 2 = 4 \text{ kg}$$

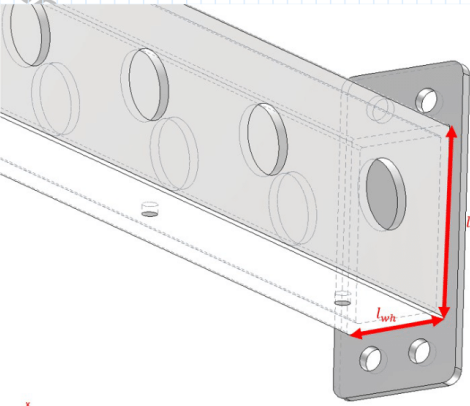
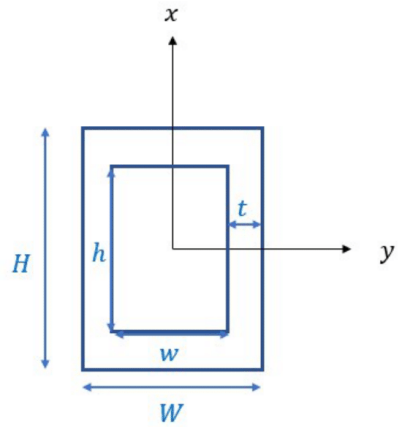
Total weight for top beam

$$m_{tot} := m_{MBE} + m_B + m_{laser} + m_{CTD} + m_{TxRx}$$

2 Kinetic energy and elastic energy to forces		
Kinetic energy of MUX:	$E_{k.MUX} := 0.5 \cdot m_{MUX} \cdot v^2$	$E_{k.MUX} = 1.721 \text{ J}$
Elastic potential energy in MUX drawer:	$U_{p.MUX} := 0.5 \cdot 2.6 \text{ kN} \cdot 1.317 \text{ mm} = 1.712 \text{ J}$	$U_{p.MUX} = 1.712 \text{ J}$
		$F_{MUX} := 2.6 \text{ kN}$
Kinetic energy of doppler:	$E_{k.Doppler} := 0.5 \cdot m_{Doppler} \cdot v^2$	$E_{k.Doppler} = 1.154 \text{ J}$
Elastic potential energy in doppler holder:	$U_{p.Doppler} := 0.5 \cdot 1.18 \text{ kN} \cdot 1.96 \text{ mm} = 1.156 \text{ J}$	$U_{p.Doppler} = 1.156 \text{ J}$
		$F_{Doppler} := 1.18 \text{ kN}$
Kinetic energy of sensors and beam:	$E_{k.B} := 0.5 \cdot \frac{m_{tot}}{2} \cdot v^2$	$E_{k.B} = 1.489 \text{ J}$
Elastic potential energy in beam:	$U_{p.B} := 0.5 \cdot 2.13 \text{ kN} \cdot 1.397 \text{ mm}$	$U_{p.B} = 1.488 \text{ J}$
		$F_B := 2.13 \text{ kN}$

Appendix S Weld check of critical weld 1

1 Weld section 1

2 Assumptions

- Conservatively let the moment be taken by the horizontal welds by making a force couple of the moment. Vertical load are taken by the vertical welds.
- Assume fixed support at each end with load applied at L/2 of beam.

2 Input Parameters

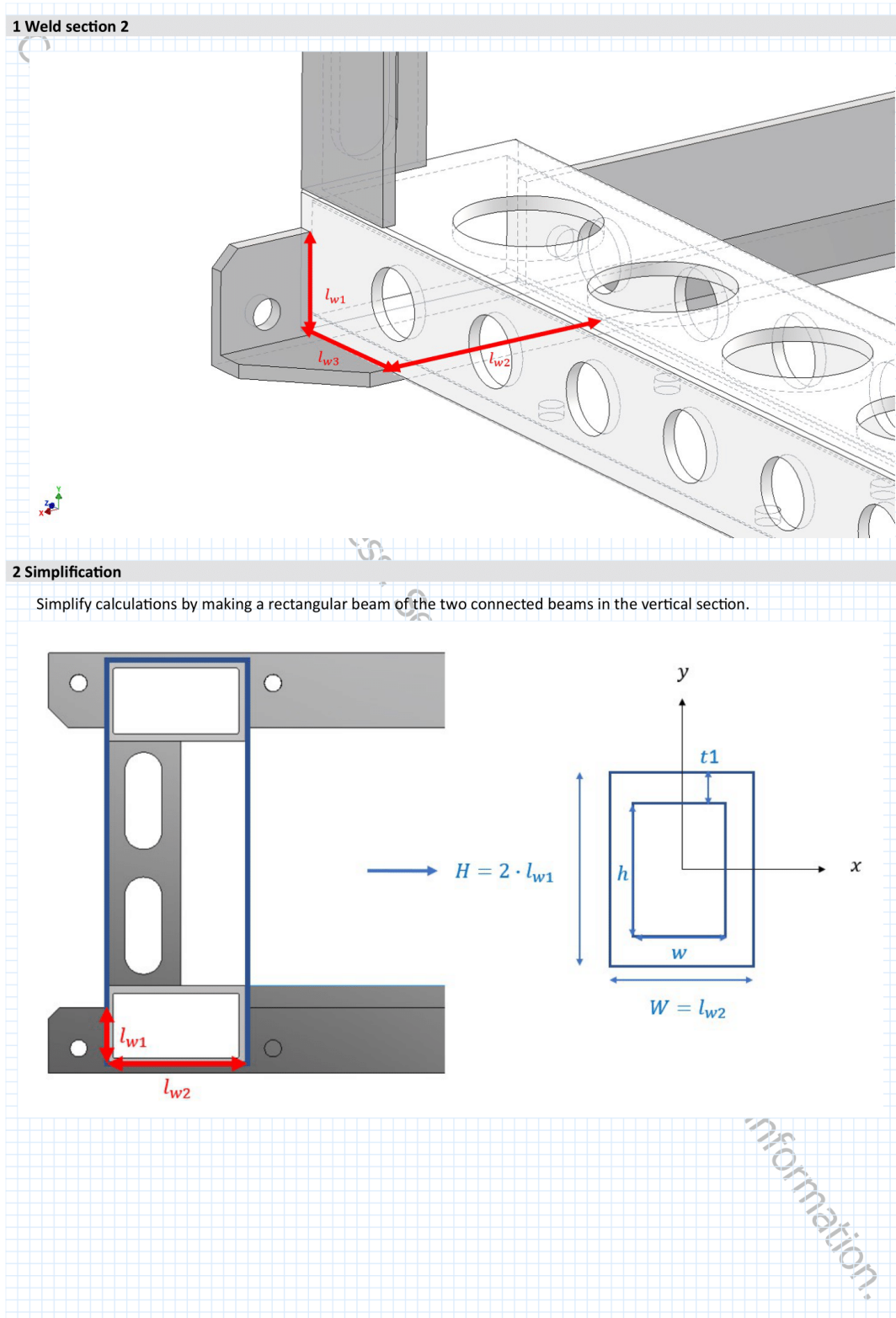
Height of beam:	$H := 140 \text{ mm}$	
Width of beam:	$W := 80 \text{ mm}$	
Thickness of beam:	$t := 7 \text{ mm}$	
Inner height	$h := H - 2 t = 126 \text{ mm}$	
Inner width:	$w := W - 2 t = 66 \text{ mm}$	
Length of horizontal weld:	$l_{wh} := W = 80 \text{ mm}$	
Length of vertical weld:	$l_{wv} := H = 140 \text{ mm}$	
Weld throat thickness:	$a := 8 \text{ mm}$	
Number of welds:	$n_w := 2$	
Material yield strength:	$f_{u,haz} := 185 \text{ MPa}$	
Material Factor for Weld	$\gamma_{mw} := 1.3$	
Length from weld to load:	$L_1 := 677 \text{ mm}$	

3 Intermediate Calculations

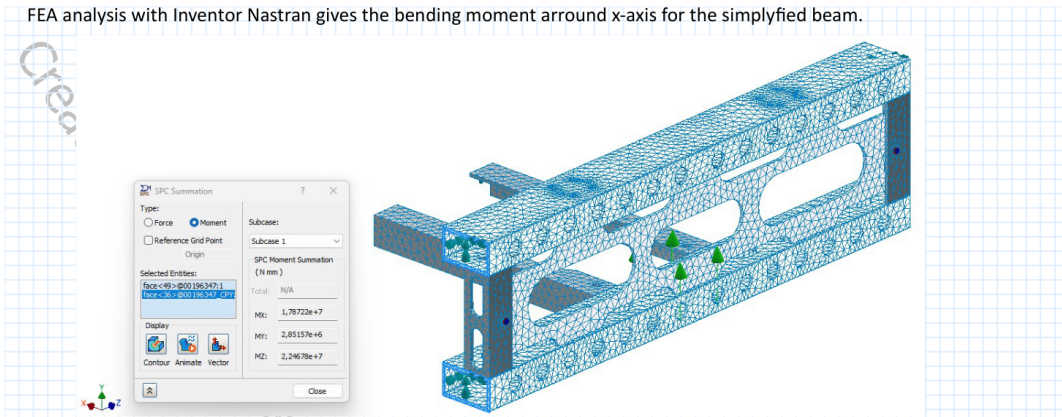
Allowable stress:	$f_{all} := \frac{f_{u,haz}}{\gamma_{mw}}$	$f_{all} = 142.308 \text{ MPa}$
Effective horizontal weld length:	$l_{wh,eff} := l_{wh} - 2 \cdot a$	$l_{wh,eff} = 64 \text{ mm}$
Effective vertical weld length:	$l_{wv,eff} := l_{wv} - 2 \cdot a$	$l_{wv,eff} = 124 \text{ mm}$
Axial Section modulus:	$W_{ey} := \frac{(W + 2 a) \cdot (H + 2 a)^3 - (w + 2 a) \cdot (h + 2 a)^3}{6 \cdot (H + 2 a)}$	$W_{ey} = 138532.393 \text{ mm}^3$
Cross sectional area:	$A := W \cdot H - w \cdot h$	$A = 2884 \text{ mm}^2$
Vertical shear area:	$A_s := \frac{A \cdot H}{(W + H)}$	$A_s = 1835.273 \text{ mm}^2$

4 Forces Considered		
ULS-b vertical force impact:	$F_Y := 78 \text{ kN} = 78 \text{ kN}$	
Moment due to vertical force:	$M_V := F_Y \cdot \frac{L_l}{8} = 6.601 \text{ kN} \cdot \text{m}$	
Distance between horizontal welds:	$d_h := H$	$d_h = 140 \text{ mm}$
Axial force due to moment on horizontal weld:	$F_h := \frac{M_V}{d_h}$	$F_h = 47.148 \text{ kN}$
5 Horizontal Weld Stress		
Axial stress to the horizontal weld:	$\sigma_a := \frac{F_h}{\sqrt{2} \cdot l_{wh,eff} \cdot a}$	$\sigma_a = 65.115 \text{ MPa}$
	$\tau_n := \sigma_a$	$\tau_n = 65.115 \text{ MPa}$
Equivalent von-Mises stress:	$\sigma_{vm} := \sqrt{\sigma_a^2 + 3 \cdot \tau_n^2}$	$\sigma_{vm} = 130.2 \text{ MPa}$
Utilization Factor:	$\eta_h := \frac{\sigma_{vm}}{f_{all}} = 0.915$	
6 Vertical Weld Stress		
Shear stress:	$\tau_{par} := \frac{F_Y}{n_w \cdot a \cdot l_{vw,eff}}$	$\tau_{par} = 39.3 \text{ MPa}$
Equivalent von-Mises stress:	$\sigma_{vm} := \sqrt{3 \cdot \tau_{par}^2}$	$\sigma_{vm} = 68.1 \text{ MPa}$
Utilization Factor:	$\eta_v := \frac{\sigma_{vm}}{f_{all}} = 0.479$	
6 Check of connection weld stress		
Bending stress to the horizontal weld:	$\sigma_b := \frac{M_V}{\sqrt{2} \cdot W_{ey}}$	$\sigma_b = 33.692 \text{ MPa}$
	$\tau_n := \sigma_b$	$\tau_n = 33.692 \text{ MPa}$
Shear stress:	$\tau_{par} := \frac{F_Y}{A_s}$	$\tau_{par} = 42.5 \text{ MPa}$
Equivalent von-Mises stress:	$\sigma_{vm} := \sqrt{\sigma_b^2 + 3 \cdot \tau_n^2 + 3 \cdot \tau_{par}^2}$	$\sigma_{vm} = 99.8 \text{ MPa}$
Utilization Factor:	$\eta_c := \frac{\sigma_{vm}}{f_{all}} = 0.701$	

Appendix T Weld check of critical weld 2



FEA analysis with Inventor Nastran gives the bending moment around x-axis for the simplified beam.



3 Assumptions

- Conservatively let the moment be taken by the horizontal welds by making a force couple of the moment. Vertical load are taken by the vertical welds.
- Symmetry in the model divide the the load present in each weld in two, with load applied at L/2 of beam.

4 Input Parameters

Length of horizontal weld:	$l_{wh} := 140 \text{ mm}$
Length of vertical weld:	$l_{wv} := 58 \text{ mm}$
Thickness of beam:	$t := 7 \text{ mm}$
Height of beam:	$H := 2 \cdot l_{wv} = 116 \text{ mm}$
Width of beam:	$W := 140 \text{ mm}$
Inner height	$h := H - 2 \cdot t = 102 \text{ mm}$
Inner width:	$w := W - 2 \cdot t = 126 \text{ mm}$
Weld throath thickness:	$a := 6 \text{ mm}$
Number of welds:	$n_w := 2$
Material yield strength:	$f_{u,haz} := 185 \text{ MPa}$
Material Factor for Weld	$\gamma_{mw} := 1.3$

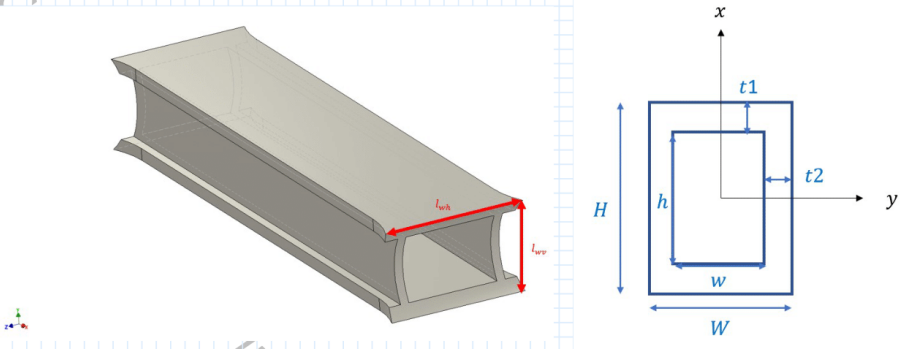
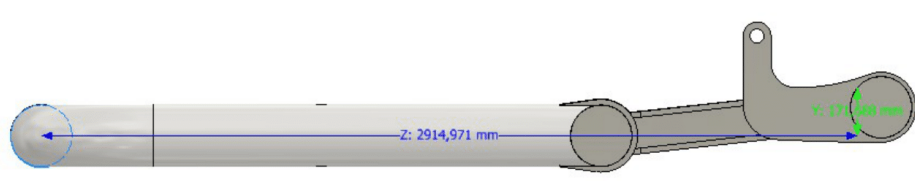
5 Intermediate Calculations

Allowable stress:	$f_{all} := \frac{f_{u,haz}}{\gamma_{mw}}$	$f_{all} = 142.308 \text{ MPa}$
Effective horizontal weld length:	$l_{wh,eff} := l_{wh} - 2 \cdot a$	$l_{wh,eff} = 128 \text{ mm}$
Effective vertical weld length:	$l_{wv,eff} := l_{wv} - 2 \cdot a$	$l_{wv,eff} = 46 \text{ mm}$
Axial Section modulus:	$W_{ey} := \frac{(W + 2a) \cdot (H + 2a)^3 - (w + 2a) \cdot (h + 2a)^3}{6 \cdot (H + 2a)}$	$W_{ey} = 148846.396 \text{ mm}^3$
Cross sectional area:	$A := W \cdot H - w \cdot h$	$A = 3388 \text{ mm}^2$
Vertical shear area:	$A_s := \frac{A \cdot H}{(W + H)}$	$A_s = 1535.188 \text{ mm}^2$

6 Forces Considered		
ULS-b vertical force:	$F_Y := \frac{I \cdot \omega}{2} \text{ kN} = 39 \text{ kN}$	
Moment due to vertical force:	$M_V := 17.872 \text{ kN} \cdot \text{mm}$	
Distance between neutral axis:	$d_h := 405 \text{ mm}$	
Axial force due to moment on horizontal weld:	$F_h := \frac{M_V}{d_h}$	$F_h = 0.044 \text{ kN}$
7 Horizontal Weld Stress		
Axial stress to the horizontal weld:	$\sigma_a := \frac{F_h}{\sqrt{2} \cdot l_{wh,eff} \cdot a}$	$\sigma_a = 0.041 \text{ MPa}$
	$\tau_n := \sigma_a$	$\tau_n = 0.041 \text{ MPa}$
Equivalent von-Mises stress:	$\sigma_{vm} := \sqrt{\sigma_a^2 + 3 \cdot \tau_n^2}$	$\sigma_{vm} = 0.1 \text{ MPa}$
Utilization Factor:	$\eta_h := \frac{\sigma_{vm}}{f_{all}} = 0.001$	
8 Vertical Weld Stress		
Shear stress:	$\tau_{par} := \frac{F_Y}{n_w \cdot a \cdot l_{vw,eff}}$	$\tau_{par} = 70.7 \text{ MPa}$
Equivalent von-Mises stress:	$\sigma_{vm} := \sqrt{3 \cdot \tau_{par}^2}$	$\sigma_{vm} = 122.4 \text{ MPa}$
Utilization Factor:	$\eta_v := \frac{\sigma_{vm}}{f_{all}} = 0.86$	
9 Check of connection weld stress		
Bending stress to the horizontal weld:	$\sigma_b := \frac{M_V}{\sqrt{2} \cdot W_{ey}}$	$\sigma_b = 0.085 \text{ MPa}$
	$\tau_n := \sigma_b$	$\tau_n = 0.085 \text{ MPa}$
Shear stress:	$\tau_{par} := \frac{F_Y}{A_s}$	$\tau_{par} = 25.4 \text{ MPa}$
Equivalent von-Mises stress:	$\sigma_{vm} := \sqrt{\sigma_b^2 + 3 \cdot \tau_n^2 + 3 \cdot \tau_{par}^2}$	$\sigma_{vm} = 44 \text{ MPa}$
Utilization Factor:	$\eta_c := \frac{\sigma_{vm}}{f_{all}} = 0.309$	

Appendix U Weld check of critical weld 3

1 Weld section 3

2 Assumptions

- Simplify the box beam weld cross section as a rectangular weld.
- Conservatively let the moment be taken by the horizontal welds by making a force couple of the moment. Vertical load are taken by the vertical welds.
- Conservatively let the sum of forces in ULS-a and ULS-b be applied
- The two box beams in the hatch divide the load

3 Input Parameters

Height of beam:	$H := 150 \text{ mm}$
Width of beam:	$W := 240 \text{ mm}$
Thickness of upper flange:	$t_1 := 25.63 \text{ mm}$
Thickness of lower flange:	$t_2 := 15 \text{ mm}$
Inner height	$h := H - 2 t_1 = 98.74 \text{ mm}$
Inner width:	$w := W - 2 t_2 = 210 \text{ mm}$
Length of horizontal weld:	$l_{wh} := W = 240 \text{ mm}$
Length of vertical weld:	$l_{wv} := H = 150 \text{ mm}$
Weld throat thickness:	$a := 8 \text{ mm}$
Number of welds:	$n_w := 2$
Material yield strength:	$f_y := 700 \text{ MPa}$
Correlation factor:	$\beta := 1.0$
Material Factor for Weld	$\gamma_{mw} := 1.3$
Length from load to weld:	$L_1 := 2915 \text{ mm}$

4 Intermediate Calculations		
Allowable stress:	$f_{all} := \frac{f_y}{\beta \cdot \gamma_{mw}}$	$f_{all} = 538.462 \text{ MPa}$
Effective horizontal weld length:	$l_{wh,eff} := l_{wh} - 2 \cdot a$	$l_{wh,eff} = 224 \text{ mm}$
Effective vertical weld length:	$l_{wv,eff} := l_{wv} - 2 \cdot a$	$l_{wv,eff} = 134 \text{ mm}$
Axial Section modulus:	$W_{ey} := \frac{(W + 2a) \cdot (H + 2a)^3 - (w + 2a) \cdot (h + 2a)^3}{6 \cdot (H + 2a)}$	$W_{ey} = (8.33 \cdot 10^5) \text{ mm}^3$
Cross sectional area:	$A := W \cdot H - w \cdot h$	
Vertical shear area:	$A_s := \frac{A \cdot H}{(W + H)}$	$A_s = 5871 \text{ mm}^2$
5 Forces Considered		
Vertical forces ULS-a:	$F_{Y,ULSA} := 43.76 \text{ kN}$	
Vertical forces ULS-b:	$F_{Y,ULSB} := 68.38 \text{ kN}$	
Largest vertical force:	$F_Y := \max(F_{Y,ULSA}, F_{Y,ULSB})$	$F_Y = 68.38 \text{ kN}$
Moment due to vertical force:	$M_V := \frac{F_Y}{2} \cdot L_l = 99.664 \text{ kN} \cdot \text{m}$	
Distance between horizontal welds:	$d_h := 150 \text{ mm}$	
Axial force due to moment on horizontal weld:	$F_h := \frac{M_V}{d_h}$	$F_h = 664.426 \text{ kN}$
6 Horizontal Weld Stress		
Axial stress to the horizontal weld:	$\sigma_a := \frac{F_h}{\sqrt{2} \cdot l_{wh,eff} \cdot a}$	$\sigma_a = 262.176 \text{ MPa}$
	$\tau_n := \sigma_a$	$\tau_n = 262.176 \text{ MPa}$
Equivalent von-Mises stress:	$\sigma_{vm} := \sqrt{\sigma_a^2 + 3 \cdot \tau_n^2}$	$\sigma_{vm} = 524.4 \text{ MPa}$
Utilization Factor:	$\eta_h := \frac{\sigma_{vm}}{f_{all}} = 0.974$	
7 Vertical Weld Stress		
Shear stress:	$\tau_{par} := \frac{F_Y}{n_w \cdot a \cdot l_{wv,eff}}$	$\tau_{par} = 31.9 \text{ MPa}$
Equivalent von-Mises stress:	$\sigma_{vm} := \sqrt{3 \cdot \tau_{par}^2}$	$\sigma_{vm} = 55.2 \text{ MPa}$
Utilization Factor:	$\eta_v := \frac{\sigma_{vm}}{f_{all}} = 0.103$	

8 Check of connection weld stress

Bending stress to the horizontal weld:

$$\sigma_b := \frac{M_V}{\sqrt{2} \cdot W_{ey}}$$

$$\sigma_b = 84.605 \text{ MPa}$$

$$\tau_n := \sigma_b$$

$$\tau_n = 84.605 \text{ MPa}$$

Shear stress:

$$\tau_{par} := \frac{F_V}{A_s}$$

$$\tau_{par} = 11.6 \text{ MPa}$$

Equivalent von-Mises stress:

$$\sigma_{vm} := \sqrt{\sigma_b^2 + 3 \cdot \tau_n^2 + 3 \cdot \tau_{par}^2}$$

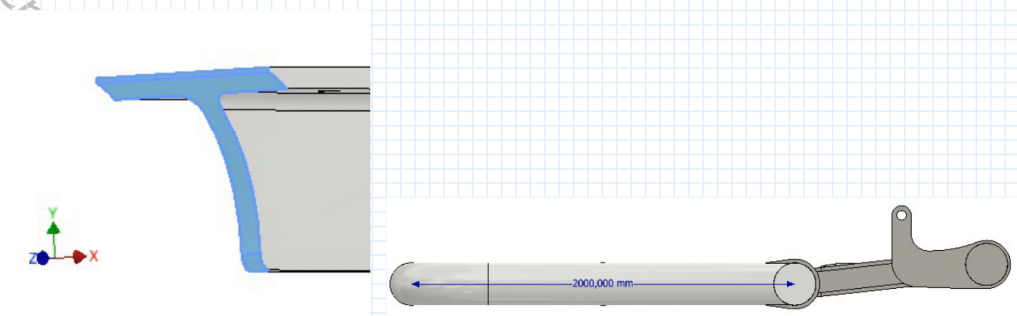
$$\sigma_{vm} = 170.4 \text{ MPa}$$

Utilization Factor:

$$\eta_c := \frac{\sigma_{vm}}{f_{all}} = 0.316$$

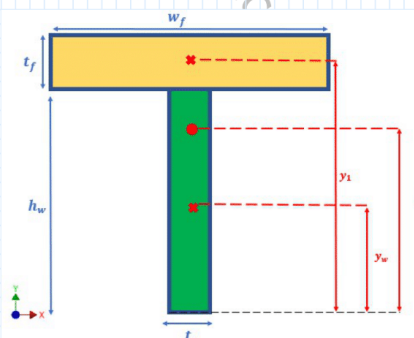
Appendix V Weld check of critical weld 4

1 Weld section 4



2 Simplifications

- Simplify T-bar geometry to crosssection.



3 Assumptions

- Conservatively let the moment be taken by the horizontal welds. Vertical load are taken by the vertical welds.
- The T-bar with the largest moment is to be calculated
- Assume that the load is spread equal over all 8 beams and 2 pipes

4 Input Parameters

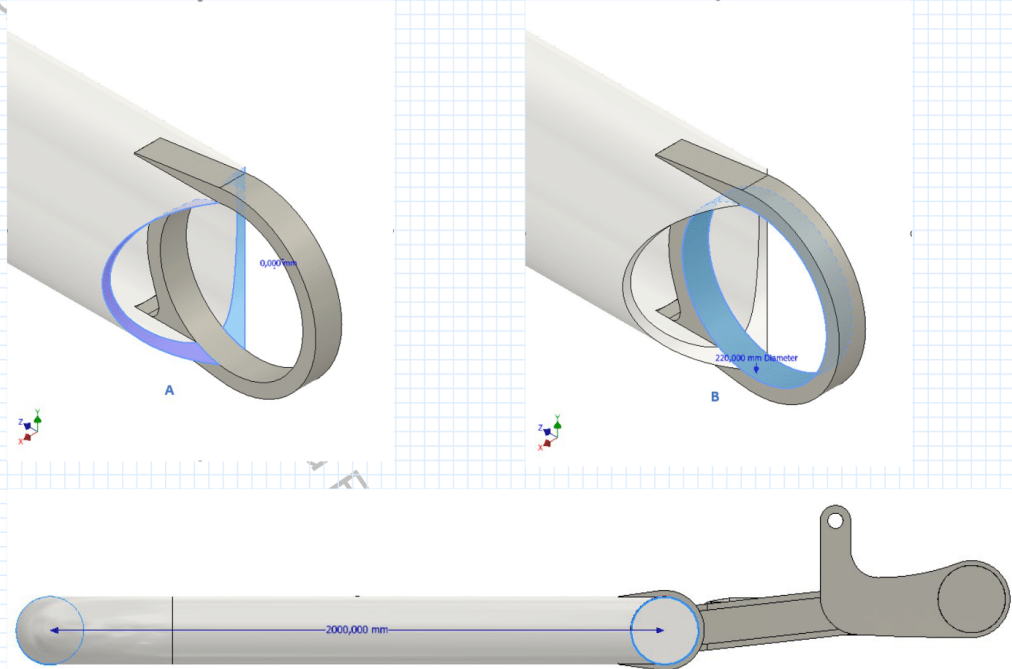
thickness of flange:	$t_f := 13 \text{ mm}$
Width of flange:	$w_f := 120 \text{ mm}$
Thickness of web:	$t_w := 13 \text{ mm}$
height of web:	$h_w := 107 \text{ mm}$
Distance from load to weld section:	$L_1 := 2000 \text{ mm}$
Length of horizontal weld:	$l_{wh} := w_f = 120 \text{ mm}$
Length of vertical weld:	$l_{wv} := h_w = 107 \text{ mm}$
Weld throat thickness:	$a := 10 \text{ mm}$
Number of welds:	$n_w := 2$
Material yield strength:	$f_y := 420 \text{ MPa}$
Correlation factor:	$\beta := 1.0$
Material Factor for Weld	$\gamma_{mw} := 1.3$

5 Intermediate Calculations - Weld dimension		
thickness of flange:	$t_{fw} := t_f + 2 \cdot a$	$t_{fw} = 33 \text{ mm}$
Width of flange:	$w_{fw} := w_f + 2 \cdot a$	$w_{fw} = 140 \text{ mm}$
weld Thickness of web:	$t_{wv} := t_w + 2 \cdot a$	$t_{wv} = 33 \text{ mm}$
weld height of web:	$h_{wv} := h_w + 2 \cdot a$	$h_{wv} = 127 \text{ mm}$
6 Intermediate Calculations - other		
Allowable stress:	$f_{all} := \frac{f_y}{\beta \cdot \gamma_{mv}}$	$f_{all} = 323.077 \text{ MPa}$
Effective horizontal weld length:	$l_{wh,eff} := l_{wh} - 2 \cdot a$	$l_{wh,eff} = 100 \text{ mm}$
Effective vertical weld length:	$l_{wv,eff} := l_{wv} - 2 \cdot a$	$l_{wv,eff} = 87 \text{ mm}$
Area of flange:	$A_f := w_{fw} \cdot t_{fw}$	$A_f = 4620 \text{ mm}^2$
Area of web:	$A_w := t_{wv} \cdot h_{wv}$	$A_w = 4191 \text{ mm}^2$
Shear area:	$A_s := 0.9 \cdot ((A_f + A_w) - w_{fw} \cdot t_{fw})$	$A_s = 3771.9 \text{ mm}^2$
Distance to centroid of flange	$y_f := h_{wv} + \frac{t_{fw}}{2}$	$y_f = 143.5 \text{ mm}$
Distance to centroid of web	$y_w := \frac{h_{wv}}{2}$	$y_w = 63.5 \text{ mm}$
Distance to centroid of T-bar:	$y_c := \frac{y_f \cdot A_f + y_w \cdot A_w}{A_f + A_w}$	$y_c = 105.448 \text{ mm}$
Second moment of area for flange:	$I_{xf} := w_{fw} \cdot \frac{t_{fw}^3}{12}$	$I_{xf} = 419265 \text{ mm}^4$
Second moment of area for web:	$I_{xw} := t_{wv} \cdot \frac{h_{wv}^3}{12}$	$I_{xw} = 5633053.25 \text{ mm}^4$
Total moment of inertia of T-bar:	$I_x := (I_{xw} + A_w \cdot (y_c - y_w)^2) + (I_{xf} + A_f \cdot (y_f - y_c)^2)$	$I_x = (2.012 \cdot 10^7) \text{ mm}^4$
Lower section modulus:	$W_l := \frac{I_x}{y_c}$	$W_l = (1.908 \cdot 10^4) \text{ m}^3$
Upper section modulus:	$W_u := \frac{I_x}{\left(h_w + \frac{t_f}{2}\right) - y_c}$	$W_u = (2.498 \cdot 10^6) \text{ mm}^3$
7 Forces Considered		
Vertical force ULS-a:	$F_{Y,ULSA} := 43.76 \text{ kN}$	
Vertical force ULS-b:	$F_{Y,ULSB} := 68.38 \text{ kN}$	
Largest vertical force:	$F_Y := \max(F_{Y,ULSA}, F_{Y,ULSB})$	$F_Y = 68.38 \text{ kN}$
Moment due to vertical force:	$M_V := F_Y \cdot L_l$	$M_V = 136.76 \text{ kN} \cdot \text{m}$
Moment on one T-bar	$M_{VT} := \frac{M_V}{10}$	$M_{VT} = 13.676 \text{ kN} \cdot \text{m}$

Distance between horizontal welds:	$d_h := \left(h_{ww} + \frac{t_{fw}}{2} \right) - y_c$	$d_h = 38.052 \text{ mm}$
	$d_h := \frac{(h_w + t_f + 2 \cdot a)}{2}$	$d_h = 70 \text{ mm}$
Axial force due to moment on horizontal weld:	$F_h := \frac{M_{VT}}{d_h}$	$F_h = 195.371 \text{ kN}$
8 Horizontal Weld Stress		
Axial stress to the horizontal weld:	$\sigma_a := \frac{F_h}{\sqrt{2} \cdot l_{wh.eff} \cdot a}$	$\sigma_a = 138.148 \text{ MPa}$
	$\tau_n := \sigma_a$	$\tau_n = 138.148 \text{ MPa}$
Equivalent von-Mises stress:	$\sigma_{vm} := \sqrt{\sigma_a^2 + 3 \cdot \tau_n^2}$	$\sigma_{vm} = 276.3 \text{ MPa}$
Utilization Factor:	$\eta_h := \frac{\sigma_{vm}}{f_{all}} = 0.855$	
9 Vertical Weld Stress		
Shear stress:	$\tau_{par} := \frac{F_Y}{n_w \cdot a \cdot l_{wv.eff}}$	$\tau_{par} = 39.3 \text{ MPa}$
Equivalent von-Mises stress:	$\sigma_{vm} := \sqrt{3 \cdot \tau_{par}^2}$	$\sigma_{vm} = 68.1 \text{ MPa}$
Utilization Factor:	$\eta_v := \frac{\sigma_{vm}}{f_{all}} = 0.211$	
10 Check of connection weld stress		
Bending stress to the horizontal weld:	$\sigma_b := \frac{M_{VT}}{\sqrt{2} \cdot W_i}$	$\sigma_b = 50.691 \text{ MPa}$
	$\tau_n := \sigma_b$	$\tau_n = 50.691 \text{ MPa}$
Shear stress:	$\tau_{par} := \frac{F_Y}{A_s}$	$\tau_{par} = 18.1 \text{ MPa}$
Equivalent von-Mises stress:	$\sigma_{vm} := \sqrt{\sigma_b^2 + 3 \cdot \tau_n^2 + 3 \cdot \tau_{par}^2}$	$\sigma_{vm} = 106.1 \text{ MPa}$
Utilization Factor:	$\eta_c := \frac{\sigma_{vm}}{f_{all}} = 0.329$	

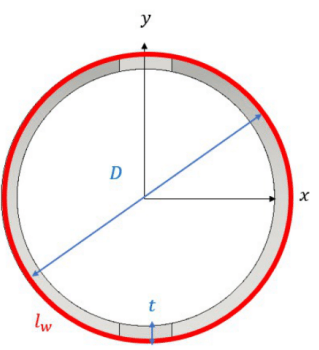
Appendix W Weld check of critical weld 5

1 Weld section 5



2 Simplification

Simplify section A by making a circular cross section area of the weld.



3 Assumptions

- Conservatively let the sum of forces in ULS-a and ULS-b be applied at the end of the hatch.
- Conservatively let the two pipe connections in the hatch divide the load

4 Input Parameters		
Diameter:	$D := 219.1 \text{ mm}$	
Thickness:	$t := 23.01 \text{ mm}$	
Inner diameter	$d := D - 2 \cdot t = 173.08 \text{ mm}$	
Length of weld:	$l_w := 140 \text{ mm}$	
Distance from load to weld section:	$L_l := 2000 \text{ mm}$	
Weld throath thickness:	$a := 10 \text{ mm}$	
Number of welds:	$n_w := 2$	
Material yield strength API 5L X65:	$f_{u,A} := 448 \text{ MPa}$	
Material yield strength Strenx 700 OME:	$f_{u,B} := 700 \text{ MPa}$	
Material Factor for Weld	$\gamma_{mw} := 1.3$	
Correleation factor:	$\beta := 1.0$	
5 Intermediate Calculations		
Material with lowest yield strength:	$f_u := \min(f_{u,A}, f_{u,B})$	$f_u = 448 \text{ MPa}$
Allowable stress:	$f_{all} := \frac{f_u}{\gamma_{mw} \cdot \beta}$	$f_{all} = 344.615 \text{ MPa}$
Effective horizontal weld length:	$l_{w,eff} := l_w - 2 \cdot a$	$l_{w,eff} = 120 \text{ mm}$
Axial Section modulus:	$W_{ey} := \frac{\pi \cdot (D^4 - d^4)}{32 \cdot D}$	$W_{ey} = (6.305 \cdot 10^{-4}) \text{ m}^3$
Twist section modulus:	$W_p := \frac{\pi \cdot (D^4 - d^4)}{16 \cdot D}$	$W_p = 1260955.428 \text{ mm}^3$
Cross sectional area:	$A := \pi \cdot \frac{(D^2 - d^2)}{4}$	$A = 14174.963 \text{ mm}^2$
Vertical shear area:	$A_s := 2 \cdot \frac{A}{\pi}$	$A_s = 9024.062 \text{ mm}^2$
6 Forces Considered		
Vertical forces ULS-a:	$F_{Y,ULSA} := 43.76 \text{ kN}$	
Vertical forces ULS-b:	$F_{Y,ULSB} := 68.38 \text{ kN}$	
Largest vertical force:	$F_Y := \max(F_{Y,ULSA}, F_{Y,ULSB})$	$F_Y = 68.38 \text{ kN}$
Moment due to vertical force:	$M_V := \frac{F_Y}{2} \cdot L_l$	$M_V = 68.38 \text{ kN} \cdot \text{m}$
Torsion due to vertical force:	$T_V := M_V$	$T_V = 68.38 \text{ kN} \cdot \text{m}$
7 Check of connection weld section A		
Bending stress to the horisontal weld:	$\sigma_b := \frac{M_V}{\sqrt{2} \cdot W_{ey}}$	$\sigma_b = 76.691 \text{ MPa}$
	$\tau_n := \sigma_b$	$\tau_n = 76.691 \text{ MPa}$
Parallel shear stress:	$\tau_{par} := \frac{F_Y}{A_s}$	$\tau_{par} = 7.6 \text{ MPa}$

Equivalent von-Mises stress: $\sigma_{vm} := \sqrt{\sigma_b^2 + 3 \cdot \tau_n^2 + 3 \cdot \tau_{par}^2}$ $\sigma_{vm} = 153.9 \text{ MPa}$

Utilization Factor: $\eta_c := \frac{\sigma_{vm}}{f_{all}} = 0.447$

8 Check of connection weld section B

Torsional shear stress: $\tau_t := \frac{T_V}{n_w \cdot W_p}$ $\tau_t = 27.1 \text{ MPa}$

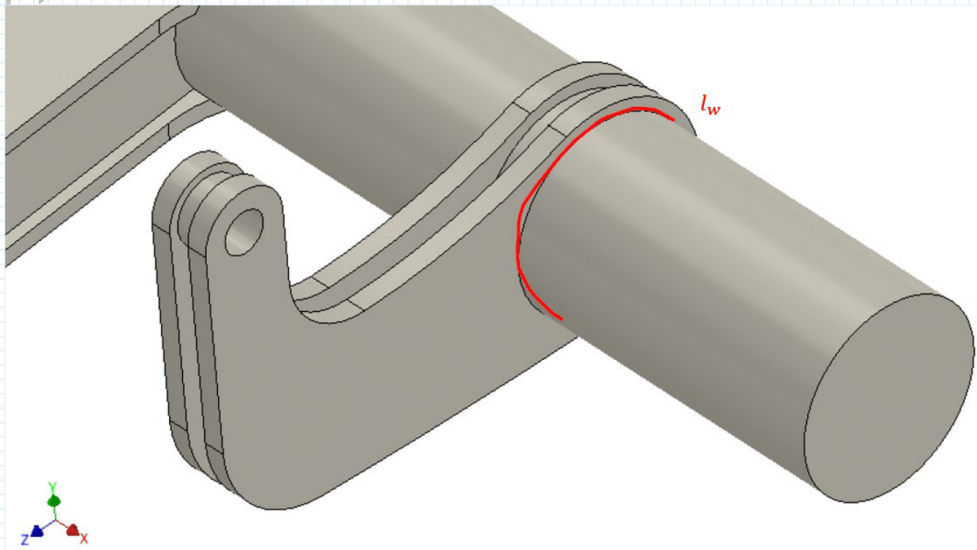
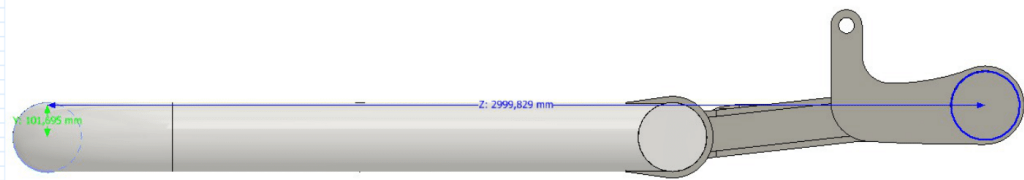
Equivalent von-Mises stress: $\sigma_{vm} := \sqrt{3 \cdot \tau_t^2}$ $\sigma_{vm} = 47 \text{ MPa}$

Utilization Factor: $\eta_c := \frac{\sigma_{vm}}{f_{all}} = 0.136$

Created with PTC Mathcad Express. See www.mathcad.com for more information.

Appendix X Weld check of critical weld 6

1 Weld section 6

2 Simplification

- Assume both welds to experience same torsional force
- Let the largest of sum of ULS-a and ULS-b be applied
- The two hinges in the hatch divide the load

3 Input Parameters

Diameter:	$D := 219.1 \text{ mm}$
Thickness:	$t := 23.01 \text{ mm}$
Inner diameter	$d := D - 2 \cdot t = 173.08 \text{ mm}$
Length of weld:	$l_w := \pi \cdot D = 688.323 \text{ mm}$
Weld throath thickness:	$a := 10 \text{ mm}$
Number of welds:	$n_w := 2$
Material yield strength Strenx 700 OME:	$f_u := 700 \text{ MPa}$
Material Factor for Weld	$\gamma_{mw} := 1.3$
Correleation factor:	$\beta := 1.0$
Length from weld to load:	$L_h := 3000 \text{ mm}$

4 Intermediate Calculations

Allowable stress: $f_{all} := \frac{f_u}{\gamma_{mw} \cdot \beta}$ $f_{all} = 538.462 \text{ MPa}$

Effective horizontal weld length: $l_{w,eff} := l_w - 2 \cdot a$ $l_{w,eff} = 668.323 \text{ mm}$

Twist section modulus: $W_p := \frac{\pi \cdot (D^4 - d^4)}{16 D}$ $W_p = 1260955.428 \text{ mm}^3$

Cross sectional area: $A := \pi \cdot \frac{(D^2 - d^2)}{4}$ $A = 14174.963 \text{ mm}^2$

5 Forces Considered

Vertical forces ULS-a: $F_{Y,ULSA} := 43.76 \text{ kN}$

Vertical forces ULS-b: $F_{Y,ULSB} := 68.38 \text{ kN}$

Largest vertical force: $F_Y := \max(F_{Y,ULSA}, F_{Y,ULSB})$ $F_Y = 68.38 \text{ kN}$

Torsion due to vertical force: $T_V := \frac{F_Y}{2} \cdot L_h$ $T_V = 102.57 \text{ kN} \cdot \text{m}$

6 Check of connection weld stress

Torsional shear stress: $\tau_t := \frac{T_V}{W_p}$ $\tau_t = 81.3 \text{ MPa}$

Equivalent von-Mises stress: $\sigma_{vm} := \sqrt{3 \cdot \tau_t^2}$ $\sigma_{vm} = 140.9 \text{ MPa}$

Utilization Factor: $\eta_c := \frac{\sigma_{vm}}{f_{all}} = 0.262$

Appendix Y Damping of rubber materials

Damping of rubber materials for the hatch and skid

Square profiles:

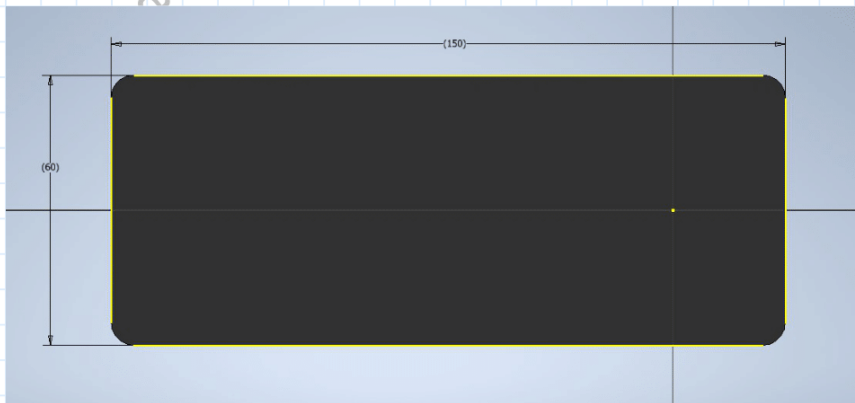
Load: $F := 60 \text{ kN}$

Width of load area $W_s := 200 \text{ mm}$

Length of load area $L_s := 400 \text{ mm}$

Load area: $A_{ls} := W_s \cdot L_s = 80000 \text{ mm}^2$

Thickness of rubber: $t_s := 60 \text{ mm}$



Shape factor:

$$S_s := \frac{(L_s \cdot W_s)}{2 \cdot t_s \cdot L_s + 2 \cdot t_s \cdot W_s} = 1.111$$

Young's modulus:
Tabulated acc. to
A. N. Gent, Engineering with Rubber

$$E_0 := \begin{bmatrix} 896 \\ 1158 \\ 1469 \\ 1765 \\ 2137 \\ 3172 \\ 4344 \\ 5723 \\ 7170 \\ 9239 \end{bmatrix} \text{ kPa} = \begin{bmatrix} 0.896 \\ 1.158 \\ 1.469 \\ 1.765 \\ 2.137 \\ 3.172 \\ 4.344 \\ 5.723 \\ 7.17 \\ 9.239 \end{bmatrix} \text{ MPa}$$

Elastomer compression coefficient:
Tabulated acc. to
A. N. Gent, Engineering with Rubber

$$\phi := \begin{bmatrix} 0.93 \\ 0.89 \\ 0.85 \\ 0.80 \\ 0.73 \\ 0.64 \\ 0.57 \\ 0.54 \\ 0.53 \\ 0.52 \end{bmatrix}$$

Created with PTC Mathcad Express. See www.mathcad.com

Compressive modulus: $E_c := E_0 \cdot (1 + \phi \cdot S_s^2) =$

1.925
2.43
3.011
3.508
4.063
5.678
7.401
9.538
11.861
15.17

MPa

Rubber deformation: $d_{cs} := F \cdot \frac{t_s}{A_{ls} \cdot E_c} =$

23.38
18.516
14.947
12.827
11.076
7.925
6.08
4.718
3.794
2.966

mm

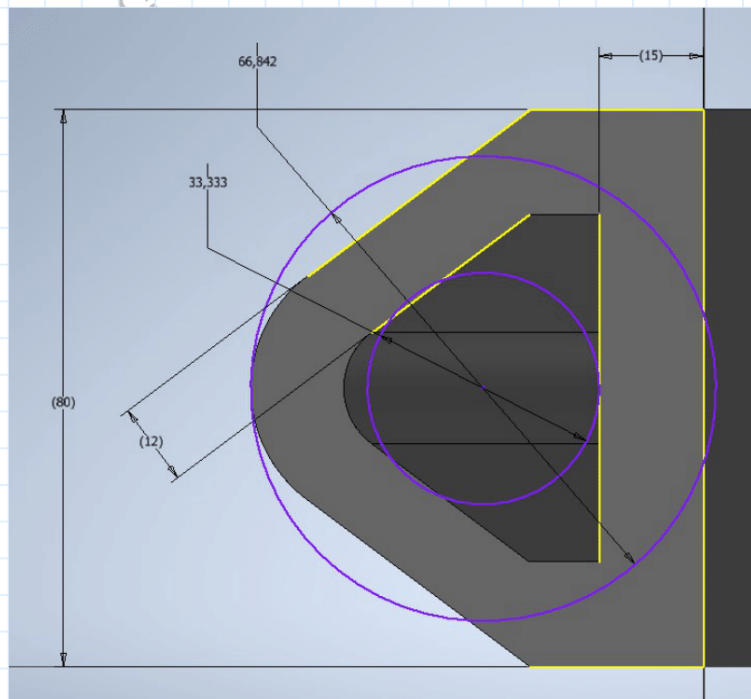
Elastic potential energy absorbed in one square rubber profile: $U_{srs} := 0.5 \cdot F \cdot d_{cs} =$

701.393
555.471
448.424
384.812
332.272
237.748
182.411
141.534
113.814
88.99

J

Hollow profiles:

- Width of load area: $W_h := 80 \text{ mm}$
- Length of load area: $L_h := 400 \text{ mm}$
- Load area: $A_{th} := W_h \cdot L_h = 32000 \text{ mm}^2$
- Inner diameter of rubber: $d_i := 33 \text{ mm}$
- Outer diameter of rubber: $d_o := 66 \text{ mm}$
- Thickness: $t_h := 12 \text{ mm}$



Shape factor for hollow tube profiles:

$$S_t := \frac{(d_o - d_i) \cdot L_h}{2 \cdot \pi \cdot \left(\frac{(d_o)^2}{4} - \frac{(d_i)^2}{4} \right)} = 2.572$$

Compressive modulus:

$$E_c := \overline{E_0 \cdot (1 + \phi \cdot S_t^2)} = \begin{bmatrix} 6.409 \\ 7.977 \\ 9.73 \\ 11.107 \\ 12.458 \\ 16.603 \\ 20.726 \\ 26.17 \\ 32.312 \\ 41.025 \end{bmatrix} \text{ MPa}$$

Created with PTC Mathcad Express. See www

Rubber deformation: $d_{cs} := F \cdot \frac{t_h}{A_{th} \cdot E_c} =$

3.511
2.821
2.312
2.026
1.806
1.355
1.086
0.86
0.696
0.548

mm

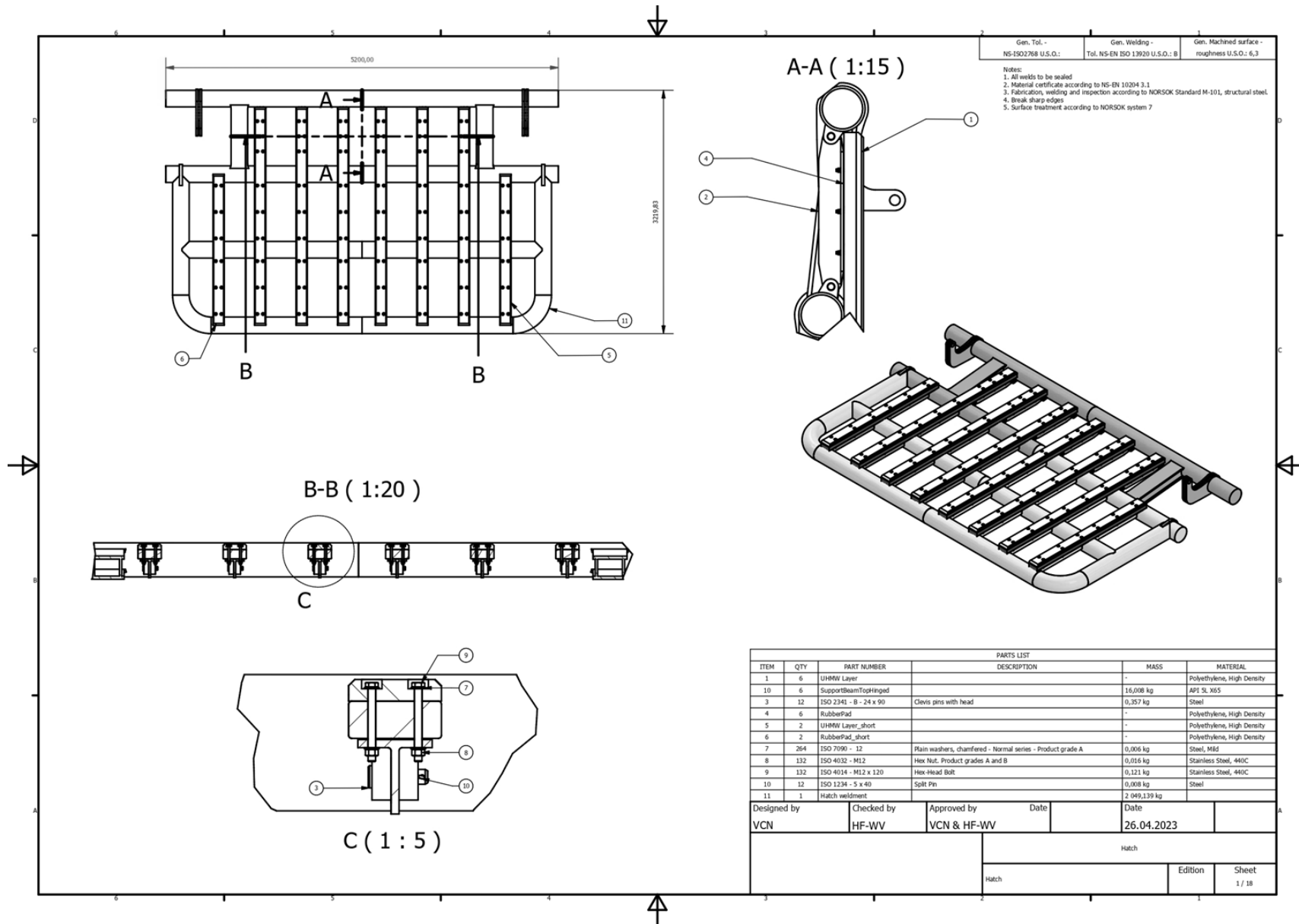
Correction factor for geometry uncertainty: $\beta := 0.7$

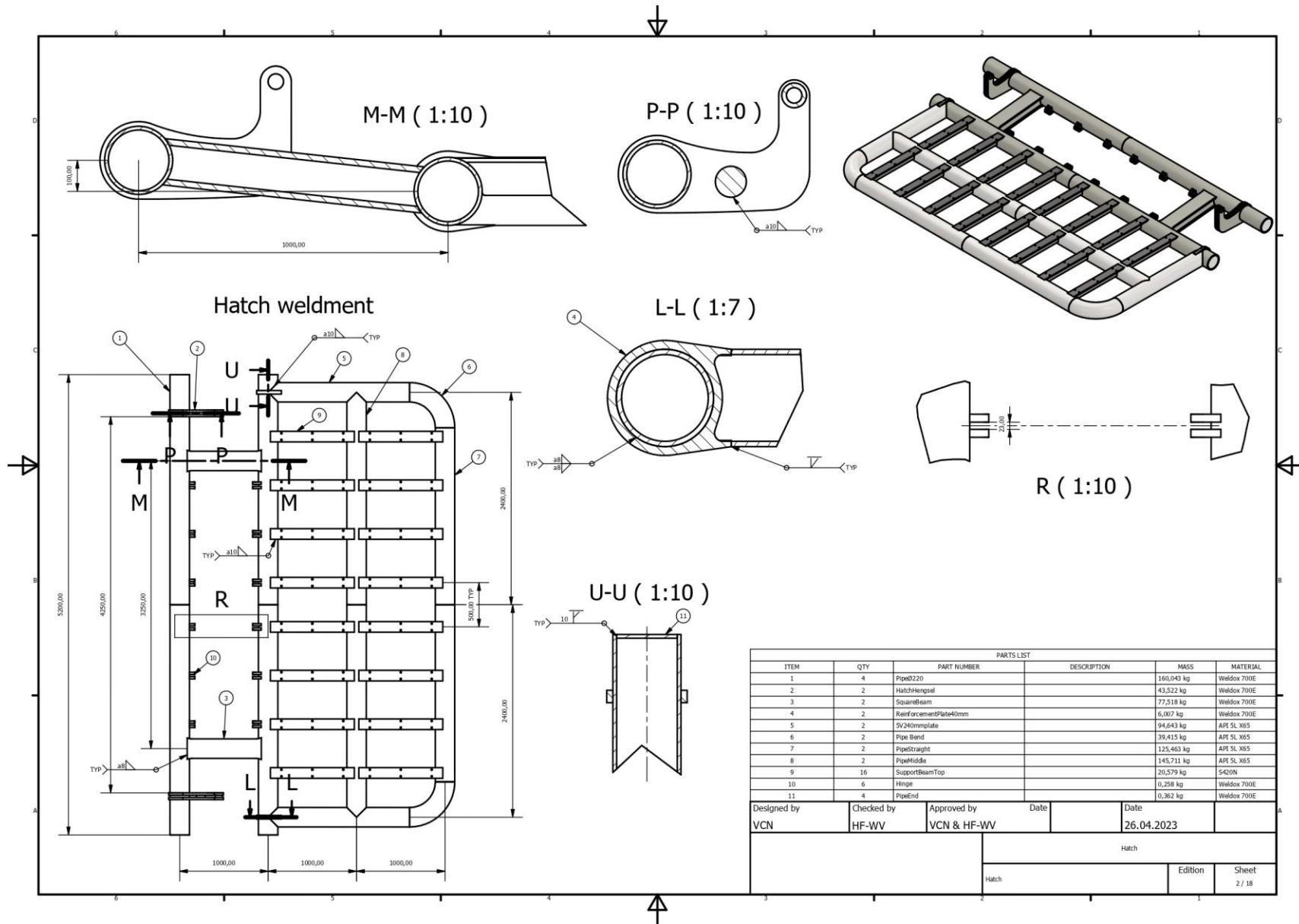
Elastic potential energy absorbed in one hollow rubber profile: $U_{srs} := 0.5 \cdot F \cdot d_{cs} \cdot \beta =$

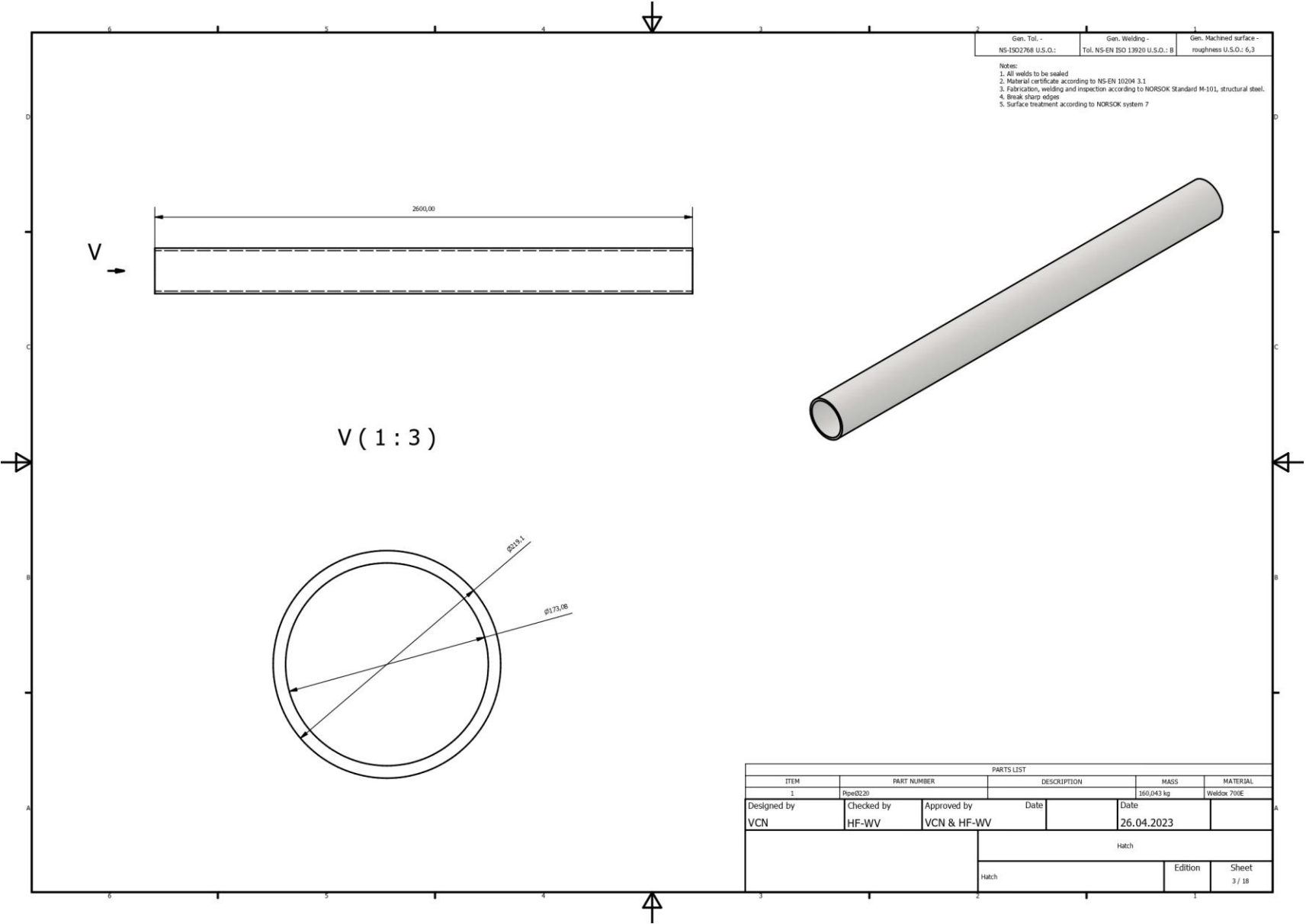
73.723
59.234
48.559
42.54
37.926
28.458
22.797
18.055
14.623
11.517

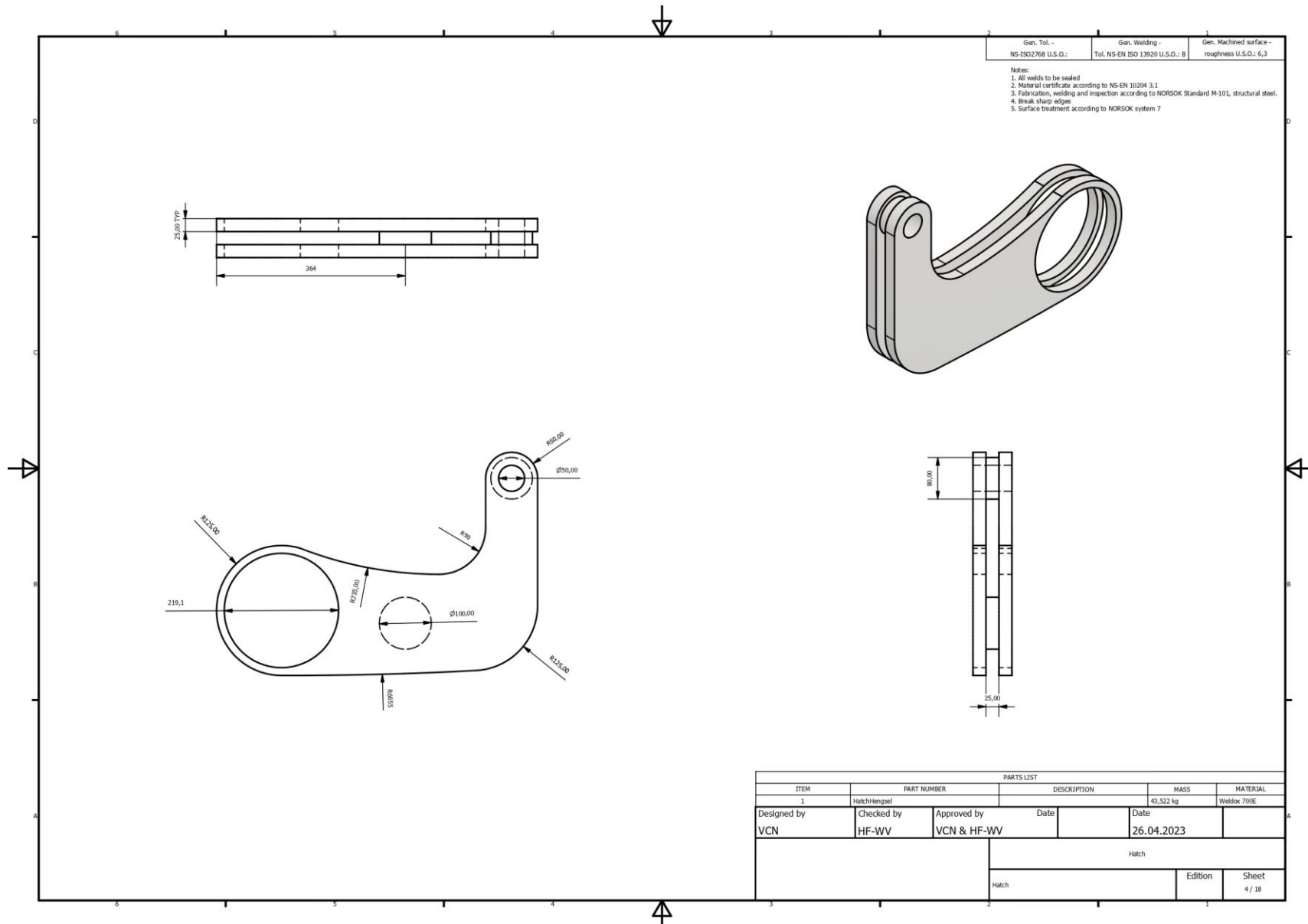
J

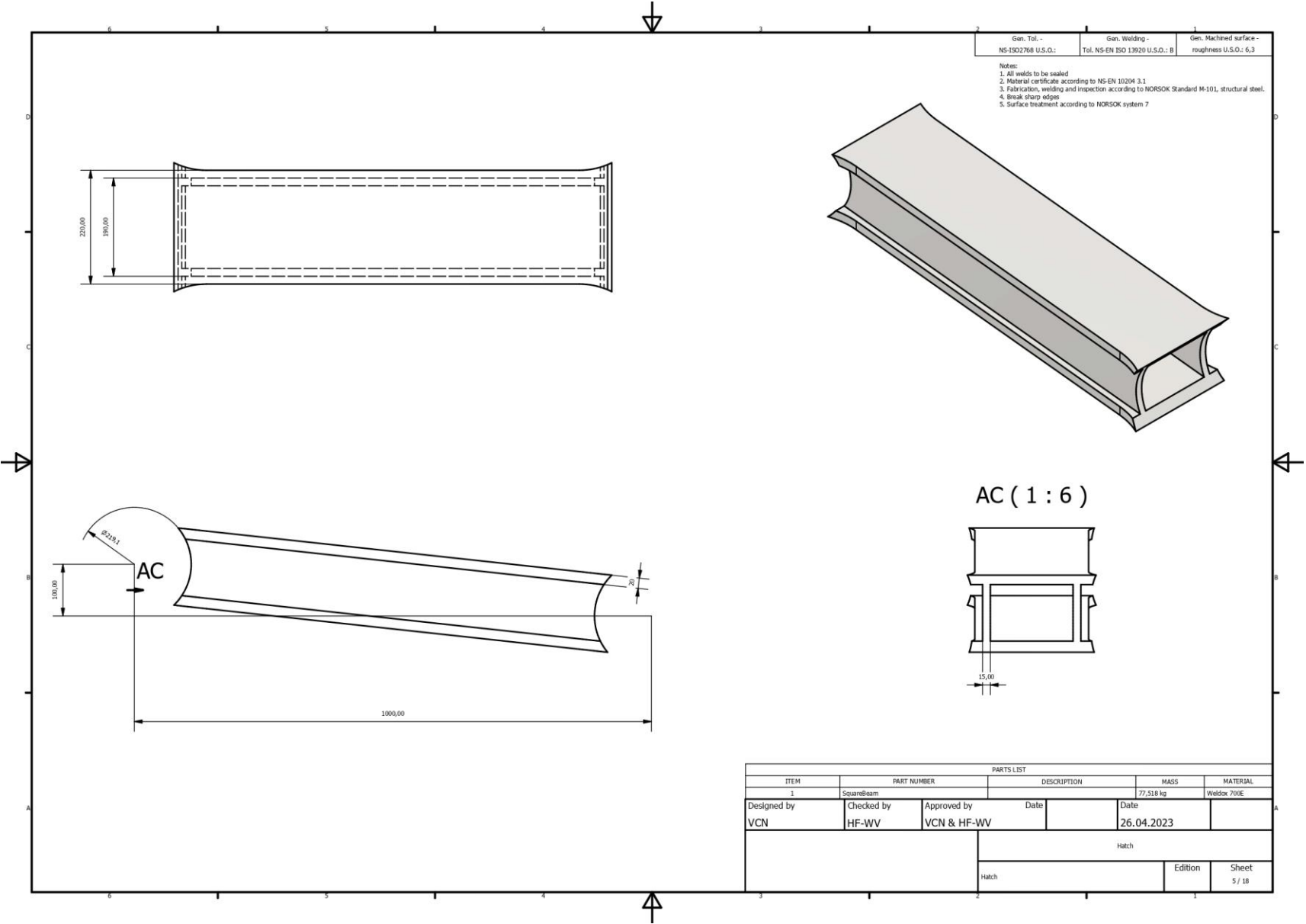
Appendix Z Hatch Drawings

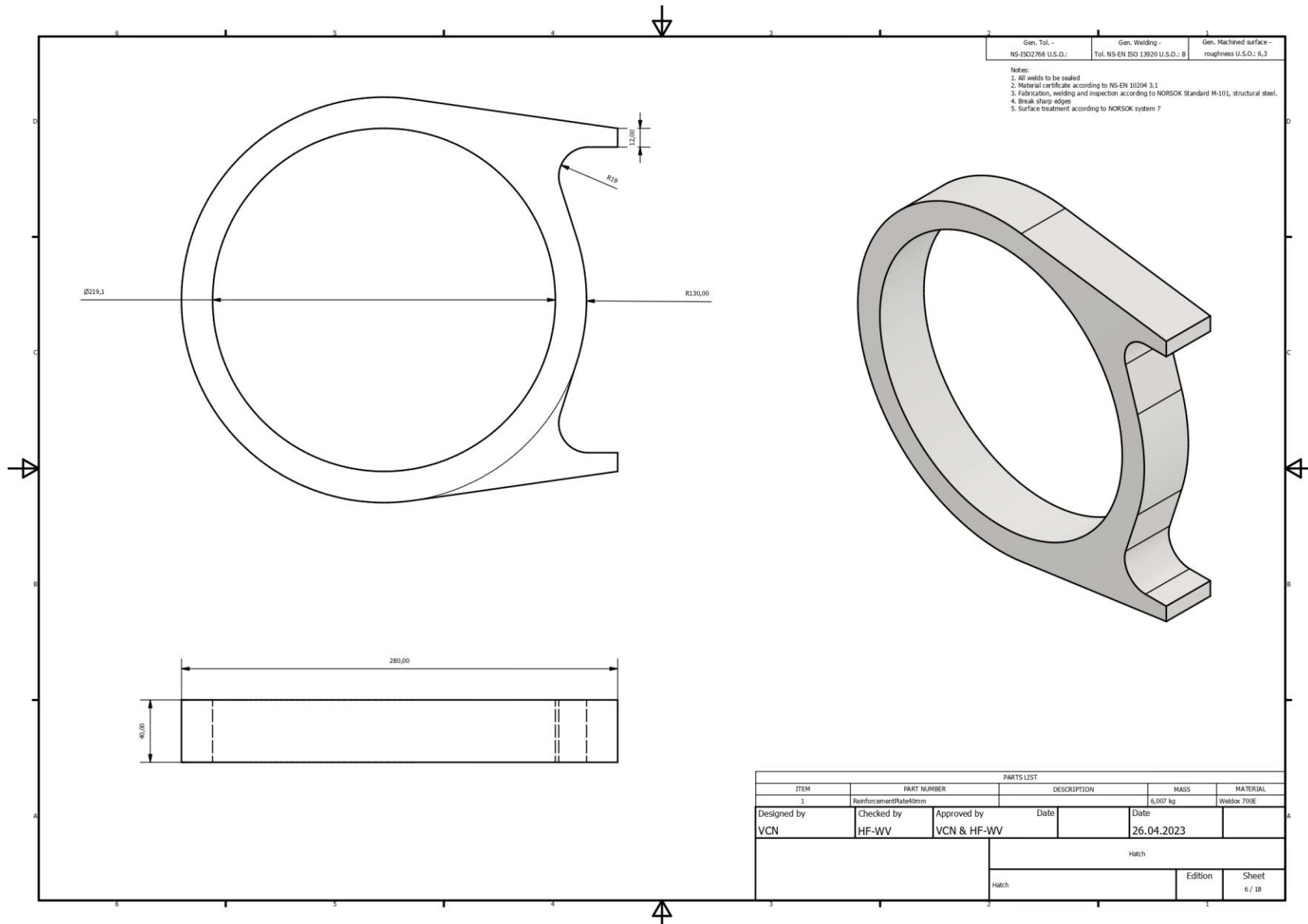


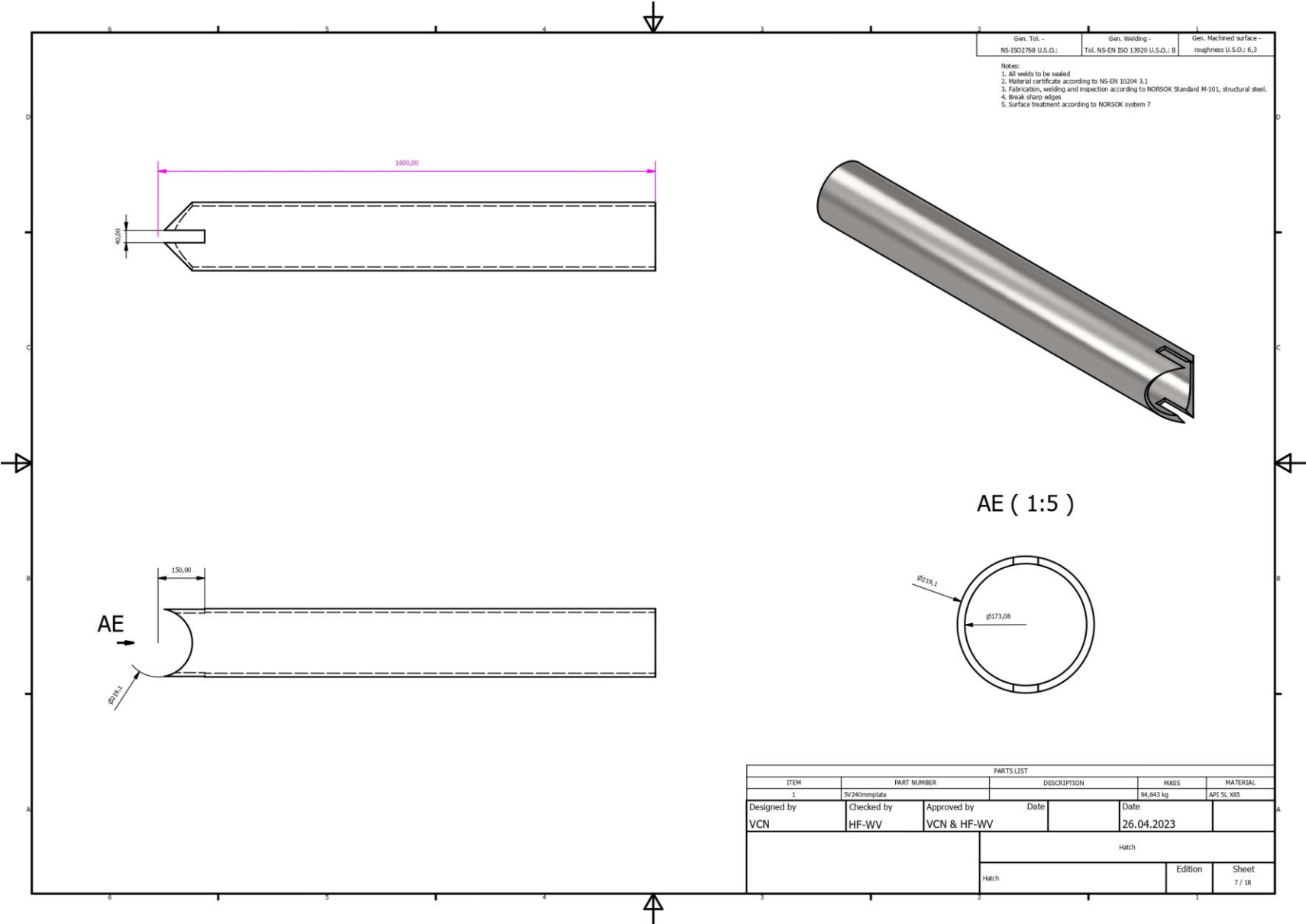








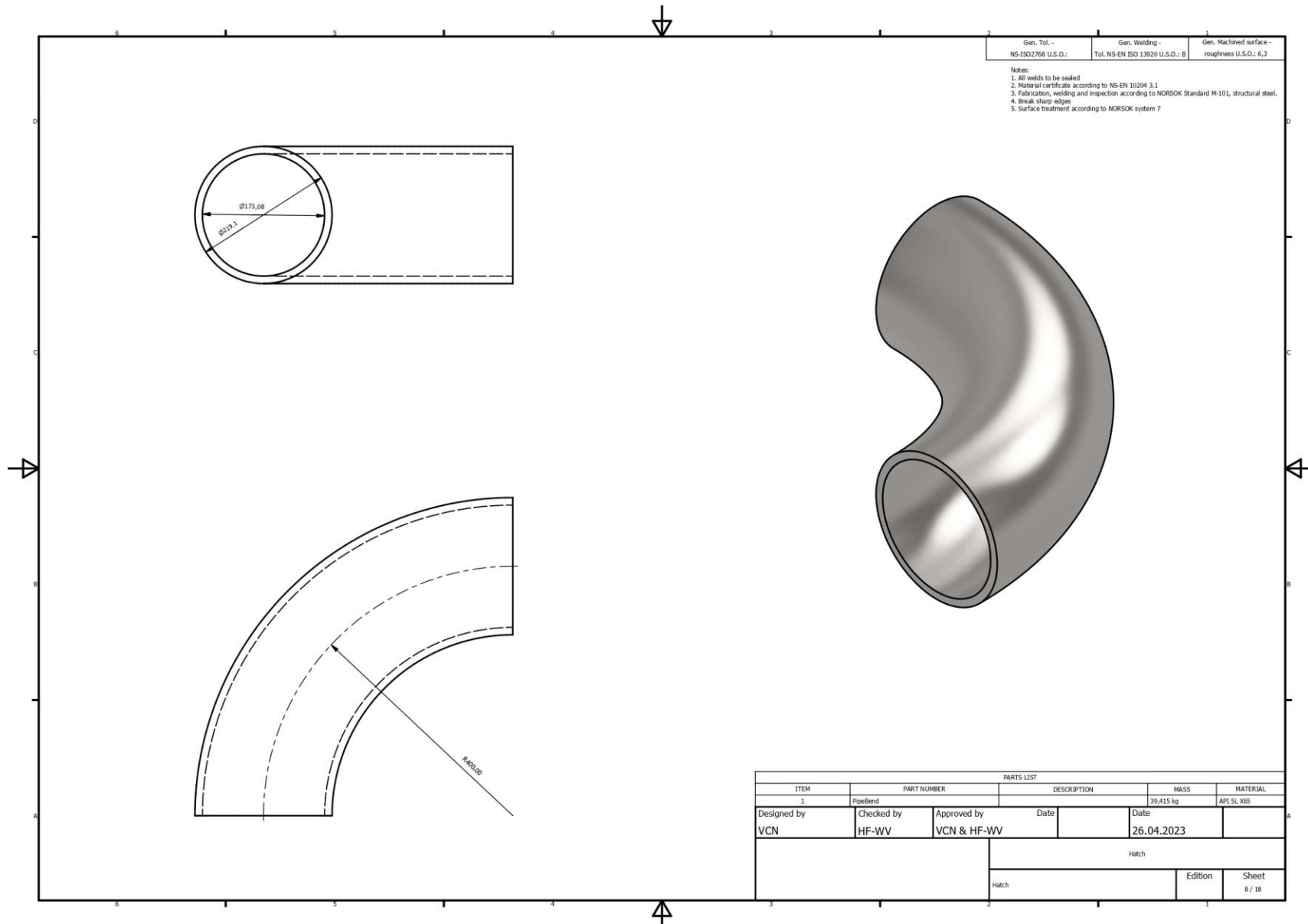


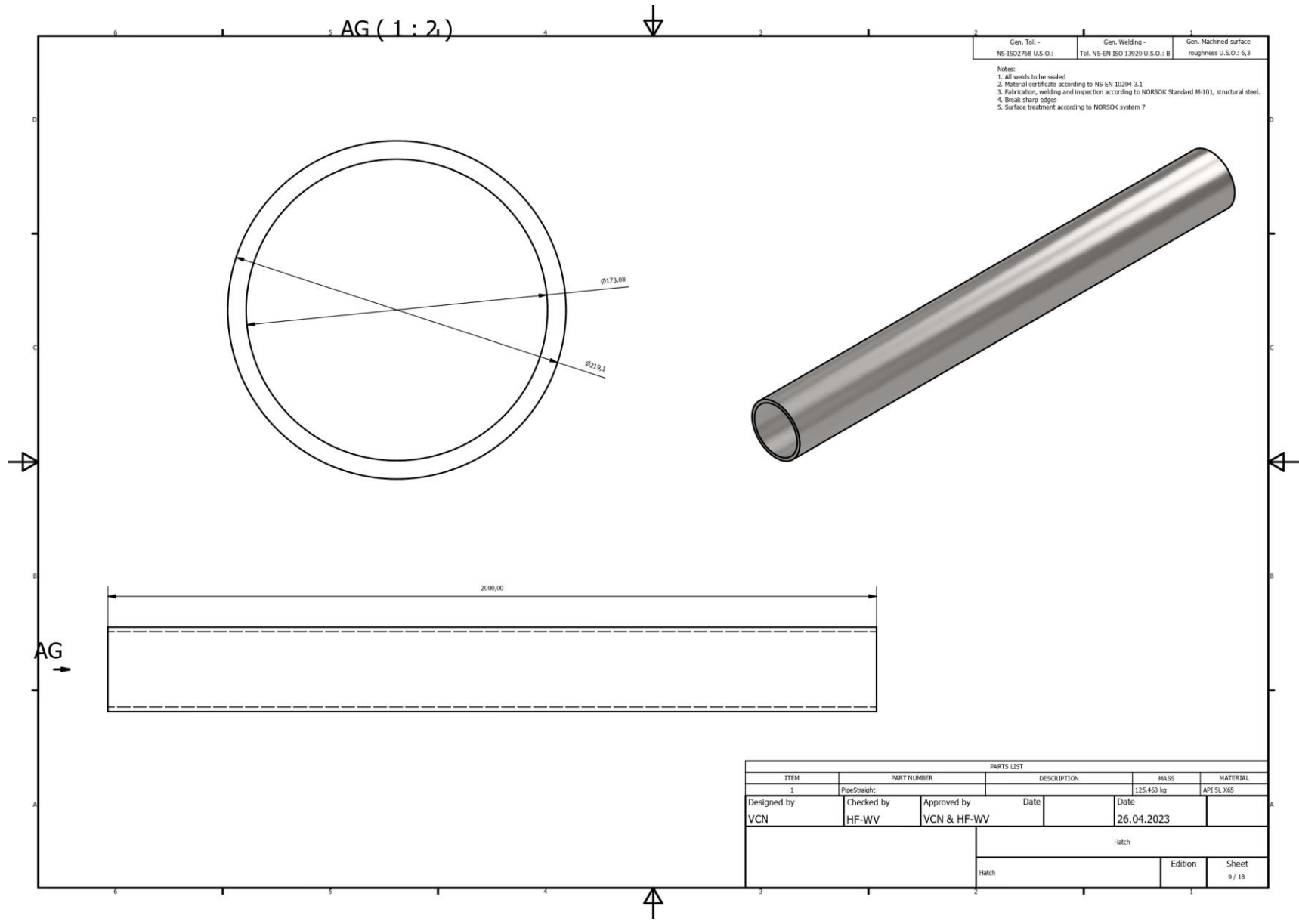


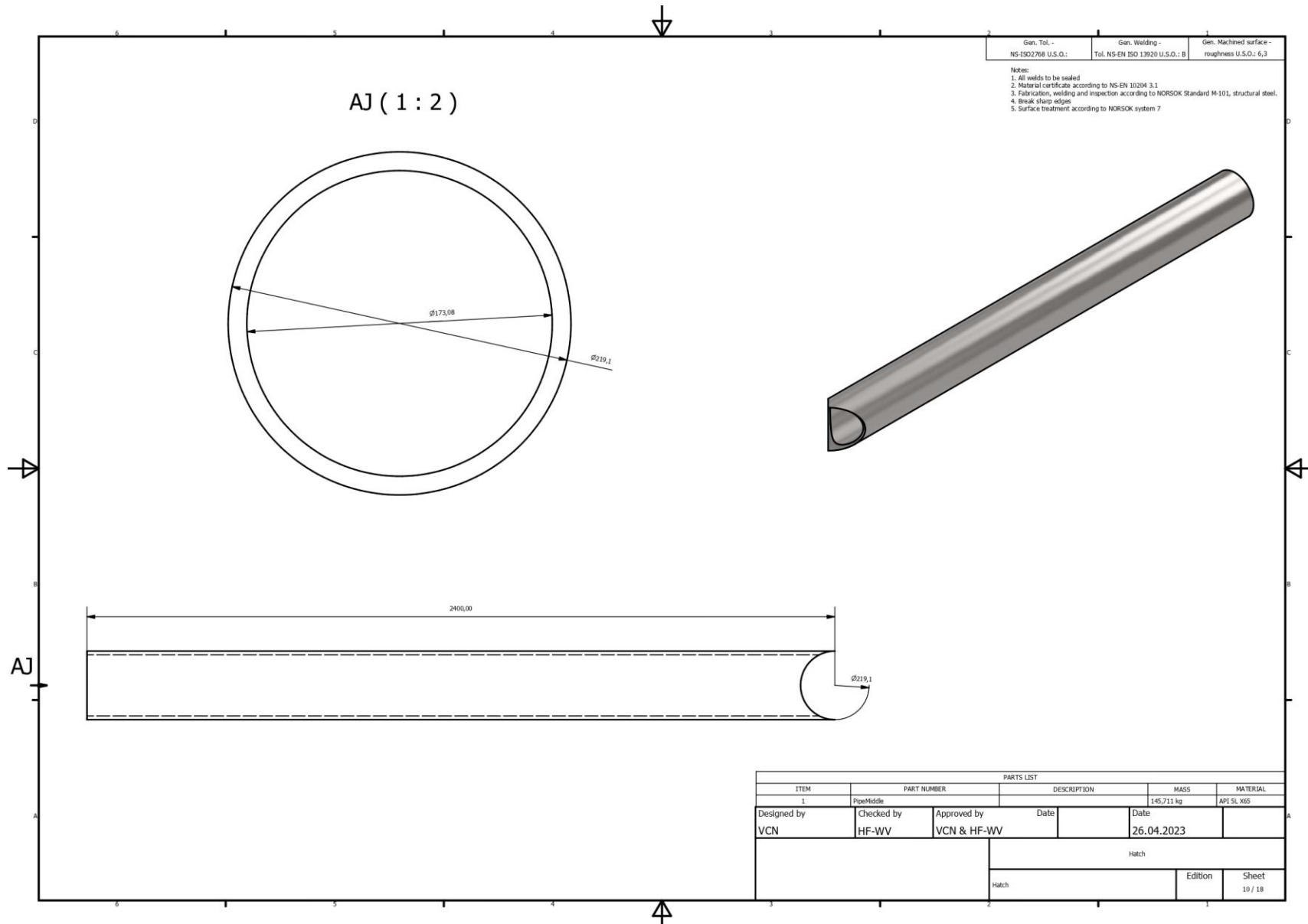
Gen. Tol. - NS-1502798 U.S.O.:
 Gen. Welding - Tol. NS-EN ISO 13920 U.S.O.: B
 Gen. Machined surface - roughness U.S.O.: 6,3

Notes:
 1. All welds to be sealed
 2. Material certificate according to NS-EN 10204 3.1
 3. Fabrication, welding and inspection according to NORSOK Standard M-101, structural steel.
 4. Break sharp edges
 5. Surface treatment according to NORSOK system 7

PARTS LIST					
ITEM	PART NUMBER	DESCRIPTION	MASS	MATERIAL	
1	SV240mplate		94,643 kg	API 5L X65	
Designed by	Checked by	Approved by	Date	Date	
VCN	HF-WV	VCN & HF-WV		26.04.2023	
Hatch			Hatch		
Hatch			Edition	Sheet	
Hatch				7 / 18	



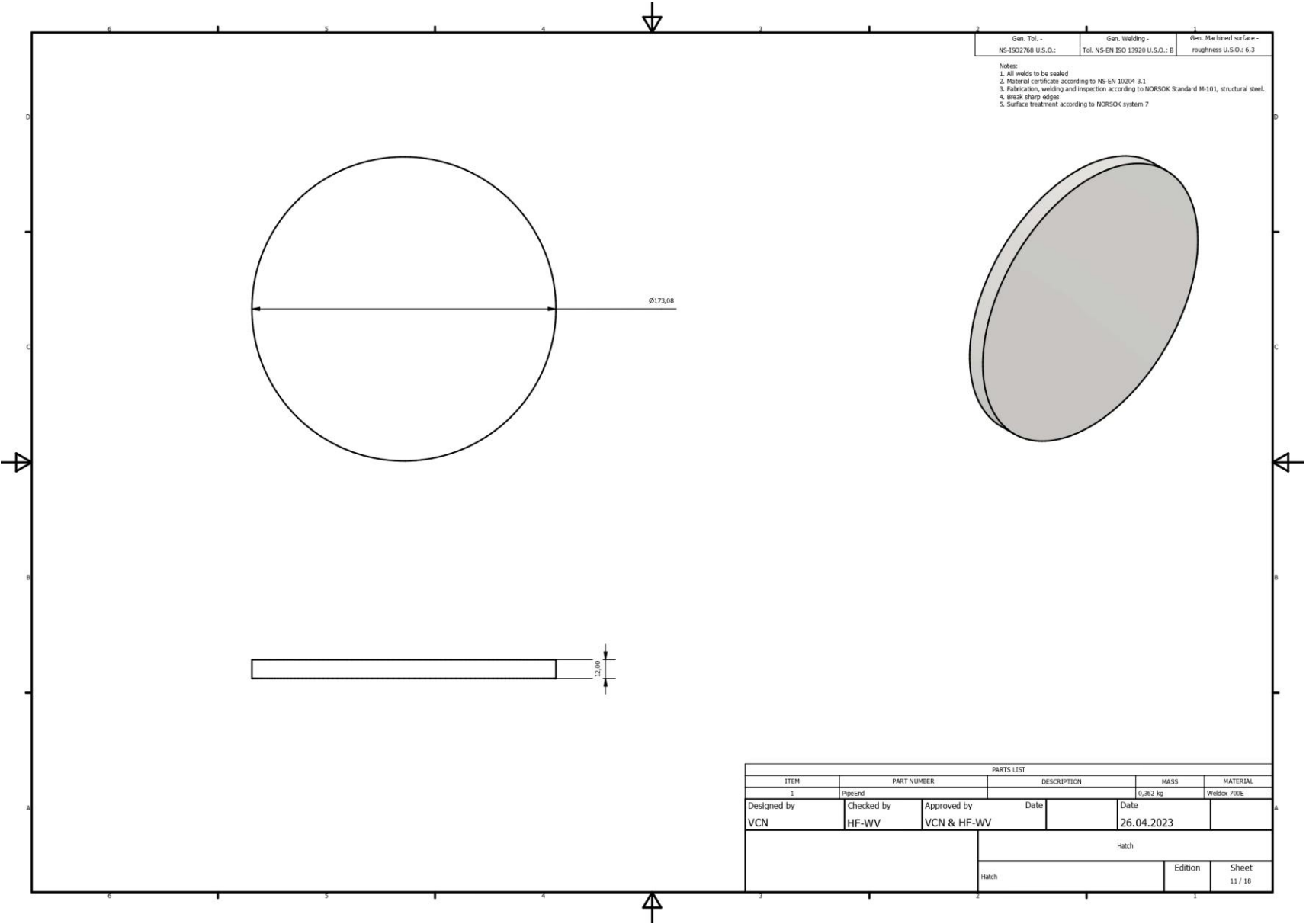




Gen. Tol. -
NS-ISO2768 U.S.O.:
Gen. Welding -
Tol. NS-EN ISO 13920 U.S.O.: B
Gen. Machined surface -
roughness U.S.O.: 6,3

Note:
1. All welds to be sealed
2. Material certificate according to NS-EN 10204 3.1
3. Fabrication, welding and inspection according to NORSOK Standard M-101, structural steel.
4. Break sharp edges
5. Surface treatment according to NORSOK system 7

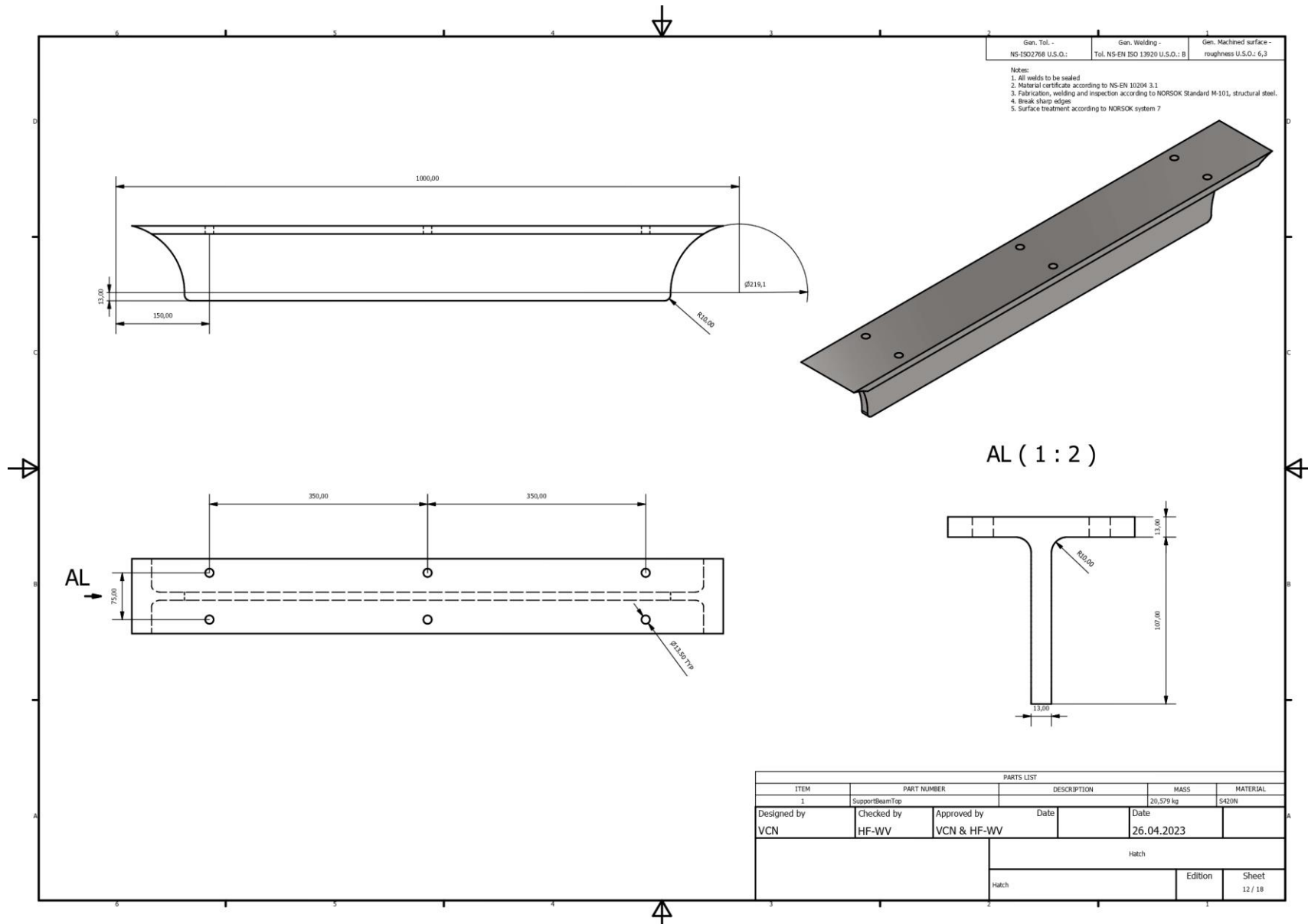
PARTS LIST					
ITEM	PART NUMBER	DESCRIPTION	MASS	MATERIAL	
1	PipeMiddle		145,711 kg	API 5L X65	
Designed by		Checked by	Approved by	Date	Date
VCN		HF-WV	VCN & HF-WV		26.04.2023
			Hatch		
			Hatch	Edition	Sheet
					10 / 18



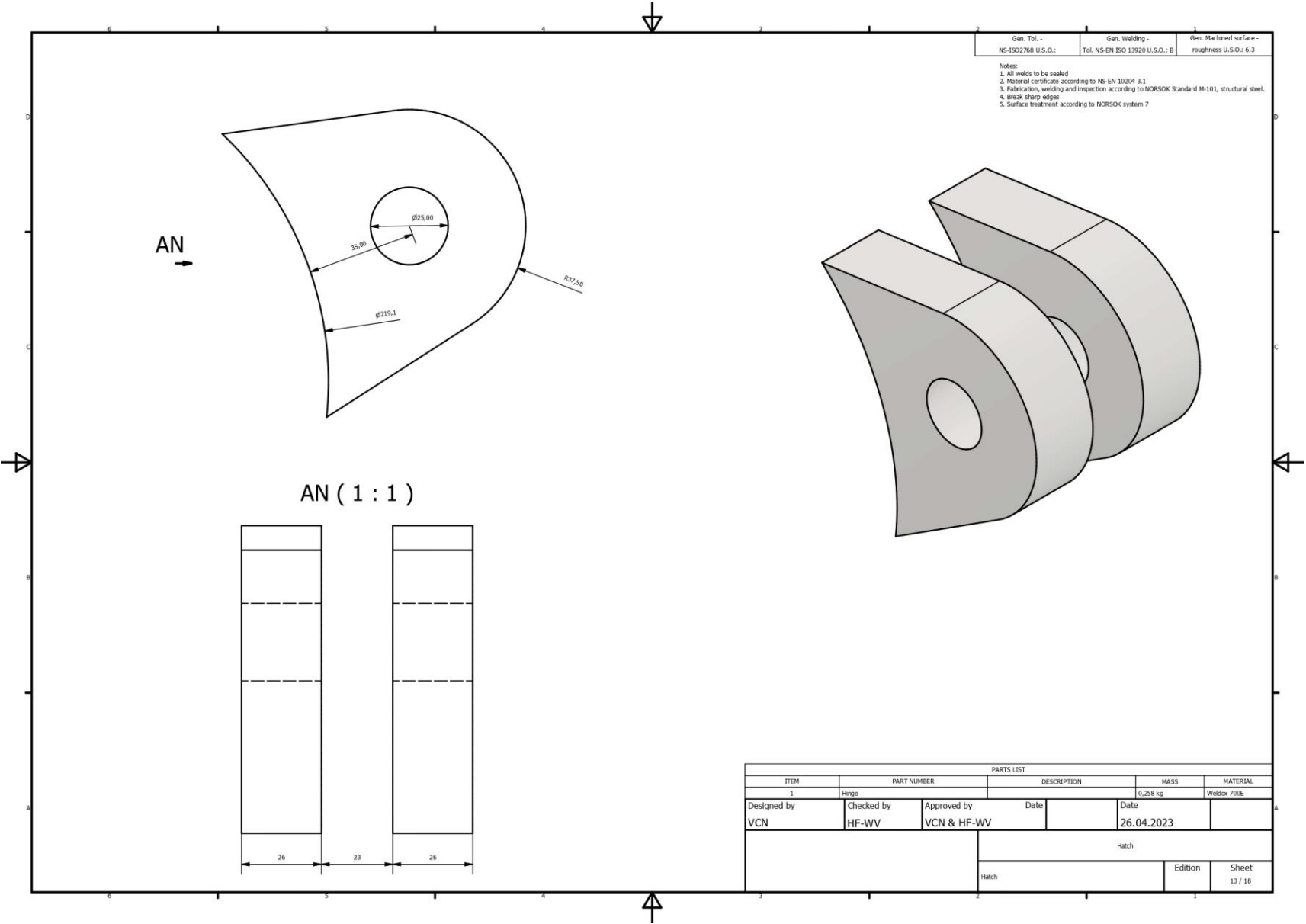
Gen. Tol - NS-1502768 U.S.O.:
 Gen. Welding - Tol. NS-EN ISO 13920 U.S.O.: B
 Gen. Machined surface - roughness U.S.O.: 6,3

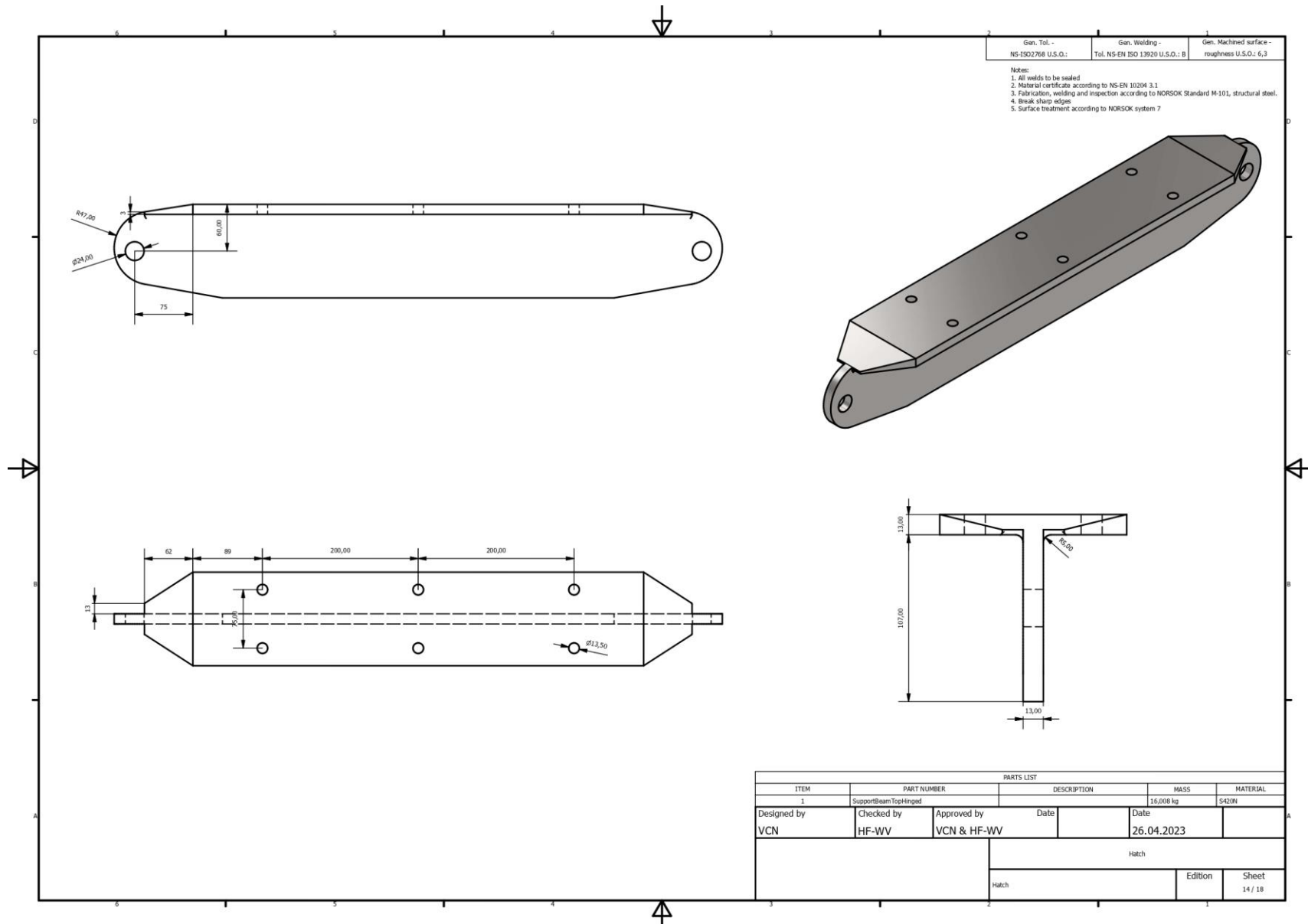
Notes:
 1. All welds to be sealed
 2. Material certificate according to NS-EN 10204 3.1
 3. Fabrication, welding and inspection according to NORSOK Standard M-101, structural steel.
 4. Break sharp edges
 5. Surface treatment according to NORSOK system 7

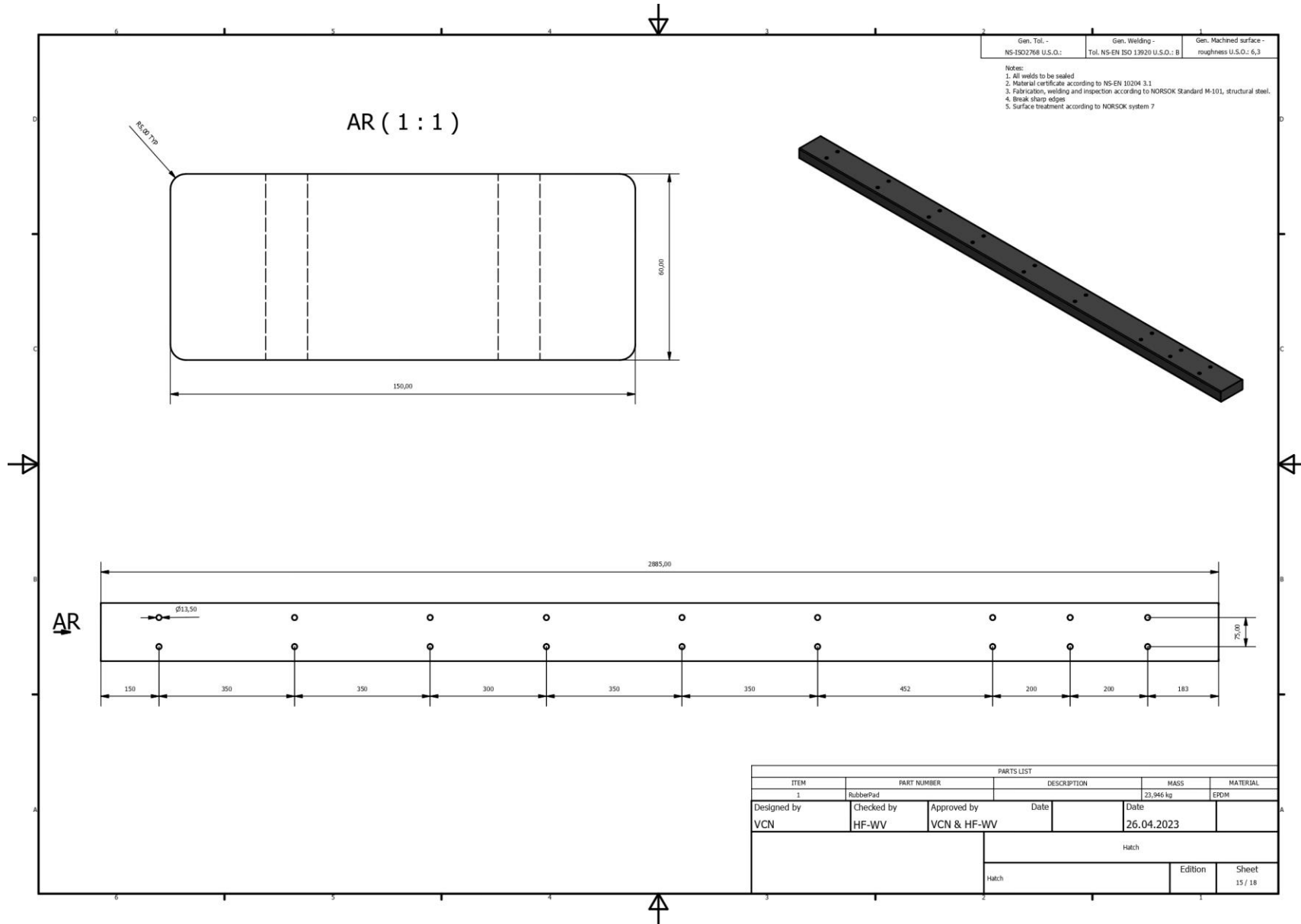
PARTS LIST					
ITEM	PART NUMBER	DESCRIPTION	MASS	MATERIAL	
1	PipeEnd		0,362 kg	Weldox 700E	
Designed by	Checked by	Approved by	Date	Date	
VCN	HF-WV	VCN & HF-WV		26.04.2023	
Hatch			Hatch		
Hatch			Edition	Sheet	
Hatch				11 / 18	

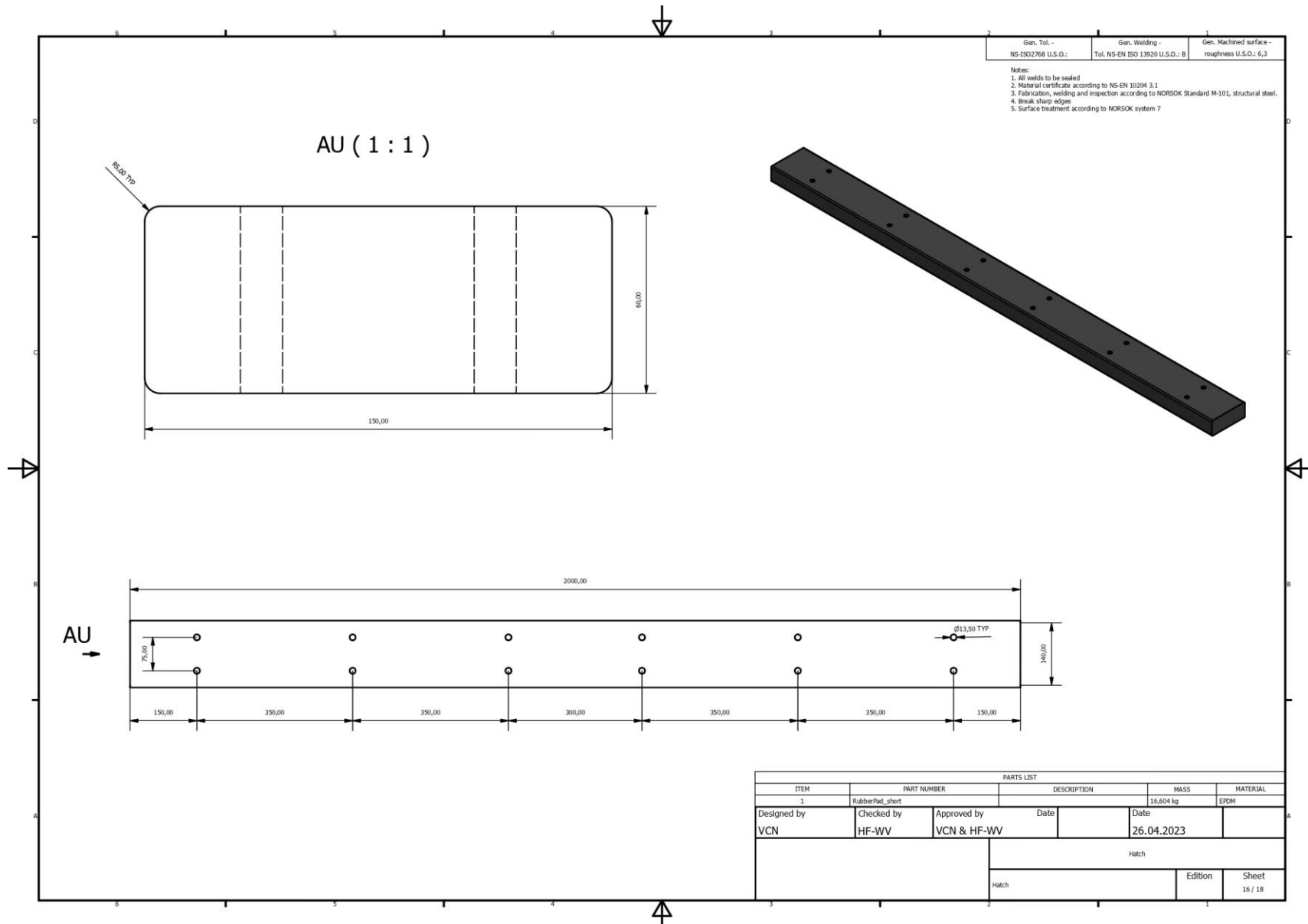


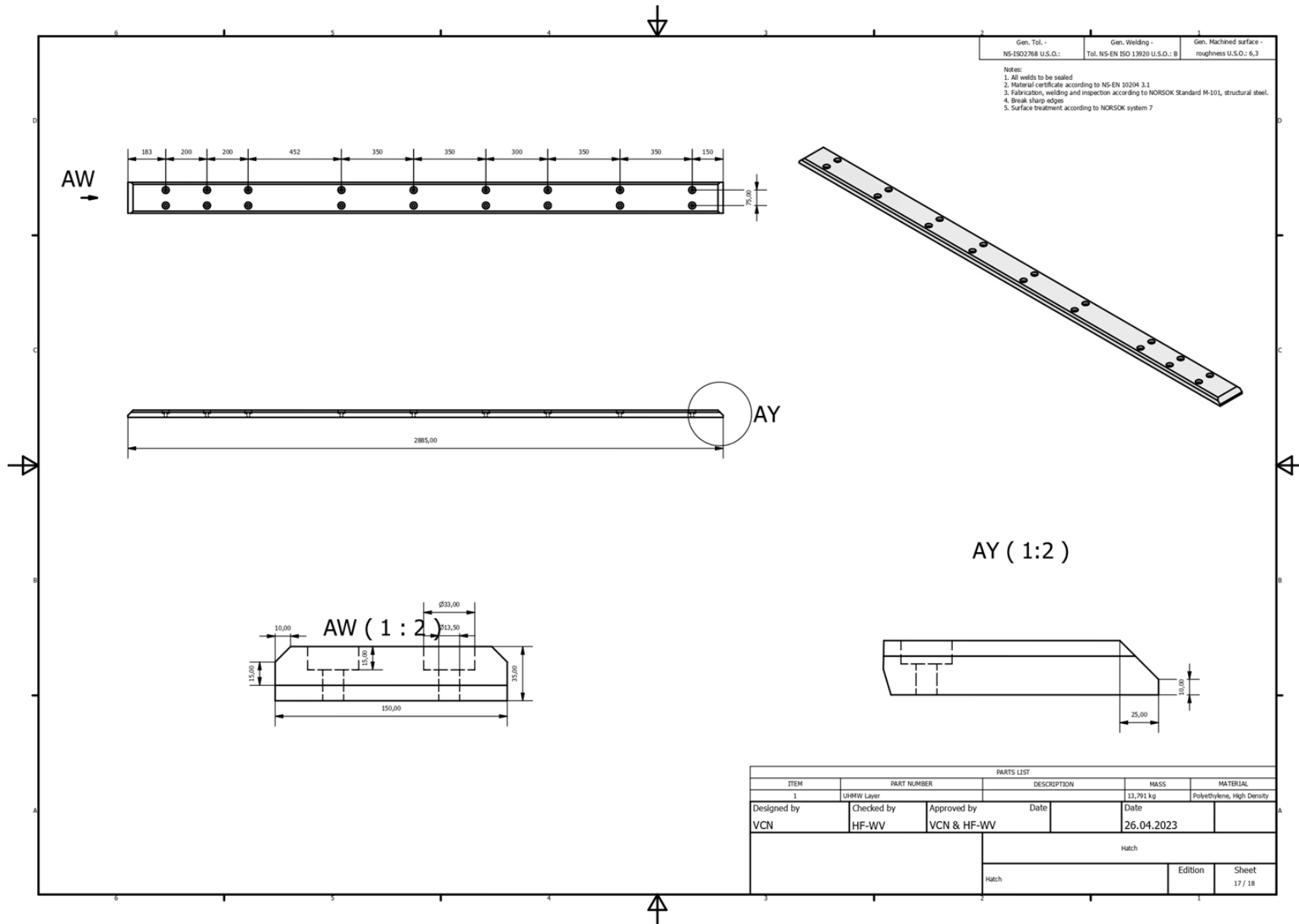
PARTS LIST					
ITEM	PART NUMBER	DESCRIPTION	MASS	MATERIAL	
1	SupportBeamTop		20,579 kg	S420N	
Designed by	Checked by	Approved by	Date	Date	
VCN	HF-WV	VCN & HF-WV		26.04.2023	
Hatch					
Hatch				Edition	Sheet
					12 / 18

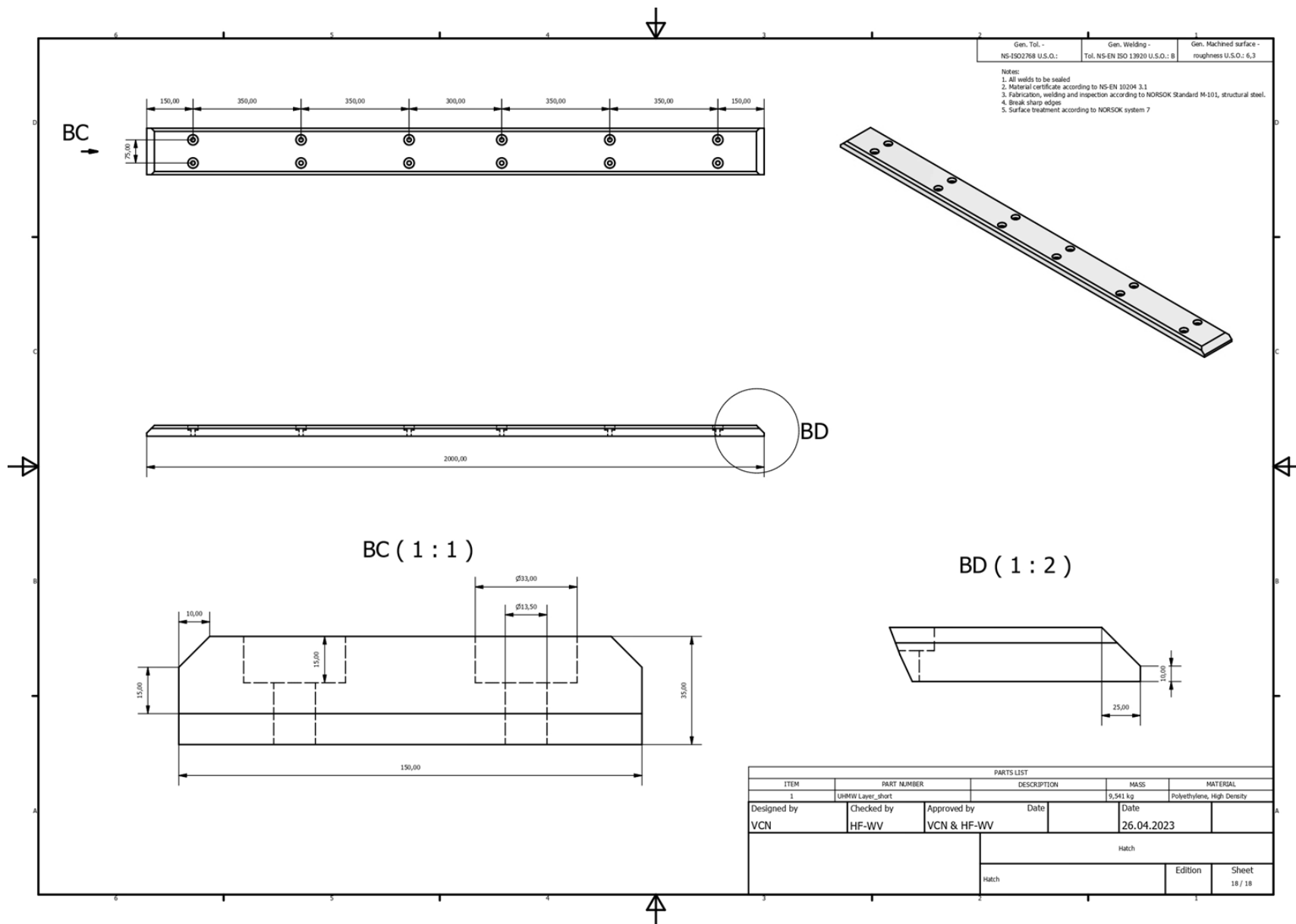




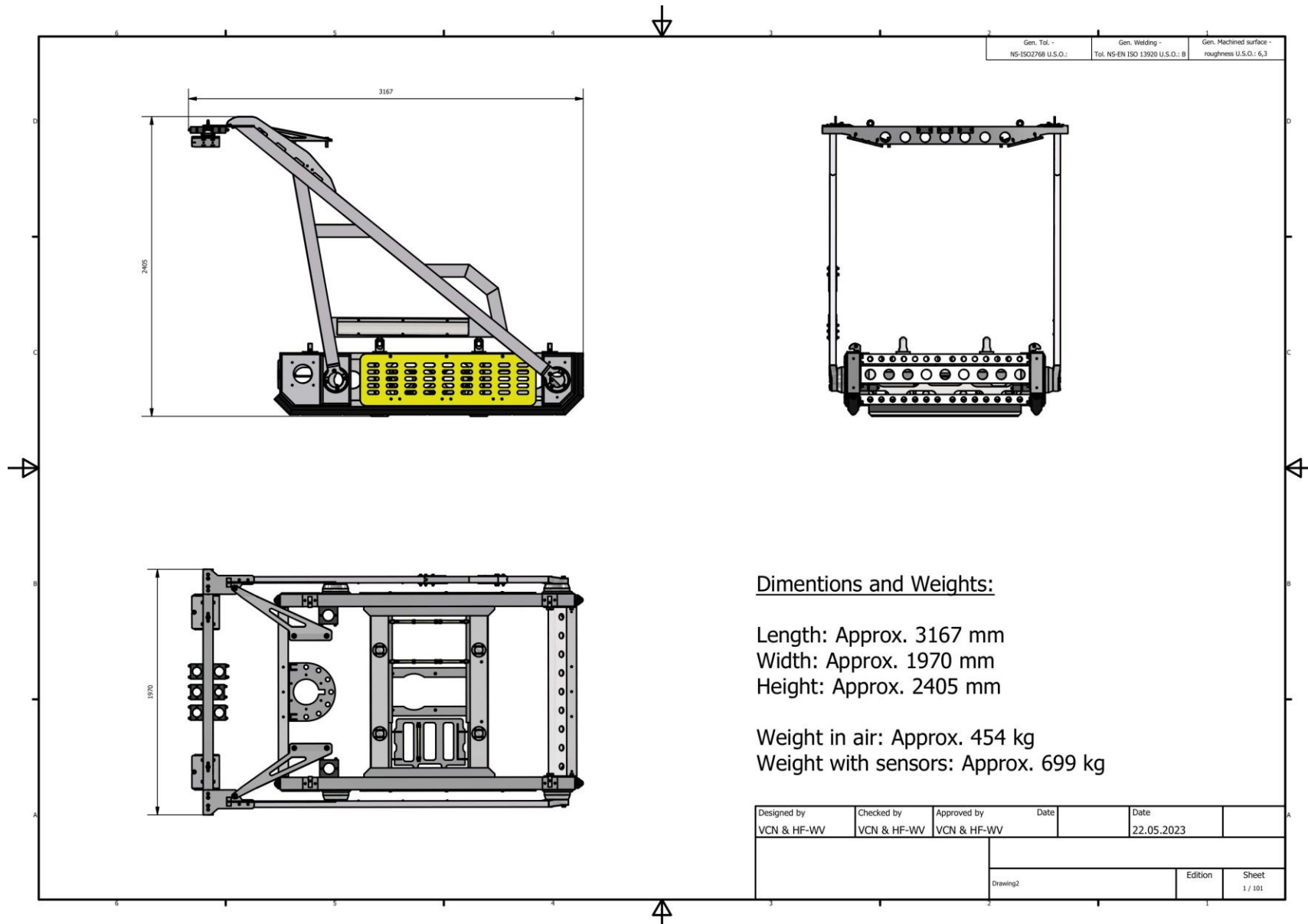








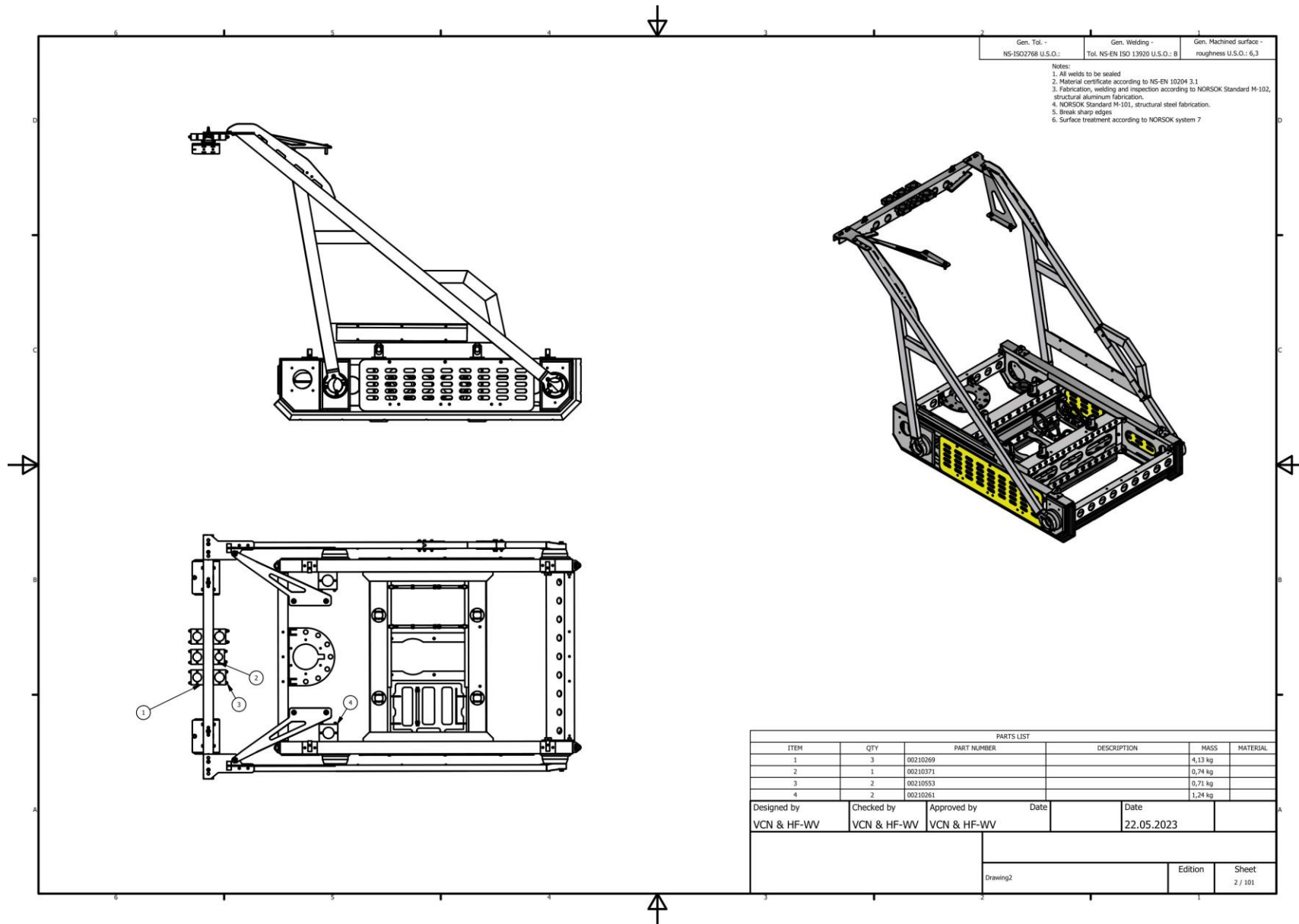
Appendix AA Skid Drawings

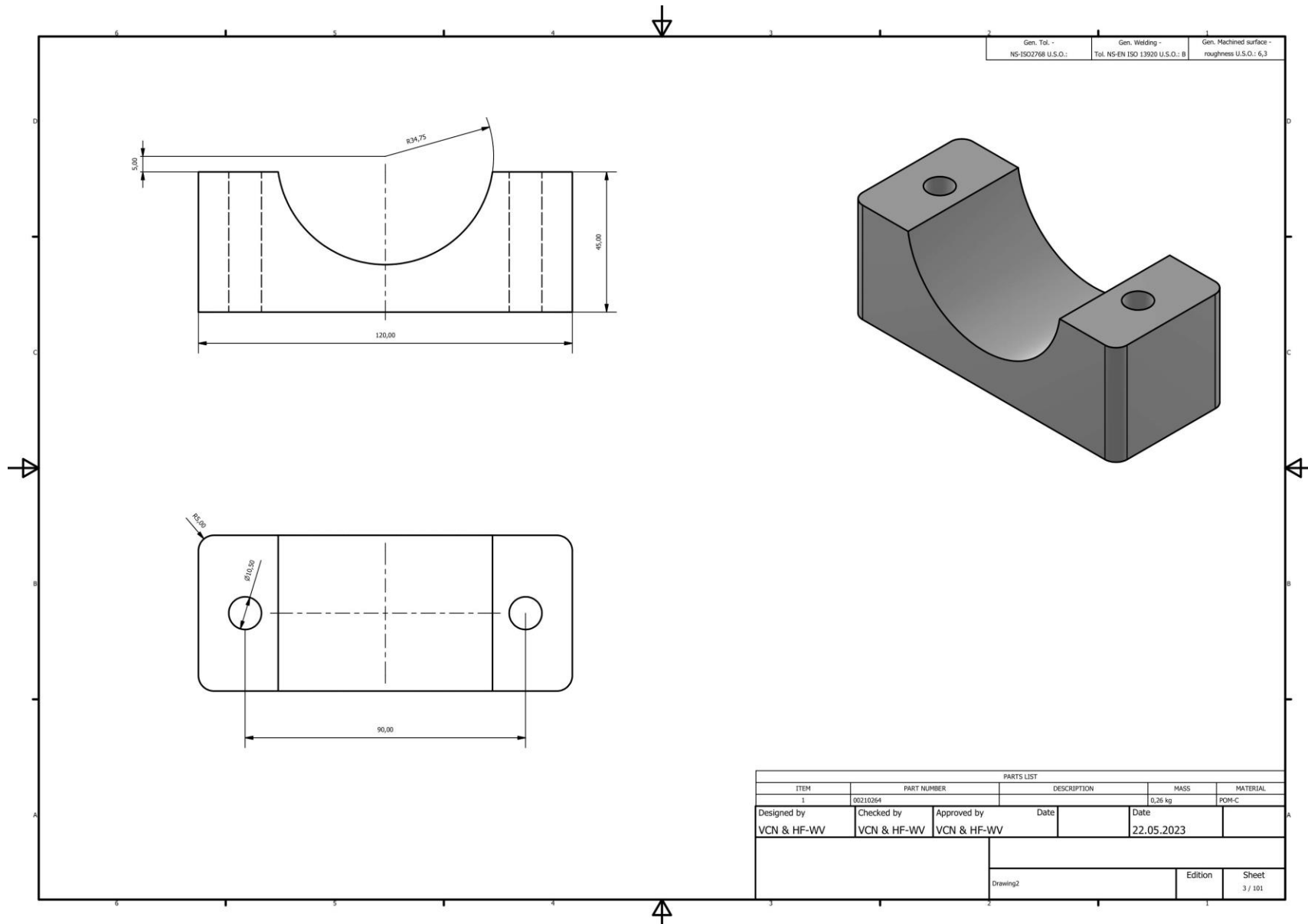


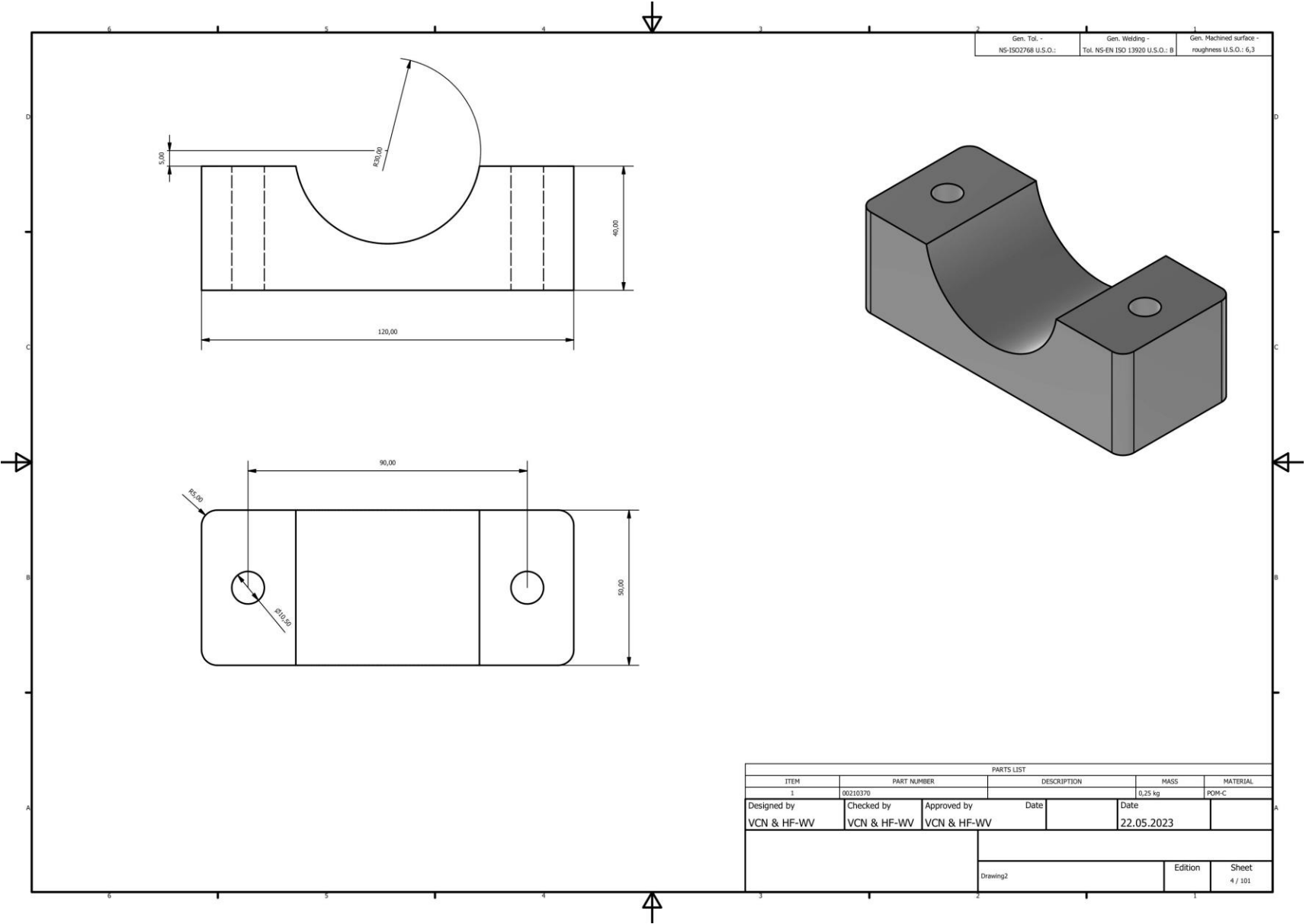
Dimensions and Weights:

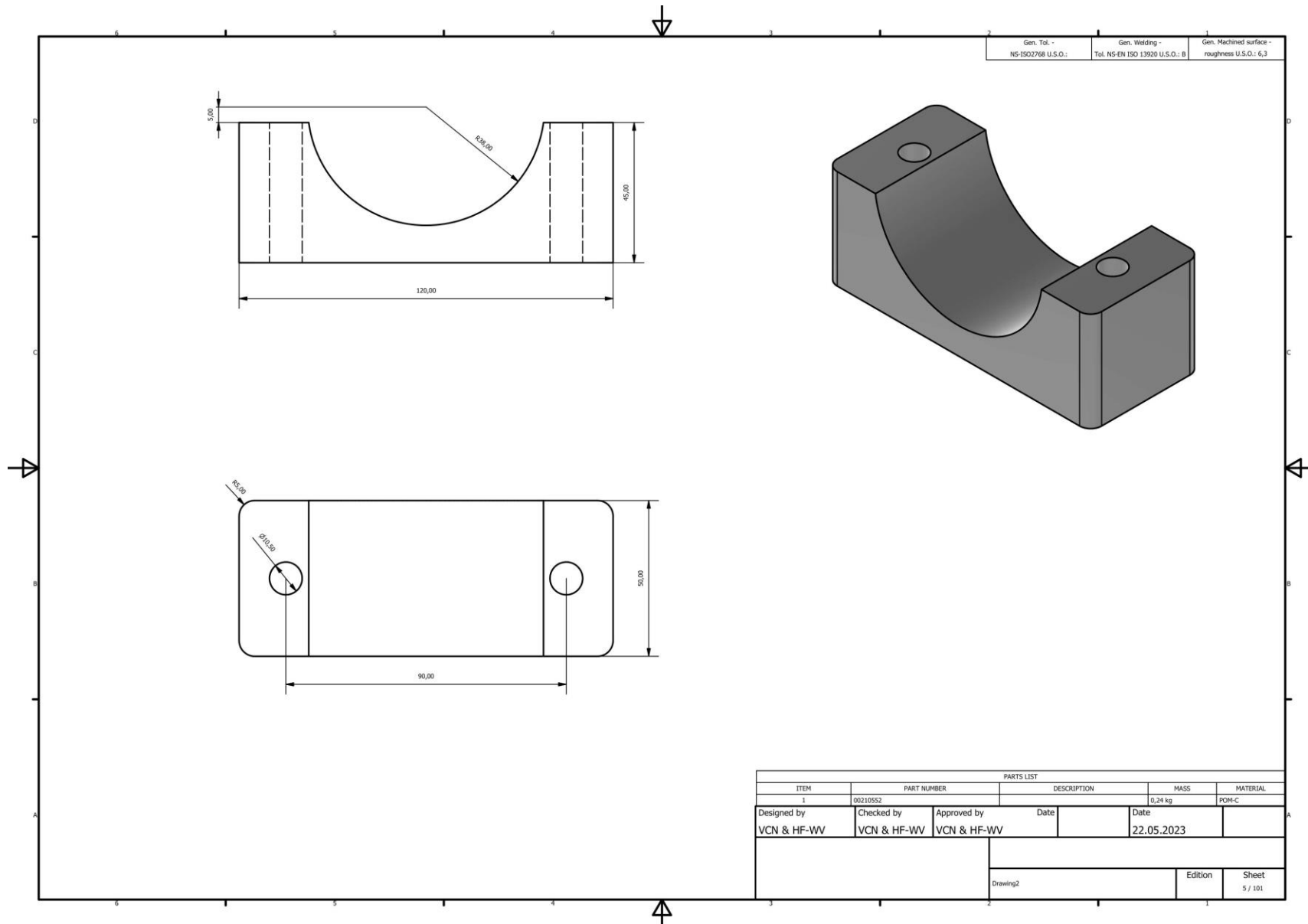
Length: Approx. 3167 mm
 Width: Approx. 1970 mm
 Height: Approx. 2405 mm

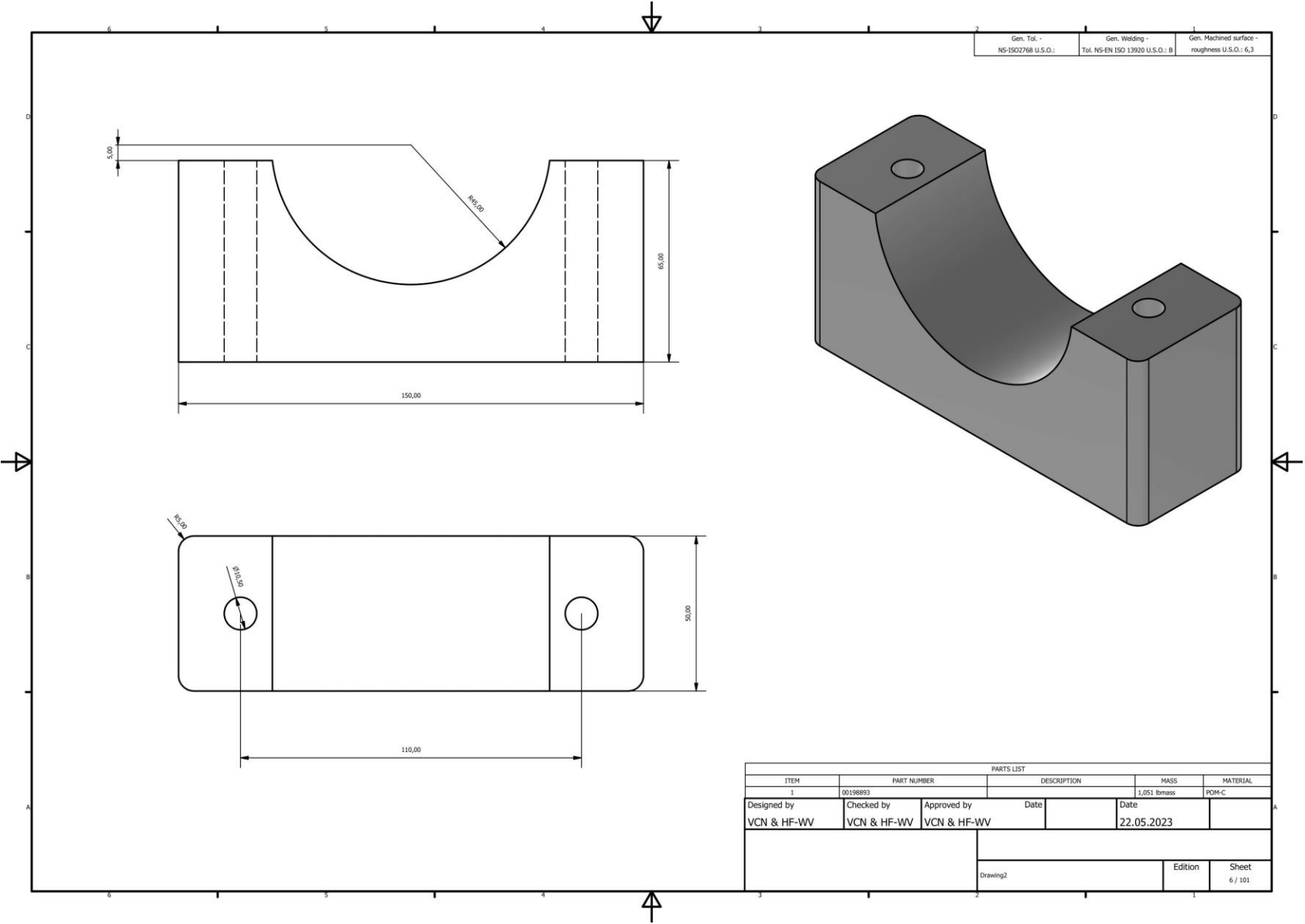
Weight in air: Approx. 454 kg
 Weight with sensors: Approx. 699 kg



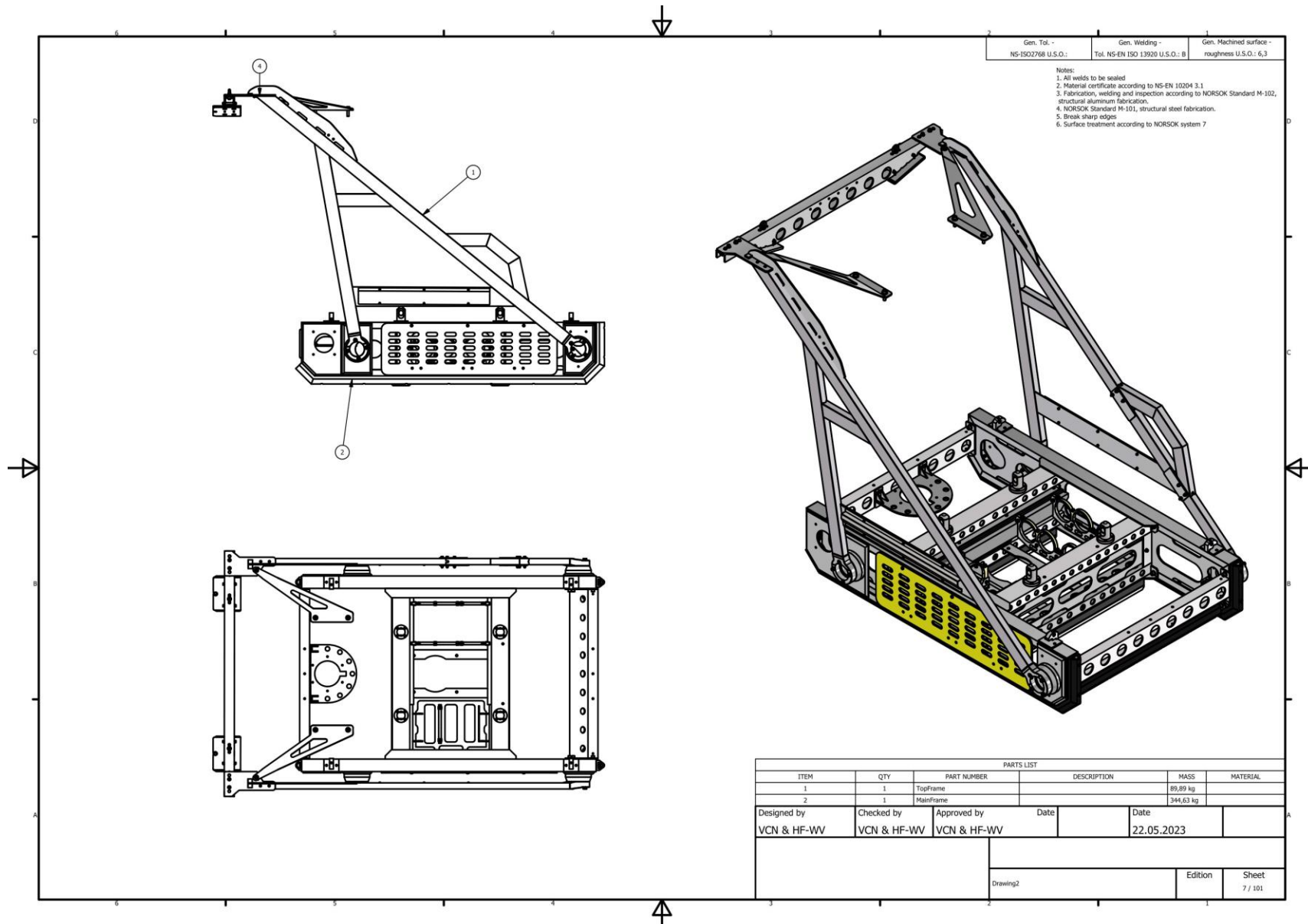


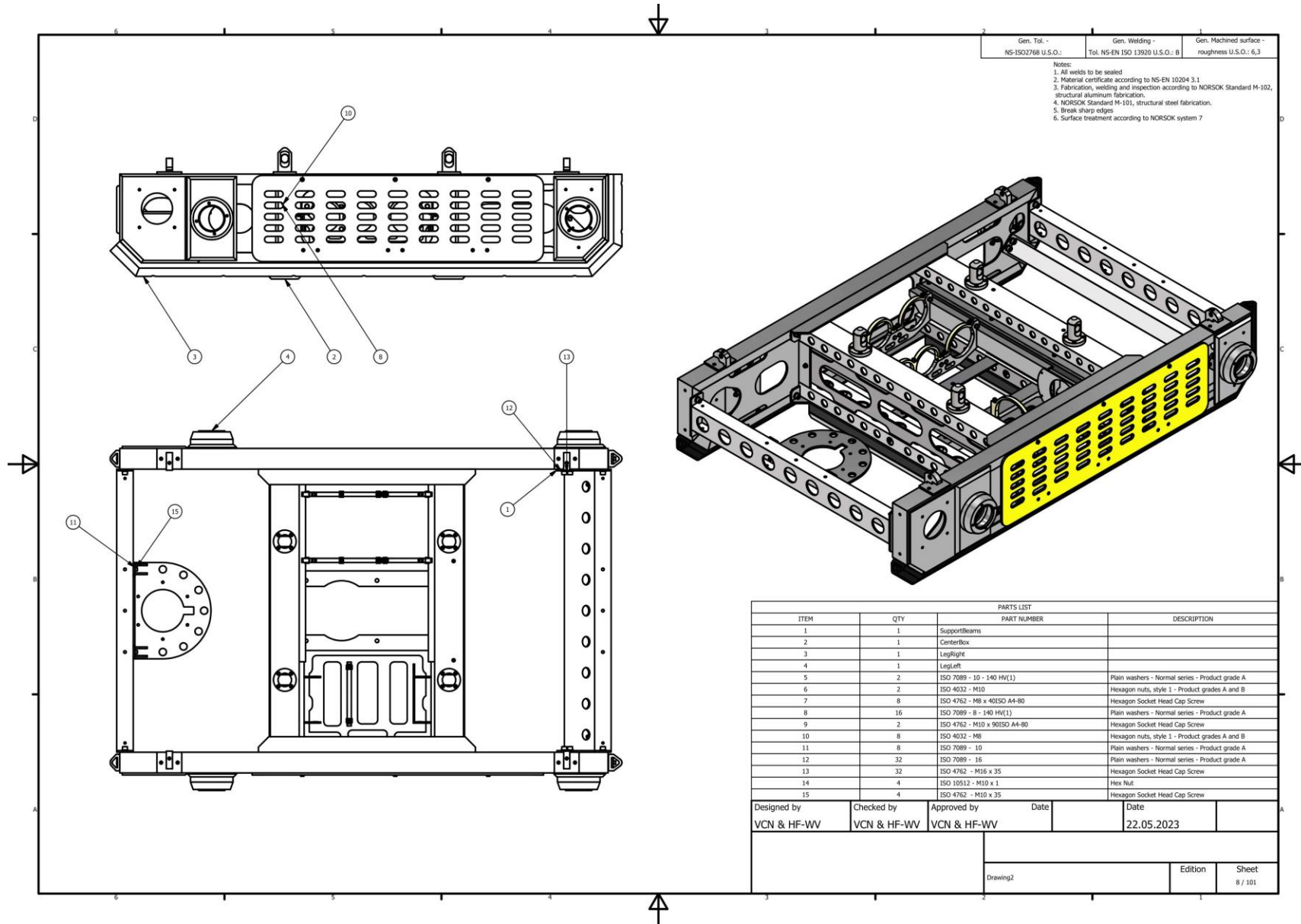






Integration of a Skid and Hatch-Based Launch and Recovery System for ROVs on USVs



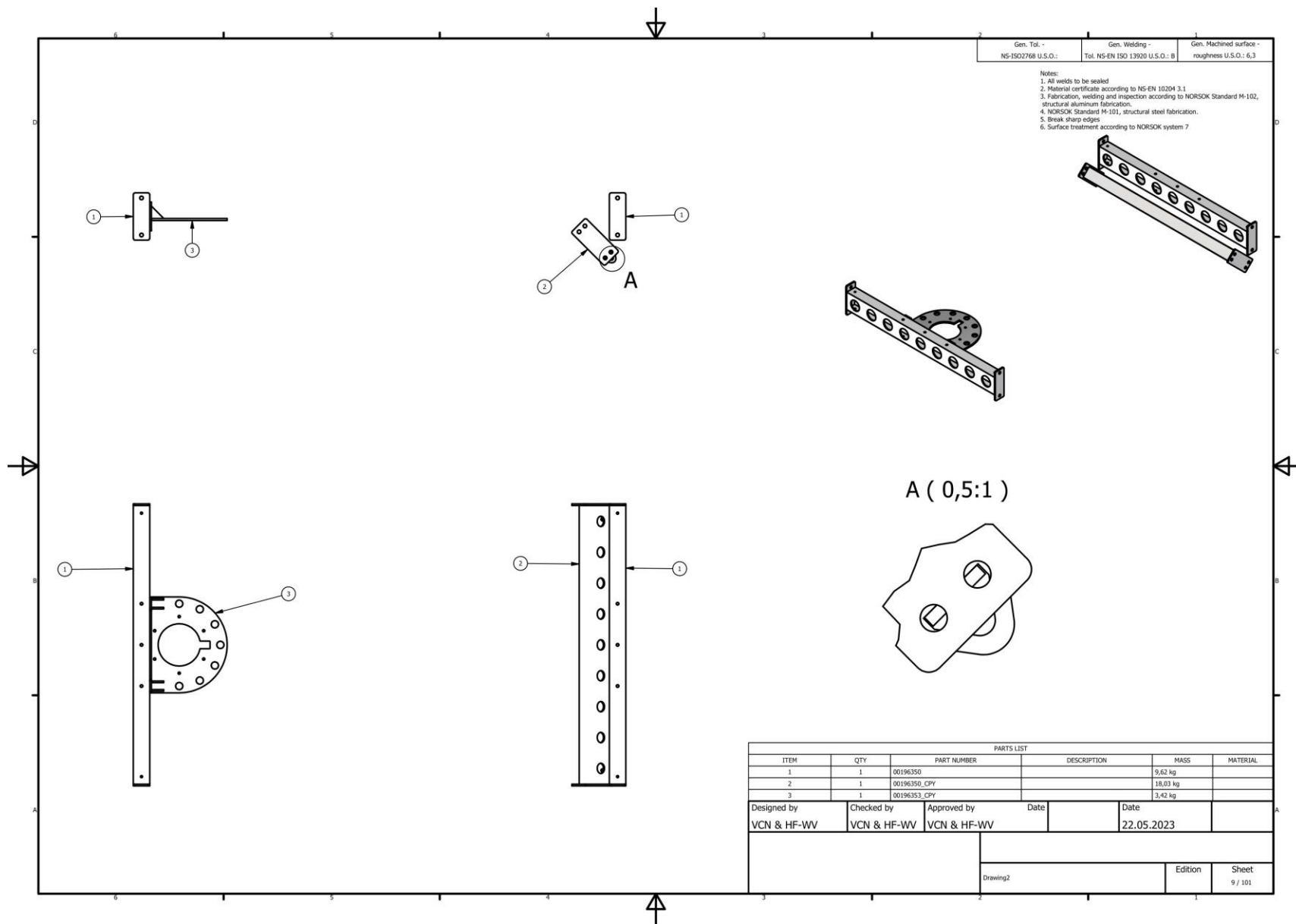


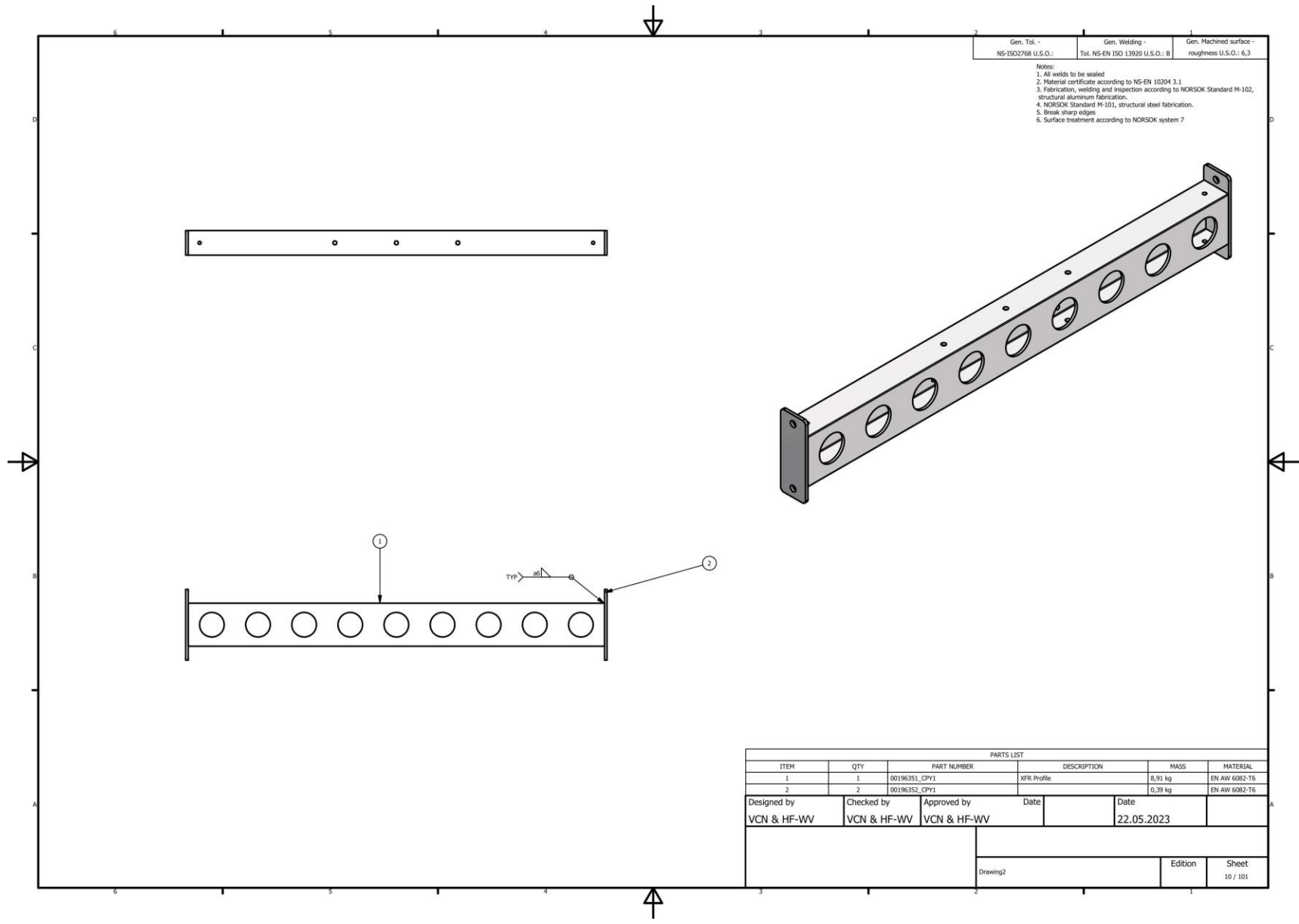
Gen. Tol - NS-ISO2768 U.S.O.; Gen. Welding - Tol. NS-EN ISO 13920 U.S.O.: B Gen. Machined surface - roughness U.S.O.: 6,3

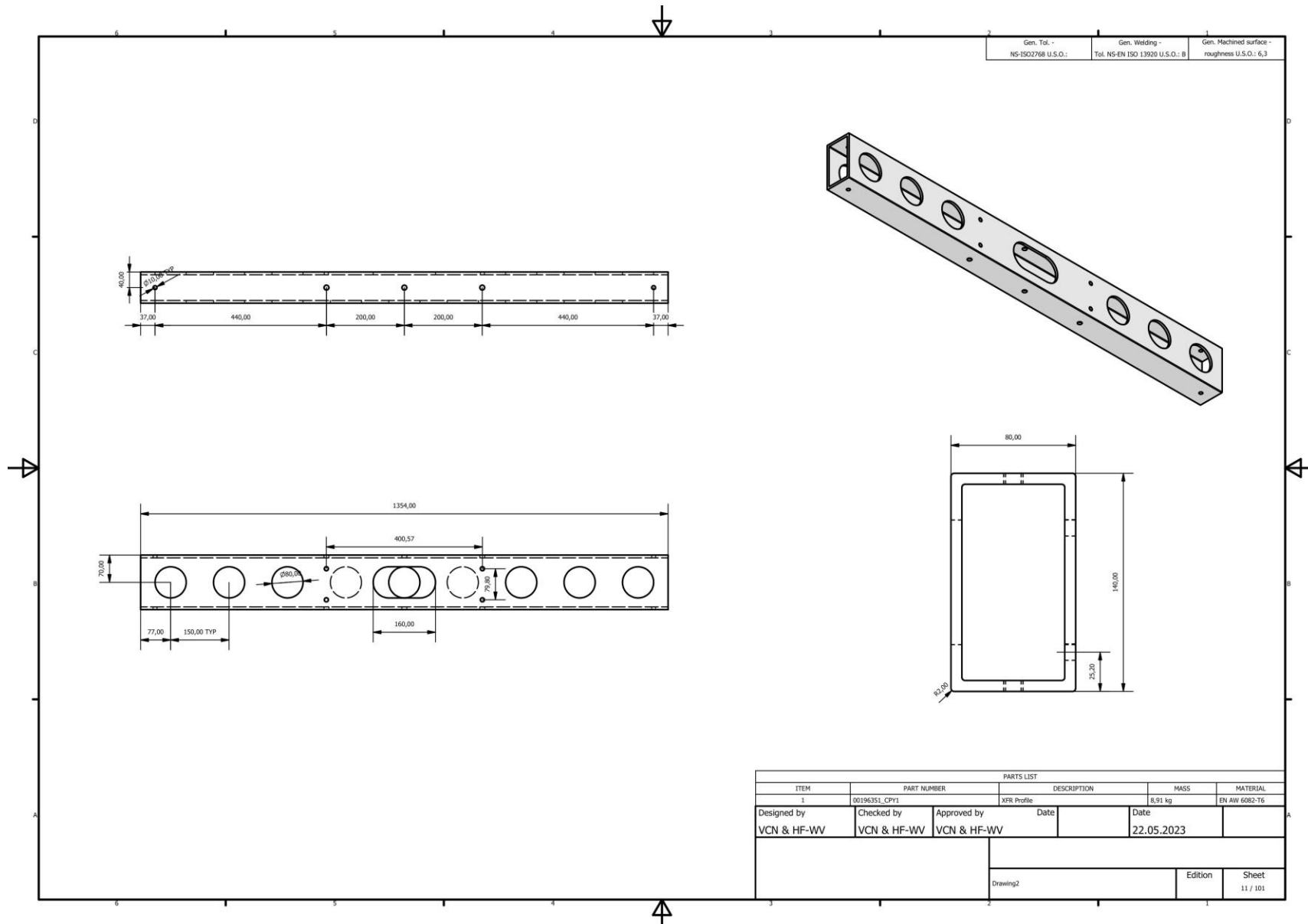
Notes:
 1. All welds to be sealed
 2. Material certificate according to NS-EN 10204 3.1
 3. Fabrication, welding and inspection according to NORSOK Standard M-102, structural aluminum fabrication.
 4. NORSOK Standard M-101, structural steel fabrication.
 5. Break sharp edges
 6. Surface treatment according to NORSOK system 7

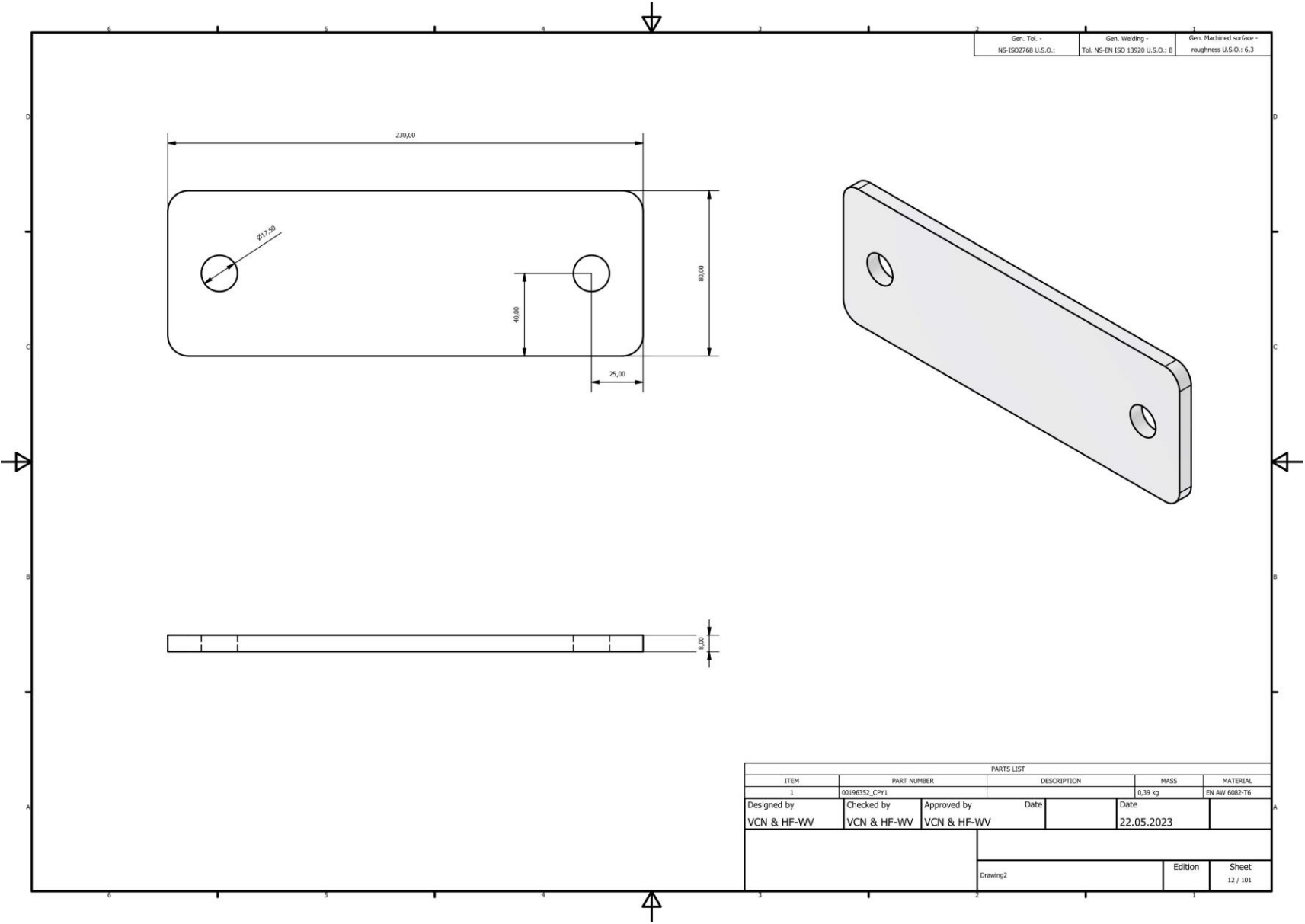
PARTS LIST				
ITEM	QTY	PART NUMBER	DESCRIPTION	
1	1	SupportBeams		
2	1	CenterBox		
3	1	LegRight		
4	1	LegLeft		
5	2	ISO 7089 - 10 - 140 HV(1)	Plain washers - Normal series - Product grade A	
6	2	ISO 4032 - M10	Hexagon nuts, style 1 - Product grades A and B	
7	8	ISO 4762 - M8 x 40ISO A4-80	Hexagon Socket Head Cap Screw	
8	16	ISO 7089 - 8 - 140 HV(1)	Plain washers - Normal series - Product grade A	
9	2	ISO 4762 - M10 x 90ISO A4-80	Hexagon Socket Head Cap Screw	
10	8	ISO 4032 - M8	Hexagon nuts, style 1 - Product grades A and B	
11	8	ISO 7089 - 10	Plain washers - Normal series - Product grade A	
12	32	ISO 7089 - 16	Plain washers - Normal series - Product grade A	
13	32	ISO 4762 - M16 x 35	Hexagon Socket Head Cap Screw	
14	4	ISO 10512 - M10 x 1	Hex Nut	
15	4	ISO 4762 - M10 x 35	Hexagon Socket Head Cap Screw	
Designed by	Checked by	Approved by	Date	Date
VCN & HF-WV	VCN & HF-WV	VCN & HF-WV		22.05.2023
			Drawing2	Edition
				Sheet
				8 / 101

Integration of a Skid and Hatch-Based Launch and Recovery System for ROVs on USVs

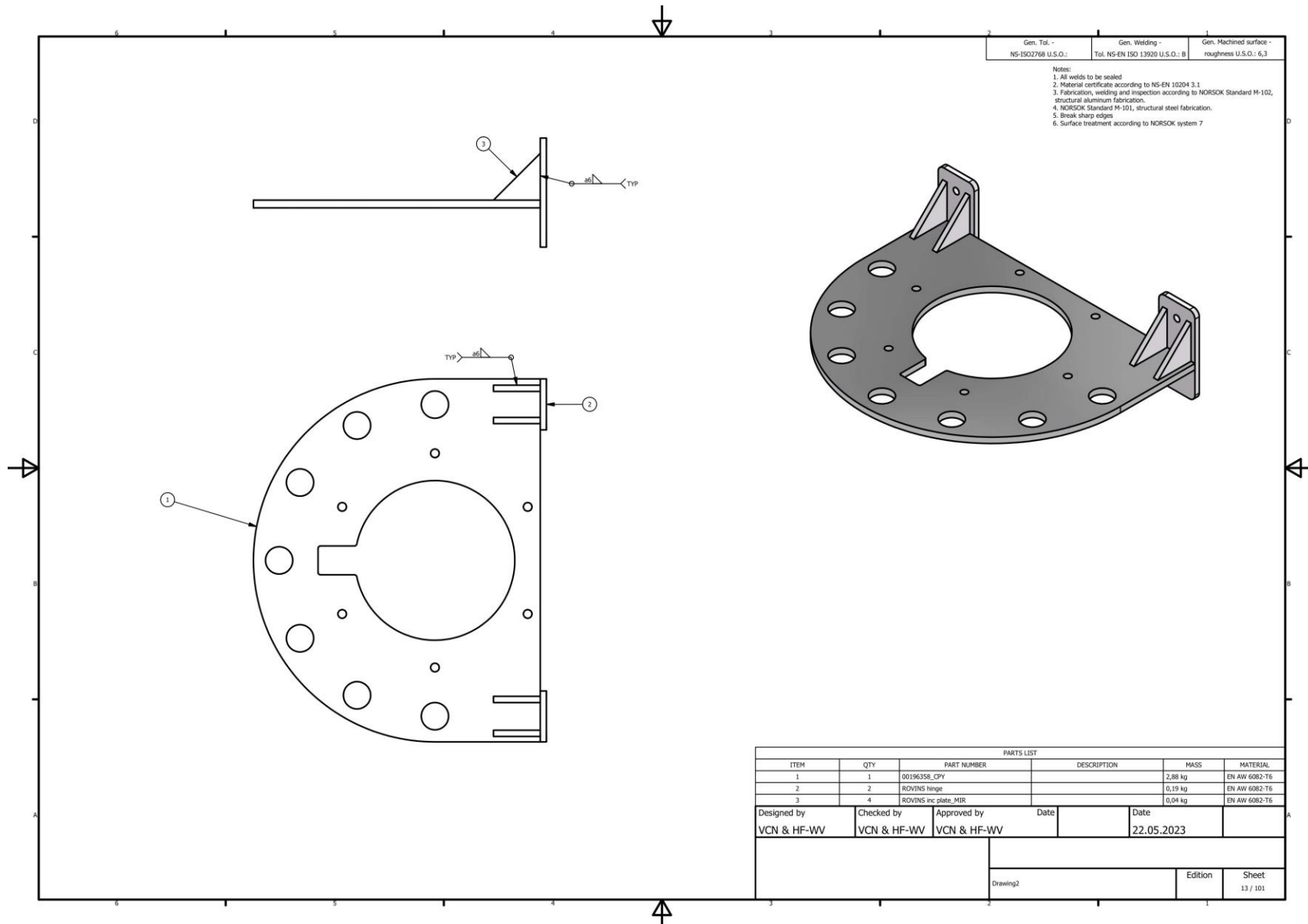








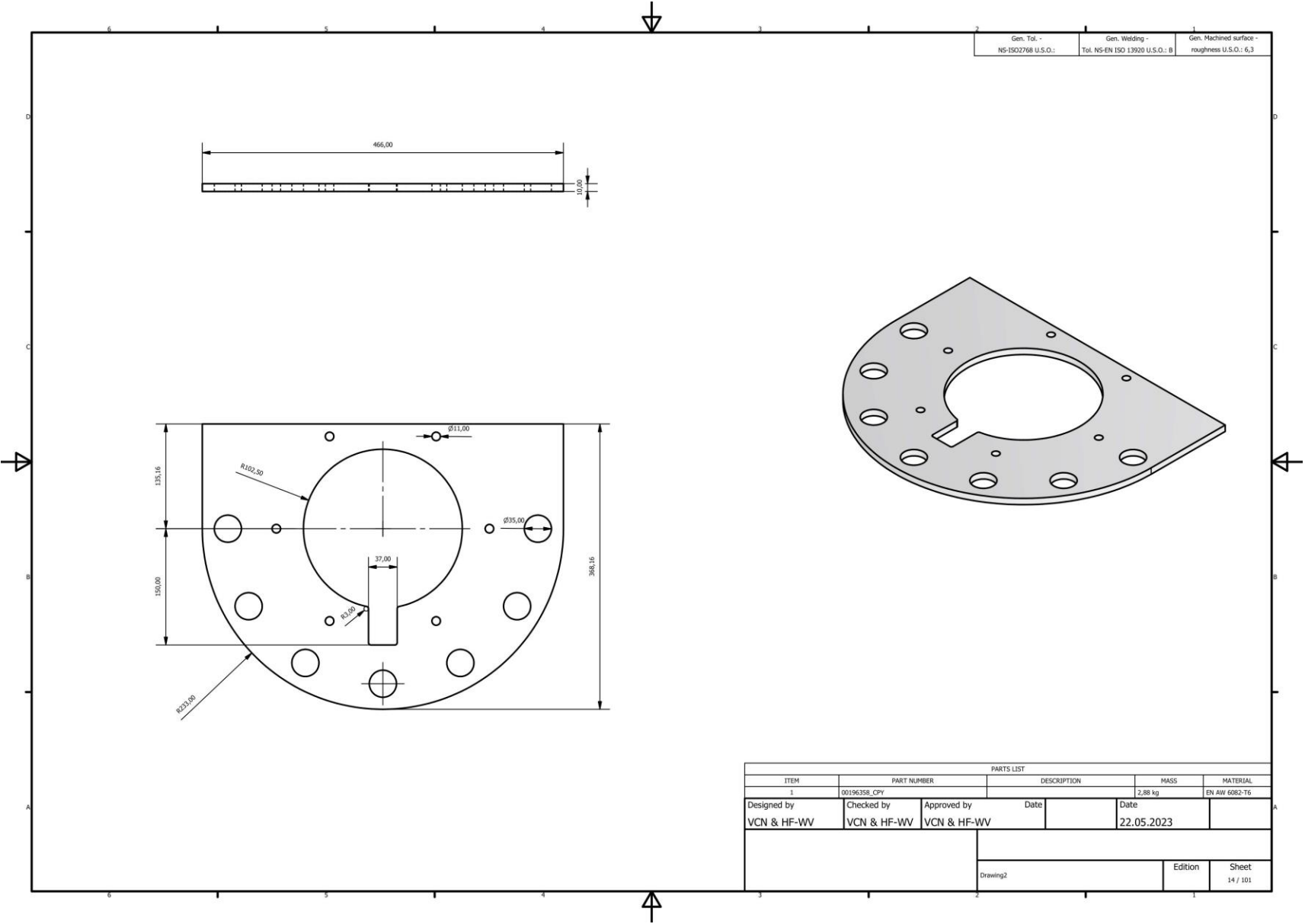
Integration of a Skid and Hatch-Based Launch and Recovery System for ROVs on USVs



Gen. Tol. -
NS-ISO2768 U.S.O.:
Gen. Welding -
Tol. NS-EN ISO 13920 U.S.O.: B
Gen. Machined surface -
roughness U.S.O.: 6,3

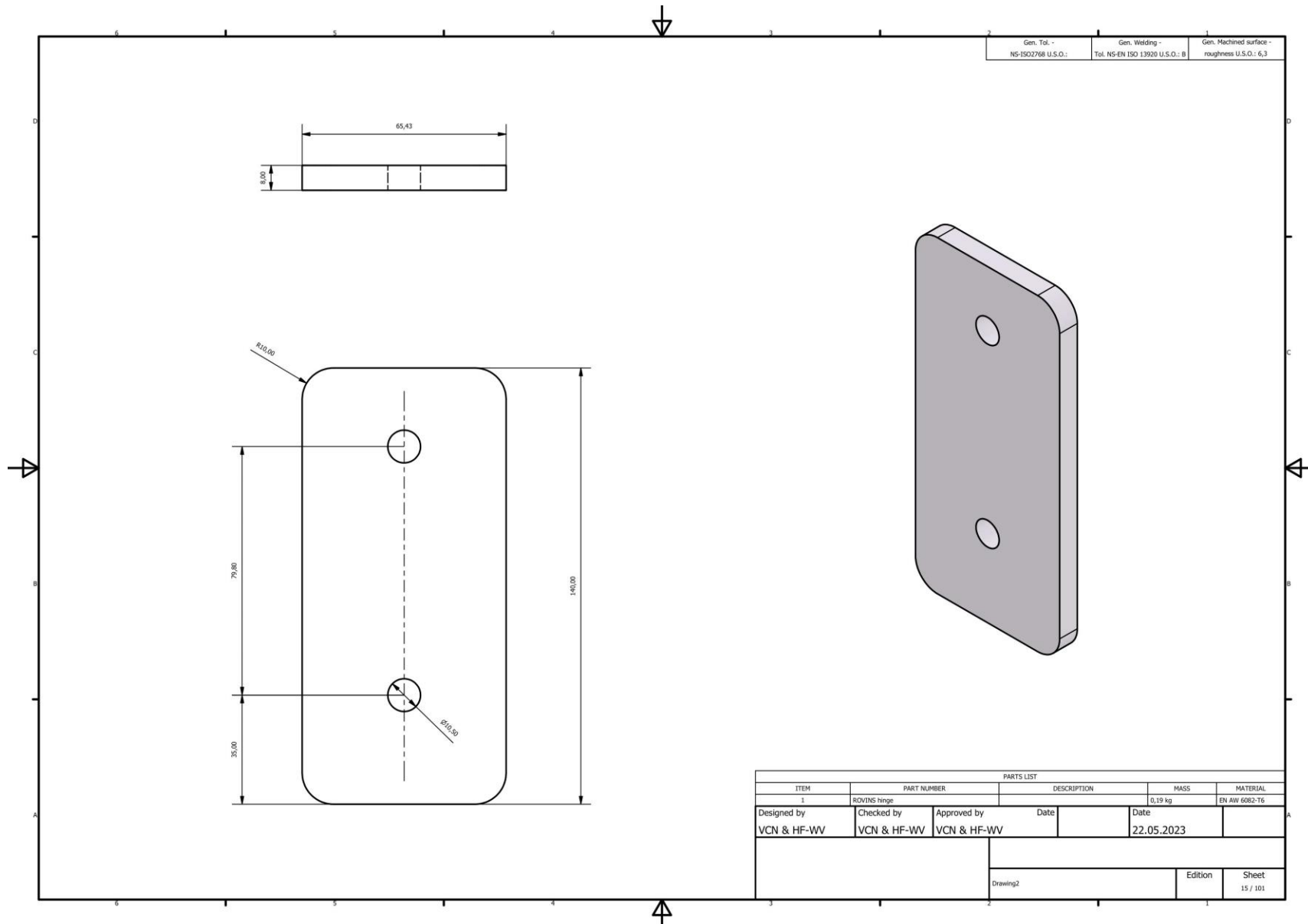
Notes:
1. All welds to be sealed
2. Material certificate according to NS-EN 10204 3.1
3. Fabrication, welding and inspection according to NORSOK Standard M-102, structural aluminum fabrication.
4. NORSOK Standard M-101, structural steel fabrication.
5. Break sharp edges
6. Surface treatment according to NORSOK system 7

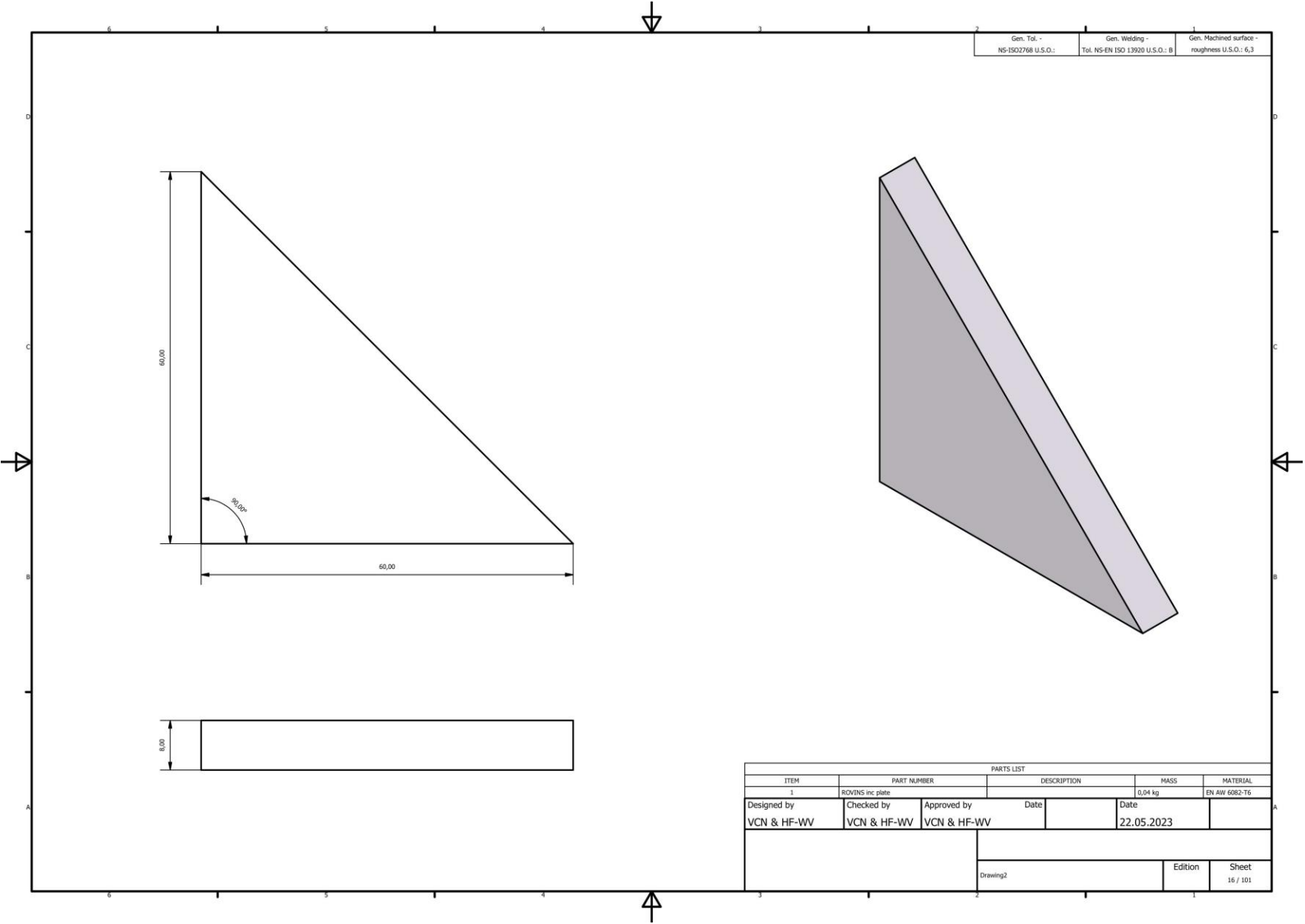
PARTS LIST						
ITEM	QTY	PART NUMBER	DESCRIPTION	MASS	MATERIAL	
1	1	00196358_COPY		2,88 kg	EN AW 6082-T6	
2	2	ROVINS Hinge		0,19 kg	EN AW 6082-T6	
3	4	ROVINS Inc plate_MIR		0,04 kg	EN AW 6082-T6	
Designed by		Checked by	Approved by	Date	Date	
VCN & HF-WV		VCN & HF-WV	VCN & HF-WV		22.05.2023	
				Drawing2	Edition	Sheet
						13 / 101



Gen. Tol - NS-ISO2768 U.S.O.:	Gen. Welding - Tol. NS-EN ISO 13920 U.S.O.:	Gen. Machined surface - roughness U.S.O.:
	B	6,3

PARTS LIST				
ITEM	PART NUMBER	DESCRIPTION	MASS	MATERIAL
1	00196358_CPY		2,88 kg	EN AW 6082-T6
Designed by	Checked by	Approved by	Date	Date
VCN & HF-WV	VCN & HF-WV	VCN & HF-WV		22.05.2023
			Edition	Sheet
			Drawing2	14 / 101

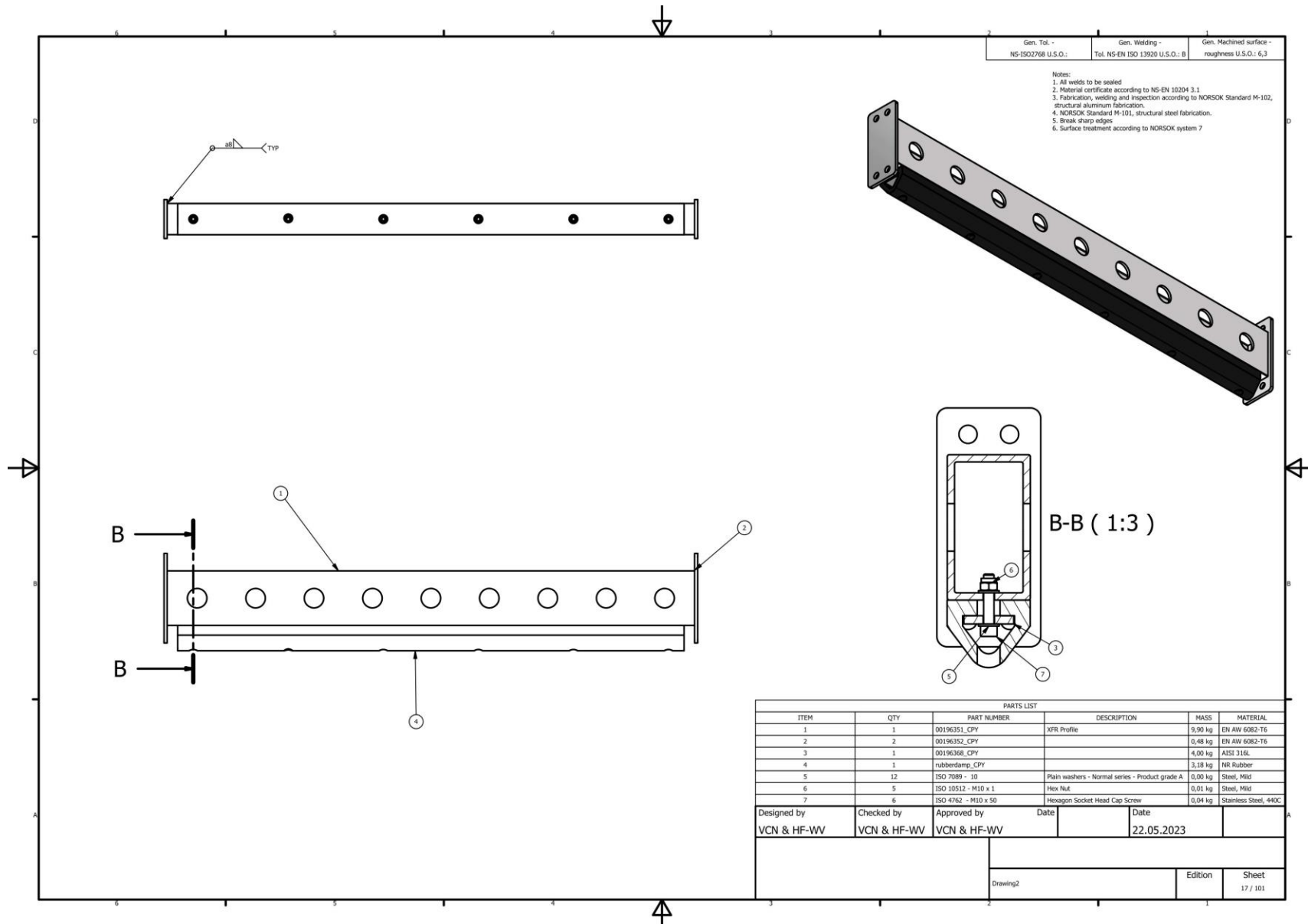


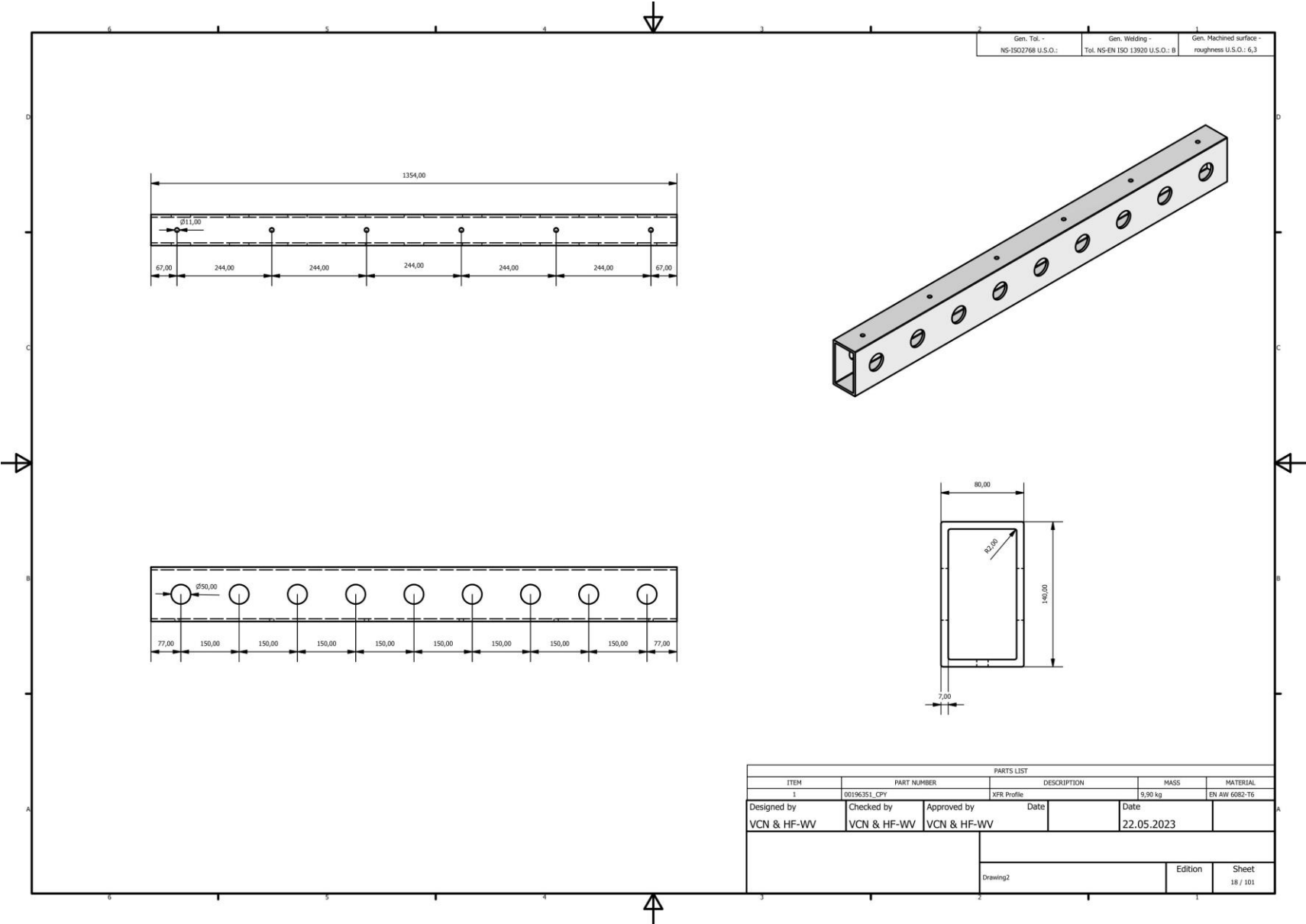


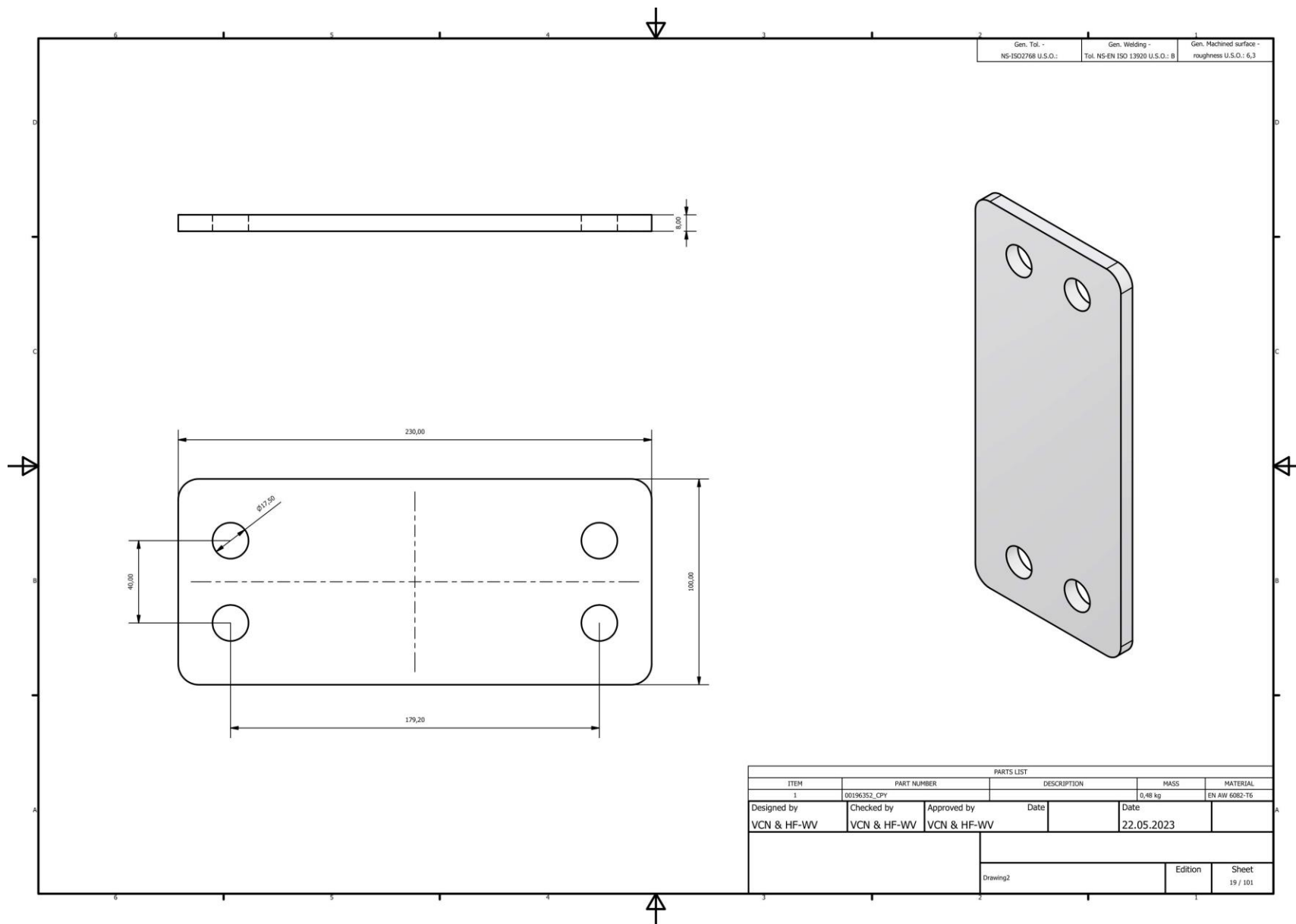
Gen. Tol - NS-ISO2768 U.S.O.:	Gen. Welding - Tol. NS-EN ISO 13920 U.S.O.:	Gen. Machined surface - roughness U.S.O.:
	B	6,3

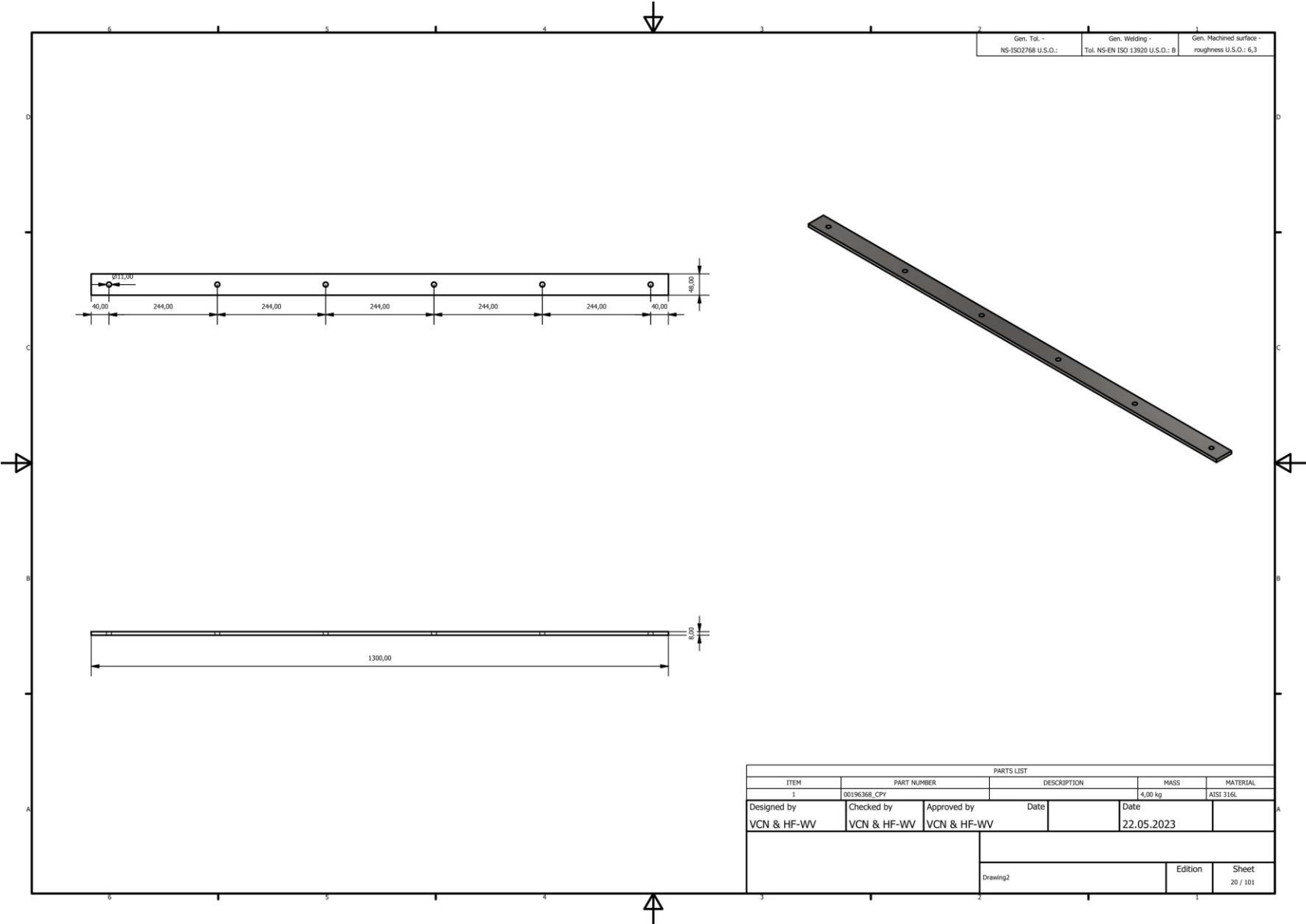
PARTS LIST				
ITEM	PART NUMBER	DESCRIPTION	MASS	MATERIAL
1	ROVINS inc plate		0,04 kg	EN AW 6082-T6
Designed by	Checked by	Approved by	Date	Date
VCN & HF-WV	VCN & HF-WV	VCN & HF-WV		22.05.2023
			Edition	Sheet
			Drawing2	16 / 101

Integration of a Skid and Hatch-Based Launch and Recovery System for ROVs on USVs

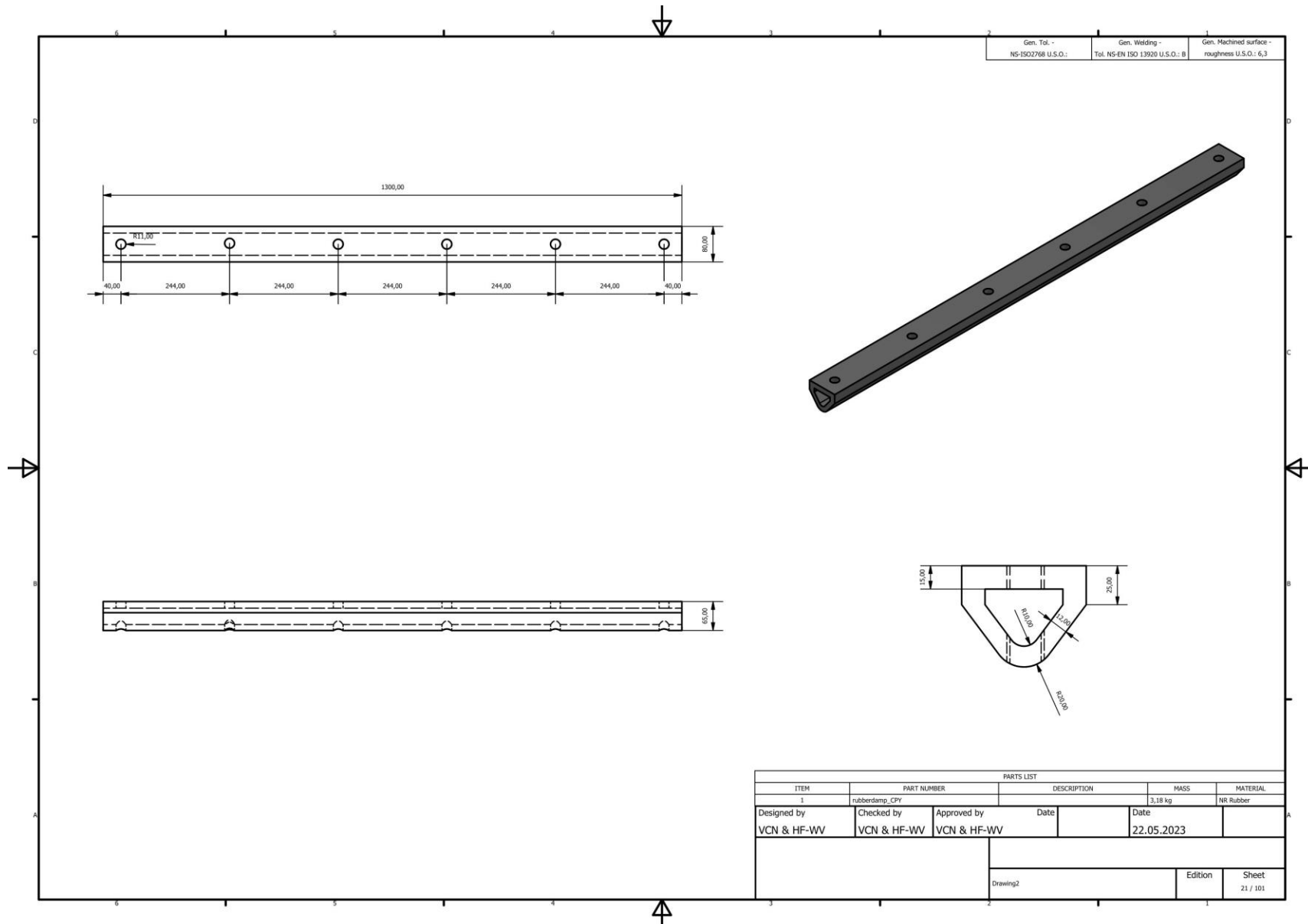


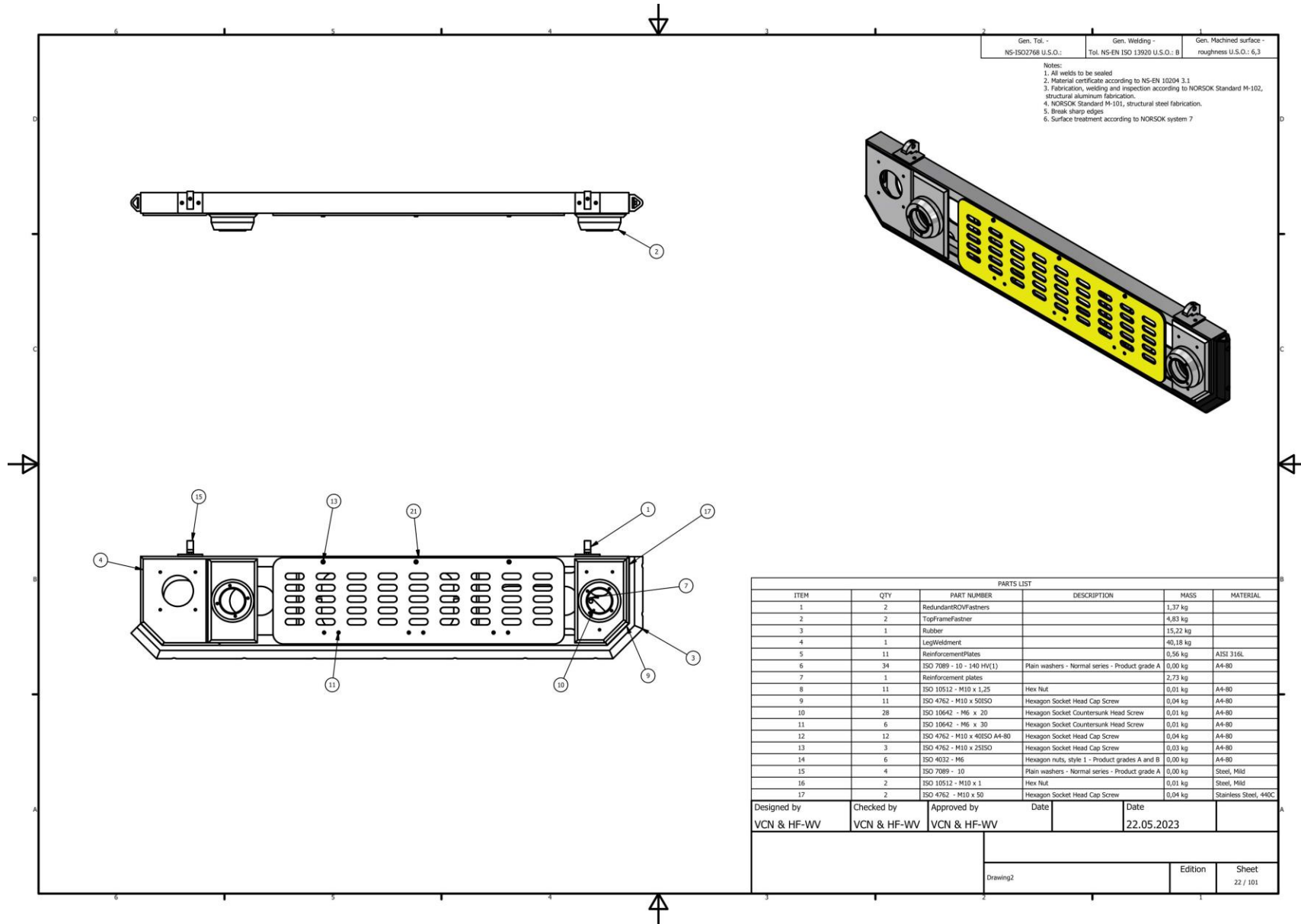




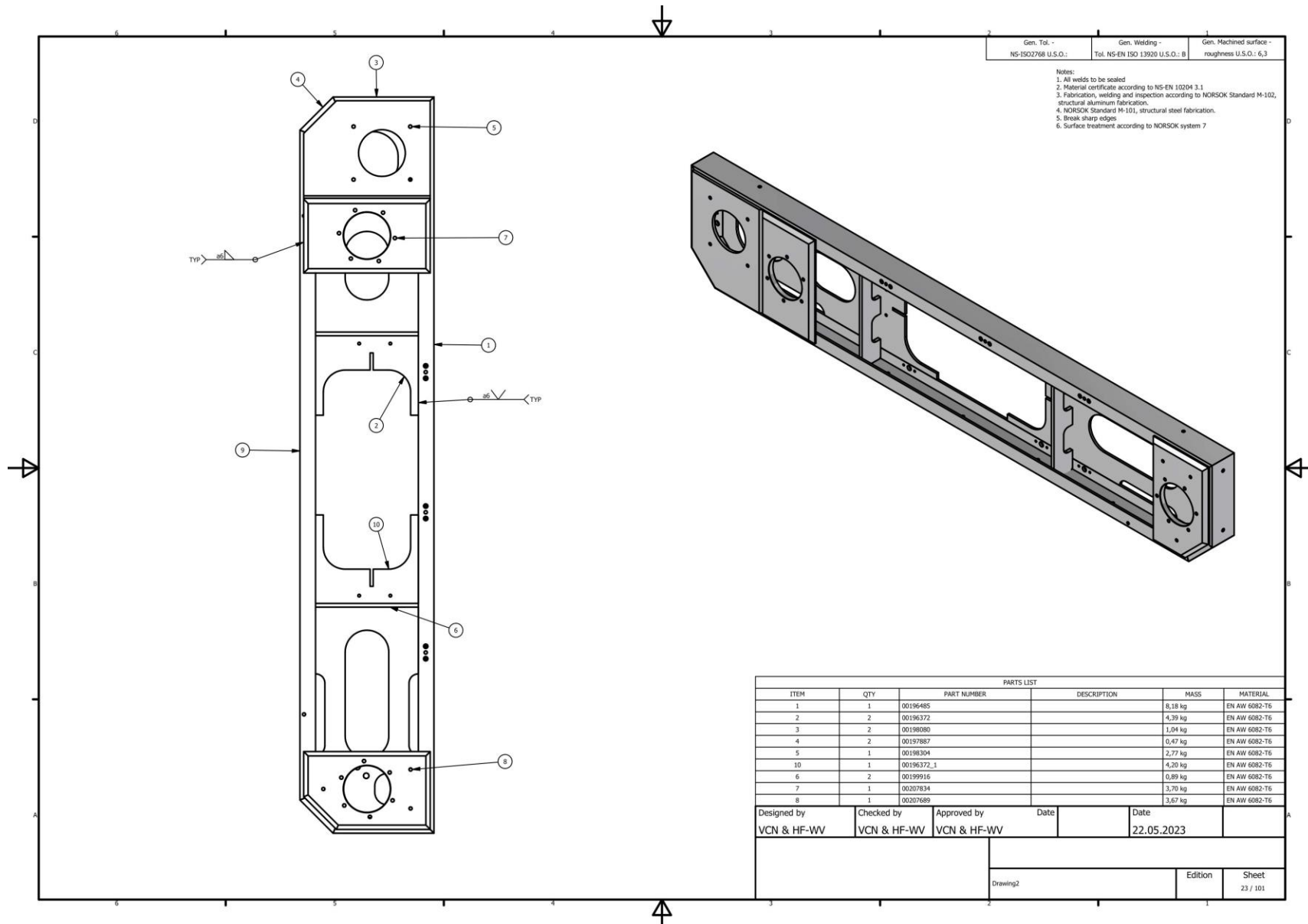


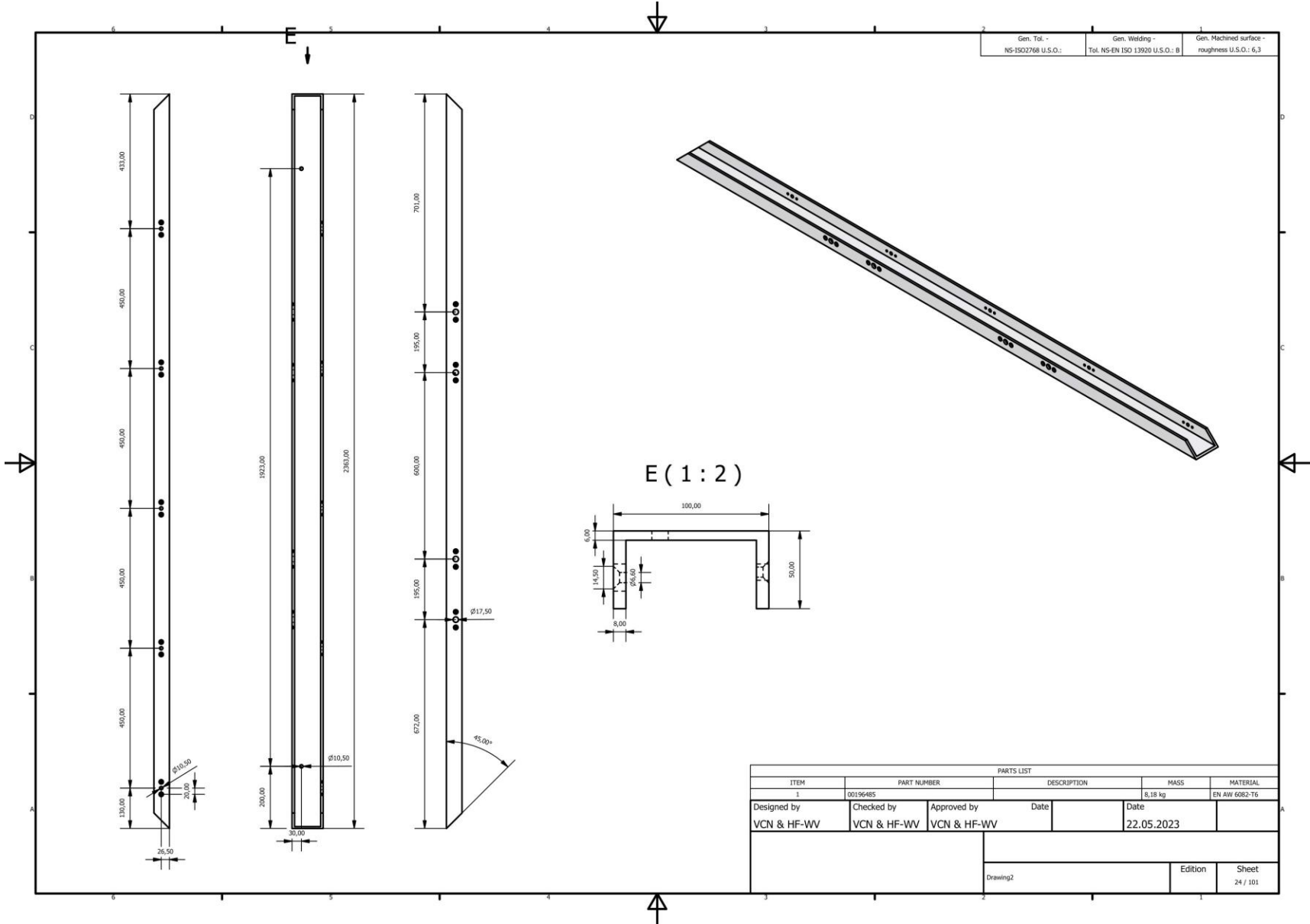
PARTS LIST					
ITEM	PART NUMBER	DESCRIPTION	MASS	MATERIAL	
1	00196368_CPY		4,00 kg	AISI 316L	
Designed by	Checked by	Approved by	Date	Date	
VCN & HF-WV	VCN & HF-WV	VCN & HF-WV		22.05.2023	
			Edition		Sheet
			Drawing2		20 / 101

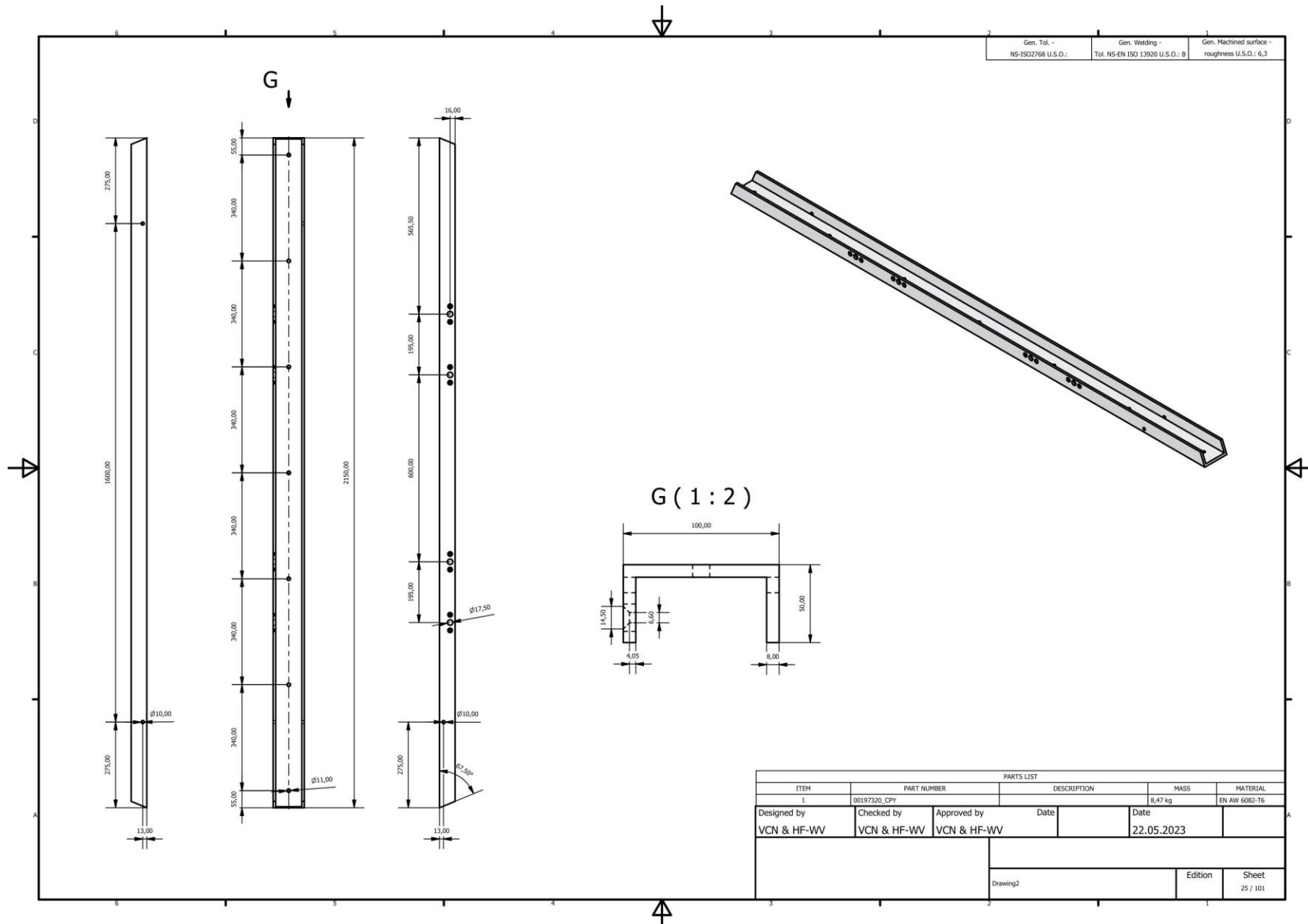


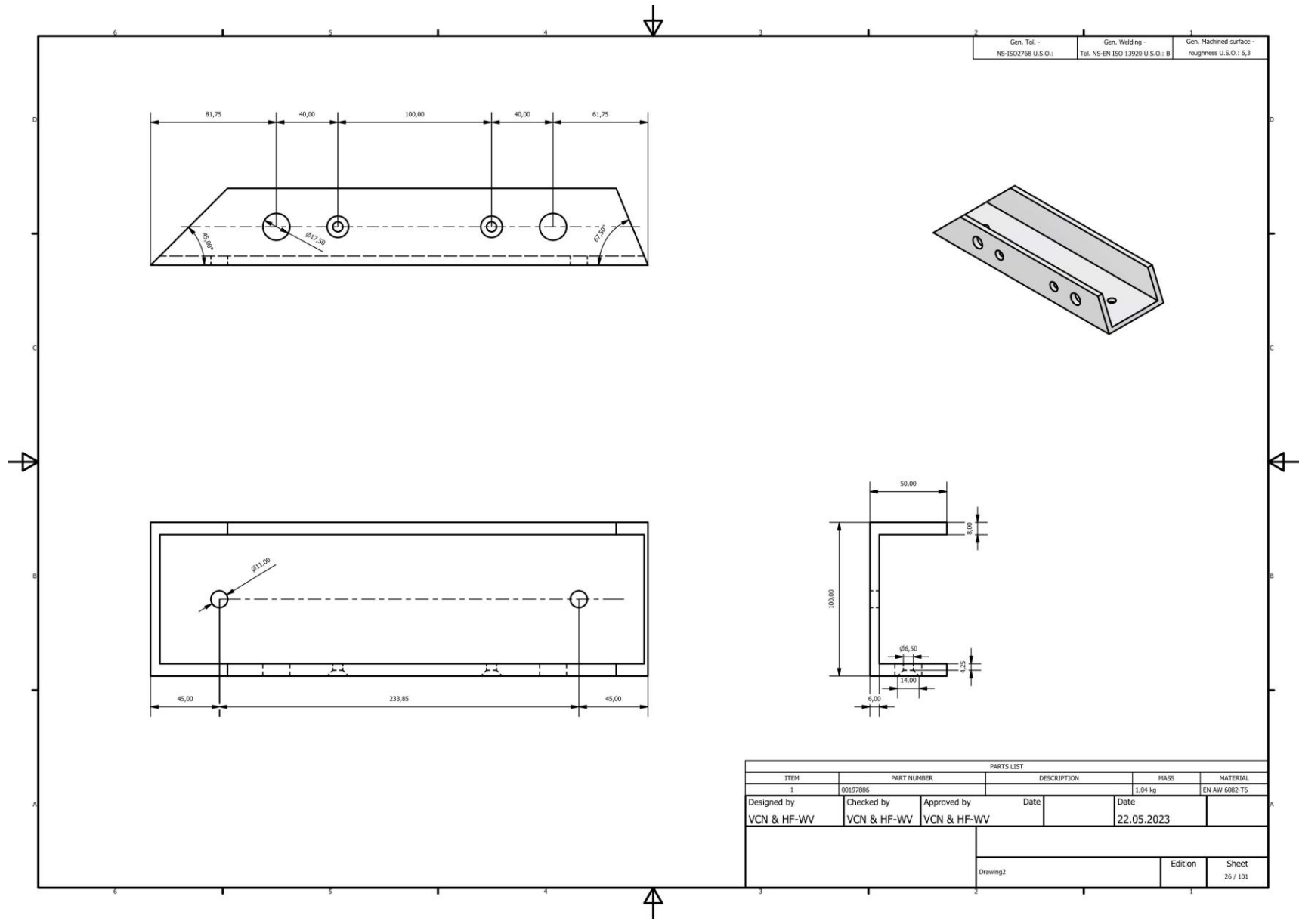


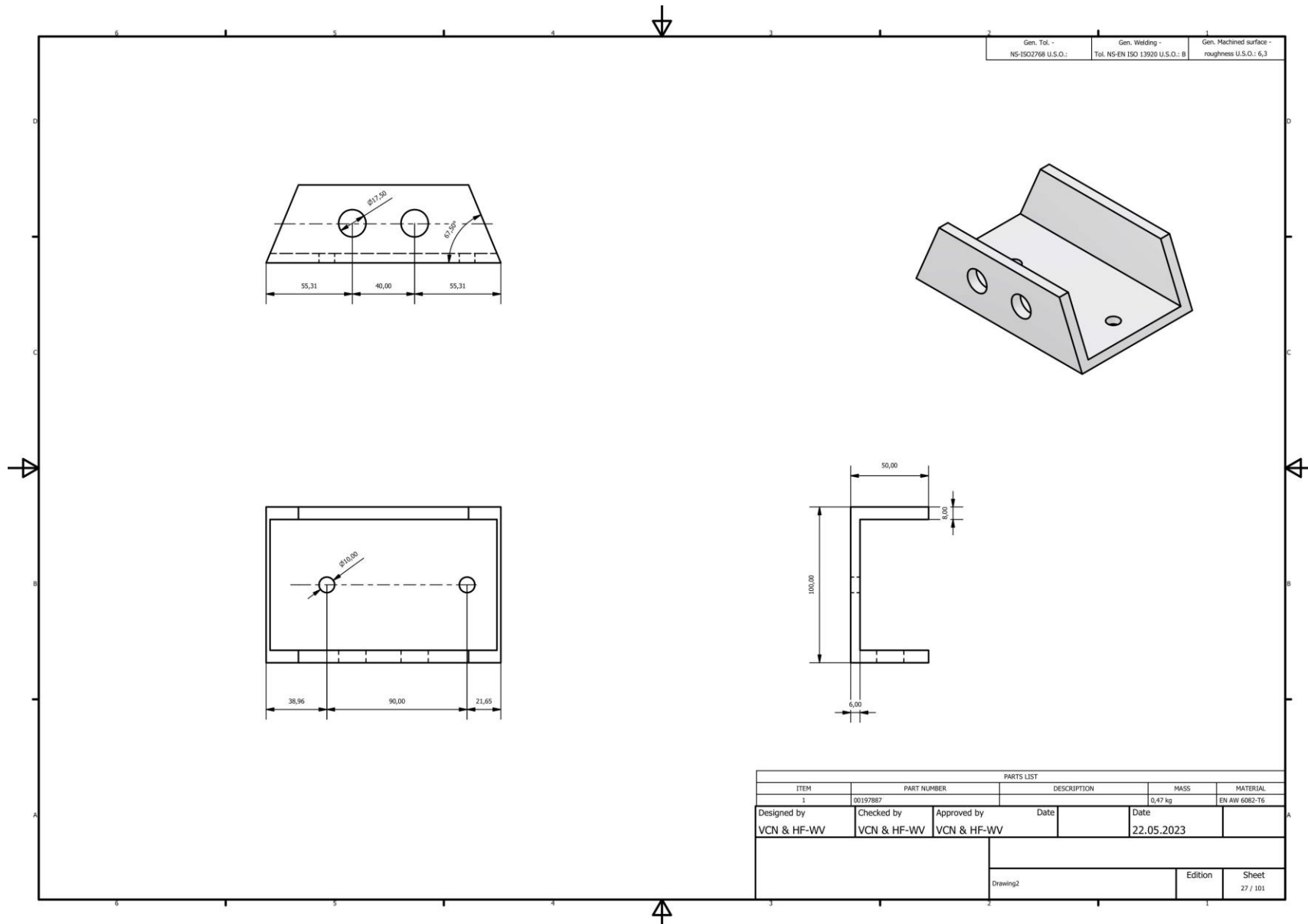
Integration of a Skid and Hatch-Based Launch and Recovery System for ROVs on USVs

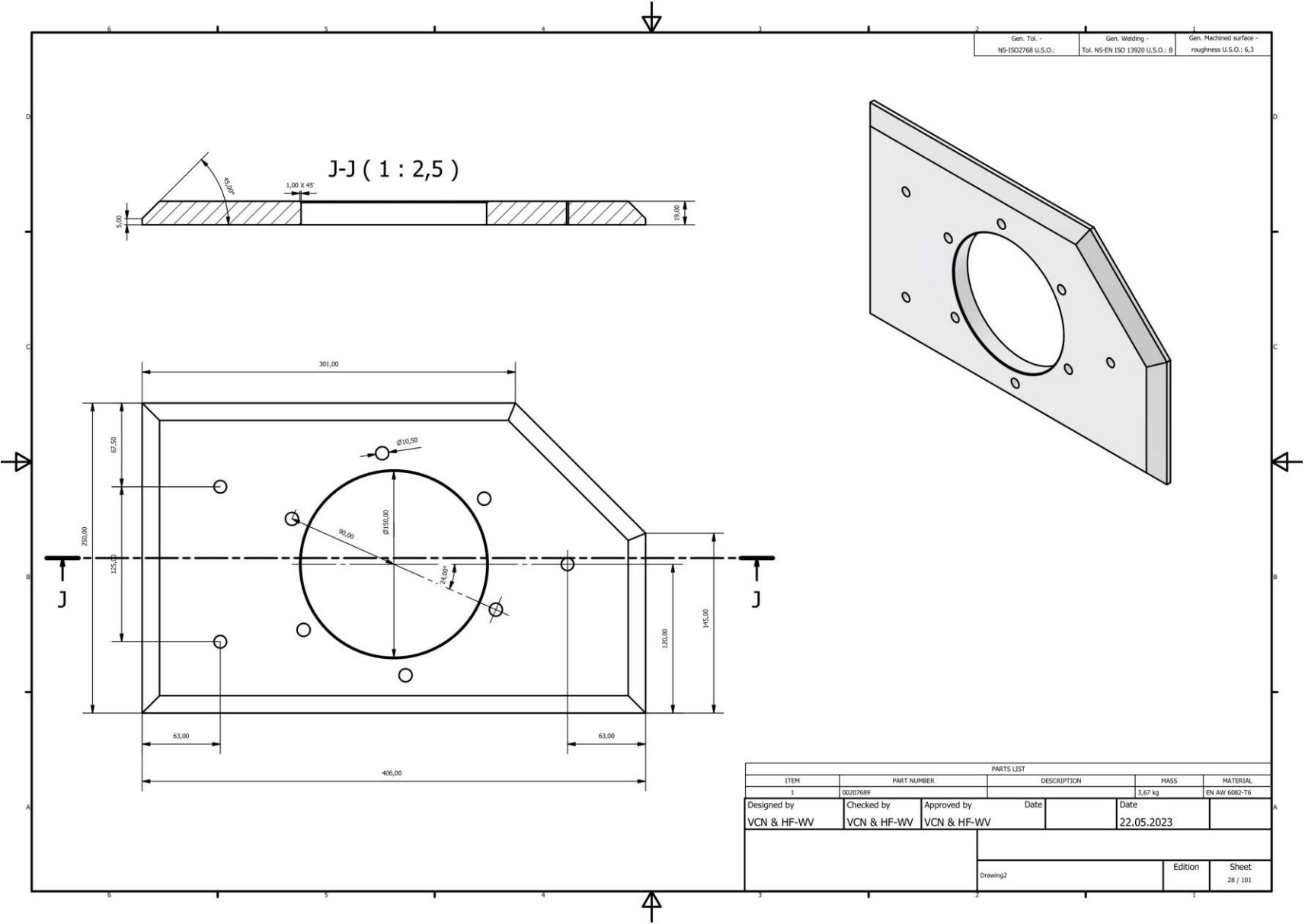


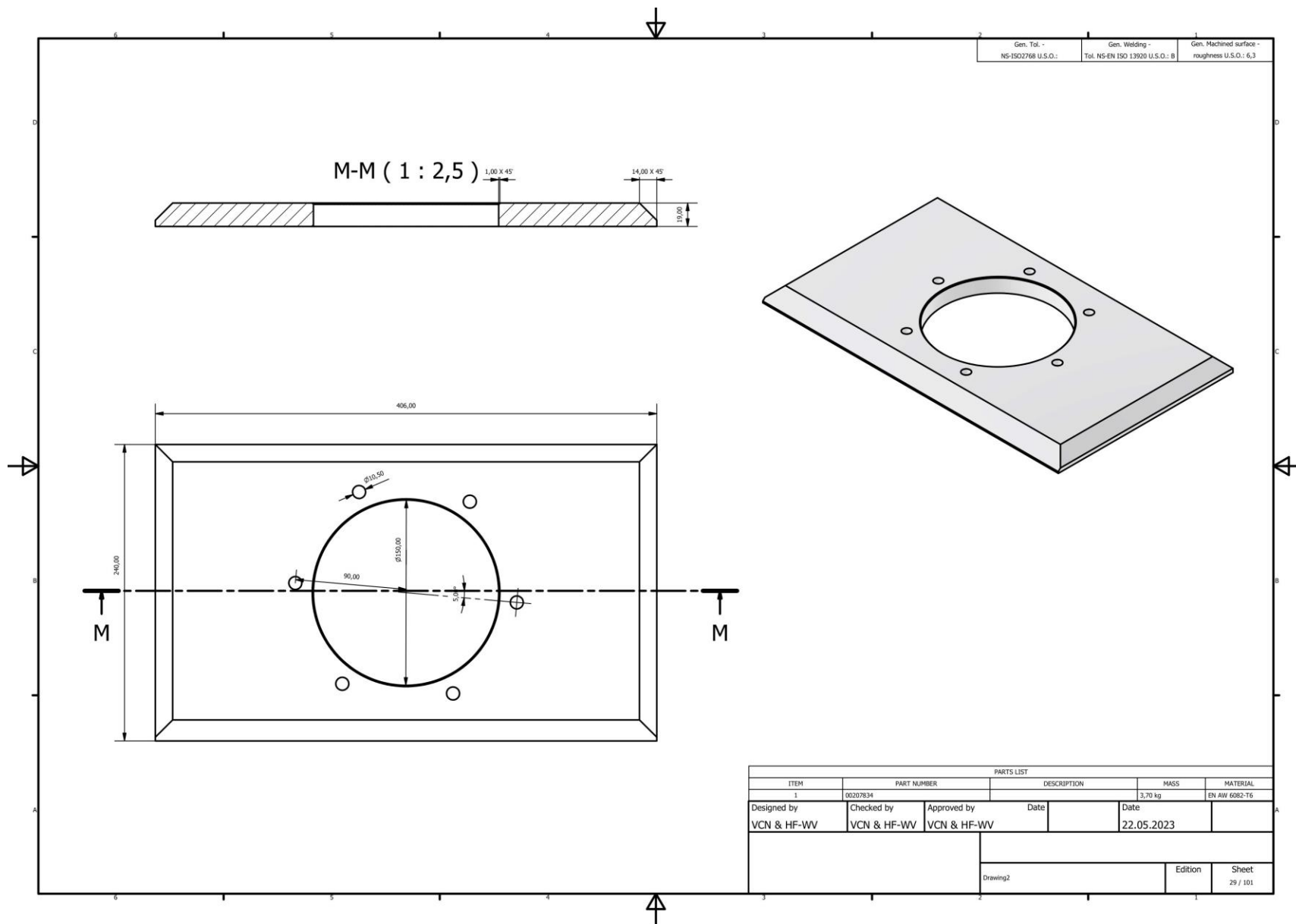


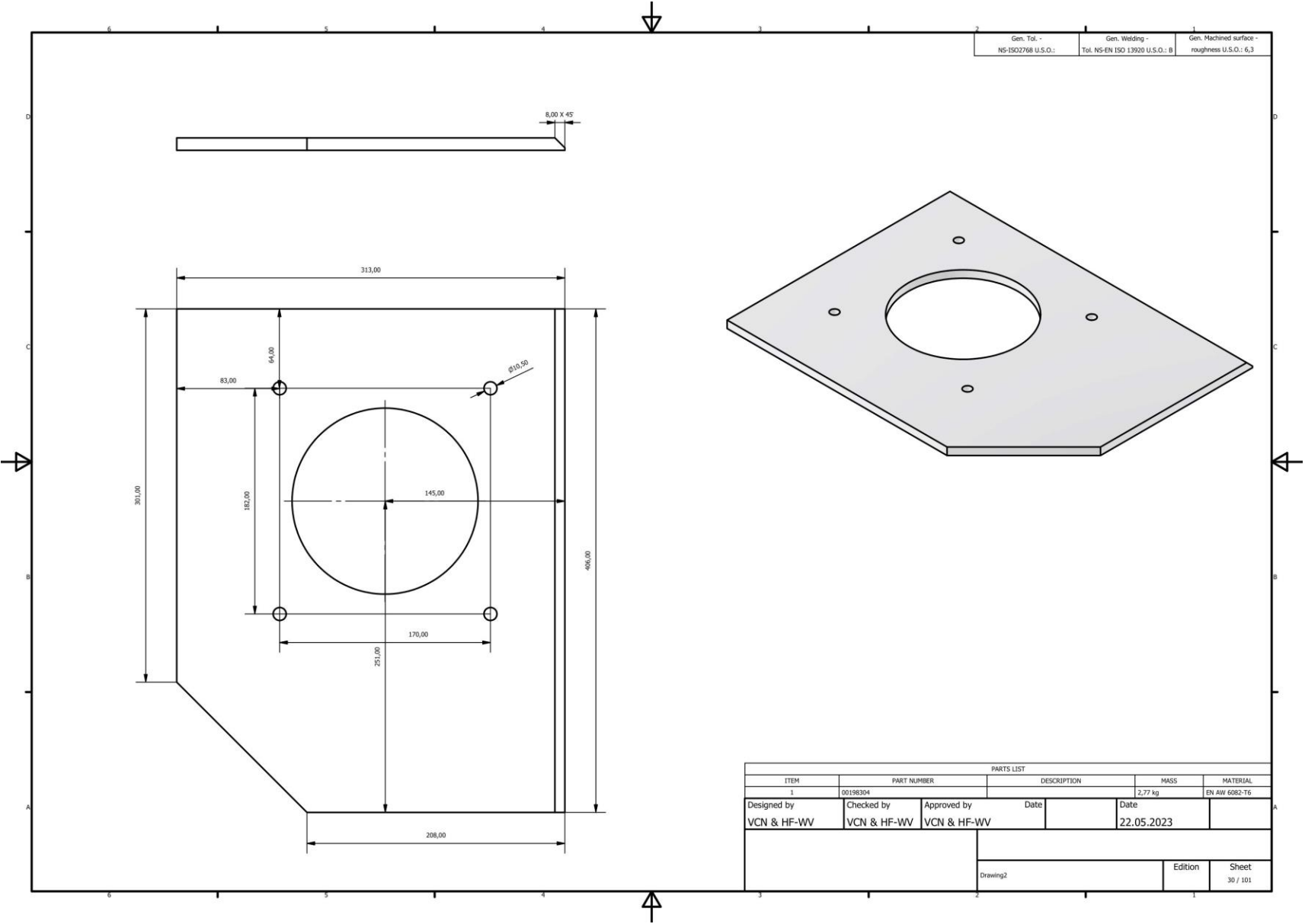






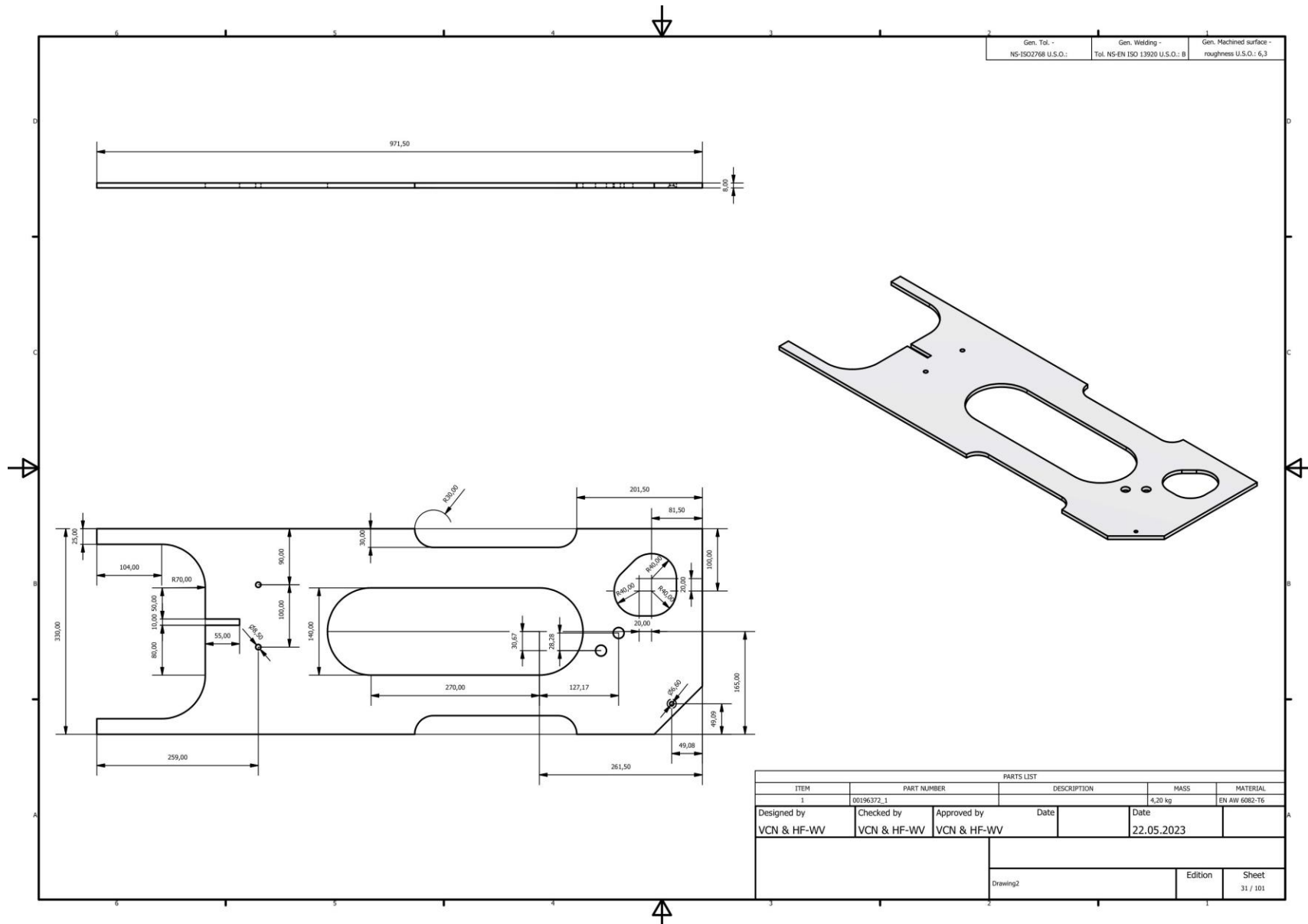


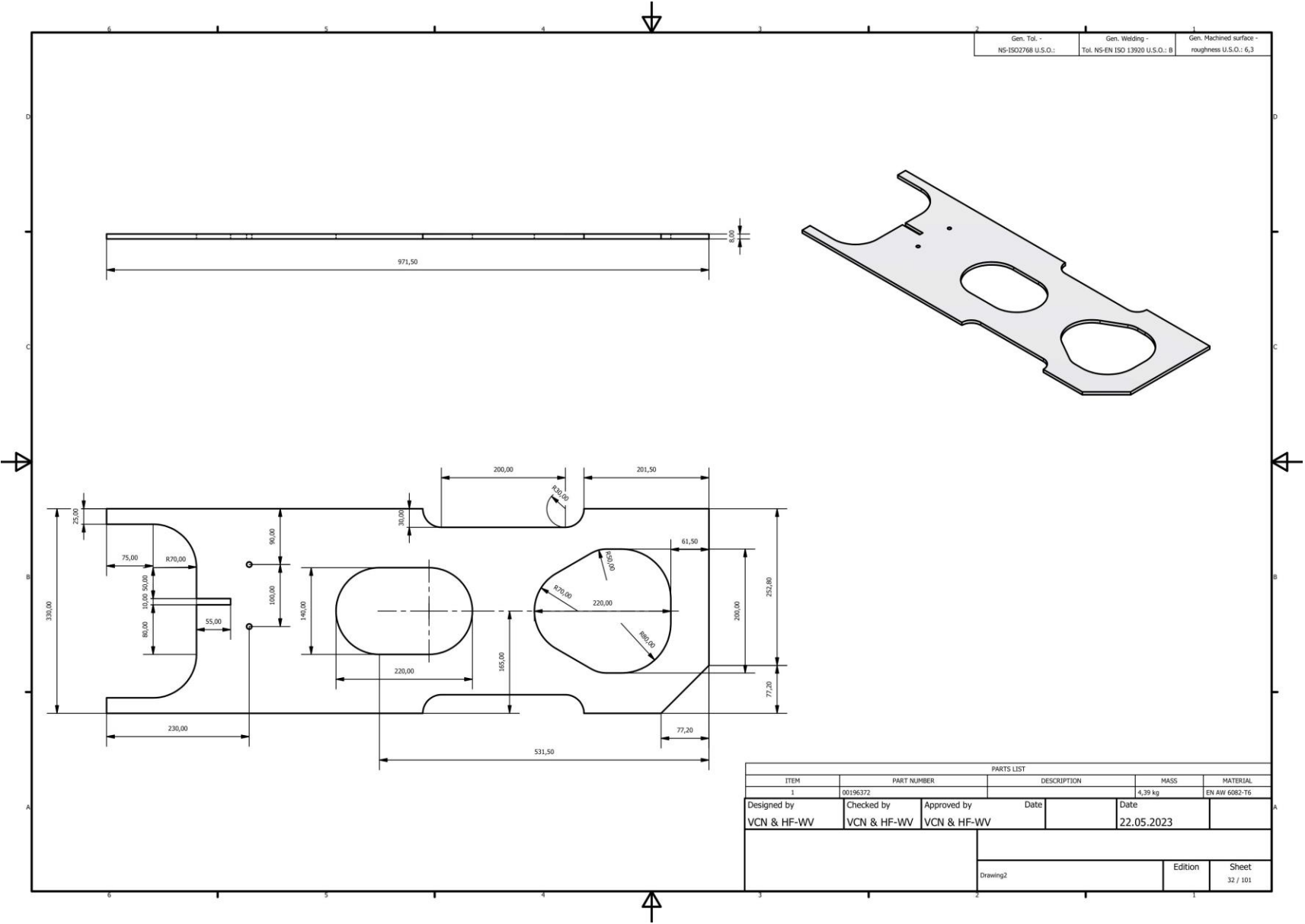




Gen. Tol - NS-ISO2768 U.S.O.:	Gen. Welding - Tol. NS-EN ISO 13920 U.S.O.:	Gen. Machined surface - roughness U.S.O.:
	B	6,3

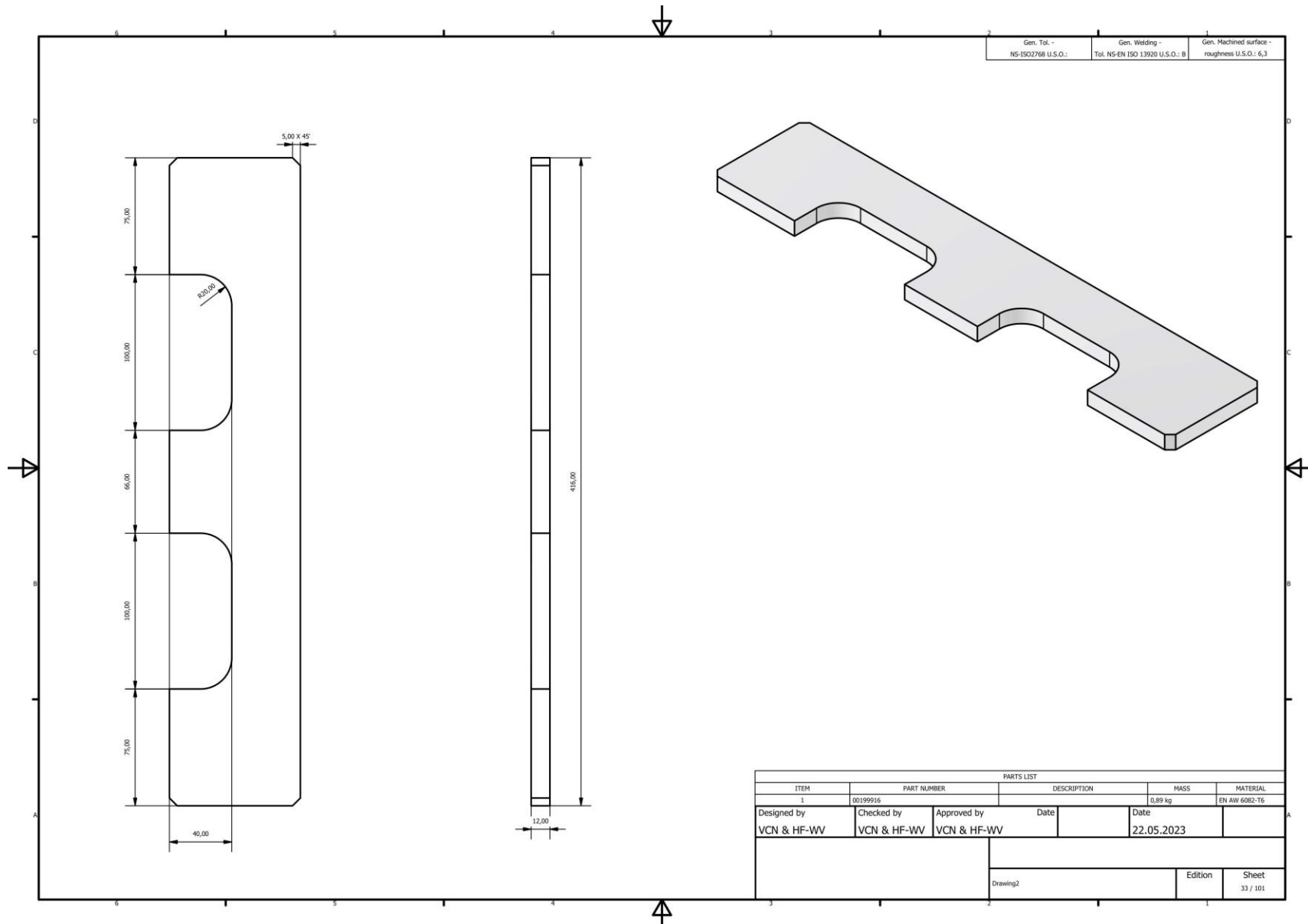
PARTS LIST					
ITEM	PART NUMBER	DESCRIPTION	MASS	MATERIAL	
1	00198304		2,77 kg	EN AW 6082-T6	
Designed by	Checked by	Approved by	Date	Date	
VCN & HF-WV	VCN & HF-WV	VCN & HF-WV		22.05.2023	
			Edition	Sheet	
Drawing2				30 / 101	

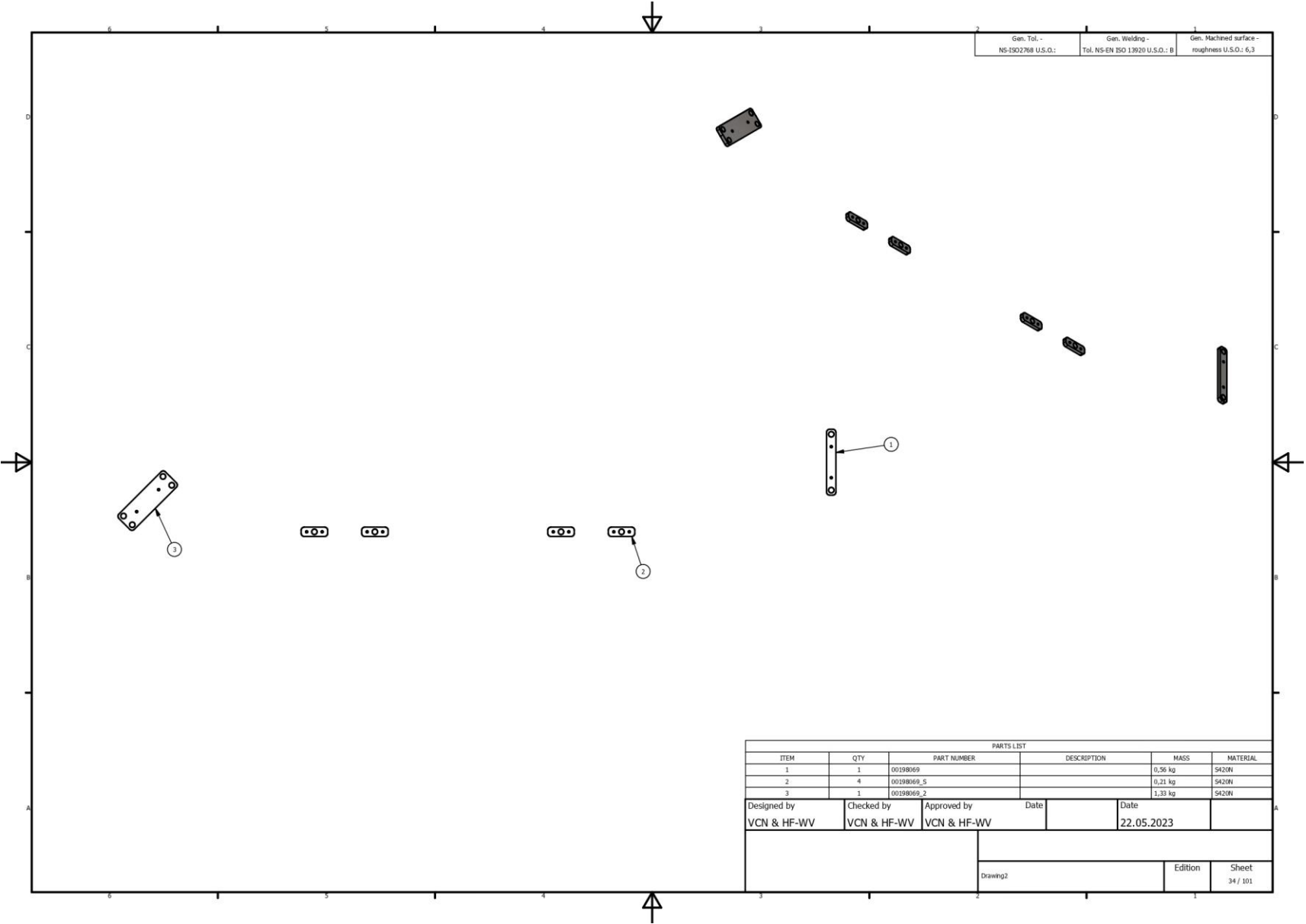


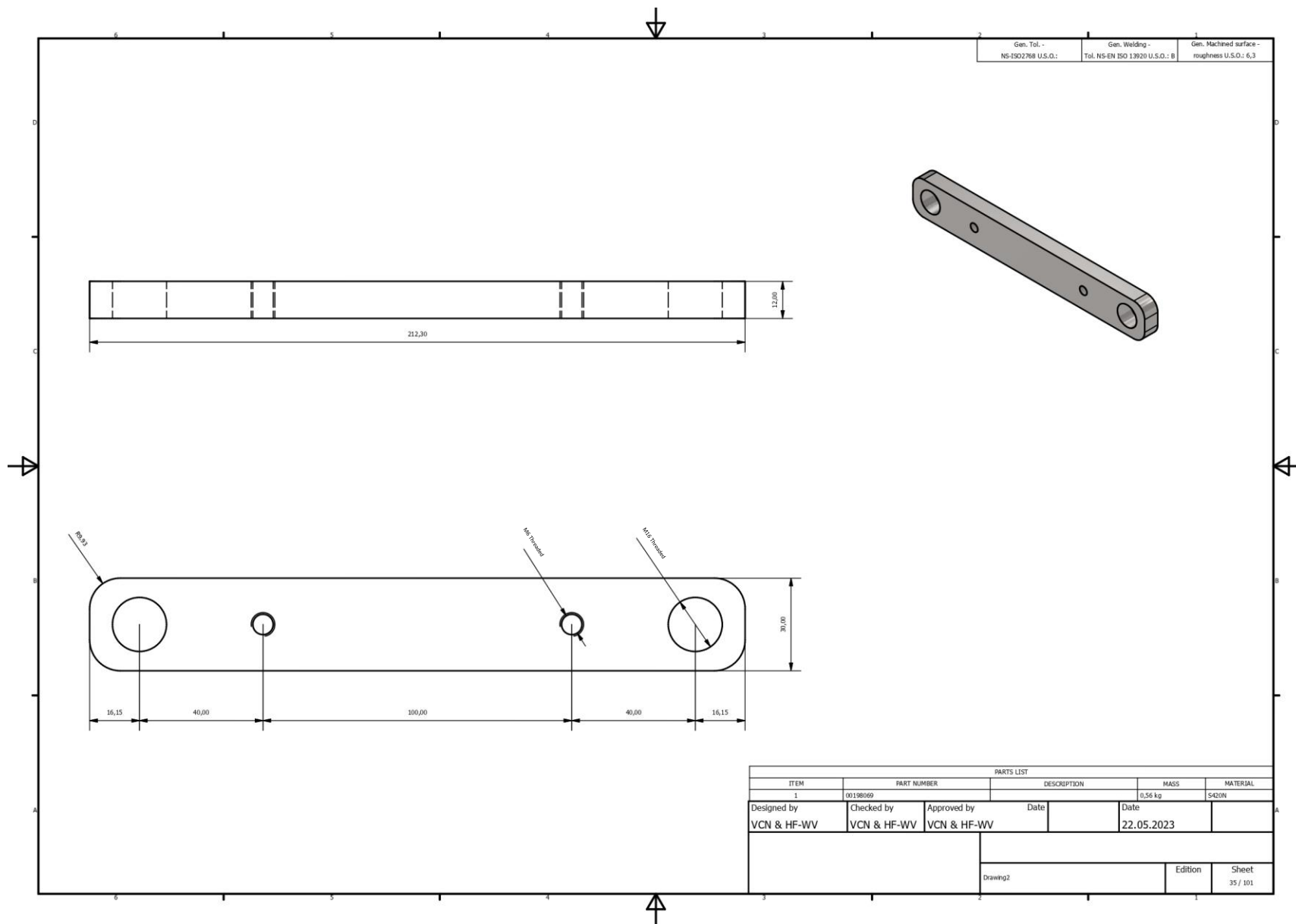


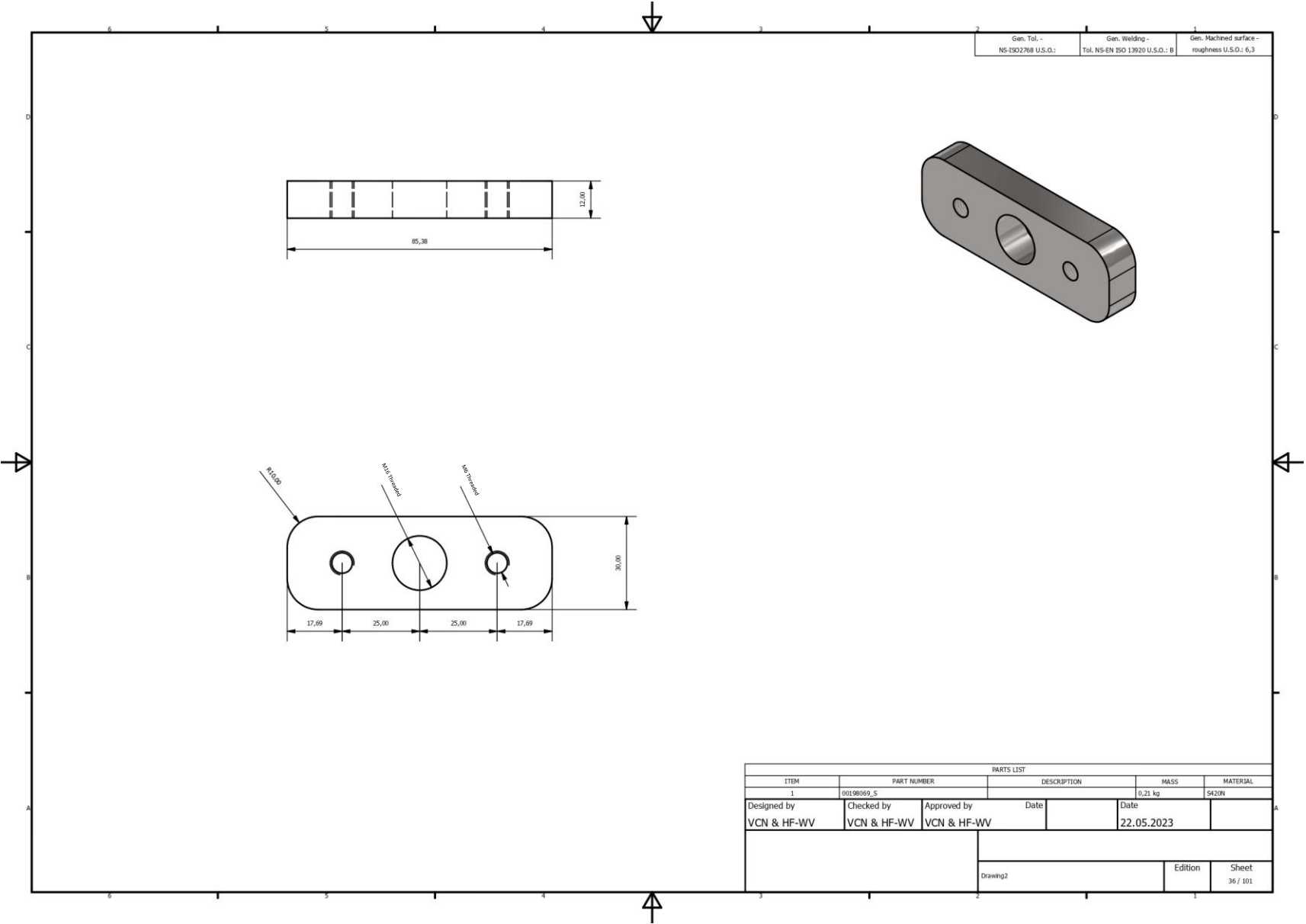
Gen. Tol - NS-ISO2768 U.S.O.:	Gen. Welding - Tol. NS-EN ISO 13920 U.S.O.:	Gen. Machined surface - roughness U.S.O.:
	B	6,3

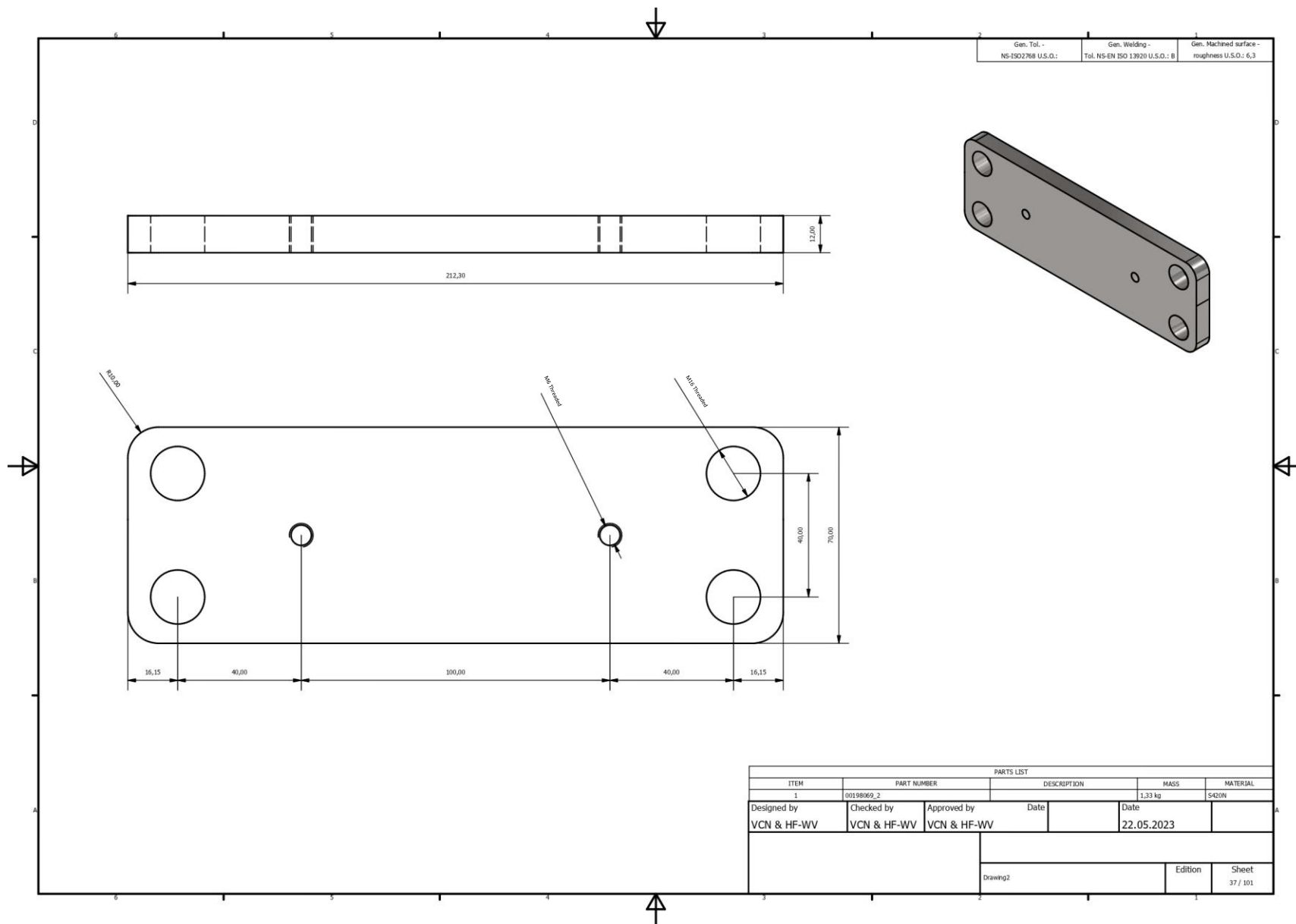
PARTS LIST					
ITEM	PART NUMBER	DESCRIPTION	MASS	MATERIAL	
1	00196372		4,39 kg	EN AW 6082-T6	
Designed by	Checked by	Approved by	Date	Date	
VCN & HF-WV	VCN & HF-WV	VCN & HF-WV		22.05.2023	
			Edition		
Drawing2			Sheet		
			32 / 101		

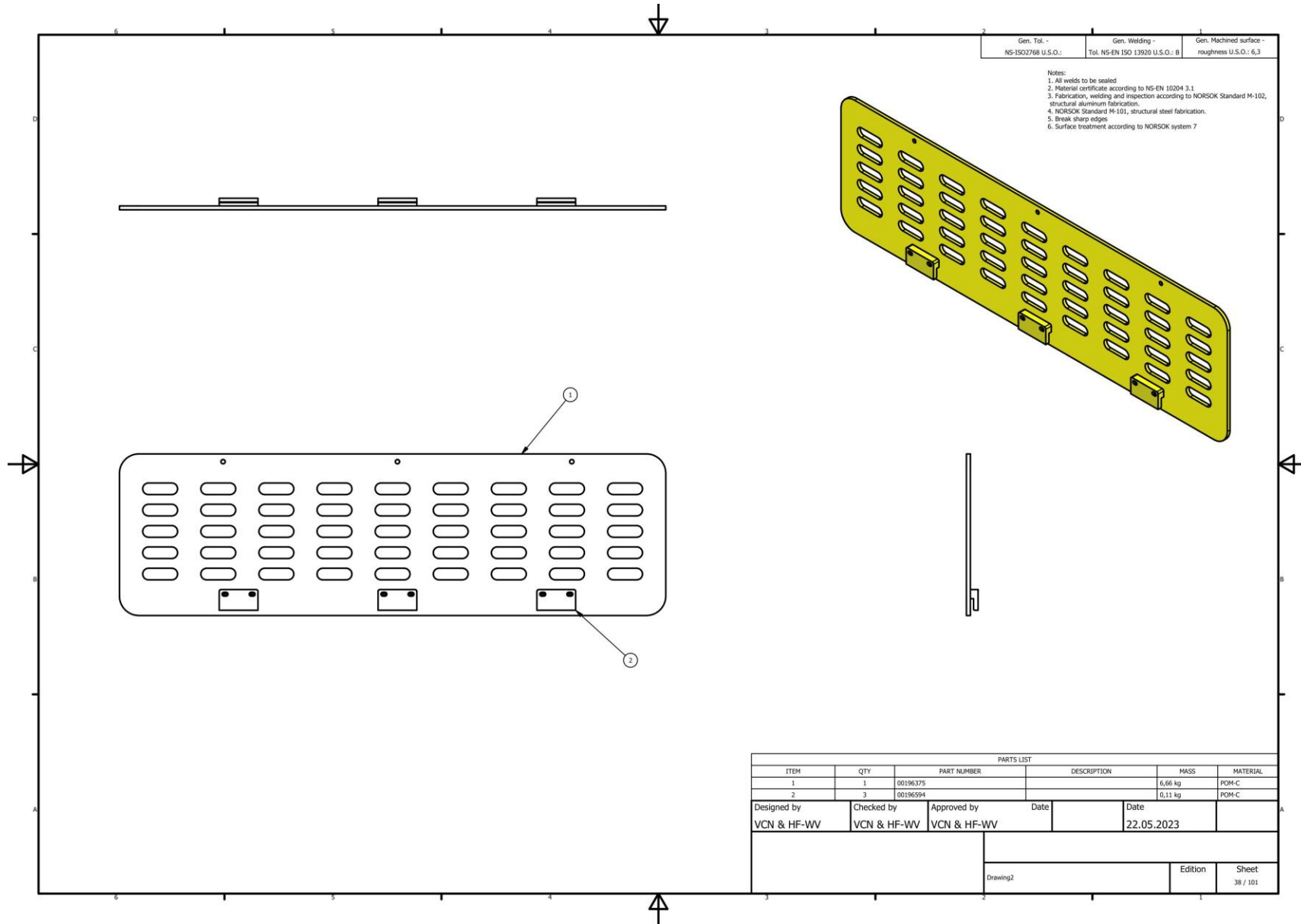








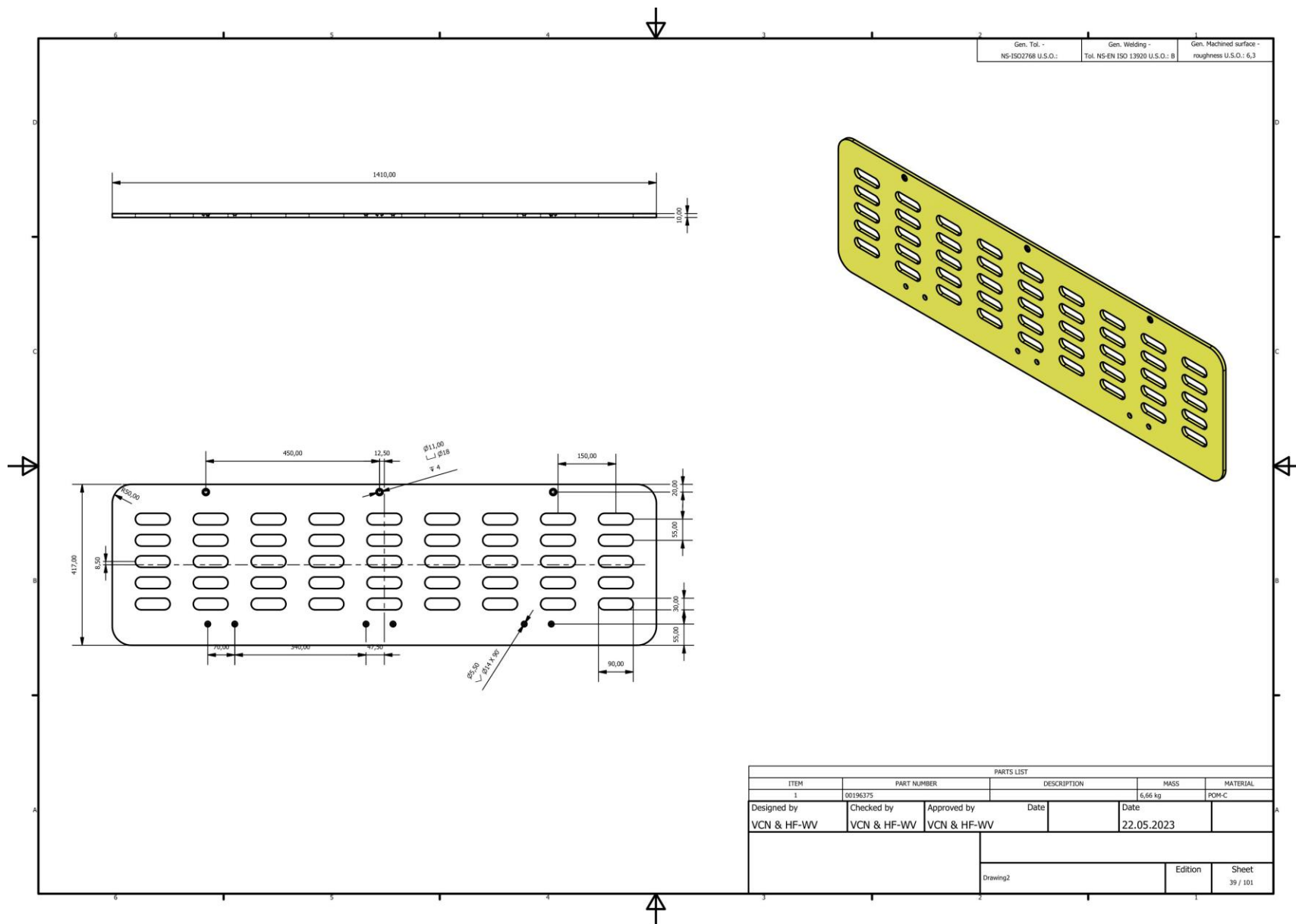


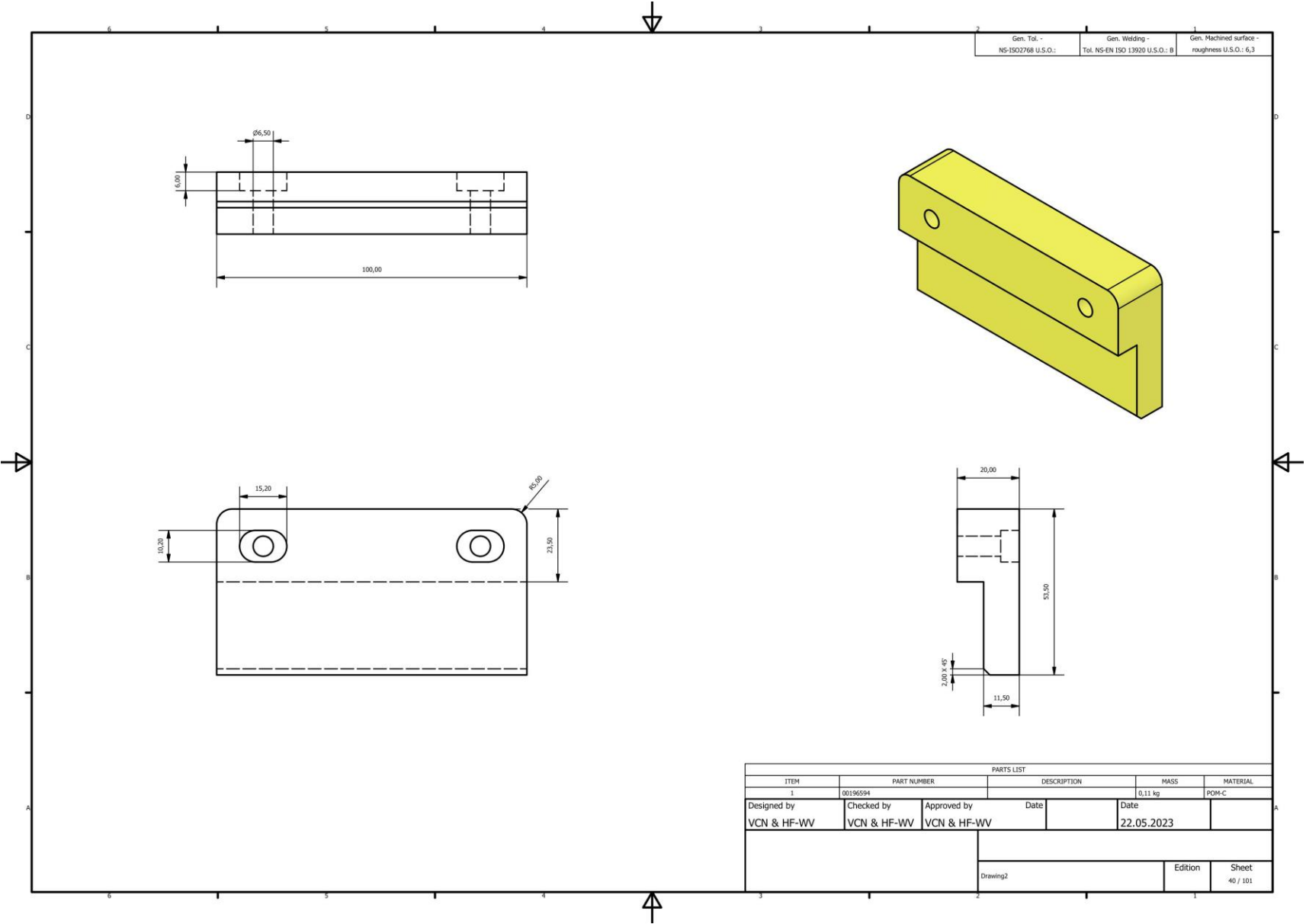


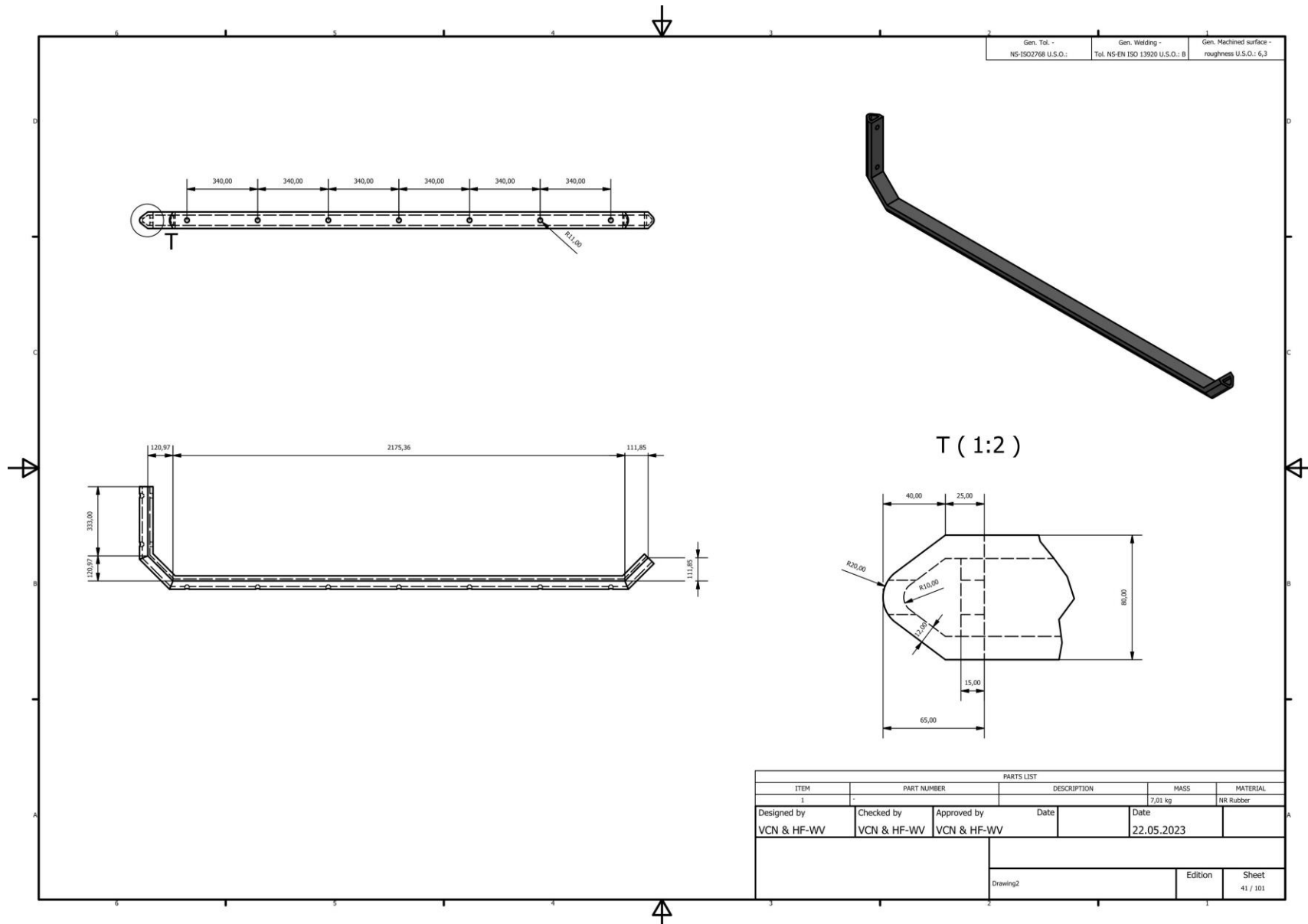
Gen. Tol - NS-ISO2768 U.S.O.:	Gen. Welding - Tol. NS-EN ISO 13920 U.S.O.: B	Gen. Machined surface - roughness U.S.O.: 6,3
----------------------------------	--	--

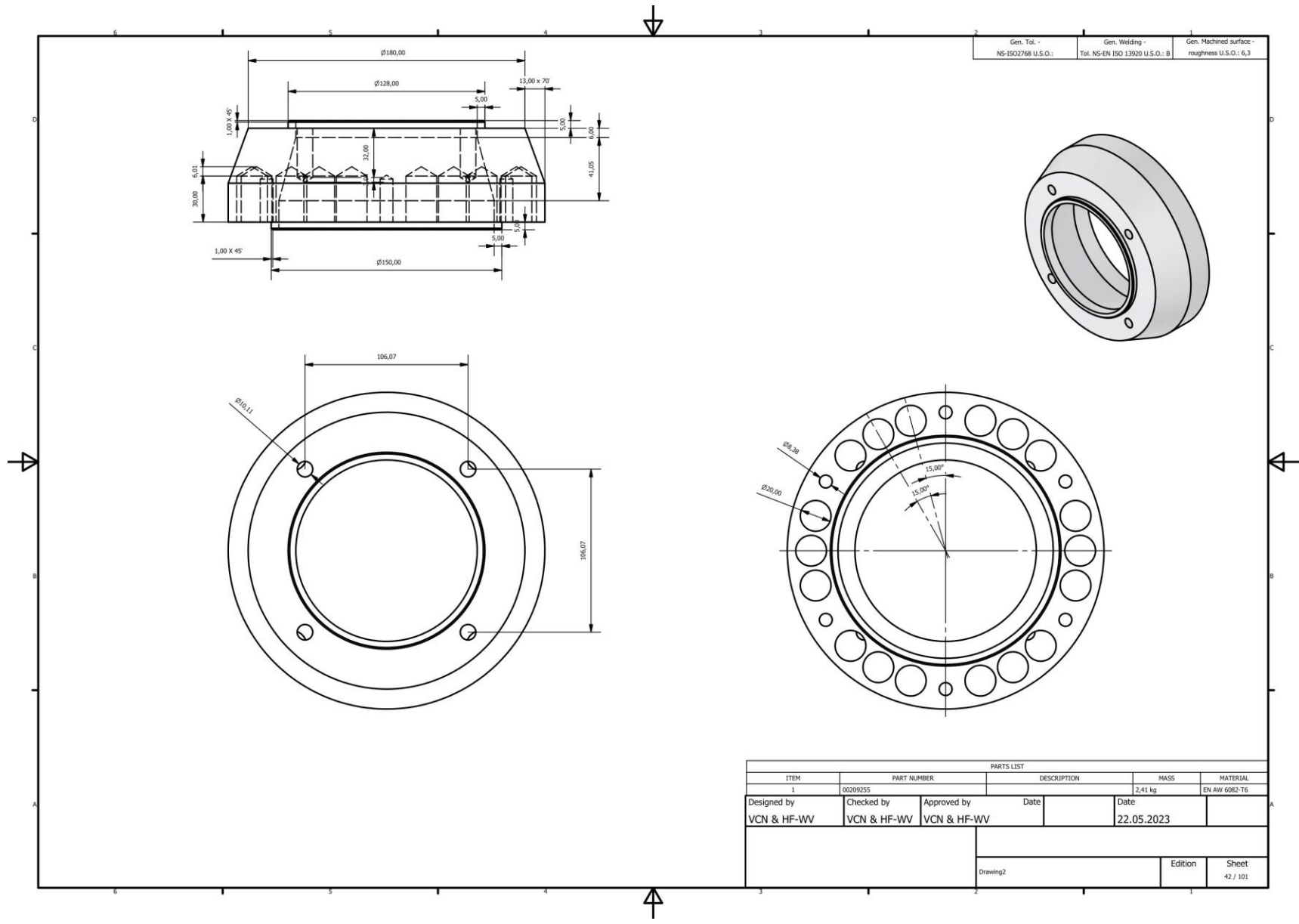
- Notes:
1. All welds to be sealed
 2. Material certificate according to NS-EN 10204 3.1
 3. Fabrication, welding and inspection according to NORSOK Standard M-102, structural aluminum fabrication.
 4. NORSOK Standard M-101, structural steel fabrication.
 5. Break sharp edges
 6. Surface treatment according to NORSOK system 7

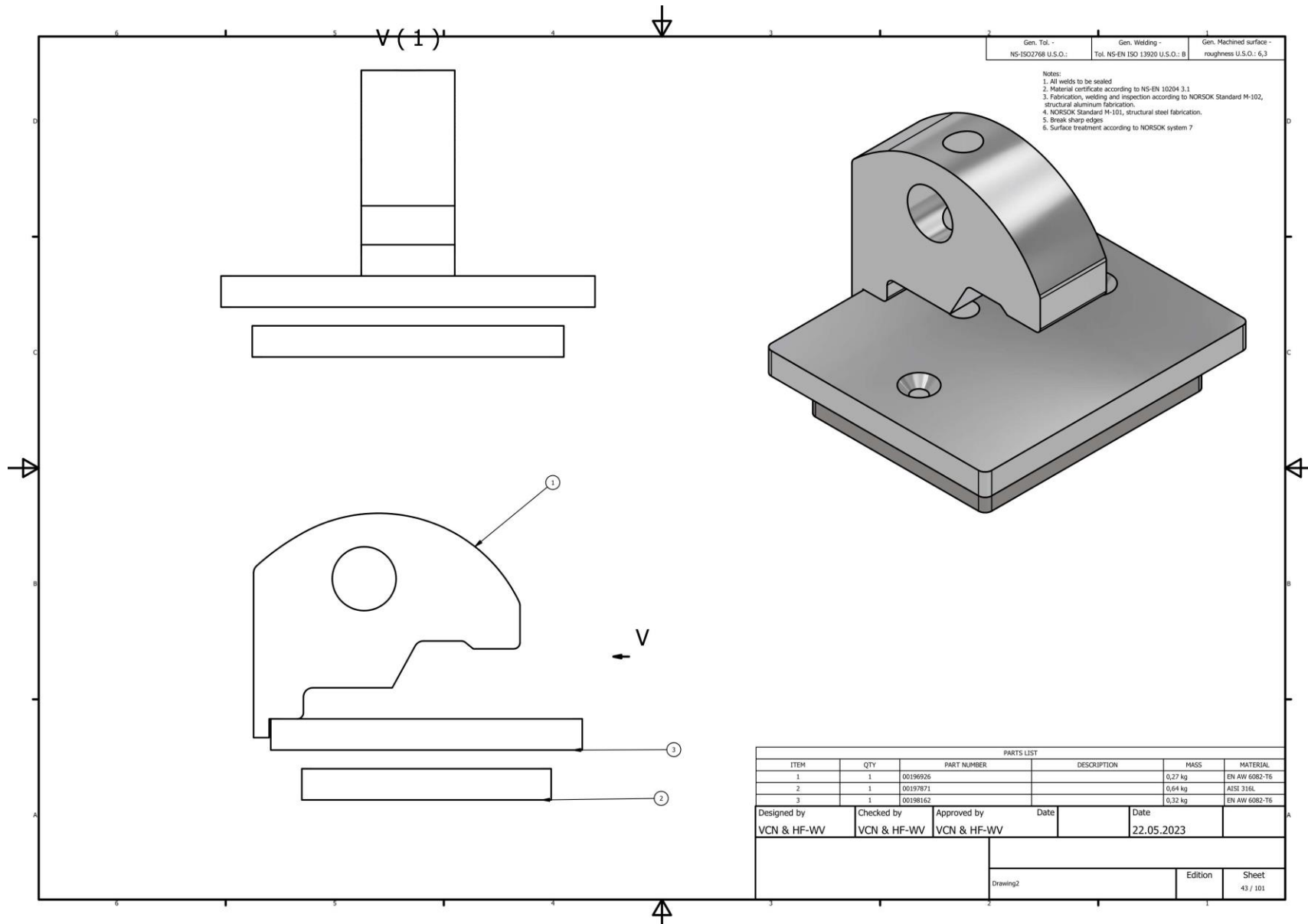
PARTS LIST					
ITEM	QTY	PART NUMBER	DESCRIPTION	MASS	MATERIAL
1	1	00196375		6,66 kg	PDM-C
2	3	00196594		0,11 kg	PDM-C
Designed by VCN & HF-WV		Checked by VCN & HF-WV	Approved by VCN & HF-WV	Date 22.05.2023	
			Drawing2	Edition	Sheet 38 / 101

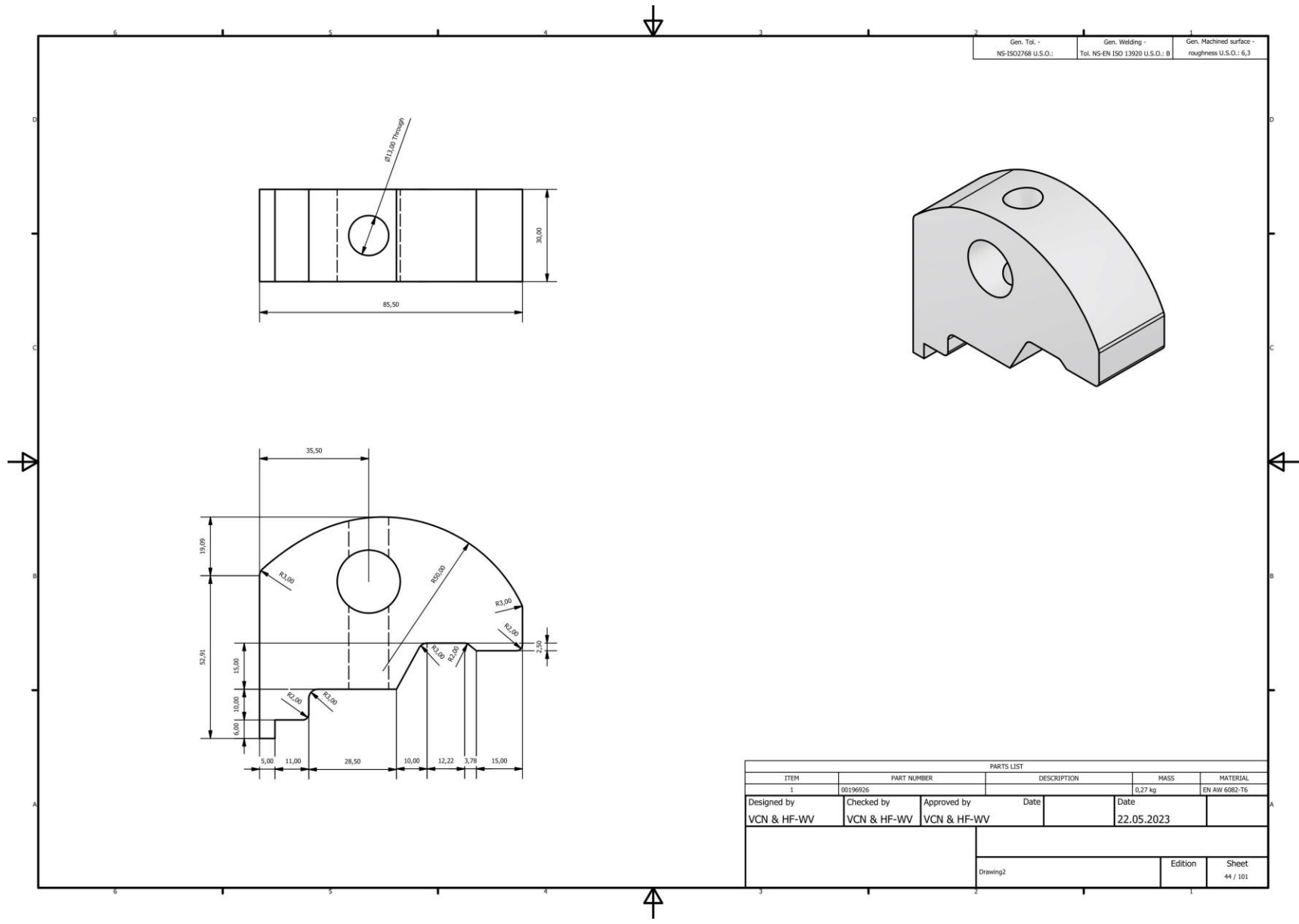


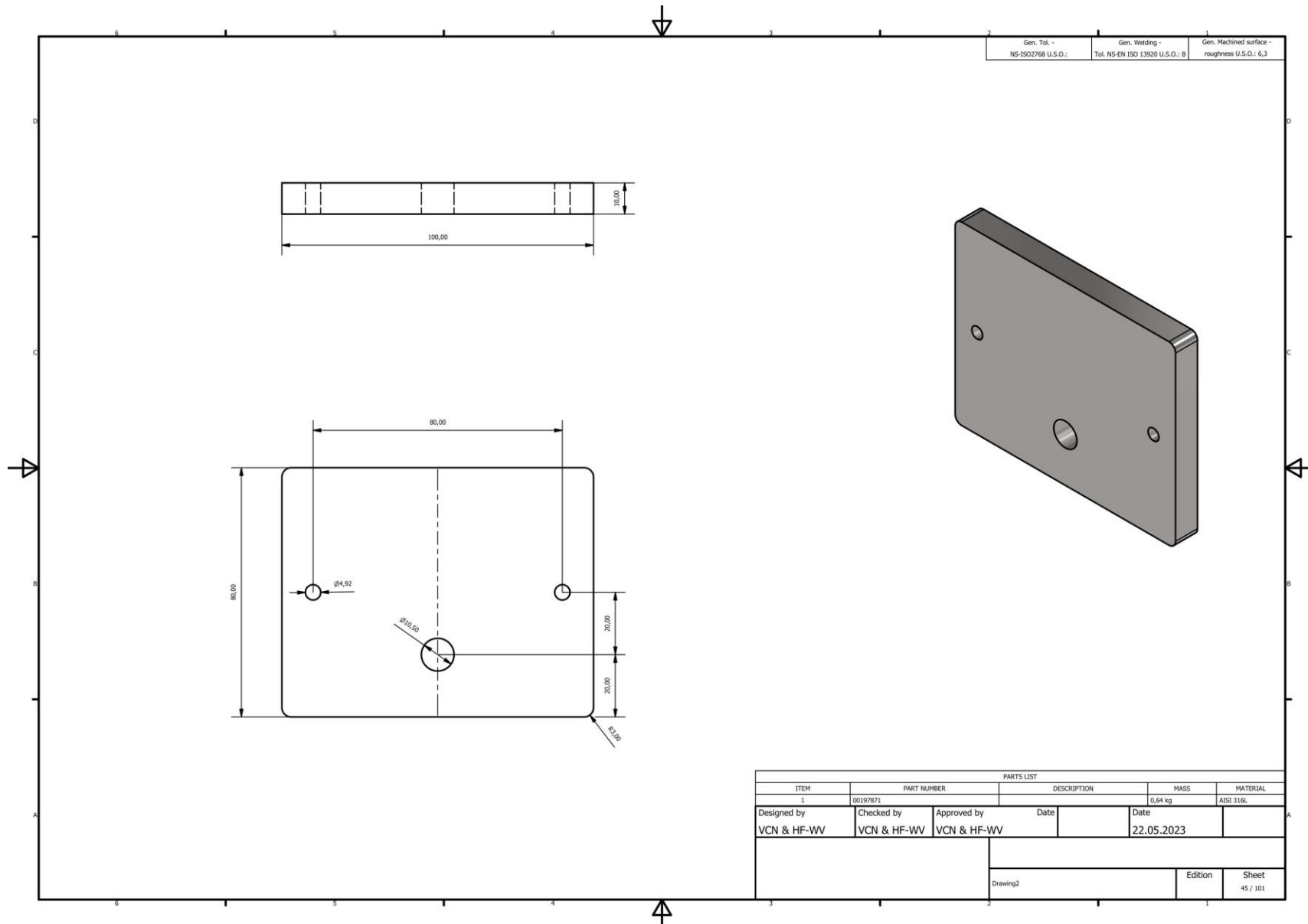






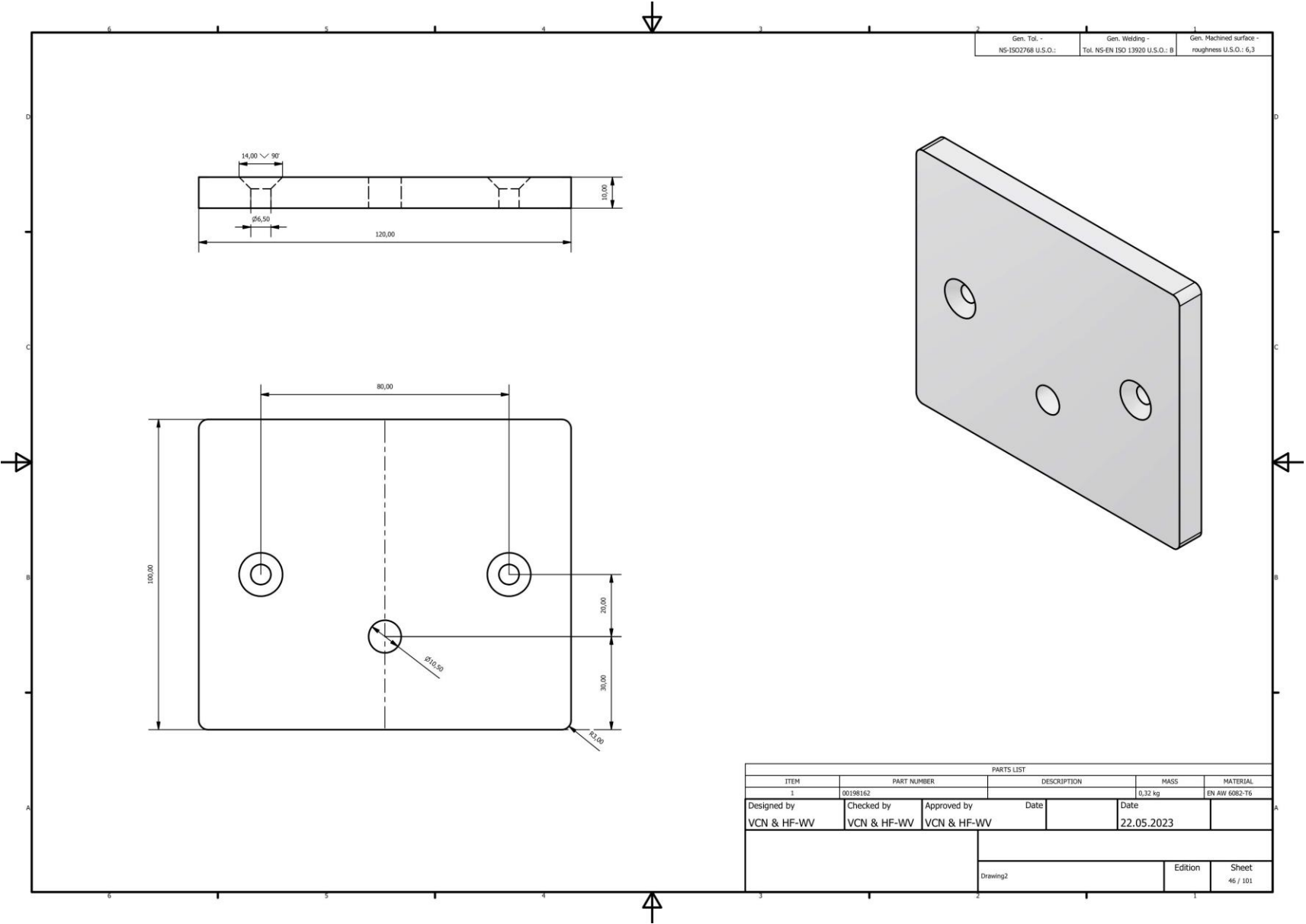




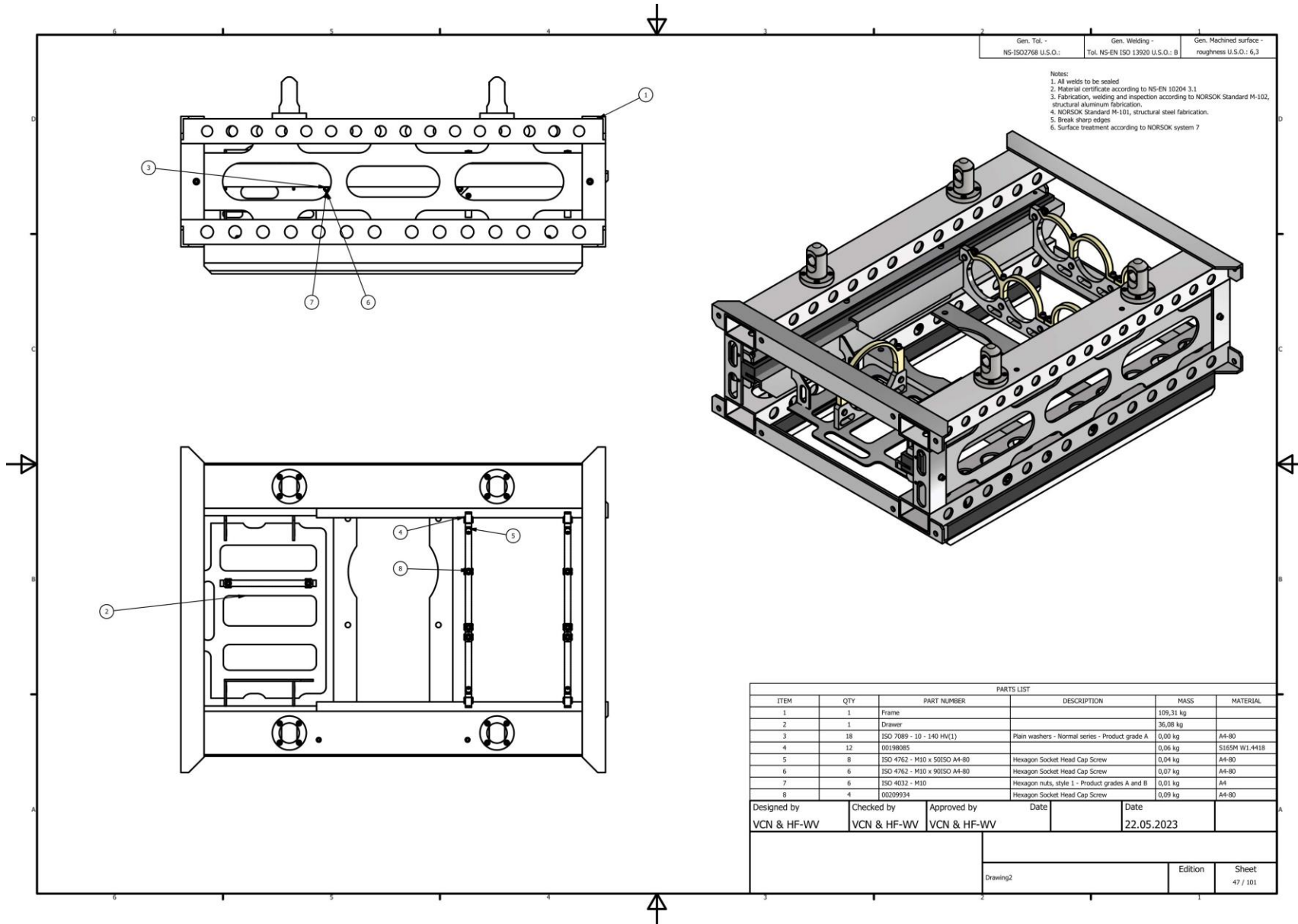


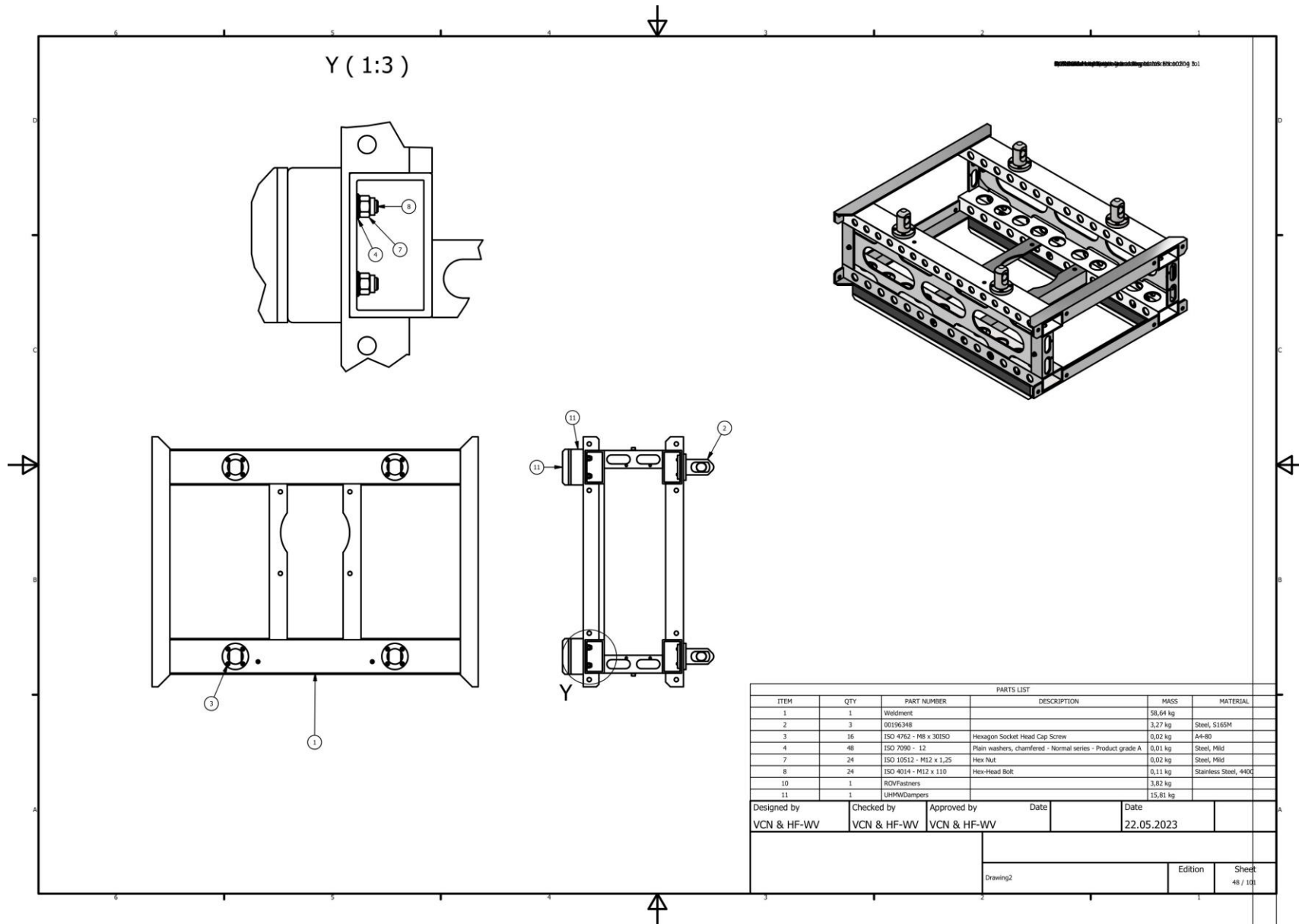
Gen. Tol. -
NS-ISO2768 U.S.O.:
Gen. Welding -
Tol. NS-EN ISO 13920 U.S.O.: B
Gen. Machined surface -
roughness U.S.O.: 6,3

PARTS LIST					
ITEM	PART NUMBER	DESCRIPTION	MASS	MATERIAL	
1	00197871		0,64 kg	AISI 316L	
Designed by	Checked by	Approved by	Date	Date	
VCN & HF-WV	VCN & HF-WV	VCN & HF-WV		22.05.2023	
			Drawing2	Edition	Sheet
					45 / 101



Integration of a Skid and Hatch-Based Launch and Recovery System for ROVs on USVs



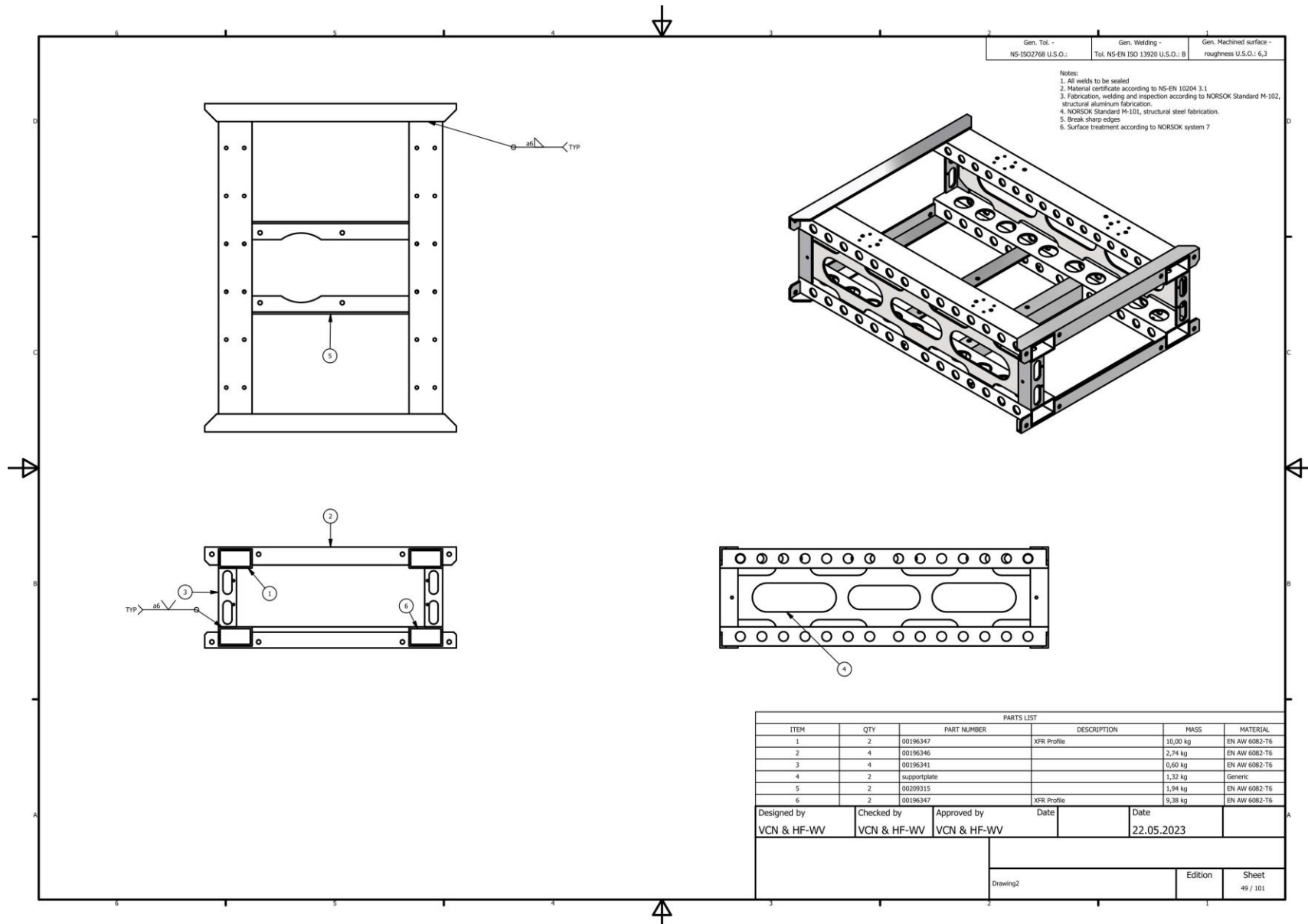


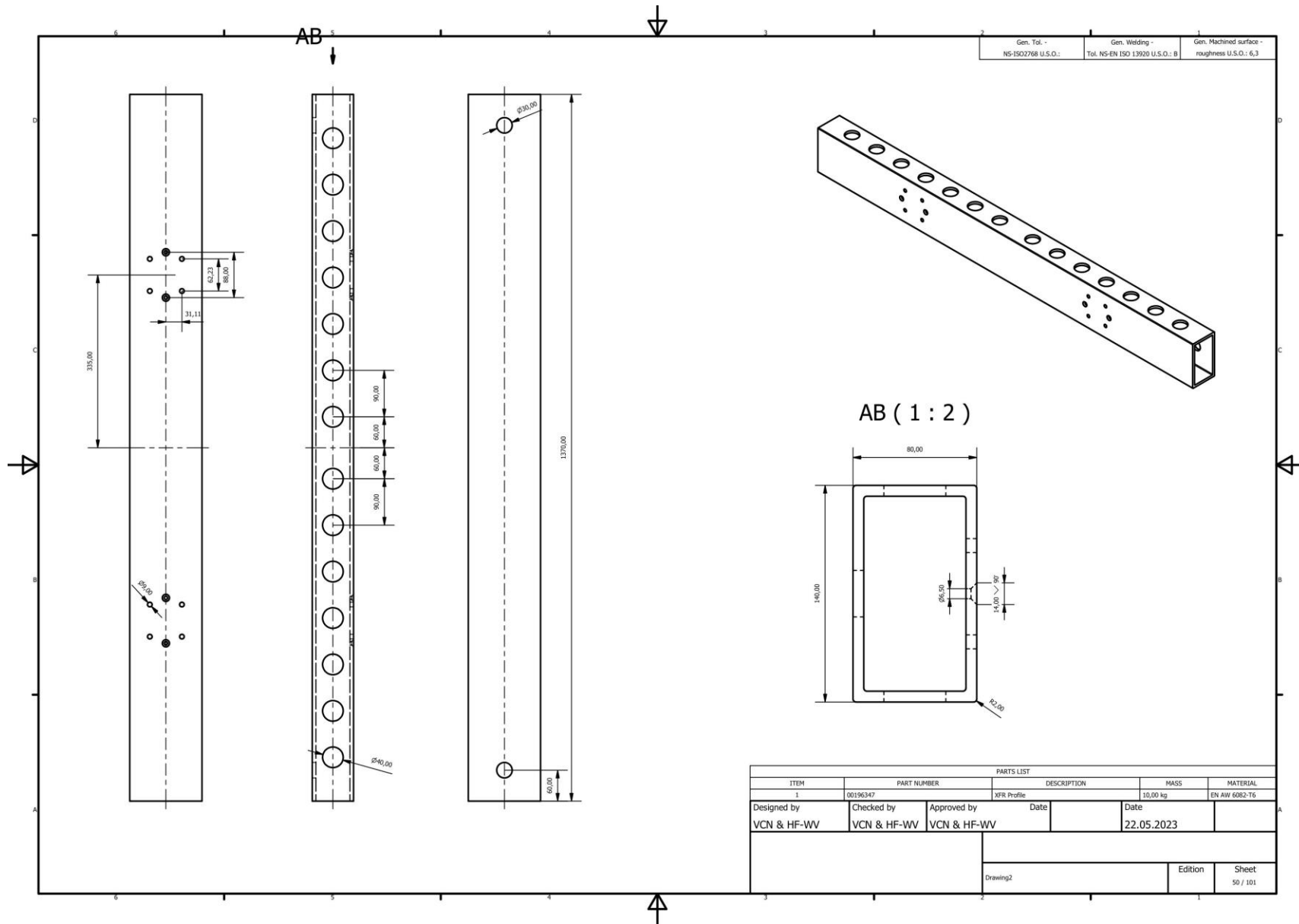
PARTS LIST					
ITEM	QTY	PART NUMBER	DESCRIPTION	MASS	MATERIAL
1	1	Weldment		58,64 kg	
2	3	00196348		3,27 kg	Steel, S165M
3	16	ISO 4762 - M8 x 30ISO	Hexagon Socket Head Cap Screw	0,02 kg	A4-80
4	48	ISO 7090 - 12	Plain washers, chamfered - Normal series - Product grade A	0,01 kg	Steel, Mild
7	24	ISO 10512 - M12 x 1,25	Hex Nut	0,02 kg	Steel, Mild
8	24	ISO 4014 - M12 x 110	Hex-Head Bolt	0,11 kg	Stainless Steel, 440C
10	1	ROVFastners		3,82 kg	
11	1	UHMW-Dampers		15,81 kg	

Designed by	Checked by	Approved by	Date	Date
VCN & HF-WV	VCN & HF-WV	VCN & HF-WV		22.05.2023

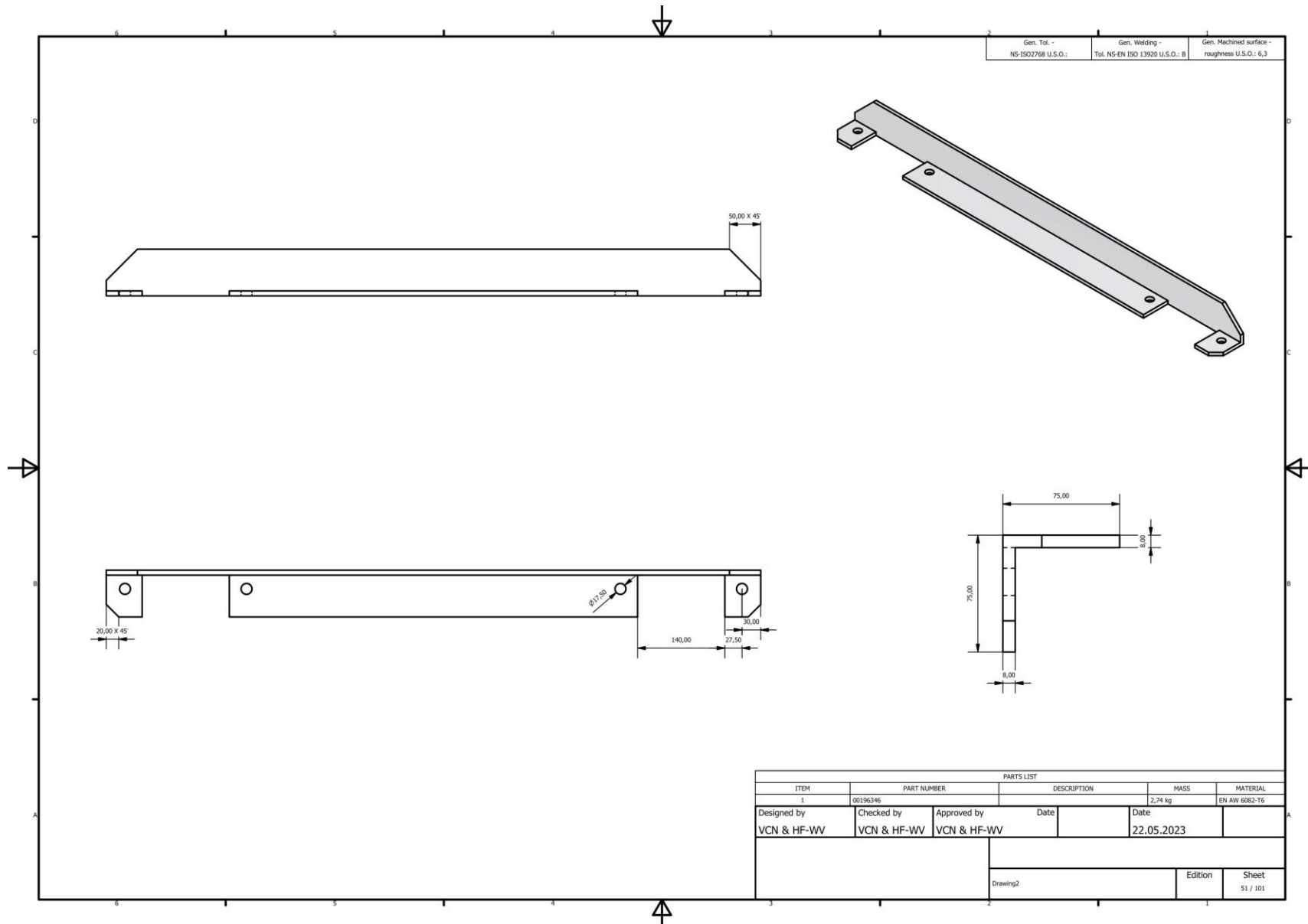
Drawing2	Edition	Sheet
		48 / 101

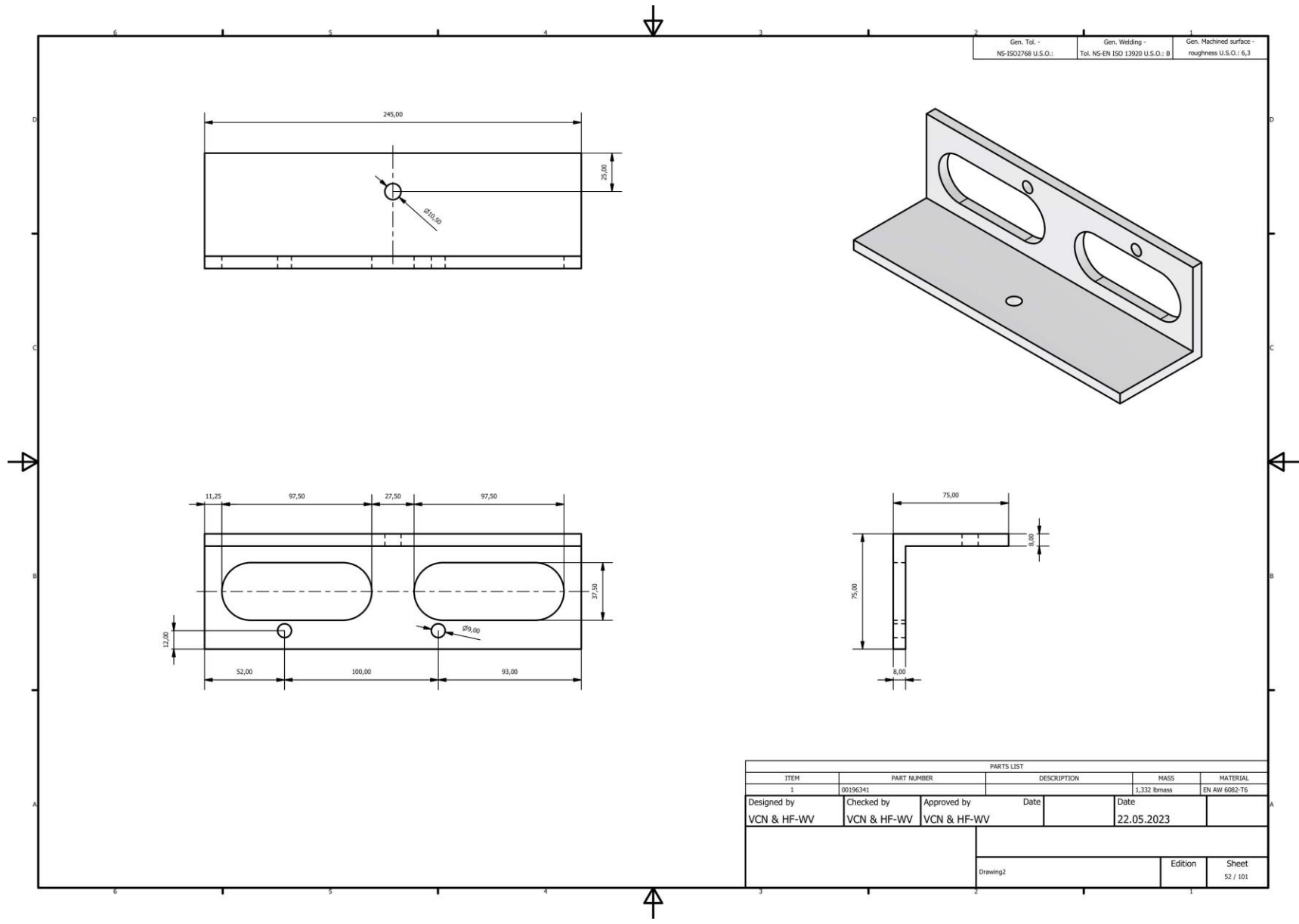
Integration of a Skid and Hatch-Based Launch and Recovery System for ROVs on USVs

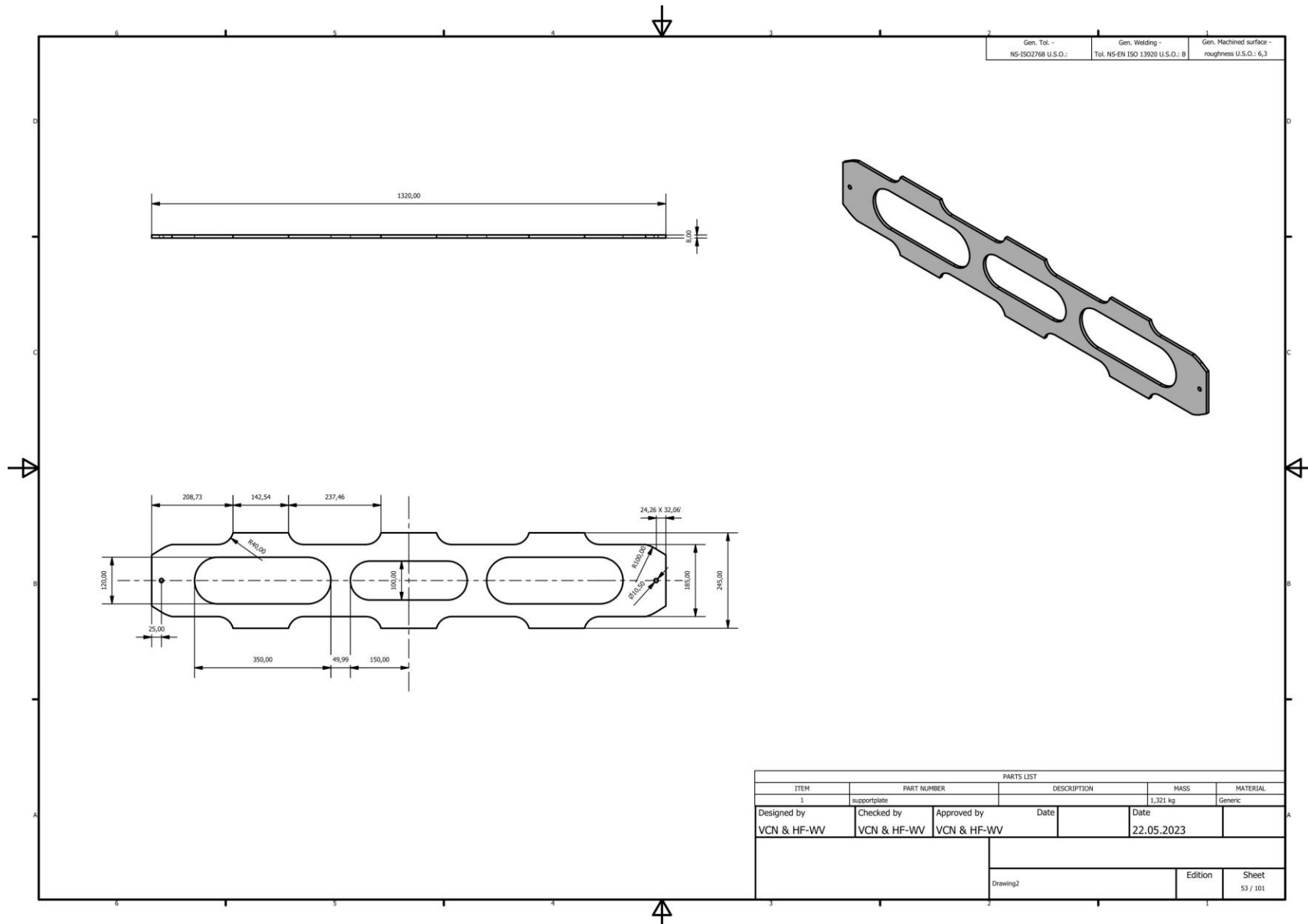




Integration of a Skid and Hatch-Based Launch and Recovery System for ROVs on USVs

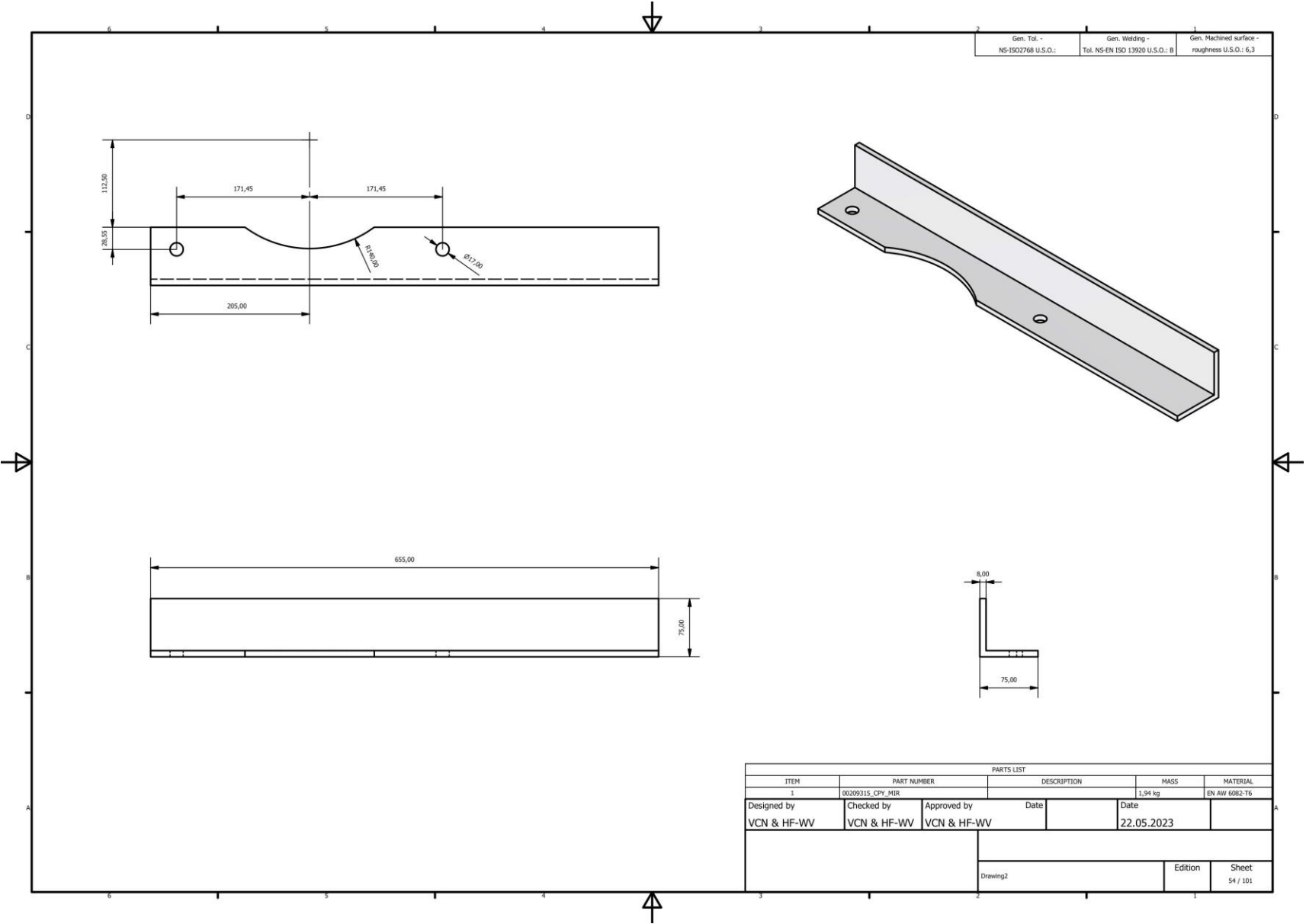


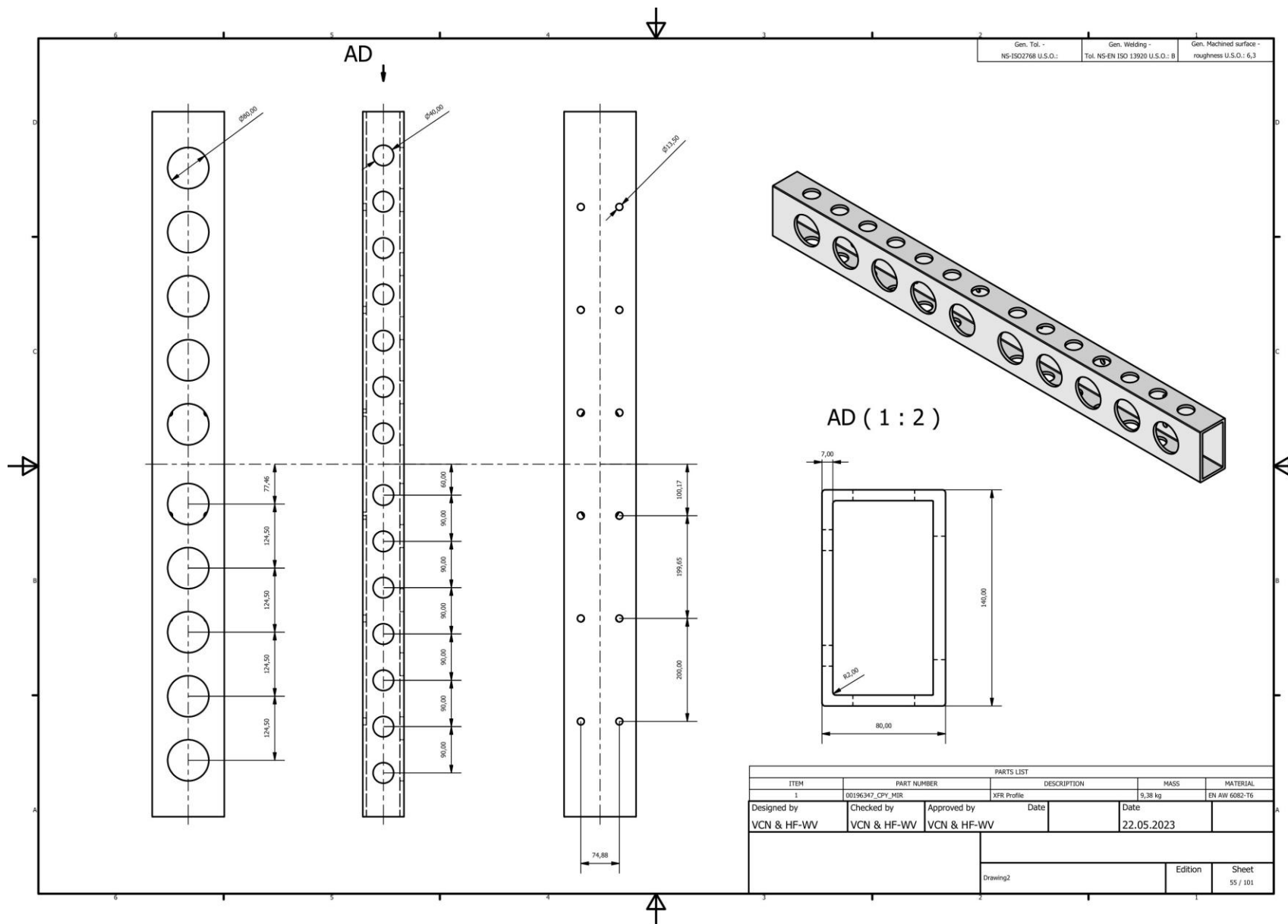




Gen. Tol. - NS-ISO2768 U.S.O.: M	Gen. Welding - Tot. NS-EN ISO 13920 U.S.O.: B	Gen. Machined surface - roughness U.S.O.: 6,3
-------------------------------------	--	--

PARTS LIST					
ITEM	PART NUMBER	DESCRIPTION	MASS	MATERIAL	
1	supportplate		1,321 kg	Generic	
Designed by	Checked by	Approved by	Date	Date	
VCN & HF-WV	VCN & HF-WV	VCN & HF-WV		22.05.2023	
			Drawing2	Edition	Sheet 53 / 101





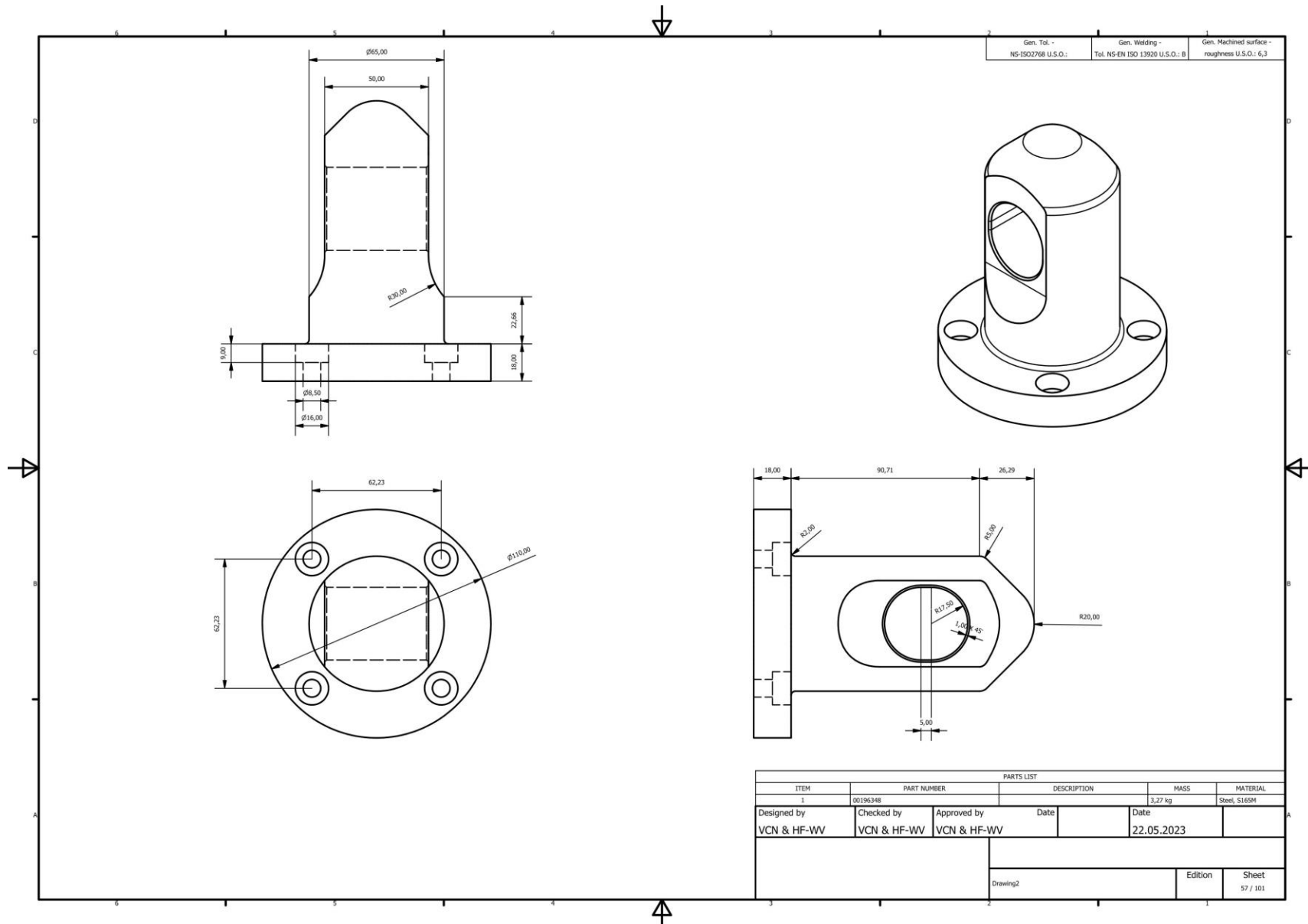
Gen. Tol -
NS-ISO2768 U.S.O.:

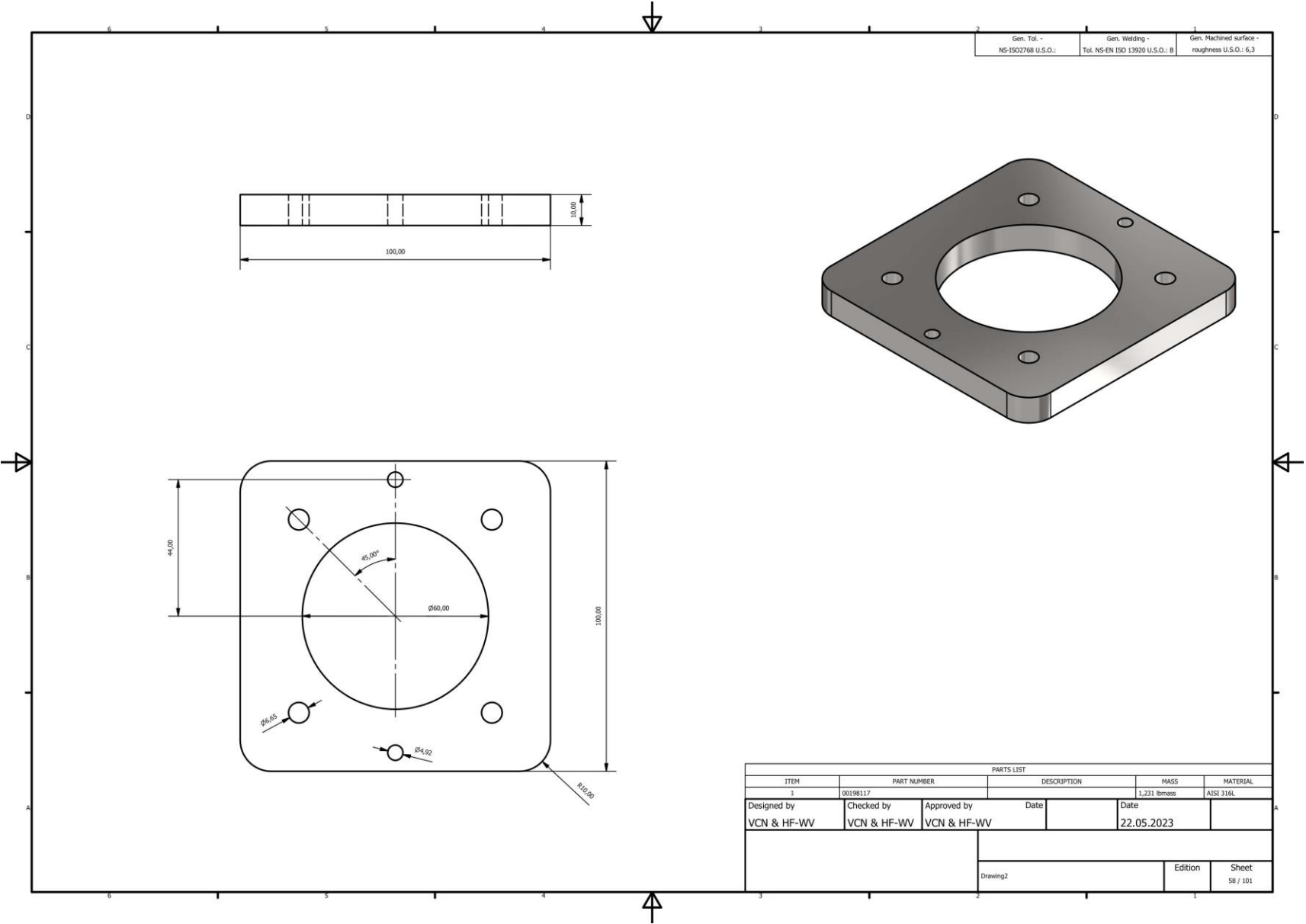
Gen. Welding -
Tol. NS-EN ISO 13920 U.S.O.: B

Gen. Machined surface -
roughness U.S.O.: 6,3

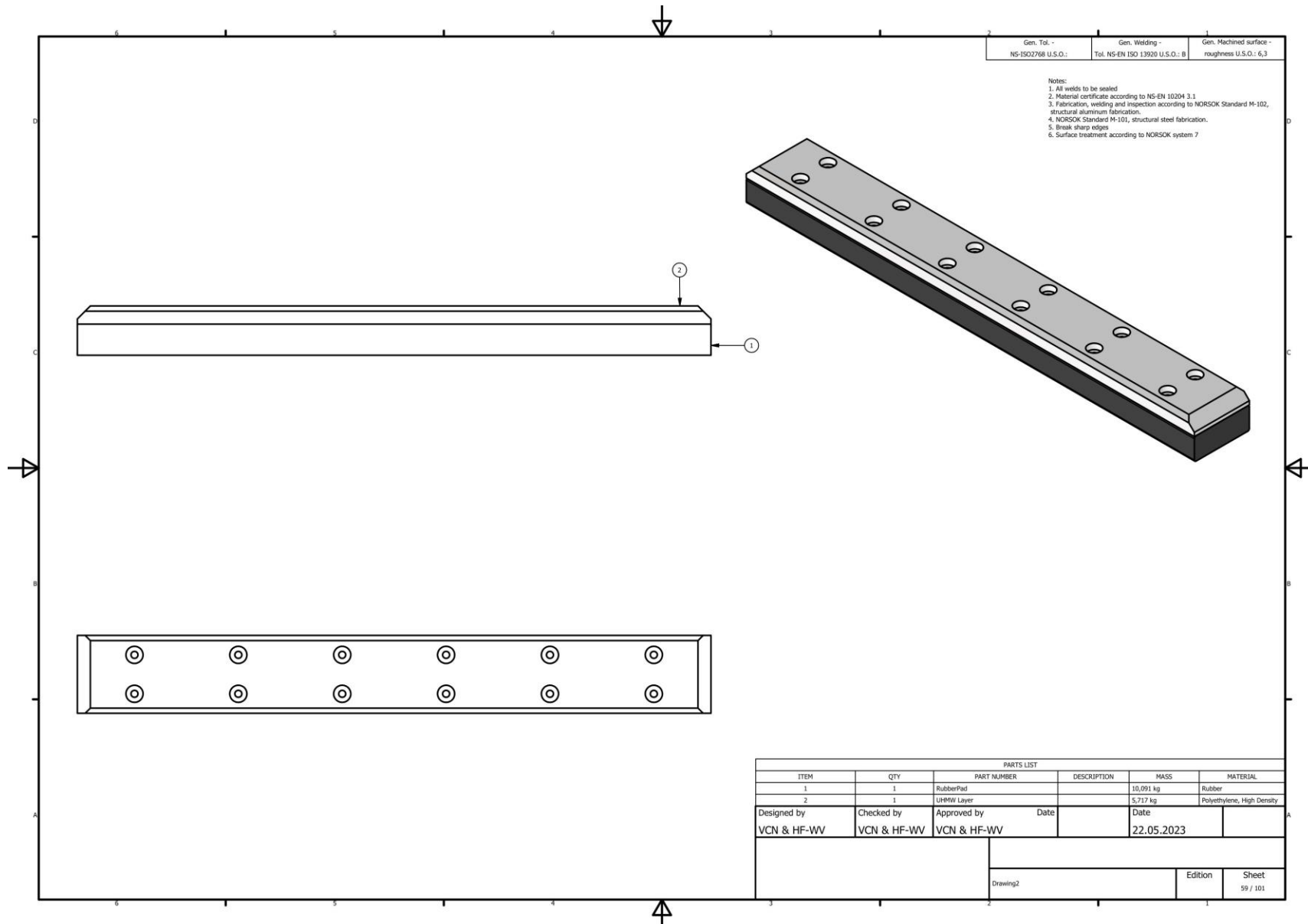
Notes:
 1. All welds to be sealed
 2. Material certificate according to NS-EN 10204 3.1
 3. Fabrication, welding and inspection according to NORSOK Standard M-102, structural aluminum fabrication.
 4. NORSOK Standard M-101, structural steel fabrication.
 5. Break sharp edges
 6. Surface treatment according to NORSOK system 7

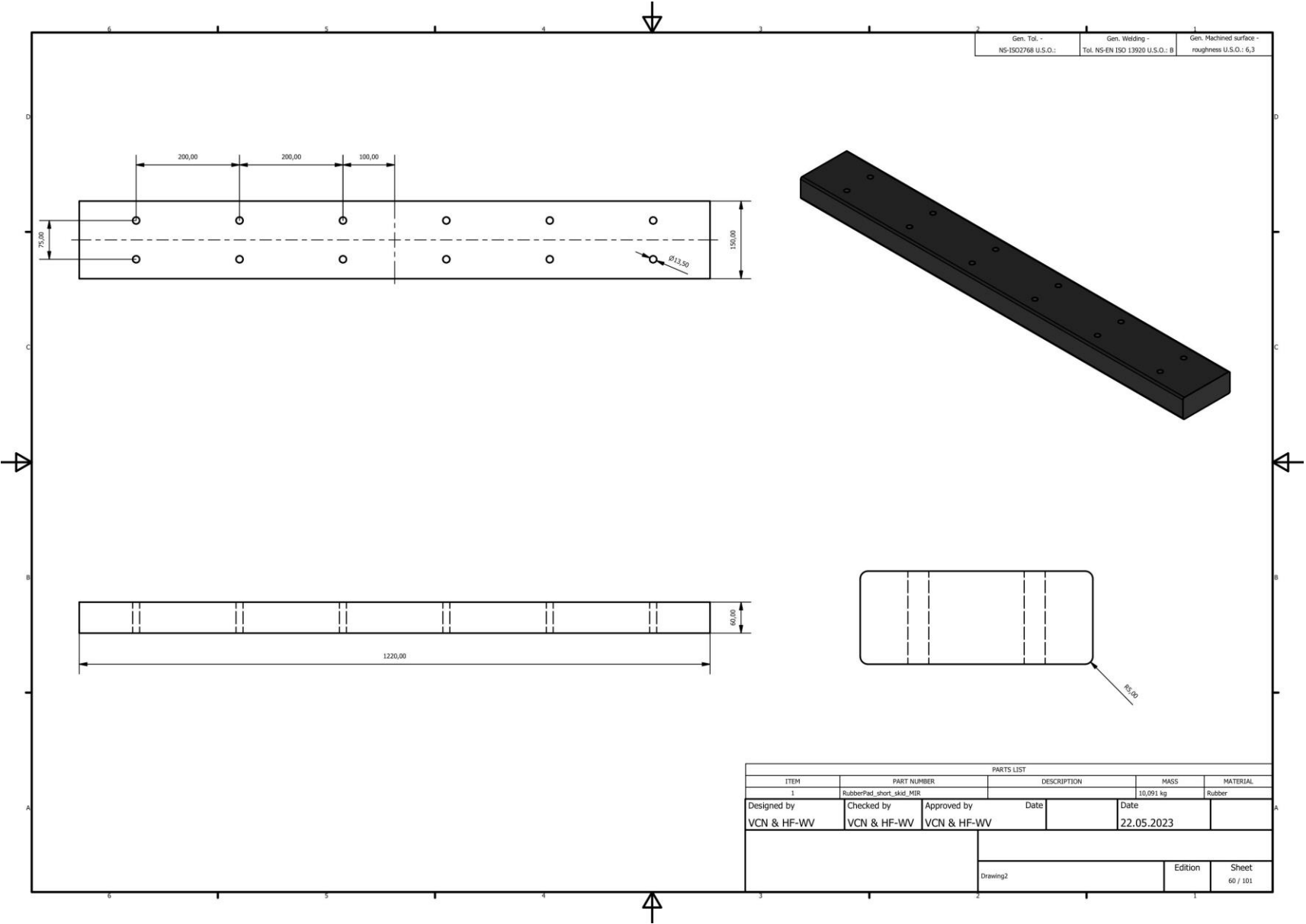
PARTS LIST					
ITEM	QTY	PART NUMBER	DESCRIPTION	MASS	MATERIAL
1	1	00196348		3,27 kg	Steel, S165M
2	1	00198117		0,56 kg	AISI 316L
Designed by VCN & HF-WV		Checked by VCN & HF-WV	Approved by VCN & HF-WV	Date 22.05.2023	
			Drawing2	Edition	Sheet 56 / 101

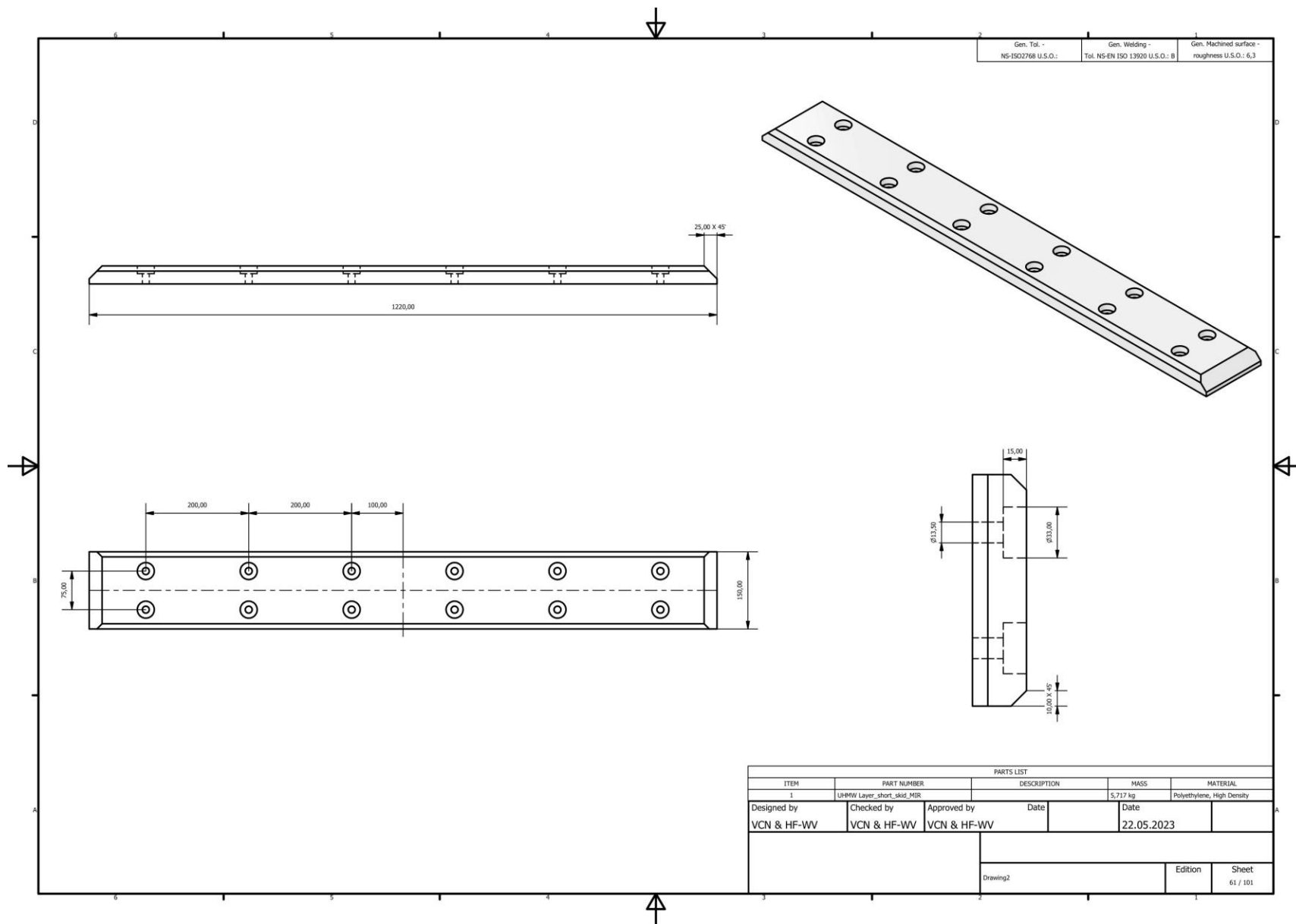


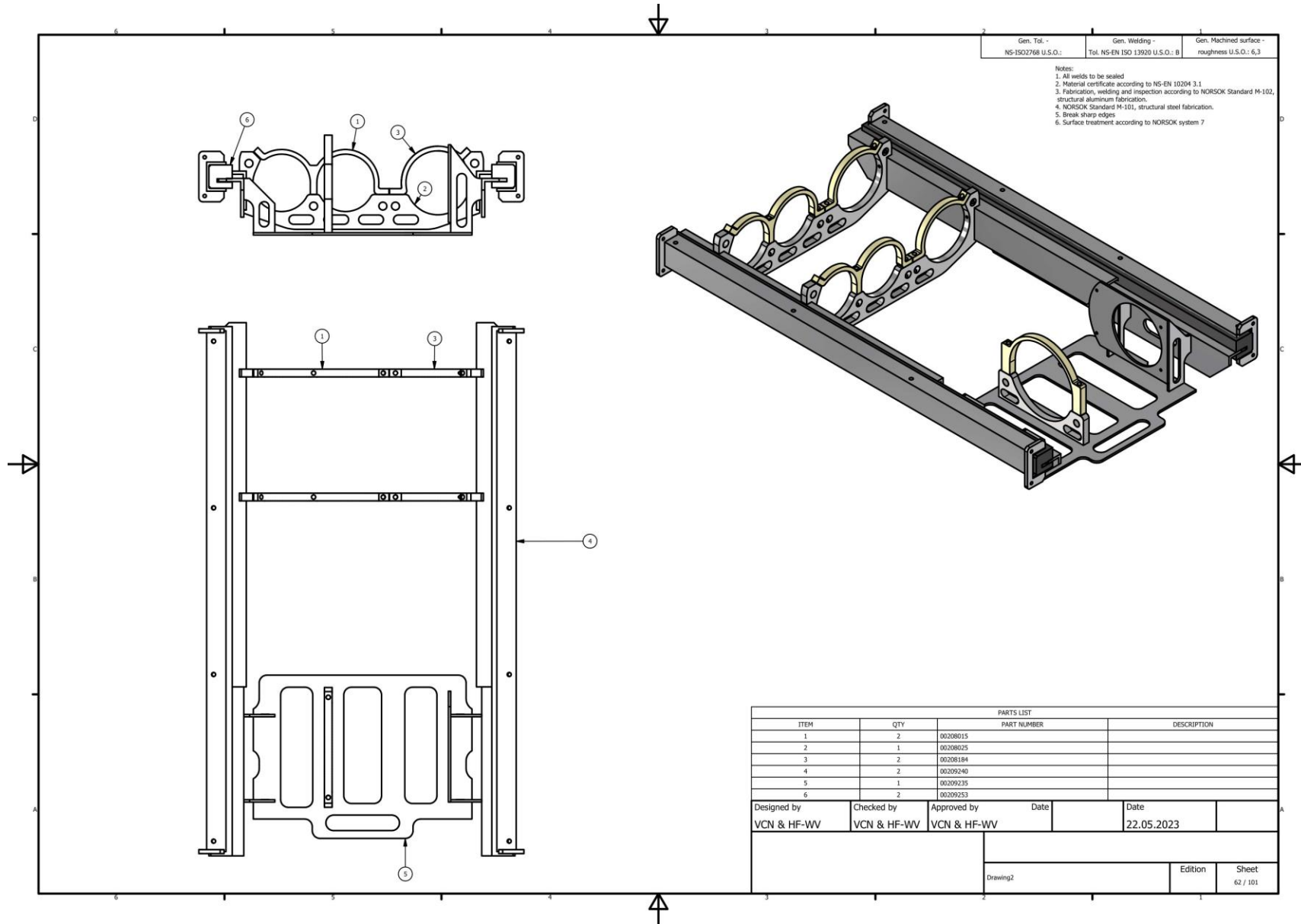


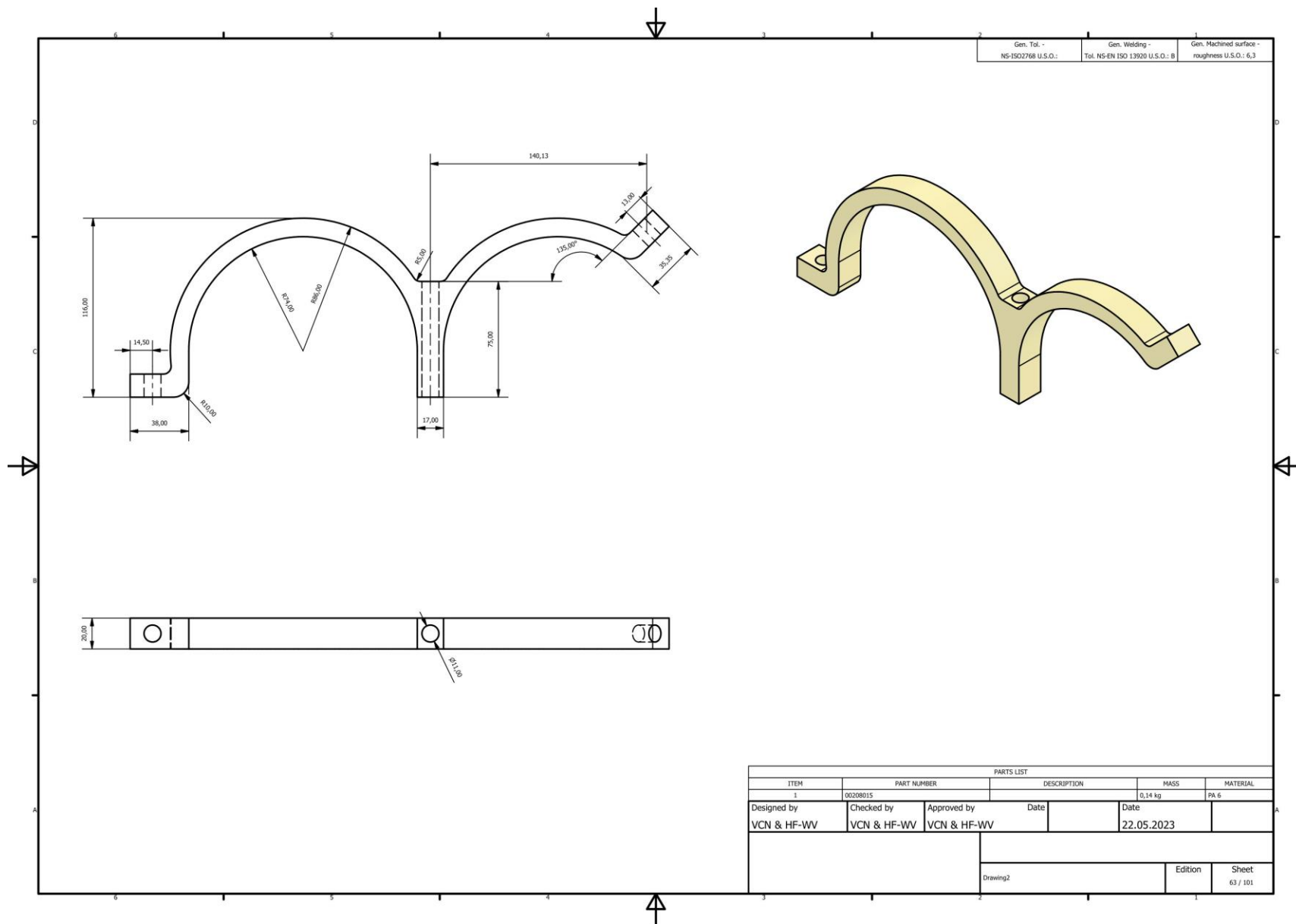
Integration of a Skid and Hatch-Based Launch and Recovery System for ROVs on USVs

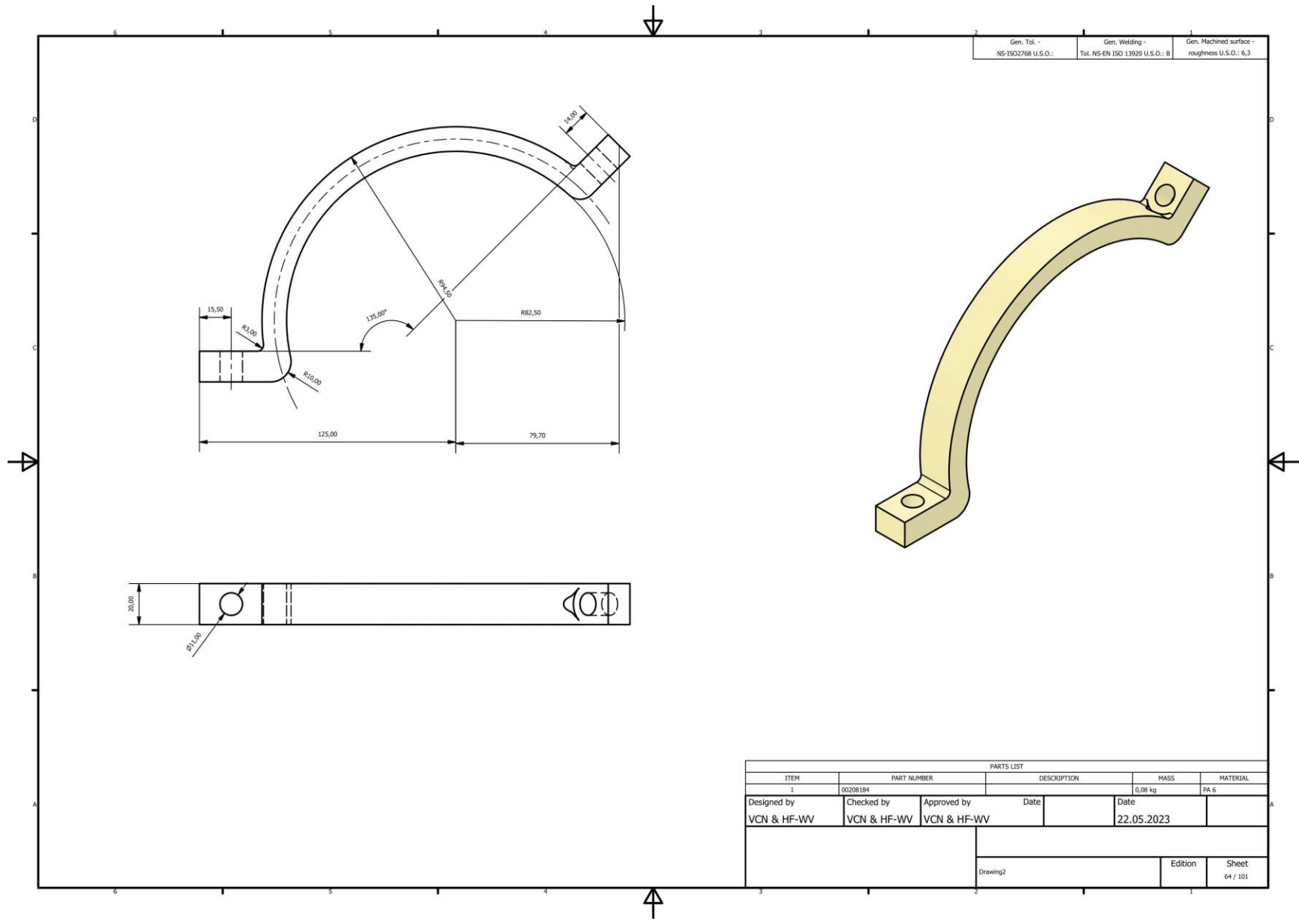






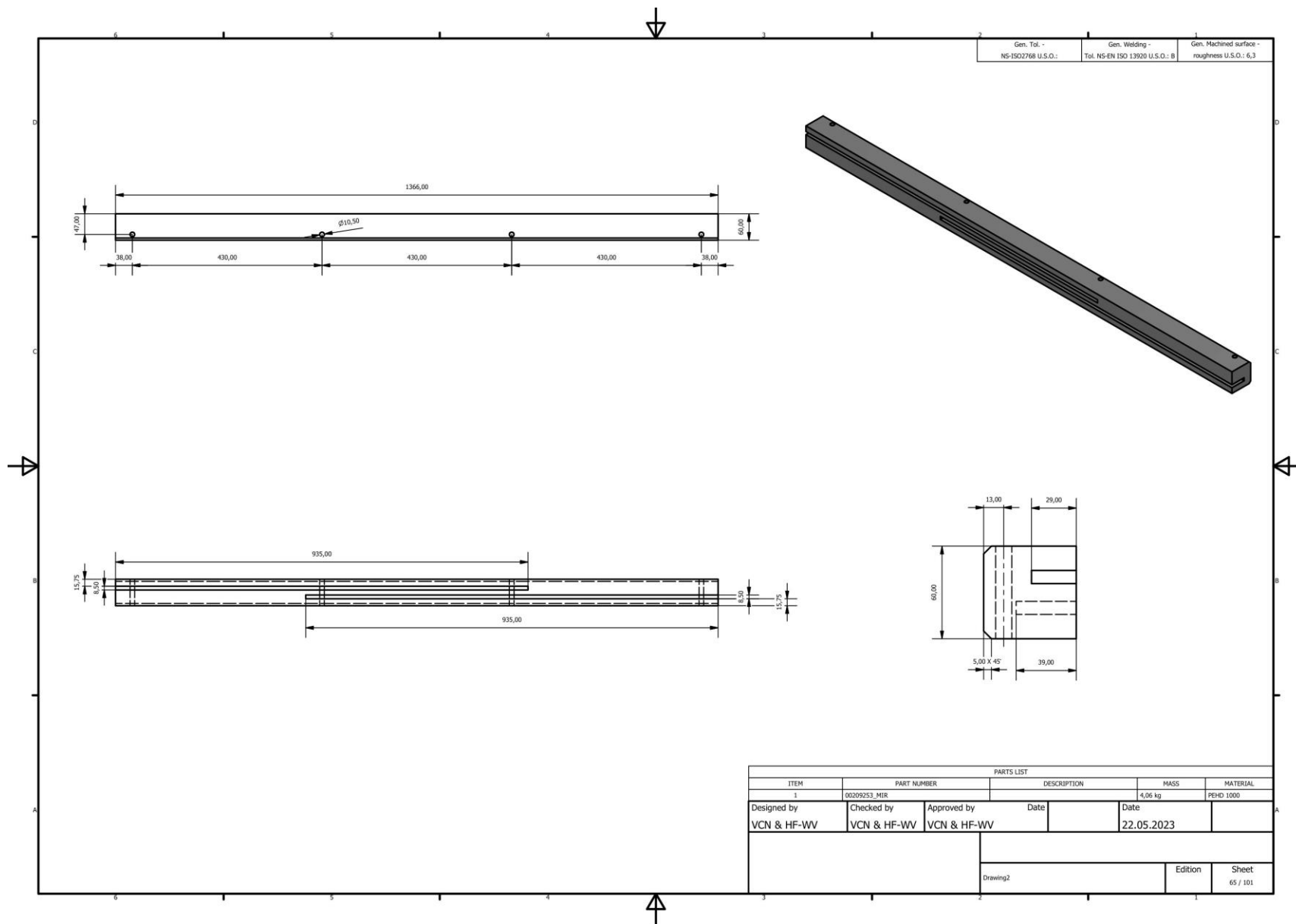


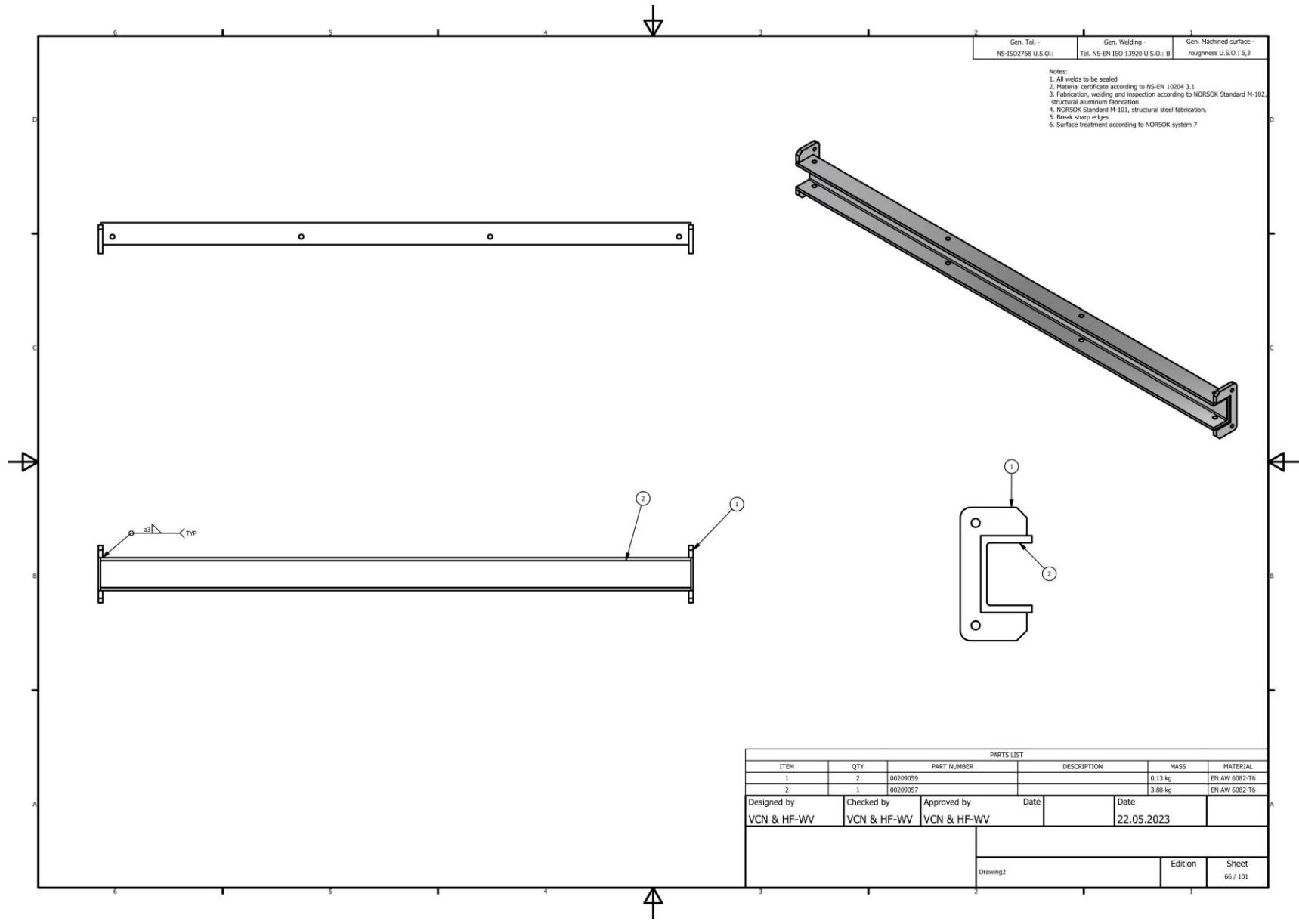


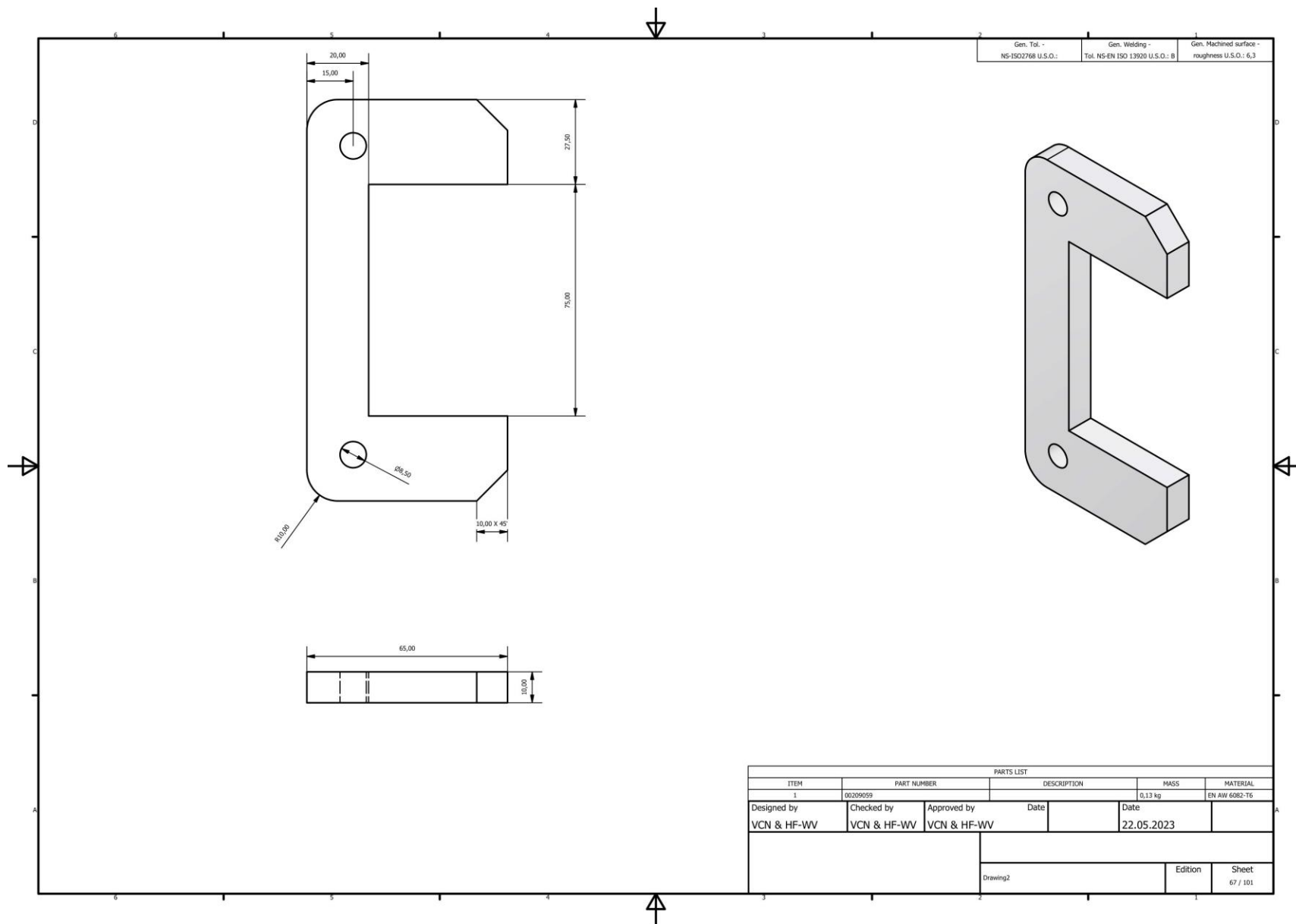


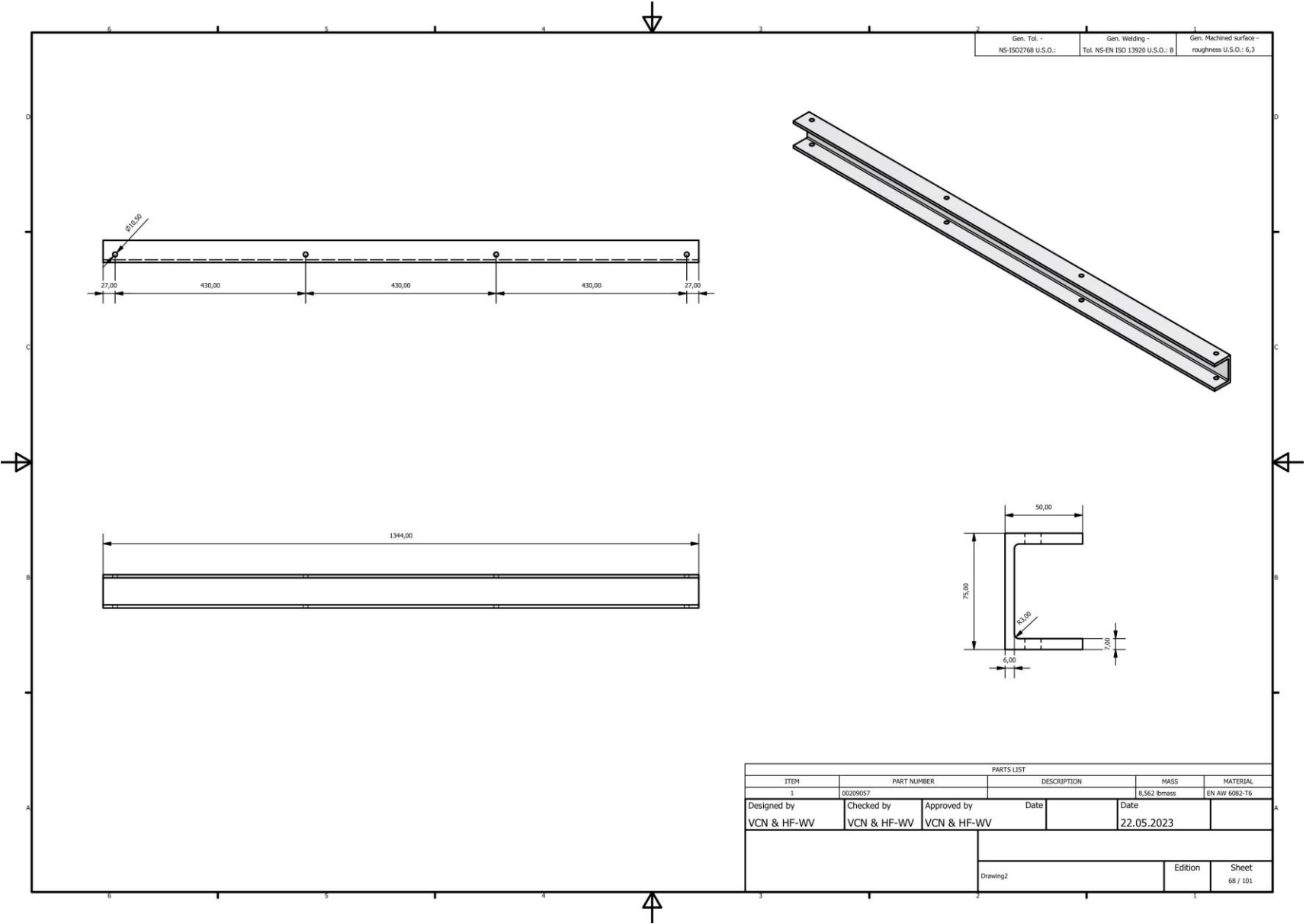
Gen. Tol - NS-ISO2768 U.S.O.:	Gen. Welding - Tol. NS-EN ISO 13920 U.S.O.:	Gen. Machined surface - roughness U.S.O.:
	B	6,3

PARTS LIST					
ITEM	PART NUMBER	DESCRIPTION	MASS	MATERIAL	
1	00208184		0,08 kg	PA 6	
Designed by	Checked by	Approved by	Date	Date	
VCN & HF-WV	VCN & HF-WV	VCN & HF-WV		22.05.2023	
			Drawing2	Edition	Sheet
					64 / 101

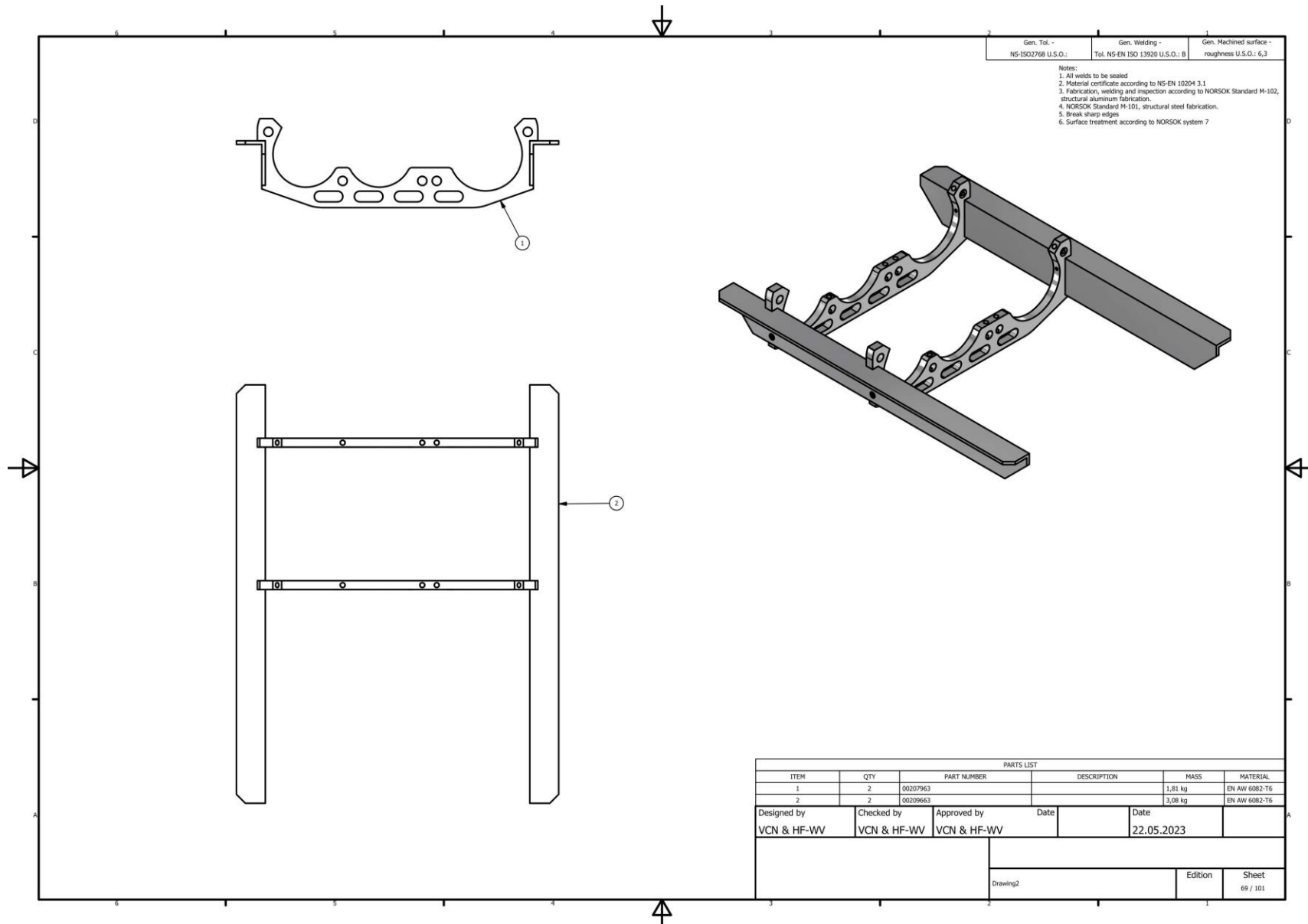


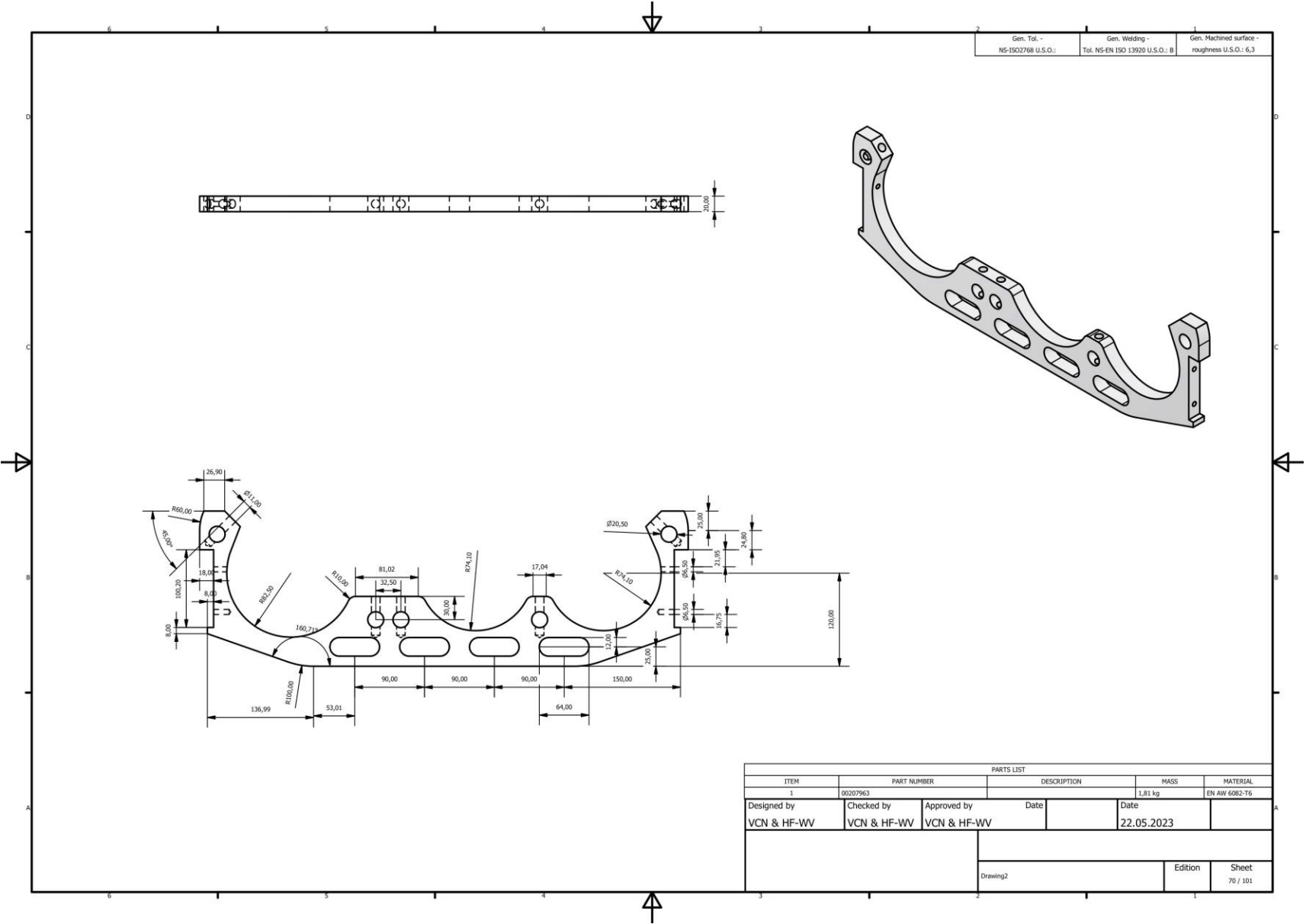


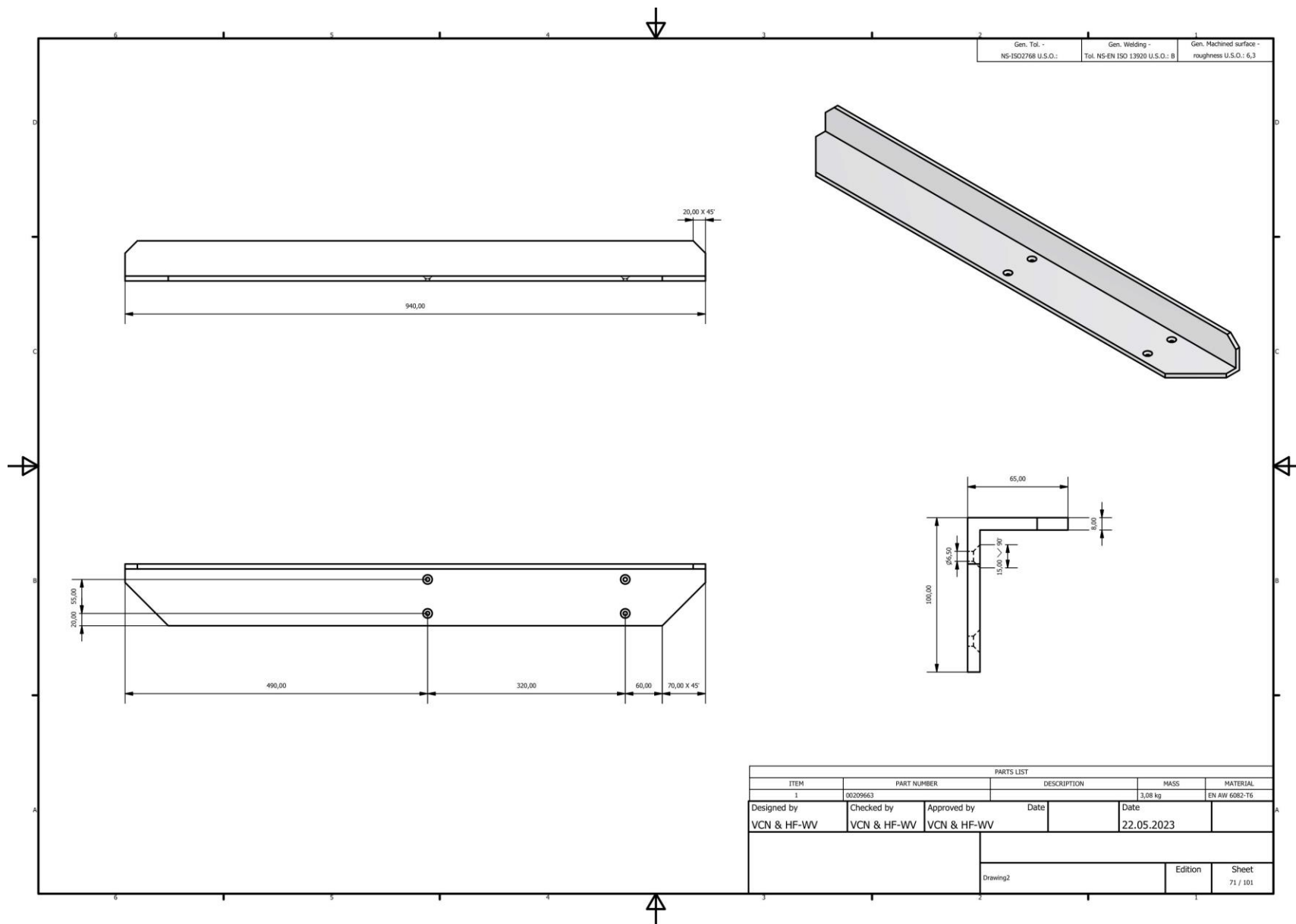


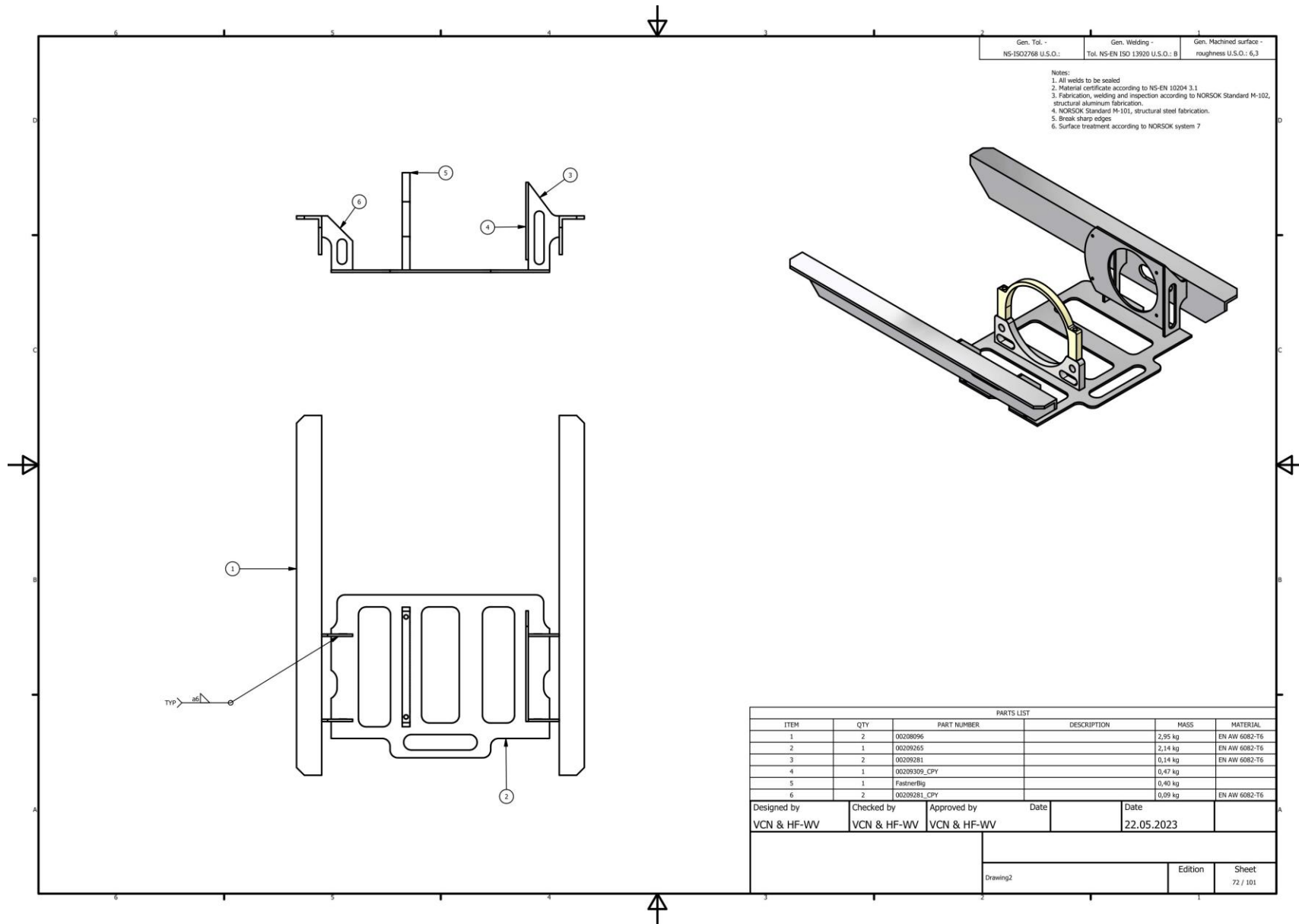


Integration of a Skid and Hatch-Based Launch and Recovery System for ROVs on USVs









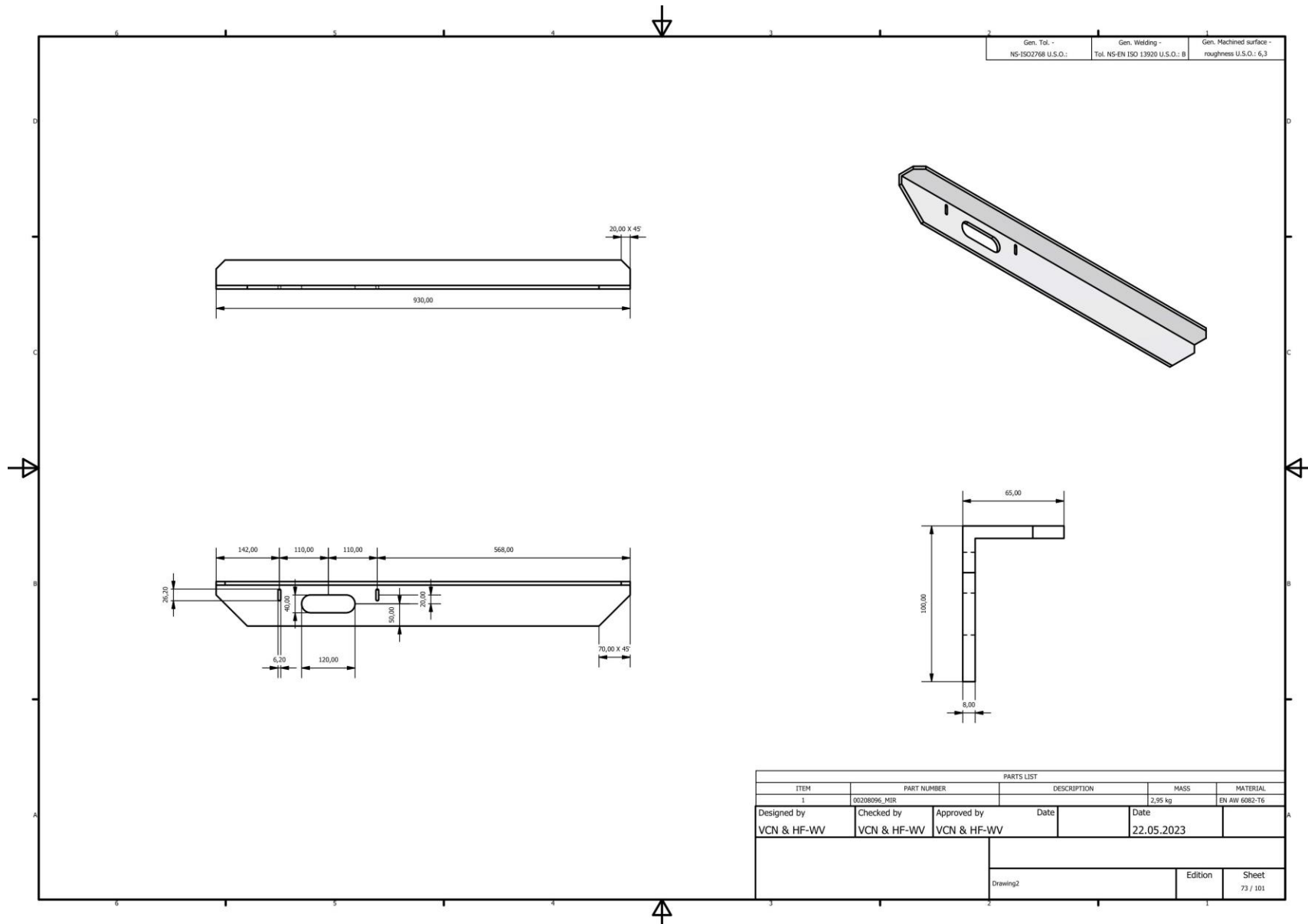
Gen. Tol. - NS-ISO2768 U.S.O.:
 Gen. Welding - Tol. NS-EN ISO 13920 U.S.O.: B
 Gen. Machined surface - roughness U.S.O.: 6,3

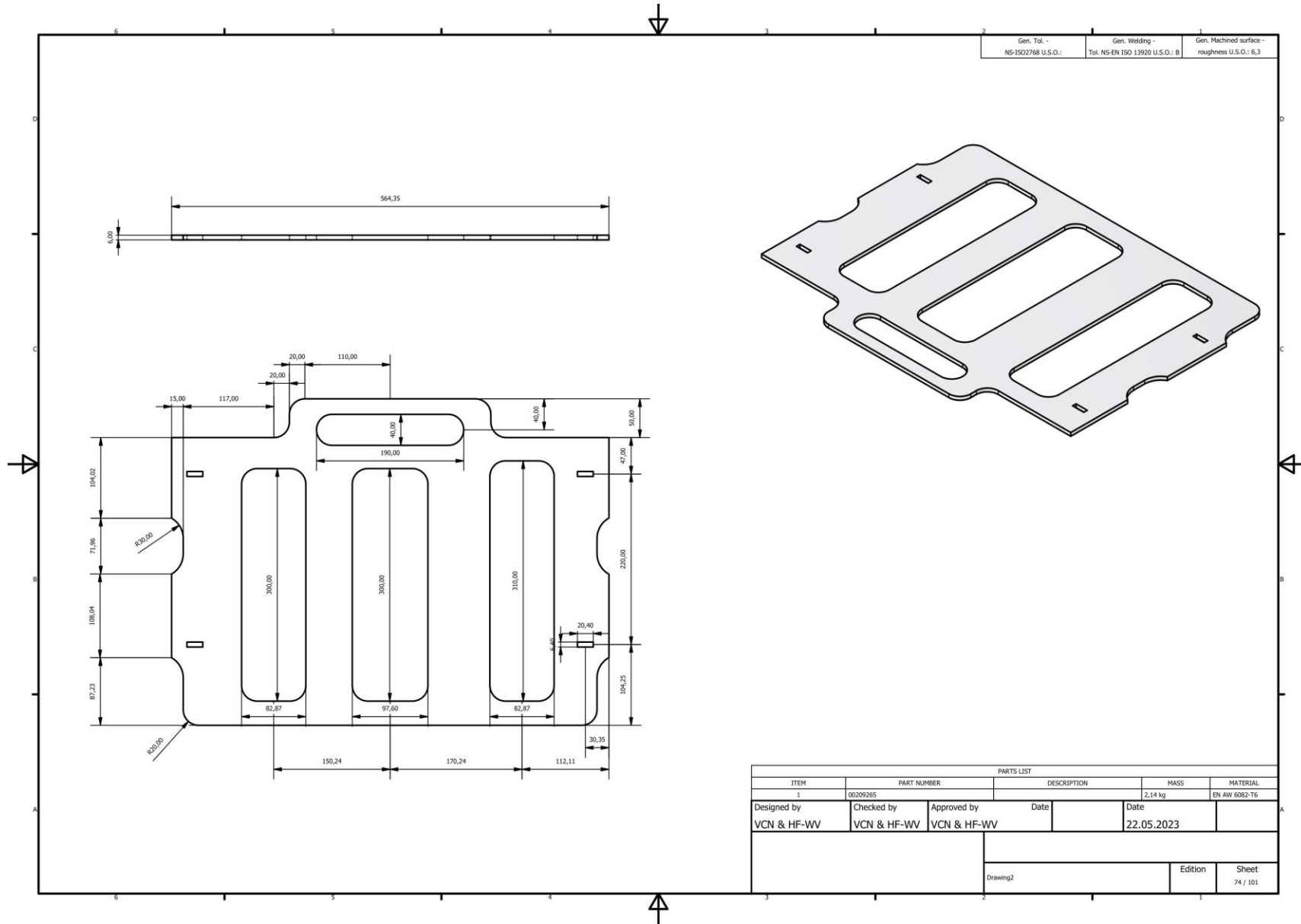
- Notes:
 1. All welds to be sealed.
 2. Material certificate according to NS-EN 10204 3.1.
 3. Fabrication, welding and inspection according to NORSOK Standard M-102, structural aluminum fabrication.
 4. NORSOK Standard M-101, structural steel fabrication.
 5. Break sharp edges.
 6. Surface treatment according to NORSOK system 7.

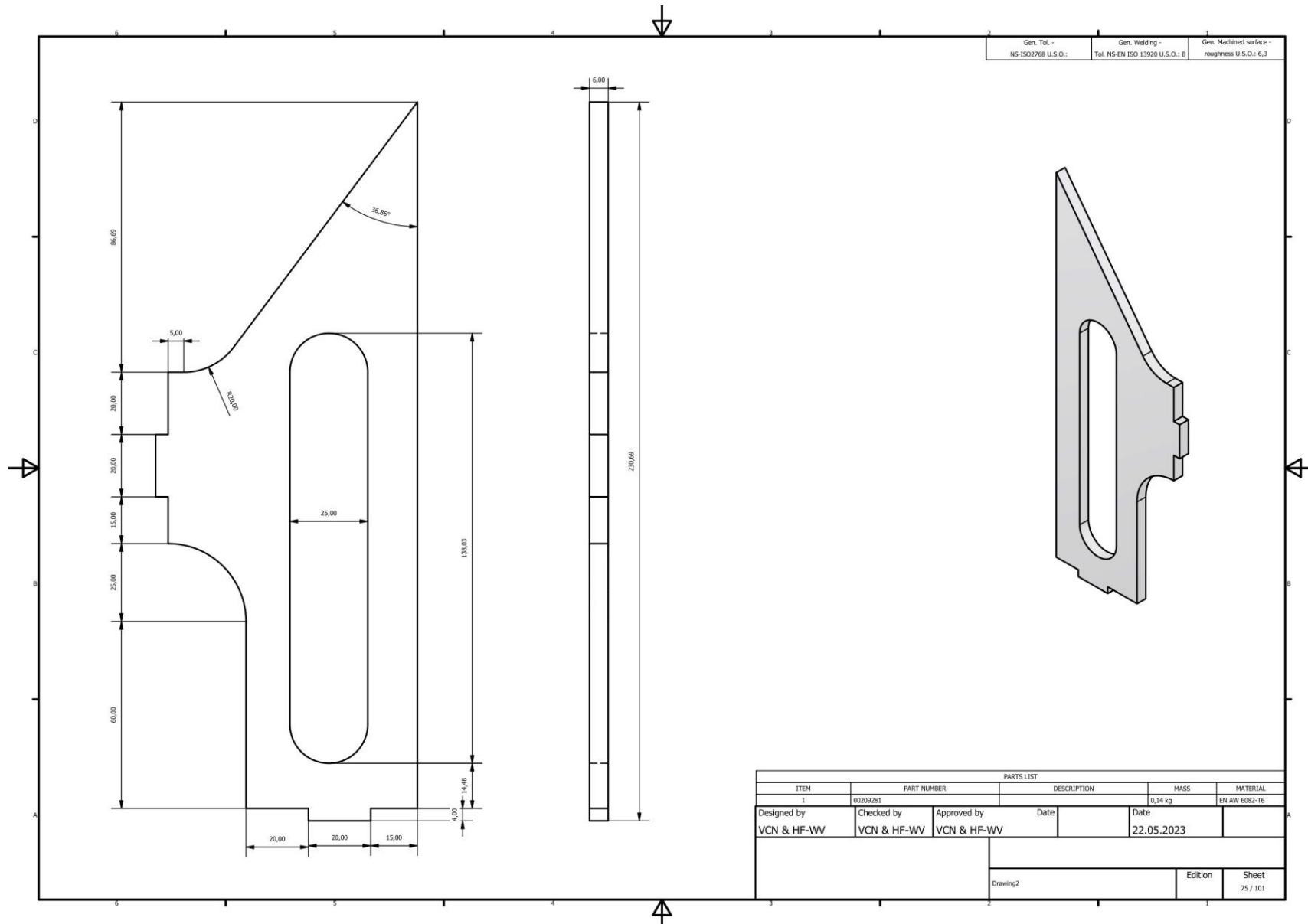
PARTS LIST					
ITEM	QTY	PART NUMBER	DESCRIPTION	MASS	MATERIAL
1	2	00208096		2,95 kg	EN AW 6082-T6
2	1	00209265		2,14 kg	EN AW 6082-T6
3	2	00209281		0,14 kg	EN AW 6082-T6
4	1	00209309_CPY		0,47 kg	
5	1	FastnerBig		0,40 kg	
6	2	00209281_CPY		0,09 kg	EN AW 6082-T6

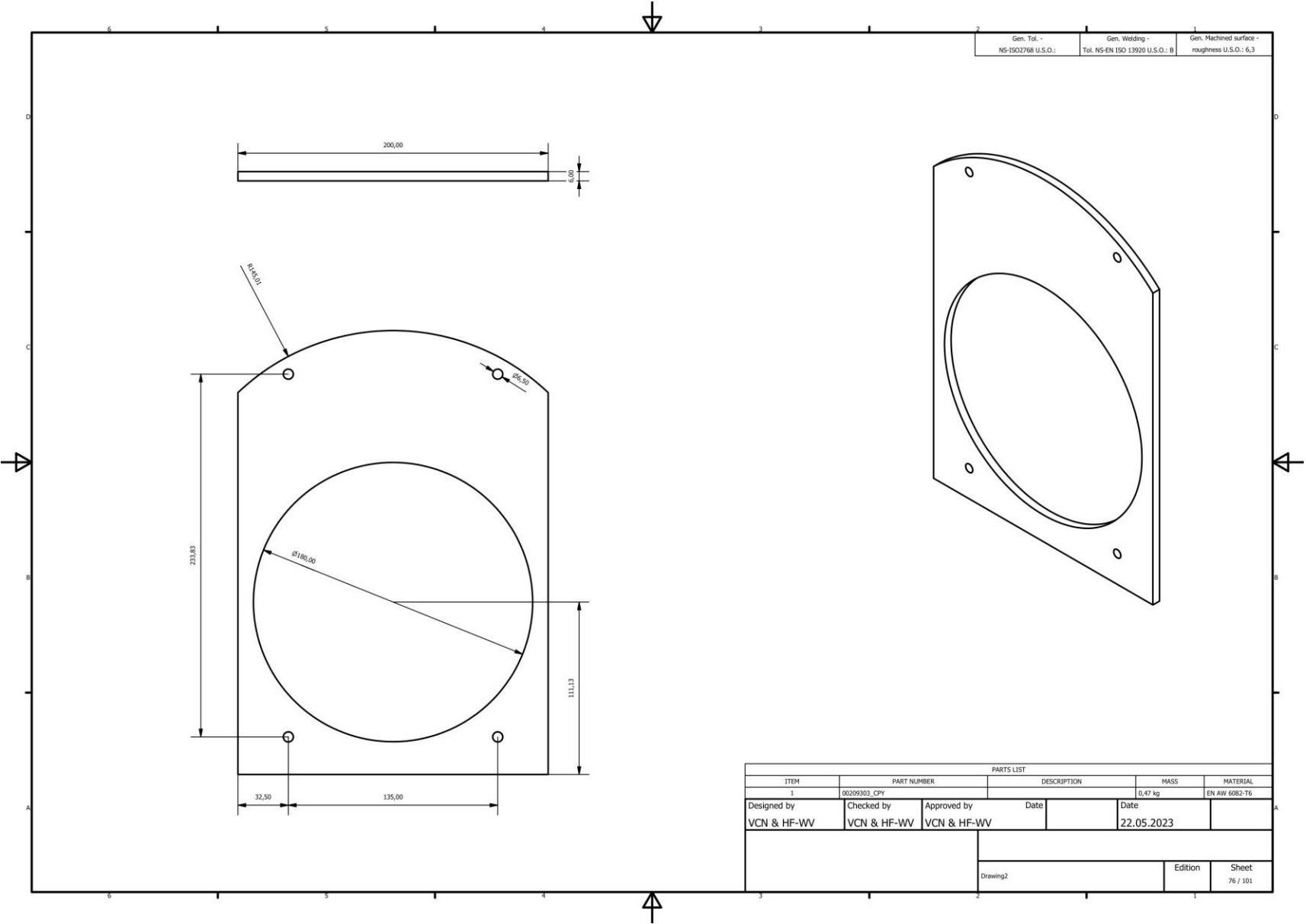
Designed by VCN & HF-WV	Checked by VCN & HF-WV	Approved by VCN & HF-WV	Date	Date	
				22.05.2023	
			Drawing2	Edition	Sheet 72 / 101

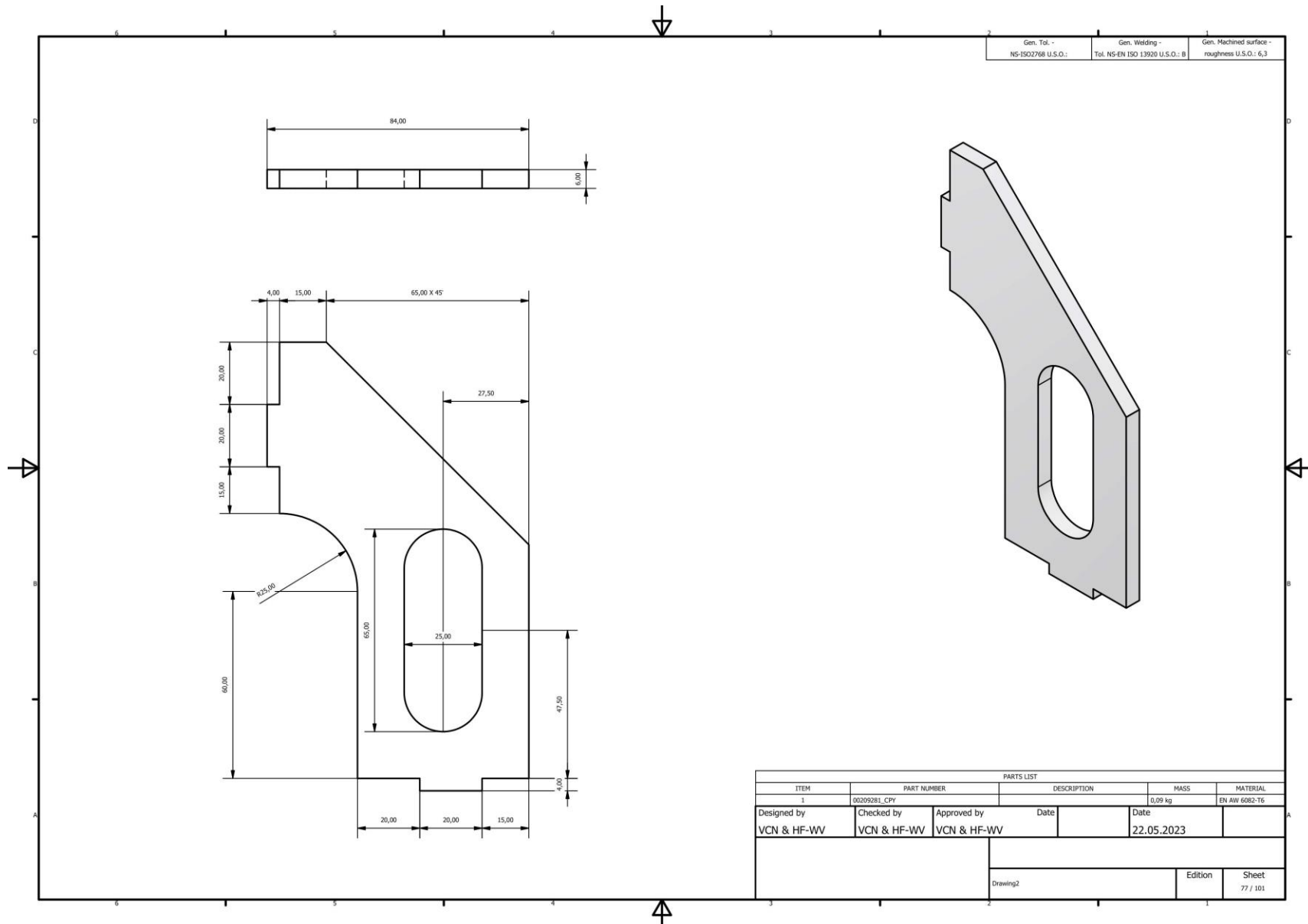
Integration of a Skid and Hatch-Based Launch and Recovery System for ROVs on USVs

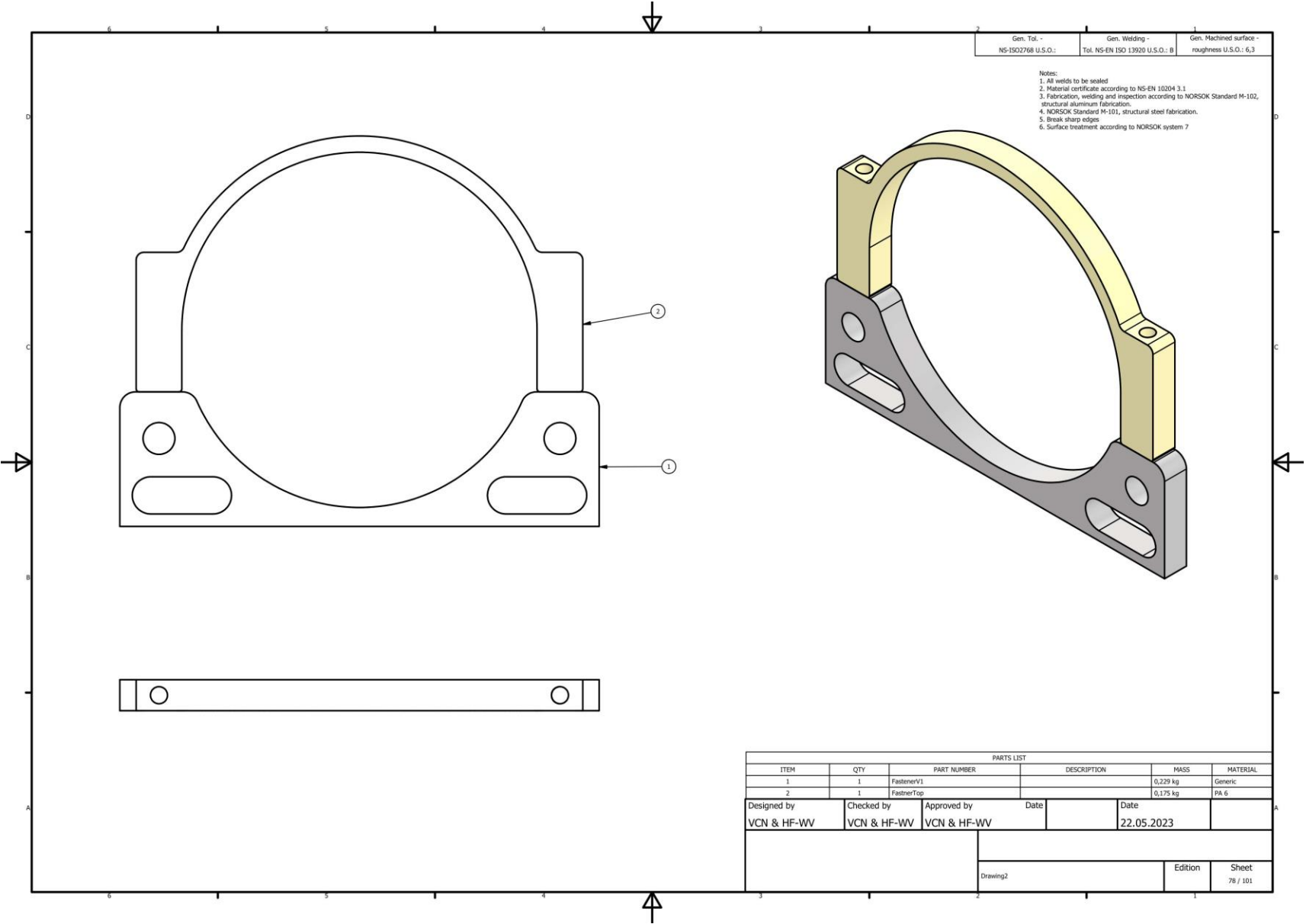


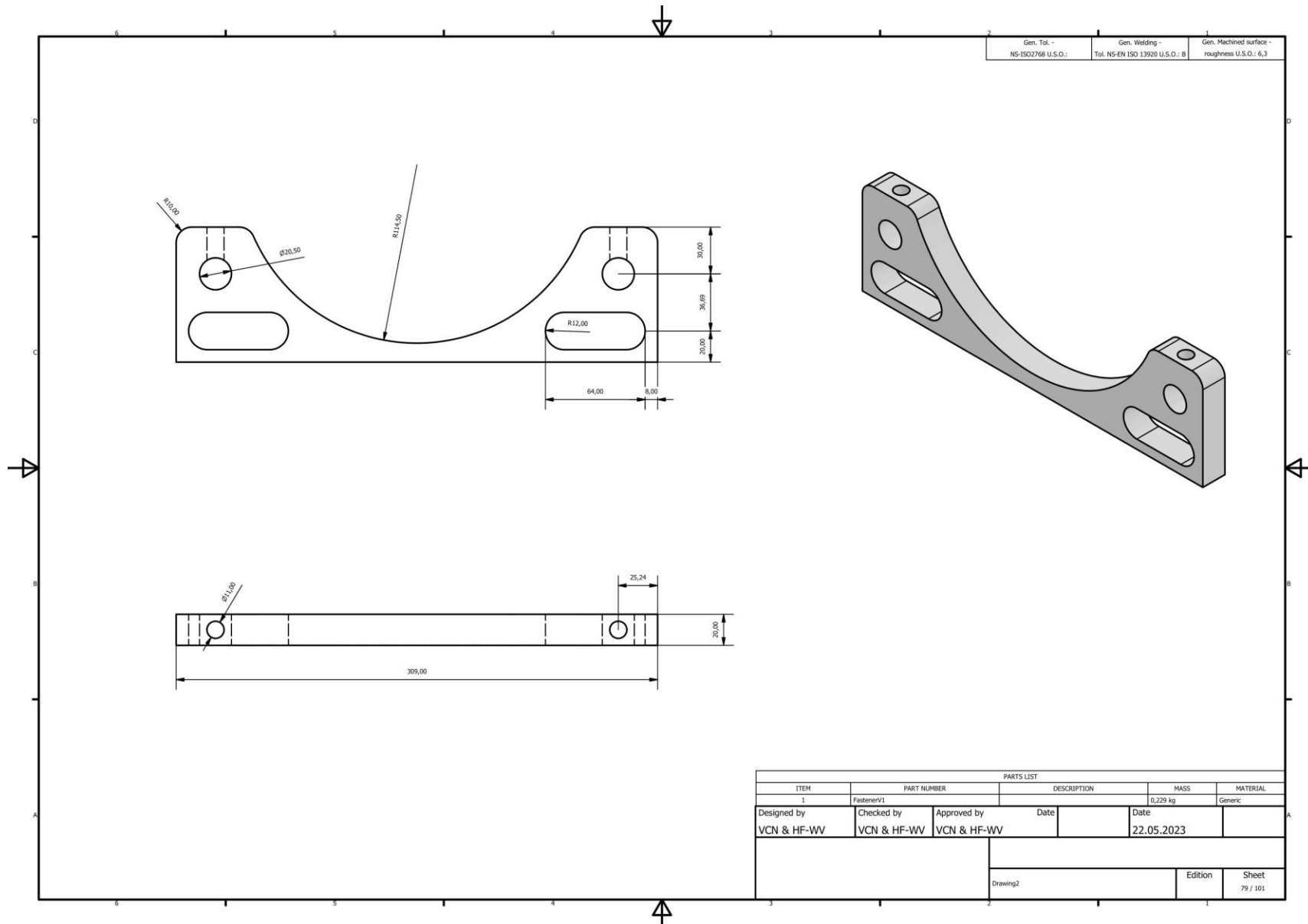


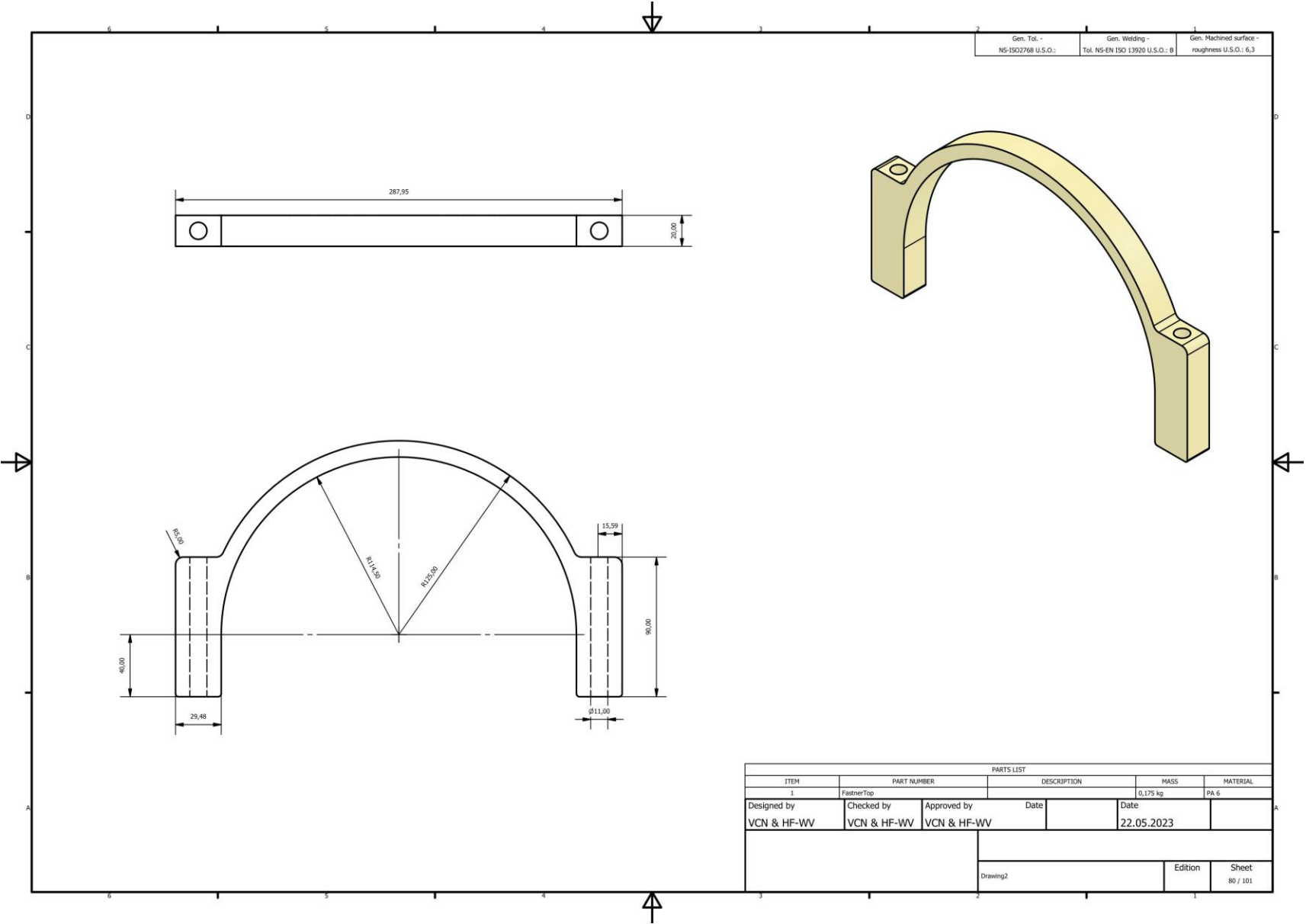






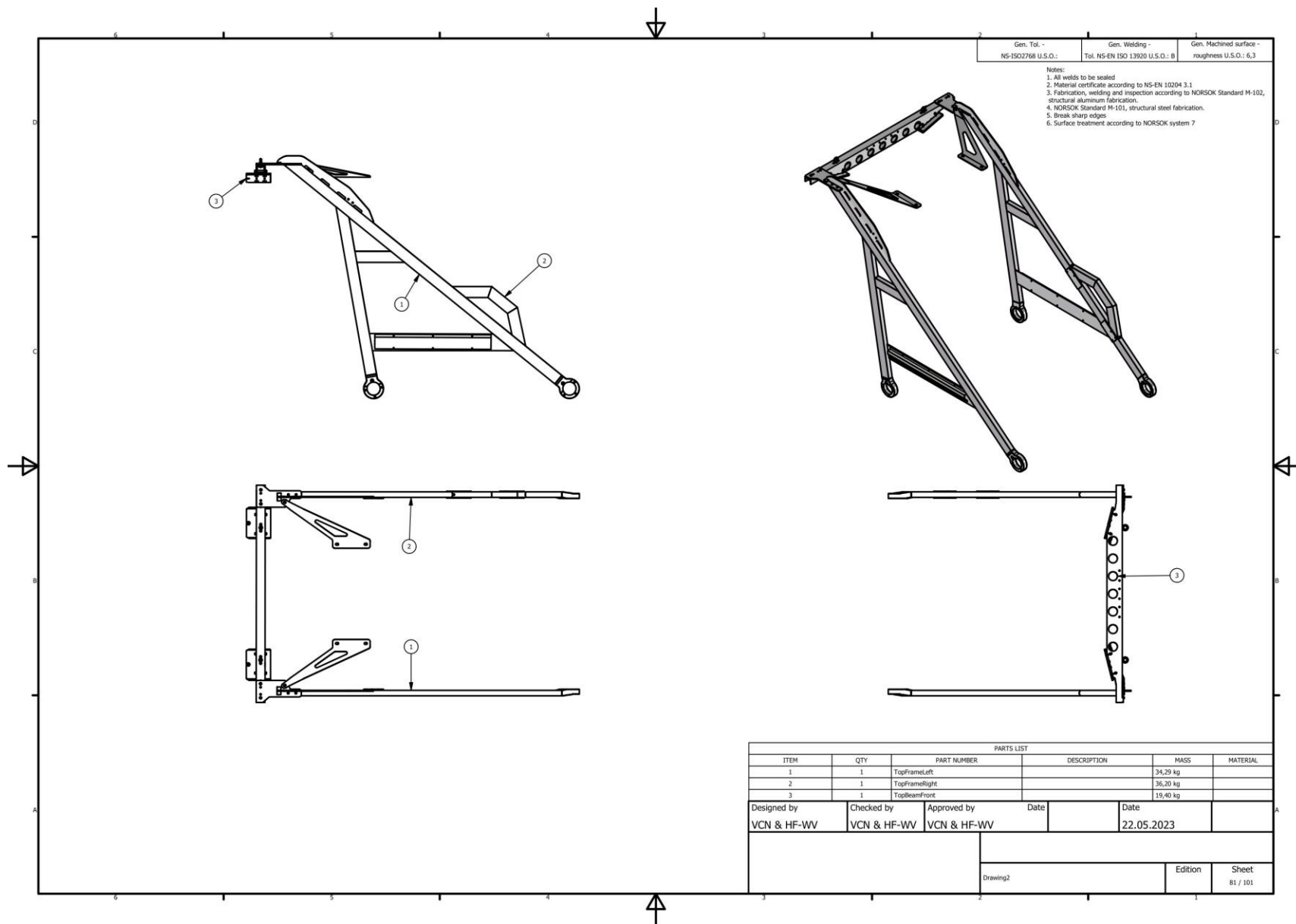


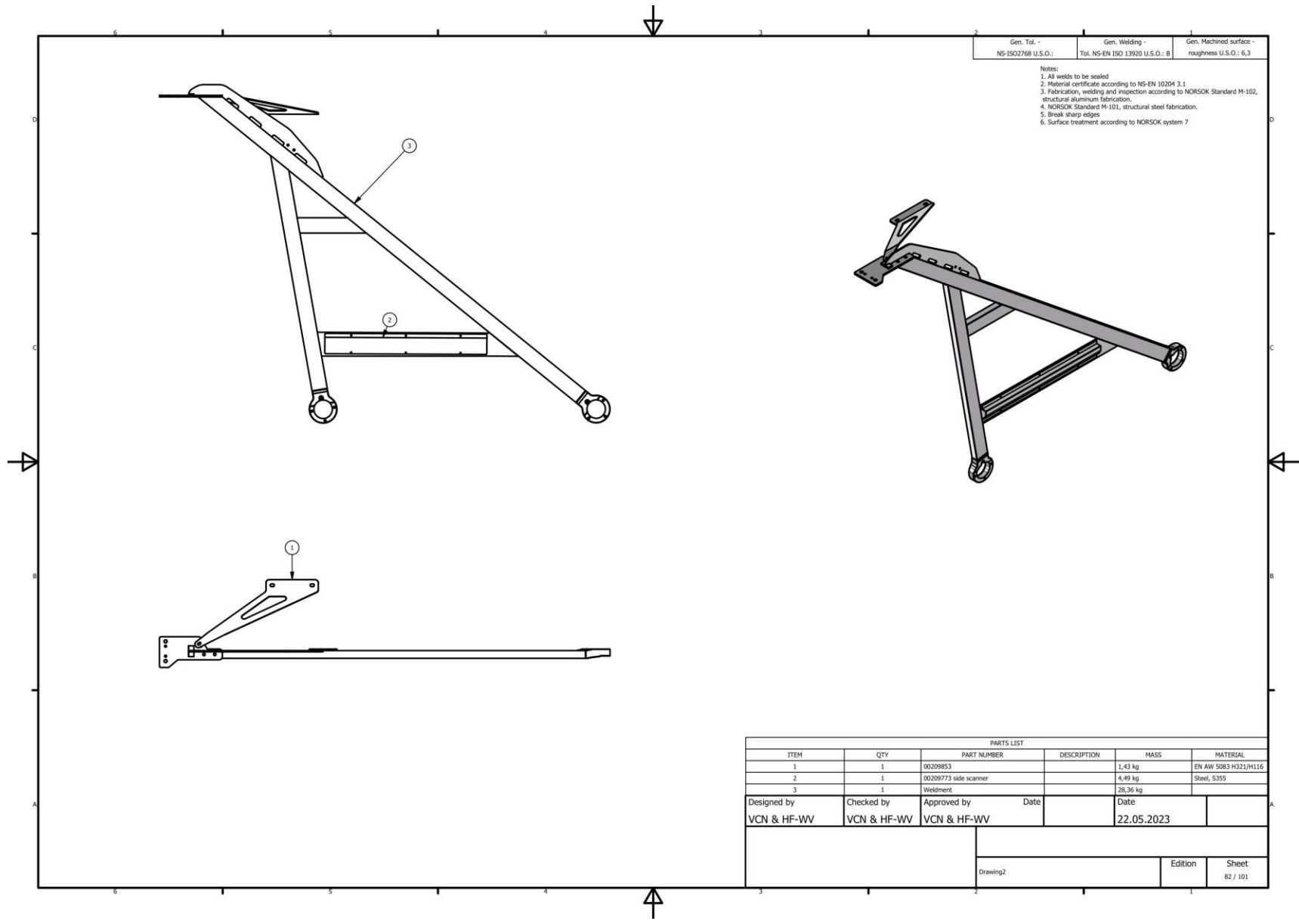


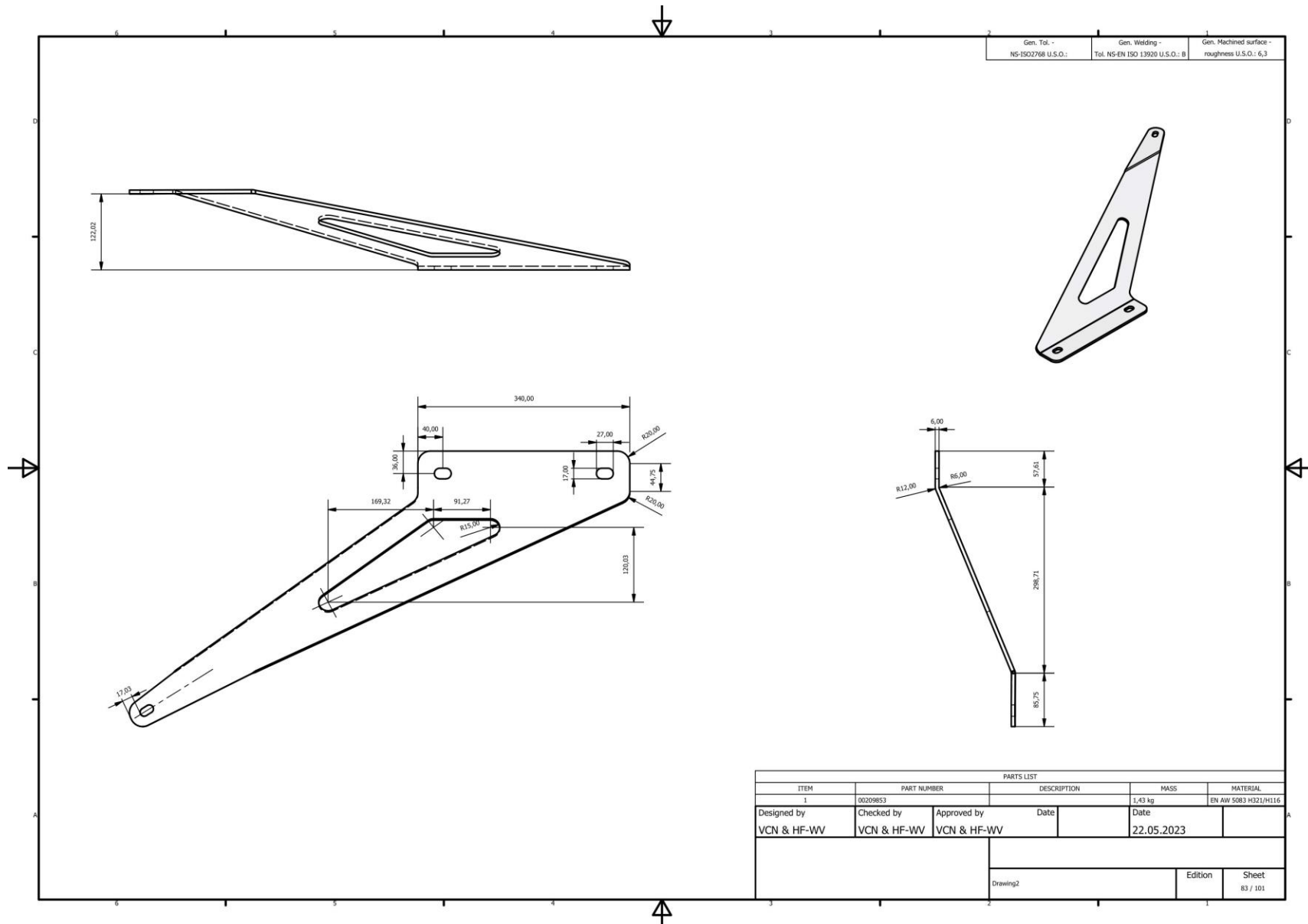


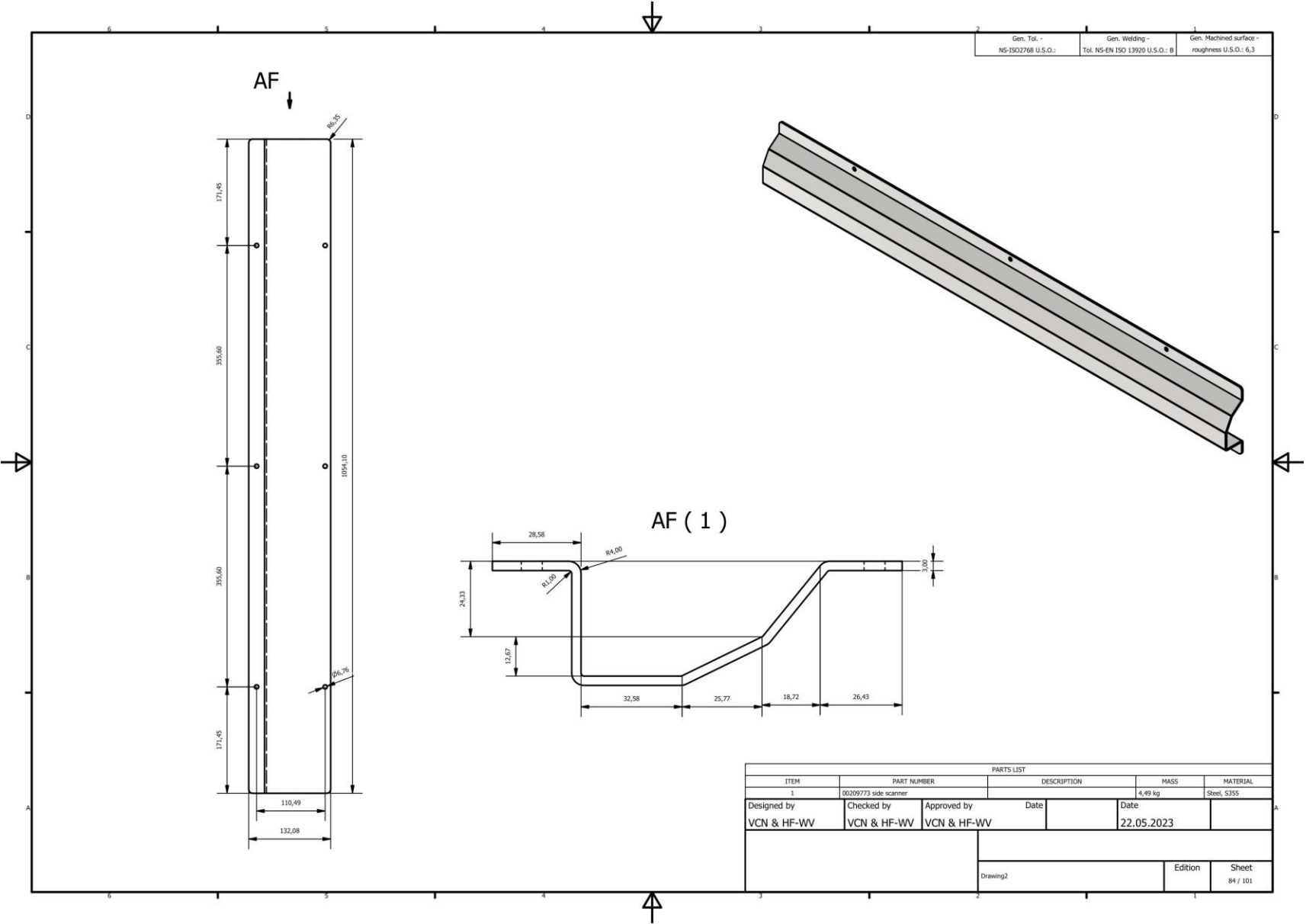
PARTS LIST					
ITEM	PART NUMBER	DESCRIPTION	MASS	MATERIAL	
1	FastnerTop		0,175 kg	PA 6	
Designed by	Checked by	Approved by	Date	Date	
VCN & HF-WV	VCN & HF-WV	VCN & HF-WV		22.05.2023	
			Drawing2	Edition	Sheet
					80 / 101

Integration of a Skid and Hatch-Based Launch and Recovery System for ROVs on USVs

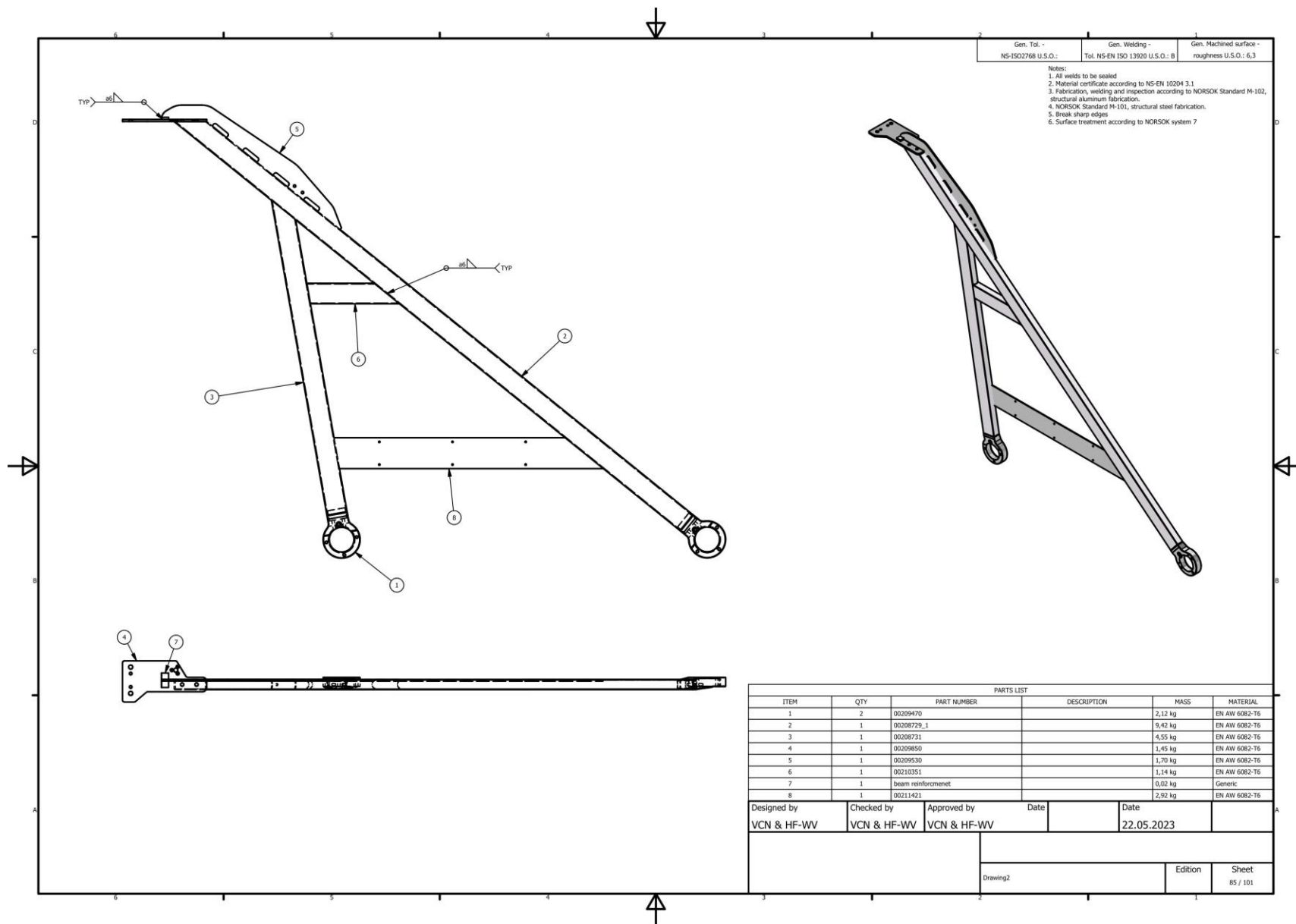


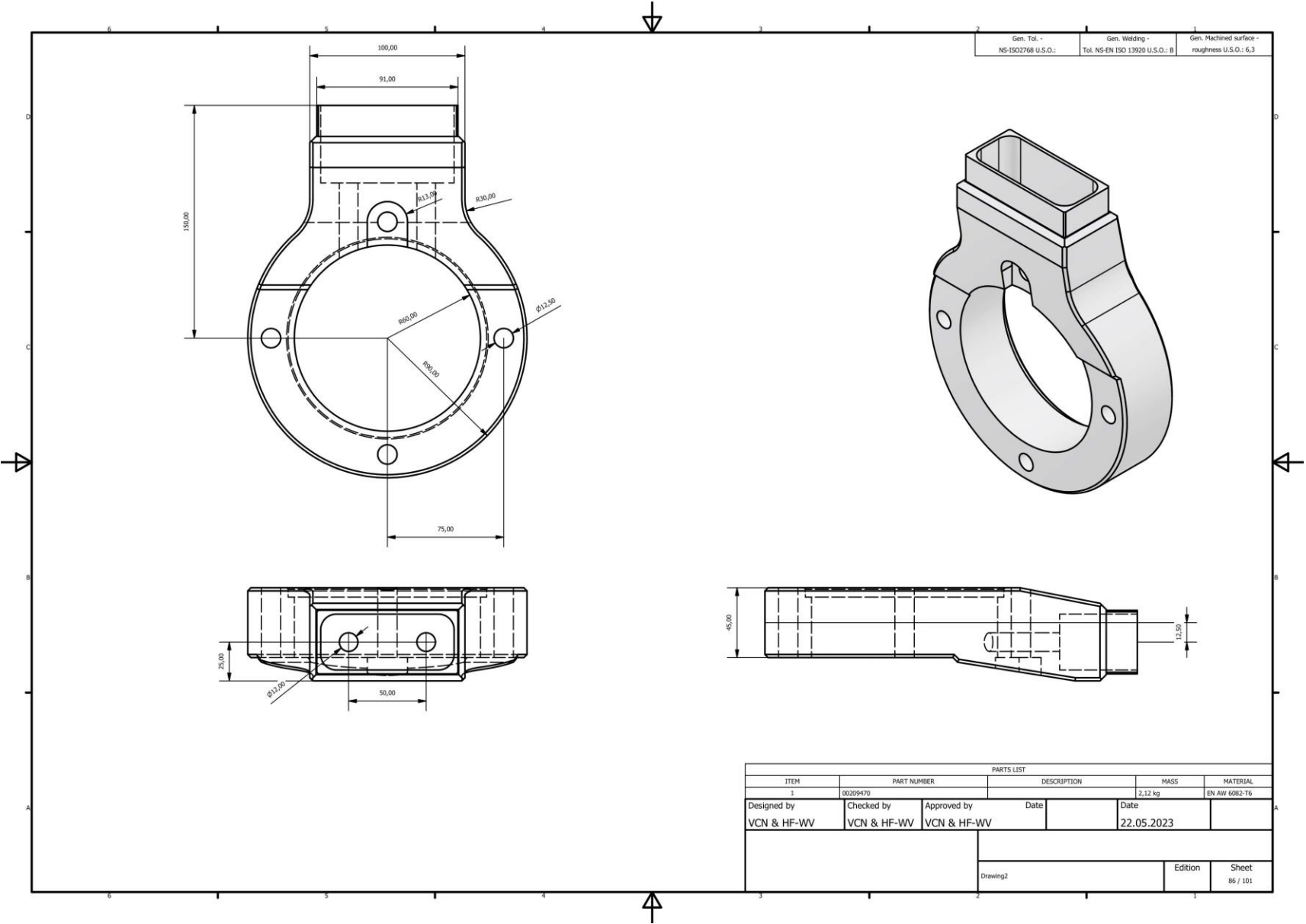


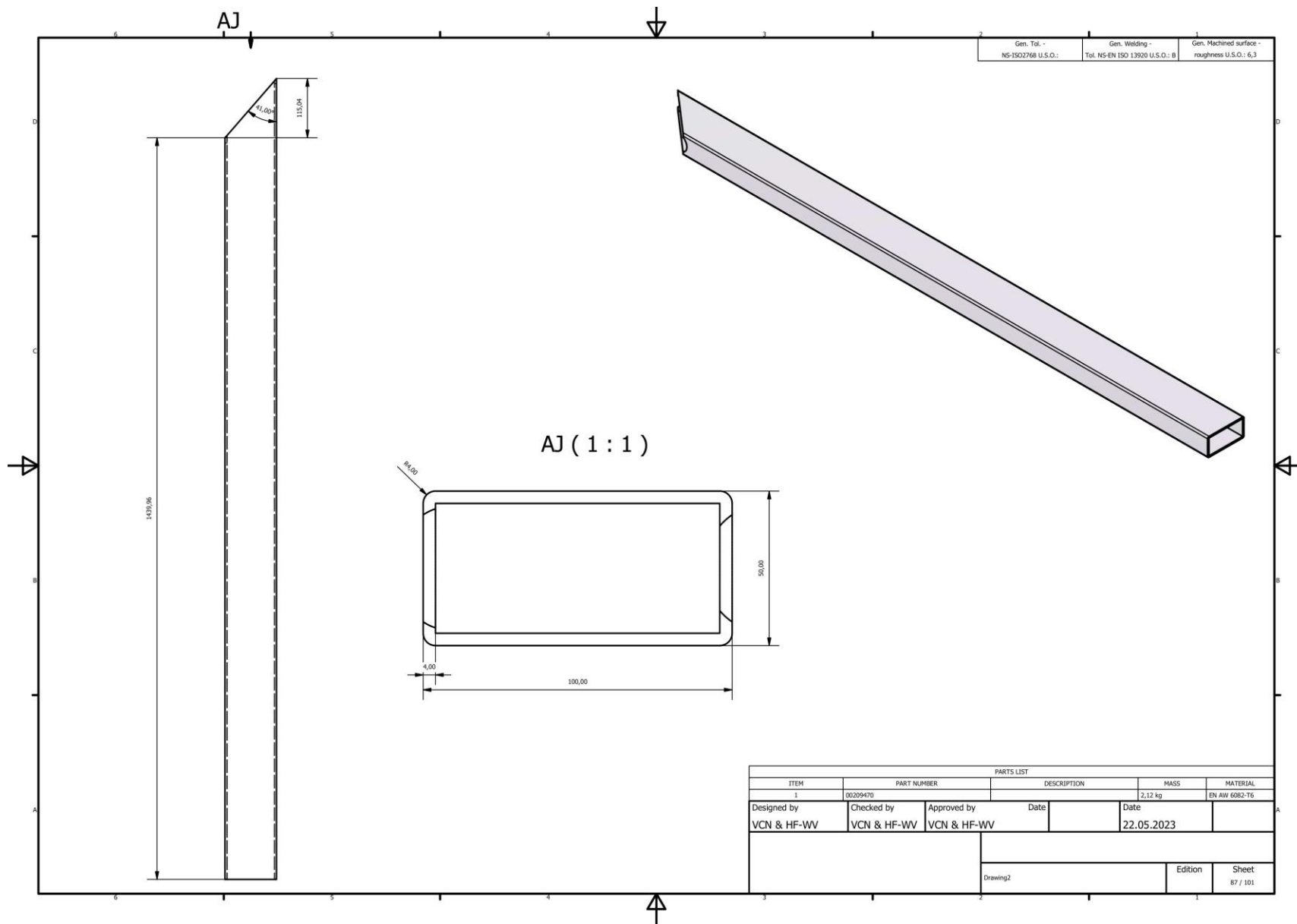


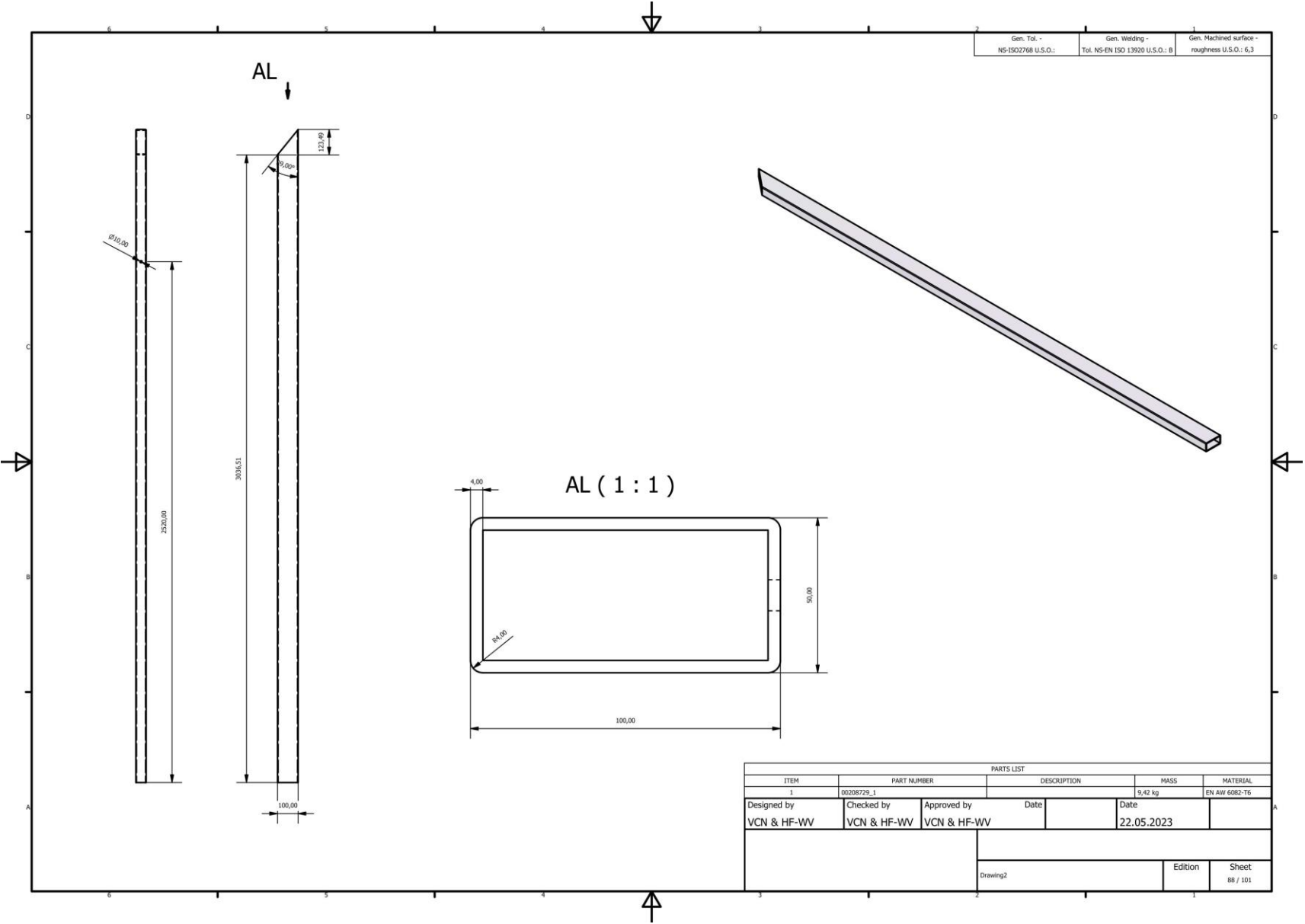


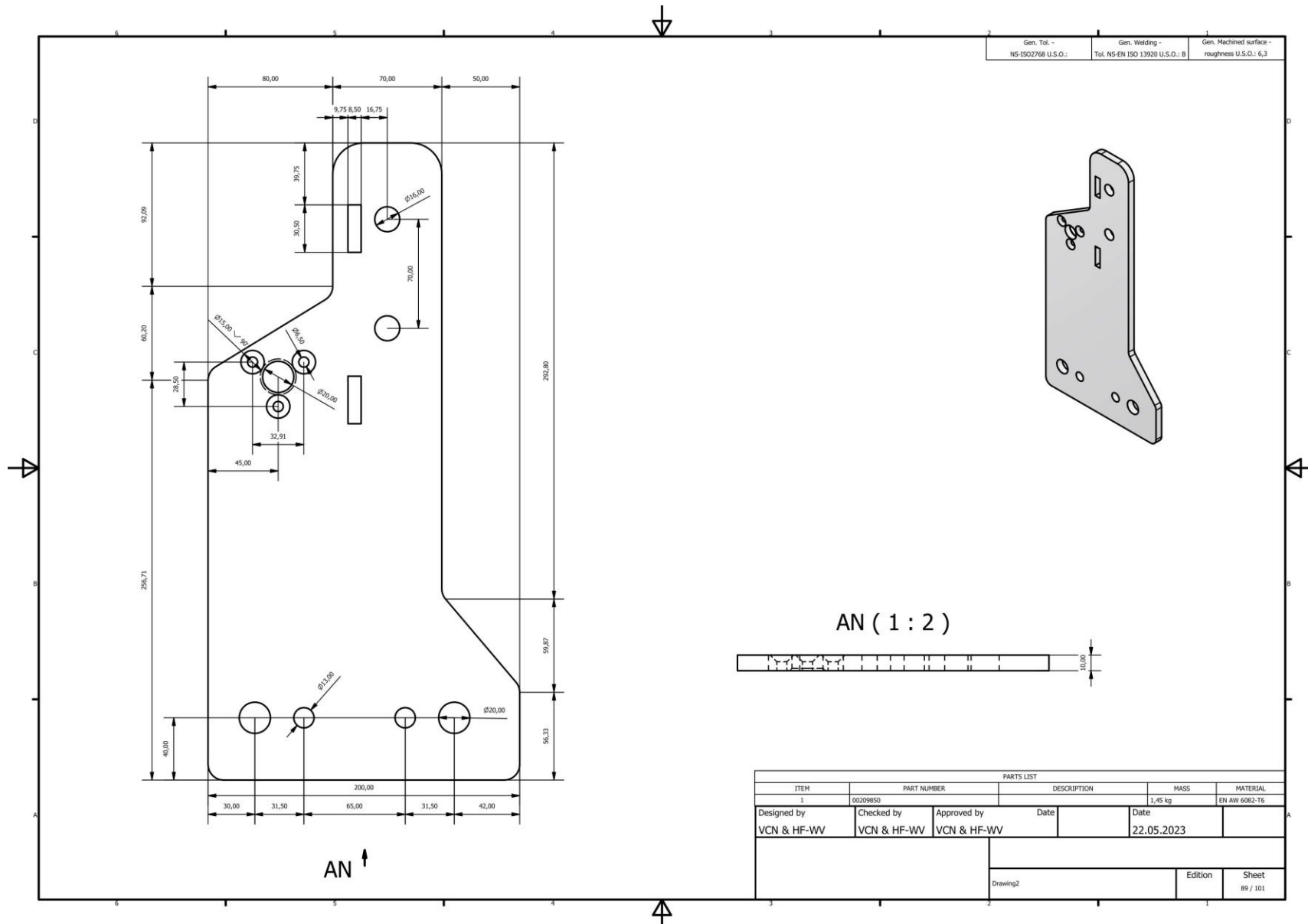
Integration of a Skid and Hatch-Based Launch and Recovery System for ROVs on USVs

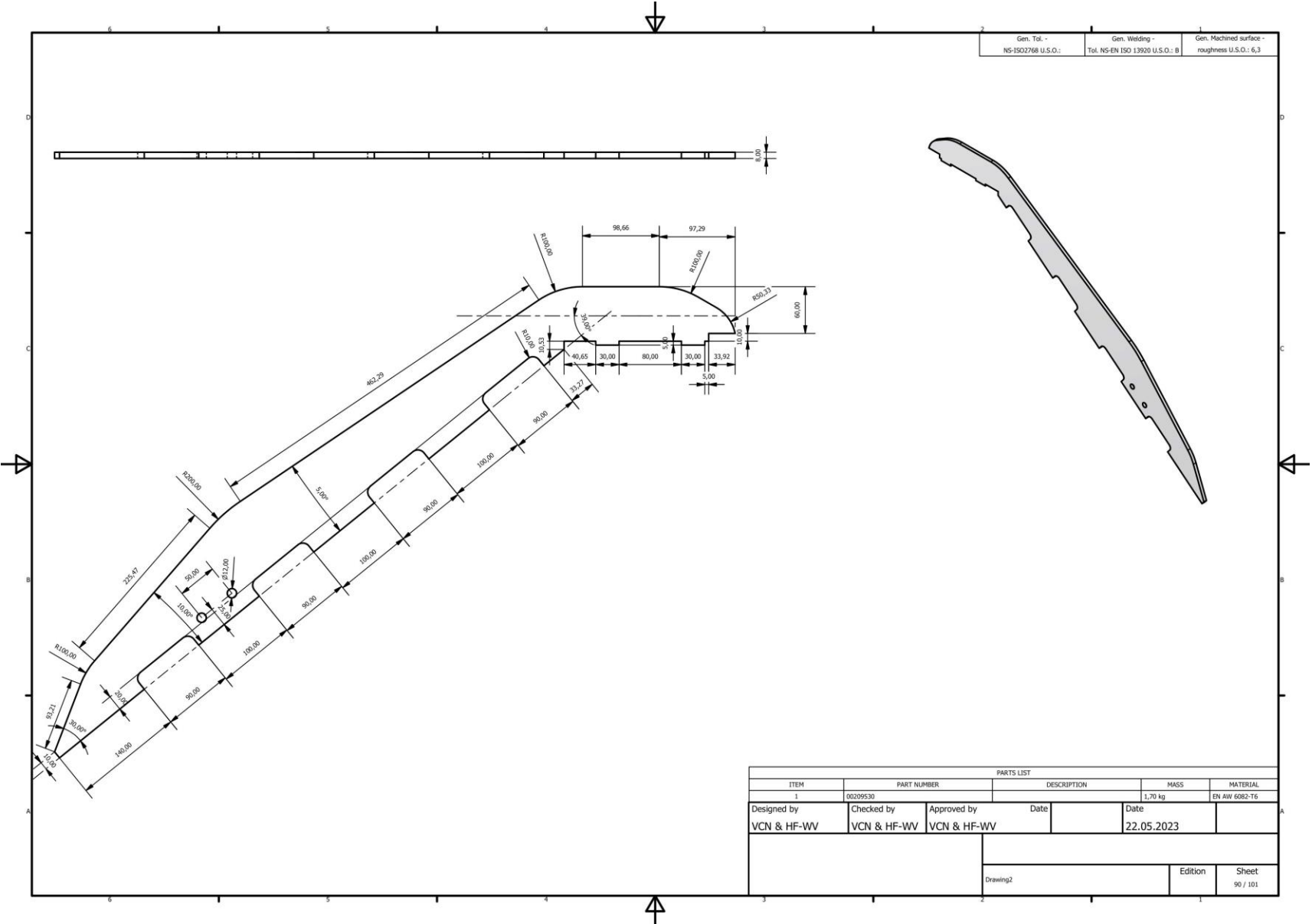


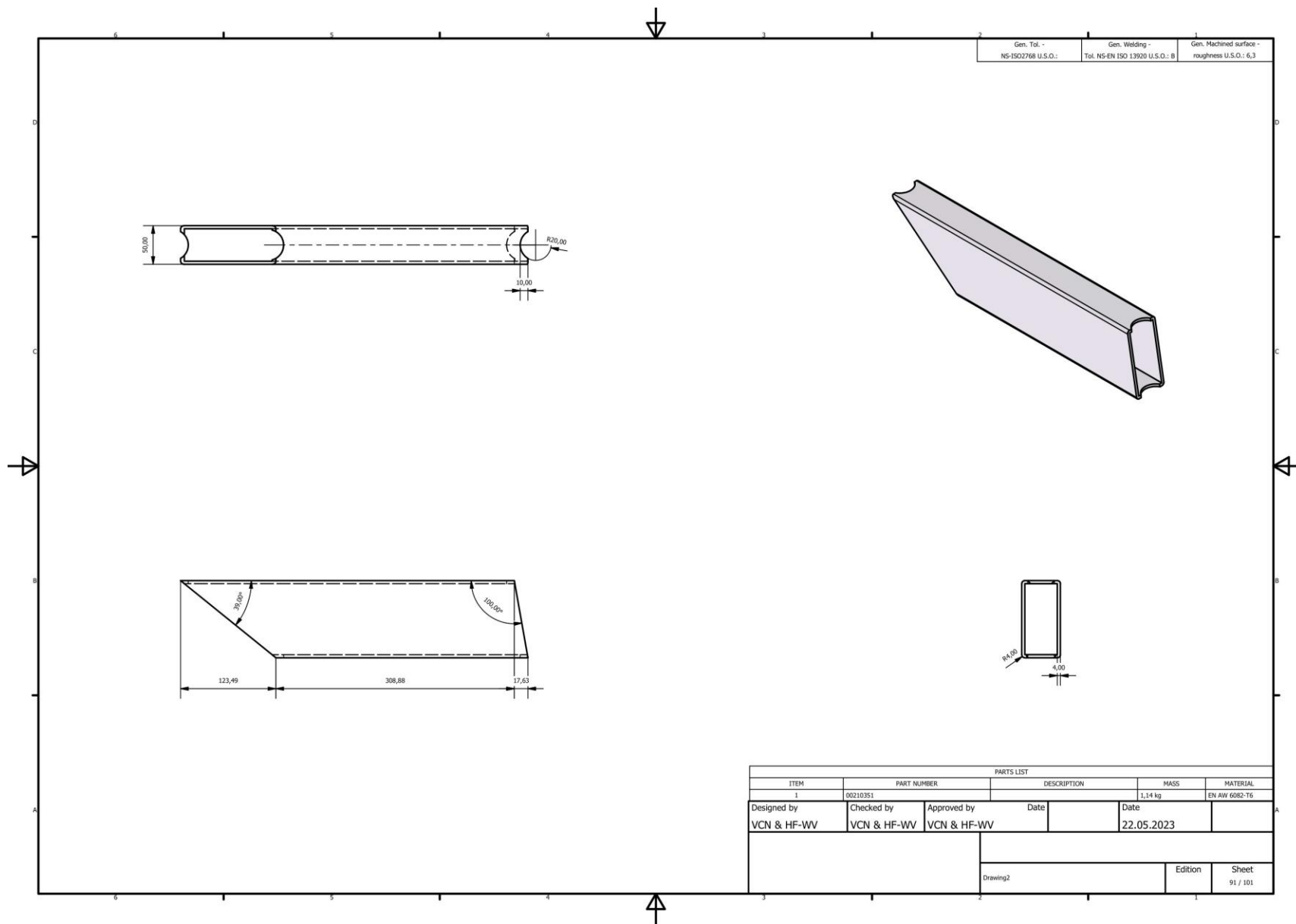


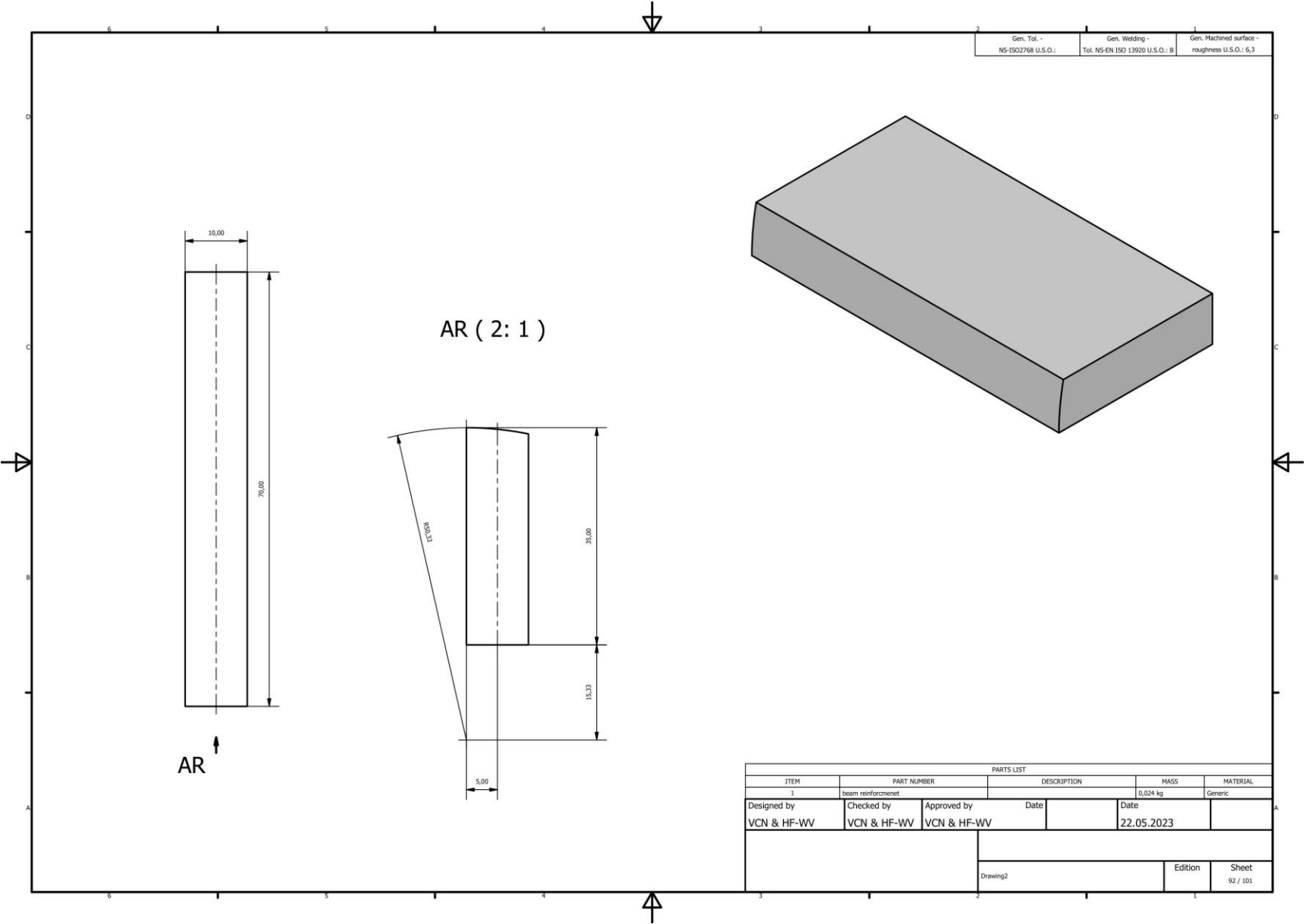


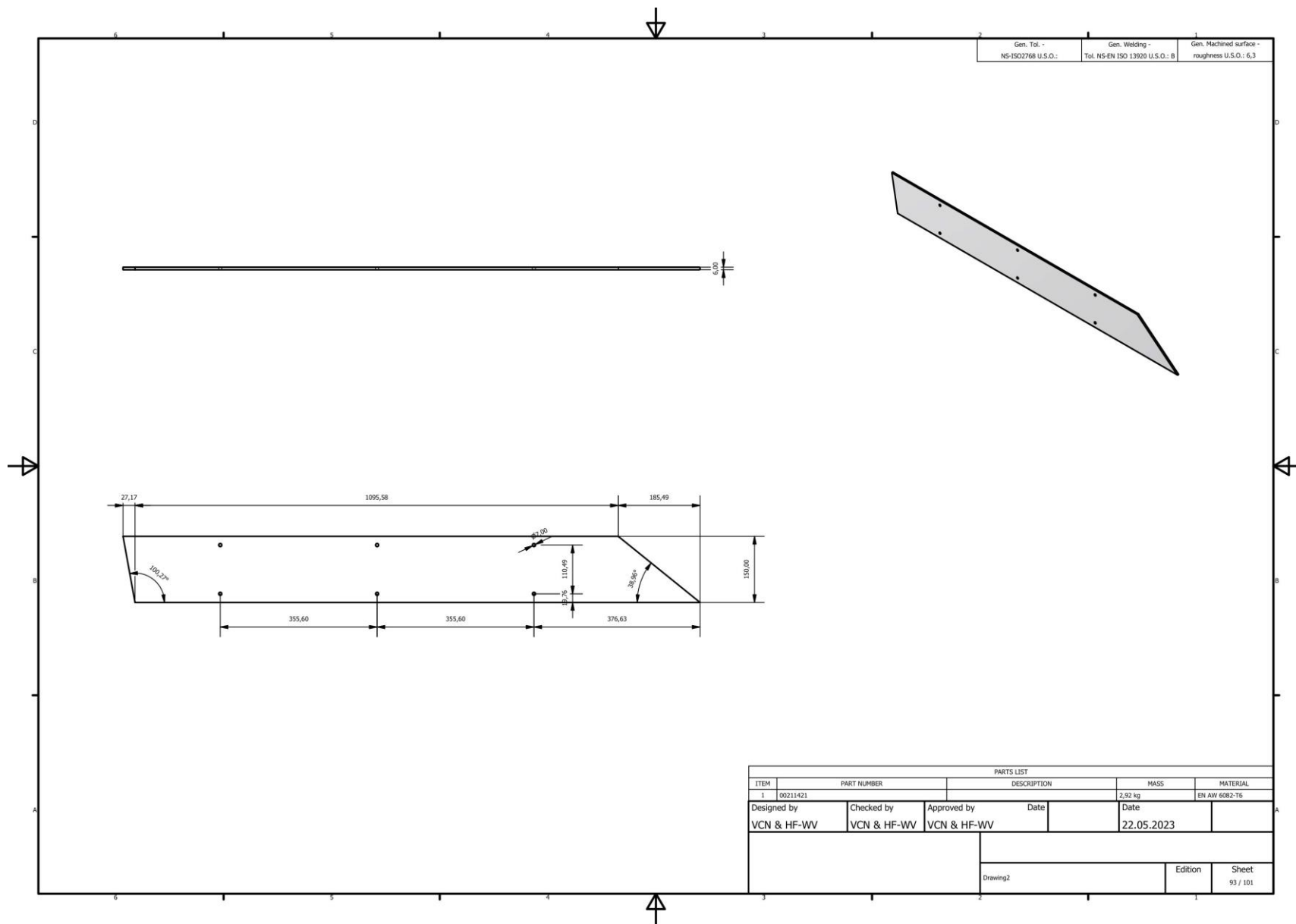


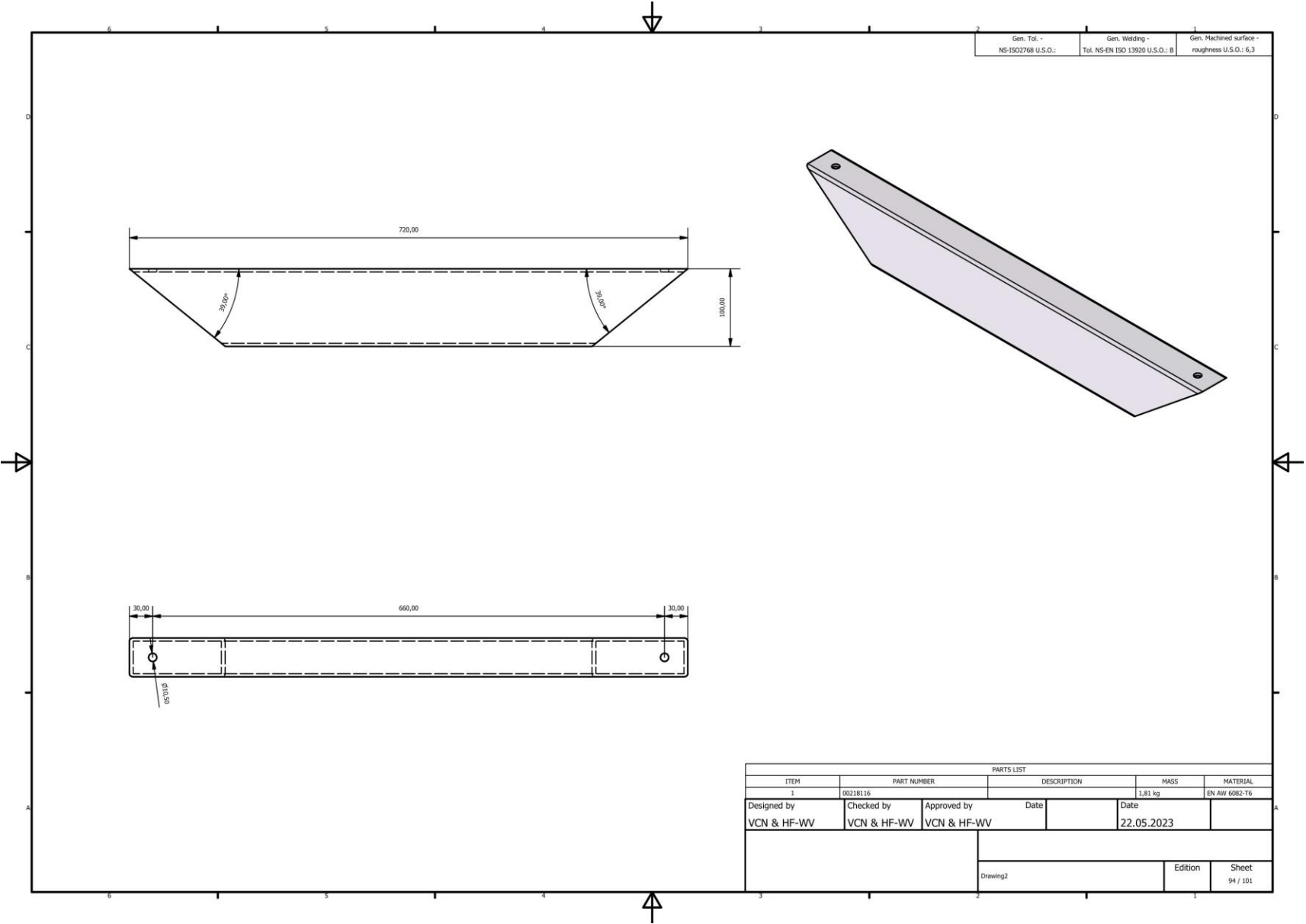


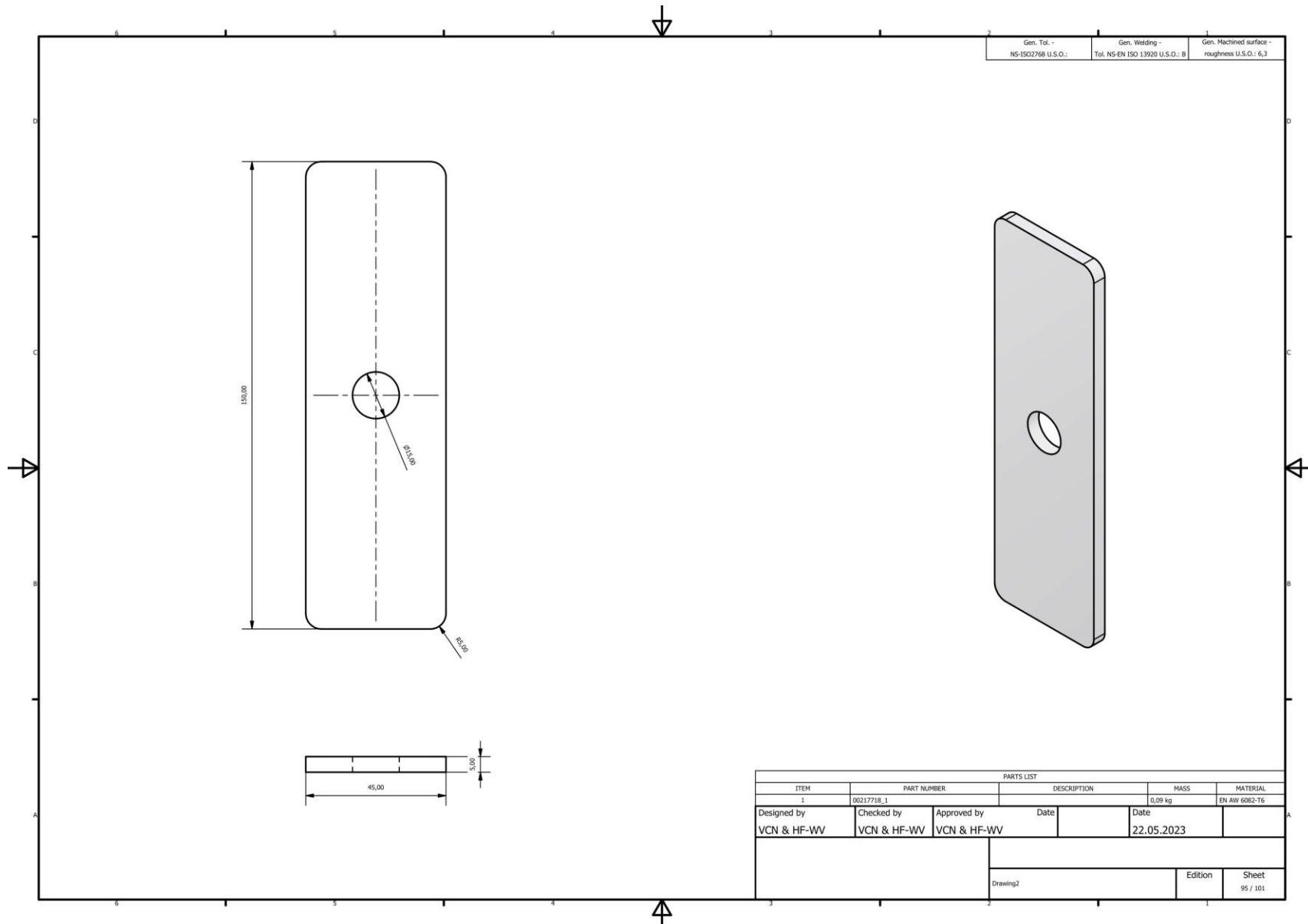


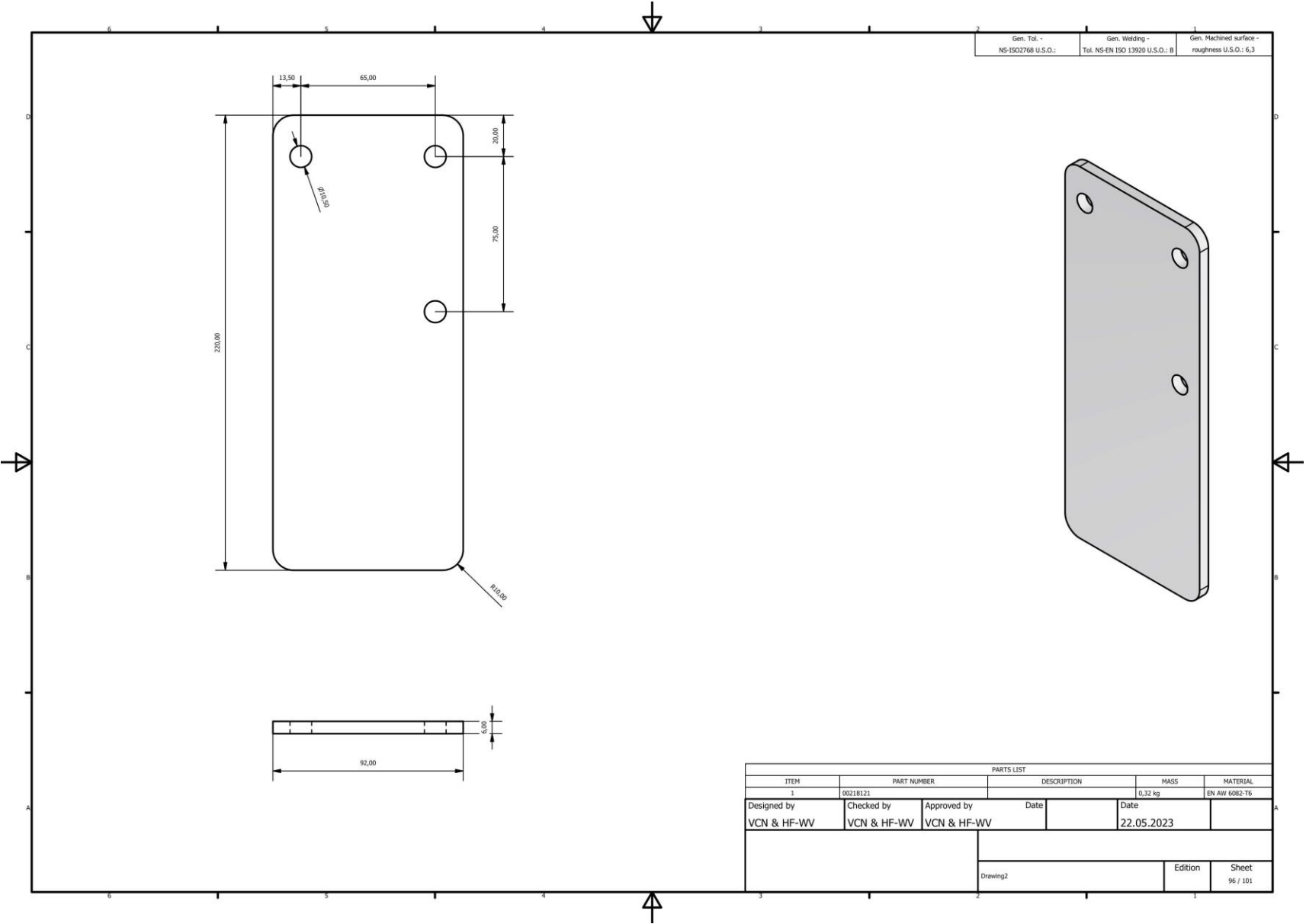


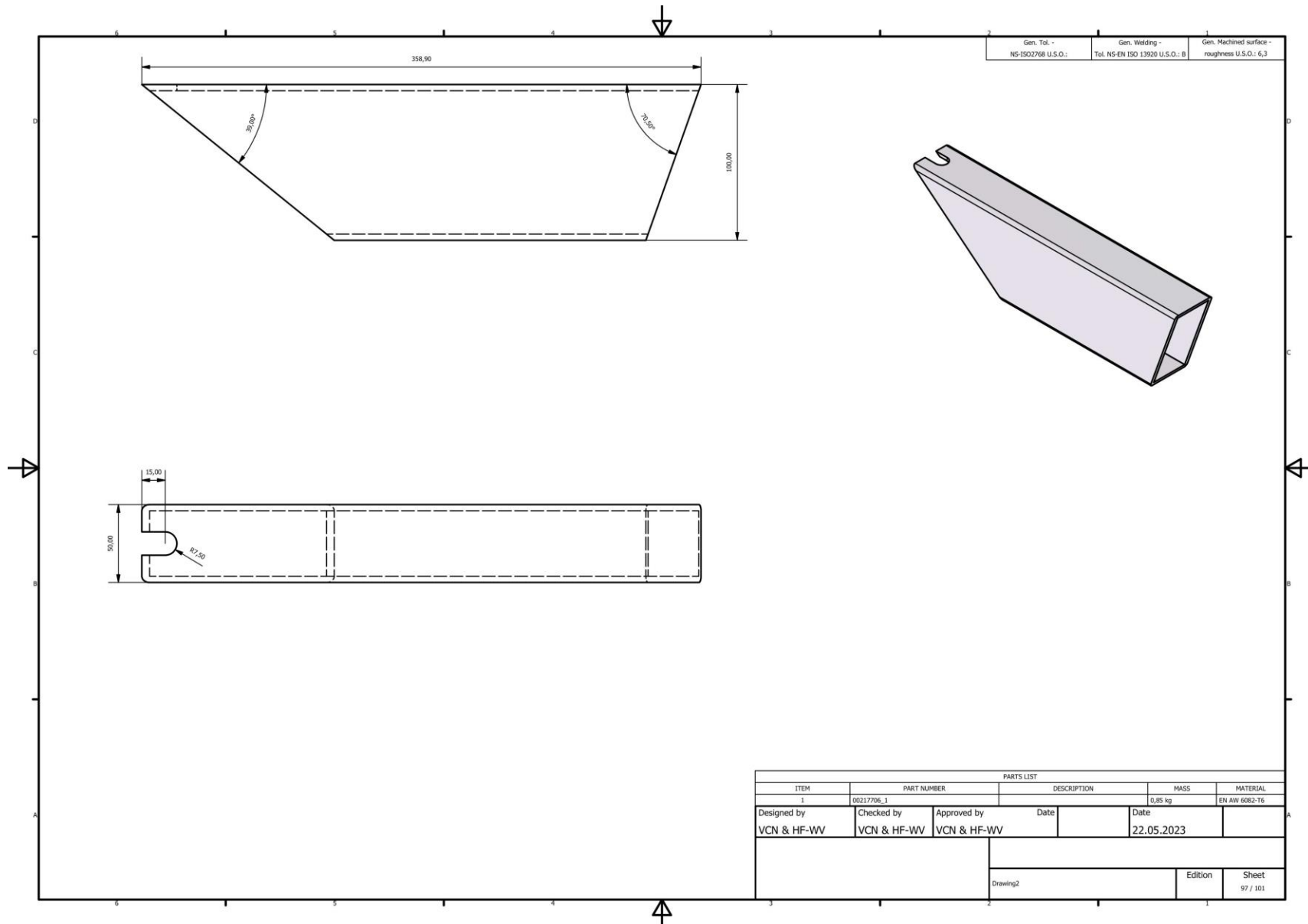


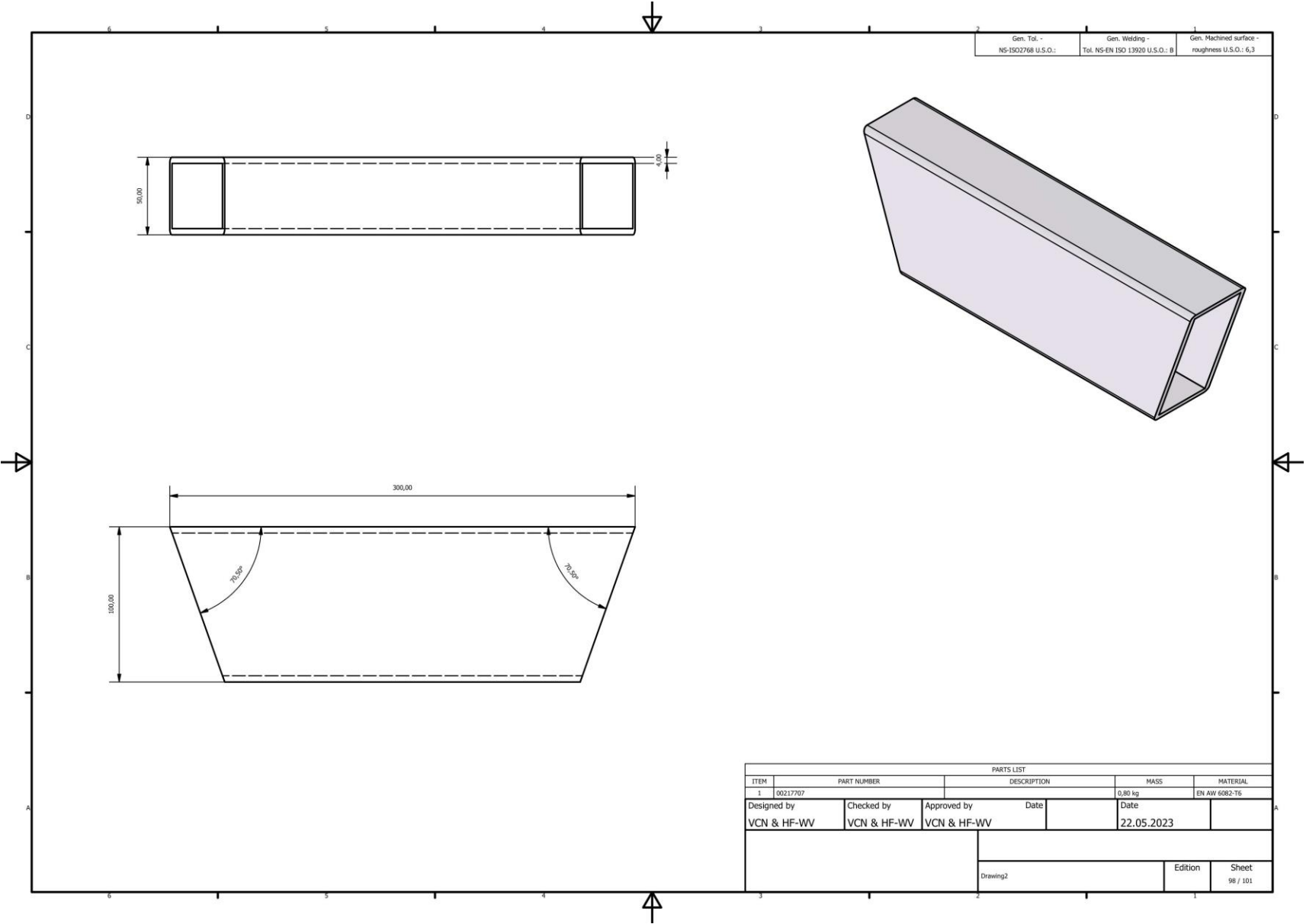




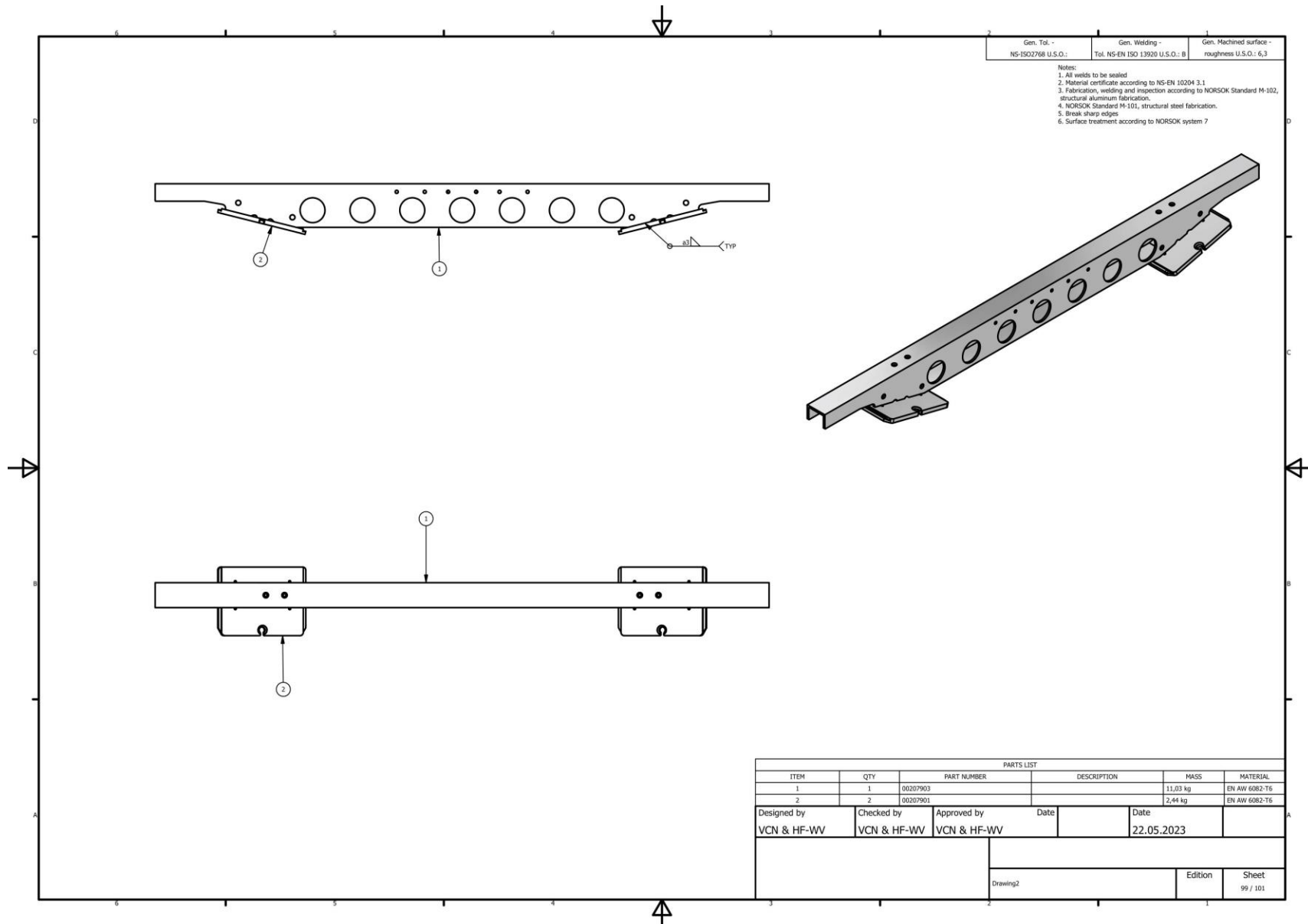


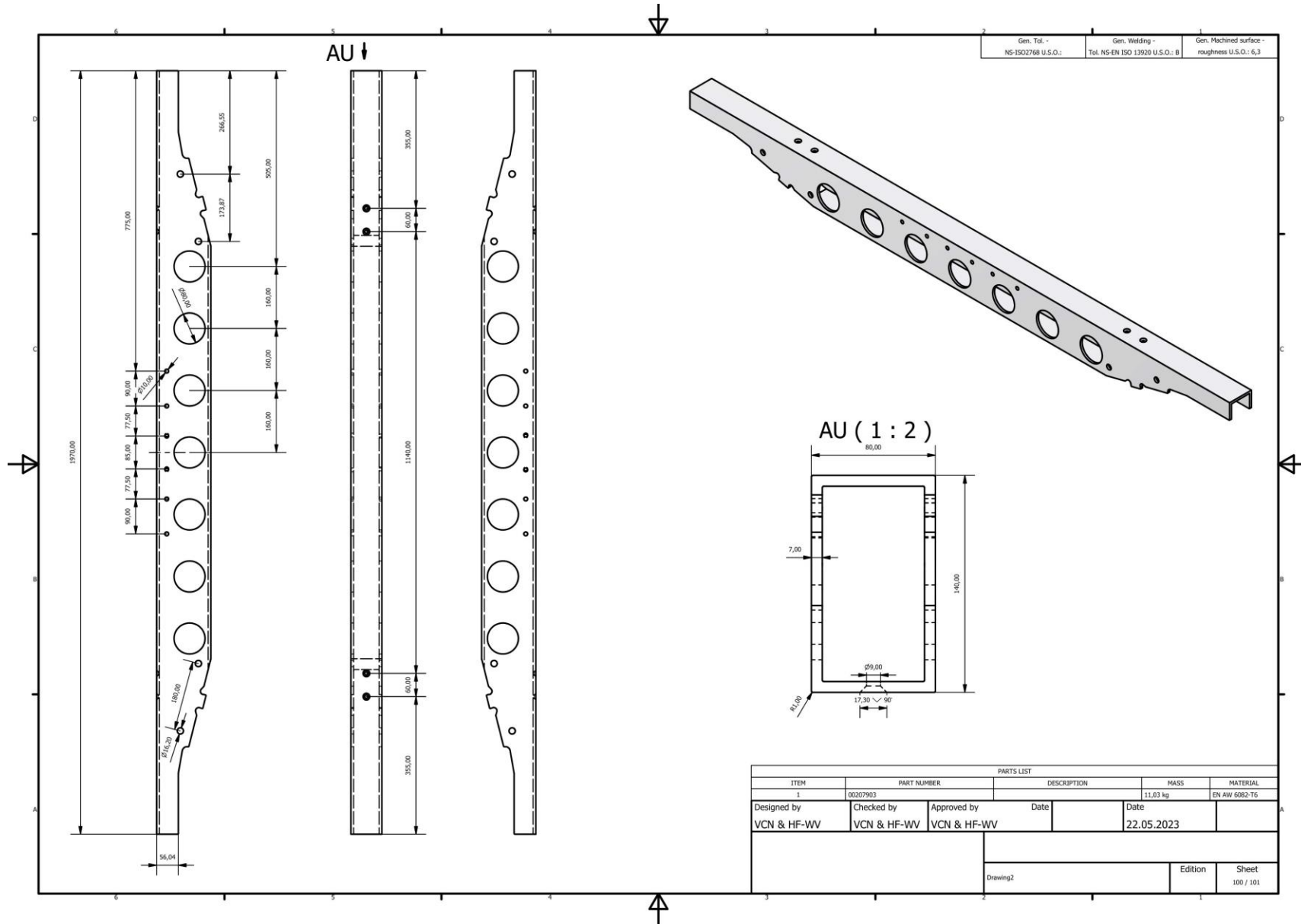


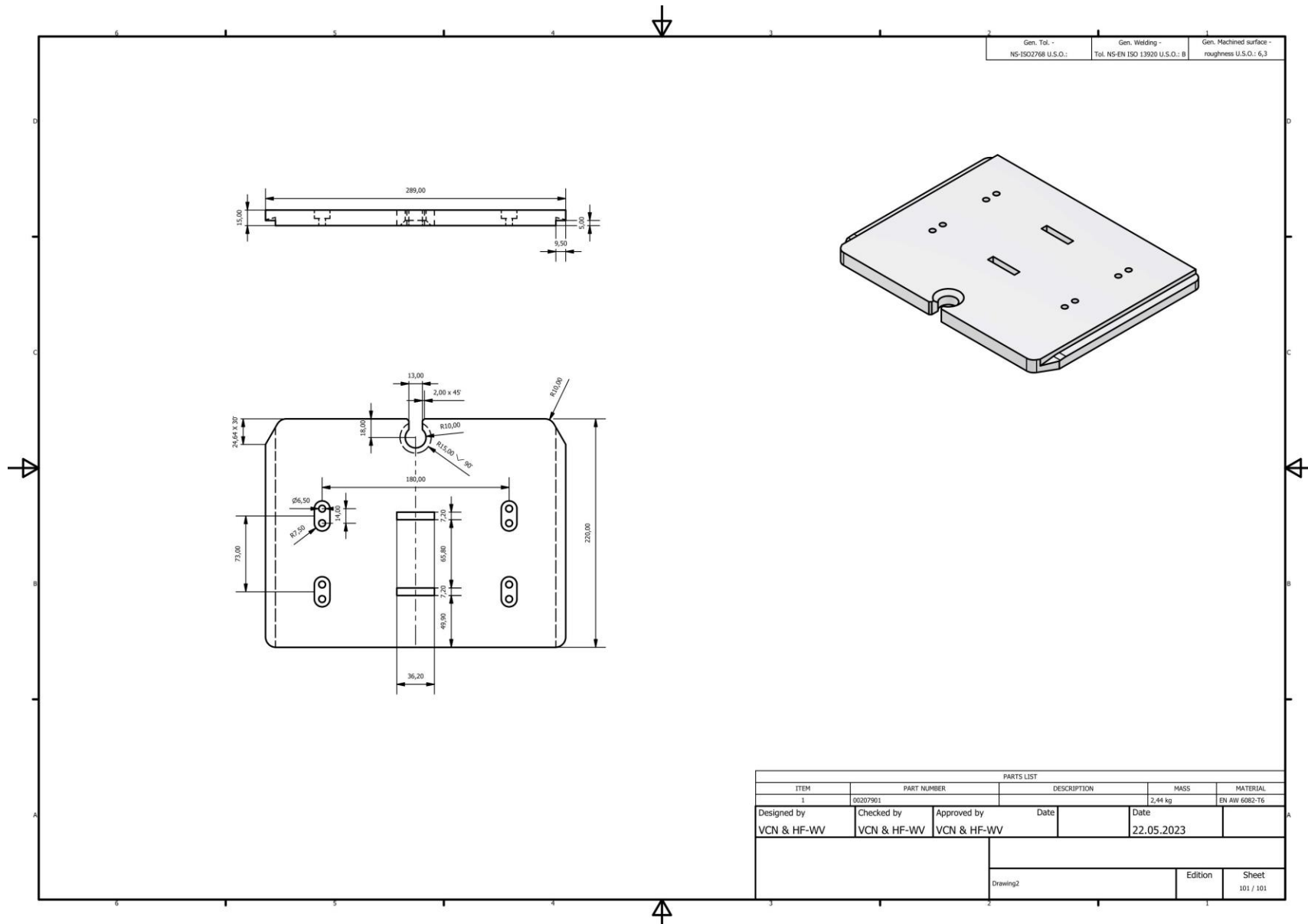




Integration of a Skid and Hatch-Based Launch and Recovery System for ROVs on USVs







Gen. Tol. - NS-ISO2768 U.S.O.:	Gen. Welding - Tol. NS-EN ISO 13920 U.S.O.: B	Gen. Machined surface - roughness U.S.O.: 6,3
-----------------------------------	--	--

PARTS LIST				
ITEM	PART NUMBER	DESCRIPTION	MASS	MATERIAL
1	00207901		2,44 kg	EN AW 6082-T6
Designed by	Checked by	Approved by	Date	Date
VCN & HF-WV	VCN & HF-WV	VCN & HF-WV		22.05.2023
Drawing2			Edition	Sheet
				101 / 101